Encoding of Object Presence and Manipulation Affordances in the Frontoparietal Grasp Network

by

Rex N. Tien

B.S.E., Mechanical Engineering, Princeton University, 2011

Submitted to the Graduate Faculty of

the Swanson School of Engineering in partial fulfillment

of the requirements for the degree of

Doctor of Philosophy

University of Pittsburgh

2021

UNIVERSITY OF PITTSBURGH

SWANSON SCHOOL OF ENGINEERING

This dissertation was presented

by

Rex N. Tien

It was defended on

December 17 2020

and approved by

Jennifer L. Collinger, PhD, Associate Professor, Department of Bioengineering

Zhi-Hong Mao, PhD, Professor, Department of Electrical and Computer Engineering

Peter L. Strick, PhD, Distinguished Professor and Chair, Department of Neurobiology

Carl R. Olson, PhD, Professor, Center for the Neural Basis of Cognition, Carnegie Mellon University

Dissertation Director: Andrew B. Schwartz, PhD, Professor, Department of Neurobiology

Encoding of Object Presence and Manipulation Affordances in the Frontoparietal Grasp Network

Rex N. Tien, PhD

University of Pittsburgh, 2021

The ability to grasp and manipulate objects is a fundamental human capacity. Loss of this function due to injury or disease can result in the inability to independently perform tasks of daily living. Brain computer interfaces (BCIs), which decode neural activity to control assistive devices, represent a new class of potential therapies to restore arm and hand function. Recent efforts to implement BCI control of a robotic hand for grasping have been hindered by unexpected neural modulations in primary motor cortex (M1) related to the contextual factor of whether movements were made with or without an object present.

We designed and carried out three experiments in healthy rhesus macaque monkeys to characterize the influence of various object-related contextual factors on movement features (MFs — kinematics and muscle activity of the arm and hand) and on neural activity in three grasp-related brain areas: M1, ventral premotor cortex (PMV) and anterior intraparietal area (AIP). A novel method was devised to implant intracortical microelectrode arrays in PMV and AIP for these experiments. In Experiment 1, monkeys performed similar reaching movements with or without an object present. In Experiment 2, monkeys performed similar grasps on a set of objects with different grip affordances (objects could be grasped in multiple ways). In Experiment 3, monkeys performed similar grasps on two objects with different use affordances (one was stationary and one could be lifted). All object-related contextual factors were found to evoke small but significant differences in MFs despite task requirements remaining constant across contexts. These context-dependent behavioral differences were accompanied by proportionately larger neural differences in all three brain areas. The presence or absence of an object resulted in changes in neuronal firing rates that could not be accounted for by linear encoding of MFs. This object presence signal was found to interact with MF encoding in M1 in a way that

was detrimental for BCI-style MF decoding. Object grip affordance differences resulted in similar but smaller neural modulations that did not impact MF decoding. Neural modulations related to object use affordance were prominent only in PMV.

Table of Contents

List of Tables

List of Figures

Preface

This dissertation is dedicated to my family, who have provided me with endless support throughout my doctoral journey. I am incredibly grateful for their love, advice and guidance, and I am lucky to have such caring and insightful role models so close at hand.

I must also thank my advisor, Andy, for bestowing monumental amounts of knowledge upon me and allowing me the freedom and resources to forge my own academic path. I have greatly enjoyed my time working with Andy in the MotorLab, from performing monkey brain surgery to seeing the first spikes on a freshly implanted array to sharing exciting discoveries and subsequently discussing them for hours.

None of the work in this dissertation would have been possible without the formal and informal training I have received from the brilliant postdocs, PhD students and staff of the MotorLab, the Chase Lab, and the Center for the Neural Basis of Cognition. Engaging with such a rich range of scientific perspectives has made me the researcher I am today.

I am ever indebted to the industrious and attentive staff of the Pitt Bioengineering Department, the Division of Laboratory Animal Resources and the McGowan Institute for Regenerative Medicine for providing superb research support and a world-class academic experience.

Finally, I credit my ability to complete this work to the inspiration and energy I garner from my inimitable friends. Throughout my time in Pittsburgh, I have been surrounded by a vibrant and eclectic community that has nurtured me as a person, enriched my creativity and imagination, and propelled me ever onward and upward toward success.

1.0 Introduction

The ability to grasp and manipulate objects is a fundamental human capacity that forms the basis of our technological achievements and is central to many of the tasks of daily living. The effortlessness with which we regularly grasp and manipulate objects belies the complex problem that the brain faces in controlling the arm and hand.

While much has been learned about how the brain controls the hand to interact with objects, a great deal is left to be understood. A frontoparietal network of brain regions has been identified as critical for the control of visually guided grasp in primates. At the core of this grasp network are primary motor cortex (M1), ventral premotor cortex (PMV) and anterior intraparietal area (AIP). These areas are thought to implement a visuomotor transformation by which visual information about an object is transformed into a motor command to grasp it.

Understanding of how the brain naturally controls movement has enabled the development of therapeutic technologies for those who have lost arm and hand function due to injury or disease. In recent years, brain computer interfaces (BCIs) have emerged as a promising potential new therapy for individuals with paralysis. These BCIs can restore function by decoding movement intentions from brain signals, often recorded in M1, to drive assistive devices such as a computer cursor or a robotic prosthetic arm. While early BCIs have been largely successful in controlling robotic arms for broad reaching movements, recent efforts have faced difficulties in implementing BCI control of a robotic hand to dexterously interact with objects. These difficulties are due in part to unexpected changes in M1 neural activity which relate to the contextual factor of whether grasping movements were made on a real physical object or in open space, with no object present. In order to build future BCI systems that can successfully enable all of the various grasp-related tasks performed in daily life, such context-dependent neural activity needs to be understood and accounted for.

Graspable objects, especially those with known uses such as tools, have been found to be especially strong contextual drivers of activity in the frontoparietal grasp network. Human

brain imaging studies suggest that merely seeing an object or reading the name of an object can activate grasp network regions. Human behavioral evidence suggests that this activation relates to the object's affordances — those actions which are available to be performed on the object given its perceived properties and the capabilities and knowledge of the grasping individual. Moreover, contextual factors such as an object's overall shape, the known uses associated with the object, or the way in which the object will be manipulated after grasp all affect how the object is grasped. These contextual effects have rarely been studied at the level of single neurons and population spiking activity.

The goal of this dissertation is to characterize the influence of object affordance related contextual factors on grasping behavior and spiking neural activity in M1, PMV and AIP in a healthy rhesus macaque model (*macaca mulatta*). Three experiments were designed and carried out to investigate three possible object affordance related contextual factors. Throughout all experiments, movement features (MFs — detailed kinematics and muscle activity of the arm and hand) and neural activity in M1, PMV and AIP were recorded. The overall strategy of each experiment was the same: to elicit very similar behaviors in different object affordance contexts in order to isolate and characterize the component of neural activity related to object context.

In the Object Presence Experiment, monkeys performed similar reaching movements with or without an object present and also grasped the object. Moderate differences in MFs were observed between reaches with our without the object present. The presence or absence of an object evoked proportionately large modulations in neural activity throughout the grasp network which could not be accounted for by linear tuning to MFs. This object presence related neural signal interfered with the ability to decode MFs from M1 neuronal firing rates. We propose a modified decoder architecture to mitigate these effects. Further, when the object was present, reach behavior and neural activity throughout the grasp network was biased toward the behavior and activity patterns that were normally observed when the object was grasped, suggesting that the mere presence of the object activated the neural representations of the grasp actions afforded by the object, even when it was not grasped.

In the Grip Affordance Experiment, monkeys performed similar grasps on objects with different grip affordances. Objects could differ in terms of their perceived grip affordances

— the multiple ways in which the objects could be grasped based on their shape — or in terms of their learned grip affordances — the ways that the objects were habitually grasped. Small but significant differences in MFs were observed for grasps on the different objects, despite the fact that the grasped portions of the objects were identical. Grip affordance differences evoked small but significant changes in neural activity, some of which could not be accounted for by linear tuning to MFs. This grip affordance related signal did not impact the ability to decode MFs. There was weak evidence for the automatic activation of grip affordance representations in background M1 activity.

In the Use Affordance Experiment, monkeys grasped two objects over two separate sessions. In the first session, both objects were mechanically fixed in place. In the second session, one object remained fixed, while the other was released and was intermittently lifted by the subjects. Thus, in the second session, the movable object gained the learned use affordance of lifting. In the pre-learning session, small but significant differences were observed in MFs and neural activity when the two objects were grasped. In the post-learning session, relatively larger differences were observed in behavior and neural activity for grasps on the different objects. The neural differences in PMV were larger than could be accounted for by linear encoding of MFs, and thus constituted encoding of the learned use affordance. Strong use affordance encoding was not observed in M1 or PMv, suggesting that PMV played a special role in storing and processing the learned use affordance of the movable object. When the movable object was grasped and held (but not lifted), behavior and neural activity was similar to that observed when the object was actually lifted, suggesting that the representation of the lifting affordance may have been automatically activated when the movable object was grasped.

PMV and AIP were identified as potential sources of object context information in M1. In a few instances, PMV and AIP units displayed extreme firing rate modulations for contextual differences. Preparatory activity related to object context was prominent in these areas, especially with regards to object presence. The relative timecourses of population modulation in M1, PMV and AIP suggested that contextual information may be processed in a feedforward manner from AIP to PMV to M1.

This dissertation represents several novel contributions to the fields of grasp neuroscience and neural engineering. While many studies have explored the relationship between neural activity and MFs, fewer have directly inquired into the presence of context-dependent activity in motor cortical areas. Those studies which have found context-related activity often did not monitor behavior in detail, and were thus unable to determine the extent to which neural changes reflected contextual factors or encoding of behavioral differences. In the experiments of this dissertation, behavioral differences were minimized across contexts and detailed features of the behavior were recorded, allowing context-related changes in behavior and neural activity to be measured and compared.

Several novel behavioral tasks were developed and employed in the experiments of this dissertation. To our knowledge, no published study has examined both grasping and reaching in free space in the same experiment. This comparison is enabled by the task design of the Object Presence Experiment. The design of the Grip Affordance Experiment represents a unique dissociation of perceived and learned grip affordances. The design of the Use Affordance Experiment reveals the neural changes associated with the learning and processing of object use knowledge.

Additionally, few studies have recorded neural activity simultaneously in M1, PMV and AIP. Those that have were focused on movement-related activity in these areas. The experiments of this dissertation grant insights into the comparative levels of context-related activity in these areas as well as the timing and directionality of context-related information flow through the grasp network.

Lastly, a novel method was devised and used to position and implant penetrating intracortical microelectrode arrays in PMV and AIP to obtain neural data for the experiments described herein. PMV and AIP are located in the banks of the arcuate and intraparietal sulci, which are not immediately accessible on the cortical surface. Magnetic resonance imaging was used to visualize the morphology of the sulci. Segmentation software was used to extract this morphological information, which was subsequently transferred to computer-aided design software. The stereotaxic surgical equipment was modeled alongside the brain structures in the virtual model, and this information was used to design and 3D print insertion alignment guides. The guides were sterilized and used

during surgery to rapidly and accurately implant eight microelectrode arrays in PMV and AIP in two separate procedures. This method represents a low-cost solution for array implantation in sulcal brain areas which can be extended to other brain regions or devices.

1.1 Structure and Contents of this Dissertation

Chapter 2 contains an in-depth review of the scientific literature relevant to the experiments carried out for this dissertation. Studies concerning the general aspects of grasping behavior are presented in Section 2.1. M1, PMV and AIP are then introduced individually in Sections 2.2, 2.3 and 2.4. The history, anatomical connectivity and function of each area are discussed. Progress in the field of BCI is discussed in Section 2.2.1. M1, PMV and AIP are then discussed in terms of their functioning as critical nodes of the frontoparietal grasp network in monkeys and humans in Section 2.5, with a focus on the processing of affordances in the grasp network and other frontoparietal networks (Section 2.5.1) and evidence for the automatic activation of affordance representations (Section 2.5.2). Section 2.6 contains a review of studies which describe context-dependency in grasp behavior. Section 2.7 contains a review of studies which describe context-dependent neural activity in M1, PMV and AIP, with general cases of context-dependent neural activity discussed first, and grasp-specific instances of context-dependent neural activity described subsequently in Section 2.7.1. Finally, the motivations for the three experiments of this dissertation are presented in Sections 2.8, 2.9 and 2.10, with reference to the gaps in the existing literature that these experiments address.

Chapter 3 contains a general description of the experimental design of the three experiments of this dissertation. Section 3.1 concerns the physical setup of the experiment room and the construction of the behavioral apparatus with which the monkeys interacted. Section 3.2 describes the behavioral tasks employed in the three experiments, including the task timing and progression, the visual feedback delivered during the tasks and the scheduling of task condition blocks within each session. Section 3.3 contains a brief description of the data streams that were recorded during the experiments.

Results from the Object Presence Experiment, Grip Affordance Experiment and Use Affordance Experiment are presented in Chapters 4, 5 and 6. These chapters contain results concerning M1 data, while the results concerning PMV and AIP data for all three experiments are presented in Chapter 7.

The findings of the three experiments are discussed in Chapter 8. The results are first summarized and interpreted in Section 8.1. Additional analyses which were run as controls are noted in Section 8.2. Section 8.3 addresses the limitations of the current experiments. Future research directions are considered in Section 8.4. Final conclusions are presented in Section 8.5.

The Appendix contains detailed descriptions of the experimental methods and data analyses employed for this dissertation. Section A.1 describes the surgical methods used to implant recording microelectrode arrays in M1, PMV and AIP. The novel method used for planning and inserting arrays in PMV and AIP is described in detail in Section A.1.2. The design and fabrication of the instrumented objects is presented in Section A.2. Section A.3 concerns the animal behavioral training strategies that were employed to achieve the desired behavioral outcomes. Section A.4 contains detailed descriptions of the methods used to acquire and preprocess the various data streams. The custom software used to automate the behavioral task is outlined in Section A.5. Finally, mathematical descriptions of the statistical methods used to analyze the data are presented in Section A.6.

2.0 Background and Review of Related Work

Grasping and using objects can seem routine and effortless. However, this belies the computational complexity entailed in controlling the intricate musculature and mechanics of the arm and hand. Over the last century, a large body of research has been devoted to studying the behavioral aspects of reaching, grasping and object manipulation and the neural mechanisms which enable and control these behaviors.

The cortical networks involved in grasping appear to be similar in humans and other dexterous primates such as monkeys. Three cortical areas in particular have been identified as critical nodes of the cortical grasp network: primary motor cortex (M1), ventral premotor cortex (PMV) and the anterior intraparietal area (AIP).

This chapter contains a review of the scientific literature concerning grasping behavior and the three brain areas at the core of the cortical grasp network. A particular focus is given to contextual effects in behavior and neural activity, as these are pertinent to the experiments performed for this dissertation.

This chapter is organized as follows. Section 2.1 contains a brief overview of general aspects of grasping behavior. Section 2.2 contains a review of the anatomical and functional properties of M1, including an overview of progress in brain computer interfaces and neuroprosthetics. Sections 2.3 and 2.4 concern the anatomical and functional properties of PMV and AIP, respectively. Section 2.5 explores the functioning of M1, PMV and AIP as a coherent network which implements the visuomotor transformations necessary for object interaction, including an overview of evidence for the automatic activation of motor representations in the network when graspable objects are viewed. Section 2.6 describes the context sensitivity of grasp behaviors. Section 2.7 describes contextual effects in neural activity in M1, PMV and AIP, with additional discussion of context dependent activity due to object-related factors in Section 2.7.1. Finally, Sections 2.8, 2.9 and 2.10 contain more detailed discussions of select studies with particular relevance to the three experiments described in this dissertation, and outlines the motivations for each experiment.

2.1 Grasping Behavior

The human hand is a specialized, highly complex neuromusculoskeletal system which enables a vast array of ways to interact with and manipulate the environment. One of the main ways that this interaction proceeds is through prehension — the closing of the hand around an object for subsequent transport or use. Despite the variety of potentially graspable objects and ways they can be grasped, grasping actions are executed with a certain regularity, and aspects of movement are conserved across different grasping actions.

In an early analysis of grasp in humans, Napier observed in 1956 that grasps could be classified into two broad categories [1]. He deemed these general categories "precision grip" and "power grip." Precision grips are characterized by the use of the pads of the thumb and one or more of the long digits to pinch the object. Examples of precision grips include holding a pen for writing and grasping a sheet of paper to feed it into a mail slot. Power grips are characterized by the long digits pressing the object against the palm, with or without assistance from the thumb. Examples of power grips include holding a hammer by the handle and holding a soda can to take a drink. Though these categories describe the two general classes of grips, a vast array of intermediate and modified versions of these grasps are observed in human behavior. The particular grasp is dictated by the size and shape of the object, as well as the intended use of the object.

In the 1980s, Jeannerod published a landmark study in which videos of human subjects reaching to grasp a series of objects were analyzed [2, 3]. It was observed that reach-to-grasp actions proceeded in two phases: an initial high-velocity phase in which the hand was accelerated toward the object and the fingers were extended followed by a low-velocity phase in which the hand was decelerated and the fingers were closed until contacting the object. In addition, the grip aperture (distance between thumb and index finger) was scaled to the size of the object to be grasped, even during the early part of the movement. The grip aperture increased during the reach and reached a maximum after the peak reach velocity, at which point the aperture decreased until contact was made wtih the object. The object-specific early scaling of the grip aperture was deemed "preshaping," and was present even without visual feedback of the hand.

A later study by Santello and Soechting examined finger kinematic trajectories in greater detail while subjects reached toward and grasped 15 geometrically complex objects [4]. Preshaping was found to occur gradually over the course of the reach. Significant correlation to the final hand posture was observed even at the midpoint of the reach. The object-specificity of the hand posture increased monotonically throughout the reach and was maximal at the time of object contact.

Further human behavioral studies have elaborated on these two main concepts (grip categories and preshaping). Based on photographs of hands grasping objects, Kamakura described 14 grip patterns in seven different categories [5]. Kroemer identified 10 postural couplings between hands and objects [6]. An exhaustive list of grasp postures would be difficult to achieve, as transitions between posture categories are continuous and each instance of grasping reflects the unique combination of the individual's idiosyncratic hand morphology, the object's physical characteristics and the intended use of the object. Nevertheless, grasping movement diversity appears to reflect variations on a set of basic grasp motifs.

Other efforts have been made to mathematically describe grasp movement variability using dimensionality reduction techniques. While the hand has roughly 25 kinematic degrees of freedom controlled by some 40 muscles [7], hand movements have been found to be coordinated along a smaller set of dimensions, or "hand synergies." Principal Components Analysis of detailed hand and finger kinematics revealed that during static pantomimed grasps, over 80% of the variance in 15 joint angles could be explained by two dimensions [8]. Analysis of dynamic reach-to-grasp trajectories toward 16 different objects revealed that over 90% of variance could be explained by a single hand synergy [9]. A further study revealed that naturalistic hand motions were more complex, with two hand synergies capturing about 60% of kinematic variance [10]. The number of hand synergies needed to capture kinematic variance is dependent on the complexity of the task and may be a hallmark of optimal control [11]. The low dimensionality in hand kinematics may reflect a combination of biomechanical and neural constraints [12].

Studies of grasping in rhesus macaque monkeys have revealed similar behavioral strategies to those found in humans. Video analysis of unconstrained monkey behavior

revealed the use of 15 different grip categories [13], as well as preshaping dependent on objects' physical characteristics [14]. Monkeys also exhibit object size specific preshaping, and display low dimensionality in dynamic hand kinematic variability [15, 16]. Monkeys display hand preshaping and show consistent object-specific kinematics when grasping different objects [17, 18]. Preshaping is evident in muscle activity as well as kinematics, as EMG recordings in arm and hand muscles of monkeys grasping six different objects were object specific, even during the early reach phase [19].

In daily life, it is rare to simply grasp and hold objects. Instead, objects are usually used for a purpose, often as tools. The learned and intended uses of an object affect the way in which the object is grasped (see Section 2.6). Human tool use is unparalleled in nature in terms of extent, flexibility and capacity to manufacture novel tools to accomplish specific goals.

Nevertheless, macaques are capable of cognitive complex object manipulation behaviors to a degree. Wild long-tailed macaques have been observed using stones to break open nuts and shellfish against anvils, or to detach shellfish from boulders and trees [20]. The stones used for the different actions were shaped differently and were grasped according to their use. In another instance, Tonkean macaques were observed transporting and using a long pole to scale the wall of a nature reserve [21]. In laboratory settings, rhesus macaques are capable of learning to use a rake to retrieve food that would otherwise be out of reach, though induction of this behavior often requires extensive training [22–29].

Controlling the arm and hand to successfully grasp and manipulate objects presents a difficult problem for the brain to solve. Though limited, the similarities in grasping behaviors in humans and monkeys suggest that similar neural mechanisms may be employed. Indeed, studies have identified a frontoparietal network of cortical areas with particular involvement in grasp and object manipulation in both monkeys and humans. The three critical nodes of this network are M1, PMV and AIP. The following sections will describe the anatomical and functional properties of these cortical areas based on results from human and monkey neuroscience.

2.2 Anatomical and Functional Properties of M1

In humans and monkeys, M1 is the cortical area most directly linked to the production of voluntary movement. M1 is located in the anterior bank of the central sulcus and on the adjacent convexity of the precentral gyrus, and corresponds to Brodmann Area 4 [30].

The earliest investigations of the functions of motor cortex involved electrical stimulation of the brain. In 1870, Fritsch and Hitzig identified an area of the dog brain that, when stimulated with current from a battery, evoked muscular contractions on the contralateral side of the body [31]. Stimulating different areas of the cortex reliably caused different muscles to contract, suggesting an organized map of the different body parts in cortex. In 1875 these results were extended to monkeys in a study by Ferrier [32]. Ferrier noted a progression through contralateral leg, trunk, arm, hand and face muscle contractions as the stimulation was applied starting from more medial portions of the precentral gyrus and moving to more lateral portions. Ferrier also noted that brief stimulus evoked localized muscle twitches, but stimulus applied for a longer period (several seconds) evoked more complex, multi-joint movements.

In 1937, Penfield and Boldrey published a detailed functional map of the human motor and sensory cortices [33]. They stimulated the brains of epilepsy patients and recorded the resulting muscle contractions and sensations reported by the patient. The authors identified an organized map of the contralateral side of the body along the mediolateral aspect of the precentral gyrus, and illustrated a motor "homunculus" to describe this somatotopic map. They noted that disproportionately large regions of cortex were related to face, tongue and hand movements.

Subsequent studies in monkeys [34–36] and humans [37] have replicated the ability to evoke muscle twitches by focal electrical stimulation of M1 at relatively low thresholds. These studies confirm the presence of a gross homuncular map in M1, but reveal that the somatotopy of M1 is more complicated than initially believed, as particular muscles can be activated from multiple separate regions in M1. Recent studies have confirmed Ferrier's finding that long duration stimulation of M1 can evoke complex, multi-joint movements which appear similar to some natural behaviors including grasping [38–40].

Anatomical tracer histology studies reveal that the hand area of M1 receives projections from other areas within M1, a range of premotor areas including ventral and dorsal premotor cortex, supplementary motor area and cingulate motor areas, primary and secondary somatosensory cortices, posterior parietal cortex areas including AIP, and the insula [40, 41], as well as the ventrolateral thalamus, which receives cerebellar and pallidal inputs [42].

The influence of M1 on muscle activity is largely mediated by the corticospinal projections of the pyramidal tract. Kuypers identified this projection in monkeys by lesioning M1 and observing a degeneration of pyramidal tract axons projecting to the gray matter and motoneuron pools in the spinal cord [43]. Projections from M1 constitute a large portion of the corticospinal tract (35–50%) [44–47].

In monkeys and humans, the corticospinal projections from M1 include "corticomotoneurons" — cells which originate in M1 and synapse directly on motoneurons in the ventral horn of the spinal cord [48]. Anatomical tracer studies indicate that these corticomotoneurons are predominantly located in the caudal portion of M1 in the anterior bank of the central sulcus [49]. The direct synaptic link between these corticomotoneurons and their target motoneurons and muscles can be revealed using spike-triggered averaging [50–54].

M1 and its corticospinal projections in the pyramidal tract, including the corticomotoneurons, are particularly critical for producing the individuated finger movements necessary for grasping small objects [55, 56]. Complete bilateral lesion of the pyramidal tracts in monkeys resulted in a global motor control deficit from which nearly all movements were eventually recovered except for the fine dexterous control of the fingers necessary for precision grasps, which remained permanently abolished [57]. Very similar results were observed when M1 of adult or juvenile monkeys was permanently lesioned [58]. Transiently inactivating monkey M1 hand and arm area using muscimol results in paresis of the contralateral arm, hand and fingers, marked reduction in grip strength and an inability to perform precision grips [59–62] or independent finger movements [63]. Similarly, M1 or corticospinal tract damage in humans is associated with hemiparesis on the contralateral side, reduced independence of finger movements and reduced performance

on tasks of daily living [64]. Comparative anatomy studies reveal that the prevalance and extent of the corticomotoneuronal system in a given species coincides with its capacity for manual dexterity, especially among primates [65, 66].

The connectivity between M1 and spinal interneurons and motoneurons is complex, as single neurons in M1 can synapse in multiple locations in the spine and the motoneurons of a single muscle receive input from multiple regions in M1 [67]. Axons from M1 corticospinal neurons branch in the spinal cord to innervate multiple regions in the spinal gray matter and the motoneurons of multiple different muscles [68]. Accordingly, spike-triggered averages reveal that single corticomotoneurons can facilitate a "muscle field" comprising multiple muscles acting across proximal and distal joints [53, 69]. Stimulation in any particular region in M1 activates a set of muscles acting on multiple joints [70], often including multiple opposing muscles across a single joint [71]. Retrograde tracers injected in hand muscles reveal that a single muscle's motoneurons can receive direct and indirect input from neurons spanning the entire hand/arm area of M1 [72]. A further complication is that individual spinal interneurons can influence multiple muscles in complex ways [73–75].

Given the relatively direct anatomical linkages between M1 neurons and motoneurons, and the readiness with which muscle activity can be evoked by stimulating M1, neural activity in M1 was initially hypothesized to be directly related to muscle activity and the production of force. Accordingly, neurons projecting in the corticospinal tract have been referred to as "upper motor neurons" [76, 77]. This designation suggests an overly simplistic view of M1 neurons, as a large number of electrophysiological investigations have revealed that M1 neural activity "encodes" not only muscle activity, but many features of movement at multiple levels of abstraction.

M1 neuronal firing rates (FRs) have been found to encode force, both in terms of grip force when grasping an object [78–82] as well as directional force applied isometrically through the hand [83–85]. M1 neural activity is also correlated with muscle activity [54, 86, 87] and functional muscle synergies [88]. However, even in early studies, it was evident that the relation between M1 neural activity and muscle activity was not straightforward. For instance, corticomotoneurons were often found to have higher FRs during precision grasps than during power grasps despite muscle activity being much

higher for power grasps in general [89]. This discrepancy was hypothesized to represent the contribution of corticomotoneurons to the fractionation of finger movements necessary to execute the precision grasps [90].

In a series of studies in the 1980s, the Georgopoulos research group showed that M1 neurons encode a more abstract, extrinsic feature of movement: the direction of reach. They utilized a "center-out" reaching task in which a monkey held a manipulandum and made outward movements to targets dispersed radially around a central starting location. The FRs of individual M1 neurons were found to be maximal for reaches in a certain direction (the "preferred direction" of the neuron), and decreased for movements away from that direction according to the cosine of the angle between the movement direction and the preferred direction. This "cosine tuning" was found for reaches in a plane [91] as well as in 3D space [92]. Based on this property of individual neurons, the intended movement direction could be "decoded" from a population of M1 neurons by computing a vector sum of the neurons' FR modulations projected onto their preferred directions to generate the "population vector" [93–95]. This encoding of an extrinsic, more abstract feature of movement suggests that M1 neural activity is related to high-level aspects of movement.

In the years since, a flurry of experiments have shown M1 neural activity to be related to an array of movement features. With respect to reaching movements, these encoded features include reach target direction and distance [96], reach direction and speed and their interaction [97], combinations of target direction and hand kinematics [98], temporally extended movement fragments [99], final limb posture [100, 101] and isometric loads at the endpoint and across the joints of the arm [102]. In general, during reaching, hand velocity is encoded more strongly than hand position [103, 104]. Direction encoding is not fixed to a particular reference frame, as different neurons can encode direction in extrinsic, hand-centered or shoulder-centered frames [105]. Studies comparing the encoding of intrinsic (muscle-related) features to extrinsic (direction-related) features show that individual neurons often display one type of encoding, but can encode a mixture of both, [106–108]. M1 is most strongly activated for reaches of the contralateral arm, though some activity can be observed during ipsilateral arm reaches [109]. M1 activity is also related to the impedance of the arm during interaction with a dynamic object [110, 111].

With regards to reach-to-grasp movements, M1 neural activity has been observed to coincide with the preshaping, grasping and lifting phases of manipulation actions [112]. Human M1 is active for both real and imagined contralateral hand movements [113, 114]. M1 neurons encode grasp dimension [81], and modulate differentially for different objects, with maximal discriminability of objects at the time of object contact [115, 116]. Individual M1 neuron FRs relate to combinations of kinematics across multiple joints of the arm and hand [16, 17, 117–120]. M1 neurons may also encode time-extended, coordinated trajectories of combinations of hand and arm joint motions [121, 122]. In contrast to the velocity-oriented encoding of reaching movements, hand joint angle positions are encoded more strongly than joint angle velocities in M1 [117, 120, 123]. M1 activity is not well-related to the low dimensional grasp synergies that capture much of the kinematic variance during grasp, suggesting that M1 activity acts to fractionate and elaborate on these grasp synergies, rather than controlling them directly [124].

More recently, the Shenoy research group has posited that given the temporal complexity of FR modulation in M1 neurons, perhaps no movement feature encoding model can adequately describe M1 neural activity [125]. Instead, they propose, M1 may act as a dynamical system which generates a basis set suitable for driving muscle activity [126]. In support of this concept is the fact that a large amount of neural variance in M1 during reaching movements manifests as smooth rotational dynamics [127], though a recent study has shown that these rotational dynamics are not present in M1 during grasping behaviors [128].

Although the studies listed above suggest a complicated encoding scheme in M1, they all generally portray M1 neural activity as directly related to some intrinsic or extrinsic aspect of the immediate, ongoing movement. However, neural activity in M1 can also be uncoupled from behavior [129]. In these cases, neural activity may reflect cognitive processing. One prominent instance of such activity is preparatory activity in the period before movement onset. Many neurons in M1 begin modulating hundreds of milliseconds before movement, even when the subject is intentionally withholding movement during a delay period after presentation of an instruction [130]. This preparatory activity is related to the upcoming movement [131], though on a population level, it resides in a subspace orthogonal to the

activity observed during movement [132, 133]. The M1 preparatory activity may represent cognitive processing related to the task, such as mentally rotating the intended movement direction from an initially presented target [134]. Others have suggested that preparatory activity may act to set the initial conditions to drive the FR modulation dynamics of the subsequent movement period [135].

Another instance in which M1 neural activity becomes uncoupled from behavior is when different neural activity is observed when the same movements are executed in different cognitive contexts. These instances of context sensitivity are discussed in more detail in Section 2.7.

In accordance with the corticocortical connectivity between M1 and primary somatosensory cortex, M1 neurons also respond robustly to cutaneous stimulation, muscle palpation and passive joint motion of the hand [136–140]. Afferent skin contact and grip force signals were even present in the M1 of a human with spinal cord injury [141]. These somatosensory signals are critical to the execution of dexterous movements, as a patient with a neurodegenerative disease affecting only afferent nerves was unable to manipulate small or complex objects, though overall strength and motility were spared [142]. In addition, inactivation of primary somatosensory cortex with muscimol impaired manual coordination and the ability to accurately place the fingers during grasp and maintain a grip, though muscle strength was spared [61].

M1 is critically involved in the motor learning that occurs after injury or due to motor skill acquisition. The homoncular map in M1 adapts after the loss of a body part, with the representation of adjacent body parts subsuming the cortical area that was previously linked to the lost body part [143–145]. Learning of new motor skills is associated with rapid reorganization and adaptation in M1 followed by a longer-term consolidation process [146–152]. When an action involving a particular body part is practiced for long periods, the cortical area associated with that body part expands [153, 154].

The scientific understanding of M1 gained in the last decades has enabled the development of assistive devices that allow users to control computers and robots directly with signals recorded from the brain. These developments are discussed in the next section.

2.2.1 Brain Computer Interfaces and Neuroprosthetics

There are over 200000 individuals living with spinal cord injury in the United States [155]. Spinal cord damage can often lead to paralysis and subsequent loss of the ability to perform the tasks of daily living. Surveys of quadriplegic patients revealed that recovery of hand function was the most important and desired outcome for quality of life improvement [155, 156]. Advances in the understanding of the motor system as well as chronic electrophysiology techniques have enabled a new class of therapies for these patients: brain computer interfaces (BCIs) and neuroprosthetics.

Motor BCIs function by "decoding" an intended movement signal from neural activity — typically in M1 — and translating this signal to drive the motion of a computer cursor or robotic neuroprosthesis. The subject must be able to volitionally modulate M1 neural activity for this method to work.

In a set of pioneering studies, Fetz demonstrated that monkeys could learn to modulate the FRs of single neurons in M1 on demand to receive a reward [157–159]. The subjects received auditory and visual feedback linked to the FR of a selected neuron, and were required to drive the FR past some threshold. This served as a proof of concept for the BCIs, and laid the groundwork for future progress. The ability of humans, even those with spinal cord injuries, to volitionally modulate M1 neurons on command was later confirmed [160].

Subsequent studies initially focused on the ability to decode movements "offline." That is, neural activity was recorded while the subject performed movements, and the movements were reconstructed post-hoc. This was initially done with sequentially recorded populations of neurons and later with simultaneously recorded neural populations. Decoding can be performed with a variety of statistical and machine learning techniques. For example reach direction can be predicted offline using the population vector approach [94,95]. Later studies showed the ability to decode locomotion [161], simplified reach-to-grasp movements [162], high-dimensional reach-to-grasp trajectories [16,163], detailed hand kinematics during grasp [123,164–166] and individual finger movements [167–170] offline.

Based on initial successes in offline decoding, a growing number of BCIs have been implemented to give subjects real-time control of electronic devices. Monkeys have been able

to control on-screen cursors [171–173], a three degree-of-freedom (DoF) robot arm (remotely) [174], the aperture of a virtual hand [175], a four DoF robot arm with a gripper [176] and their own paralyzed hands via functional electrical stimulation (FES) of the muscles [177]. Paralyzed human subjects implanted with recording microelectrode arrays have been able to control on-screen cursors [160, 178, 179], a highly constrained robotic arm [160], a cursor with a "click" function [180, 181], a virtual hand controlled with two hand synergies [182], a four DoF robot arm with a gripper [183], a seven DoF robot arm with a gripper [184], a robot arm with 10 DoF in the arm and hand [119], the grip force of a virtual hand [185] and their own paralyzed hand via FES [186–189].

Recent efforts have seen some success in delivering touch feedback to the subject. Monkeys receiving intracortical microstimulation in primary somatosensory cortex were able to distinguish between different virtual textures [190]. Supplying human subjects with touch feedback via vibrations on the skin [141] or intracortical microstimulation in primary somatosensory cortex [191] increased neuroprosthetic performance.

Along with the promise of restoration of function, BCIs provide a unique opportunity to learn about the functioning of the motor system. The ability to fully control of the mapping between neural activity and output in BCIs allows for unique experiments. Perturbing this mapping and observing the resulting changes in neural activity has provided valuable insight into how motor learning is implemented in M1 [150–152, 192–195].

While most motor BCIs utilize neural activity recorded from M1, recent efforts have investigated the use of recordings from posterior parietal cortex to create a "cognitive neural prosthetic" [196]. Signals from parietal cortex may allow rapid decoding of more abstract action goals [197, 198].

While BCIs controlling cursors and robotic arms for reaching have shown promising success, dexterous grasping neuroprostheses have been more difficult to implement. Most successful grasping BCIs feature a one-dimensional gripper which can simply be opened or closed. The Battelle NeuroLife research group has achieved decoding of seven different grasp by using classifiers, but this did not allow continuous control of the many degrees of freedom of the hand [188]. The recent 10-dimensional robot arm control (three dimensions of hand control) demonstrated by Wodlinger et al [119] revealed one potential reason for the difficulty

in controlling hand kinematics for grasping objects. They report a strong influence of context in the neural signal in M1 specifically related to whether the intended movement was made in the presence or absence of an object. This result serves as a primary motivation for the experiments of this dissertation, and is discussed further in Section 2.8.

2.3 Anatomical and Functional Properties of PMV

The term "premotor" was initially used by Fulton in 1935 [199] to describe the part of cortex anterior to M1, in the anterior portion of the precentral gyrus corresponding essentially with Brodmann area 6 [30]. Based on cytoarchitectonics, Matelli further subdivided premotor cortex in the monkey into regions F2–F5 (with F1 corresponding to M1) [200]. PMV typically corresponds with Matelli's areas F4 and F5. For the purpose of this dissertation, PMV is used to refer to Matelli's area F5, which is located in the posterior bank of the lower limb of the arcuate sulcus lateral to the spur, and in the immediately posterior convexity of the precentral gyrus. In humans, PMV can refer to the inferior portion of Brodmann area 6 as well as the posterior portion of the inferior frontal gyrus pars opercularis corresponding with Brodmann area 44 and sometimes also includes Brodmann area 45 [30, 201].

PMV is one of six premotor cortical areas in the frontal lobe which projects to the digit representations in M1 [202]. PMV is connected corticocortically to M1, the other premotor areas, AIP and other inferior parietal regions and regions in the intraparietal sulcus, the superior parietal lobule, secondary somatosensory cortex, the insula, prefrontal areas in the inferior frontal gyrus including Brodmann areas 46 and 12, and the thalamus and claustrum [202–208]. PMV also contributes between 4% and 10% of the axons in the corticospinal tract, though these projections synapse almost exclusively in the upper cervical segments, with few reaching the cervical enlargement, where they would be able to directly influence hand and finger movements [44–47, 209–213].

Brief electrical stimulation of PMV results in muscle twitches in the contralateral arm, hand and face, though the size of the stimulus needed to evoke a response is greater for

PMV than for M1 [34, 36, 214–217]. Stimulating for a longer duration ($>$ 500ms) results in coordinated, multijoint movements of the arm, often involving manipulatory actions such as bringing the hand toward the body and moving the wrist, or moving the hand toward the mouth and opening the mouth [38–40]. In humans, the muscle activity evoked from transcranial magnetic stimulation (TMS) of PMV occurs at a longer lag than that evoked from M1 [37].

Lesion studies suggest that PMV is critical for visually guided dexterous control of the hand. Reversibly inactivating PMV in a monkey led to an inability to appropriately shape the hand to grasp objects, though objects could be grasped after some tactile exploration [62]. Lesions of PMV also interfered with the ability to perform a visually cued grasp task [218]. In humans, inactivating PMV using theta-burst TMS resulted in the fingers being placed inaccurately and inappropriately on the object during attempted grasp [219].

Initial characterization of the functional properties of PMV neurons was carried out by the Rizzolatti research group in the 1980s. The found that PMV neurons could have sensory responses to touches of the hand or face [220], or to visually presented objects in the subject's peripersonal space [221]. In a later experiment, they showed that PMV neurons fired during object-oriented grasping movements, and individual neurons preferred certain grips [222]. The most common class of neurons in PMV responded for grasps, but neurons were also found which preferred actions such as bringing an object to the mouth or manipulating the object in some way, such as tearing. They initially posited that these neurons encoded the actions at a high level and were unrelated to the particulars of the movements, and thus PMV contained a "vocabulary" of manual actions [214].

In a more comprehensive study, Murata et al described the types of "canonical" neurons in PMV [223]. In their experiment, monkeys were presented with a set of objects which they subsequently grasped. They found three classes of neurons that had task-related activity: visual neurons, motor neurons and visuomotor neurons. Visual neurons responded most strongly during the visual presentation of objects, whereas motor neurons responded during the movement made to grasp the objects. Visuomotor neurons were active during both visual presentation and movement. Neurons of all types showed preference for either a single object or a group of objects that were grasped similarly.

PMV neuronal preference for certain grip types during both object presentation and movement has been confirmed by several subsequent studies [224–226]. Similar activation of PMV for grasps has been observed in humans [227]. In a study in which a monkey grasped 50 differently shaped objects, PMV activity was preferentially related to the grip required to grasp the object, rather than object shape, suggesting that PMV neurons encode the motor act of grasping rather than the visual appearance of the object [116, 228]. PMV neurons are also modulated by the orientation of the object to be grasped [224, 225, 229], and the 3D visual contours of the object [230]. Visual and visuomotor responses are only present when the object is within reach of the subject [231]

Despite the initial proposal by Rizzolatti et al that PMV neural activity represents only the overall grasp or manipulation goal [214], further experiments have revealed that PMV neurons encode the details of ongoing movements. Neural activity patterns in PMV is strikingly similar to that observed in M1 during the execution of grasping movements [81]. PMV neurons encode grasp force [79, 80, 82], limb biomechanics [232], and hand movement direction [215, 217, 233, 234]. Continuous kinematic trajectories can be decoded from PMV at an accuracy only slightly worse than that obtained from M1 decoding [116, 162, 163, 166].

In contrast to M1, PMV neurons often encode the outcome of a movement moreso than the details of the movement. Studies in which the visual outcome of motion is dissociated from motion itself reveal that PMV neuronal activity is more closely associated with the visual feedback of motion than with the actual movement [235, 236]. In addition, in a study where wrist movement direction was dissociated from muscle activation, PMV neurons were found to mostly encode the extrinsic feature of movement direction as opposed to the intrinsic features of the muscle activations [237]. This suggests that PMV is selectively involved in the visual guidance and coordination of movement [238], and may implement a visuomotor transformation [108] in that it transforms visual stimuli into appropriate motor commands.

Furthermore, PMV neurons are often sensitive to abstract aspects of a task. PMV neurons respond differently when the same movement is made with a different end goal in mind (e.g. eating vs. placing an object) [239–241]. PMV is also involved with linking arbitrary cues to movement, as PMV neurons respond to visual, auditory and vibrotactile cues that have been learned to be associated with certain motor responses [242].

To an apparently greater extent than M1, neural activity in PMV can become dissociated from immediate movement. One dramatic instance of this dissociation is the existence of "mirror neurons" in PMV, which are active during both observation of an action and when the subject performs that same action [243–250]. Mirror neuron activity is discussed further in Section 2.5.2.

Whereas mirror neurons represent activity which is present in two vastly different contexts, PMV neural activity is also context sensitive in that different activity can be observed when the same movement is made in different contexts. These instances of context sensitivity are further discussed in Section 2.7.

Finally, a growing literature suggests that PMV area F5 may be further subdivided into a more cognitive area F5a and a more motor area F5p [251]. Differential cytoarchitecture [204, 252] and anatomical connectivity [253] support this division. Functional studies of neural activity in the two areas suggest that neural activity in F5a is more closely related to the visual stimulus or outcome of action, and neural activity in F5p is more closely related to the movement, similarly to M1 [116, 163, 228, 230, 251].

2.4 Anatomical and Functional Properties of AIP

AIP is one of several areas in the intraparietal sulcus of the posterior parietal cortex which are involved with sensorimotor transformations for action [254–256]. AIP is located in the anterior extent of the lateral bank of the intraparietal sulcus in both monkeys and humans [257].

AIP is anatomically connected with areas PF and PFG in the convexity of the inferior parietal lobule, the rostral lateral intraparietal area, areas in the caudal intraparietal sulcus, PMV, secondary somatosensory cortex, areas in the superior temporal sulcus and middle temporal gyrus, the frontal eye fields and areas 46 and 12 in the prefrontal cortex [258]. While corticospinal projections have been identified originating from the interconnected and adjacent intraparietal region PEip [259] AIP appears to contain very few, if any projections to the spinal cord [45, 47].

Lesion studies reveal that AIP plays an important role in matching the shape of the hand to features of a graspable object. In monkeys, broad lesions of posterior parietal cortex resulted in disuse of the contralateral arm and inability to accurately reach to or grasp objects [260]. More focal, transient lesions obtained with microinjections of muscimol in monkey AIP caused deficits in hand preshaping during grasp, though the reaching component of the movement was preserved [261]. In humans, damage to AIP results in an inability to properly shape the hand for grasp [262, 263]. Additionally, a patient with bilateral inferior parietal damage was unable to properly grasp and manipulate novel objects [264]. Virtual lesions of human AIP using theta-burst TMS disrupts object-specific hand muscle activation during grasp [265], accurate finger placements and grip force scaling [266], grasp kinematics in general [267], as well as the ability to correct for rapid perturbations in object orientation or size [267–269].

The presence of grasping related neural activity in AIP was first identified by Mountcastle et al in 1975 [270]. The experimenters recorded single neurons in areas of the posterior parietal cortex of monkeys while the subjects executed different eye, arm and hand movements. They found that AIP contained many "hand-manipulation" related neurons, which were active for specific reach-to-grasp and manipulate actions such as grooming or tactile exploration of an object in a box. They posited that these neurons were related to the overall goal of the movement, rather than the specifics of the action used to obtain that goal.

The classes of neuronal responses in AIP were further characterized by Sakata and colleagues. They recorded from single neurons as monkeys viewed and subsequently grasped a set of objects. They identified three classes of neurons, similar to those classes observed in PMV (see Section 2.3). The classes were "visual-dominant" neurons, which responded preferentially during visual presentation of the object, "motor-dominant" neurons, which responded preferentially during the movement phase of trials, even when movements were made in the dark, and "visuomotor" neurons, which responded both during presentation and movements made with lights on [271, 272]. Importantly, these neurons showed sustained firing for just one object, or a set of objects which were shaped similarly and thus required a similar grip. A further investigation suggested that the

visual-dominant neurons distinguished objects based more on their geometry and orientation, where motor-dominant neurons distinguished objects based more on the hand movement required to grasp them [273]. Many neurons showed sustained activity during a delay period in the dark, suggesting a potential role for AIP in short-term memory or motor planning [274].

Later studies have largely confirmed and extended these findings. Many AIP neurons are sensitive to fragmented images of 3-dimensional visual contours and edges, both naturalistic and synthetic [275–278]. Object identity and orientation can be decoded with high accuracy from AIP, even during the pre-movement delay period [116, 229, 279]. Additionally, human brain imaging suggests that AIP is active during both tactile exploration of objects and visual object perception [280].

Despite the initial proposal that AIP neurons only encode the overall action goal, several studies have shown that AIP neurons are sensitive to detailed aspects of movement. AIP activity is time-locked to movement, and activity is generally maximal at the time of object contact [281]. AIP neurons also encode grip force [82] and target position [234], and detailed continuous grasp kinematics can be decoded from AIP, albeit at a level slightly lower than decoding from PMV or M1 [163].

AIP is integral to the learning and comprehension required for tool use. When monkeys were trained to use a rake in order to retrieve food, structural [27, 28], histochemical [26] and functional [24] changes were observed in AIP and in adjacent parietal areas. In humans, functional brain imaging studies suggest that AIP is selectively involved with linking tools to the appropriate use actions [282], and for understanding both the identity and functional use of tools [283].

As in PMV and M1, context-dependent activity has been observed in AIP, where different neural activity is observed for the same movements made in different contexts. These observations will be discussed further in Section 2.7.

2.5 The Cortical Grasp Network in Monkey and Man

In Sections 2.2, 2.3 and 2.4, cortical areas M1, PMV and AIP were introduced and reviewed independently. This section contains a review of data supporting the idea that these networks act together as a coherent cortical grasp network which implements the visuomotor transformations necessary for successful grasping behavior.

M1, PMV and AIP are considered part of the "dorsal visual stream," which extracts spatial features from vision for pragmatic use in generating appropriate actions, as opposed to the "ventral visual stream" which performs object recognition for semantic understanding [284–286]. M1, PMV and AIP constitute one of several parallel but interconnected parietofrontal pathways of the dorsal stream which implement visuomotor transformations for grasps, reaches, saccades and defensive movements [287, 288]. Jeannerod et al provided an early description of M1, PMV and AIP as the essential nodes in a network which performs visuomotor transformation for grasping [255]. This framing is now largely accepted (see [117, 247, 289] for reviews), though additional parietal, prefrontal and temporal cortical areas are involved with some aspects of grasping behavior [40, 290].

Monkey functional brain imaging studies reveal that M1, PMV and AIP are preferentially engaged during grasping as opposed to reaching [291] and that different grasps could be decoded from activity in these areas [292]. Similarly, human functional brain imaging studies reveal that AIP and PMV are preferentially activated together when grasping actions are performed [262, 293, 294] and specifically when small objects are grasped [295], complex objects are manipulated [296], or when precision grips are executed in a controlled manner [297, 298]. Further studies in humans show that these areas are also activated simply by imagining or observing grasping actions [299, 300]. AIP and PMV are active even when making judgments about appropriate use actions for tools [301] or simply viewing and naming images of tools [302] (see [201, 303, 304] for review), suggesting a role for AIP and PMV in object use affordance comprehension, in addition to the on-line control of grasp.

Substantial evidence suggests that the AIP-PMV-M1 network acts in a hierarchical, feedforward manner in that the visuomotor output of the network proceeds from AIP through PMV to M1, which outputs the resulting motor command to the arm and hand muscles.

The relative prevalence of corticospinal projections originating from M1, PMV and AIP also suggest that corticospinal motor output driving hand muscles is primarily mediated by M1. AIP has few if any corticospinal projections [45, 47]. PMV contains some corticospinal neurons, though these neurons project primarily to the upper cervical segments, whereas hand muscle motoneurons are primarily located in the cervical enlargement [44–47, 209–213]. Contrastingly, projections from M1 constitute approximately half of the corticospinal tract [44–47] and in primates this projection includes corticomotorneurons which synapse directly on spinal motoneurons which drive hand muscles [48, 55, 56].

Anatomical studies in monkeys show that AIP projects strongly to PMV [205, 207, 305] and PMV projects strongly to M1 [305–308] in a topographically organized manner [309], while M1 receives only sparse projection from AIP [308]. Stimulation in area PF (adjacent to AIP) can directly excite PMV neurons, and stimulation in PMV can antidromically activate neurons in AIP [305]. Similarly, PMV can be activated antidromically from stimulation in M1 [305]. When electrical stimulation is applied in PMV, rapid excitation can be observed in M1, followed by slow inhibition [310–312]. However, bidirectional feedback connections do exist between the areas, and stimulation in M1 can excite PMV neurons at short lags [312].

Stimulation in PMV evokes weaker muscle activity at a longer lag compared to equivalent stimulation in M1 [37, 313]. Detailed stimulation studies have revealed that the primary route by which PMV influences hand muscle is through facilitation of M1 corticospinal output. This is revealed by studies in which the strength of motor evoked potentials (MEPs) due to stimulation in M1 is measured with or without a preceding conditioning stimulus in PMV. When PMV is stimulated just before M1, the MEP in thumb muscles can be greatly facilitated [314]. These influences can also be inhibitory, and the timing of the effect suggests that the increase in MEPs is mediated by PMV-M1 corticocortical interactions as opposed to direct corticospinal output from PMV [315]. This enhancement of M1 output by a conditioning stimulus in PMV is muscle- and grasp-specific, in that the size and pattern of the effect changes when the conditioning and test stimuli are applied during the preparation and execution of different grasping actions [316]. In further support of the necessity of M1 to mediate PMV output to hand muscles, MEPs evoked from stimulation only in PMV are largely abolished when M1 is inactivated with muscimol [216, 315].

Very similar effects are observed in humans when M1 is stimulated with TMS with or without a conditioning TMS stimulation in PMV. The effect of conditioning stimuli in PMV on MEPs evoked from M1 is inhibitory during rest, neutral during power grasps and excitatory during precision grasps [317]. When the stimuli were applied during the grasp of different objects, the effects were found to be object-specific [318]. Furthermore, disruption of AIP using theta burst TMS reduced the facilitatory effect of PMV conditioning stimuli on M1 evoked MEPs [265]. Disruption of AIP during the pre-movement period decreased the usual reduction of beta oscillation magnitude in M1 [319]. Finally, conditioning stimuli in AIP could facilitate M1 output to hand muscles, and this effect was abolished when PMV was inactivated using theta burst TMS [320].

The functional properties of neural activity in M1, PMV and AIP further support the hierarchical structure of the grasp network. The correlations between movement parameters and neural activity are strongest in M1, followed by PMV and then AIP. This order holds for correlations with grip force [82], hand and arm kinematics [163] and hand direction in M1 and PMV [233]. Conversely, visual information is most strongly represented in AIP, followed by PMV and then M1. Selectivity for 3D visual contours was present mostly in AIP and area F5a of PMV, and absent in area F5p of PMV [230,321]. Responses to visual presentation of objects are most common in AIP, present in PMV but largely absent in M1 [115, 214, 272]. AIP neurons tend to cluster objects based on their visual appearance, whereas M1 clusters objects based on the kinematics necessary to grasp them, and the PMV representation is intermediate between visual and motor [228].

Finally, the relative timing of neural activity in M1, PMV and AIP further suggests a predominantly feedforward relationship between the areas. AIP shows the earliest onset of modulation after visual presentation of the object, followed shortly by PMV activity, which subsequently becomes correlated with M1 activity just before movement [228]. Selectivity for objects during the pre-movement period is greater in PMV and AIP than in M1 [115,116].

In the Results Section 7.4, the timing of modulation in M1, PMV and AIP populations is examined for evidence that information related to object context is transmitted sequentially from AIP to PMV to M1.

2.5.1 Affordance Processing in Frontoparietal Areas

The functional properties of M1, PMV and AIP and the deficits resulting from damage to these areas have led to theories which posit that the grasp network extracts and selects grasp affordances. As first defined by Gibson, affordances are the actions made possible by the combination of the physical features of the environment and the subject's capabilities and knowledge [322]. Any manipulable object has a number of grasp affordances based on it's shape and has a further set of use affordances, especially if the object is a tool.

One prominent theory for how affordances are processed in frontoparietal networks is the "affordance competition hypothesis," first put forth by Cisek in 2007 [323]. Based on neurophysiological data [279, 324] (see [325] for review), this theory posits that multiple potential action affordances are extracted in parallel from sensory data. The representations of these potential actions compete within the frontoparietal dorsal stream brain regions, with further sensory information and internally generated goals biasing neural activity toward one particular action, which eventually wins out to become the enacted behavior. This hypothesis is supported by experiments such as that of Baumann et al [279], in which an object with multiple grasp affordances (power grasp and precision grasp) was presented, followed by a grip cue. During the time before the grip cue was presented, neural activity in AIP represented both the power grasp and the pinch grasp. Only after the grip cue was delivered did neural activity converge to the representation of the single, cued grasp. This experiment is discussed further in Section 2.9.

A number of computational theories have been developed to model the affordance processing in M1, PMV and AIP (for review, see Thill et al [326]). The FARS model by Fagg and Arbib posits that AIP extracts the grasp affordances of the object based on it's visual appearance, and the appropriate grasp is selected via interaction with PMV [247, 327]. The selection of the appropriate grasp action may be influenced by information from other brain areas in prefrontal cortex [290]. The TRoPICALS model by Calligiore et al posits that potential affordances are automatically extracted and the appropriate action is selected by dynamic neural competitions that integrate these affordances with top-down information about goals and context from the prefrontal

cortex [328]. The TRoPICALS model is heavily motivated by findings that the motor representations in the grasp network are automatically activated by object-related stimuli. This "automatic activation" of the grasp network is discussed in the following section.

2.5.2 Automatic Activation of the Grasp Network

An array of behavioral and neurophysiological data indicate that the grasp network motor representations of an object's affordances are automatically activated when that object is perceived. One main line of evidence for this automatic activation is human behavioral studies showing compatibility effects between stimuli and the motor responses required to complete the task. An early example of this stimulus-response compatibility effect is the "Simon effect," as first described by Simon and Wolf in 1963 [329]. In that task, subjects were seated, with each hand on a button, in front of a board with two lights attached to it. The subjects were simply required to lift their left hand off of the button if the left-hand light came on, or lift their right hand if the right-hand light came on. However, the board with the lights could be rotated, such that the left-hand light cued the subject to lift their right hand and the right-hand light cued the subject to lift their left hand. In the case that the stimuli and responses were compatible (left light-left hand, right light-right hand), the subjects' reaction times were shorter and they made few errors. When the stimuli and responses were incompatible (left light-right hand, right light-left hand), the subjects displayed longer reaction times and made many more errors.

The classical Simon effect concerns the spatial compatibility of the cue and response. A number of behavioral studies have shown that a similar effect can be observed when the stimulus is a large or small object and the subject must respond by making a power grasp or a precision grasp. In one early study showing such effects, subjects were required to judge whether images depicted man-made or natural objects by executing either a power grasp or a precision grasp on a handle [330]. Subjects responded more quickly and accurately when the object was large and the response required a power grasp and when the object was small and the response required a precision grasp. Conversely, responses were slower and more error prone when a large object required a precision grasp response and when a

small object required a power grasp response. Importantly, the subjects were not explicitly instructed to judge the size of the objects or imagine grasping them, but simply to judge whether or not they were man-made objects. The authors suggest that the representations of the grasp actions afforded by an object are integral to that object's representation, and are automatically activated when the object is perceived [330]. When the action afforded by the presented object is compatible with the required response, that response is facilitated. When the action afforded by the presented object is incompatible with the response, it interferes with and slows that response.

Subsequent studies have shown that grasp related stimulus-response compatibility effects can be observed in a wide range of situations. The grasp compatibility effect was observed when subjects planned certain grasps, and images of objects with congruent or incongruent affordances were shown in order to trigger the action [331]. Grasp compatibility effects were observed when using grasps to respond to an auditory tone while passively viewing images of objects, even though the objects were completely irrelevant to the behavioral task [332]. Grasp compatibility effects were present even when images of objects were flashed only briefly [333]. Images of objects are not required to trigger grasp compatibility effects; the effect can be observed even when subjects simply read words corresponding to large or small objects [333, 334]. Grasp compatibility effects were present even when the images of objects were masked and presented so briefly that they were not consciously perceived [335]. Grasp compatibility effects depended on how the stimuli objects were habitually grasped by the subject, indicating the activation of stored object use knowledge along with the visually extracted grasp affordances [336]. Grasp compatibility effects were also observed when stimuli were not images of objects but were instead images of hands performing power grasps or precision grasps [337]. Additionally, similar compatibility effects have been observed for wrist rotation responses when the stimuli were images of congruently or incongruently oriented bars [338, 339] or objects [340]. Grasp compatibility effects could be observed not only in reaction time and error rate but also in grasp kinematics. Such effects are discussed in Section 2.6.

Human functional brain imaging studies have contributed further evidence of automatic activation in the grasp network. Several of these studies found that simply viewing images

of tools or naming tools, without the intention to grasp, resulted in activation of PMV and AIP or surrounding regions in the inferior parietal lobule [341–343]. While images of graspable objects in general could drive activation, images of tools activated a greater cortical area [344]. Automatic activation was observed even when the images of manipulable objects were suppressed from conscious awareness using continuous flash suppression [345] or binocular rivalry [346]. In some studies, automatic activation from observation or naming of tool images was only observed in PMV [215, 347, 348]. In addition, when subjects were engaged in a stimulus-response compatibility task, AIP and PMV were activated when the grasp affordance of the stimulus object was incompatible with the response behavior [349].

Intracortical electrophysiology in monkeys can reveal the signatures of automatic activation at the level of individual neurons. While it is well established that object-selective visually responsive neurons exist in AIP [272] and PMV [214], the studies which identified those neurons involved behavioral tasks in which the subjects were always required to grasp the objects. Thus, it cannot be ruled out that the visual responses observed in those neurons represented an early phase of motor planning. A recent study utilized a modified version of the task such that on some trials the subject was required to reach out and grasp the object after it was presented ("go trials"), but on other trials, before the object was presented, the subjects were instructed to not move ("no-go trials"). Neurons in PMV that were found to have motor responses during go trials displayed similar but slightly weaker object-specific responses even for no-go trials, suggesting they were activated by vision of the objects even when no motor intent was present [350, 351].

Another aspect of neural activity that is related to automatic activation is "mirror neuron" activity. Mirror neurons were first identified by the Rizzolatti research group and first described in a study by Di Pellegrino et al in 1992 [243]. The authors observed that a subset of neurons in PMV area F5 which fired when the monkey performed a certain goal-direct action (such as grasping, holding or tearing) also fired when the monkey observed the human experimenter executing the same action. Crucially, the monkey made no movement of its own body. Further studies have affirmed the presence of mirror neuron activity in monkey PMV [244–248, 250] as well as in area PF of the monkey inferior parietal lobule adjacent to AIP [208], monkey M1 [352–354] and human M1 [355].

In the Results Sections 4.7, 5.7, 6.7 and 7.5 of this dissertation, evidence is considered for the hypothesis that neural activity in M1, PMV and AIP populations reflect automatic activation of the perceived and learned affordances of objects.

2.6 Context-Dependent Grasp Behavior

Behavioral studies of grasping performed in different contexts reveal that grasp kinematics consistently differ in a context-dependent manner. This contextual effect on grasp kinematics is revealed in experiments where the overall requirements for a grasping movement are held constant and the context within which the movement is performed is altered.

One relevant contextual factor is the artificiality or naturalness of the movement. Grasp kinematics were different when humans performed repetitive, stereotyped grasping movements typical of laboratory experiments compared to more unconstrained functional grasping movements akin to those performed regularly in daily life [356]. Grasp kinematics were also different when grasping a real object compared to pantomiming the same grasp next to the object [357].

The kinematics of a grasp movement can also be affected by the presence of other, ungrasped objects in the workspace. Grasp kinematics were different when subjects had to avoid an obstacle placed between their hand and the object, despite the object remaining the same in the two conditions [358]. Grasp kinematics were also affected by the visual presence of distractor objects in the workspace, even when they did not present an obstacle to the target object [359]. The timecourses of reach and grasp kinematics and the size of peak grip aperture were altered when "flanker" objects were placed adjacent to the object to be grasped, indicating a possible avoidance strategy [360]. When grasping fruits in the presence of other, ungrasped fruits, grasp kinematics were altered when subjects were required to attend to the distractor fruits by counting how many times they were illuminated, indicating potential automatic activation of the representations of the grasp affordances of the distractor fruits [361]. Similarly, grasp kinematics were different when identical grasp targets were

attached to differently shaped objects [362]. This experiment is discussed further in Section 2.9. Grasp kinematics could also be affected by semantic information; subjects displayed smaller grip apertures when reaching to grasp an object with the word "small" printed on it, and larger grip apertures when reaching to grasp an object of the same shape, but with the word "large" printed on it [363]. This suggests the potential that grasp movement representations can be automatically activated by perceived objects.

Many studies of human behavior have identified alterations in grasp kinematics dependent on the subsequent intended use of the object after it is grasped, even though the requirements of the initial grasping phase of the movement are the same. Even in the early study of Napier, it was noted that where the subjects placed their thumbs when grasping objects depended on the intended action to be performed with the objects [1]. Studies in which objects were grasped and transported suggest that objects are initially grasped in such a way to maximize comfort in the final posture after the transport action [364–366] (see [367] for review).

Other studies have shown that initial grasp kinematics vary based on a wide array of subsequent intended manipulation actions. When grasping an object prior to transport, grasp kinematics depend on the proximity of the final transport target [368] or the height of the final transport target [369]. When grasping an object to lift it, grasp kinematics depend on whether the object was lifted in isolation or lifted in order to show it to another person [370]. Objects are grasped differently when they were subsequently lifted, or placed into a small or large receptacle [356]. When grasping a bottle, grasps differed depending on whether the subject intended to subsequently drink from, hold, throw, move, pour or pass it [371]. Grasps on a food morsel were different depending on the object was to be eaten or moved [372]. Although these kinematic differences are typically small in magnitude, they can be detected by human observers, who can reliably identify the intended use of the item based only on the initial grasp kinematics [373,374] or kinematics after object contact [372]. The observation of these grasps and detection of intention appears to involve regions in the inferior parietal lobule, based on human brain imaging studies [375].

Intrinsic object properties can also affect grasp kinematics. Reach trajectories were different when grasping fragile or robust objects [376]. Differences in grasp kinematics can

also be observed even for seemingly arbitrary differences in object characteristics. In a study where subjects grasped objects that were colored red or green, but were otherwise identical, larger peak grip apertures were observed for the red object [377].

In the three experiments of this dissertation, significant differences in grasp kinematics and muscle activity were observed when similar grasps were performed in different object contexts. These results are presented in Sections 4.1, 4.2, 5.1, 5.2, 6.1 and 6.2.

The consistent differences in grasp kinematics suggest that grasping behaviors performed in different contexts were driven by different central neural signals. Evidence for context-related differences in neural activity relating to object context is reviewed in Section 2.7.1.

2.7 Context-Dependent Neural Activity in M1, PMV and AIP

Though neural activity in M1, PMV and AIP reliably encodes an array of movement features (see Sections 2.2, 2.3 and 2.4), the instantaneous relationships between neural activity and movement features have been found to be labile across contexts. Many studies have shown evidence for context-dependent activity in M1, PMV and AIP in which neural activity differs for the same or similar movements, muscle activity or behaviors performed in different contexts. This flexibility of the relationship between neural activity and behavior is possible due to the redundancy of the cortical motor system (there are many more neurons in cortex than there are muscles in the arm and hand) and the indirect, and divergent-convergent nature by which cortex influences the spine and muscles (individual corticospinal neurons synapse in multiple locations in the spinal gray matter, individual corticomotoneuronal neurons branch to synapse on multiple motoneurons driving different muscles and spinal interneurons and individual motoneurons receive input from many cortical and subcortical neurons and spinal interneurons) [67, 129]. In addition, motor cortex projects to many other cortical and subcortical structures. This means that any given motor act is realizable by multiple different patterns of cortical activity.

This section contains a review of studies that show evidence for context-dependency in M1 and PMV as defined by instances in which cortical activity in M1 or PMV neurons differs

for similar behaviors performed in different contexts. Section 2.7.1 discusses studies which reveal context-dependency of M1, PMV and AIP activity with specific regards to grasping behaviors.

A number of studies have shown that the linkage between M1 cortical activity and muscle activity is malleable to an extent. Natural M1 neuron to muscle correlations can be abolished using operant conditioning [158]. Conversely, the throughput from an M1 corticomotoneuron as measured by spike-triggered averaging can be increased with operant reinforcement [378]. In a task in which monkeys made wrist movements, many corticomotoneurons were found to be "functionally tuned" to muscle activity in that the linkage between specific neuron-muscle pairs was only evident when the muscle was used for a specific function such as accelerating, braking or stabilizing [379]. In another study of wrist movements, M1 neuron correlations with EMG were found to vary based on the underlying instantaneous EMG of the muscles [380] or on the concurrent posture of the arm and hand [118]. In chronic M1 and EMG recordings, neuron-muscle correlations were found to change depending on whether the monkey subjects were engaged in a structured behavioral task, unconstrained free movements or sleep [381]. Similarly, in mice, focal inactivation of M1 using optogenetic techniques revealed that M1 only directly influenced muscle activity during a trained, difficult task and not during treadmill walking [382].

Other studies have shown that behaviors are encoded differently when they are embedded in a sequence as opposed to performed in isolation. 40% of M1 neurons displayed different activity when reaching to targets as part of a highly practiced memorized sequence vs. performing the same movements in a randomly cued fashion [383]. Metabolic activity in M1 was also reduced during execution of the memorized sequences [384]. The correlational structure in a population of M1 neurons differed between performance of a sequential vs. cued reaching task [385]. This sequence vs. cued contextual effect was also observed in the preparatory period before movement onset [386, 387]. Another study found that a sequence effect was not detectable in M1, but was present in PMV, which was preferentially active for visually cued movements over sequences [238]. When potential targets were presented sequentially, many M1 neurons encoded the serial order of target presentation along with target direction [388].

Contextual effects also emerge when the location of a visual cue is dissociated from the instructed movement direction. In a task where arm movement was instructed to the left or right using either congruent cues (same side as required movement) or incongruent cues (opposite side from required movement), in the preparatory period, 40% of M1 neurons were tuned to the cue position and 15% were tuned to movement direction, and in the movement period, 14% were tuned to the cue position and 71% were tuned to the actual movement [389]. In a similar task in which colored lights on the left or right cued whether the movement should be made toward or away from the light, the majority of M1 neurons showed different firing rates for the same movement depending on how it was cued [390]. In a center-out reaching task, when the cue was presented at a location rotated a consistent amount from the required movement direction, activity in many M1 neurons reflected the cue position during the preparatory period and a smaller number of neurons retained this cue sensitivity during the movement [391]. During a similar visuomotor cue-target dissociation adaptation task, half of M1 neurons altered their relationship to hand movement direction [392]. Many M1 neurons changed their relation to hand movement direction when switching from a standard center-out task to a task in which the color of the cue, and not the location, instructed the movement direction [393]. Some of this color sensitivity remained when the task was reverted to the standard center-out paradigm, even though color was no longer task-relevant [393].

The relations of M1 neurons to hand movement direction can also change when the posture of the arm is manipulated. In reaching and isometric force tasks, M1 preferred directions (the correlative relationship between M1 neuron FRs and hand movement direction) changed depending on whether the arm was held with the elbow against the body or abducted to the side [394, 395]. M1 preferred directions also changed when center out movements were performed with the entire target set centered around different regions of space in front of the subject [396]. Similar location-dependency of preferred directions was observed in an isometric force task [397]. In addition, visuomotor rotation learning effects were only found in M1 in the region of space where the perturbation was practiced, and the skill did not generalize to movements made in distant regions in space [398]. M1 preferred directions and baseline firing rates also changed when viscous loads were applied to the elbow and shoulder joints during reaching [399].

BCI experiments have also revealed contextual effects. M1 preferred directions changed when progressing from controlling a cursor using the hand to controlling the cursor directly with brain signals [171]. This change reflected a transition from encoding of hand motion to encoding of cursor motion [400]. M1 preferred directions also changed when learning a new neuron-to-cursor BCI mapping after practicing another BCI mapping [192]. M1 neurons displayed dynamic range adaptation when moving from a 2D cursor control task to a 3D cursor control task [401].

Contextual effects are also observed when different effectors were used to complete an action. M1 preferred directions changed when behaviors were performed using the ipsilateral or contralateral arm [109], and when monkeys performed unimanual or bimanual BCI tasks [402].

Finally, the relationship between M1 neural activity and movement parameters can change over the different behavioral epochs of a single action. M1 activity is markedly different when the arm is at rest compared to when it is actively controlled for reaching, with some neurons increasing their activity during rest periods [403]. During the transition from the preparatory period to movement onset, M1 population correlational structure undergoes a large change [133] and neural correlations with the upcoming movement direction change [132, 232]. Large-scale modulation in M1 FRs is observed between the acceleration and deceleration phases of a movement [404]. In a center-out reaching task, M1 neurons were found to have multiple sequential periods of stable cosine tuning corresponding roughly to preparation, early reach and target acquisition, with preferred directions of individual neurons changing between each period [405]. The final phase of tuning stability was largely abolished when visual feedback of the hand position was withheld [406]. These changes in preferred directions over the course of a reach may be related to the evolving dynamical biomechanics of the limb [232]. Responses of M1 neurons to loads applied to the shoulder and elbow joints were different depending on whether the subject was moving dynamically or holding a static posture [407].

2.7.1 Grasp-Specific Context-Dependent Neural Activity

The previous section concerned context-dependent neural activity during the performance of similar behaviors in different behavioral contexts with reference mostly to M1 activity during reaching behaviors. In this section context-dependency in M1, PMV and AIP is discussed when the contextual behavioral difference is related to grasping. Object differences appear to be particularly potent drivers of contextual effects in the cortical grasp network.

Human brain imaging studies have highlighted differences in neural activity that occur during grasping actions made toward real objects as opposed to pantomimed grasping actions. Grasping real objects evoked greater activity in AIP as opposed to pantomimed grasping, and AIP and M1 were preferentially activated for grasps on real objects vs. reaches toward that object, but not for pantomimed grasps in empty space vs. reaching into empty space [408]. AIP was found to be preferentially active when planning grasps on real objects vs. planning pantomimed grasps to pictures of objects [409].

The importance of a presence of a real object has been noted in monkey electrophysiology studies. In PMV, the number of neurons with mirror responses was lower when monkeys observed grasp actions without an object present [248]. In AIP, preparatory tuning to grip type was only present at a very weak level when grip was cued without a visible object, and activity increased when an object became visible [279].

Human BCI studies have suggested an effect of object presence on neural activity in M1. In a 10D robot arm control task, a decoder trained on isolated hand movements with no object present performed poorly when used to grasp real objects, indicating differential neural activity for real grasps vs. pantomimed grasp actions [119]. This effect was ameliorated by training grasp decoders in a virtual environment with objects present. In a human BCI experiment where FES was used to activate arm and hand muscles to execute grasps, grasp decoders were most successful when trained with a real object present [189]. Analysis of neural activity in human M1 during real and pantomimed grasps revealed a global increase in M1 firing rates when grasps were made toward real objects [410].

Several studies have identified facilitation of the throughput from cortex to muscles specifically during grasp or preparation for grasp. In monkeys, 20% of corticomotoneuron-muscle linkages changed sign or disappeared, and many others changed magnitude when comparing linkages during an isometric push-pull task and a reach-to-grasp task [411]. In humans, M1 throughput to intrinsic hand muscles as evoked by TMS was greater during precision grips than during more simple finger abduction tasks which required similar magnitudes of EMG [412–415]. This increased throughput was found to be object- and muscle-specific and was only present during preparation for grasp on real objects [416, 417] and required vision of the object [418]. Another study found that throughput from M1 to muscles varied over the course of a reach-to-grasp movement; low-intensity TMS delivered to M1 during the transport phase excited shoulder, arm and extrinsic hand muscles, while the same stimulus delivered at the time of object contact preferentially excited intrinsic hand muscles [419].

The functional linkages between neural activity and movement parameters have also been found to change during the execution of different types of grasps on different objects. Many corticomotoneurons in M1 display higher FRs during precision grasps compared to power grasps despite power grasps requiring greater overall EMG activity [89, 90]. The muscle fields of M1 corticomotoneurons were largely consistent between precision and power grips, but corticomotoneuron-muscle pairings had greater spike-triggered average amplitude and peak to noise ratio during precision grips [52]. Muscle activity could be decoded with high accuracy from M1 neurons when training and testing the decoder only on precision grasp data, but when testing the same decoder on power grasp data, performance was degraded [86]. Similarly, in a task where a monkey grasped four different objects, training a kinematic decoder on grasps of only three objects and testing on data from grasps of the fourth object resulted in significant drops in performance [121], though this effect was not observed in a subsequent study [122]. In a study where monkeys grasped several different objects, encoding and decoding models which incorporated object-specific changes in ensemble M1 activity performed better than static models [420].

Grasp-related neural activity can differ when two similar grasps are made with a different intended end goal. Even in Mountcastle's early investigation of AIP, neurons were identified

that were engaged during grooming but not for similar movements made in an aggressive context [270]. In PMV and areas PF and PFG of the inferior parietal lobule, different FRs were observed in many neurons when the same grasp was followed by an eating action vs. a placing action, even when the placing receptacle was located near the mouth in order to make the kinematics of the subsequent actions similar [239–241,351,421]. PMV neurons also showed differential activity when grasping an object in order to place it in a receptacle or to give the object to an experimenter [422]. In humans, functional brain imaging reveals that AIP and PMV are differentially activated for grasping and holding actions compared to grasping and manipulating actions [423], even during the preparatory period [424]. In a human BCI subject, M1 activity was found to differ for grasp-to-hold actions and grasp actions followed by transport of the object [186].

Neural activity has also been found to differ based on the intrinsic properties and learned uses of the grasped object. PMV neural populations distinguished between the same grasp actions made on objects with multiple different grasp affordances [425]. PMV and inferior parietal lobule neurons were modulated by object identity (food vs. synthetic) even when the objects were grasped and transported in the same way [239, 241, 421] — though this effect was not observed in two studies [240, 426]. Similar effects were observed in neurons in inferior parietal lobule region PF [421]. In humans, larger regions of parietal and premotor cortex were activated for imagined grasps of tools with known uses compared to neutral objects [344]. Similar effects were observed when viewing novel objects that had only recently been learned to have tool functions as opposed to viewing novel non-tool objects [427].

Context dependency was also observed in a grip-force step tracking task [80]. Neurons in M1 and PMV encoded the same grip force differently depending on the serial order of the grip force steps or the direction of the steps, despite EMG showing no such context effect. The neurons displayed signatures of dynamic range adaptation. Greater contextual effects were observed in PMV compared to M1.

Goal-directed tool use in particular can be a strong driver of context-related changes in neural activity. Correlations between many corticospinal neurons in M1 and muscle activity were different when monkeys performed a simple precision grip or used a rake object as a tool to retrieve food [29]. In a task where monkeys were trained to use normal pliers (opening

the hand opened the pliers) and reverse pliers (opening the hand closed the pliers), nearly all PMV neurons and about half of M1 neurons were found to preferentially encode the motion of the tool tip, while only half of M1 neurons were more closely related to the actual hand motion [428]. When humans observed the use of similar normal and reverse pliers, TMS-evoked thumb muscle activity reflected the tool tip motion when observing the pliers used to grasp an object, but reflected the actual observed hand movement when the pliers were operated in empty space.

Many of the experiments reviewed in this section have direct implications for the experiments performed in this dissertation. In the following sections, the studies with particular relevance to each experiment are discussed. The motivations for each experiment are then put forth with reference to how these experiments will contribute to the existing literature.

2.8 Motivation for the Object Presence Experiment

For the Object Presence Experiment of this dissertation, kinematics and EMG of the arm and hand and neural data in M1, PMV and AIP were recorded while monkeys grasped an object in two ways, reached toward but did not grasp that object, and reached into empty space with the object absent from the workspace.

Though reaching and grasping have both been studied extensively in isolation, relatively few studies have compared reaching and grasping directly. Those few studies which have compared neural activity during reaches and grasps have use whole-brain functional imaging techniques in monkeys [291, 292] or humans [357, 408, 409] or were focused on subcortical brain regions such as the cerebellum and red nucleus [429, 430], and thus leave open the question of how neural activity differs between reaches and grasps on the level of single neurons and populations of single neurons in M1, PMV and AIP. Extant monkey intracortical electrophysiology studies which purport to find signals related to reaching and grasping in grasp network regions (e.g. [122, 217, 234, 431]) only examined reaching movements which

were embedded within a reach-to-grasp movement. In the Object Presence Experiment, neural activity, kinematics and EMG during reach-to-grasp and isolated reaching behavior are directly compared.

The trial conditions of the Object Presence Experiment were designed to elicit very similar reach-only behaviors in two different contexts: in the presence or absence of a previously grasped object. Several studies have highlighted the importance of the presence of a real, physical object in driving neural activity in the cortical grasp network [279, 409, 416, 417] and mirror neuron activity [248]. Of particular interest are recent BCI experiments which have identified object-related changes in M1 neural activity that, if left unaccounted for, degrade reach and grasp decoding performance [119, 189]. Preliminary analysis of M1 activity revealed a global increase in FRs when grasps were performed on an object as opposed to pantomimed in free space [410].

The analyses of data collected in the Object Presence Experiment were designed to more comprehensively characterize the object presence effect. The magnitude of the object presence effect, its interaction with movement feature encoding and its impact on decoding are established with the goal of confirming and elaborating on the human BCI findings [119, 189, 410]. Critically, detailed kinematics and EMG of the arm and hand were also recorded during the behavior in order to separate the neural modulation due to object presence from the encoding of movement features, revealing robust object presence encoding. A novel decoder architecture is proposed to retain high-accuracy decoding across object presence contexts. Unfortunately, the exact task used in human studies [119, 410] could not be replicated, as monkeys were unable to be trained to pantomime grasps (see Section 8.3). However, the results from the Object Presence Experiment remain highly relevant to future BCI implementations.

Finally, the question of what information may be represented in the object presence signal remains an open one. Several studies have suggested that vision of graspable objects and especially tools can automatically activate motor representations of the object's affordances in the cortical grasp network (see Section 2.5.2). In a particularly relevant experiment, Baumann et al showed that presentation of an object with multiple grasp affordances before any action cue was given caused AIP and PMV neurons to represent

both of the possible grasps of the object [279]. However, the structure of their task did not allow them to determine whether these effects persisted throughout movement, nor did they examine potential activation of grasp affordance representations in M1. Additionally, in an experiment in which objects were presented without a required action, the same PMV neurons were active in much the same way as when a reach-to-grasp action was required [350, 351]. This suggests that PMV neurons automatically encode the representations of the grasps afforded by objects even when they were not grasped, though this study could not determine whether such activation persists throughout a reaching movement in which no grasp is performed. In the analyses of the Object Presence Experiment, neural activity in M1, PMV and AIP is examined for evidence of automatic activation of the grasp affordance of the object when the object was present and reached toward, but not grasped.

2.9 Motivation for the Grip Affordance Experiment

In the Grip Affordance Experiment of this dissertation, kinematics and EMG of the arm and hand and neural data in M1, PMV and AIP were recorded while monkeys grasped objects with different perceived and learned grip affordances. These objects were shaped so that they could afford only a power grasp, or only a precision grasp (simple objects) or both types of grasp (compound objects) based on their perceived shape. Two of the compound objects were only ever grasped with one grip type, meaning that these objects had two perceived grip affordances and only one learned grip affordance. The third compound object was regularly grasped using both grip types, and thus had two perceived grip affordances and two learned grip affordances. The objects of the Grip Affordance Experiment are depicted in Figure 5.1.

Only a few studies have examined grasping under circumstances in which the grasped portion of two objects is identical, but the ungrasped portions of the objects differ. One behavioral study of particular relevance is that of Gentilucci 2002 [362]. In this series of experiments, humans grasped two identical sticks that were attached to the tops of differently

shaped objects. In the first experiment, the sticks were attached to the tops of two pieces of fruit (an apple and a strawberry) where the stems would otherwise be located. In subsequent experiments, the two identical grasped sticks were attached to a variety of differently shaped objects such as a tall and short stick, and a large and small sphere. The shape, size and familiarity of the ungrasped portion of the object was found to have an influence on grasp kinematics. When the grasped stick was attached to a large object, maximum grip aperture was larger than when the grasped stick was attached to a small object, even though the grasped sticks were identical on the two objects. This behavioral difference suggests that the central neural command differed for the two grasps. This influence of the ungrasped portion of the object on neural activity in M1, PMV and AIP is directly addressed in the analyses of the Grip Affordance Experiment. Additionally, more detailed grasp kinematics as well as EMG were collected for the Grip Affordance Experiment, allowing verification and further exploration of the behavioral differences evoked by differences in the ungrasped portions of compound objects.

Another highly relevant study by Vargas-Irwin et al in 2015 examined neural activity in PMV during grasps of two objects which featured identical upper power grasp portions and differing lower portions; the lower portion of one object was a pinch grasp tab, and the lower portion of the other object was a disk which afforded a key grip (with the thumb opposed against the side of the pointer finger) [425]. It was found that individual PMV neurons and the PMV population as a whole distinguished between power grasps executed on the two objects, even though the portions of the objects that were grasped with a power grasp were exactly the same. This differential neural activity for the two objects began early after object presentation and persisted throughout the entire grasping movement. The Grip Affordance Experiment expands on these findings in three ways. First, kinematics and EMG were not recorded in that study, and so it was impossible to determine whether the power grasp behaviors differed systematically for the two objects, and therefore it was also impossible to determine how much of the difference in neural activity for the different objects was due to a "true" context effect or was due to encoding of differences in movement features. Recording of detailed arm and hand kinematics and EMG for the Grip Affordance Experiment enables such analyses. Second, as neural activity was recorded in M1, PMV and

AIP for the Grip Affordance Experiment, it can be determined whether similar contextual effects can be observed in the other core nodes of the cortical grasp network. Third, perceived and learned grip affordances were not dissociated in the study of Vargas-Irwin et al; each object had two perceived grip affordances and two learned grip affordances. Thus, the study could not determine whether the differences in neural activity were due simply to the shape of the object or due to association of the object with a certain set of grasp behaviors. In the Grip Affordance Experiment, more object conditions are utilized to determine whether contextual effects of grasp encoding are driven by perceived grip affordances, learned grip affordance or both. The importance of habitual favoring of one possible grip affordance over others is evident in human behavior; humans spontaneously grasp the "handle" portion of tools, even when no specific grip instruction is provided and when the handle is positioned in such a way that its grasp would result in an uncomfortable posture [432].

Finally, in the analyses of the Grip Affordance Experiment, neural activity in M1, PMV and AIP are examined for evidence that the neural representation of the unused grip affordance is automatically activated. In the study of Baumann et al 2009 [279], it was noted that preparatory activity in AIP reflected both potential grasps (power grasp and precision grasp) which had been learned to be used on the object. However, the structure of the task did not enable the experimenters to determine whether activity related to the unused grasp persisted throughout movement. Evidence for automatic activation of the ungrasped affordance of compound objects throughout the preparatory and movement periods is considered in the Grip Affordance Experiment.

2.10 Motivation for the Use Affordance Experiment

In the Use Affordance Experiment of this dissertation, kinematics and EMG of the arm and hand and neural data in M1, PMV and AIP were recorded while monkeys grasped to hold two objects, both of which afforded a power grasp and a precision grasp, over two separate sessions. In the first session, the two objects were both mechanically fixed in place and were identical other than their color. In the second session, one object remained fixed,

while the other object was released from fixation and allowed to slide up and down on guide rods. In the second session, the subjects simply grasped and held both objects with both types of grasp, and additionally grasped the movable object with a power grasp and lifted it. Thus, in the first session, the same grasps were executed in the two different contexts of differently colored objects. In the second session, the same grasps were executed with the additional contextual factor that one object had a newly learned use affordance in that it could be lifted.

In the first session of the Use Affordance Experiment, the objects differed only by color. Human grasp kinematics have been found to be different for objects of different color. In a study in which subjects grasped red or green objects with a precision grip, grip apertures were larger during reach for red objects [377]. Analyses of kinematic and EMG data from the first session of the Use Affordance Experiment allow this effect to be verified, and analyses of the neural data from the first session of the Use Affordance Experiment reveal the potential neural signatures of this color context effect.

In the second session of the Use Affordance Experiment, the objects differed by color and in their learned use affordances; one object was mechanically fixed while one object had been learned to be lifted. Human functional brain imaging studies suggest that use affordance knowledge may be stored and processed in the cortical grasp network. Imagining grasping tools with known uses compared to neutral objects activates larger regions of premotor and parietal cortex [344]. Viewing novel objects for which a tool use had been learned compared to novel graspable objects without a known use also activated larger regions of premotor and parietal cortex [427]. The analyses of the Use Affordance Experiment allow this effect to be examined on the single neuron and population level in M1, PMV and AIP.

Natural grasping behavior reveals the influence of learned use knowledge on grasp planning. When tools with known uses were presented to human subjects, they naturally grasped the tools in a way that was appropriate to their use (usually, by the handle), even when such a grasp resulted in an uncomfortable arm posture [432]. Interestingly, this natural behavior was abolished when subjects were engaged in a task with high cognitive load, suggesting that the integration of use affordance knowledge into the grasp action plan may rely on high-level cognitive resources. The kinematics and EMG recorded in the Use

Affordance Experiment allow verification of this habitual, spontaneous use-associated grasp behavior. Additionally, analyses of the neural data from the Use Affordance Experiment were designed to find signatures of use affordance knowledge encoding during grasp planning in M1, PMV and AIP.

Learned information about object characteristics may be retained and processed in M1. In one study, human subjects lifted a set of objects which differed in weight but were otherwise shaped the same and visually identical. The objects were presented in a random fashion and thus the subject did not know on each trial whether the object would be heavy or light. Hand muscle activity evoked from TMS applied to M1 revealed that the cortical excitability of M1 was greater if the object lifted on the previous trial was heavy, even just after the object was presented and before movement onset [433]. The Use Affordance Experiment was designed to look for similar effects of retention of object properties (mobility vs. fixation) in M1, PMV and AIP.

Many studies have shown that when similar grasps were part of different grasp-and-manipulate action chains with different goals, differences are observed in grasp behavior [356, 368–374] and neural activity in M1 [186], PMV [239–241, 351, 422–424], AIP [270, 423, 424] and areas of the inferior parietal lobule adjacent to AIP [240, 421]. However, in most of these experiments, object identity was not dissociated from behavior, and thus neural and behavioral differences may have been evidence of preparatory motor planning related to the entire action chains, as opposed to a "true" contextual effect of object identity based on learned use knowledge. Important exceptions are the studies of the Rizzolatti group [239–241, 351, 421, 426]. In these experiments, a monkey was trained to grasp a food morsel and subsequently eat it or to grasp a synthetic pellet and subsequently place it in a receptacle near the mouth. Critically, on some trials, monkeys were instructed to grasp a food morsel and place it into the receptacle instead of eating it. Thus, in the trials in which both food morsels and synthetic pellets were grasped and placed in the receptacle, the only difference was the contextual difference of the identity of the object to be grasped. In some instances, neurons in PMV and inferior parietal lobule were found to fire more for grasp-and-place actions made with the food compared to the same actions made with the pellet object [239, 421], though such effects were not found in other studies [240, 426]. These findings

indicate potential encoding of object identity based on learned use affordances in these neurons. However, though the overall requirements of the grasp-and-place actions were the same for food and pellet items in these trials, the researchers did not record kinematics or EMG of the arm and hand, and thus subtle variability in behavior may have accounted for the neural differences. Additionally, neural activity was not recorded in M1. The analyses of the Use Affordance Experiment were specifically designed to find and characterize contextual encoding of object identity based on learned use affordances in M1, PMV and AIP, and to measure and account for the neural differences that were attributable to encoding of differences in kinematics and EMG.

3.0 Experimental Approach

Three novel experiments were designed for this dissertation: the Object Presence Experiment, the Grip Affordance Experiment and the Use Affordance Experiment. All experiments were designed with the same basic goal of evoking very similar reaching or grasping behaviors in different object contexts while recording detailed kinematics and muscle activity of the arm and hand and neural activity in M1, PMV and AIP. By holding overall behavioral requirements constant and varying only contextual factors, the behavioral and neural differences related specifically to these contextual factors can be isolated and characterized.

This chapter contains general descriptions of the three experiments. More specific descriptions of the behavioral outcomes of each individual experiment are presented in the Results Sections 4.1, 5.1 and 6.1. Section 3.1 describes the physical apparatus and equipment used in the experiments. Section 3.2 describes the behavioral tasks employed in the three experiments, including the progression of the task phases and the visual feedback shown to the subjects. Section 3.2.1 describes the task presentation block structure and schedule. Finally, Section 3.3 describes the data recorded during each experiment.

3.1 Physical Apparatus

The experiments were performed in a dedicated room outfitted with laboratory Biosafety Level 2 precautions. The primate chair, object, feedback monitor and kinematic motion tracking cameras were all mounted in an aluminum frame (80/20 Inc., Columbia City, IN). A photograph of Monkey R in the experiment room is shown in Figure 3.1.

Monkeys sat in a custom primate chair, with one arm free and the other restrained in a tube. A plastic barrier was placed around the monkey's head in order to protect the neural recording hardware. A drink tube was affixed in front of the monkey's mouth to deliver rewards. A start button was placed on the side of the chair, near the monkey's waist.

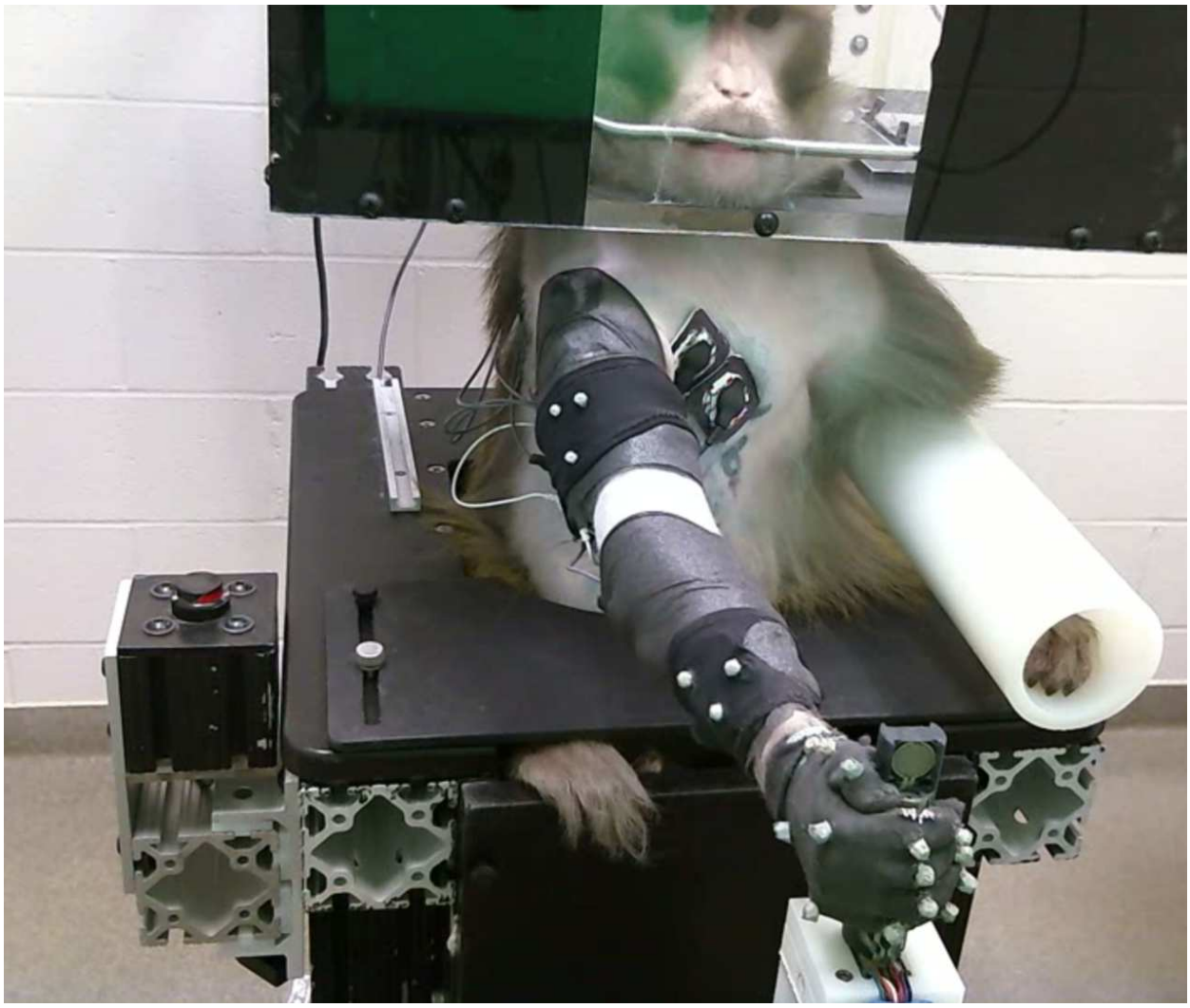

Figure 3.1: **Monkey R in the Experiment Room.** Subject is shown performing a Power Grasp in the Object Presence Experiment.

In each experiment, monkeys grasped or reached toward an object or set of objects. Each object was presented about 25 cm directly in front of the monkey at chest height. The distance to the object was adjusted for each monkey to accommodate the different sizes of the monkeys. The objects were designed to elicit power grasps, pinch grasps, or both. Objects were manufactured using 3D printing and CNC milling and were instrumented with force sensors to detect the appropriate grasps. The design of the objects is detailed in Section A.2, and descriptions of the objects are also provided in the Results Sections 4.1, 5.1 and 6.1. The objects were mounted on the aluminum frame and fixed in place (save for Object 2 in the Use Affordance Experiment post-learning session, which was designed to slide vertically). The objects were always presented in the same location, in order to promote consistent behavior between the different objects. Different objects were presented sequentially in blocks. The block scheduling is detailed in Section 3.2.1.

An LCD monitor was mounted 50 cm directly in front of the monkey at eye level. The monitor was used to deliver visual feedback during the task. Details of the visual feedback are presented in Section 3.2.

3.2 Behavioral Task

The tasks employed in the three experiments were variations of a simple delayed reach-to-grasp task. For all experiments, objects were grasped and held with a power grasp or a pinch grasp. For the Object Presence Experiment, subjects either grasped and held a single object with a power grasp or a pinch grasp, reached into a target area in space next to the object, or reached into the same target area in space with no object present. For the Grip Affordance Experiment, the subjects grasped a series of objects with power grasps or pinch grasps. For the Use Affordance Experiment, the subjects grasped two objects with power grasps and pinch grasps, and in the post-learning session, also lifted one of the objects. The lights in the experiment room were on and the object was visible throughout all trials and inter-trial periods. The phases of the task are depicted in Figure 3.2.

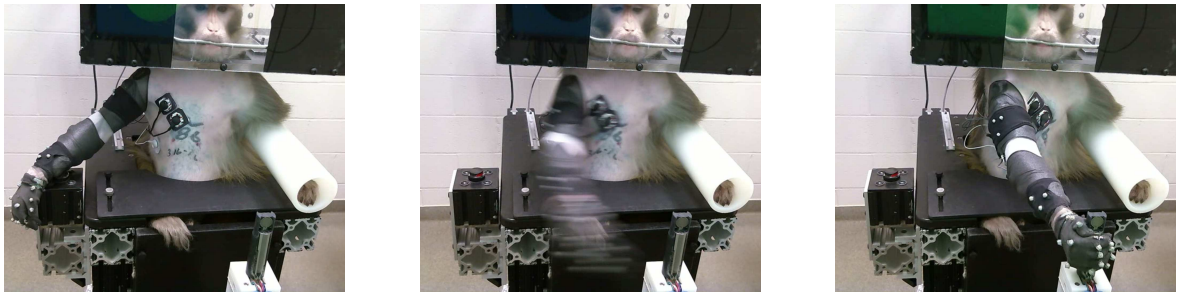

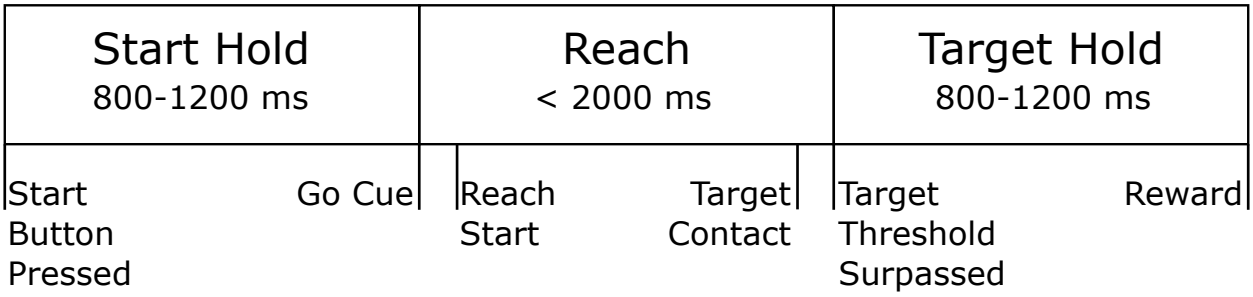

Figure 3.2: **Task phases, reach and reach to grasp and hold trials.** Top: still frames of Monkey R performing the different task phases. Bottom: Timeline of task phases and task events (not to scale).

Each trial proceeded as follows. The subject initiated the trial by pressing the start button, entering the "Start Hold" phase. The subject was then required to hold the start button down for 800–1200 ms (time drawn from a uniform distribution on each trial). After the delay period, a "Go Cue" was delivered, initiating the "Reach" phase. The subject was required to reach forward and grasp the object (or reach into the target sphere in the reach trials of the Object Presence Experiment). For grasping trials, the subjects were required to apply a small force to the appropriate part of the object, corresponding with the instructed grasp. For the reach trails of the Object Presence Experiment, the subject was required to bring the hand into a 3 cm radius target sphere in space.

Monkeys were required to initiate grasp or enter the target sphere within 2000 ms after the Go Cue, initiating the "Target Hold" phase. The subject was then required to maintain the grasp or maintain the hand within the target sphere for 800–1200 ms, after which a reward was delivered through the drink tube.

For the lift trials of the Use Affordance Experiment post-learning session, an additional "Lift" task phase was appended after the Target Hold phase. The lift was required to be completed within 2000 ms. The task progression of lift trials is displayed in Figure 3.3.

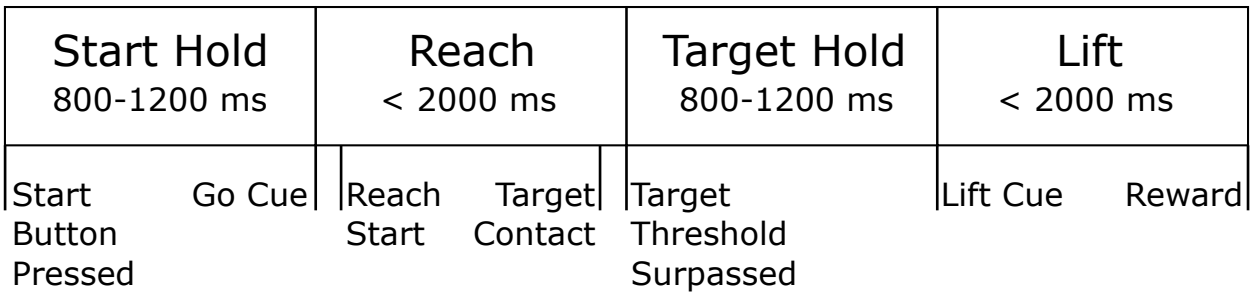

Figure 3.3: **Task phases, lift trials.** Timeline of task phases and task events (not to scale).

The task progression was controlled automatically via custom software which detected behavioral events and tracked elapsed time to step through the task phases. Details of the task control software are provided in Section A.5. Trials were automatically aborted if timing requirements were not met or if inappropriate grasp force sensors were activated.

Visual feedback was provided to the subject via an LCD monitor. Depictions of the visual feedback are shown in Figure 3.4.

During the inter-trial period, the screen was gray with a white central circle. During the Start Hold phase, a green central circle was displayed and the background changed to a color. The background color cued the grip type or reach that was required for the task. Blue or turquoise colors were used to cue power grasps, red or orange colors cued pinch grasps, and yellow or white colors cued reaches with no grasps (in the Object Presence Experiment). At the end of the Start Hold phase, the central circle switched from green to black, serving as the "Go Cue," instructing the subject to begin the reach.

For all grasp and hold trials, as the subject began to apply force to the object, a green feedback circle appeared in the center of the display and grew in size. The radius of the green feedback circle was proportional to force sensor signals. The outer black circle represented the target force threshold. For the reach trials of the Object Presence Experiment, the radius of the green feedback circle was proportional to the inverse of the distance between the current hand position and the center of the target sphere. In those cases, the black circle represented the positional target threshold.

After the target force or position threshold was attained, a smaller black circle was superimposed over the green feedback circle. The green feedback circle radius remained related to the force sensor signal or inverse distance between the current hand position and the target. The black circle indicated the lower threshold that the subject was required to hold above. After successful completion of the Target Hold phase, the reward was delivered and the monitor displayed the inter-trial pattern, indicating the end of the trial.

For the lift trials of the Use Affordance Experiment, an additional triangular shape was displayed on the feedback monitor. These modified displays are shown in Figure 3.5.

This triangle was present throughout the entire trial for lift trials. The triangle remained black and stationary throughout the Start Hold, Reach and Target Hold periods. At the end of the Target Hold period, the triangle changed from black to green, serving as the "Lift Cue." At this point, the height of the triangle on the screen was linked to the sensor from the linear potentiometer lift sensor. As the subject lifted the object, the triangle moved upward. The triangle reaching the top of the screen corresponded with the lift distance threshold.

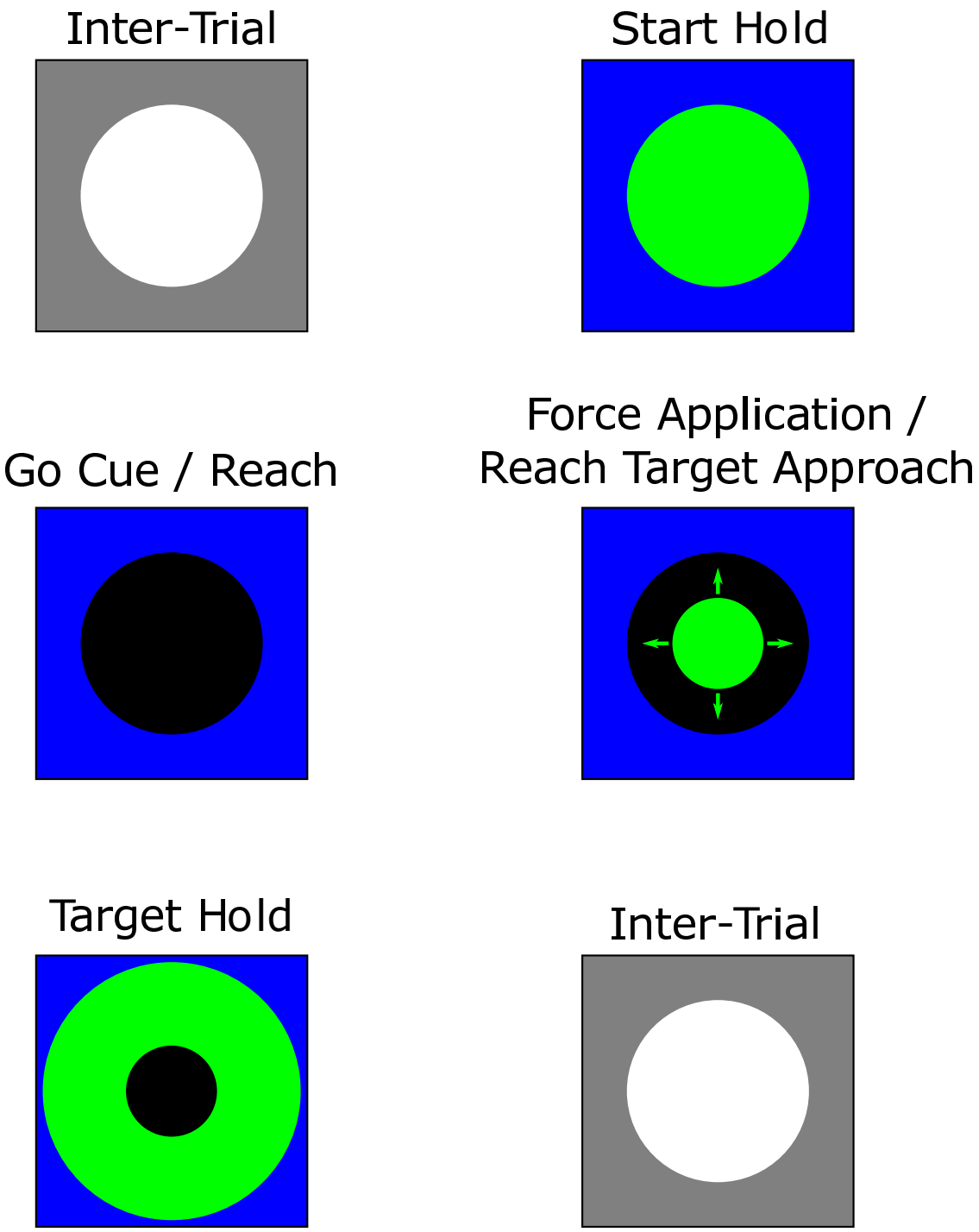

Figure 3.4: **Visual feedback for reach and reach to grasp and hold trials.** The blue color corresponded to a power grasp. Other colors were used to cue different grasps or reaches. Green arrows indicate motion and were not displayed during the task.

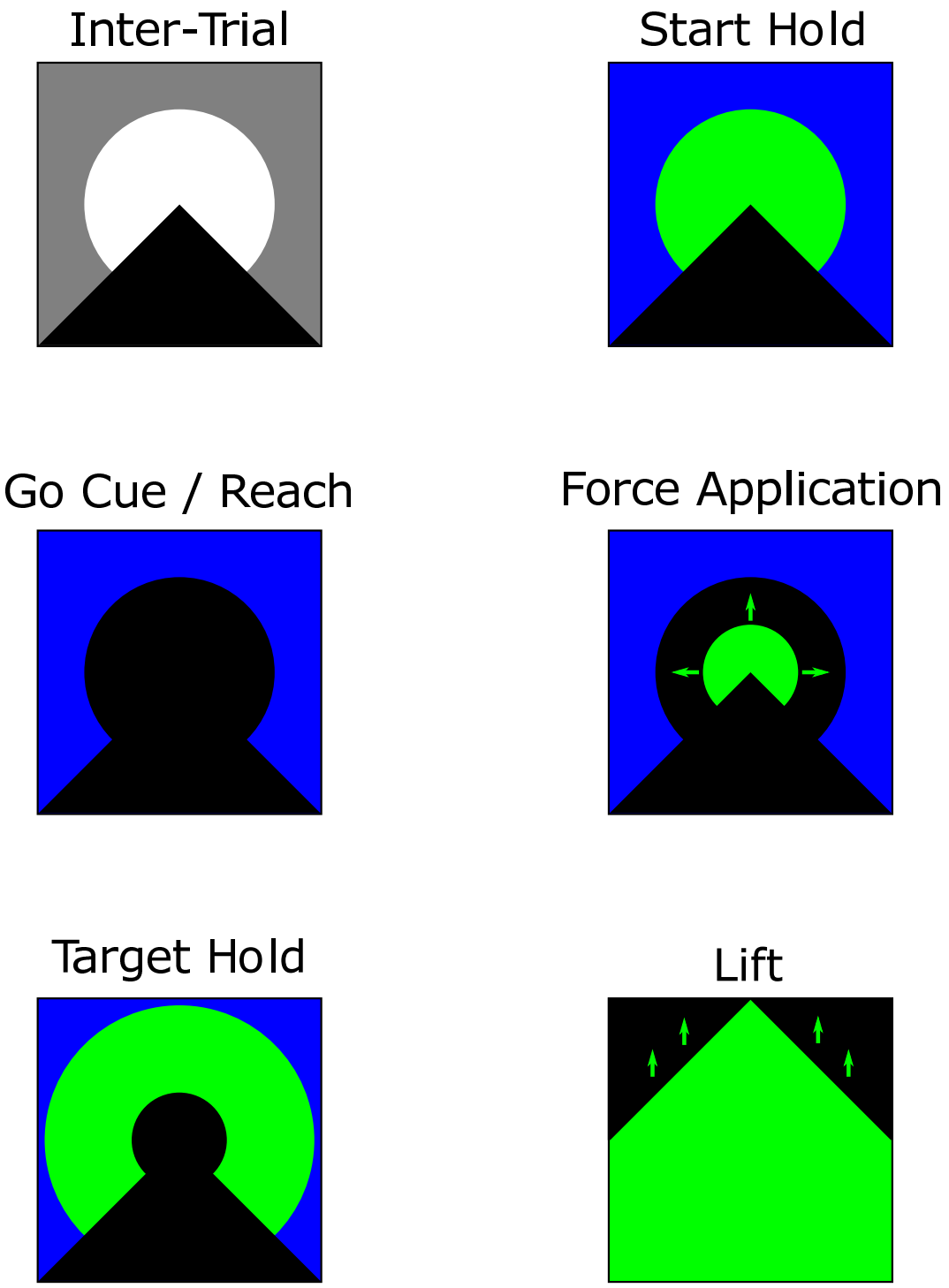

Figure 3.5: **Visual feedback for lift trials.** Green arrows indicate motion and were not displayed during the task.

3.2.1 Block Scheduling

The objects were presented in blocks in order to keep inter-trial times low and encourage high trial counts. Objects were changed by the experimenter between blocks, with the subject's view blocked by an opaque barrier. Blocks could contain a single trial type, or in the case that an object afforded multiple behaviors, blocks could contain multiple trial types. In the case that multiple trial types were presented in the same block, trials were presented in a pseudorandom interleaved fashion.

The blocks of the Object Presence Experiment were:

1. Compound Object Grasp (Power Grasps and Pinch Grasps interleaved)
2. Object Reach
3. No-Object Reach

The blocks of the Grip Affordance Experiment were:

1. Simple Power Object (Power Grasps only)
2. Simple Pinch Object (Pinch Grasps only)
3. Compound Power Object (Power Grasps only)
4. Compound Pinch Object (Pinch Grasps only)
5. Compound Multi-grasp Object (Power Grasps and Pinch Grasps interleaved)

The blocks of the Use Affordance Experiment pre-learning session were:

1. Object 1 (Power Grasps and Pinch Grasps interleaved)
2. Object 2 (Power Grasps and Pinch Grasps interleaved)

The blocks of the Use Affordance Experiment post-learning session were:

1. Object 1 (Power Grasps and Pinch Grasps interleaved)
2. Object 2 (Power Grasps, Pinch Grasps and Lift Trials interleaved)

The analyses conducted for this dissertation critically depend on comparisons of behavioral measures and neural activity between different blocks. However, behavioral and neural activity may change during the course of the session due to factors such as motivation,

wakefulness [434], impulsivity [435] or thirst and satiety [436]. To mitigate the effects of such potential temporal drift in behavior and neural activity, each block was presented twice, with the sequence of blocks in the first half of the session repeated backwards in the second half of the session, producing a palindromic sequence.

For example, consider a session consisting of three block types, A, B and C. These blocks were split into halves, A1, A2, B1, B2, C1 and C2. The blocks were the presented in a balanced order: A1–B1–C1–C2–B2–A2. Thus, the trial types performed at the beginning of the session were performed again at the end of the session.

Such a structure was chosen to minimized the effect of any slow drift in behavior or neural activity over the course of the session. For all experiments, 140 trials of each type were performed in each session (with 70 trials in each half task block), except for Monkey I in the Grip Affordance Experiment, in which 130 trials of each type were performed.

3.3 Data Streams

Throughout all experiments, neural activity, kinematics of the arm and hand, EMG from shoulder and arm muscles, and behavioral events were recorded. Kinematic data consisted of 22 joint angles of the arm and hand (three shoulder angles, elbow flexion, three wrist angles and 15 finger joint angles) which were obtained using an infrared motion tracking system (Vicon, Oxford, UK). EMG was obtained from eight sites (pectoralis or trapezius, deltoid, biceps, triceps, proximal and distal forearm flexors and proximal and distal forearm extensors) using adhesive skin surface electrodes and a dedicated EMG amplifier (Bortec Biomedical, Calgary, Canada). Details of the data acquisition and processing for each of the data streams are provided in Section A.4.

Spiking neural activity was recorded using penetrating intracortical microelectrode arrays. All M1 recordings were obtained with Utah Arrays (Blackrock Microsystems, Salt Lake City, UT) and all PMV and AIP recordings were obtained with Floating Microelectrode Arrays (FMAs; Microprobes for Life Science, Gaithersburg, MD). The approximate array locations in each subject are portrayed in Figure 3.6.

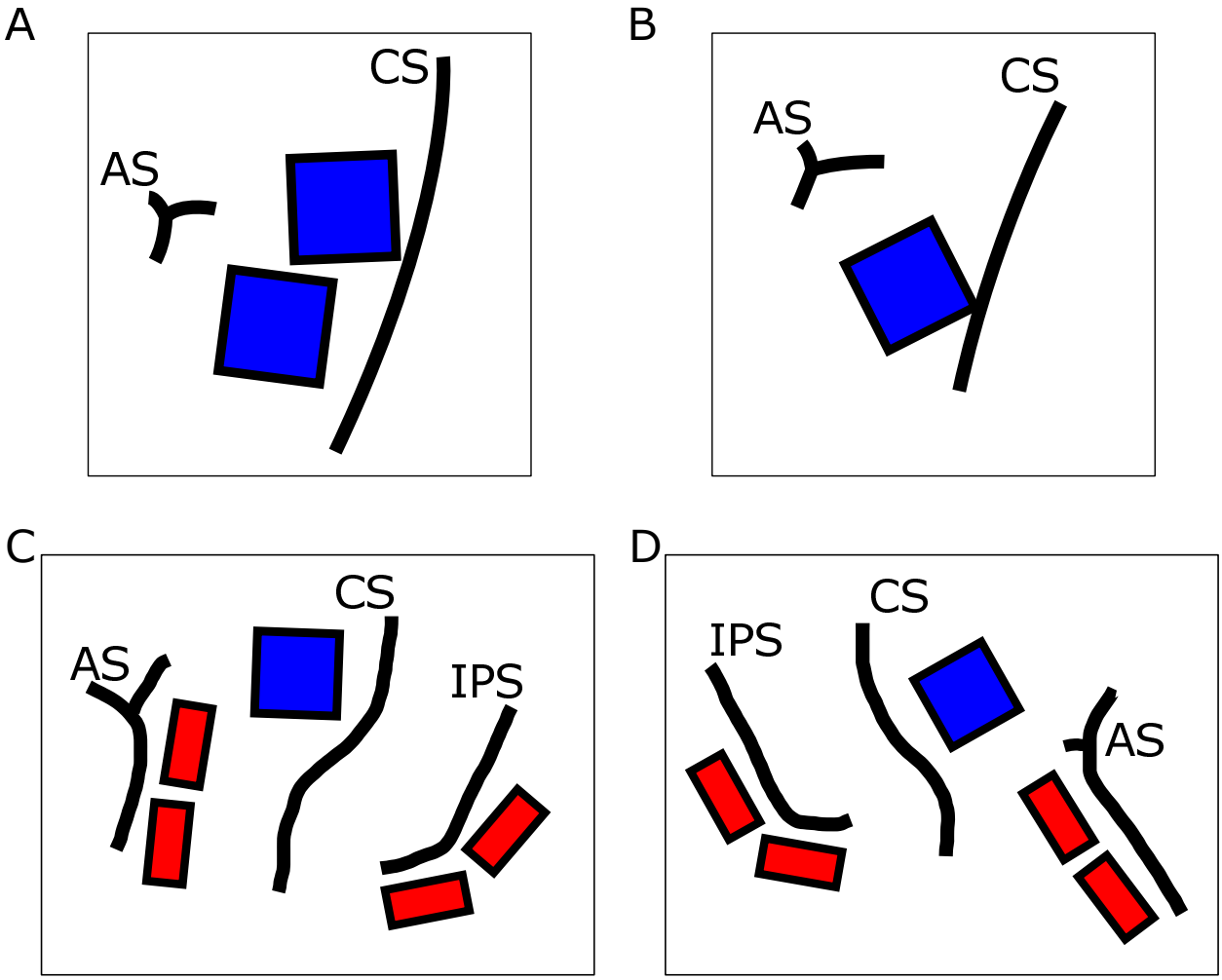

Figure 3.6: **Microelectrode array locations.** Drawings were traced from photographs taken during the implant surgeries. Blue: Utah Arrays. Red: Floating Microelectrode Arrays. A: Monkey R. B: Monkey I. C: Monkey T left hemisphere. D: Monkey T right hemisphere. CS: central sulcus. AS: arcuate sulcus. IPS: intraparietal sulcus

The implantation surgical procedures for the microelectrode arrays are detailed in Section A.1. A novel method was used to target and implant the FMAs in PMV and AIP. This method is described in Section A.1.2.

Neural data were always recorded from the hemisphere contralateral to the hand used for the experiments. For Monkey R and Monkey I, neural activity was recorded only from left hemisphere M1, and the tasks were performed with the right hand. For Monkey T, neural activity was recorded from M1, PMV and AIP. Neural activity was recorded sequentially from both hemispheres of Monkey T. Recording microelectrode arrays were implanted in each hemisphere in separate procedures approximately six months months apart. Thus, Monkey T performed all experiments twice, once with the right hand and once with the left hand.

Monkey R and Monkey T completed all three experiments, while Monkey I completed only the Grip Affordance Experiment and the Use Affordance Experiment. For Monkey T, left hemisphere M1 data were only obtained for the Grip Affordance Experiment, as the recording pedestal was damaged, precluding further recordings. The neural data which were recorded for each subject in the three experiments is summarized in Table 3.1.

Table 3.1: **Neural data streams for each subject in each experiment.** Green cells indicate experiments for which neural data from each brain area were recorded. Gray cells indicate instances where the subject participated in the experiment, but neural data from that brain area were unavailable. Blank cells indicate that the subject did not participate in the experiment. OPE: Object Presence Experiment. GAE: Grip Affordance Experiment. UAE: Use Affordance Experiment. Pre: pre-learning session. Post: post-learning session.

		Experiment			
Subject	**Area**	**OPE**	**GAE**	**UAE Pre**	**UAE Post**
Monkey R	M1				
Monkey I	M1				
Monkey T	M1 Left				
	M1 Right				
	PMV Left				
	PMV Right				
	AIP Left				
	AIP Right				

4.0 Results — Object Presence Experiment — M1

The Object Presence Experiment was designed to study how behavior and neural activity differ when similar reaching actions are performed in the presence or absence of an object. Two subjects (Monkey R and Monkey T) completed the Object Presence Experiment. Monkey R completed the task with the right hand, while Monkey T utilized first the right, then in another session, the left hand. Neural data were always recorded from the hemisphere contralateral to the hand used. This section describes results from a single Monkey R session and a single Monkey T left hand (right hemisphere) session only, for which M1 neural data were collected. The results of this experiment from Monkey T PMV and AIP are presented in Chapter 7.

The main findings of this chapter are summarized as follows. Subjects performed reaches to the same spatial location in different object contexts (with or without an object present), and also grasped the object. The behaviors, in terms of kinematics and EMG, for the two reach conditions (with and without an object present) were similar. Despite this similarity in behavior, the spiking activity of the majority of M1 units differed significantly between reaches made with or without the object present. The difference in population neural activity observed between the two reach conditions was relatively large compared to the difference in behavior. This difference in neural activity could not be fully accounted for by fixed linear encoding of kinematics and EMG, and was therefore taken as evidence for the explicit encoding of object presence. For the majority of M1 units, activity was better fit by models in which the linear tuning to kinematics and EMG were allowed to change depending on object presence, as opposed to being fixed across contexts. Decoding performance decreased markedly when training a simple linear decoder in one context and testing in the other. Accurate decoding could be recovered by using a context classifier with context-specific decoders. When the object was present, behavior and neural activity were biased toward the activity associated with the grasping actions afforded by that object, even when it was not grasped.

Section 4.1 contains a detailed description of each subject's behavior during the different task conditions. The behavior is described in terms of the observed movement features (MFs), comprised of 22 joint angles and joint angular velocities of the arm, wrist and fingers, 3D hand position and hand velocity, and EMG from eight muscle groups. Section 4.2 characterizes the differences in the MFs between the different task conditions. Section 4.3 describes the single unit and population level M1 neuronal firing rate (FR) responses recorded during the experiment, highlighting the differences in neural activity between conditions in which the object was present vs. the condition in which the object was absent. Section 4.4 concerns the relation between the M1 FRs and the MFs, with specific focus on the evidence for contextual object presence encoding in M1, defined as neural modulation beyond that which can be accounted for by fixed linear tuning to MFs. Section 4.5 concerns the interaction between object presence encoding and linear MF encoding in M1. Section 4.6 characterizes the impact of the object presence encoding signal on decoding accuracy. Finally, section 4.7 explores the possibility that the object presence related differences in behavior and neural activity were related to the grasp affordances of the object.

4.1 Behavioral Results of the Object Presence Experiment

Each subject completed 140 repetitions of each of the following 4 task conditions, for a total of 560 trials:

1. Power Grasp
2. Pinch Grasp
3. Object Reach
4. No-Object Reach

Still images from videos of Monkey R completing each of these tasks are shown in Figure 4.1. In all conditions, the subject began each trial with its hand on the start button and awaited the go cue. During this time, the subject was cued as to which behavior was required by a

colored indicator on the feedback monitor: blue for Power Grasp, orange for Pinch Grasp, yellow for Object Reach and white for No-Object Reach. After 800–1200 ms, a go cue was presented, and the subject reached forward to grasp the object or reached into the target sphere in space. Section 3.2 contains further details of the trial structure, visual feedback and block schedule.

In the Power Grasp condition, the subject reached forward and grasped the object around the base with a whole-hand power grip, in which digits 2–5 and the palm were opposed. Successful grasp required the simultaneous activation of two force sensors embedded in the left and right sides of the object at a low force threshold, while not activating the pinch grip sensors (see Section A.2 for details of object design and force sensors). The subject was required to maintain the grasp for 800–1200 ms to complete the trial and receive a reward.

In the Pinch Grasp condition, the subject reached forward and grasped the upper tab of the object with a precision grip, in which the thumb and pointer finger were opposed. In this case, successful grasp required the simultaneous activation of two force sensors on the front and back of the tab at a low force threshold, while not activating the power grip sensors. Again the subject was required to maintain the grasp for 800–1200 ms to receive a reward.

In the Object Reach condition, the subject reached forward toward the object but did not make contact with it. A successful reach was judged by the hand position (defined as the mean x-y-z coordinates of motion tracking markers HAN1, HAN2, HAN3 and HAN4, see Section A.4.1) breaching a 3cm radius sphere around the mean hand position obtained from the Target Hold periods of previous successful Power Grasp and Pinch Grasp trials (the Mean Grasp Position). After breaching the initial 3cm radius target sphere, the subject was required to maintain its hand position within a 6cm radius sphere around the Mean Grasp Position for 800–1200 ms to complete the trial and receive a reward. The trial was automatically aborted if any force sensor was activated, including the extra strip force sensor on the back of the object. The task was monitored by video in real time, and trials were manually aborted if there was any indication that the subject made contact with the object which the force sensors failed to detect. In addition, videos were carefully reviewed after each session in order to exclude any trial in which the subject touched the object at all, though such occurrences were rare.

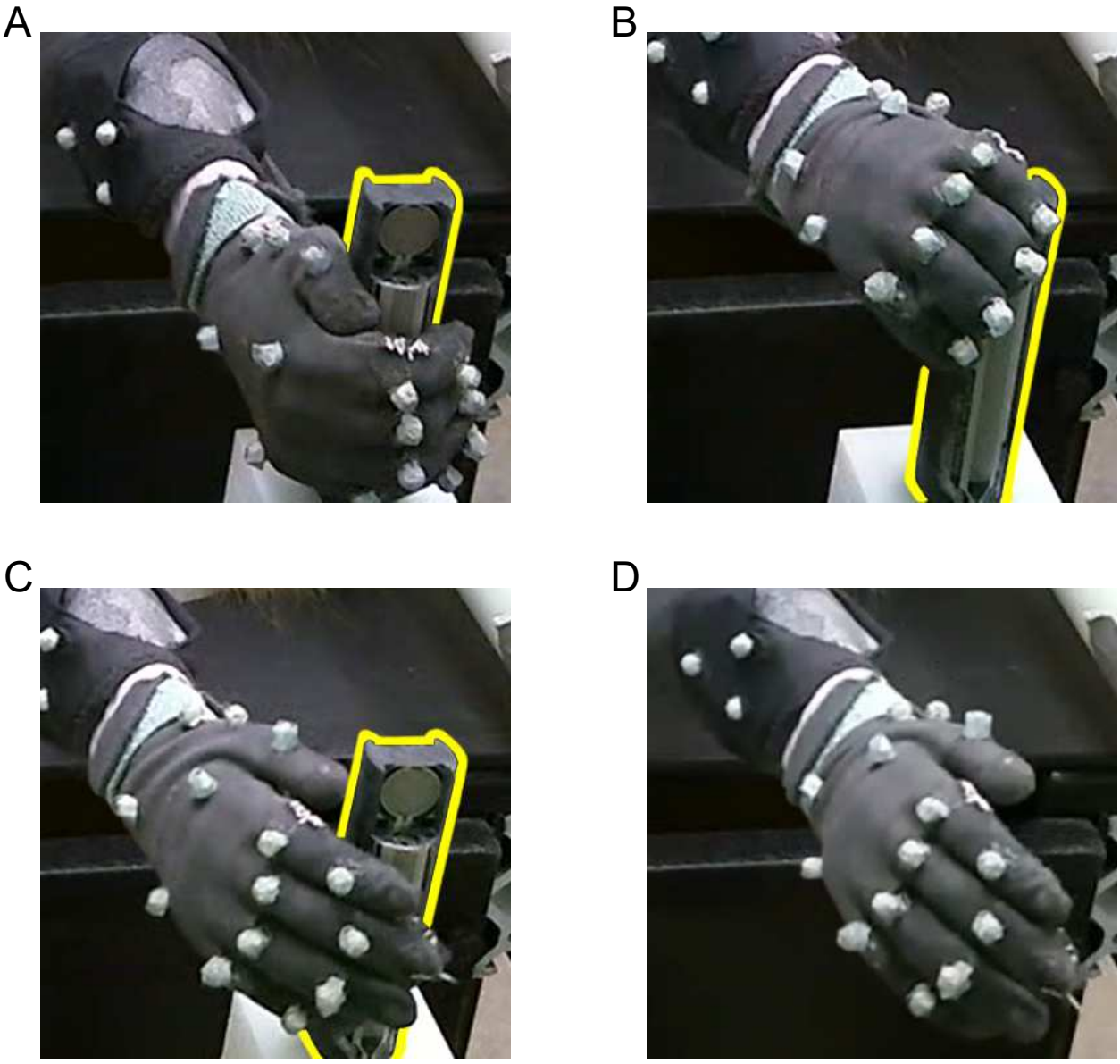

Figure 4.1: **Task conditions of the Object Presence Experiment.** Single frames from video recordings of Monkey R Session 270 performing successful trials of the four conditions of the Object Presence Experiment. The object has been highlighted in yellow. A: Power Grasp. B: Pinch Grasp. C: Object Reach. D: No-Object Reach.

In the No-Object Reach condition, the object was removed and the subject reached forward to breach the initial 3cm target sphere around the Mean Grasp Position. The subject was then required to maintain a hand position within the 6cm radius sphere around the Mean Grasp Position for 800–1200 ms in order to receive a reward. The target spheres in No-Object Reach trials were exactly the same as those in Object Reach trials.

For all conditions, the Reach Start time was defined as the time point of the first kinematic sample in which the hand velocity exceeded 1 mm/s for a sustained period. For the Power Grasp and Pinch Grasp conditions, the Target Contact time was defined by the initial uptick of the appropriate force sensors. For Object Reach and No-Object Reach conditions, the Target Contact time was defined by the first kinematic sample in which hand position was inside the 3cm target sphere around the Mean Grasp Position. See Section A.4.5 for more details of data alignment to task epochs.

In each condition, the subject received visual feedback in the form of a variable-radius green circle on the feedback monitor. In the Power Grasp and Pinch Grasp conditions, the radius of the feedback circle was linked to the signals from the appropriate force sensors. In the Object Reach and No-Object Reach conditions, the radius of the circle was proportional to the inverse of the distance between the current hand position and the Mean Grasp Position. Thus, in all cases, successful behavior resulted in a sustained increase in the size of the green feedback circle. Further details of the visual feedback are provided in Section 3.2. Details on real-time hand position calculation and streaming are provided in Section A.4.1 and descriptions of the training strategies to induce these behaviors are provided in Section A.3.

The subjects exhibited somewhat different reach times (the time between Reach Start and Target Contact) for each condition. Monkey R performed Power Grasp, Pinch Grasp, Object Reach and No-Object Reach reaches in 404.7 ± 33.9, 425.0 ± 29.7, 467.8 ± 100.2 and 530.4 ± 167.5 ms (mean $\pm$ standard deviation) respectively. Monkey T performed the reaches in 310.9 ± 33.2, 344.0 ± 15.0, 472.4 ± 52.9 and 495.7 ± 189.0 ms respectively. In order to compare across conditions, trials were resampled at variable rates within the reach period to produce an equal number of samples for each trial (see Section A.4.5 for details).

Trial-averaged hand positions and hand velocities are shown in Figure 4.2 for both subjects. The trial-averaged values were calculated by averaging the values at each time

point across all 140 trials of each condition. The hand position was defined as the average x-y-z coordinates of markers HAN1, HAN2, HAN3 and HAN4 (see Section A.4.1), relative to the mean hand position on the start button. The coordinate axes corresponded to the workspace as follows: positive X pointed to the right of the subject, positive Y pointed forward from the subject and positive Z pointed upward.

For both subjects, the Power Grasp hand position was lower and further forward than the Pinch Grasp position, reflecting the spatial separation of the portions of the object being grasped. For the Object Reach and No-Object Reach trials, Monkey R maintained an hand position intermediate between those observed in the Power Grasp and Pinch Grasp Trials. Monkey T's hand position during Object Reach and No-Object Reach trial was more similar to the position observed during Pinch Grip trials.

Both subjects exhibited overshoot in the hand Z position, especially for Power Grasps. This reflected the fact that the hand was initially raised upward to lift off of the start button, and then brought downward to make contact with the object.

Both subjects displayed slower hand velocities during the Object Reach and No-Object Reach trials compared to the grasp trials. In addition, both subjects' hand speeds decreased earlier during Object Reach, No-Object Reach and Pinch Grasp trials compared to the Power Grasp trials, reflecting the fact that the subjects had to slow and stop their own movements during non-Power Grasp trials, whereas the subject could use contact with the object to stop the hand during Power Grasp trials.

Trial-averaged joint angle trajectories of the arm and fingers are shown in Figures 4.3 and 4.4 for Monkey R and Figures 4.5 and 4.6 for Monkey T. Details of the calculation of these joint angles are presented in Section A.4.1.

For Monkey R, shoulder angle trajectories were largely similar across all conditions, reflecting elevation, adduction and inward rotation to raise the arm from a position at the subject's side toward the target at the center of the workspace. The elbow flexion angle remained steady throughout the trials for the Object Reach and No-Object Reach conditions, while slight flexion, followed by extension before object contact was observed for Power Grasp and Pinch Grasp trials. The wrist was brought from an extended initial position to a flexed target position, with less final flexion for Power Grasps. The wrist was abducted (radial

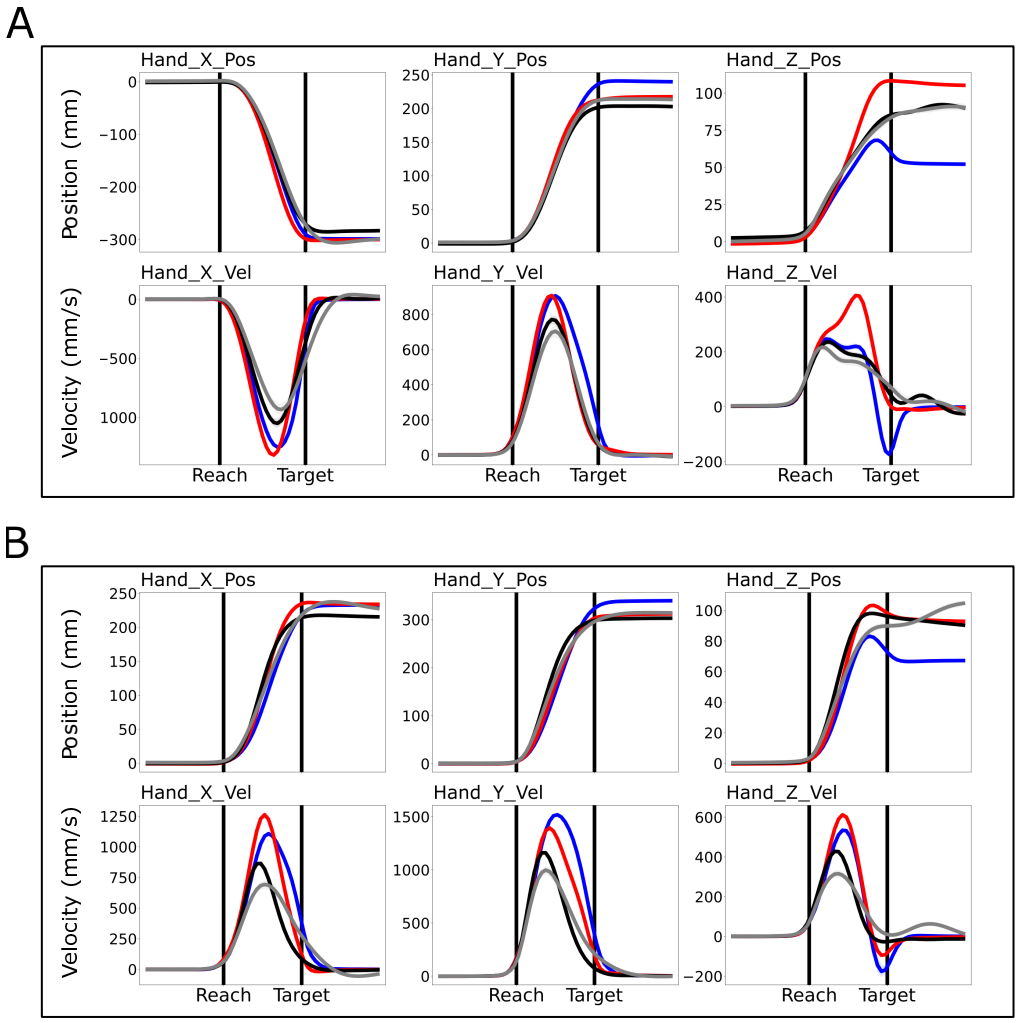

Figure 4.2: **Trial-averaged hand positions and velocities in the Object Presence Experiment.** Hand positions are relative to the mean hand position 400 ms before Reach Start. A: Monkey R. B: Monkey T. Blue: Power Grasp. Red: Pinch Grasp. Black: Object Reach. Gray: No-Object Reach.

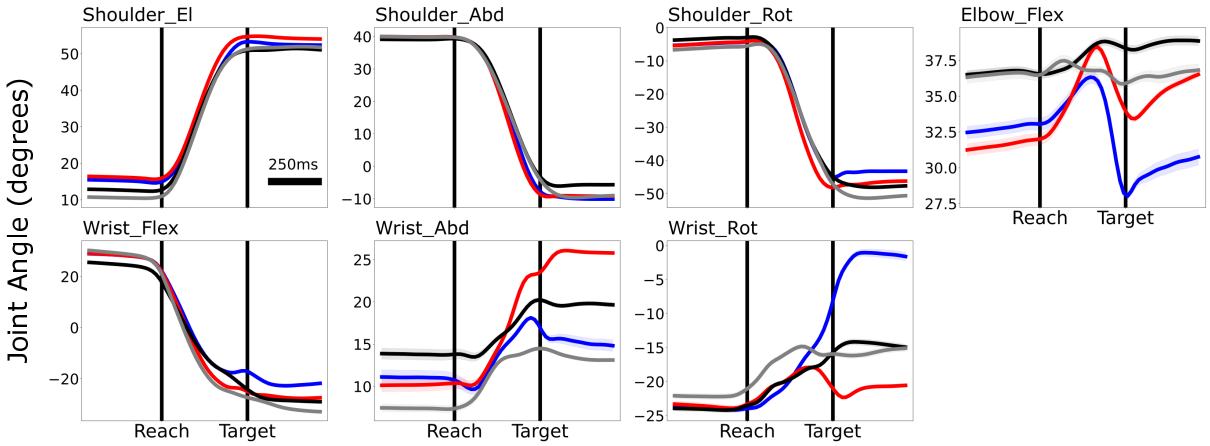

Figure 4.3: **Trial-averaged arm joint angle trajectories for Monkey R in the Object Presence Experiment.** Blue: Power Grasp. Red: Pinch Grasp. Black: Object Reach. Gray: No-Object Reach. El: elevation. Abd: abduction. Rot: rotation. Flex: flexion.

deviation) when approaching the target, with greater abduction for Pinch Grasps. The wrist was initially supinated, then pronated for Pinch Grasp trials and further supinated for Power Grasp trials, while remaining neutral for Object Reach and No-Object Reach trials.

Finger postures were highly condition-dependent. For Power Grasp trials, the thumb was extended and abducted at the CMC joint, while remaining neutral at the MCP joint. This reflected the thumb being placed against the object on the same side as the palm, rather than wrapping around the object to oppose the palm (Figure 4.1 A). Power Grasps also coincided with major MCP flexion and adduction (towards the thumb) and moderate PIP flexion in digits 2–5. For Pinch Grasp trials, the thumb was flexed and adducted at the CMC joint to bring it under the palm, and flexed at the MCP joint in order to engage the object. The digit 2–5 MCP joints exhibited much less flexion than in Power Grasp trials and remained abducted (away from the thumb), while the PIP joints exhibited greater flexion. For Object Reach and No-Object Reach trials, the fingers remained extended and abducted, with somewhat greater extension in the MCP joints for Object Reach trials as the hand was opened to avoid contact with the object.

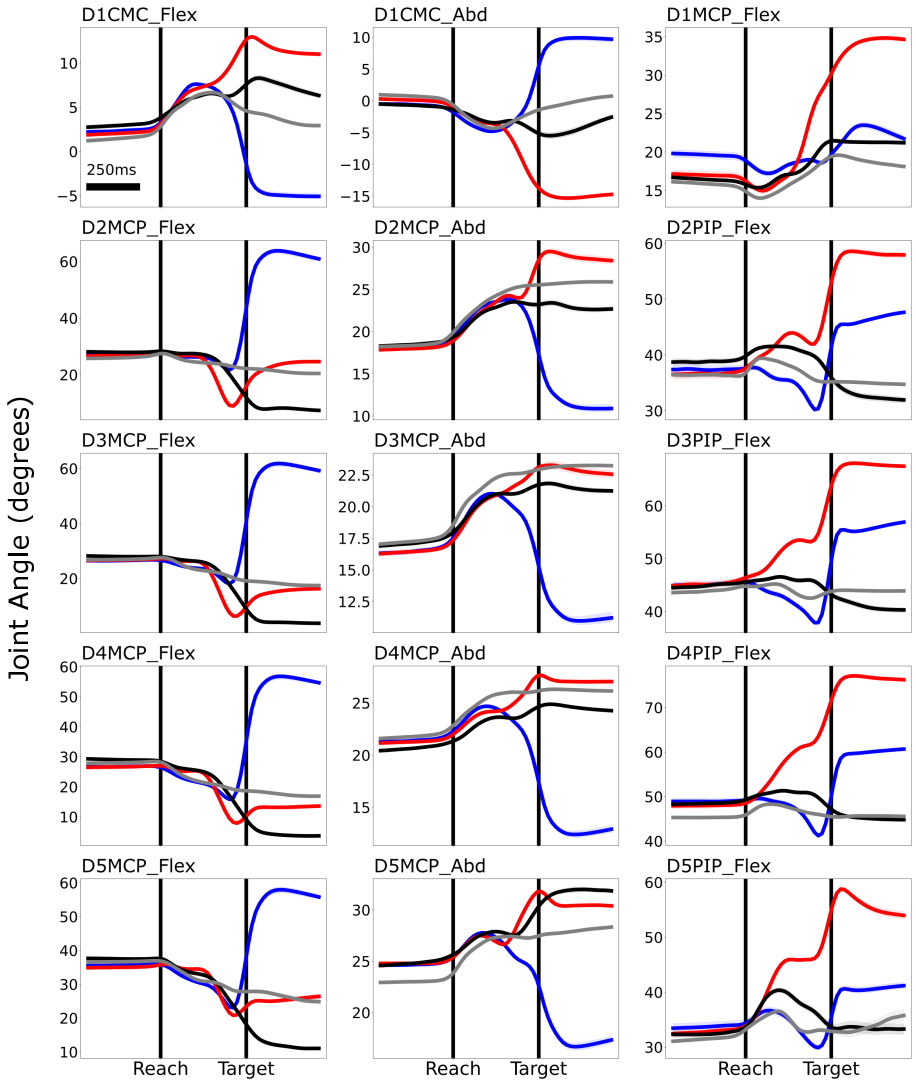

Figure 4.4: **Trial-averaged finger joint angle trajectories for Monkey R in the Object Presence Experiment.** Blue: Power Grasp. Red: Pinch Grasp. Black: Object Reach. Gray: No-Object Reach. CMC: carpometacarpal joint. MCP: metacarpophalangeal joint. PIP: proximal interphalangeal joint. Flex: flexion. Abd: abduction.

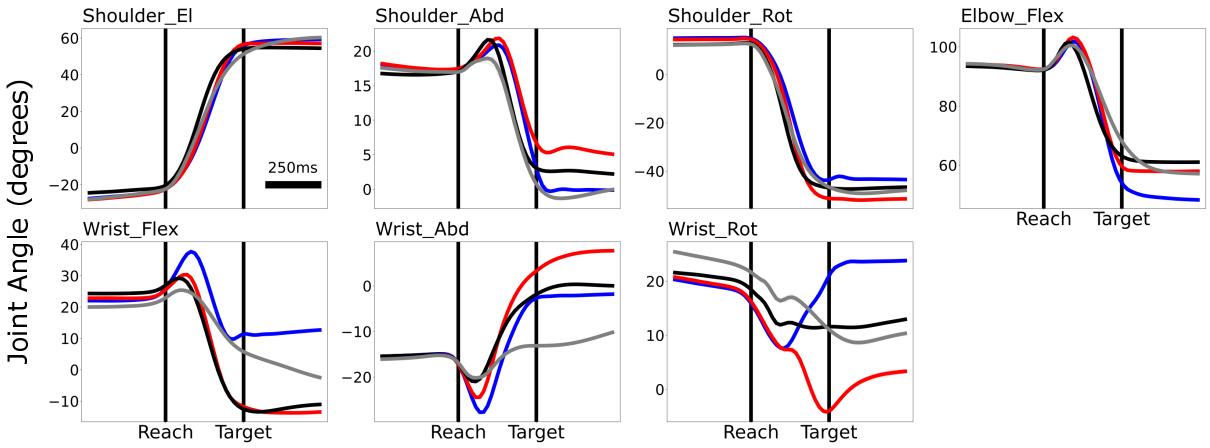

Figure 4.5: **Trial-averaged arm joint angle trajectories for Monkey T in the Object Presence Experiment.** Blue: Power Grasp. Red: Pinch Grasp. Black: Object Reach. Gray: No-Object Reach. El: elevation. Abd: abduction. Rot: rotation. Flex: flexion.

Monkey T exhibited qualitatively similar joint angles to Monkey R with some exceptions. Monkey T displayed a greater range of elbow motion, with flexion followed by extension for all conditions. The wrist remained more extended for Power Grasp and No-Object Reach. During Power Grasps, the thumb exhibited greater MCP flexion, and digits 3 and 4 showed greater PIP flexion. During Pinch Grasps, the thumb was held in a more extended position, and digits 2–5 weref adducted (toward the thumb). The most marked difference was that for the Object Reach condition, Monkey T exhibited PIP flexion in digits 2–5, while keeping those digits extended in the No-Object Reach condition.

Trial-averaged muscle activity recorded from surface EMG electrodes is shown in Figure 4.7 for both subjects. Details of surface EMG data collection are presented in Section A.4.2.

Monkey R displayed an initial burst of activity in the deltoid and biceps coincident with Reach Start for all conditions. Power Grasp trials were associated with high activity across all muscles, especially the deltoid, triceps, and proximal and distal wrist flexors. Pinch Grasps evoked much less activity in the deltoid, triceps and wrist flexors, and greater activity in the wrist extensors, likely to help exert force through the thumb and to stabilize the finger

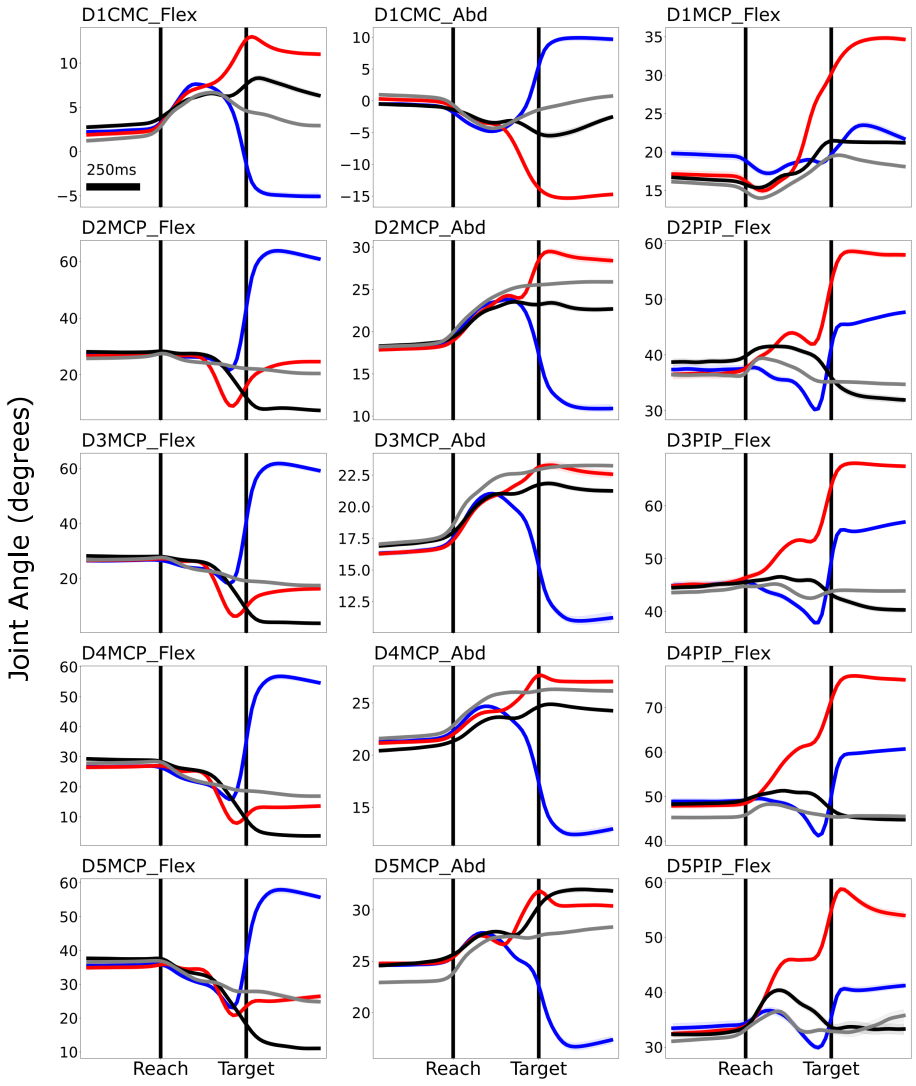

Figure 4.6: **Trial-averaged finger joint angle trajectories for Monkey T in the Object Presence Experiment.** Blue: Power Grasp. Red: Pinch Grasp. Black: Object Reach. Gray: No-Object Reach. CMC: carpometacarpal joint. MCP: metacarpophalangeal joint. PIP: proximal interphalangeal joint. Flex: flexion. Abd: abduction.

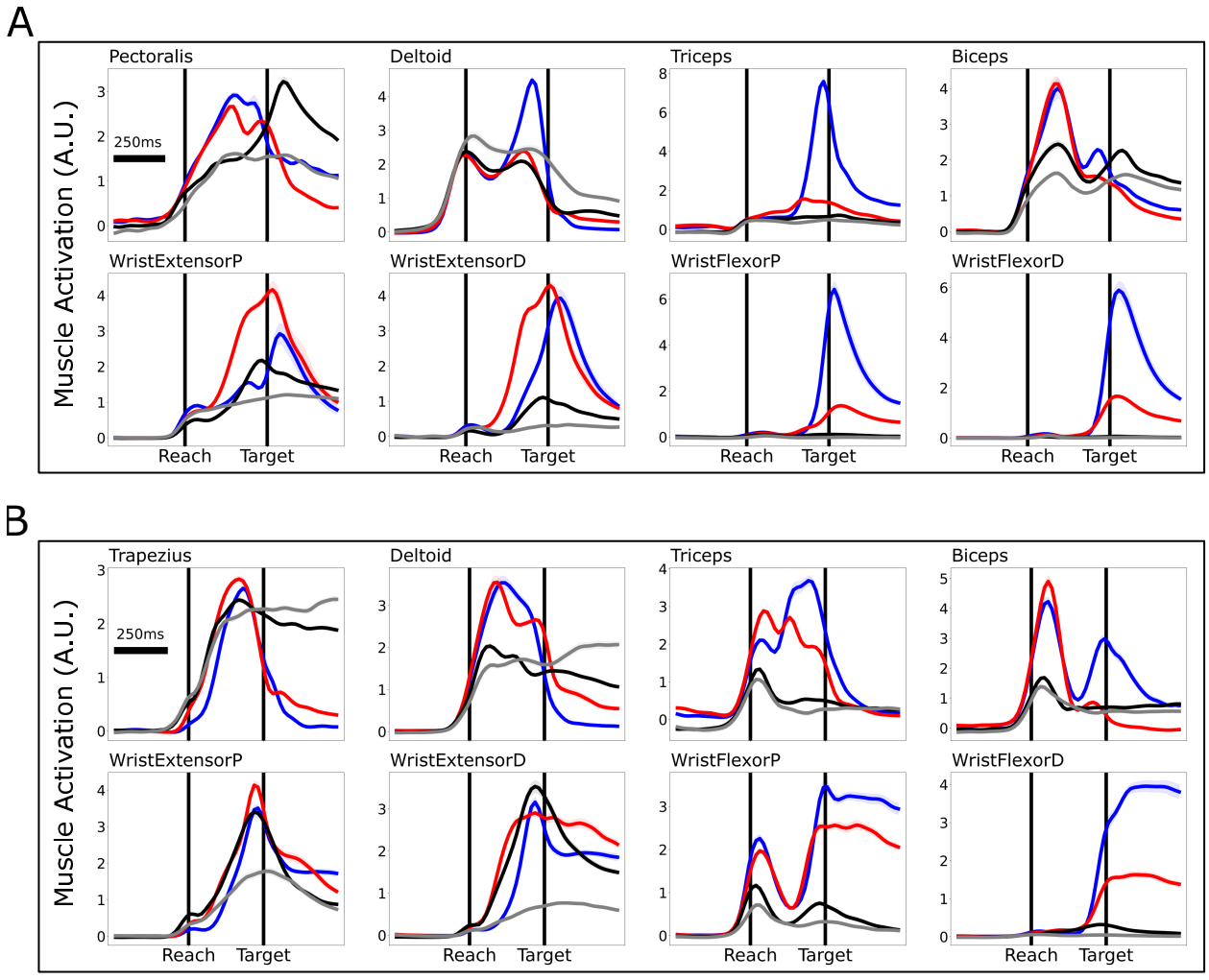

Figure 4.7: **Trial-averaged EMG muscle activations in the Object Presence Experiment.** EMG values are relative to the mean EMG values 400 ms before Reach Start. A: Monkey R. B: Monkey T. Blue: Power Grasp. Red: Pinch Grasp. Black: Object Reach. Gray: No-Object Reach. P: proximal. D: distal.

posture during grasp. Object Reach and No-Object Reach trials evoked comparable shoulder and upper arm muscle activities during the course of the reach, and in general much lower activity in the forearm muscles, with minimal activation of the wrist flexors. Object Reach trials evoked higher activity during the target hold period in the pectoralis, biceps and wrist extensors compared to No-Object Reach, likely reflecting the increased need to brake and stabilize the arm to prevent the hand from touching the object.

Monkey T displayed early activity in trapezius, deltoid, triceps, biceps and proximal wrist flexors and extensors coinciding with Reach Start. In general, Power Grasp activity was more similar to Pinch Grasp activity in Monkey T, with slightly higher Power Grasp evoked activity in the triceps, biceps and proximal and distal wrist flexors, while Pinch Grasp evoked activity was slightly higher in deltoid and proximal and distal wrist flexors. For most muscle groups, Object Reach and No-Object Reach evoked activity was very similar, with the exception of the proximal and distal wrist flexors where activity was much higher for Object Reach trials. This, along with slightly higher proximal wrist flexor activity in Object Reach trials vs. No-Object Reach trials, likely reflected the flexed PIP, extended MCP finger posture observed during Object Reach trials in Monkey T (Figure 4.6).

In summary, the hand was brought to a similar point in space for all conditions. Kinematics and EMG were very consistent across trials within each condition, but differed between conditions. The Power Grasp and Pinch Grasp conditions evoked divergent finger postures and muscle activity. The Object Reach and No-Object Reach behaviors were generally similar to each other, and distinct from the grasping conditions. The next section contains direct comparisons of the behaviors observed during the different conditions.

4.2 Movement Feature Differences Across Conditions

The Object Presence Experiment was designed to elicit similar reaching movements in different object contexts (with or without the object present). However, reaching movements were significantly different depending on whether or not the object was present. The observed variation in MFs across the experimental conditions is characterized in this section.

To measure the differences in MFs between different conditions, the Euclidean distance between each pair of conditions was calculated at each time point in subsets of MFs. The 5 MF subsets considered were the 3D hand position, 3D hand velocity, 22 joint angles, 22 joint angular velocities, and eight EMGs. These distances were calculated only in the peri-movement time window (from 100 ms before Reach Start to 400 ms after Target Contact).

The trial-averaged MF values were calculated by averaging over all trials within each condition at each time point. Within each MF subset, each MF was treated as a separate dimension. Thus, for the 22 joint angles, the trial-averaged values for a single condition at a single time point constituted a 22-dimensional vector. The Euclidean distance between a pair of vectors, corresponding to a pair of conditions, could then be calculated in joint angle space at each time point. For hand position, this distance corresponded to the actual distance between hand positions in 3D space. The inter-condition MF subset distances D_{MFS} were calculated according to Equation 4.1:

$$D_{\mathrm{MFS},i,j,t} = \sqrt{\sum_{p=1}^{N_{\mathrm{MFS}}} \left(\overline{m}_{i,p,t} - \overline{m}_{j,p,t}\right)^2} \tag{4.1}$$

where $D_{\mathrm{MFS},i,j,t}$ is the distance in MF subspace MFS between the values for conditions i and j at time t, N_{MFS} is the number of MFs in subspace MFS, $\overline{m}_{i,p,t}$ is the average value of MF m_p for condition i at time t and $\overline{m}_{j,p,t}$ is the average value of MF m_p for condition j at time t. For the hand positions and hand velocities, $N_{\mathrm{MFS}} = 3$, for the joint angles and joint angular velocities, $N_{\mathrm{MFS}} = 22$, and for the EMGs, $N_{\mathrm{MFS}} = 8$. The resulting inter-condition MF subset distances are plotted in Figures 4.8 and 4.9 for Monkeys R and T, respectively.

For both subjects, all pairs of conditions began close together in MFs before Reach Start, as the subject's hand rested on the start button. Hand positions and joint angles diverged over the course of the reach, and maintained separation during the target hold period. Hand speeds were most divergent during the reach, and decreased around target contact, while joint angular velocities exhibited a sharp peak of divergence around target contact, as the fingers closed differently for different grasps. For Monkey R, inter-condition distances in EMG peaked around target contact and subsequently decreased, while for Monkey T, the EMG distances remained high throughout the target hold period.

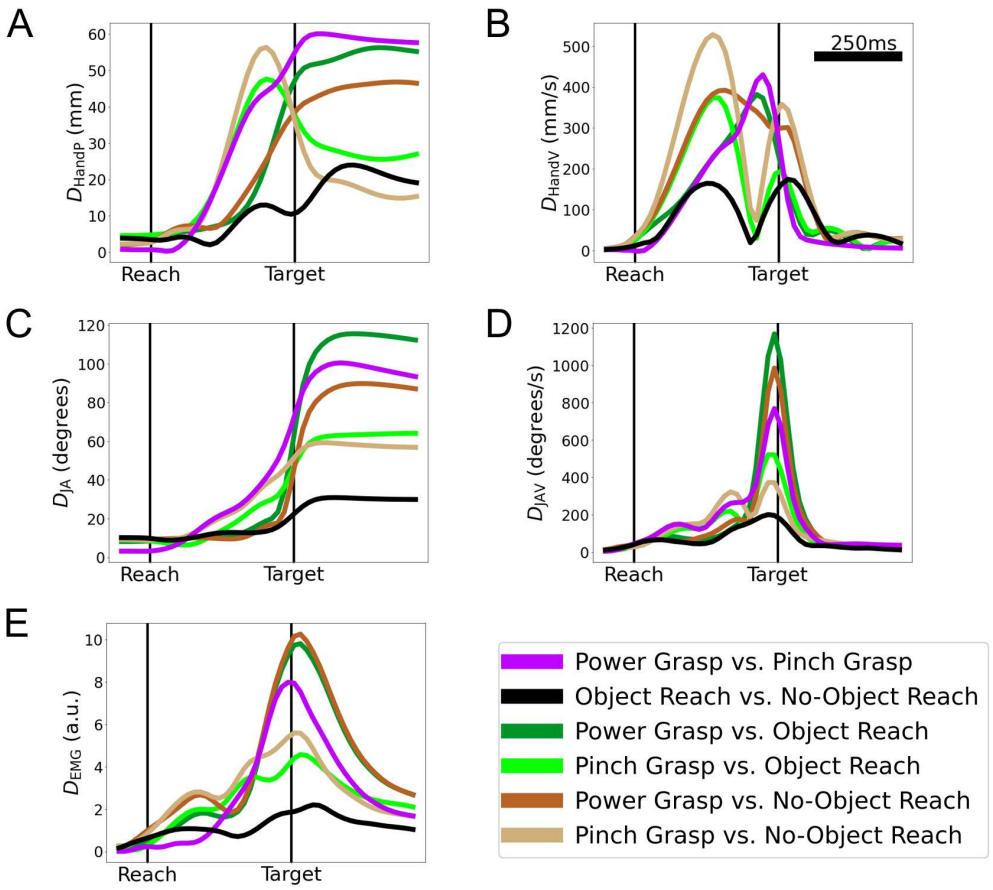

Figure 4.8: **Inter-condition distances in MF subsets for the Object Presence Experiment, Monkey R.** A: distances in hand position. B: distances in hand velocity. C: distances in joint angles. D: distances in joint angular velocities. E: distances in EMGs.

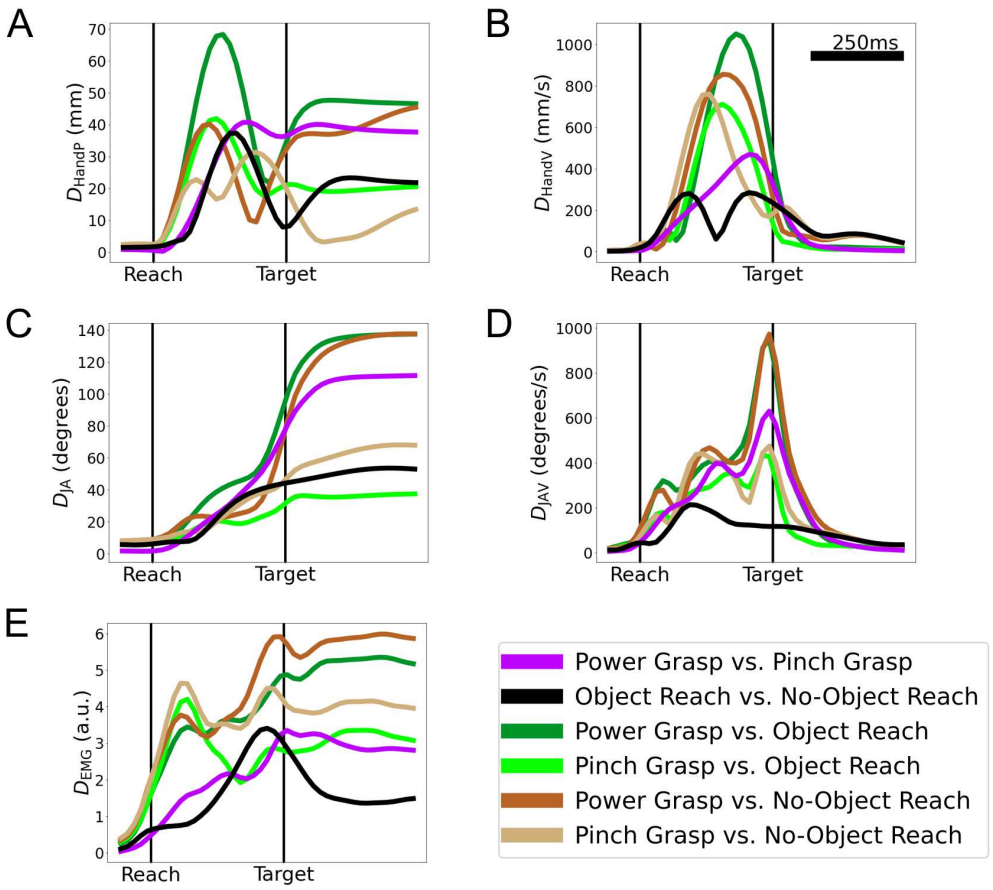

Figure 4.9: **Inter-condition distances in MF subsets for the Object Presence Experiment, Monkey T.** A: distances in hand position. B: distances in hand velocity. C: distances in joint angles. D: distances in joint angular velocities. E: distances in EMGs.

In general, distances between MF values for the Power Grasp and Pinch Grasp conditions were relatively large (Figures 4.8 and 4.9, purple traces) compared to distances between MF values for the Object Reach and No-Object Reach conditions (Figures 4.8 and 4.9, black traces). For instance, for Monkey R, the difference in hand position for Power Grasp and Pinch Grasp conditions peaked at about 60 mm, whereas the difference in hand position for Object Reach and No-Object Reach conditions peaked at about 25 mm.

For Monkey R, the Object Reach and No-Object Reach conditions were the most similar condition pair across all MF subsets, save for the difference in hand positions during the target hold period, for which the Pinch Grasp and No-Object Reach conditions were slightly more similar. In addition, the large peaks in distances between conditions with different hand shapes (Figure 4.8, colored traces) were largely absent for the Object Reach vs. No-Object Reach distances (Figure 4.8, black traces). For Monkey T, the Object Reach vs. No-Object Reach distances were relatively larger. This was attributed to the bent-finger posture used during the Object Reach trials versus the open-hand posture used during the No-Object Reach trials. Despite this, for Monkey T, the Object Reach vs. No-Object Reach distances remained small compared to the Power Grasp vs. Pinch Grasp distances.

In order to characterize inter-condition distances across all of the MFs together, the MFs were combined in a dimensionally-reduced form using Principal Components Analysis (PCA). To this end, the 3D hand positions, 3D hand velocities, 22 joint angles, 22 joint angular velocities, and eight EMGs were combined as a 58-dimensional vector of MFs at each time point. To focus on the differences between conditions, the condition-independent timecourse in each MF was removed (MFs were centered across time) by subtracting the average of each MF across all conditions at each time point in the peri-movement time window. The MFs were then trial-averaged by taking the mean across all trials within each condition. The resulting trial-averaged, centered MFs were then Z-scored by subtracting the mean and dividing by the standard deviation.

PCA was performed on the full matrix of Z-scored trial-averaged centered MFs, and the top PCs explaining 99% of the total variance were extracted. This equated to 16 PCs for Monkey R and 14 PCs for Monkey T, which formed the bases of the MF PC Space. Varimax rotation was then applied to the PCs for increased interpretability (See Section

A.6.1). The resulting varimax-rotated MF PCS (MF VPCs) were sorted by proportion of variance explained. The scores of the first 12 MF VPCs are shown in Figure 4.10 for Monkey R and Figure 4.11 for Monkey T, with scores for each condition plotted separately.

For both subjects, the MF VPCs could be grouped into three broad categories. The first were 'tonic' MF VPCs with strong loadings on hand positions, joint angles and EMGs, in which condition separations began late in the reach and were sustained throughout the target hold period (MF VPCs 1, 5, 7 and 11, Monkey R; MF VPCs 1, 2 and 5, Monkey T). The second were 'phasic' MF VPCs with strong loadings on joint velocities and EMGs, in which condition separations began earlier in the reach period, peaked sharply around the time of target contact and were absent from the target hold period (MF VPCs 2, 3, 6, 9 and 12 Monkey R; MF VPCs 3, 4, 9 and 11 Monkey T). The final group were 'mixed' MF VPCs with loadings on several different MF subsets. The 'mixed' MF VPCs often reflected preshaping and differences in reach speed.

In general, separation between Object Reach and No-Object Reach conditions (Figures 4.10 and 4.11 black and gray traces) was relatively small in the MF VPCs, especially for Monkey R. Though Monkey T displayed moderately more separation between Object Reach and No-Object Reach conditions, this separation was largely constrained to certain MF VPCs (i.e. MF VPCs 2 and 10). The Monkey T MF VPC 2 eigenvector suggests that MF VPC 2 was related to thumb CMC abduction and flexion, digit 2–5 PIP flexion and wrist extensor EMGs, thus capturing the more closed hand posture exhibited during Object Reach trials and Pinch Grasp trials as compared to the open hand posture exhibited during the No-Object Reach trials and Power Grasp trials for Monkey T. Despite this, the separability of Object Reach and No-Object Reach Trials in Monkey T MF VPCs was still generally small compared to the separation between Power Grasp and Pinch Grasp conditions or the separation between Grasp conditions and Reach conditions.

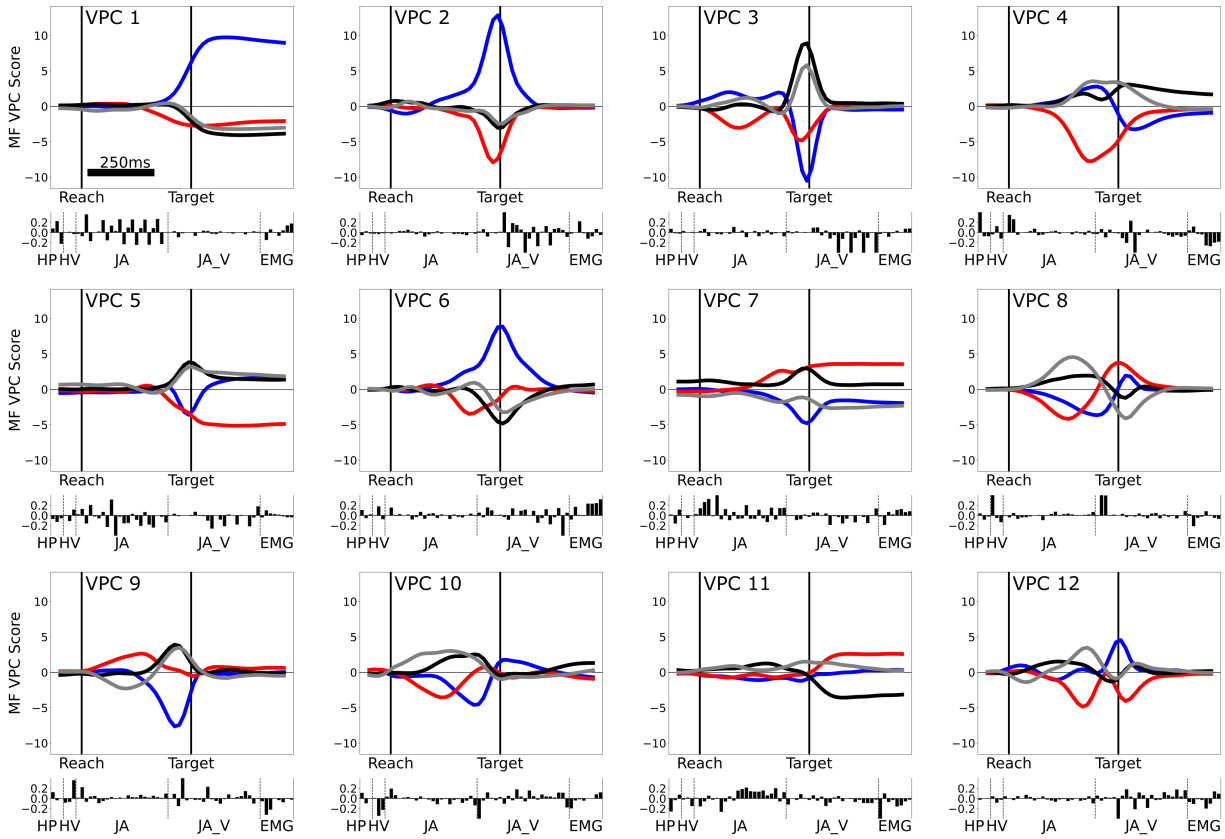

Figure 4.10: **Varimax PCA of the MFs in the Object Presence Experiment, Monkey R.** Trial-averaged scores in the first 12 VPCs. Blue: Power Grasp. Red: Pinch Grasp. Black: Object Reach. Gray: No-Object Reach. Bar graph insets below each VPC score plot denote the loading vector corresponding to the VPC.

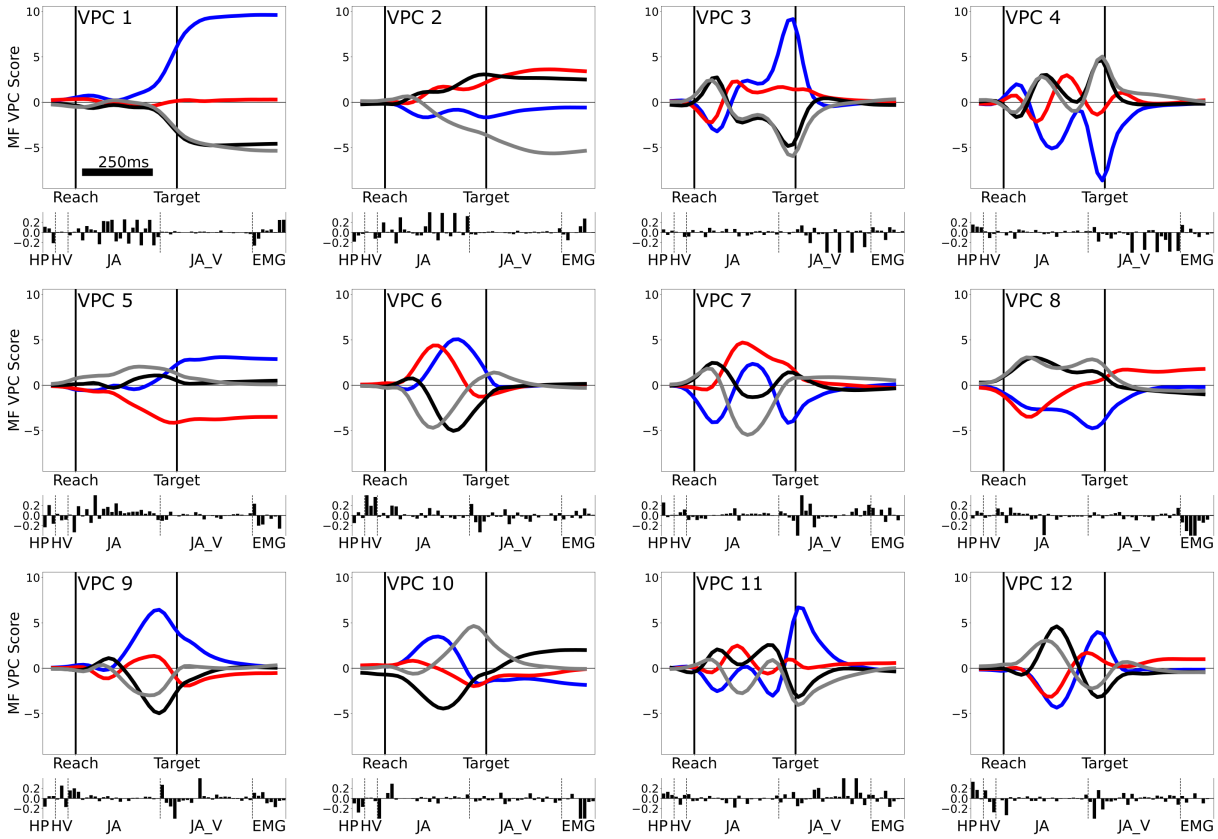

Figure 4.11: **Varimax PCA of the MFs in the Object Presence Experiment, Monkey T.** Trial-averaged scores in the first 12 VPCs. Blue: Power Grasp. Red: Pinch Grasp. Black: Object Reach. Gray: No-Object Reach. Bar graph insets below each VPC score plot denote the loading vector corresponding to the VPC.

To characterize the inter-condition variability across all of the the MF PCs, the Euclidean distance in MF PC space, D_{MFPC}, was calculated for each pair of conditions according to Equation 4.2:

$$D_{\mathrm{MFPC},i,j,t} = \frac{1}{\sqrt{N_{\mathrm{MFPC}}}} \sqrt{\sum_{p=1}^{N_{\mathrm{MFPC}}} \left(\overline{s}_{i,p,t} - \overline{s}_{j,p,t}\right)^2} \tag{4.2}$$

where $D_{\mathrm{MFPC},i,j,t}$ is the Euclidean distance in MF PC space between conditions i and j at time point t, N_{MFPC} is the number of MF PCs, $\overline{s}_{i,p,t}$ is the score of MF PC p for condition i at time point t and $\overline{s}_{j,p,t}$ is the score of MF PC p for condition j at time point t. Values were scaled by $1/\sqrt{N_{\mathrm{MFPC}}}$ to facilitate comparison across subjects. The average MF PC distances $\overline{D}_{\mathrm{MFPC},i,j}$ were also calculated by averaging $D_{\mathrm{MFPC},i,j,t}$ across time in the peri-movement period. The MF PC distances are shown in Figure 4.12.

Before movement, all conditions began close together in MF PC space, reflecting the fact that each trial started with the subject's hand on the start button. The MF PC scores for the different conditions steadily diverged over the course of the reach, reaching peak divergence just before target contact, and decreased to sustained levels during the target hold period. The large peaks in inter-condition distances around target contact corresponded to the large differences in finger joint angular velocities and in EMGs observed in that period. The sustained distances during the target hold period corresponded to the consistent static joint angle and EMG differences.

In general, the largest distances were observed in Power Grasp vs. Object Reach (dark green traces) and Power Grasp vs. No-Object Reach (dark brown traces). The Power Grasp vs. Pinch Grasp distances (purple traces) were also consistently large. Distances corresponding to Pinch Grasp vs. Object Reach (light green traces) and Pinch Grasp vs. No-Object Reach were moderate.

Critically, the distances between Object Reach and No-Object Reach were consistently low compared to distances for other condition pairs. In other words, the Object Reach and No-Object Reach conditions were the most similar condition pair in the MFs. For Monkey R, Object Reach vs. No-Object Reach always evoked the lowest MF PC distance, indicating that the kinematics and EMGs observed in these two conditions were very similar. For

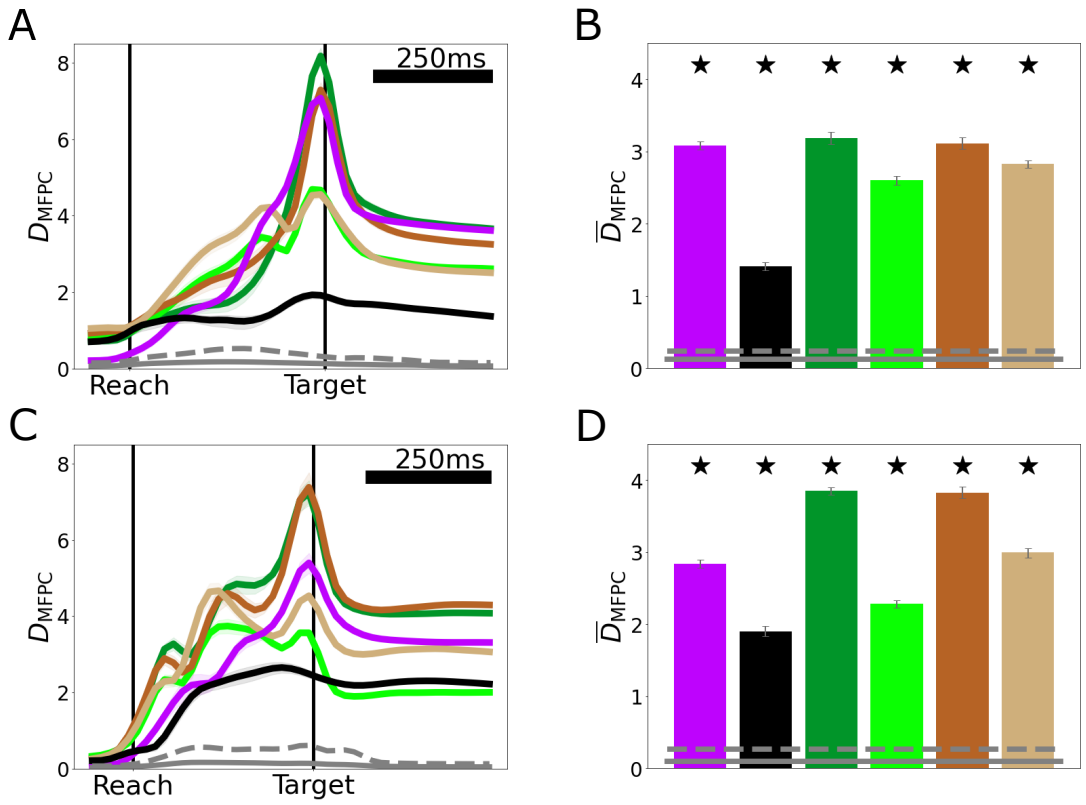

Figure 4.12: **Scaled Euclidean distances D_{MFPC} and $\overline{D}_{\mathrm{MFPC}}$ between pairs of trial-averaged MF PC scores in the Object Presence Experiment.** Distances were calculated in the 99% MF PC space. A, B: Monkey R. C, D: Monkey T. A, C: D_{MFPC}, the distances in MF PC space over time. B, D: $\overline{D}_{\mathrm{MFPC}}$, D_{MFPC} averaged over time. Star: $\overline{D}_{\mathrm{MFPC},i,j}$ significantly greater than within condition $\overline{D}_{\mathrm{MFPC}}$ variability ($p < 0.05$, one-sided bootstrap interval). Purple: Power Grasp vs. Pinch Grasp, Black: Object Reach vs. No-Object Reach, Dark Green: Power Grasp vs. Object Reach, Light Green: Pinch Grasp vs. Object Reach, Dark Brown: Power Grasp vs. No-Object Reach, Light Brown: Pinch Grasp vs. No-Object Reach. Gray: mean and upper 95% one-sided confidence interval of within-condition D_{MFPC} variability. 95% confidence intervals (shaded regions A and C, error bars B and D) are bootstrap intervals, trials resampled 10000 times.

Monkey T, the Pinch Grasp vs. Object Reach distance was similar to the Object Reach vs. No-Object Reach distance, especially during the target hold period, reflecting the fact that Monkey T exhibited a finger posture with bent fingers during the Object Reach trials, whereas the fingers were held straight during the No-Object Reach trials.

To determine if the inter-condition distances in MF PC space were due to the differences in task conditions rather than natural trial-to-trial variability in MFs, within-condition distances were calculated by comparing halves of trials from a single condition (Figure 4.12 gray lines). For all condition pairs, the inter-condition distances were greater than the within-condition distances ($p < 0.05$), suggesting that MF PCs were significantly different for the different task conditions, including the Object Reach vs. No-Object Reach condition pair. Details of the within-condition distance calculations are provided in Section A.6.6.

In summary, the behaviors in terms of kinematics and EMG during the Object Reach and No-Object Reach trials were similar, but significantly different. The behavioral differences in terms of MF PCs between Power Grasp and Pinch Grasp trials were comparatively large (2.18 and 1.49 times as large as Object Reach vs. No-Object Reach distances on average for Monkey R and Monkey T respectively, Figure 4.12 B and D purple vs. black bars).

Power Grasps and Pinch Grasps evoked highly divergent hand postures and muscle activity, whereas the behaviors observed during Object Reach and No-Object Reach trials were very similar (see Figure 4.1). Based on the hypothesis that M1 neural activity is closely and directly related to behavior, the difference in neural activity between Power Grasp and Pinch Grasp trials should likewise be large, whereas the neural activity for Object Reach and No-Object Reach trials should be similar. However such a pattern was not observed; Object Reach and No-Object Reach trials evoked very different patterns of neural activity. This disparity in neural activity differences is described in the following section.

4.3 M1 Neural Activity Differences Across Conditions

This section describes the neural activity in M1 recorded during the Object Presence Experiment, with a focus on the relatively large difference in neural activity observed between Object Reach and No-Object Reach trials, despite the similarity in behavior during these two conditions as described in Section 4.2. The hypothesis that M1 neural activity is closely and directly linked to motor output only would predict that neural activity should generally be similar for Object Reach and No-Object Reach trials. However, in single- and multi-units and on a population level, we observed a substantial difference in activity between the two reach conditions.

After excluding channels with crosstalk and low FR units (see Section A.4.4), a total of 124 and 57 units were analyzed from M1 in Monkey R and Monkey T, respectively. These units consisted of both multi-unit spiking activity and well-isolated single-units.

Spiking units displayed remarkably varied activity patterns. The trial-averaged FRs of four example units are plotted in Figure 4.13.

Panels A and B of Figure 4.13 portray units with activity patterns that adhere to the classical understanding of M1; FRs appear qualitatively similar to EMG (Figure 4.7). Panel C presents a unit which fired much more during grasp trials and Object Reach trials compared to No-Object Reach trials. This unit also exhibited marked preparatory activity, with conditions becoming significantly separable shortly after cue onset (Start) and well before movement onset (Reach). Panel D shows another unit that strongly distinguished between the Object Reach and No-Object Reach conditions around the time of movement onset. This unit displayed a higher FR for No-Object trials. The units in panels C and D displayed another common feature: the FRs associated with all trials in which an object was present were similar and distinct from FRs associated with the No-Object Reach condition.

To assess the overall trends in the population, average normalized (Z-scored) FRs across all units were calculated for each condition at each time point, and plotted in Figure 4.14.

During Power Grasp and Pinch Grasp trials, both subjects showed a general pattern of mild increase in FRs before reach initiation, with a much larger peak just before object

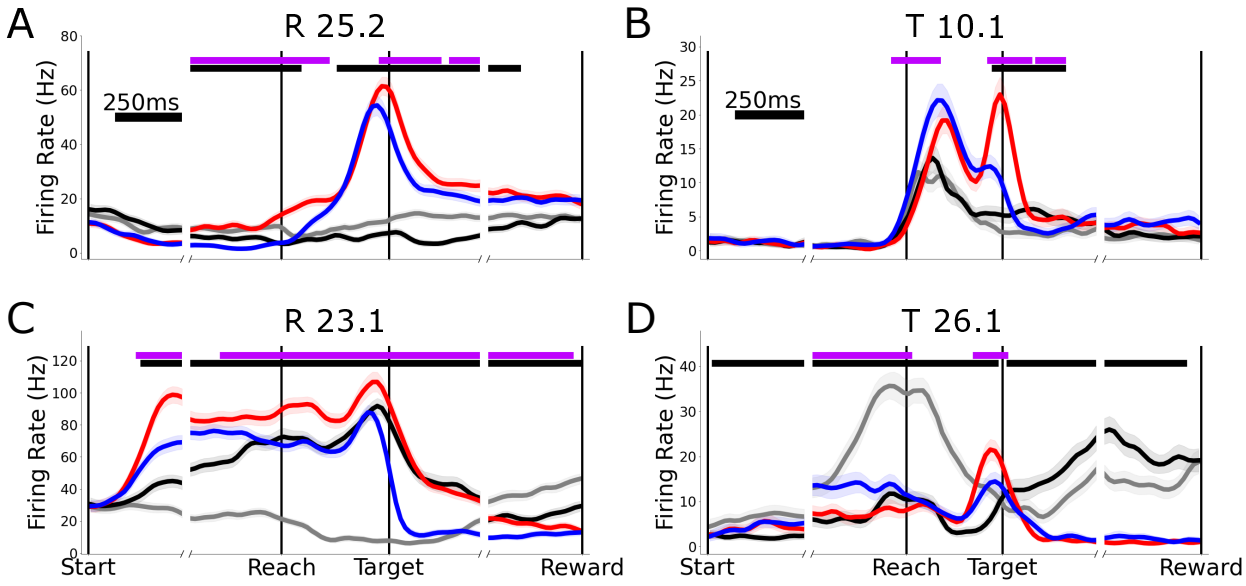

Figure 4.13: **Trial-averaged FRs of four example units during the Object Presence Experiment.** A: Monkey R Unit 25.2. B: Monkey T Unit 10.1. C: Monkey R Unit 23.1. D: Monkey T Unit 92.2. Blue: Power Grasp, Red: Pinch Grasp, Black: Object Reach, Gray: No-Object Reach. Purple horizontal bars: Power Grasp significantly different than Pinch Grasp. Black horizontal bars: Object Reach significantly different than No-Object Reach (permutation test of difference in mean FRs, n=10000, $p < 0.01$)

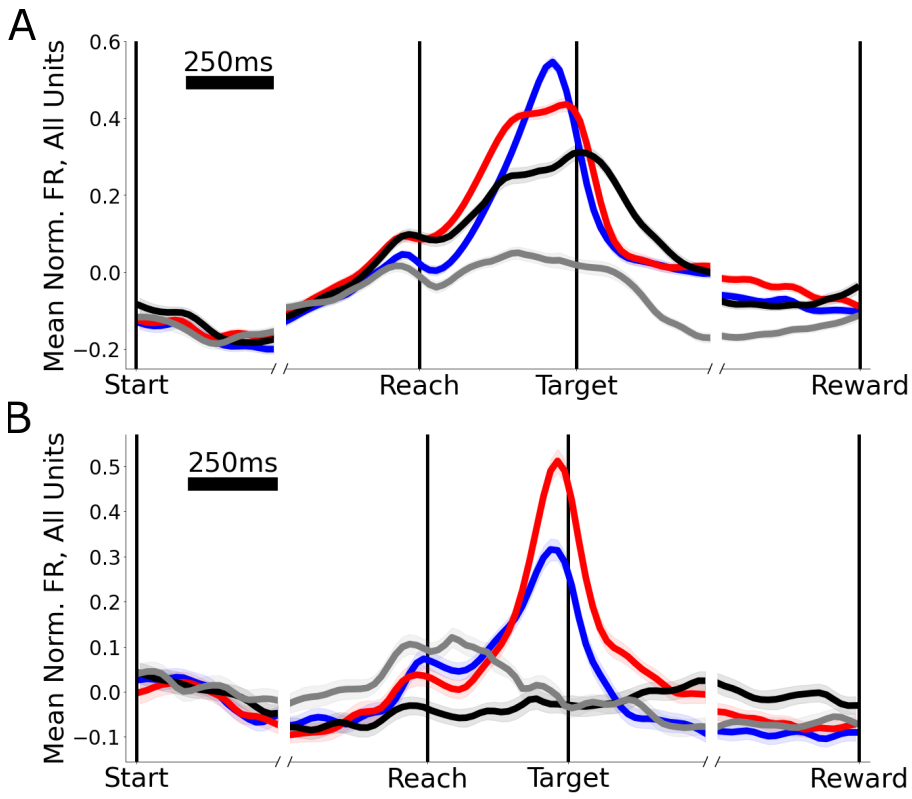

Figure 4.14: **Mean normalized FRs across all neurons for each condition in the Object Presence Experiment.** A: Monkey R. B: Monkey T. Blue: Power Grasp. Red: Pinch Grasp. Black: Object Reach. Gray: No-Object Reach

contact. Monkey R had similar average normalized FRs for Power Grasps and Pinch Grasps, while Monkey T had higher average normalized FRs for Pinch Grasps compared to Power Grasps.

Monkey R displayed higher average normalized FRs for Object Reach trials compared to No-Object Reach trials. This is in line with the findings from Downey et al 2017 [410]; FRs were higher on average for actions performed on an object, compared to similar actions performed with no object present. However Monkey T displayed the opposite effect in that average normalized FRs were somewhat higher before movement and throughout the reach phase for No-Object Reach trials as compared to Object Reach trials. In addition, in Monkey R the Object Reach trials were associated with average normalized FRs that were similar to those attained from Power Grasp and Pinch Grasp trials. In Monkey T, Object Reach trials were associated with generally low average normalized FRs.

The overall averages portrayed in Figure 4.14 present an overly simplified view of M1 spiking activity. Individual unit FR patterns were heterogeneous, and many individual units displayed higher firing rates for reaches than for grasps. Figure 4.15 portrays the percentage of units with preference for each condition, based on which condition evoked the highest mean FR in the peri-movement period.

To determine the prevalence of condition-dependent differences in the FRs of individual units, permutation tests for a difference in mean FRs were performed at each time point between each pair of conditions for each unit ($p < 0.01$, labels shuffled 10000 times). The percentage of neurons displaying significant modulation (significantly different mean FRs) for each pair of conditions is shown in Figure 4.16.

A sizeable proportion (10–40%) of units showed significant modulation during the preparatory period, especially for Monkey R. In both subjects, the number of simultaneously significantly modulated units for all condition pairs steadily increased during the pre-movement period and early reach. For Monkey R, the number of significantly modulated units peaked around early reach and plateaued through target contact, then moderately decreased during the target hold period. For Monkey T, the number of significantly modulated units peaked around the time of target contact and decreased through the target hold period.

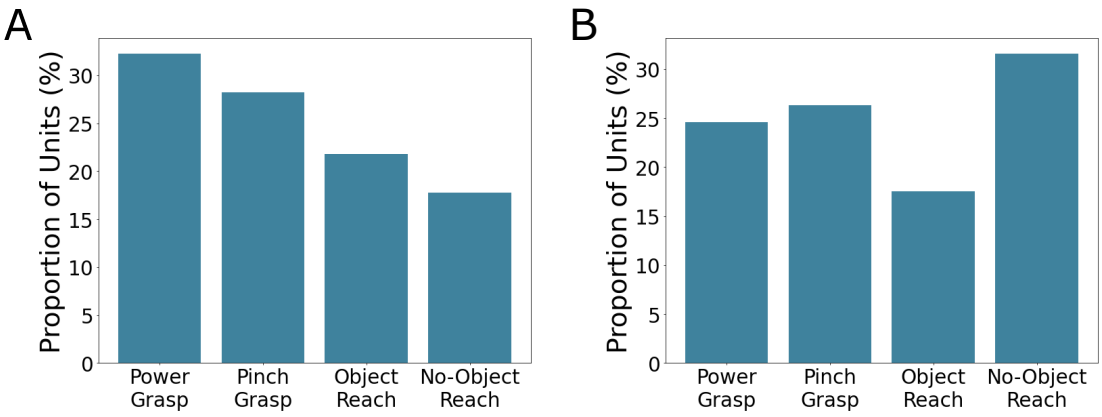

Figure 4.15: **Preferred conditions of individual units.** Bars portray the percentage of units which displayed the highest mean peri-movement FRs for each condition. A: Monkey R. B: Monkey T.

Surprisingly, for both subjects, the number of units that were significantly modulated for Object Reach vs. No-Object Reach (Figure 4.16 A and C black traces) was approximately equal to or greater than the number of units significantly modulated for Power Grasp vs. Pinch Grasp (Figure 4.16 A and C purple traces) at any single time point. To assess the prevalence of sustained modulation, the number of neurons that were significantly modulated for at least 500 ms was calculated (Figure 4.16 B and D). For both subjects, the majority of units (94/124 or 75.8% for Monkey R, 34/57 or 59.7% for Monkey T) showed sustained significant modulation for Object Reach vs. No-Object Reach, and a greater number of units were significantly modulated for Object Reach vs. No-Object Reach than for Power Grasp vs. Pinch Grasp. This was unexpected, given the much larger MF differences observed for Power Grasp vs. Pinch Grasp compared to Object Reach vs. No-Object Reach (Figure 4.12). In addition, the majority of units that showed sustained significant modulation for Object Reach vs. No Object Reach also showed sustained significant modulation for Power Grasp vs. Pinch Grasp, and vice-versa.

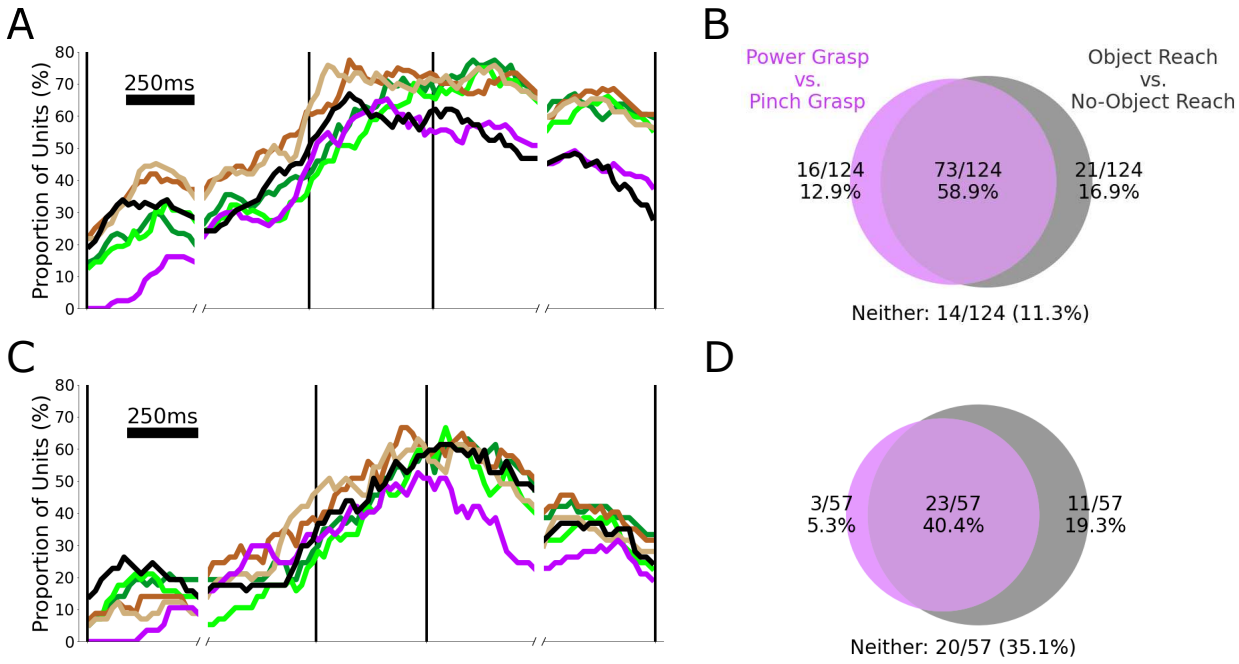

Figure 4.16: **Percentage of units with significantly modulated activity for each pair of conditions in the Object Presence Experiment.** A, B: Monkey R. C, D: Monkey T. A, C: percentage of units with significant modulation for each pair of conditions at each time point ($p < 0.01$, permutation test, 10000 shuffles). Purple: Power Grasp vs. Pinch Grasp, Black: Object Reach vs. No-Object Reach, Dark Green: Power Grasp vs. Object Reach, Light Green: Pinch Grasp vs. Object Reach, Dark Brown: Power Grasp vs. No-Object Reach, Light Brown: Pinch Grasp vs. No-Object Reach. B, D: number of units with ≥ 500 ms of significantly modulated activity for Power Grasp vs. Pinch Grasp (purple) and Object Reach vs. No-Object Reach (black).

To examine the patterns and magnitudes of FR variability of the neural population as a whole, varimax PCA was performed on the FRs. Similarly to the varimax PCA performed for the MFs in Section 4.2, the condition-independent timecourse was subtracted from each unit's FR (FRs were centered across time), and FRs were trial-averaged by calculating the mean FR for all trials in each condition at each time point. The trial-averaged centered FRs were then normalized and the top components explaining at least 99% of neural variance due to conditions were extracted. This resulted in 25 components for Monkey R and 26 components for Monkey T. Varimax rotation was then performed on the PCs to generate the FR VPCs. The scores of the top 16 FR VPCs are plotted in Figure 4.17 for Monkey R and Figure 4.18 for Monkey T, with the scores for each condition plotted separately.

Many of the FR VPCs reflected separation between grasp trials (Power Grasp and Pinch Grasp) and reach trials (Object Reach and No-Object Reach) in general (FR VPCs 1, 2, 8, 11 and 15, Monkey R; FR VPCs 1, 5, 9 and 15, Monkey T). Notably, a large separation between Object Reach and No-Object Reach conditions could be observed throughout many of the FR VPCs (Figures 4.17 and 4.18 black and gray traces), whereas such separation was rare and small in the MF VPCs (Figures 4.10 and 4.11). Additionally, separation between conditions was more prevalent during the pre-movement and early portion of the reaches in FR VPCs compared to MF VPCs, suggesting the presence of preparatory neural activity. Several FR VPCs differed between No-Object Reach trials and all other trials, suggesting the possibility of an object presence related signal (FR VPCs 10 and 12, Monkey R; FR VPCs 8, 10 and 12, Monkey T). Finally, the variations in the FR VPCs were temporally complex.

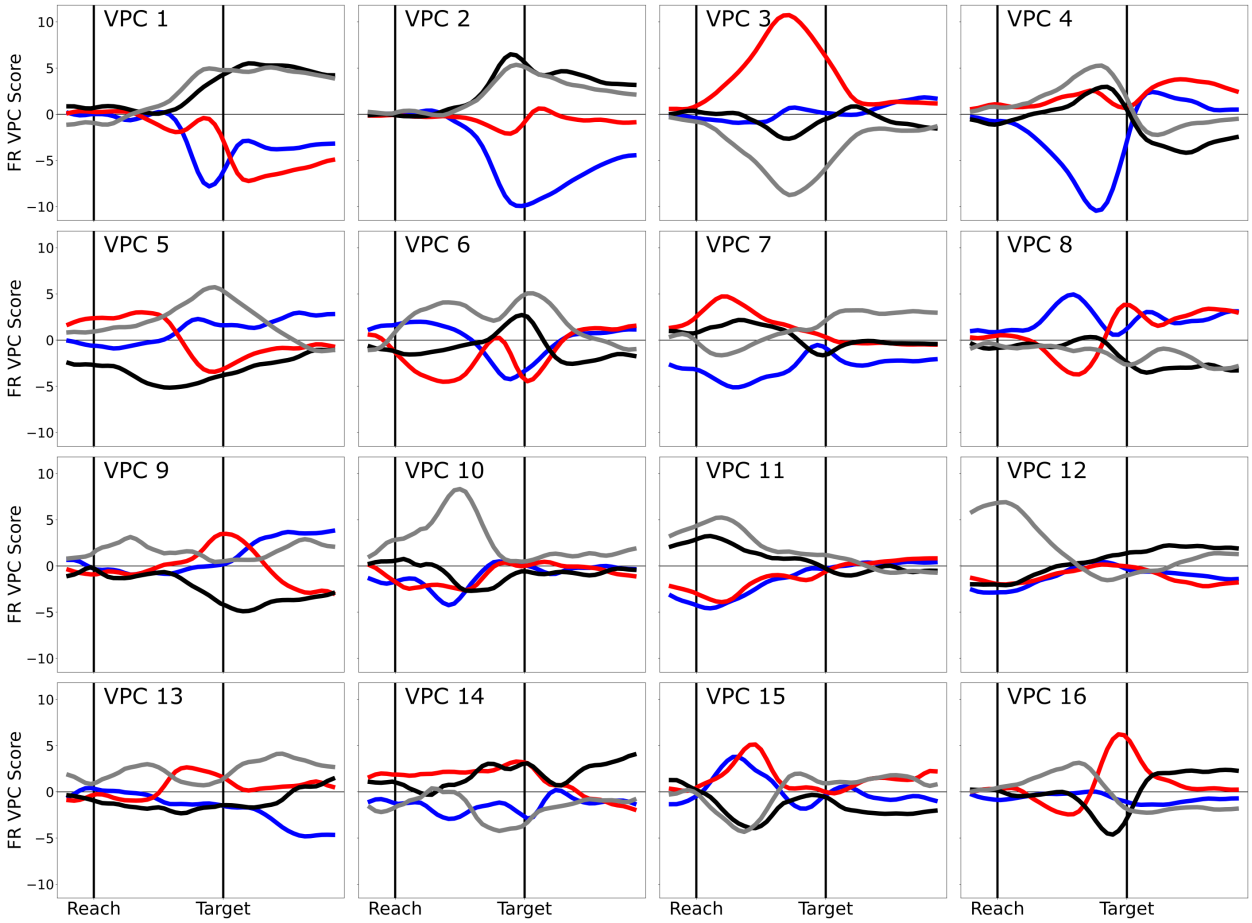

Figure 4.17: **Varimax PCA of the FRs in the Object Presence Experiment, Monkey R.** Scores in the top 16 FR VPCs. Blue: Power Grasp, Red: Pinch Grasp, Black: Object Reach, Gray: No-Object Reach.

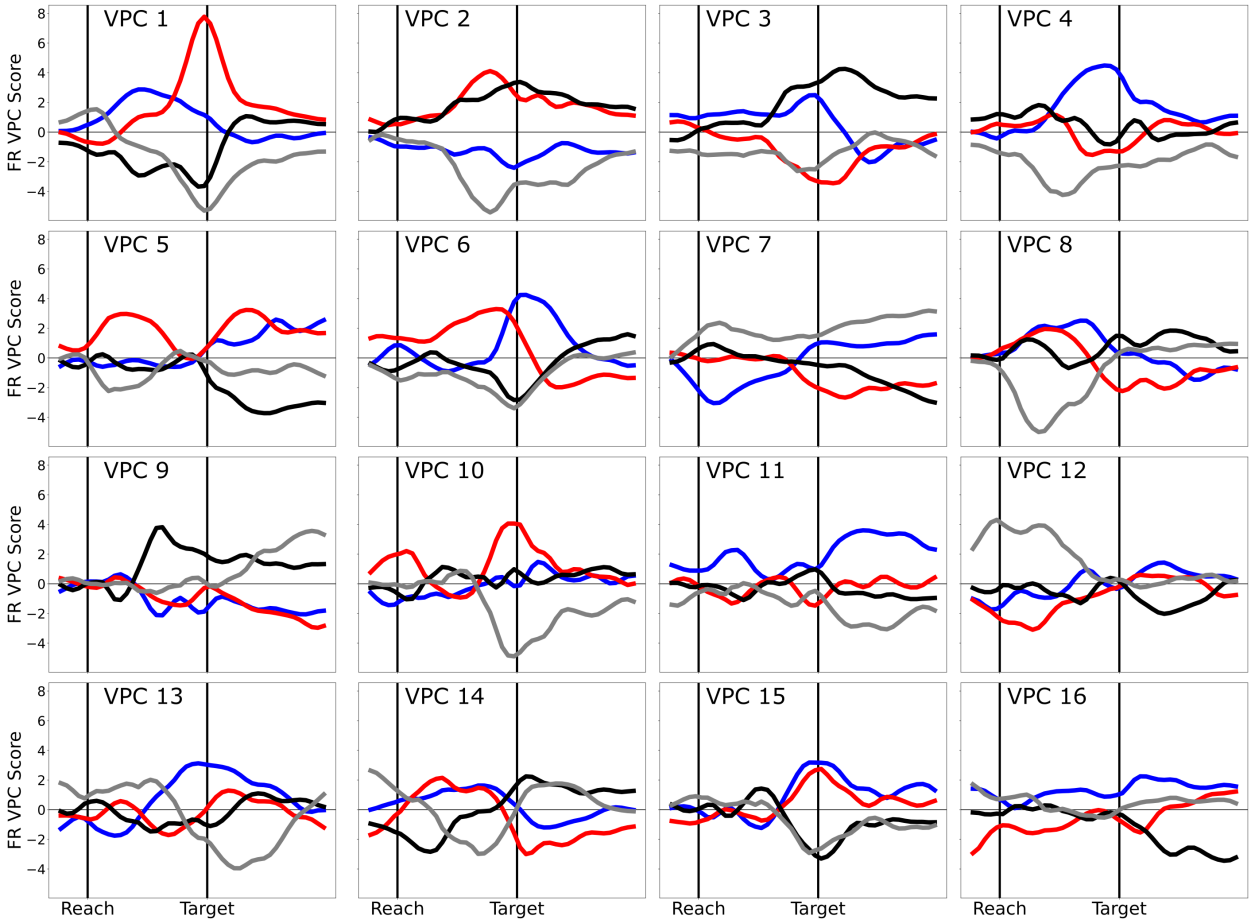

Figure 4.18: **Varimax PCA of the FRs in the Object Presence Experiment, Monkey T.** Scores in the top 16 FR VPCs. Blue: Power Grasp, Red: Pinch Grasp, Black: Object Reach, Gray: No-Object Reach.

The FR VPCs suggest that neural population activity was markedly different in the different task conditions. To visualize the magnitude of inter-condition modulation in the population FRs, the Euclidean distances between each pair of conditions were calculated in neural state space. The distances were first calculated in full FR space, treating the FR of each unit as a separate dimension. The result, the population modulation Δ, was calculated by combining the individual unit modulations, δ according to Equations 4.3 and 4.4.

$$\delta_{i,j,n,t} = |\overline{f}_{i,n,t} - \overline{f}_{j,n,t}| \tag{4.3}$$

$$\Delta_{i,j,t} = \frac{1}{\sqrt{N_{\mathrm{U}}}} \sum_{n=1}^{N_{\mathrm{U}}} \delta_{i,j,n,t}^2 \tag{4.4}$$

where $\delta_{i,j,n,t}$ is the modulation of unit n for conditions i and j at time t, $\overline{f}_{n,i,t}$ is the mean FR for unit n at time t over all trials in condition i, $\overline{f}_{n,j,t}$ is the mean FR for unit n at time t over all trials in condition j, $\Delta_{i,j,t}$ is the population modulation for conditions i and j at time t, and N_{U} is the number of units. The population modulation was scaled by a factor of $(1/\sqrt{N_{\mathrm{U}}})$ to facilitate comparison between subjects. The resulting Δ values are plotted in Figure 4.19.

For both subjects, for all condition pairs, $\Delta_{i,j,t}$ steadily increased during the pre-movement period and throughout the reach, peaking just before target contact, and decreasing thereafter. Power Grasp vs. Pinch Grasp separation (Figure 4.19, purple trace) was not apparent until 200–300 ms after the cue onset, since these conditions were presented in interleaved fashion. By contrast, the other conditions, which were presented in separate blocks, showed some neural separation already at the start of the trials.

For both subjects, $\Delta_{\mathrm{ObjectReach,No-ObjectReach},t}$ was very similar in magnitude to $\Delta_{\mathrm{PowerGrasp,PinchGrasp},t}$, often greater in the case of Monkey T, except for the period around object contact. This contrasted markedly with the pattern observed in the MF PCs, where D_{MFPC} for Object Reach vs. No-Object Reach was much less than D_{MFPC} for Power Grasp vs. Pinch Grasp (Figure 4.12). The size of neural modulation between Object Reach and No-Object Reach trials was surprising, and suggests that neural activity in M1 may relate not only to behavior but also to the contextual factor of object presence.

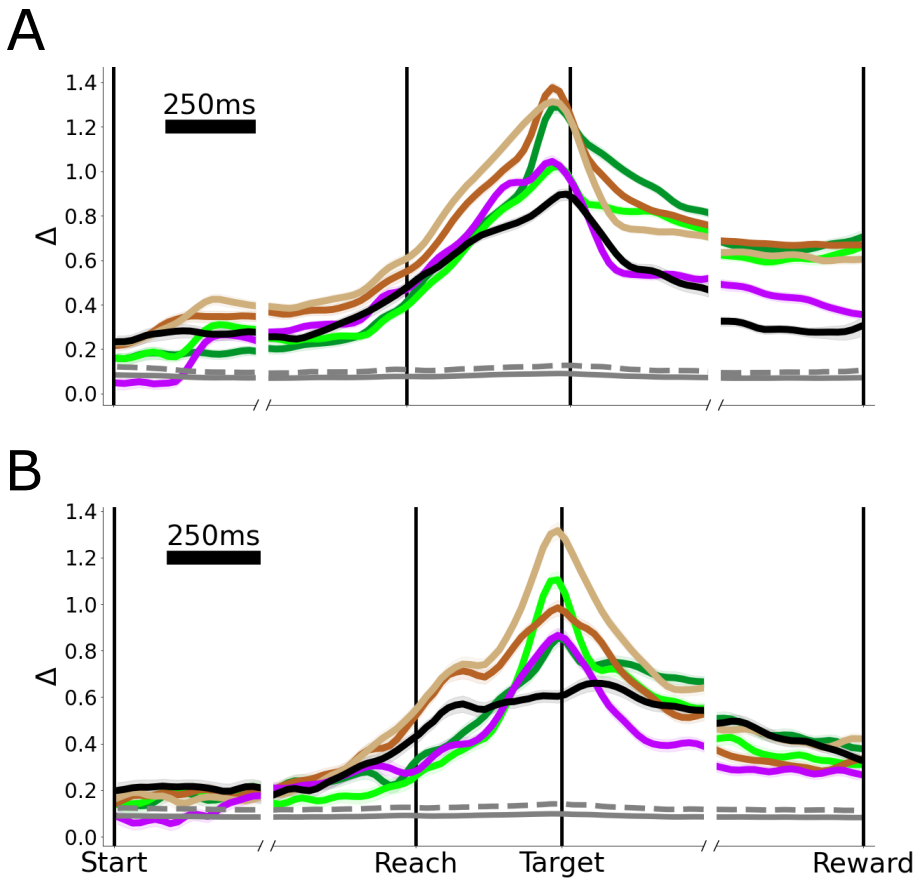

Figure 4.19: **Population modulation Δ for each pair of conditions in the Object Presence Experiment.** A: Monkey R. B: Monkey T. Purple: $\Delta_{\text{PowerGrasp,PinchGrasp},t}$. Black: $\Delta_{\text{ObjectReach,No-ObjectReach}}$. Dark Green: $\Delta_{\text{PowerGrasp,ObjectReach}}$. Light Green: $\Delta_{\text{PinchGrasp,ObjectReach}}$. Dark Brown: $\Delta_{\text{PowerGrasp,No-ObjectReach}}$. Light Brown: $\Delta_{\text{PinchGrasp,No-ObjectReach}}$. Gray: mean and upper 95% one-sided confidence interval of within-condition Δ variability.

For more direct comparison with the inter-condition distances in MF PC space D_{MFPC}, the inter-condition distances were also calculated in FR PC space, according to equation 4.5:

$$D_{\mathrm{FRPC},i,j,t} = \frac{1}{\sqrt{N_{\mathrm{FRPC}}}} \sqrt{\sum_{p=1}^{N_{\mathrm{FRPC}}} \left(\overline{s}_{i,p,t} - \overline{s}_{j,p,t}\right)^2} \tag{4.5}$$

where $D_{\mathrm{FRPC},i,j,t}$ is the Euclidean distance in FR PC space between conditions i and j at time point t, N_{FRPC} is the number of FR PCs, $\overline{s}_{i,p,t}$ is the score of FR PC p for condition i at time point t and $\overline{s}_{j,p,t}$ is the score of FR PC p for condition j at time point t. Values were scaled by $1/\sqrt{N_{\mathrm{FRPC}}}$ to facilitate comparison across subjects. The average FR PC distances $\overline{D}_{\mathrm{FRPC},i,j}$ were also calculated by averaging $D_{\mathrm{FRPC},i,j,t}$ across time in the peri-movement period. The FR PC distances are shown in Figure 4.20.

For all condition pairs, mean inter-condition FR PC distances $\overline{D}_{\mathrm{FRPC}}$ were significantly greater than estimated within-condition $\overline{D}_{\mathrm{FRPC}}$ variability (Figure 4.20 gray lines).

Comparing the inter-condition distances in FR PC space (Figure 4.20) to the inter-condition distances in MF PC space (Figure 4.12) reveals key differences. First, in both FR PC space and MF PC space, inter-condition distances peaked around the time of object contact. However, this peak was much less pronounced for the distances in FR PC space, owing to an earlier, more steady rise in distances and less pronounced drop after target contact. Second, the Object Reach vs. No-Object Reach distances were relatively larger in FR PC space compared to those in MF PC space. In MF PC space, the Object Reach vs. No Object Reach distances were consistently lower than the Power Grasp vs. Pinch Grasp distances, whereas in FR PC space, the Object Reach vs. No Object Reach distances were comparable to the Power Grasp vs. Pinch Grasp distances, or greater in the case of Monkey T (Figures 4.12 and 4.20 black and purple traces). On average, FR PC distances for Power Grasp vs. Pinch Grasp were 1.03 and 0.84 times as large as Object Reach vs. No-Object Reach distances for Monkey R and Monkey T (compared to 2.18 and 1.49 for MF PC distances).

In summary, despite the relative similarity of Object Reach and No-Object Reach conditions in behavior (Figure 4.12 black traces), the majority of units in both subjects displayed significant modulation in FRs between the Object Reach and No-Object Reach

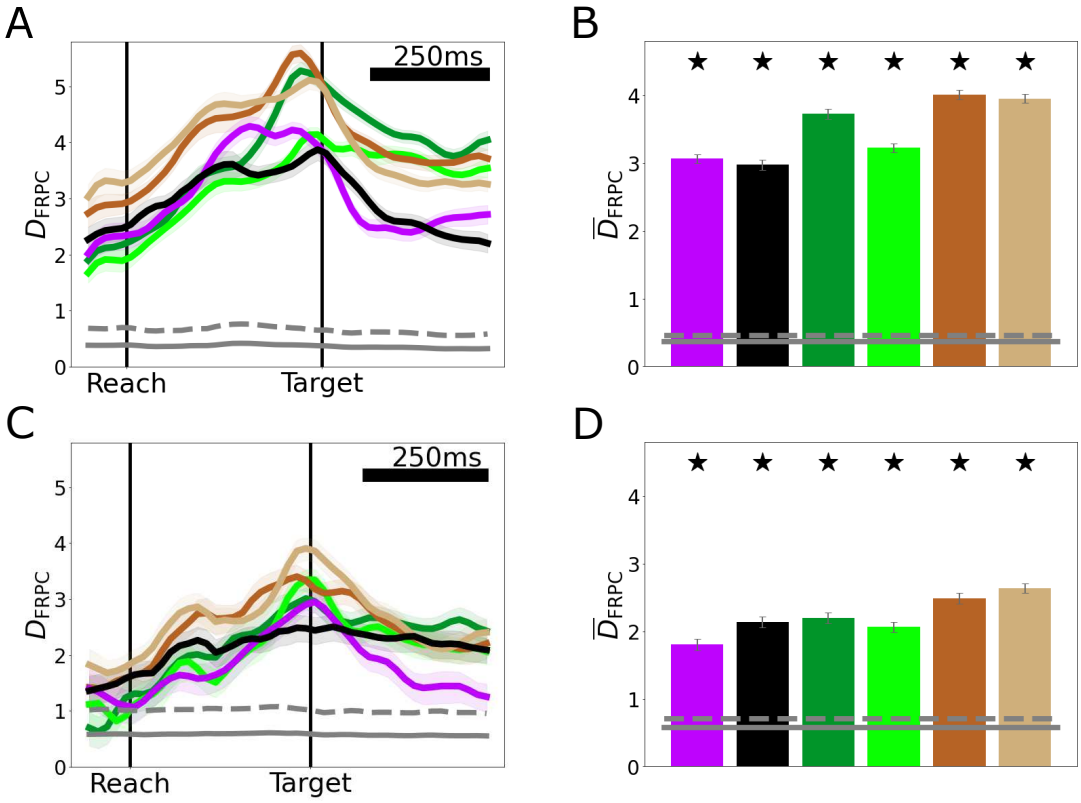

Figure 4.20: **Scaled Euclidean distances D_{FRPC} and $\overline{D}_{\mathrm{FRPC}}$ between pairs of trial-averaged FR PC scores in the Object Presence Experiment.** Distances were calculated in the 99% FR PC Space. A, B Monkey R. C, D Monkey T. A, C D_{FRPC}, the distances in FR PC space over time. B, D $\overline{D}_{\mathrm{FRPC}}$, D_{FRPC} averaged over time. Star: $\overline{D}_{\mathrm{FRPC},i,j}$ significantly greater than within condition $\overline{D}_{\mathrm{FRPC}}$ variability ($p < 0.05$, one-sided bootstrap interval). Purple: Power Grasp vs. Pinch Grasp, Black: Object Reach vs. No-Object Reach, Dark Green: Power Grasp vs. Object Reach, Light Green: Pinch Grasp vs. Object Reach, Dark Brown: Power Grasp vs. No-Object Reach, Light Brown: Pinch Grasp vs. No-Object Reach. Gray: mean and upper 95% one-sided confidence interval of within-condition $\overline{D}_{\mathrm{FRPC}}$ variability. 95% confidence intervals (shaded regions A and C, error bars B and D) are bootstrap intervals, trials resampled 10000 times.

conditions for sustained periods (Figure 4.16 black traces and black circles), and the magnitude of FR modulation for this condition pair across the population was large (Figures 4.19 and 4.20, black traces). A useful point of comparison is the neural difference observed between Power Grasp and Pinch Grasp conditions, which elicited relatively dissimilar behaviors while holding the object context constant. Thus, the Power Grasp vs. Pinch Grasp contrast serves as a benchmark of the neural activity difference that can be expected for largely different behaviors. The number of significantly modulated units and magnitude of population modulation were remarkably as large or larger for the Object Reach vs. No-Object Reach condition pair as for the Power Grasp vs. Pinch Grasp condition pair, despite the similarity of behaviors for Object Reach and No-Object Reach conditions.

The findings in this section suggest the possibility of a contextual signal in M1 related to the presence or absence of the object, which acts to separate the neural representations of the Object Reach and No-Object Reach actions more than would be expected from the differences in MFs associated with the two conditions. The next section will explore the relation between neural activity and MFs, with a focus on the finding that a model assuming linear, fixed tuning of FRs to MFs fails to account for the large neural modulation observed between the Object Reach and No-Object Reach conditions.

4.4 Evidence for Contextual Object Presence Encoding

Historically, M1 neural activity has been thought to be directly related to movement, given the direct axonal projections from M1 to motoneuron pools in the spinal cord [55, 56] and the readiness with which movement can be evoked from electrical stimulation in M1 [34–36] (see Section 2.2). However, many studies have found evidence for contextual changes in M1 neural activity, where different neural activity was observed in M1 in different contexts, even when the movements made in each context were similar (see Section 2.7).

As noted in Sections 4.2 and 4.3, both MFs and FRs were significantly different for Object Reach trials and No-Object Reach trials. However, the differences in FRs were relatively

large compared to the differences in MFs; relative to the Power Grasp vs. Pinch Grasp distances, the average Object Reach vs. No-Object Reach FR PC distances were 2.12 and 1.77 times as large as the corresponding MF PC distances for Monkey R and Monkey T respectively.

This disparity in distances can be visualized using multi-dimensional scaling (MDS), which takes as input a multi-dimensional dissimilarity matrix and plots classes in a 2D plane in a way that attempts to accurately capture the relative distances between classes. MDS was performed separately on the $\overline{D}_{\mathrm{MFPC}}$ values of Figure 4.12 and the $\overline{D}_{\mathrm{FRPC}}$ values of Figure 4.20 to generate the plots shown in Figure 4.21.

The relatively large differences between Object Reach and No-Object Reach neural activity compared to the relatively smaller differences between Object Reach and No-Object Reach MFs (Figure 4.21 black and gray markers) suggest that the neural differences not only correspond to encoding of MF differences, but may also include explicit encoding of the contextual factor of whether or not the object was present.

In this section, evidence is put forth for the existence in M1 of context encoding related to the presence or absence of an object. For the purpose of these analyses, contextual object presence encoding is defined as neural modulation due to the factor of whether or not the object was present, which exceeds the neural modulation that can be explained by linear neural tuning to MFs. Thus, for the Object Presence Experiment, the key condition comparison is between the Object Reach condition and the No-Object Reach condition, as similar movements were made in different contexts (the object was present or absent), but large differences in neural activity were observed. The evidence for object presence encoding is presented first from an encoding perspective (Section 4.4.1), in which individual unit FRs are related to linear combinations of MFs, and then from a decoding perspective (Section 4.4.2), in which MFs are related to linear combinations of FRs.

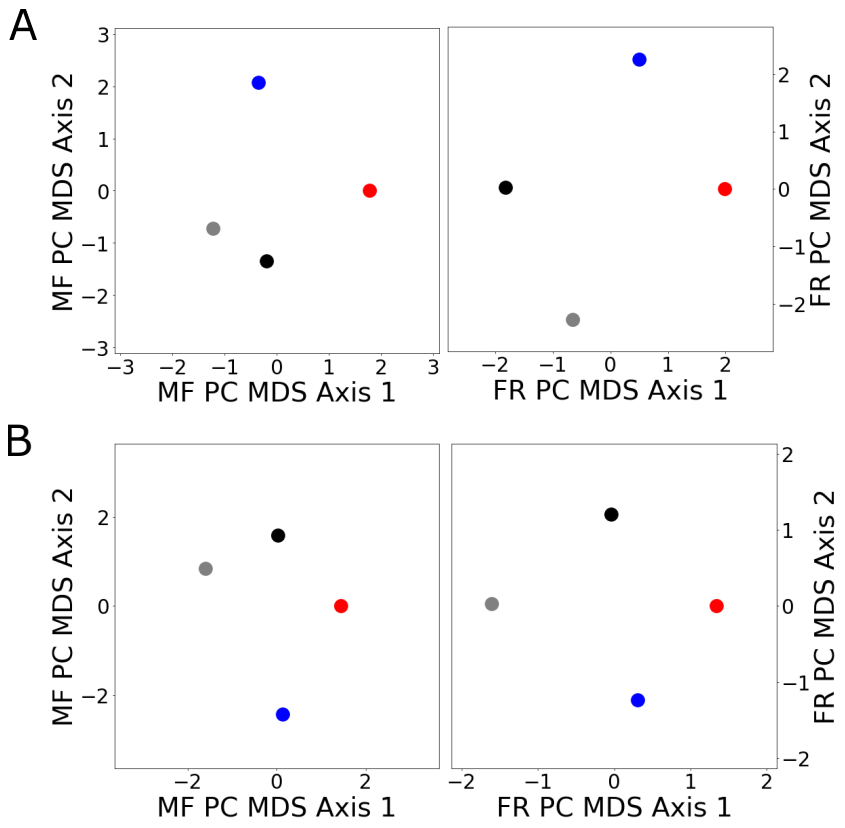

Figure 4.21: **MDS of MF PC and FR PC inter-condition distances in the Object Presence Experiment.** A: Monkey R. B: Monkey T. Left-hand plots: MDS of MF PC distances. Right-hand plots: MDS of FR PC distances. Blue: Power Grasp. Red: Pinch Grasp. Black: Object Reach. Gray: No-Object Reach. Plots were rotated to align Pinch Grasps with the x-axis, and scaled so that the MF PC and FR PC distances between Power Grasp and Pinch Grasp were visually equal.

4.4.1 Encoding Perspective

Given the hypothesis that M1 neural activity is simply and directly related to movements and muscle activity, a common way to model M1 FRs is with a fixed linear tuning model as that shown in Equation 4.6:

$$f_{n,t} = \beta_{0,n} + \sum_{k=1}^{N_{\mathrm{M}}} \beta_{k,n} m_{k,t+\tau} + \epsilon_n \tag{4.6}$$

where $f_{n,t}$ is the FR of unit n at time t, $\beta_{0,n}$ is a constant intercept term, N_{M} is the number of movement features, $\beta_{k,n}$ is a constant weight term, $m_{k,t+\tau}$ is MF k at time $t+\tau$ where τ is a fixed lag, and ϵ_n is an error term.

To evaluate the degree to which such a model applies to the current data, for each neuron, weights β_0 and β_k and noise for each unit were estimated via linear regression, which assumes a Gaussian error distribution, $\epsilon_n \sim \mathcal{N}(0,\, \sigma_n^2)$. The terms m_k were replaced by MF PC scores s calculated by performing PCA on the MFs, and N_{M} was replaced by N_{MFPC}. Unlike in Section 4.2, full normalized MF data were used as inputs to the PCA, without subtracting the condition-independent timecourse or trial-averaging the data. The scores of the top MF PCs that explained 99% of the variance in MFs were used ($N_{\mathrm{MFPC}} = 31$ PCs for Monkey R and $N_{\mathrm{MFPC}} = 24$ PCs for Monkey T). The lag term τ was set to 40 ms (neural activity preceding movements), which was found to be an acceptable value in other studies [63, 87, 104, 163]. Results were qualitatively similar for other reasonable values of τ.

This resulted in the model of Equation 4.7, which was then used for regression:

$$f_{n,t} = \beta_{0,n} + \sum_{p=1}^{N_{\mathrm{MFPC}}} (\beta_{p,n} s_{p,t+40ms}) + \epsilon_n \tag{4.7}$$

where $s_{p,t+\tau}$ is the score of MF PC p at time $t + 40ms$.

The regression was performed on data from the peri-movement period, with t ranging from 100 ms before reach onset to 400 ms after target contact. The resulting R^2 values from the regression analysis are reported in Figure 4.22.

The mean regression R^2 was 0.35 for Monkey R and 0.21 for Monkey T when considering all datapoints (Figure 4.22 A and C). This measure was dominated by trial-to-trial variability,

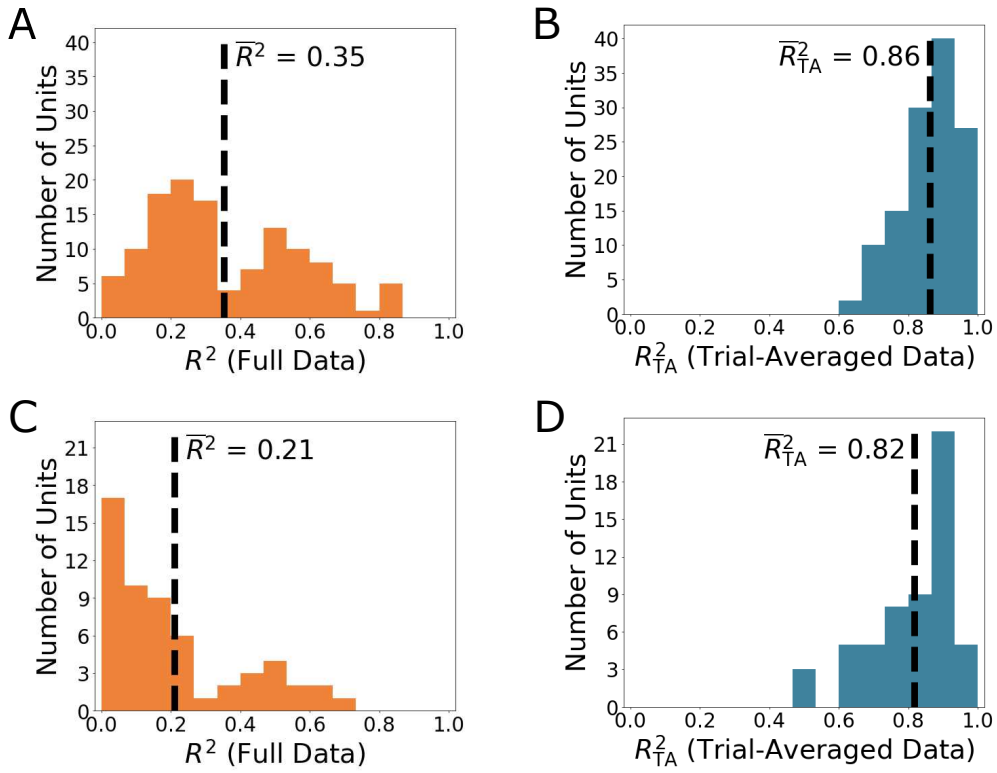

Figure 4.22: **Regression R^2 distributions for the linear tuning of unit FRs to MF PCs in the Object Presence Experiment.** A, B: Monkey R. C, D: Monkey T. A, C Regression R^2 values obtained from the full neural data (including trial-to-trial variability). B, D: R^2_{TA} obtained from trial-averaged neural data and predictions (trial-to-trial variability excluded). Black dashed lines: mean values.

as the trial-averaged R^2 values, R^2_{TA} (Figure 4.22 B and D), which were calculated from the squared correlation of trial-averaged FRs and predicted FRs, were much higher on average. Trial-averaged predicted FRs were calculated via Equation 4.8:

$$\overline{\hat{f}}_{i,n,t} = \hat{\beta}_{0,n} + \sum_{p=1}^{N_{\text{MFPC}}} \hat{\beta}_{p,n} \overline{s}_{i,p,t+40\text{ms}} \tag{4.8}$$

where $\overline{\hat{f}}_{i,n,t}$ is the mean predicted FR of unit n for condition i at time t, $\hat{\beta}$ are the regression weights, N_{MFPC} is the number of MF PC scores, and $\overline{s}_{i,p,t+\tau}$ is the mean score of MF PC p for condition i at time $t + 40$ms. The noise term, $\hat{\epsilon}_n$ was excluded for prediction.

The mean trial-averaged R^2, R^2_{TA} was 0.86 for Monkey R and 0.82 for Monkey T. Thus linear tuning to MF PC scores generally explained a large percentage of FR variance when averaged over conditions, ignoring trial-to-trial variability.

Relatively large neural population modulation was observed in both subjects when comparing FRs for Object Reach trials and No-Object Reach trials (Figure 4.19 black traces and bars) despite the relative similarity of these conditions in MFs. We hypothesize that along with MF encoding, M1 units additionally explicitly encode the context of whether or not the object is present, in that the FR modulations observed between the Object Reach and No-Object Reach conditions are greater than can be accounted for by a linear MF tuning model alone. Such "extralinear modulation" would manifest as systematic structure in the residuals of the FR predictions from linear models of the form described above, in that the predicted FRs would consistently underestimate the actual separation observed between FRs for Object Reach and No-Object Reach trials.

To test the hypothesis of object presence encoding in M1 units, the extralinear modulation (modulation beyond that which can be accounted for by linear movement tuning), ξ, was calculated for each condition pair for each unit. The extralinear modulation was defined as the modulation in FRs δ minus the modulation in predicted FRs $\hat{\delta}$ generated from the linear FR to MF tuning model (Equation 4.8), according to Equations 4.9–4.11. Note that Equation 4.9 is the same as Equation 4.3.

$$\delta_{i,j,n,t} = |\overline{f}_{i,n,t} - \overline{f}_{j,n,t}| \tag{4.9}$$

$$\hat{\delta}_{i,j,n,t} = |\overline{\hat{f}}_{i,n,t} - \overline{\hat{f}}_{j,n,t}| \tag{4.10}$$

$$\xi_{i,j,n,t} = \delta_{i,j,n.t} - \hat{\delta}_{i,j,n,t} \tag{4.11}$$

where $\delta_{i,j,n,t}$ is the FR modulation for unit n for conditions i and j at time t, $\overline{f}_{i,n,t}$ is the mean FR of unit n for condition i at time t, $\overline{f}_{j,n,t}$ is the mean FR of unit n for condition j at time t, $\hat{\delta}_{i,j,n,t}$ is the predicted FR modulation for unit n for conditions i and j at time t, $\overline{\hat{f}}_{i,n,t}$ is the mean predicted FR due to linear tuning to MF PC scores of unit n for condition i at time t, $\overline{\hat{f}}_{j,n,t}$ is the mean predicted FR due to linear tuning to MF PC scores of unit n for condition j at time t, as calculated in Equation 4.8, and $\xi_{i,j,n,t}$ is the extralinear modulation for unit n for conditions i and j at time t. The resulting values were adjusted for bias using bootstrap bias correction (see Section A.6.6). The average extralinear modulation $\overline{\xi}$ for each condition pair was also calculated by averaging each ξ across time in the peri-movement period.

Figure 4.23 portrays a graphical representation of the calculation of ξ as described in Equations 4.9–4.11 for Unit R 23.1 (the same unit as in Figure 4.13 C). Unit R 23.1 had a regression R^2 of 0.58 and R^2_{TA} of 0.93.

Following Equation 4.11, the extralinear modulation ξ was calculated for each pair of conditions for each unit. To achieve a single measure of ξ for each condition pair for each unit, $\overline{\xi}_{i,j,n}$ was calculated by averaging each $\xi_{i,j,n,t}$ in time. The results of these calculations for Unit R 23.1 are shown in Figure 4.24.

As shown in Figure 4.24 B, Unit R 23.1 had relatively high values of extralinear modulation in three condition pairs: $\overline{\xi}_{\text{ObjectReach,No-ObjectReach}}$ (black bar), $\overline{\xi}_{\text{PowerGrasp,No-ObjectReach}}$ (dark brown bar) and $\overline{\xi}_{\text{PinchGrasp,No-ObjectReach}}$ (light brown bar). In other words, Unit 23.1 displayed a difference in FRs between the No-Object Reach condition and the conditions in which an object was present that could not be fully accounted for by linear tuning to MF PCs.

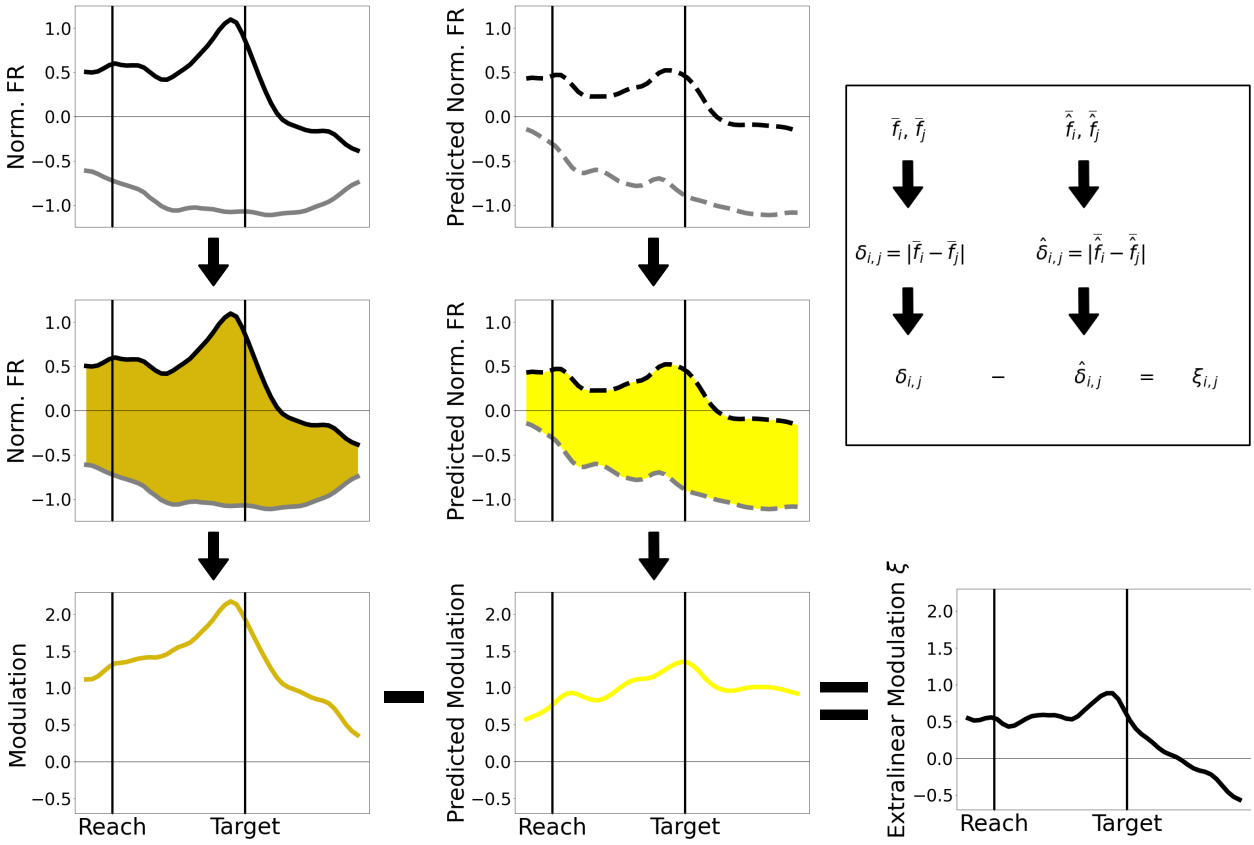

Figure 4.23: **Graphical representation of the calculation of ξ for Unit R 23.1.** The plots represent the calculation of ξ for Unit R 23.1 for the Object Reach (i)) and No-Object Reach (j) conditions. The terms in the inset panel (top right) correspond to the plots. Top left: trial-averaged normalized FRs, $\overline{f}$ for the Object Reach (black) and No-Object Reach (gray) conditions. The Power Grasp and Pinch Grasp conditions were excluded from these plots. Middle left: the absolute difference between the mean normalized FRs for the two conditions. Bottom left: the modulation δ for the two conditions. Middle column: same as the left column, but with $\hat{f}$, the FRs predicted from linear tuning to MF PCs (Equation 4.8). Bottom right: the extralinear modulation $\xi_{\text{ObjectReach,No-ObjectReach}}$.

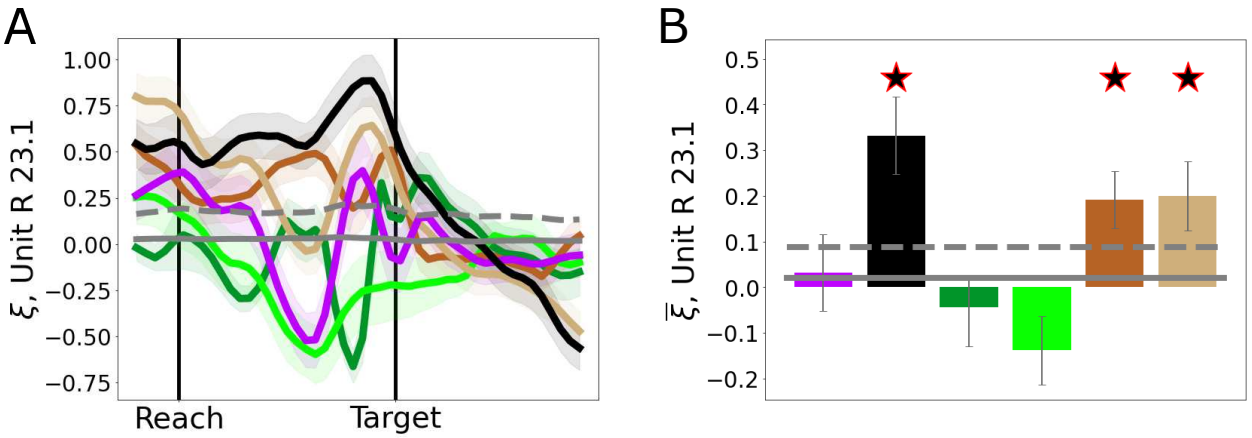

Figure 4.24: ξ **and** $\overline{\xi}$ **for each condition pair for Unit R 23.1** A: ξ, the extralinear modulation for each condition pair over time. B: $\overline{\xi}$, ξ averaged across time. Black and red star: $\overline{\xi}_{i,j}$ significantly greater than within-condition $\overline{\xi}$ variation and $\overline{\xi}_{i,j}$ greater than $\overline{\xi}_{\text{PowerGrasp,PinchGrasp}}$ ($p < 0.05$, one-sided bootstrap interval). Purple: $\xi_{\text{PowerGrasp,PinchGrasp}}$, Black: $\xi_{\text{ObjectReach,No-ObjectReach}}$, Dark Green: $\xi_{\text{PowerGrasp,ObjectReach}}$, Light Green: $\xi_{\text{PinchGrasp,ObjectReach}}$, Dark Brown: $\xi_{\text{PowerGrasp,No-ObjectReach}}$, Light Brown: $\xi_{\text{PinchGrasp,No-ObjectReach}}$. Gray: mean and upper 95% one-sided confidence interval of within-condition variability. 95% confidence intervals (shaded regions, A, error bars B) are bootstrap intervals, trials resampled 10000 times.

To determine if the inter-condition values of $\overline{\xi}$ were due to the differences in task conditions rather than natural trial-to-trial variability, the inter-condition $\overline{\xi}$ values were compared to the within-condition $\overline{\xi}$ values. To do so, a distribution of within-condition $\overline{\xi}$ values was calculated by comparing randomly selected halves of trials from the same condition. For Unit R 23.1, $\overline{\xi}_{\text{ObjectReach,No-ObjectReach}}$, $\overline{\xi}_{\text{PowerGrasp,No-ObjectReach}}$, and $\overline{\xi}_{\text{PinchGrasp,No-ObjectReach}}$ were significantly greater than the within-condition $\overline{\xi}$ values ($p < 0.01$, Figure 4.24 black, dark brown and light brown bars). The other inter-condition $\overline{\xi}$ values were not significantly greater than the within-condition $\overline{\xi}$ values. This implies that Unit R 23.1 encoded the contextual factor of whether or not an object was present, as the FR of Unit R 23.1 was modulated between conditions by an amount exceeding what could be accounted for by linear tuning to MFs, and also exceeding what could be expected from trial-to-trial variability. Thus, Unit R 23.1 was deemed "object presence encoding."

The Power Grasp vs. Pinch Grasp comparison can be taken as the paradigmatic case of conditions in which the object context was the same, but the movement was different. As seen in Figure 4.24 A, $\xi_{\text{PowerGrasp,PinchGrasp}}$ (purple trace) could also exceed 0, especially around the time of movement onset, when neural modulation was present but the MF PC scores were still very similar. Thus, some amount of extralinear modulation may be related to preparatory tuning to movements that occurred later in the trial. As some extralinear modulation could be due only to movement difference, a second criteria was added: a unit was considered "robustly object presence encoding" only if $\overline{\xi}_{\text{ObjectReach,No-ObjectReach}}$ was both significantly greater than within-condition $\overline{\xi}$ variability (see above) *and* significantly greater than $\overline{\xi}_{\text{PowerGrasp,PinchGrasp}}$ at the $p < 0.05$ level (Bootstrap one-sided 95% interval of $[\overline{\xi}_{\text{ObjectReach,No-ObjectReach}} - \overline{\xi}_{\text{PowerGrasp,PinchGrasp}}] > 0$). These criteria are denoted by the significance markers in Figure 4.24 B. This threshold can be considered conservative, as the behavioral differences observed between Power Grasp trials and Pinch Grasp trials were relatively much larger than the behavioral differences observed between Object Reach and No-Object Reach trials. Under these requirements, Unit 23.1 would thus be considered a "robustly object presence encoding" unit.

This analysis was conducted for each unit, and the number of object presence encoding units (units with mean extralinear modulation $\overline{\xi}_{\text{ObjectReach,No}-\text{ObjectReach}}$ significantly greater than $\overline{\xi}_{\text{PowerGrasp,PinchGrasp}}$) was calculated (Table 4.1).

Table 4.1: **Number of object presence encoding units based on magnitude of extralinear modulation.** Unit n is considered significantly object presence encoding if $\overline{\xi}_{\text{ObjectReach,No}-\text{ObjectReach},n}$ is significantly greater than within-condition $\overline{\xi}$ variability. Unit n is considered robustly object presence encoding if $\overline{\xi}_{\text{ObjectReach,No}-\text{ObjectReach},n}$ is also significantly greater than $\overline{\xi}_{\text{PowerGrasp,PinchGrasp},n}$ ($p < 0.05$, one-sided bootstrap interval).

			Significant		**Robust**	
Subject	**Area**	**Total Units**	**Count**	**Percent**	**Count**	**Percent**
Monkey R	M1	124	49	39.5%	36	29.0%
Monkey T	M1 Right	57	14	24.6%	9	15.8%

Object presence encoding was observed in individual units in both subjects, with 39.5% of units in Monkey R and 28.1% of units in Monkey T right hemisphere significantly encoding object presence.

To measure the strength of object presence encoding at the population level, population extralinear modulation ξ^{pop} was calculated according to Equation 4.12:

$$\xi^{\text{pop}}_{i,j,t} = \frac{1}{\sqrt{N_{\text{U}}}} \left(\sqrt{\sum_{n=1}^{N_{\text{U}}} (\delta_{i,j,n,t})^2} \; - \; \sqrt{\sum_{n=1}^{N_{\text{U}}} (\hat{\delta}_{i,j,n,t})^2} \right) \tag{4.12}$$

$\xi^{\text{pop}}_{i,j,t}$ thus corresponds to the separation of the mean normalized FRs for conditions i and j in N_{U}-dimensional neural state space which exceeds the separation of the mean predicted normalized FRs for condition i and j in neural state space. This value was scaled by $(1/\sqrt{N_{\text{U}}})$ to facilitate inter-subject comparisons. The resulting values were adjusted for bias using bootstrap bias correction (see Section A.6.6).

The average population extralinear modulation $\overline{\xi}^{\text{pop}}$for each condition pair was also calculated by averaging each ξ^{pop} over time in the peri-movement period. The population extralinear modulation results are shown in Figure 4.25.

For both subjects, mean population extralinear modulation $\overline{\xi}^{\text{pop}}_{\text{ObjectReach,No-ObjectReach}}$ exceeded both within-trial $\overline{\xi}^{\text{pop}}$ variability and $\overline{\xi}^{\text{pop}}_{\text{PowerGrasp,PinchGrasp}}$ at the $p < 0.05$ level, indicating that in both subjects, significant and robust object presence encoding was present in M1 at the population level. For Monkey R, $\xi^{\text{pop}}_{\text{ObjectReach,No-ObjectReach}}$ was largest during the latter part of the reach through target zone contact, whereas for Monkey T, $\xi^{\text{pop}}_{\text{ObjectReach,No-ObjectReach}}$ was largest early in the reach period.

For both subjects, $\xi^{\text{pop}}_{\text{PowerGrasp,PinchGrasp}}$ was relatively high at the beginning of the reach period, decreasing throughout the reach but with a transient increase around object contact. For Monkey R, $\overline{\xi}^{\text{pop}}_{\text{PowerGrasp,PinchGrasp}}$ also exceeded within-condition $\overline{\xi}$ variability. This was likely due to the presence of both strong movement related activity and preparatory activity in Monkey R.

As further confirmation of object presence encoding, in both subjects, $\overline{\xi}^{\text{pop}}_{\text{PowerGrasp,No-ObjectReach}}$ was greater than $\overline{\xi}^{\text{pop}}_{\text{PowerGrasp,ObjectReach}}$ and $\overline{\xi}^{\text{pop}}_{\text{PinchGrasp,No-ObjectReach}}$ was greater than $\overline{\xi}^{\text{pop}}_{\text{PinchGrasp,ObjectReach}}$. This would be expected given a hypothesis of object presence encoding, since Power Grasp vs. No-Object Reach includes the additional contextual difference of the object being present vs. absent, as opposed to Power Grasp vs. Object Reach, for which the object was always present (likewise for Pinch Grasp vs. No-Object Reach and Pinch Grasp vs. Object Reach). This difference was significant at $p < 0.05$ in all cases except Monkey R $\overline{\xi}^{\text{pop}}_{\text{PowerGrasp,No-ObjectReach}} > \overline{\xi}^{\text{pop}}_{\text{PowerGrasp,ObjectReach}}$, where $p = 0.0546$.

Notably, for both subjects, $\overline{\xi}^{\text{pop}}_{\text{PinchGrasp,ObjectReach}}$ was greater than $\overline{\xi}^{\text{pop}}_{\text{PowerGrasp,PinchGrasp}}$ and for Monkey R, $\overline{\xi}^{\text{pop}}_{\text{PowerGrasp,ObjectReach}}$ was greater than $\overline{\xi}^{\text{pop}}_{\text{PowerGrasp,PinchGrasp}}$. This suggests that whether or not any grasp is executed may be another contextual factor driving extralinear modulation. However, the largest extralinear modulation effect in both subjects was the pure object presence encoding effect, $\overline{\xi}^{\text{pop}}_{\text{ObjectReach,No-ObjectReach}}$, indicating the relative strength of object presence encoding at the population level.

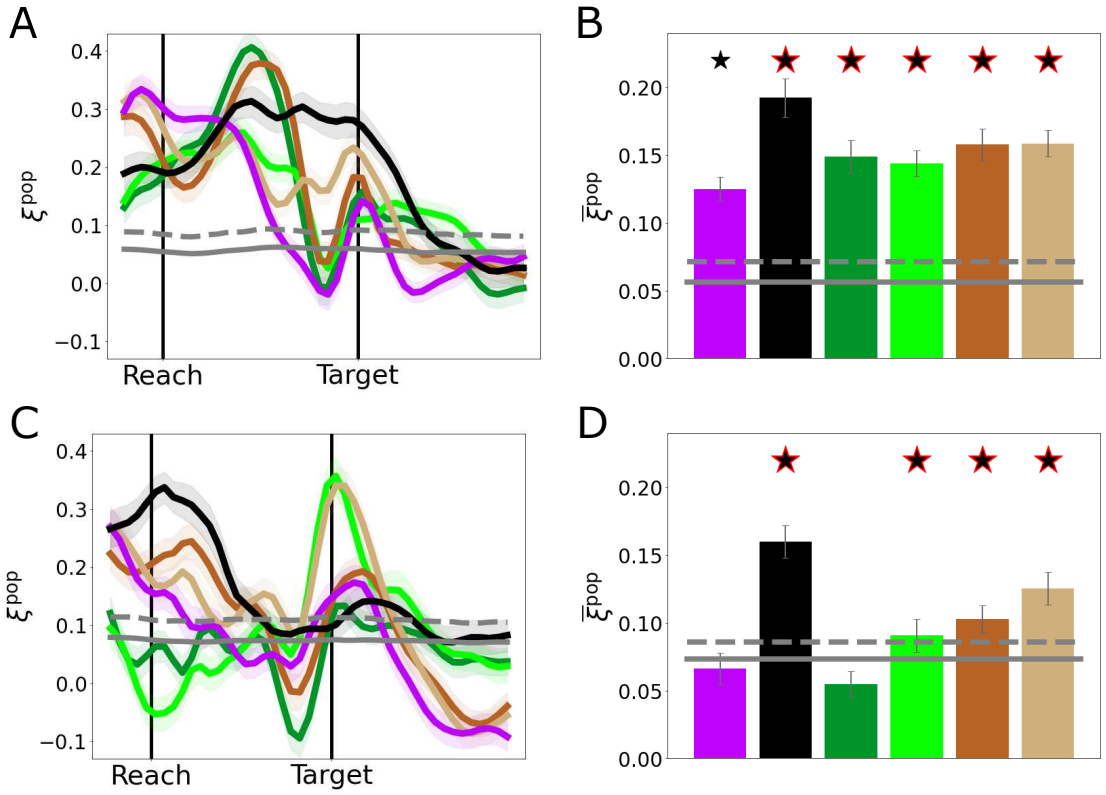

Figure 4.25: **Population extralinear modulation ξ^{pop} and $\overline{\xi}^{\text{pop}}$ for each condition pair in the Object Presence Experiment.** A, B Monkey R. C, D Monkey T. A, C ξ^{pop}, the population extralinear modulation for each condition pair over time. B, D: $\overline{\xi}^{\text{pop}}$; ξ^{pop} averaged across time. Black star: $\overline{\xi}^{\text{pop}}_{i,j}$ significantly greater than within-condition $\overline{\xi}^{\text{pop}}$ variability. Black and red star: $\overline{\xi}^{\text{pop}}_{i,j}$ additionally significantly greater than $\overline{\xi}^{\text{pop}}_{\text{PowerGrasp,PinchGrasp}}$ ($p < 0.05$, one-sided bootstrap interval). Purple: $\xi^{\text{pop}}_{\text{PowerGrasp,PinchGrasp}}$, Black: $\xi^{\text{pop}}_{\text{ObjectReach,No-ObjectReach}}$, Dark Green: $\xi^{\text{pop}}_{\text{PowerGrasp,ObjectReach}}$, Light Green: $\xi^{\text{pop}}_{\text{PinchGrasp,ObjectReach}}$, Dark Brown: $\xi^{\text{pop}}_{\text{PowerGrasp,No-ObjectReach}}$, Light Brown: $\xi^{\text{pop}}_{\text{PinchGrasp,No-ObjectReach}}$. Gray: mean and upper 95% one-sided confidence interval of within-condition variability. 95% confidence intervals (shaded regions, A and C, error bars B and D): bootstrap intervals, trials resampled 10000 times.

These extralinear modulation analyses suggest that, along with MF encoding, the contextual factor of whether or not the object was present was explicitly encoded in M1 neural activity. In the next section, a similar analysis is presented but from a decoding, rather than encoding perspective.

4.4.2 Decoding Perspective

The extralinear modulation analyses approach the question of context encoding from an "encoding" perspective, in that a linear MF PC score encoding model was built for each unit, and the extralinear modulations of individual units were interrogated for evidence of object presence encoding. The problem can also be approached from a "decoding" perspective. Recently, Kaufmann et al (2014) described a "null space" analysis in which neural activity was partitioned into two subspaces: a "potent space" from which muscle activity could be decoded, and an orthogonal "null space" in which activity always yields decoded muscle activity of zero [132]. In that study, the authors showed that preparatory activity in M1 occurred mostly in the null space, allowing for preparatory dynamics which would not result in premature muscle activity. Here, a similar null space analysis is applied to assess whether neural variation related to the context of object presence also occurs in the null space of neural activity. Where Kaufmann et al regressed neural PC scores against muscle activity PC scores to determine if preparatory activity occurred in the null space, here neural PC scores are regressed against PC scores of all MFs including joint angles, joint angular velocities, hand positions, hand velocities and muscle activity. This was done to achieve a more accurate measure of the null space as the dimensions in which neural variability is unrelated to any aspect of behavior.

For the null space analysis, PCA was first performed on both the trial-averaged peri-movement Z-scored FRs and MFs (mFRs and mMFs). The top mMR PCs accounting for 99% of the MF variance were extracted resulting in $N_{\mathrm{mMFPC}} = 15$ for Monkey R and $N_{\mathrm{mMFPC}} = 13$ for Monkey T. The top $2 * N_{\mathrm{mMFPC}}$ mFR PCs were used to reduce the mFRs, resulting in $N_{\mathrm{mFRPC}} = 30$ PCs for Monkey R and $N_{\mathrm{mFRPC}} = 26$ PCs for Monkey T. The number of

mFR PCs was selected to be twice that of the mMF PCs so that the potent and null spaces would have equal dimensionality, facilitating comparisons of the two spaces (see below). The decoding framework is expressed in Equation 4.13:

$$\mathbf{M} = \mathbf{FB} \tag{4.13}$$

where $\mathbf{M}$ is an $[(N_{\text{Samples}} * N_{\text{Conditions}}) \times N_{\text{mMFPC}}]$ matrix of mMF PC scores, $\mathbf{F}$ is an $[(N_{\text{Samples}} * N_{\text{Conditions}}) \times N_{\text{mFRPC}}]$ matrix of mFR PC scores, and $\mathbf{B}$ is an $[N_{\text{mFRPC}} \times N_{\text{mMFPC}}]$ matrix of constant weights. The number of time points in the peri-movement period, N_{Samples} was 48 for Monkey R and 45 for Monkey T (see Section A.4.5). The number of conditions, $N_{\text{Conditions}}$ was 4 for the Object Presence Experiment.

The weight matrix $\mathbf{B}$ was estimated via linear regression, resulting in $\hat{\mathbf{B}}$. This matrix was then decomposed with Singular Value Decomposition to produce $\hat{\mathbf{B}}_{\text{potent}}$ and $\hat{\mathbf{B}}_{\text{null}}$, which are matrices with dimension $[N_{mFRPC} \times N_{mMFPC}]$. The components of neural activity residing in the potent and null spaces, $\hat{\mathbf{F}}_{\text{potent}}$ and $\hat{\mathbf{F}}_{\text{null}}$ can then calculated according to Equations 4.14 and 4.15:

$$\hat{\mathbf{F}}_{\text{potent}} = \mathbf{F}\hat{\mathbf{B}}_{\text{potent}} \tag{4.14}$$

$$\hat{\mathbf{F}}_{\text{null}} = \mathbf{F}\hat{\mathbf{B}}_{\text{null}} \tag{4.15}$$

The resulting $\hat{\mathbf{F}}_{\text{potent}}$ and $\hat{\mathbf{F}}_{\text{null}}$ are both $[(N_{\text{Samples}} * N_{\text{Conditions}}) \times N_{\text{mMFPC}}]$ matrices of neural activity, partitioned into orthogonal subspaces. $\hat{\mathbf{F}}_{\text{potent}}$ describes the neural activity that can be linearly projected through $\hat{\mathbf{B}}$ to decode mMF PC scores, while $\hat{\mathbf{F}}_{\text{null}}$ describes the activity for which projection through $\hat{\mathbf{B}}$ results in a zero matrix (see Section A.6.4 for more details).

Kaufman et al showed that M1 neural variance occurred mostly in the null space during the preparatory period, suggesting a role of this null space activity in setting the initial state of a dynamical system [132]. Here, we propose that the null space activity — the population activity unrelated to MFs — encodes information related to the context of whether or not

an object was present. To approach this question, the variance due to each condition pair $V_{i,j,t}$ was calculated at each time point for the full mFR PC space, the potent space, and the null space, according to Equations 4.16, 4.17 and 4.18:

$$V_{i,j,t}^{\text{full}} = \frac{1}{4} \sum_{x=1}^{N_{\text{mFRPC}}} \left(F_{x,i,t} - F_{x,j,t}\right)^2 \tag{4.16}$$

$$V_{i,j,t}^{\text{potent}} = \frac{1}{4} \sum_{y=1}^{N_{\text{potent}}} \left(F_{y,i,t}^{\text{potent}} - F_{y,j,t}^{\text{potent}}\right)^2 \tag{4.17}$$

$$V_{i,j,t}^{\text{null}} = \frac{1}{4} \sum_{z=1}^{N_{\text{null}}} \left(F_{z,i,t}^{\text{null}} - F_{z,j,t}^{\text{null}}\right)^2 \tag{4.18}$$

where $F_{x,i,t}$ is the value of the mFR PC score x corresponding to condition i at time t, $F_{y,i,t}^{\text{potent}}$ is the value of $\hat{\mathbf{F}}_{\text{potent}}$ in potent dimension y corresponding to condition i at time t and $F_{z,i,t}^{\text{null}}$ is the value of $\hat{\mathbf{F}}_{\text{null}}$ in null dimension z corresponding to condition i at time t.

The total variance across time, $\overline{V}_{i,j}$ for each condition pair was also calculated in each subspace by averaging each $V_{i,j,t}$ across all time points in the peri-movement period. Both V and $\overline{V}$ were adjusted for bias using bootstrap bias correction, trials resampled 10000 times (see Section A.6.6).

The neural variances due to each condition pair in the full mFR PC space, potent space and null space are plotted in Figure 4.26 for Monkey R and Figure 4.27 for Monkey T.

The neural variance in the null space due to condition i and condition j is equivalent to $\frac{1}{4}$ times the squared Euclidean distance between the neural activity for condition i and j in the null space (Equation 4.18). Thus, $V_{i,j,t}^{\text{null}}$ is a similar measure to $\xi_{i,j,t}^{\text{pop}}$ (Equation 4.12) as each characterizes the separation in neural space between conditions i and j that is not accounted for by a linear relationship between neural activity and MF PC scores. The difference is that $V_{i,j,t}^{\text{null}}$ is a population level measure starting from a decoding perspective and is calculated from dimensionally-reduced trial-averaged FRs and MFs, while $\xi_{i,j,t}^{\text{pop}}$ is a population measure constructed from combining individual units FRs individually fit with encoding models using data from all trials.

Concordantly, the results for V^{null} and $\overline{V}^{\text{null}}$ (Figures 4.26 and 4.27, right-hand plots) were qualitatively similar to the results for ξ^{pop} and $\overline{\xi}^{\text{pop}}$ (Figure 4.25). As with $\overline{\xi}^{\text{pop}}$, for

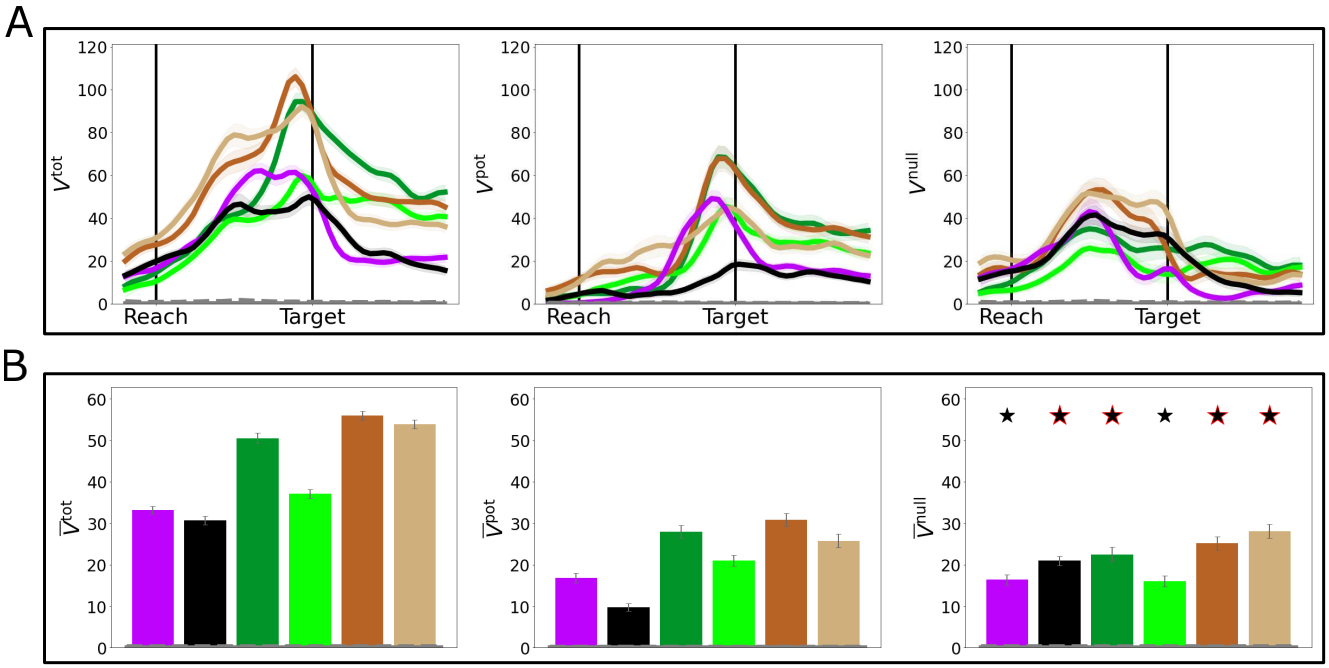

Figure 4.26: **Variances due to each condition pair in the full mFR PC space, potent space and null space for Monkey R.** A, B left column: variances in full mFR PC space; middle column: variances in the potent space; right column: variances in the null space. A: V, the variances for each condition pair over time. B: $\overline{V}$; V averaged across time. Black star: $\overline{V}^{\text{null}}_{i,j}$ significantly greater than within-condition $\overline{V}^{\text{null}}$ variability. Black and red star: $\overline{V}^{\text{null}}_{i,j}$ additionally significantly greater than $\overline{V}^{\text{null}}_{\text{PowerGrasp,PinchGrasp}}$ ($p < 0.05$, one-sided bootstrap interval). Purple: $V_{\text{PowerGrasp,PinchGrasp}}$, Black: $V_{\text{ObjectReach,No-ObjectReach}}$, Dark Green: $V_{\text{PowerGrasp,ObjectReach}}$, Light Green: $V_{\text{PinchGrasp,ObjectReach}}$, Dark Brown: $V_{\text{PowerGrasp,No-ObjectReach}}$, Light Brown: $V_{\text{PinchGrasp,No-ObjectReach}}$. Gray: mean and upper 95% one-sided confidence interval of within-condition variability. 95% confidence intervals (shaded regions, A and C, error bars B and D) are bootstrap intervals, trials resampled 10000 times.

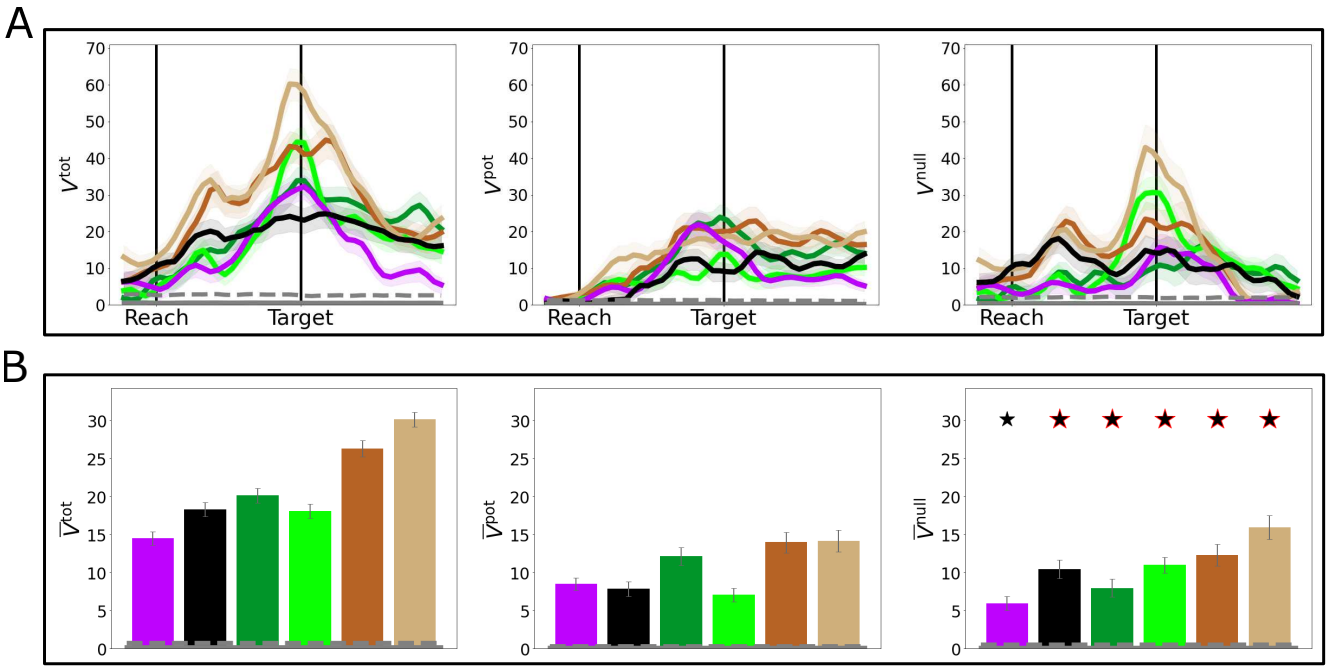

Figure 4.27: **Variances due to each condition pair in the full mFR PC space, potent space and null space for Monkey T.** Same as Figure 4.26, but for Monkey T.

both subjects, $\overline{V}^{\text{null}}_{\text{ObjectReach,No-ObjectReach}}$ was significantly greater than within-condition $\overline{V}^{\text{null}}$ variation *and* significantly greater than $\overline{V}^{\text{null}}_{\text{PowerGrasp,PinchGrasp}}$ at the $p < 0.05$ level (one-sided bootstrap interval, trials resampled 10000 times). As further confirmation of an object presence encoding effect, for both subjects, $\overline{V}^{\text{null}}_{\text{PowerGrasp,No-ObjectReach}}$ was greater than $\overline{V}^{\text{null}}_{\text{PowerGrasp,ObjectReach}}$ and $\overline{V}^{\text{null}}_{\text{PinchGrasp,No-ObjectReach}}$ was greater than $\overline{V}^{\text{null}}_{\text{PinchGrasp,ObjectReach}}$ at the $p < 0.05$ level. Taken together, these results further imply that M1 encoded object presence at the population level in both subjects. That is, both subjects displayed significantly large neural separation between conditions where the object was present and conditions where the object was absent which could not be accounted for by a linear relationship between neural activity and MFs.

Due to the orthogonality of the potent and null spaces, the full variance in mFR PC space is equal to the sum of the variances in the potent and null spaces (Equation 4.19):

$$V^{\text{full}} = V^{\text{potent}} + V^{\text{null}} \tag{4.19}$$

Thus, the proportion of full variance which occurred in the null space $\pi_{i,j,t}$ can calculated for each condition pair at each time point according to Equation 4.20:

$$\pi_{i,j,t} = \frac{V^{\text{null}}_{i,j,t}}{V^{\text{full}}_{i,j,t}} \tag{4.20}$$

The numerator is the variance due to condition pair i, j at time t in the null space, and the denominator is the variance due to condition pair i, j at time t in the full mFR PC space.

In addition, the proportion of total variance which occurred in the null space $\Pi_{i,j}$ for each condition pair was calculated according to Equation 4.21:

$$\Pi_{i,j} = \frac{\overline{V}^{\text{null}}_{i,j,t}}{\overline{V}^{\text{full}}_{i,j,t}} \tag{4.21}$$

The numerator is the total variance due to condition pair i, j in the null space, and the denominator is the total variance due to condition pair i, j in the full mFR PC space.

The proportion of variance in the null space over time π and the proportion of total variance in the null space Π are plotted in Figure 4.28.

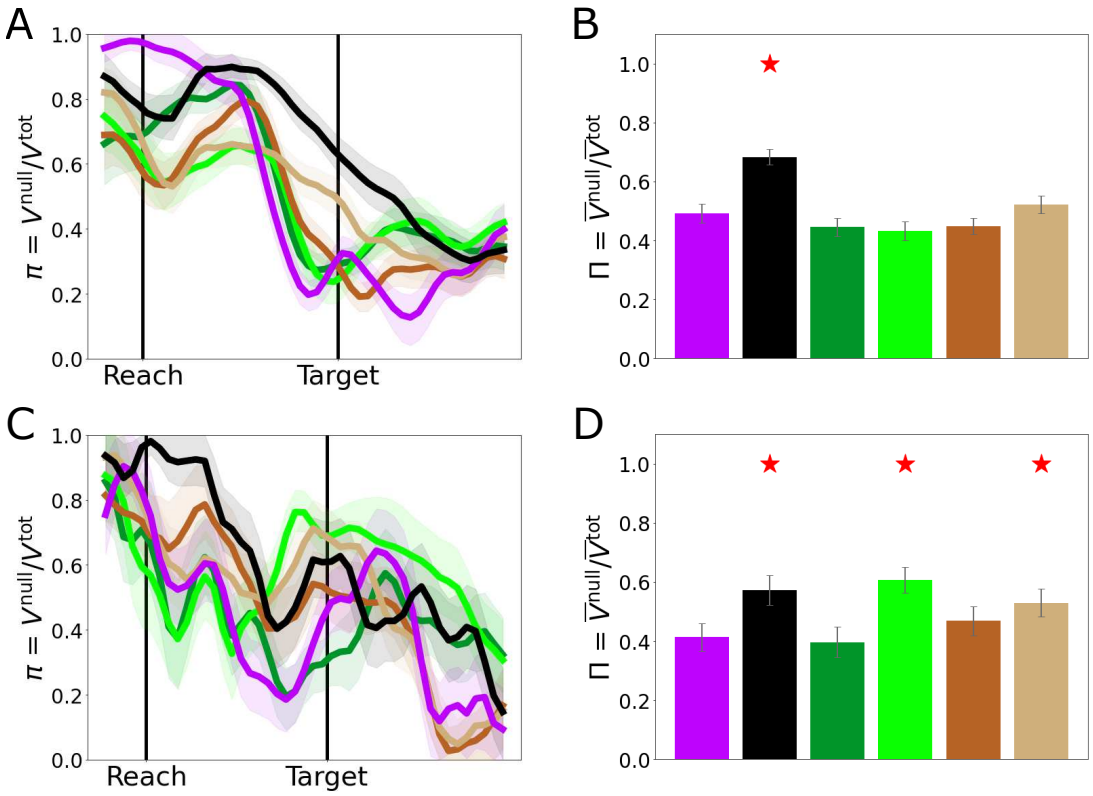

Figure 4.28: **Proportion of total variance for each condition pair which occurred in the null space π and Π.** A, B Monkey R. B, C: Monkey T. A: π, the proportion of variance in the null space for each condition pair over time. B: Π; The proportion of total variance across time in the null space for each condition pair. Red star: $\Pi_{i,j}$ significantly greater than $\Pi_{\text{PowerGrasp,PinchGrasp}}$ ($p < 0.05$, one-sided bootstrap interval). Purple: $\pi_{\text{PowerGrasp,PinchGrasp}}$, Black: $\pi_{\text{ObjectReach,No-ObjectReach}}$, Dark Green: $\pi_{\text{PowerGrasp,ObjectReach}}$, Light Green: $\pi_{\text{PinchGrasp,ObjectReach}}$, Dark Brown: $\pi_{\text{PowerGrasp,No-ObjectReach}}$, Light Brown: $\pi_{\text{PinchGrasp,No-ObjectReach}}$. Gray: mean and upper 95% one-sided confidence interval of within-condition variability. 95% confidence intervals (shaded regions, A and C, error bars B and D) are bootstrap intervals, trials resampled 10000 times.

Before reach onset, variance for all conditions occurred mostly in the null space, and some null space variance persisted throughout the trials, confirming the findings of Kaufman et al [132]. Notably, for both subjects, the majority of the neural variance due to the Object Reach vs. No-Object Reach condition pair occurred in the null space (black bars, Figure 4.28 B and D), whereas the majority of neural variance due to the Power Grasp vs. Pinch Grasp condition pair occurred in the potent space (purple bars, Figure 4.28 B and D).

Taken together, the results of the extralinear modulation analyses and the null space analyses suggest that both subjects encoded object presence in M1. That is, for both subjects, the contextual factor of object presence or absence evoked significantly large neural modulations which could not be accounted for by a linear relationship between neural activity and MFs. The extralinear modulation analysis revealed object presence encoding in many individual units and at the population level starting from an individual unit MF encoding model framework. The null space analysis revealed object presence encoding at the population level starting from a population MF decoding framework. The following section will explore the properties of the object presence encoding signal in M1 as it relates to MF encoding.

4.5 Interaction of Object Presence and MF Encoding

In Section 4.4, object presence encoding in M1 individual units and populations was discussed in terms of the instantaneous and time-averaged differences in FRs that exceeded linear tuning to MFs. In this section, the relation between FRs and MFs is explored in more detail. Specifically, we ask if and how object presence encoding interacted with the concurrent MF encoding.

The baseline hypothesis, "MF Only encoding," is that units do not alter their FRs significantly based on the contextual factor of whether or not an object is present, and are only directly related to MFs.

An alternative hypothesis, "Direct object presence encoding," is that object presence is encoded simply and directly in unit FRs. In this case, a unit would have a "preferred" context (object present or object absent), and would simply increase its firing rate during one context compared to the other. This would occur independently from MF encoding.

Another alternative hypothesis, "Interactive object presence encoding," posits that object presence is encoded in a manner that interacts with MF encoding. In this case, a unit's relation to MFs would change based on the current context (object present or object absent).

To test which of these hypotheses most accurately reflected the M1 unit activity observed in the Object Presence Experiment, linear models of several different forms were built and tested. The predictors used to fit the equations were the scores of the top MF PCs explaining 99% of the variance in MFs ($N_{\mathrm{MFPC}} = 31$ for Monkey R and $N_{\mathrm{MFPC}} = 24$ for Monkey T). The "MF Only" model takes the form of Equation 4.22 (note that Equation 4.22 is the same as Equation 4.7 from Section 4.4):

$$f_{n,t} = \beta_{0,n} + \sum_{p=1}^{N_{\mathrm{MFPC}}} (\beta_{p,n} s_{p,t+\tau}) + \epsilon_n \tag{4.22}$$

where $f_{n,t}$ is the normalized FR of unit n at time t, β are constant weights, $s_{p,t+\tau}$ is MF PC score s at time $t+\tau$, and ϵ_n is a Gaussian noise term, $\epsilon_n \sim \mathcal{N}(0, \sigma^2)$. As in Section 4.4, τ was set to 40 ms. This model assumes a fixed linear tuning to movements which ignores context.

The "Direct" model takes the form of Equation 4.23:

$$f_{n,t} = \beta_{0,n} + \sum_{p=1}^{N_{\mathrm{MFPC}}} \beta_{p,n} s_{p,t+\tau} + \beta^c_{c,n} c + \epsilon_n \tag{4.23}$$

$$c = 1 \text{ when the object is present}$$

$$c = 0 \text{ when the object is absent}$$

The Direct model contains the additional indicator variable c which has a value of 1 for all trials in which the object was present, and 0 for all trials in which the object was absent (the No-Object Reach condition). This models unit n as having a direct, constant change in FR depending on the context, in addition to MF PC score tuning.

The "Interactive" model takes the form of Equation 4.24:

$$f_{n,t} = \beta_{0,n} + \sum_{p=1}^{N_{\text{MFPC}}} (\beta_{p,n} s_{p,t+\tau}) + \beta^c_{0,n} c + \sum_{p=1}^{N_{\text{MFPC}}} \left(\beta^c_{p,n} c s_{p,t+\tau}\right) + \epsilon_n \tag{4.24}$$

$$c = 1 \text{ when the object is present}$$

$$c = 0 \text{ when the object is absent}$$

The second summation term is the interaction of the indicator variable c and the MF PC scores s. When the object is present, c "activates" the β^c terms, allowing unit n to have completely different linear relations to MF PCs when the object is present or absent.

In order to evaluate these models, each was fit separately with linear regression, using the full dataset of FRs f and MF PC scores s. The trial-averaged R^2 values, R^2_{TA} were then calculated for each model and each unit (see Section A.6.3 for details). R^2_{TA} was used instead of full R^2 in order to focus on the ability of the models to fit task-relevant activity, rather than trial-to-trial variability. Table 4.2 displays the mean and median R^2_{TA} values for each model and the R^2_{TA} values for all units are plotted in Figure 4.29.

Table 4.2: **Mean and median R^2_{TA} for the MF Only, Direct and Interactive models, Object Presence Experiment**

Subject	Measure	MF Only	Direct	Interactive
Monkey R	Mean	0.86	0.87	0.91
	Median	0.88	0.89	0.92
Monkey T	Mean	0.82	0.84	0.88
	Median	0.85	0.88	0.92

For both subjects, minor improvements in R^2_{TA} were obtained when moving from the MF Only model to the Direct model, but relatively larger improvements were obtained when moving to the Interactive model.

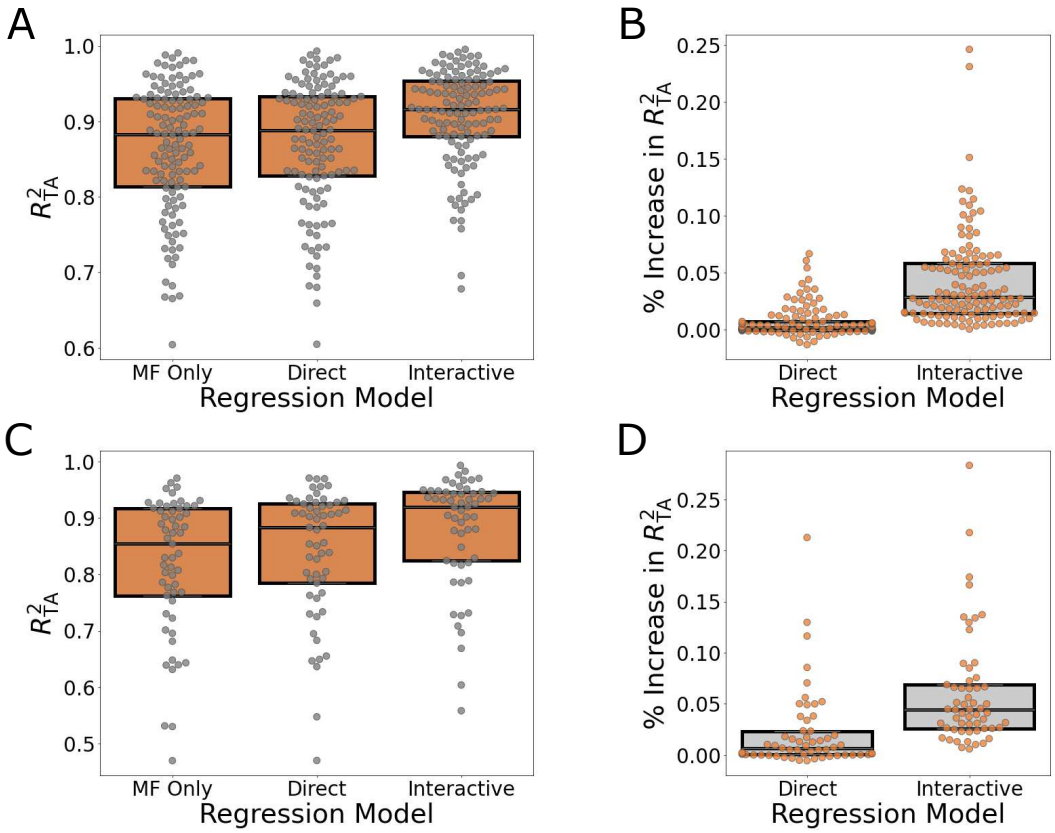

Figure 4.29: R^2_{TA} **and** R^2_{TA} **increases for the MF Only, Direct, and Interactive models, Object Presence Experiment.** A, B: Monkey R. C, D: Monkey T. A, C: R^2_{TA} values for each unit for each model. Gray circles: individual unit R^2_{TA} values. B, D: R^2_{TA} increases for the Direct and Interactive models vs. the MF Only model. Orange circles: individual unit R^2_{TA} increases. Boxplots denote the median and interquartile range.

Due to the fact that R^2_{TA} is bounded at 1, and also always increases when adding more model parameters, it alone does not make a sufficient measure for model selection. As a more informative measure, the Bayesian Information Criterion (BIC) was calculated for each model and each unit (see Section A.6.3). Model selection proceeded by choosing the model with the lowest BIC. The BIC was chosen over other similar measures such as the Akaike Information Criterion or likelihood ratio, as the BIC penalizes the number of parameters more heavily and is thus more conservative. The number of units that had minimum BIC for each of the models is reported in Table 4.3 and shown in Figure 4.30.

Table 4.3: **The proportion of units which were best fit by the MF Only, Direct and Interactive models according to BIC, Object Presence Experiment.** The model for which BIC was minimal was selected as the best model for each unit.

		MF Only		**Direct**		**Interactive**	
Subject	**Total Units**	**Count**	**Percent**	**Count**	**Percent**	**Count**	**Percent**
Monkey R	124	7	5.6%	10	8.1%	107	86.3%
Monkey T	57	11	19.3%	11	19.3%	35	61.4%

To ensure that model selection results reflected actual encoding of object context and were not simply a result of arbitrarily dividing the data into subsets, baseline frequencies of model selection were calculated by fitting the MF Only, Direct and Interactive models on datasets in which the object context labels for whole trials were randomly shuffled. The BICs of these shuffled-label models were compared to estimate the chance level of selecting each type of model. This procedure was repeated 100 times for each subject to generate the average baseline chance frequencies of selecting each model (Figure 4.30 orange lines). For both subjects, MF Only models were selected much less frequently than chance levels and Interactive models were selected at rates much higher than chance. Models which featured Direct or Indirect encoding of grip affordance factors were selected for 94.4 and 80.7% of

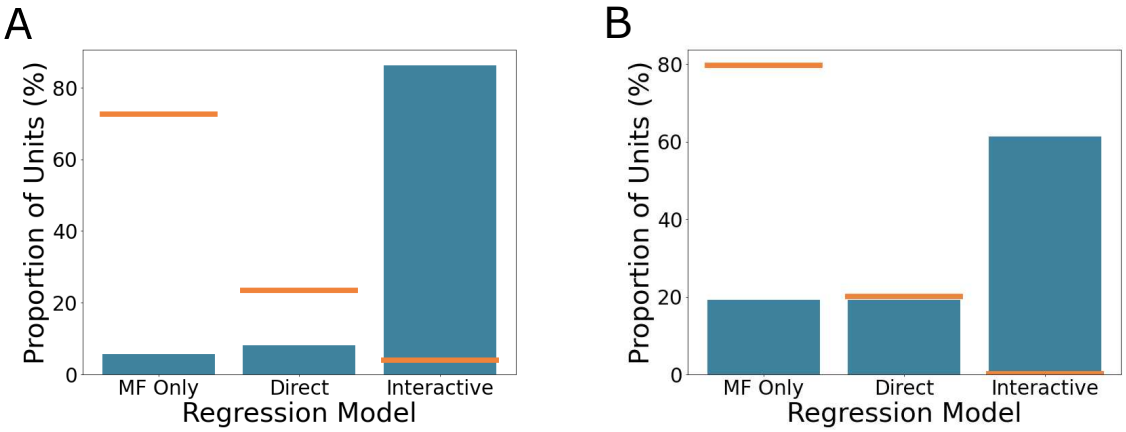

Figure 4.30: **The proportion of units which were best fit by the MF Only, Direct and Interactive models according to BIC, Object Presence Experiment.** The model for which BIC was minimal was selected as the best model for each unit. A: Monkey R. B: Monkey T. Orange lines: chance levels of selecting each model, generated by shuffling object context labels 100 times.

units for Monkey R and Monkey T respectively (chance levels: 27.4 and 20.2%). Models which featured Interactive grip affordance encoding were selected for 86.3 and 61.4% of units for Monkey R and Monkey T respectively (chance levels: 4.0 and 0.2%).

These results suggest that the analysis in Section 4.4 was conservative, as the extralinear modulation analysis identified a much lower number of units which exhibited object presence encoding (Table 4.1). These model fitting analyses suggest that object presence encoding may have been present in many more individual units, but at levels too low to be detected by the extralinear modulation analysis.

Table 4.3 and Figure 4.30 reveal that the majority of M1 units were fit best by models with Interactive object presence encoding. This suggests that these units' relations to MFs changed when the object was present or absent. To measure the magnitude of this change, the angular distance between the tuning coefficient vectors in the two contexts, Θ, was calculated for those units which preferred Interactive object presence encoding models according to Equation 4.25.

$$\Theta = \arccos\left(\frac{\hat{\boldsymbol{\beta}}_n \cdot \left(\hat{\boldsymbol{\beta}}_n + \hat{\boldsymbol{\beta}}_n^c\right)}{\|\hat{\boldsymbol{\beta}}_n\| \times \|\left(\hat{\boldsymbol{\beta}}_n + \hat{\boldsymbol{\beta}}_n^c\right)\|}\right) \tag{4.25}$$

where $\hat{\boldsymbol{\beta}}_{\boldsymbol{n}}$ is the vector of estimated MF tuning coefficients $\beta_{p,n}$ and $\hat{\boldsymbol{\beta}}_{\boldsymbol{n}}^{\boldsymbol{c}}$ is the vector of estimated MF tuning coefficients $\beta_{p,n}^c$ for $p = (1, \ldots, N_{\mathrm{MFPC}})$, as in Equation 4.24, $\cdot$ denotes the dot product operation and $\|\|$ denotes the vector norm operation. This resulted in an average tuning coefficient angular distance of 42.0 and 40.9 degrees in Monkey R and Monkey T respectively.

If a unit's MF tuning coefficients when the object was present were identical to those when the object was absent, Θ would be close to zero degrees. If tuning coefficients randomly changed between object presence and absence, Θ would be close to 90 degrees. Completely opposite tuning coefficients would result in Θ near 180 degrees. The intermediate values of 42.0 and 40.9 degrees suggest that for units that displayed Interactive object presence encoding, MF tuning coefficients with the object present were related to but markedly different from the MF tuning coefficients observed when the object was absent.

In the analyses above, trials in which the object was grasped were included in the set of trials deemed "object present". Thus, the predominantly interactive nature of object presence encoding may have been partially due to the additional contextual factor of whether or not the object was grasped. To further isolate the object presence effect, the regressions were recalculated using only data from Object Reach and No-Object Reach trials. The models were again compared using BIC to generate the model selection results shown in Figure 4.31.

As above, chance levels of model selection frequency were estimated by shuffling object context labels 100 times. Again, MF Only models were selected much less often than would be expected by chance, and Interactive models were selected much more often than chance levels. With grasp trials excluded, models which featured Direct or Indirect encoding of grip affordance factors were selected for 89.5 and 68.4% of units for Monkey R and Monkey T respectively (chance levels: 25.0 and 19.2%). Models which featured Interactive grip affordance encoding were selected for 79.0 and 38.6% of units for Monkey R and Monkey T respectively (chance levels: 1.5 and 0.1%).

When excluding grasp trials, the number of units that encoded object presence in a manner interactive with MF encoding decreased somewhat in Monkey T. However, Interactive object presence encoding remained the single most prevalent type of object presence encoding.

To measure the magnitude of Interactive object presence encoding effects, the tuning coefficient angular differences Θ were again calculated according to Equation 4.25, excluding all grasp trials. This resulted in an average angular distance of 33.4 and 37.2 degrees for Monkey R and Monkey T respectively. This again suggests that unit MF tuning coefficients were related, but somewhat different when the object was present or absent.

These results suggest that object presence encoding was common in single units in M1 and that object presence encoding most often interacts with MF encoding at the level of individual units in a complex manner, as opposed to being directly encoded in FRs or not encoded at all. Such complex context encoding should be detrimental for linear MF decoders that assume a fixed linear relationship between neural activity and MFs across contexts. This issue is directly addressed in Section 4.6.

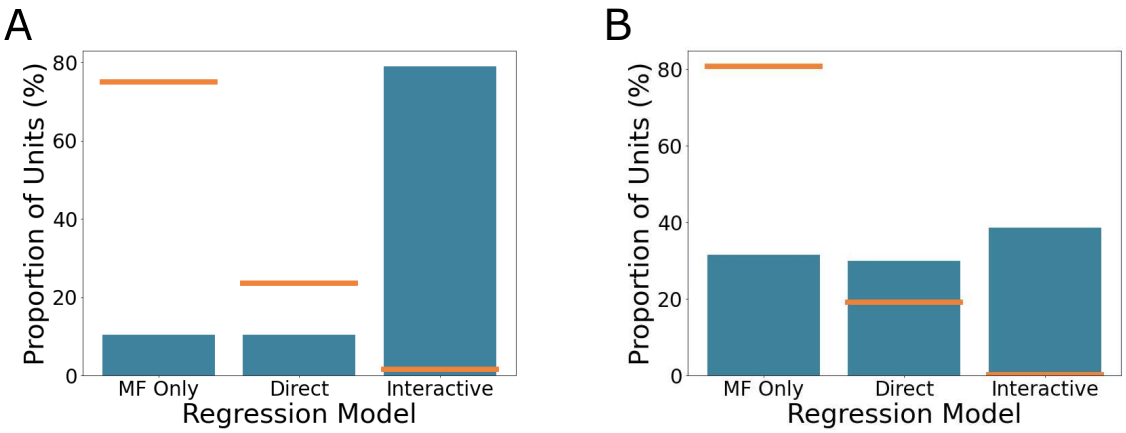

Figure 4.31: **The proportion of units which were best fit by the MF Only, Direct and Interactive models according to BIC when considering reach trials only, Object Presence Experiment.** The model for which BIC was minimal was selected as the best model for each unit. Models were fit only on Object Reach and No-Object Reach trials, excluding grasp trials. A: Monkey R. B: Monkey T. Orange lines: chance levels of selecting each model, generated by shuffling object context labels 100 times.

4.6 Impact of Object Presence on MF Decoding

Though upper limb BCI-controlled motor neuroprostheses have made great progress in recent years (see Section 2.2.1), reliable cortical control of robotic hands for object interaction has yet to be achieved. One possible reason for this difficulty is that most current neural decoders assume a fixed, linear relationship between M1 activity and the MFs to be decoded. As demonstrated in Section 4.5, the contextual factor of the presence or absence of an object may be interactive with MF encoding, resulting in changes in the relationship between neural activity and MFs that would be difficult for a fixed linear decoder to account for.

A recent study facing such problems was conducted by Wodlinger et al [119]. In this study, a neuroprosthetic decoder trained on free movements performed poorly when the subject attempted to interact with real physical objects. In this section, a similar decoding framework is constructed in order to confirm this contextual effect in a healthy primate model.

The decoder model was constructed to approximate the approach used by Wodlinger et al 2014 [119] and Clanton 2011 [437]. Thus, a linear model was used to decode each MF individually from the FRs of a population of units according to Equation 4.26:

$$y_{m,t} = W_m X_t \tag{4.26}$$

where $y_{m,t}$ is the value of normalized MF m at time t (normalized over the full data set), W_m is a vector of weights, and X_t is a vector of FRs. The FRs X_t were calculated as in previous studies [119, 437] by binning spike counts in 30 ms bins and combining the last 15 bins ocurring before time t using an exponential filter with decay constant 0.95. The decoders were trained and tested on data from the peri-movement period only (100 ms before reach onset to 400 ms after target contact).

Decoder weights W_m were fit using ridge regression, with the penalty parameter λ estimated via 10-fold cross-validation on the full, cross-context data set (see Section A.6.3 for details). The performance of this global decoder in RMSE for each of the normalized MFs is shown in Figure 4.32.

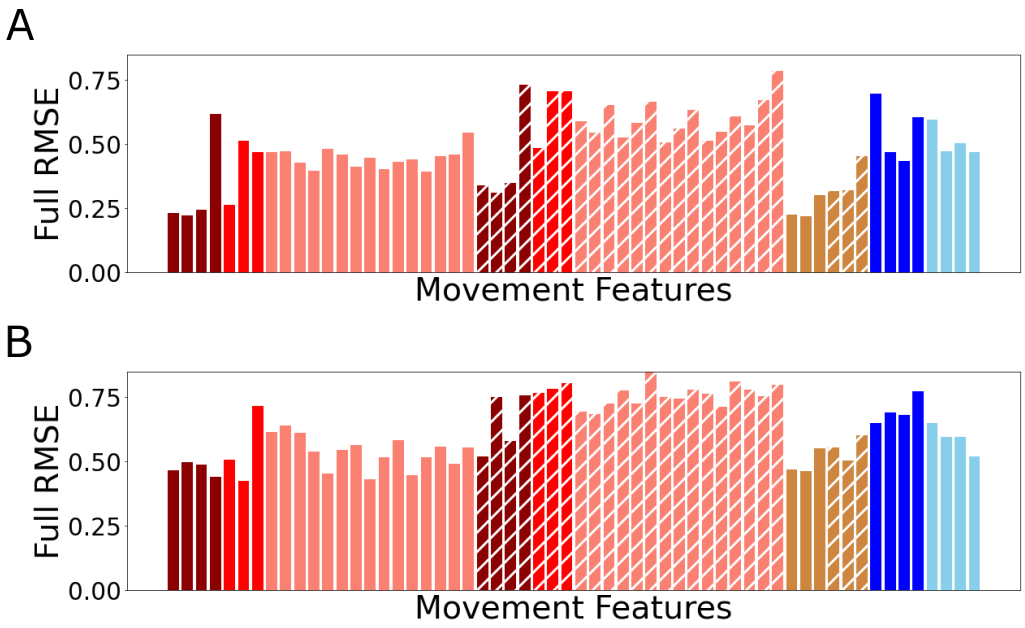

Figure 4.32: **Decoder performance in terms of RMSE when decoding normalized MFs using all data** A: Monkey R. B: Monkey T. Each bar is a different normalized MF. Hatched bars: velocities. Dark red: shoulder and elbow joint angles and joint angular velocities. Red: wrist joint angles and joint angular velocities. Light red: finger joint angles and joint angular velocities. Tan: hand positions and velocities. Dark blue: proximal EMG. Light blue: distal EMG

The most accurate decodes were observed for hand positions and shoulder joint angles, then hand velocities and wrist joint angles, then finger joint angles and EMG, with the least accurate decodes observed for wrist joint angular velocities and finger joint angular velocities. In general, joint angles and hand positions were decoded more accurately than joint angular velocities and hand velocities. For Monkey R, the elbow flexion angle and angular velocity was decoded especially poorly, likely due to the fact that this joint showed very low range of motion throughout the task (Figure 4.3). Monkey R generally had lower RMSEs, likely due to the greater number of units recorded from Monkey R and their stronger tuning to movements. (Figure 4.22)

In order to test the impact of context on the decoder performance, three different decoding models were built:

1. The "All Data" decoder, trained on data from all conditions.
2. The "Object" decoder, trained on data from conditions for which the object was present (Power Grasp, Pinch Grasp and Object Reach conditions).
3. The "No-Object" decoder, trained on data from the No-Object Reach condition.

Each decoder was then tested by decoding MFs in either of two partitions: the "Object Data," conditions for which the object was present (Power Grasp, Pinch Grasp and Object Reach conditions) or the "No-Object Data," the condition for which the object was absent (No-Object Reach condition). Thus, decoding could be done "within context," where a decoder was trained and tested on the same context partition, or "across context," where a decoder was trained on one context partition and tested on another context partition. Decoding could also be done with the "All Data" decoder, in which which a single decoder was trained on all data.

The decoders were evaluated using root mean squared error (RMSE) between decoded MFs and observed MFs. Decoder performance was evaluated using 10-fold cross-validation and averaging the resulting 10 RMSEs (see Section A.6.5).

The performance of the decoders (in terms of RMSE) for all MFs in the various decoding scenarios above is plotted in Figure 4.33.

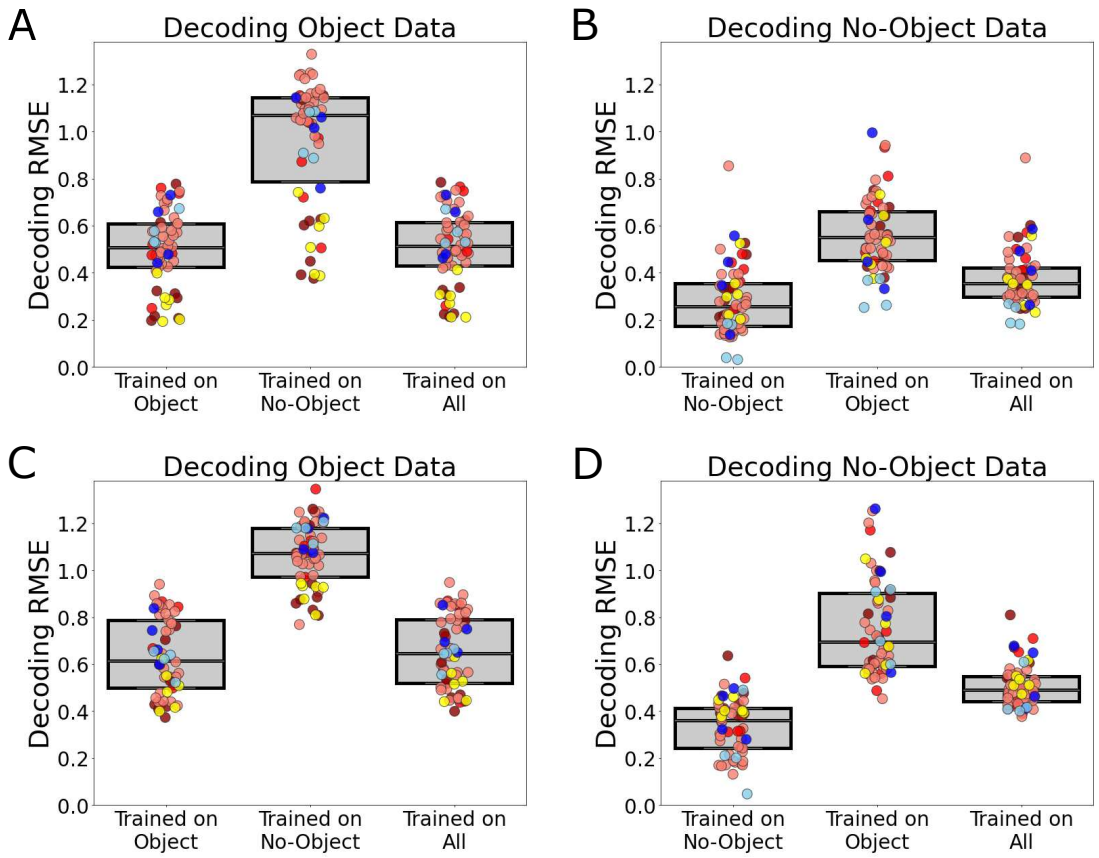

Figure 4.33: **Decoder performance in terms of RMSE when decoding within and across contexts, Object Context Experiment.** A, B: Monkey R. C, D: Monkey T. A, C: decoding Object data MFs using decoders trained on Object, No-Object or All data. B, D: decoding No-Object data MFs using decoders trained on No-Object, Object or All data. Box plots represent the median and interquartile range of all decoded MFs. Colored circles reach represent the RMSE for a single decoded MF. Red circles: joint angles and joint angular velocities. Yellow circles: hand positions and hand velocities. Blue circles: EMG. Lighter colors indicate distal MFs, darker colors are proximal MFs.

For both subjects, the best decoding performance was observed when training and testing within-context. A large increase in RMSEs (decrease in decoding performance) was observed when decoding data in one context using a decoder that was trained on the other context. The All Data decoder was comparable to the Object decoder for decoding object data, while the All Data decoder performed markedly worse than the No-Object decoder for decoding No-Object data.

To visualize the detrimental effects of decoding across contexts, the percent increase in RMSE was calculated, taking within-context decoders (Object data decoded with the Object decoder, No-Object data decoded with the No-Object decoder) as the baseline. The percent increase in RMSE when decoding across vs. within contexts is shown in Figure 4.34. The percent increase in RMSE when decoding with all data decoders vs. within-context decoders is shown in Figure 4.35.

For both subjects, decoding Object data using the No-Object decoder resulted in a substantial increase in RMSE, with RMSEs frequently doubling in size. The joint angles were more heavily affected than the joint angular velocities in general. Also of note was that hand position and velocity decodes were impacted. This echoes some of the effects seen by Wodlinger et al [119], where hand velocity was poorly decoded when trained on free movement and tested with a real object.

Decoding No-Object data using the Object decoder resulted in very large increases in RMSE, especially in the finger joint angles, finger joint angular velocities and wrist flexor EMGs. The value for the distal wrist flexor EMG for Monkey T (Figure 4.34 B lower plot, far right light blue bar) suffered in an increase of 1822.9% in RMSE when decoding No-Object data across context. This was likely due to the relative quiescence of the wrist flexor EMGs during the No-Object Reach trials, versus the strong activations observed in the grasp conditions (Figure 4.7 gray vs. colored traces).

Decoding Object data using the All data decoder resulted in only very mild increases in RMSE, often less than 5%.

Decoding No-Object data using the All data decoder still showed detrimental performance decreases, again concentrated in the finger joint angles and angular velocities and the wrist flexor EMGs.

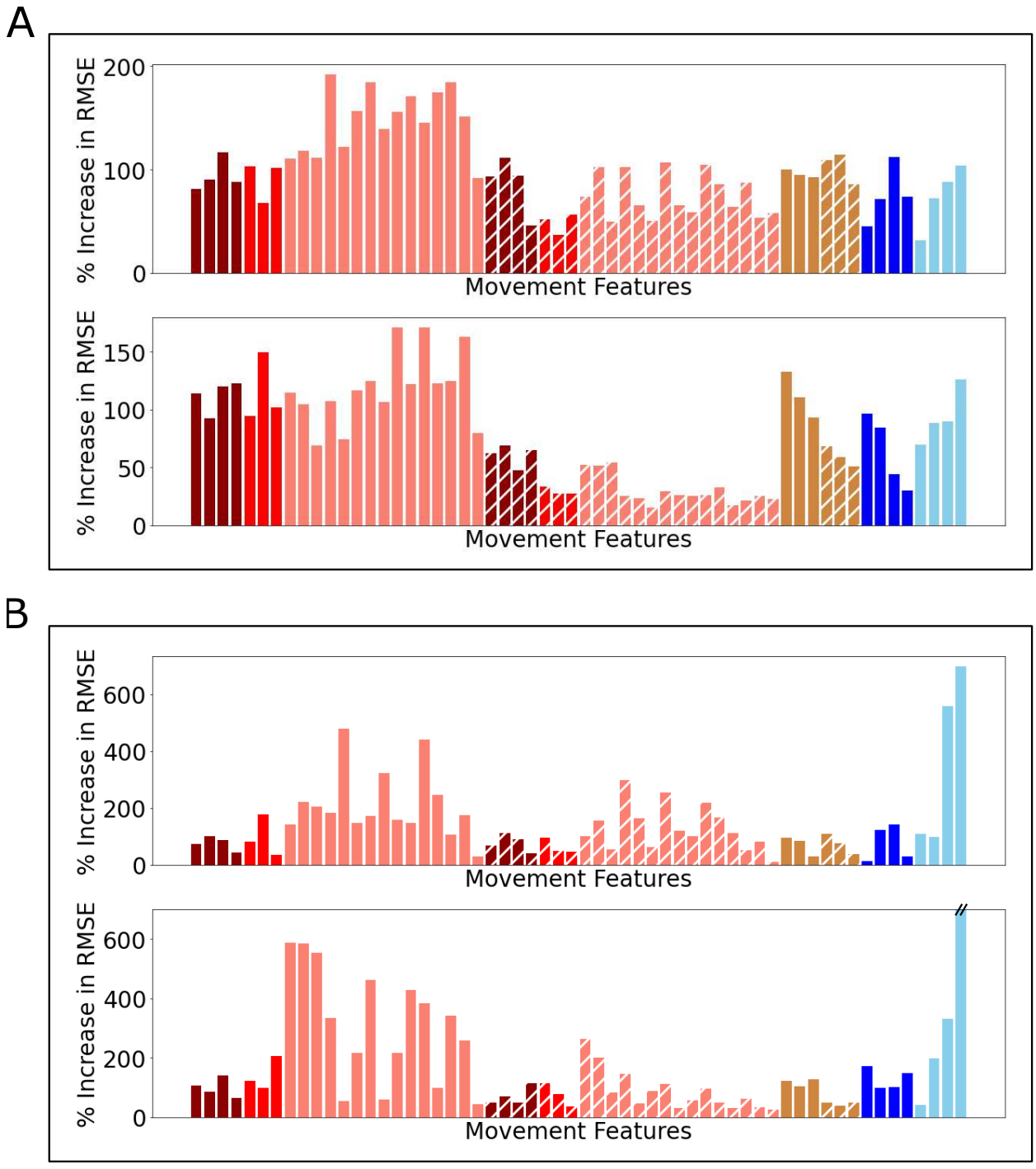

Figure 4.34: **% increase in RMSE when decoding across contexts vs. within contexts.** A: decoding Object data. B: decoding No-Object data. In each panel, the upper plot corresponds to Monkey R and the lower plot corresponds to Monkey T. Colors are the same as in Figure 4.32

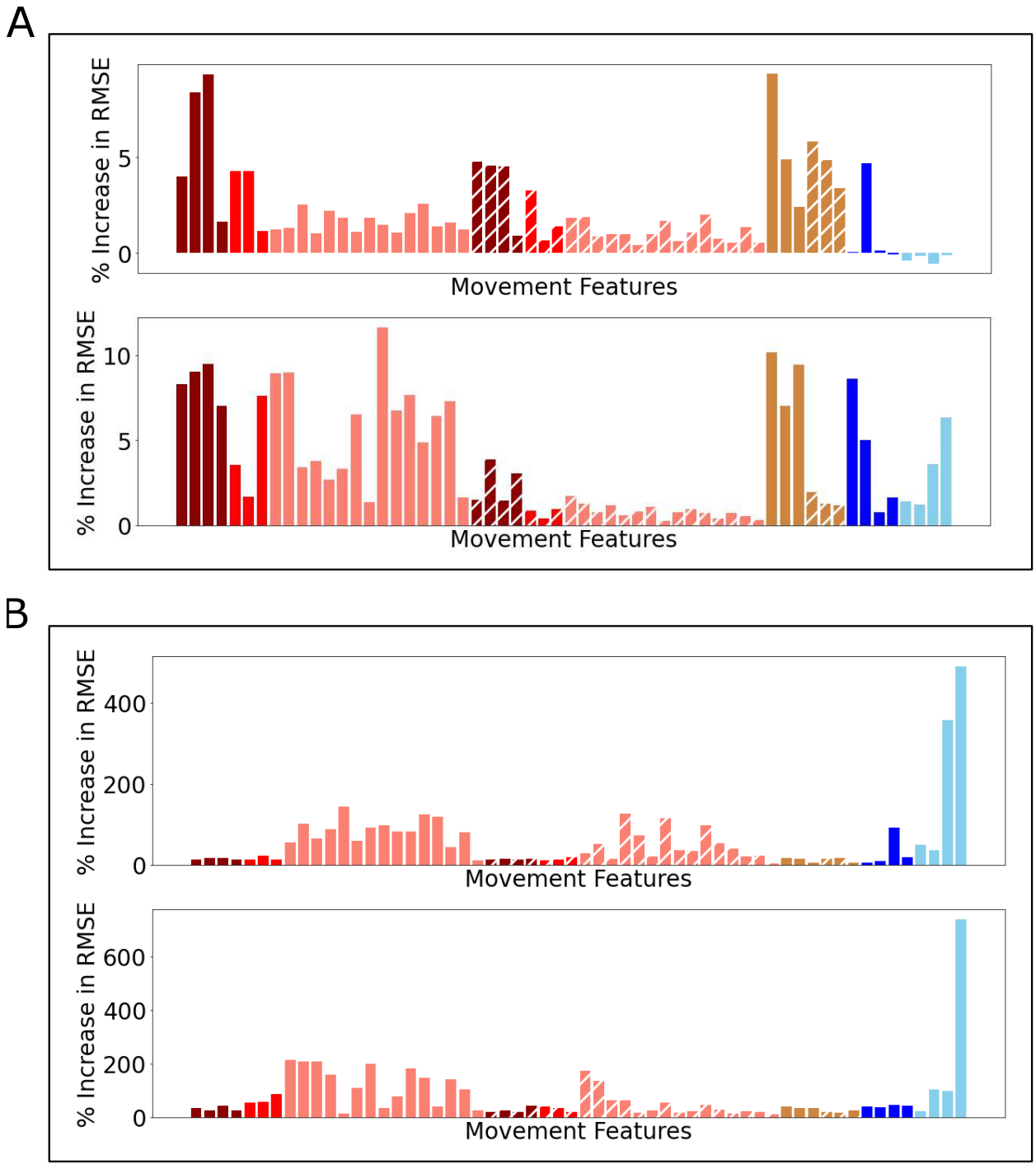

Figure 4.35: **% increase in RMSE when decoding with the All Data decoder vs. within-context decoders.** A: decoding Object data. B: decoding No-Object data. In each panel, the upper plot corresponds to Monkey R and the lower plot corresponds to Monkey T. Colors are the same as in Figure 4.32

To summarize these results, the average percent increase in RMSE across all MFs was calculated for across-context decoders compared to within-context decoders, and for full data decoders compared to within-context decoders. These average RMSE increases were calculated separately for decoding object data and decoding no object data. These results are presented in Table 4.4.

Table 4.4: **Percent increase in RMSE for across-context and full data decoders, compared to within-context decoders.**

Decoding Object Data

Subject	Area	Across-context	Full Data
Monkey R	M1	97.8%	2.2%
Monkey T	M1 Right	77.5%	3.7%

Decoding No-Object Data

Subject	Area	Across-context	Full Data
Monkey R	M1	145.8%	57.6%
Monkey T	M1 Right	184.5%	76.4%

Overall, decoding across contexts resulted in large RMSE increases for decoding both Object and No-Object data. Decoding using a decoder trained on All Data provided moderate performance when decoding Object data, but was notably worse in decoding No-Object data.

The best performance was observed when decoding within context. This could be due to the finding that object presence encoding is interactive with MF encoding (Section 4.5), in that it manifests as a change in the linear relationship between neural activity and MFs. Thus, a good solution could be to build two separate decoders, one for decoding movements made toward objects and one for free movements, and applying the appropriate decoder

in each context. Practical application of such parallel decoders would require some way to automatically detect which context was active. Here, we propose that a binary context classifier could perform this function.

As noted in Section 4.3, substantial separation between the No-Object Reach condition and the conditions for which the object was present was observed in M1 throughout the peri-movement period (Figure 4.19 black, dark brown and light brown traces). To test whether this neural information could be used to reliably classify context, Gaussian Naive Bayes classifiers were constructed to performed binary classification of context (classifying whether the trial was a No-Object Reach vs. the other three conditions, for which the object was present), using the same decoding FRs that were used as inputs to the linear MF decoders. A single classifier was constructed across all of the peri-movement data for each subject and evaluated using 10-fold cross-validation. The classifier performance at each time point is plotted in Figure 4.36.

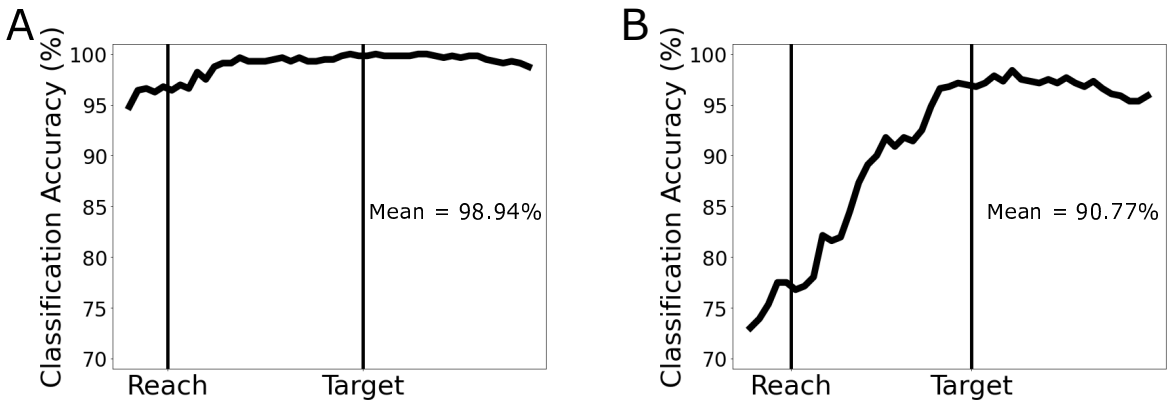

Figure 4.36: **Classification of contexts (object present vs. object absent) using a Gaussian Naive Bayes classifier.** A: Monkey R. B: Monkey T. Chance level 50%.

For both subjects, a simple Gaussian Naive Bayes classifier was able to classify context (object presence or absence) with high accuracy. Classification performance for Monkey R was near perfect throughout the peri-movement period. For Monkey T, classification

performance increased steadily throughout the reach period and remained high through object contact and target hold. This difference in performance was likely due to the higher number of units for Monkey R vs. Monkey T (124 units vs. 57 units).

The ability to consistently classify contexts suggests that the Gaussian Naive Bayes classifier could be used to select between context-specific decoders. To test such a decoding strategy, a "context-detecting decoder" was constructed and tested. The context-detecting decoder consisted of two separate context-specific linear decoders (one trained on only Object data, the other trained on only No-Object data), layered with a Gaussian Naive Bayes binary context classifier. For each decoding time step, a decoder output was obtained from each of the context-specific decoders. These decoder outputs were then scaled by the probabilities for each context class as output by the context classifier. The two scaled decoder outputs were then summed to produce the final decoded MF estimate. This decoding architecture is displayed schematically in Figure 4.37.

This decoder architecture takes advantage of the fact that the Gaussian Naive Bayes classifier can calculate the probability of each class. Weighting the context-specific decoder outputs by the context class probabilities and combining them provided a slight improvement over simply selecting the context-specific output based on which context class had a higher probability.

The performance of the context-detecting decoder was compared against a single linear decoder trained on all data, and two ideal context-specific decoders which simulated the theoretical performance of the context-detecting decoder with an 'omniscient' context classifier. All three architectures were trained and tested using 10-fold cross-validation, all using the same folds. The performance of the three decoder architectures is shown in Figure 4.38.

Both the context-detecting decoder and the theoretical perfectly applied context-specific decoders provided moderate improvements in RMSE when decoding all data. More marked improvements were observed when considering only No-Object data decoding. For Monkey R, the performance of the context-detecting decoder was very close to that of the theoretical perfectly applied context-specific decoders, owing to the near perfect performance of the

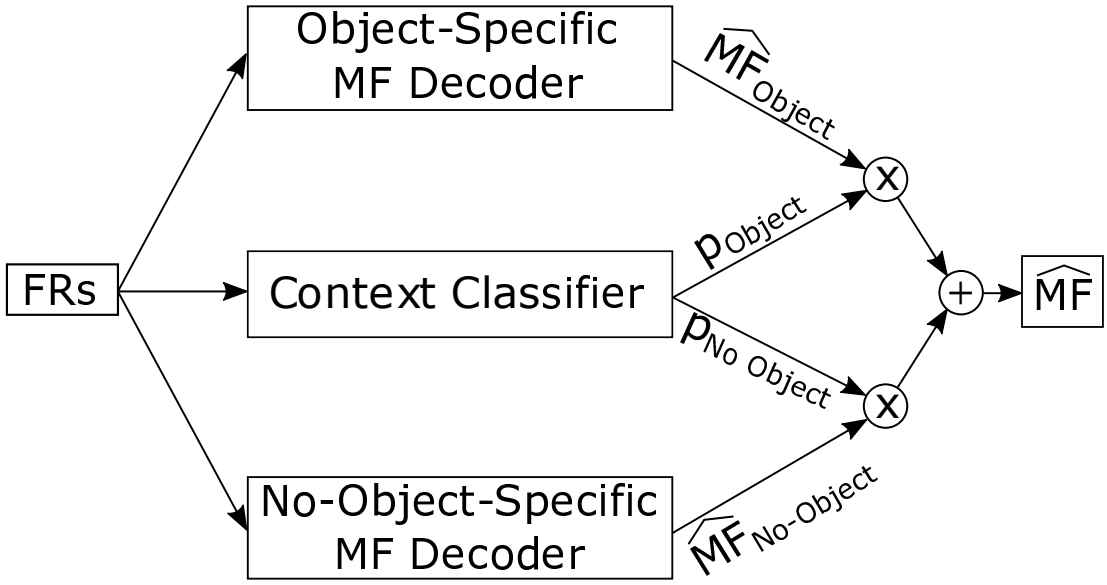

Figure 4.37: **Schematic representation of the context-detecting decoder architecture for the Object Presence Experiment.** Separate decoders were built for each MF. FRs: firing rates for decoding. $\hat{\text{MF}}_{\text{Object}}$: MF output from the object-specific MF decoder. $\hat{\text{MF}}_{\text{No-Object}}$: MF output from the no-object-specific MF decoder. p_{Object}: probability that object is present as output by the context classifier. $\text{p}_{\text{No-Object}}$: probability that object is absent as output by the context classifier, $\hat{\text{MF}}$: final decoded MF value.

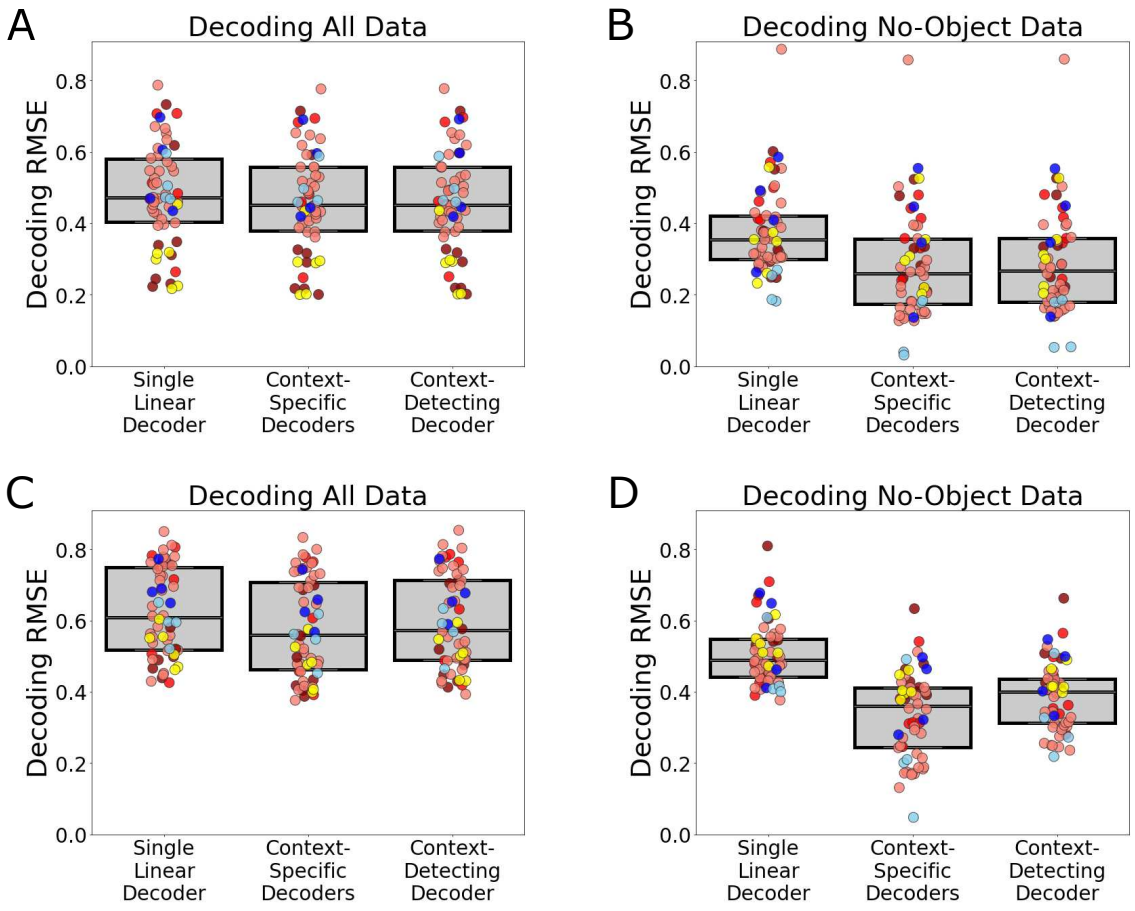

Figure 4.38: **Performance of the context-detecting decoder, compared to a single linear decoder and perfectly applied context-specific decoders.** A, B: Monkey R. C, D: Monkey T. A, C: performance when decoding all data. B, D: performance when decoding only no-object data. Colors are the same as in Figure 4.38. All groups were different at $p < 0.0001$, one-sided paired permutation test.

context classifier. For Monkey T, the performance of the context-detecting decoder was intermediate between the single linear decoder and the theoretical perfectly applied context-specific decoders, owing to the imperfect context classification for Monkey T.

The average RMSE improvements for the context-detecting decoder and the theoretical perfectly applied context-specific decoders over the single linear decoder are shown in Table 4.5.

Table 4.5: **Average RMSE improvement for the context-detecting decoders and theoretical perfectly applied context-specific decoders over single linear decoders.** Percentage is relative to the RMSE for the single linear decoders, averaged over all MFs.

Mean RMSE Improvement vs. Single Linear Decoder, All Data

Subject	Context-Specific Decoders	Context-Detecting Decoder
Monkey R	4.87%	4.55%
Monkey T	8.06%	4.73%

Mean RMSE Improvement vs. Single Linear Decoder, No-Object Data

Subject	Context-Specific Decoders	Context-Detecting Decoder
Monkey R	28.58%	26.69%
Monkey T	34.49%	24.11%

In the analyses above, relatively greater context-related decoding performance drops were observed when decoding No-Object data than when decoding Object Data. One reason for this may have been that grasp trials were included in the Object Data dataset. To verify that the decoder performance decreases were due to the object presence encoding effect and not due to the inclusion of grasping trials in the No-Object dataset, the decoding analyses above were repeated using only data from the Object Reach and No-Object Reach trials, excluding Power Grasp and Pinch Grasp trials. Decoders were trained using either

all reach data, only Object Reach data or only No-Object Reach data. Each decoder was then tested separately on either Object Reach data or No-Object Reach data. The average percent RMSE increases across all MFs when decoding reach data across-contexts (e.g. training on Object Reach data and testing on No-Object Reach data) or with decoders trained on all reach data were calculated relative to RMSEs obtained when decoding within contexts (e.g. training on Object Reach data and testing on Object Reach data). These results are shown in Table 4.6.

Table 4.6: **Percent increase in RMSE for across-context and full data decoders, compared to within-context decoders.** Only data from reaches were used for training or decoding, with grasp trials excluded.

Decoding Object Reach Data

Subject	Area	Across-context	Full Data
Monkey R	M1	56.8%	5.5%
Monkey T	M1 Right	64.7%	7.2%

Decoding No-Object Reach Data

Subject	Area	Across-context	Full Data
Monkey R	M1	85.1%	7.9%
Monkey T	M1 Right	66.1%	14.5%

Results were similar to those obtained using the full dataset, but the detrimental impact of the object presence signal on MF decoding was marginally lower in magnitude when considering only reach data (compare Table 4.6 to Table 4.4). The decoding performance penalties when training and testing decoders across context were still large in magnitude, with average RMSE increases of over 50% in each case. Decoder performance was mostly

recovered by using a single decoder trained on data from all reach trials, but this full data decoder performance was still worse than within-context decoding performance by about 5–15%.

In order to further approach within-context decoder performance, a context-detecting decoder was again built with the same structure as described in Figure 4.37, but using only Object Reach and No-Object Reach data. The Gaussian Naive Bayes context classifier retained good performance when considering only reach trials, as Object Reach vs. No-Object reach could be decoded with an average accuracy of 98.0% for Monkey R and 91.0% for Monkey T. The performance of the perfect context-specific decoders and the context-detecting decoder compared to single, all data decoders is shown in Table 4.7.

Table 4.7: **Average RMSE improvement for the context-detecting decoders and theoretical perfectly applied context-specific decoders over single linear decoders.** Percentage is relative to the RMSE for the single linear decoders, averaged over all MFs.

Mean RMSE Improvement vs. Single Linear Decoder, All Data

Subject	Context-Specific Decoders	Context-Detecting Decoder
Monkey R	5.1%	3.8%
Monkey T	7.6%	3.6%

Though modest, these results further support the finding that object presence has a detrimental impact on MF decoding performance. The somewhat smaller size of the across context decoder performance drop when considering only reaches compared to that observed when testing the full dataset including grasps suggests that whether or not a grasp was made likely represents and additional contextual factor that impacts decoder performance. This is difficult to test, given the present data, as the MFs observed during grasps were very different than the MFs observed during reaches.

The performance increases noted in Tables 4.5 and 4.7 suggest that incorporating contextual information can improve decoding results. Specifically, building separate

decoders for different contexts and combining their outputs according to a context classifier especially improves decoding of No-Object MF data. This performance increase was obtained using simple linear decoders and the relatively simple Gaussian Naive Bayes classifier, using large amounts of training data and a highly structured task with only limited and highly restricted variation in MFs. Whether similar improvements would be observed with limited training data in an actual neural prosthetic implementation remains an open question.

Thus far, object presence encoding in M1 has been characterized in terms of its relative magnitude (Section 4.4), its interaction with MF encoding (Section 4.5) and its impact on decoding performance. The final section of this chapter, Section 4.7, concerns the informational content of the object presence encoding signal, with a focus on the possibility that the object presence related changes in behavior and neural activity are related to the grasp affordances of the object.

4.7 Affordance Information in the Object Presence Signal

As first described by James Gibson [322], the affordances of an object are the potential actions that can be performed with that object, as dictated by both the physical characteristics of the object and the capabilities of the agent performing the actions. For example, in the case of the Object Presence Experiment, the object afforded the actions of grasping with a power grip and grasping with a pinch grip. Recent theoretical frameworks have postulated that the grasp and use affordances of objects are processed in the frontoparietal cortical grasp network [231, 326].

Human behavioral and brain imaging studies suggest that seeing a manipulable object may automatically activate the motor system to prime the grasping or use actions afforded by the object. In humans, viewing or naming tools activates the same grasp network areas that are activated when subjects perform actual or imagined grasping or use actions with those tools [201, 304, 343, 344]. Behaviorally, the presence of an object can prime actions or responses that are similar to those used to grasp or use the object, or can interfere with

incompatible grasp actions [330–332, 349]. A series of recent studies in macaques showed that single neurons in PMV are activated by the visual presence of an object, even when the subject makes no action toward the object [350, 351]. A more in depth review of studies concerning automatic activation is presented in Section 2.5.2. These findings suggest that the automatic activation which occurs in the presence of a graspable object may manifest in a biasing of behavior and neural activity toward the behavior and neural activity associated with the actions afforded by the object.

The results of Sections 4.2 and 4.3 suggest that behavior and population neural activity were significantly different when reaches were performed with or without an object present. However, the analyses in those sections only characterized the magnitudes of those differences. In this section, the object presence related behavioral and neural differences are further examined for evidence that they may contain information about the grasp affordance of the object in that they reflect automatic activation of motor representations of the object's afforded grasps. If the grasp affordances representations of the object are automatically activated by the object's presence, the behavior and neural activity observed on trials where the object was present but not grasped (Object Reach trials) should be more similar to the behavior and neural activity observed for trials in which the object actually was grasped (Power Grasp and Pinch Grasp trials) relative to trials in which the object was not present at all (No-Object Reach trials). That is, the presence of the object should systematically bias behavior and neural activity toward grasping behavior and neural activity, even when it is not grasped. These effects should be detectable as directional shifts of behavior and neural activity in MF PC and FR PC space when the object was present but not grasped.

Three possibilities are considered. The first is that object presence induces a pro-affordance bias, shifting behavior and neural activity toward that associated with the afforded grasps. The second possibility is that object presence induces an anti-affordance bias, shifting behavior and neural activity away from that associated with the afforded grasps. The third possibility is that object presence induces no affordance bias.

In order to characterize these biases in behavior and neural activity, the affordance shift S was calculated in both mMF PC space and mFR PC space, resulting in S^{mMFPC} and

S^{mFRPC}. The mMF PC space and mFR PC spaces were defined as the PC scores of the top PCs explaining 99% of variance in trial-averaged peri-movement MFs and in trial-averaged whole-trial FRs. The affordance shifts S^{mMFPC} and S^{mFRPC} were calculated relative to both Power Grasp and Pinch Grasp at each time point according to Equations 4.27–4.30:

$$S^{\text{mMFPC}}_{\text{Power},t} = \frac{(M_{\text{PowerGrasp},t} - M_{\text{No-ObjectReach},t}) \cdot (M_{\text{ObjectReach},t} - M_{\text{No-ObjectReach},t})}{\|M_{\text{PowerGrasp},t} - M_{\text{No-ObjectReach},t}\|^2} \tag{4.27}$$

$$S^{\text{mMFPC}}_{\text{Pinch},t} = \frac{(M_{\text{PinchGrasp},t} - M_{\text{No-ObjectReach},t}) \cdot (M_{\text{ObjectReach},t} - M_{\text{No-ObjectReach},t})}{\|M_{\text{PinchGrasp},t} - M_{\text{No-ObjectReach},t}\|^2} \tag{4.28}$$

$$S^{\text{mFRPC}}_{\text{Power},t} = \frac{(F_{\text{PowerGrasp},t} - F_{\text{No-ObjectReach},t}) \cdot (F_{\text{ObjectReach},t} - F_{\text{No-ObjectReach},t})}{\|F_{\text{PowerGrasp},t} - F_{\text{No-ObjectReach},t}\|^2} \tag{4.29}$$

$$S^{\text{mFRPC}}_{\text{Pinch},t} = \frac{(F_{\text{PinchGrasp},t} - F_{\text{No-ObjectReach},t}) \cdot (F_{\text{ObjectReach},t} - F_{\text{No-ObjectReach},t})}{\|F_{\text{PinchGrasp},t} - F_{\text{No-ObjectReach},t}\|^2} \tag{4.30}$$

where $M_{i,t}$ is the vector of mMF PC scores for condition i at time t, $F_{i,t}$ is the vector of mFR PC scores for condition i at time t, $\cdot$ denotes the dot product, and $\|\|$ denotes the vector norm operation. Thus, $S^{\text{mMFPC}}_{\text{Power},t}$ is the sign and magnitude of the projection of the vector from No-Object Reach mMF PC scores to Object Reach mMF PC scores onto the vector from No-Object Reach mMF PC scores to Power Grasp mMF PC scores, scaled by the magnitude of the latter vector. $S^{\text{mMFPC}}_{\text{Pinch},t}$ is the same, but calculated relative to Pinch Grasp instead of Power Grasp. The mFR PC affordance shifts S^{mFRPC} are analogous, but calculated in mFR PC space instead of mMF PC space.

The affordance shift related to the cosine of the angle between the vector from No-Object Reach PC scores to Object Reach PC scores and the vector between No-Object Reach PC scores to grasp PC scores. Thus, the affordance shifts are a scaled version of the correlation between the signal related to object presence, and the signal related to grasp encoding.

Additionally, the results of Section 4.4 showed that neural activity in M1 contains a robust object presence encoding signal, in that the difference in neural activity when the object was

present or absent was not fully explainable by linear tuning to MFs. In order to determine if this context-related neural activity also contains evidence of automatic activation of the unused grasp affordances, the affordance shifts were also calculated using null space neural activity. The null space neural activity is the component of neural activity which cannot be linearly combined to decode mMF PCs (see Section 4.4.2). The null space affordance shifts S^{null} were calculated according to equations 4.31 and 4.32.

$$S^{\text{null}}_{\text{Power},t} = \frac{\left(\hat{F}^{\text{null}}_{\text{PowerGrasp},t} - \hat{F}^{\text{null}}_{\text{No-ObjectReach},t}\right) \cdot \left(\hat{F}^{\text{null}}_{\text{ObjectReach},t} - \hat{F}^{\text{null}}_{\text{No-ObjectReach},t}\right)}{\|\hat{F}^{\text{null}}_{\text{PowerGrasp},t} - \hat{F}^{\text{null}}_{\text{No-ObjectReach},t}\|^2} \tag{4.31}$$

$$S^{\text{null}}_{\text{Pinch},t} = \frac{\left(\hat{F}^{\text{null}}_{\text{PinchGrasp},t} - \hat{F}^{\text{null}}_{\text{No-ObjectReach},t}\right) \cdot \left(\hat{F}^{\text{null}}_{\text{ObjectReach},t} - \hat{F}^{\text{null}}_{\text{No-ObjectReach},t}\right)}{\|\hat{F}^{\text{null}}_{\text{PinchGrasp},t} - \hat{F}^{\text{null}}_{\text{No-ObjectReach},t}\|^2} \tag{4.32}$$

where $\hat{F}^{\text{null}}_{i,t}$ is the vector of null space activity for condition i at time t. The calculation of $\hat{F}^{\text{null}}$ is described in Equation 4.15.

The three potential scenarios of pro-affordance bias, no affordance bias and anti-affordance bias are sketched out schematically in Figure 4.39.

The affordance shifts S can be thought of as a directional measure of the impact of object presence on mMF PC scores, mFR PC scores or null space activity. A positive value of S indicates that the presence of the object induced a shift in mMF PC scores, mFR PC score or null space activity toward the unused grasp. A negative value of S indicates that the presence of the object induced a shift away from the unused grasp. A value of S approximately equal to zero indicates that the differences observed due to object presence were unrelated to the grasp afforded by the object.

The affordance shift results are shown in Figure 4.40.

For both subjects, positive S values indicating pro-affordance biases relative to both afforded grasps were present in mMF PC scores, mFR PC scores and null space neural activity.

In the mMF PCs, a pro-affordance bias was observed in both subjects starting before movement onset, suggesting that during Object Reach trials, both subjects exhibited a

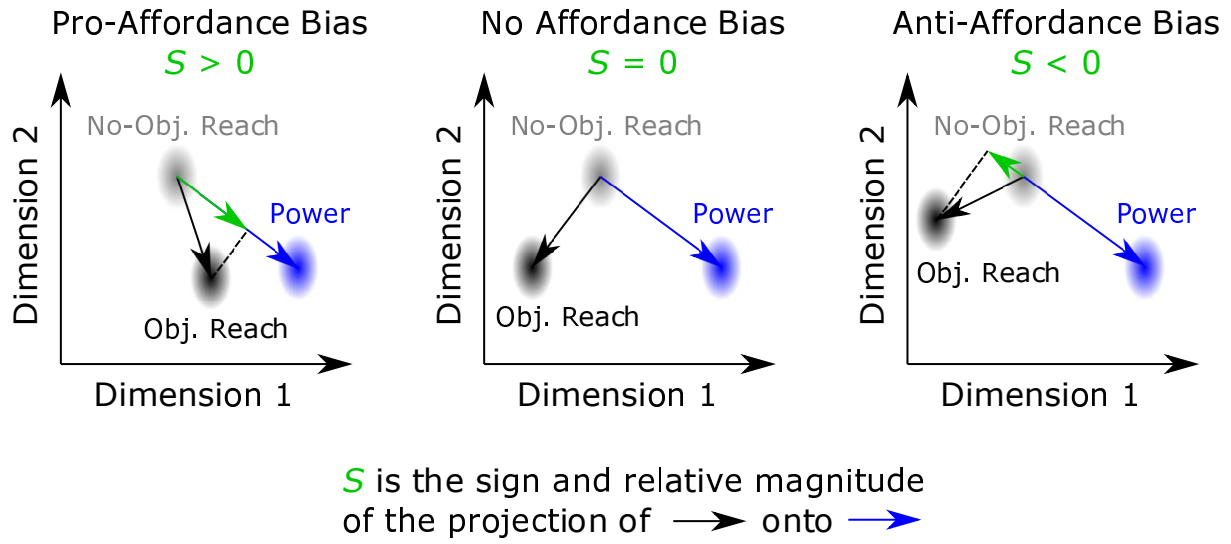

Figure 4.39: **Schematic illustration of three potential forms of affordance bias in the Object Presence Experiment.** Ellipses represent distributions of mMF PC scores, mFR PC scores or null space neural activity for different conditions. Blue ellipse: Power Grasp. Black ellipse: Object Reach. Gray ellipse: No-Object Reach. Blue vector: vector between No-Object Reach and Power Grasp. Black vector: vector between No-Object Reach and Object Reach. Green vector: the projection of the black vector onto the blue vector. The affordance shift is the magnitude of the green vector divided by the magnitude of the blue vector, with the sign positive when the green and blue vector are aligned, and negative when the green and blue vector are opposed. Dimensions could correspond to mMF PC scores for S^{mMFPC}, mFR PC scores for S^{mFRPC} and null space neural dimensions for S^{null}. The diagram shows affordance bias scenarios relative to Power Grasp at a single time point; S was also calculated relative to Pinch Grasp.

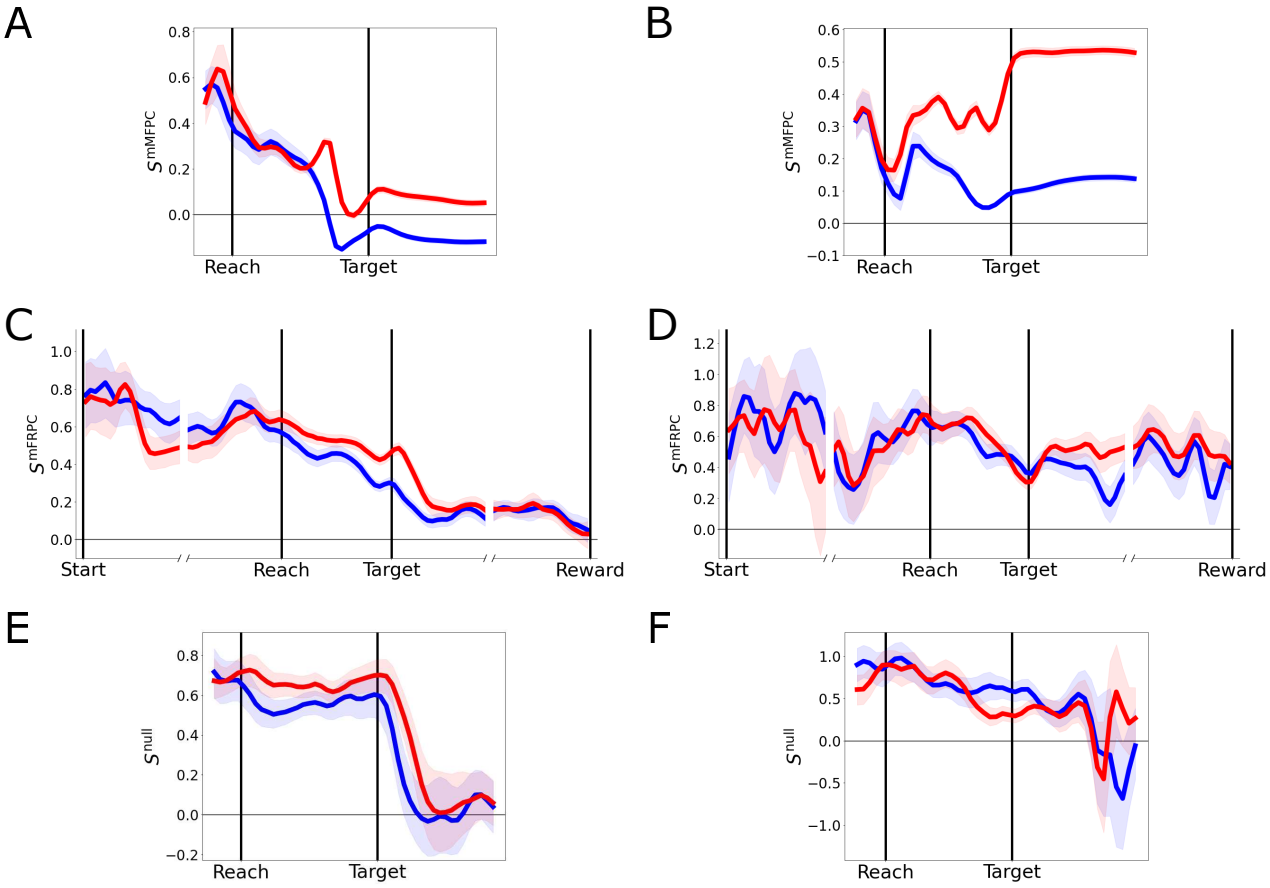

Figure 4.40: **Affordance shifts S^{mMFPC}, S^{mFRPC} and S^{null} for the Object Presence Experiment.** A, C, E: Monkey R. B, D, F Monkey T. A, B: affordance shifts S^{mMFPC} calculated in 99% mMF PC space. C, D: affordance shifts S^{mFRPC} calculated in 99% mFR PC space. E, F: affordance shifts S^{null} calculated in 99% the null space. Blue: shifts relative to Power Grasp, Red: shifts relative to Pinch Grasp. Shaded 95% confidence intervals are bootstrap intervals, trials resampled 10000 times.

starting posture that was more similar to that observed during power and pinch grasps, relative to the starting posture for No-Object Reach trials. In Monkey R, mMF PC pro-affordance bias fell over the course of the reach, leading to a small pro-affordance bias relative to Pinch Grasp and a small anti-affordance bias relative to Power Grasp during the target hold period. For Monkey T, pro-affordance bias remained high relative to Pinch Grasp throughout the reach and especially the target hold period, while a small consistent pro-affordance bias was observed relative to Power Grasp. This likely reflects the hand posture used by Monkey T during the hold period of Object Reach trials — the hand was held with the fingers relatively closed during Object Reach trials (more similar to the hand posture observed for Pinch Grasps) while the hand was held with fingers relatively straight during No-Object Reach trials.

In the full mFR PC space, pro-affordance biases were observed for both subjects relative to both grasps throughout the entire trial periods, though this pro-affordance bias was small in magnitude during the late target hold period in Monkey R. This pro-affordance bias was observed even at the start of trials, indicating that object presence could effect even background M1 activity, driving it toward the activity observed during grasping trial blocks. This is notable as Object Reach trials were presented in a separate block from Power Grasp and Pinch Grasp trials (see Section 3.2.1).

In the null space activity, pro-affordance bias was observed for both subjects during the early movement period, but decreased sharply after target acquisition, with S^{null} often not significantly different from zero during the target hold period. As the null space activity was the component of neural activity from which mMF PC scores could not be decoded, this activity likely contained the object presence encoding signal described in Section 4.4. The S^{null} results suggest that this object presence signal also served to drive neural activity toward grasp-associated neural activity, but only during the early movement period and not during the target hold period. Similar temporal shifts in M1 activity have been observed related to the different phases of reaching movements [405, 438] or dynamic vs. postural control [407].

The occurrence of pro-affordance bias in mMF PC scores, mFR PC scores and null space neural activity supports, but does not definitively confirm, the hypothesis that the

motor representations of the grasps afforded by the object were automatically activated in the presence of the object, even when it was not grasped. These results and other possible interpretations are discussed further in Chapter 8.

In summary, the results presented in this chapter suggest that strong contextual object presence encoding exists in M1. While the behaviors were similar for reaches made toward an object or without an object (Section 4.2), neural activity was markedly different in the two conditions (Section 4.3). This difference in neural activity was not accounted for by linear relation to MFs, and thus constituted contextual encoding of object presence (Section 4.4). This object presence encoding signal tended to have an interactive effect with MF encoding (Section 4.5). Object presence encoding had a detrimental effect on the performance of simple linear decoders trained in one context and tested in another, which could be mostly mitigated by a context-detecting decoder (Section 4.6). Finally, the object presence encoding signal was found to carry information about the affordances of the object, biasing behavior and neural activity toward the behavior and neural activity associated with actions afforded by the object, especially during the preparatory and early movement phases.

5.0 Results — Grip Affordance Experiment — M1

Results from the Object Presence Experiment, described in Chapter 4, reveal that behavior and neural activity significantly differed for reaches made with or without an object present, and that neural activity in M1 encoded the contextual factor of whether a single object was present or absent. In the Grip Affordance Experiment (this chapter) and the Use Affordance Experiment (Chapter 6) we seek to determine if behavior and neural activity are different for grasps made on objects with different identities, and if M1 neural activity further encodes object context related to the identity of different grasped objects.

The Grip Affordance Experiment was designed to determine how behavior and neural activity differ when the same grasps are performed on objects with different perceived or learned grip affordances.

Perceived grip affordances are those grips which could be used to grasp an object, based solely on the object's perceived size and shape. For instance, a handrail affords a power grip, whereas a credit card affords a pinch grip. It is often possible for an object to afford multiple grips. For instance, a pair of scissors affords both a modified pinch grip, with the thumb and index fingers inserted in the handles of the scissors, or a power grip, with the fingers wrapped around the closed blade portion of the scissors.

Learned grip affordances are those grips which have been learned to be associated with a certain object through use. For instance, a pen and a laser pointer have different learned grip affordances. The pen is most often associated with a tripod grip near the writing tip, whereas the laser pointer is most often associated with a power grip around the shaft, though both objects are shaped similarly and could be grasped both ways.

In the Grip Affordance Experiment, we ask whether behavior and M1 neural activity changes depending on the differences in perceived or learned grip affordances between objects, even when the objects are grasped in the same way. Further, we ask whether M1 neural activity encodes these perceived and learned grip affordances beyond the encoding of behavioral differences.

For this experiment, five objects were designed which afforded power grips or pinch grips. These objects had different perceived or learned grip affordances. Subjects grasped the different objects while kinematics, muscle activity and neural activity were recorded. In this section, results are presented for Monkey R, Monkey I and both hemispheres of Monkey T, from which M1 data were recorded. Neural data were always recorded from the hemisphere contralateral to the hand used in the task. Results for this experiment for PMV and AIP in Monkey T are presented in Chapter 7.

The main findings of this chapter are summarized as follows. Subjects performed power grasps and pinch grasps in different object contexts (objects with different perceived or learned grip affordances). The behaviors for same-grasp conditions were similar in terms of the recorded movement features (MFs), but differed significantly for different objects, despite the grasped portions of the objects being identical. Neural activity differentiated same-grasp conditions to a relatively greater extent than the MFs. The separation between same-grasp conditions in individual unit firing rates (FRs) and population neural activity was not fully accounted for by fixed linear tuning to MFs, indicating the presence of contextual grip affordance encoding in M1. The grip affordance encoding was small in magnitude. Grip affordances were found to be directly encoded in individual unit FRs in some cases, and encoded in an interactive manner with MF encoding in other cases. The grip affordance encoding signal did not substantially detract from the ability to decode MFs from neural activity using a simple linear model. Weak evidence suggested that during the preparatory period, the presence of perceived and learned grip affordances may bias neural activity toward activity associated with the unused afforded grip, suggesting weak automatic activation of the representation of the afforded grip.

Section 5.1 contains a detailed description of each subjects' behavior during the different task conditions. The behavior is described in terms of the observed movement features (MFs), comprised of 22 joint angles and joint angular velocities of the arm, wrist and fingers, 3D hand position and hand velocity, and EMG from eight muscle groups. Section 5.2 characterizes the small but significant differences in the MFs between the different task conditions. Section 5.3 describes the single unit and population level M1 neural firing rate (FR) responses recorded during the experiment, highlighting the

differences in neural activity between same-grasp conditions. Section 5.4 concerns the relation between the M1 FRs and the MFs, with specific focus on the evidence for contextual grip affordance encoding in M1, defined as neural modulation beyond that which can be accounted for by fixed linear tuning to MFs. Section 5.5 compares regression models with direct or interactive encoding of grip affordance context information. Section 5.6 characterizes the impact of the grip affordance encoding signal on MF decoding accuracy. Finally, section 5.7 explores the possibility that the grip affordance encoding signal carries information about the grips afforded by the different objects.

5.1 Behavioral Results of the Grip Affordance Experiment

Each subject performed the following six task conditions, in which Power Grasps or Pinch Grasps were performed on five different objects.

1. Power Grasp, Simple Power Object
2. Pinch Grasp, Simple Pinch Object
3. Power Grasp, Compound Power Object
4. Pinch Grasp, Compound Pinch Object
5. Power Grasp, Compound Multi-Grasp Object
6. Pinch Grasp, Compound Multi-Grasp Object

Monkey R and Monkey T (both hemispheres) performed 140 repetitions of each condition, for a total of 840 trials. Monkey I performed 130 repetitions of each condition, for a total of 780 trials.

Subjects grasped five different objects that were specifically designed for the Grip Affordance Experiment. These objects are shown in Figure 5.1.

The two "simple objects" (Simple Power Object, Figure 5.1 A; Simple Pinch Object, Figure 5.1 C) had only one perceived and one learned grip affordance each. The two "compound single-grip objects" both had two perceived grip affordances (the compound objects *could* be grasped with a power grip or a pinch grip), but only one learned

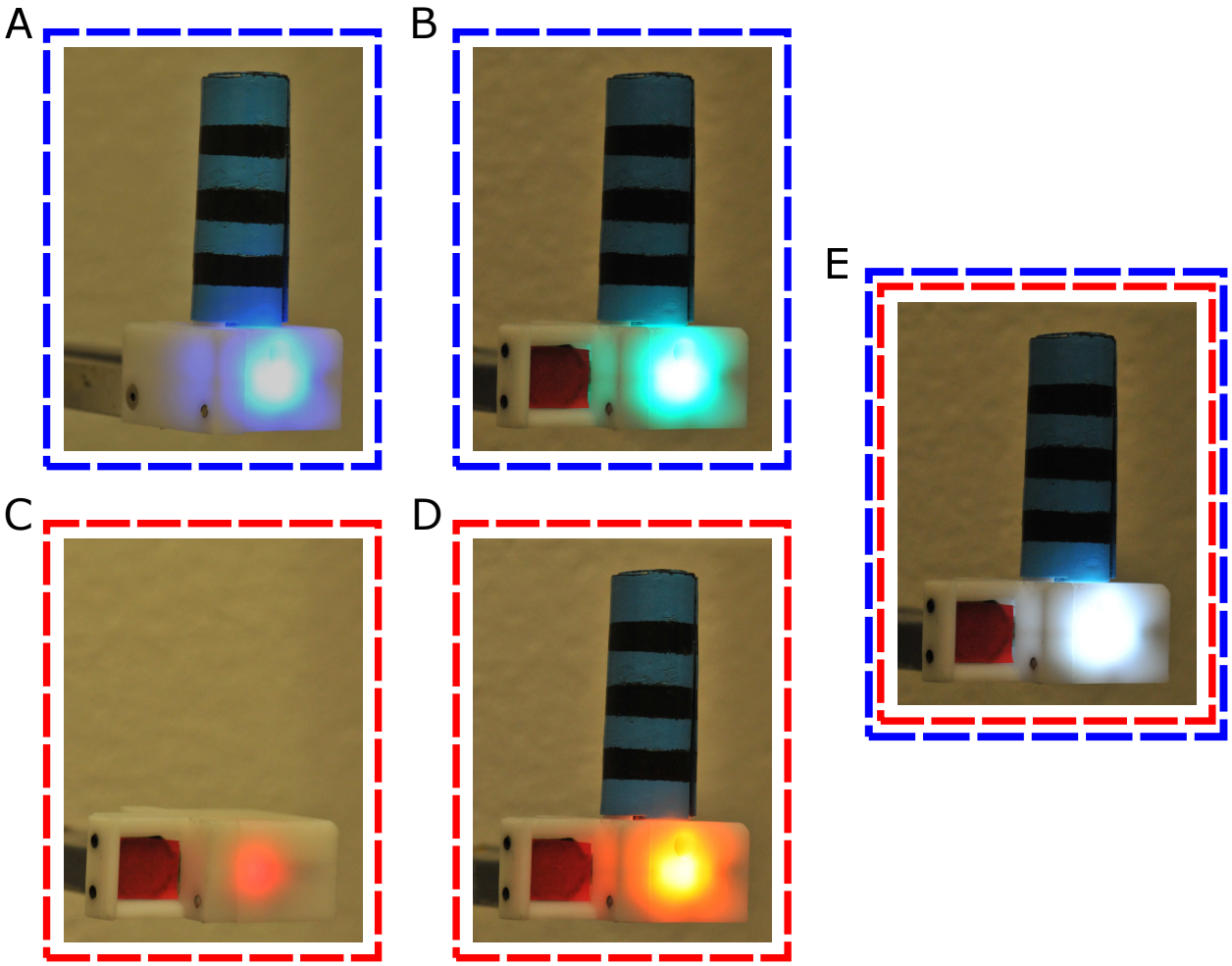

Figure 5.1: **Objects used in the Grip Affordance Experiment.** A: Simple Power Object. B: Simple Pinch Object. C: Compound Power Object. D: Compound Pinch Object. E: Compound Multi-Grasp Object. Blue dashed rectangles denote objects that were grasped with a power grip. Red dashed rectangles denote objects that were grasped with a power grip. The Compound Multi-Grasp Object (E) was grasped with both grips.

affordance each. The learned grip affordances of the compound single-grip objects were enforced through training; the Compound Power Object (Figure 5.1 B) was only ever grasped with a power grip, and the Compound Pinch Object (Figure 5.1 D) was only ever grasped with a pinch grip. The final object the "compound multi-grasp object" (Figure 5.1 E) had two perceived and two learned grip affordances. The compound multi-grasp object was grasped with either a power grip or a pinch grip, presented in an interleaved pseudorandom fashion.

The objects were designed to elicit identical grasps of each type in the different object conditions. To accomplish this, the objects were constructed with a modular design, allowing the same graspable portions of the objects to be reused for the different objects. The graspable portions of the objects were instrumented with force sensors to detect grasps (see Section A.2). The objects were differentiated using colored LEDs (Figure 5.1). Objects were presented in blocks, all in the same spatial location in front of the subject. The objects were changed by the experimenter between each block, out of view of the subject.

Trial structure was similar to that employed in the Object Presence Experiment. The subject began each trial by pressing the start button near its waist. At this time, the required grasp was cued with a colored indicator displayed on the feedback monitor. After 800-1200 ms, a go cue was presented on the monitor and the subject reached forward to grasp the object. For Power Grasp conditions, the subject grasped the upper cylindrical blue and black striped portion of the object by opposing digits 2–5 and the palm. For Pinch Grasp conditions, the subject grasped the red tab on the side of the object by opposing the thumb and digit 2. The subject was required to maintain the grasp for 800–1200 ms to receive a reward. Trials were automatically aborted if any inappropriate force sensor was activated, or if the grasp was not made within 2000 ms of the go cue. See Section 3.2 for more details of task timing and visual feedback.

For all conditions, the Reach Start time was defined as the time point of the first kinematic sample in which the hand velocity exceeded 1 mm/s for a sustained period. The Target Contact time was defined by the initial uptick of the appropriate force sensors. See Section A.4.5 for more details of data alignment to task epochs.

The subjects exhibited somewhat different reach times (the time between Reach Start and Target Contact) for different grasps, and reach times varied between trials. Power Grasp reach times were shorter than Pinch Grasp reach times on average. In order to compare across conditions and across trials, trials were resampled at variable rates within the reach period to produce an equal number of samples for each trial (see Section A.4.5 for details).

Trial-averaged hand positions and hand velocities are shown in Figure 5.2 for Monkey R. Positions were calculated relative to the hand position on the start button. The trial-averaged values were calculated by averaging the values at each time point across all 140 trials for each condition. The hand position was defined as the average x-y-z coordinates of markers HAN1, HAN2, HAN3 and HAN4 (see Section A.4.1). The coordinate axes corresponded to the workspace as follows: positive X pointed to the right of the subject, positive Y pointed forward from the subject and positive Z pointed upward.

The hand trajectories within each grasp type were very similar for the different objects. Power Grasp final hand positions were higher than Pinch Grasp final hand positions owing to the different locations of the graspable portions of the objects (Figure 5.1). Moderate overshoot was observed in the hand z-velocity, as the subject first raised its hand off of the start button and then lowered it into the power grasp position. Slightly higher velocities were observed for Power Grasps vs. Pinch Grasps. The hand z-position was slightly higher for the Power Grasps made on the compound objects vs. the Simple Power Object, as the hand was raised likely in order to avoid contacting the pinch grasp tab on the compound objects.

Trial-averaged joint angle trajectories of the arm and fingers are shown in Figures 5.3 and 5.4 for Monkey R. Details of the calculations of these joint angles are presented in Section A.4.1.

Arm and wrist joint angles were largely similar within grip types for the different objects. Some variance was observed in the elbow flexion, wrist abduction and wrist rotation angles within Pinch Grasps, indicating that Monkey R performed Pinch Grasps with a slightly different arm posture for compound objects vs. the Simple Pinch Object.

Monkey R exhibited slightly different starting hand postures for the various object conditions. These differences were small but consistent, with starting hand postures for the

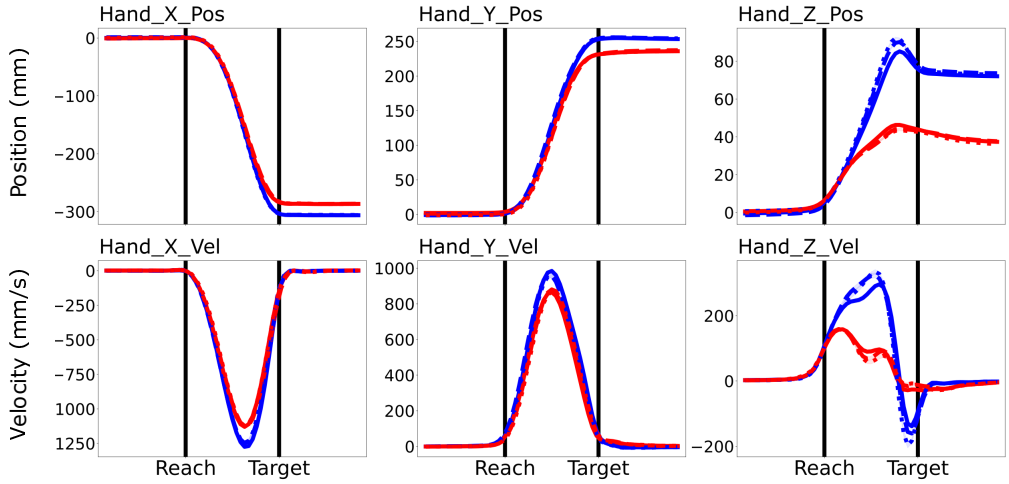

Figure 5.2: **Trial-averaged hand positions and velocities for Monkey R in the Grip Affordance Experiment.** Hand positions are relative to the mean hand position 400 ms before Reach Start. Blue: Power Grasps. Red: Pinch Grasps. Solid lines: simple objects. Dashed lines: compound single-grip objects. Dotted lines: compound multi-grasp object.

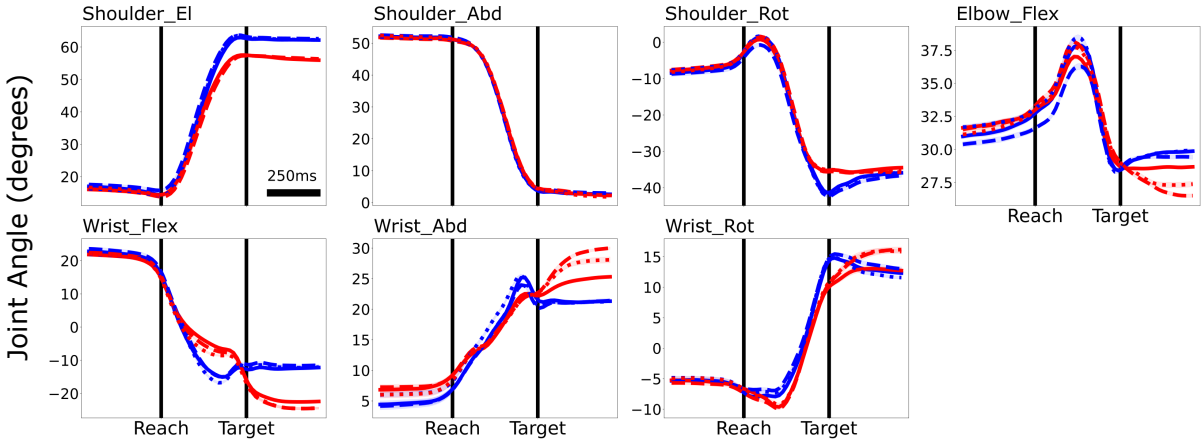

Figure 5.3: **Trial-averaged arm joint angle trajectories for Monkey R in the Grip Affordance Experiment.** Blue: Power Grasps. Red: Pinch Grasps. Solid lines: simple objects. Dashed lines: compound single-grip objects. Dotted lines: compound multi-grasp object. El: elevation, Abd: abduction, Rot: rotation, Flex: flexion.

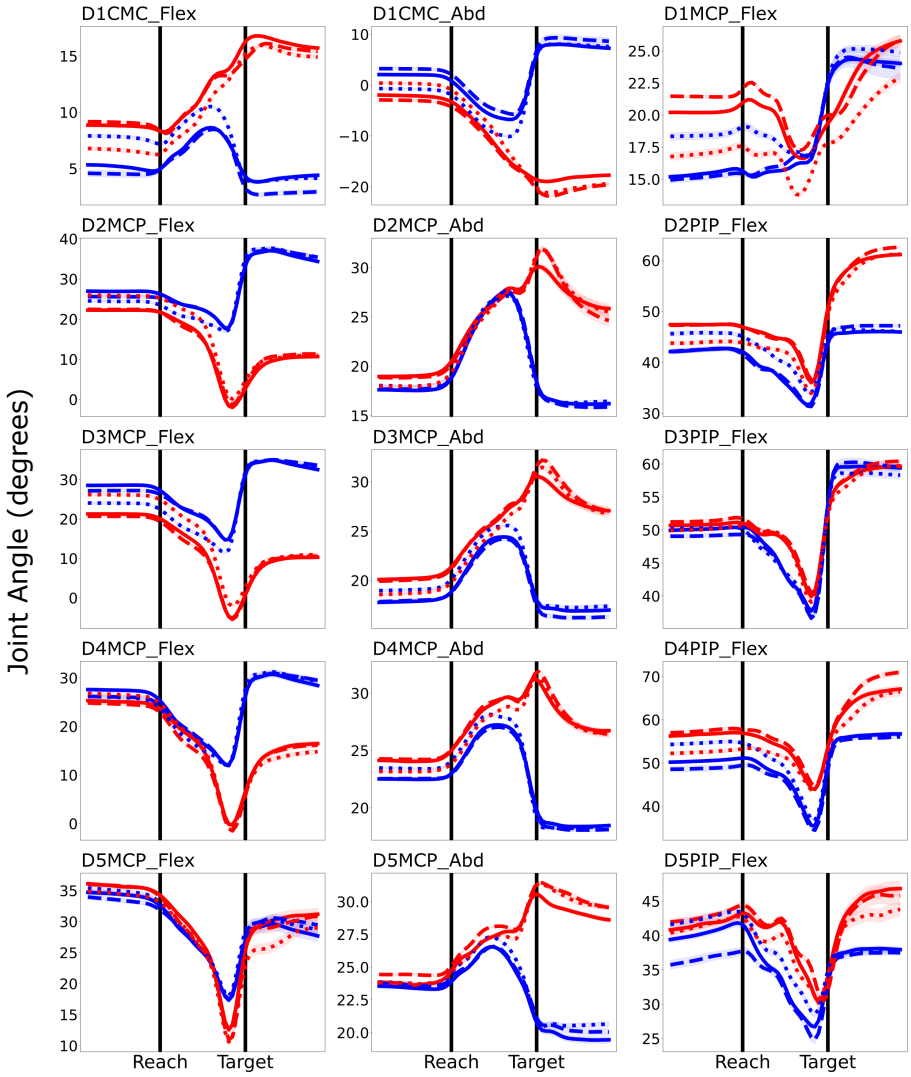

Figure 5.4: **Trial-averaged finger joint angle trajectories for Monkey R in the Grip Affordance Experiment.** Blue: Power Grasps. Red: Pinch Grasps. Solid lines: simple objects. Dashed lines: compound single-grip objects. Dotted lines: compound multi-grasp object. CMC: carpometacarpal joint, MCP: metacarpophalangeal joint, PIP: proximal interphalangeal joint. Flex: flexion, Abd: abduction.

Compound Multi-Grasp object (Figure 5.4 dotted lines) laying intermediate to the hand postures observed for the simple and compound single-grip objects. Despite this, final hand postures were largely consistent within grip types across the objects, with some variability observed in final Pinch Grasp hand positions across objects.

Trial-averaged muscle activity recorded from surface EMG electrodes are shown in Figure 5.5 for Monkey R. Details of surface EMG data collection are presented in Section A.4.2.

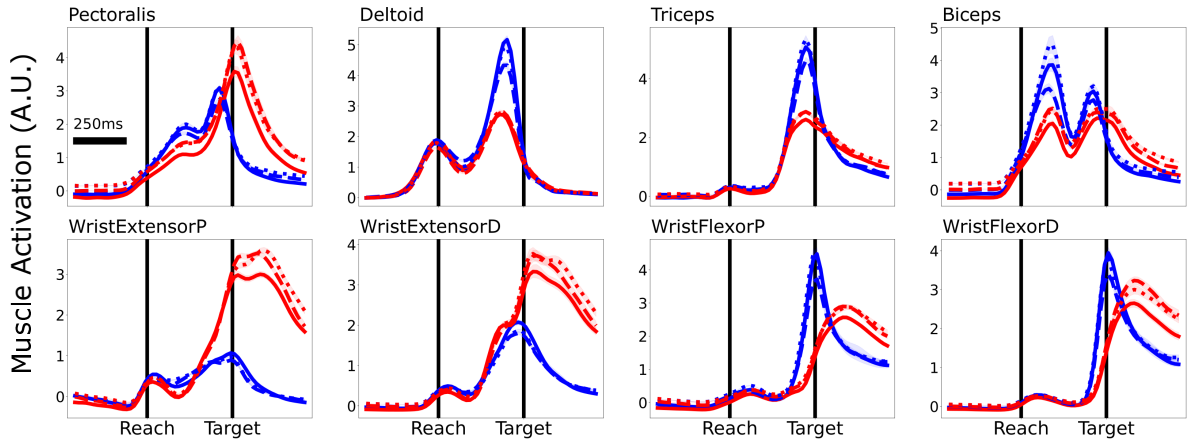

Figure 5.5: **Trial-averaged EMG muscle activations in the Grip Affordance Experiment.** EMG values are relative to the mean EMG values 400 ms before Reach Start. Blue: Power Grasps. Red: Pinch Grasps. Solid lines: simple objects. Dashed lines: compound single-grip objects. Dotted lines: compound multi-grasp object. P: proximal, D: distal.

While EMGs were mostly consistent withing grip types across the different objects, some variability was observed. Slightly higher EMG was observed in the pectoralis, biceps, triceps and forearm muscles for Pinch Grasps made on the compound objects vs. the Simple Pinch Object. In addition, some across-object variability was observed in the pectoralis, deltoid, triceps, biceps and wrist flexor muscles within Power Grasps.

In general, patterns of variability in the MFs were qualitatively consistent across all of the subjects. In all subjects, all Power Grasps were highly separable from all Pinch Grasps across the majority of MFs. Subjects often displayed a slightly different posture when pressing the start button in the different object conditions. Some relatively small variability was observed when the same grasp was made on different objects, present only in some MFs. This variability was observed both within Power Grasps and within Pinch Grasps. Such within-grasp variability was unexpected, as the grasped portions of the objects were identical between the different objects. In fact, the same physical pieces were used to construct the different objects. The next section contains direct comparisons of MFs in the different conditions, to characterize the size of the grip-type dependent and object-dependent variability in MFs.

5.2 Movement Feature Differences Across Conditions

The goal of the experimental design of the Grip Affordance Experiment was elicit very similar grasps on objects with different identities, as defined by their perceived and learned grip affordances. Despite the grasped portions of the objects being identical in shape, the objects with different overall perceived and learned grip affordances were grasped slightly differently. The analyses in this section describe the differences observed in MFs for the various conditions of the Grip Affordance Experiment.

To measure the differences in MFs between different conditions, the Euclidean distance between each pair of conditions was calculated at each time point in subsets of MFs. The MF subsets were the same as in Chapter 4, and inter-condition distances in the MF subsets were calculated according to Equation 4.1. The resulting MF subset distances are shown in 5.6 for Monkey R.

Across all MF subsets, the mean distance between Power Grasps and Pinch Grasps (Figure 5.6, purple trace) was large compared to the distances between the same grasps made on different objects. Subjects had slightly different hand trajectories when making the same grasp on different objects, partially due to the higher hand z-position observed for compound

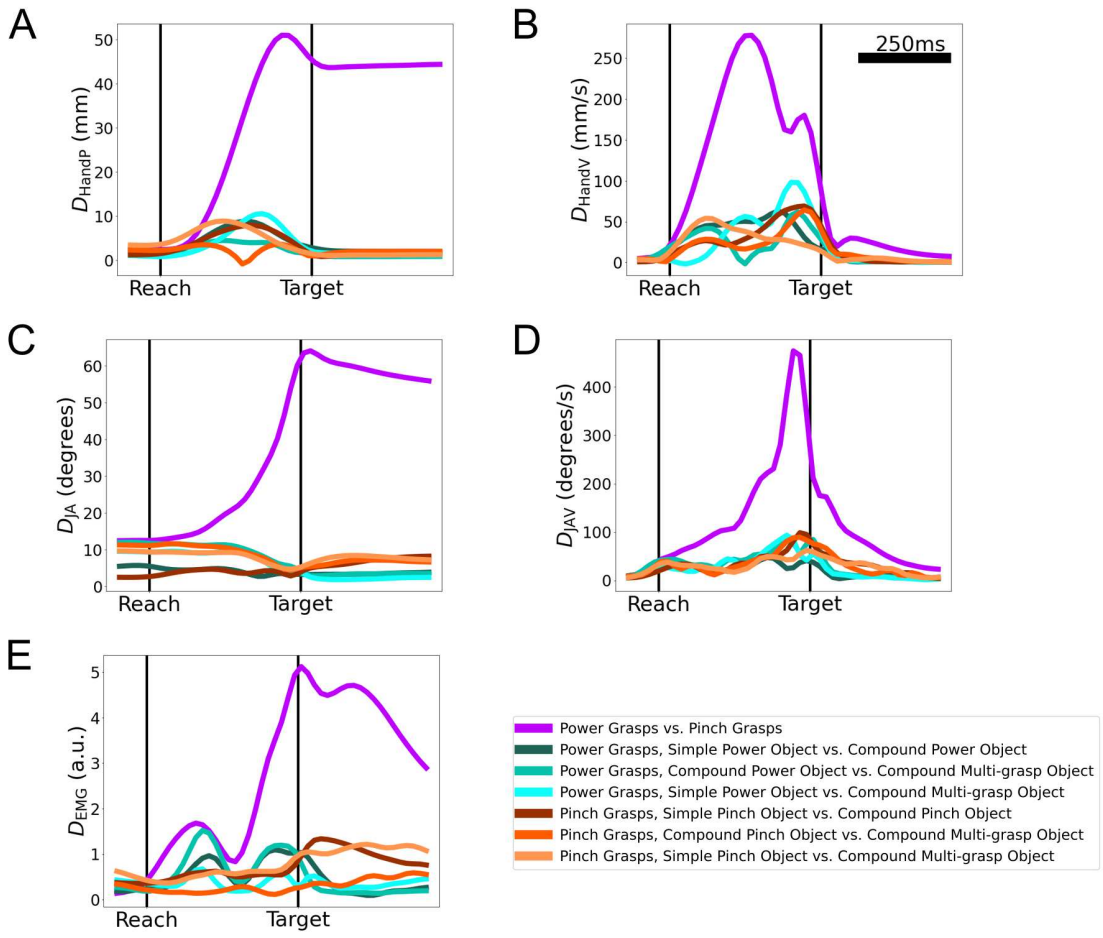

Figure 5.6: **Inter-condition distances in MF subsets for the Grip Affordance Experiment, Monkey R.** A: distances in hand position. B: distances in hand velocity. C: distances in joint angles. D: distances in joint angular velocities. E: distances in EMGs. Purple: Power Grasps vs. Pinch Grasps. Turquoise colors: Power Grasps on different objects. Orange colors: Pinch Grasps on different objects. Dark turquoise and orange: objects differed in perceived affordances. Medium turquoise and orange: objects differed in learned affordances. Light turquoise and orange: objects differed in perceived and learned affordances.

objects vs. the Simple Power Object. Many object conditions were separable in joint angles even before movement, reflecting the variation in hand postures on the start button for the different experiment blocks. Variability between Pinch Grasps made on different objects (Figure 5.6, orange traces) was more evident during the target hold period, especially in the joint angles and EMG. In contrast, the variability between Power Grasps made on different objects (Figure 5.6, turquoise traces), occurred mostly during the reach.

In order to characterize inter-condition distances across all of the MFs together, the 58 trial-averaged, centered MFs were combined in a dimensionally-reduced form using Principal Components Analysis (PCA) with varimax rotation, as in Chapter 4. For Monkey R, 19 PCs explained 99% of the variance in trial-averaged, centered MFs. The first 12 MF VPC scores and VPC loadings are shown in Figure 5.7, with each condition plotted separately. VPCs are sorted by amount of variance explained.

The first VPC accounted for 31.4% of variance in the trial-averaged, centered MFs. Any other single VPC accounted for $< 7.5\%$ of variance. The first VPC characterized the combination of hand positions, joint angles and EMGs which best accounted for the sustained difference in Power Grasps and Pinch Grasps over the course of the movements. Many of the higher VPCs (VPCs 2, 3, 4, 5, and 10) related to combinations of joint angular velocities and EMGs which captured the dynamic variability peaking just before object contact, again mostly relating to separation between all Power Grasps and all Pinch Grasps.

While small compared to the separation between all Power Grasps and all Pinch Grasps, some within-grasp separability was observed in the VPCs (comparing conditions in which the same grasp was made on different objects). One source of this within-grasp separability was the difference in starting hand postures for the different conditions, as captured by VPCs 1, 6 and 7. Within-grasp separability could also be observed in VPCs with high loadings on hand velocities (VPCS 11 and 12), due to the different reach speeds observed for the different objects. Within-grasp separability was also present in VPC 9, which largely related to the EMGs and some joint angles. Notable separability between Pinch Grasps on different objects was observed in VPC 7, which had high loading on digit 5 MCP flexion, and VPC 8, which had high loadings on wrist abduction and rotation, highlighting the slightly different hand and wrist postures observed for Pinch Grasps on the different objects.

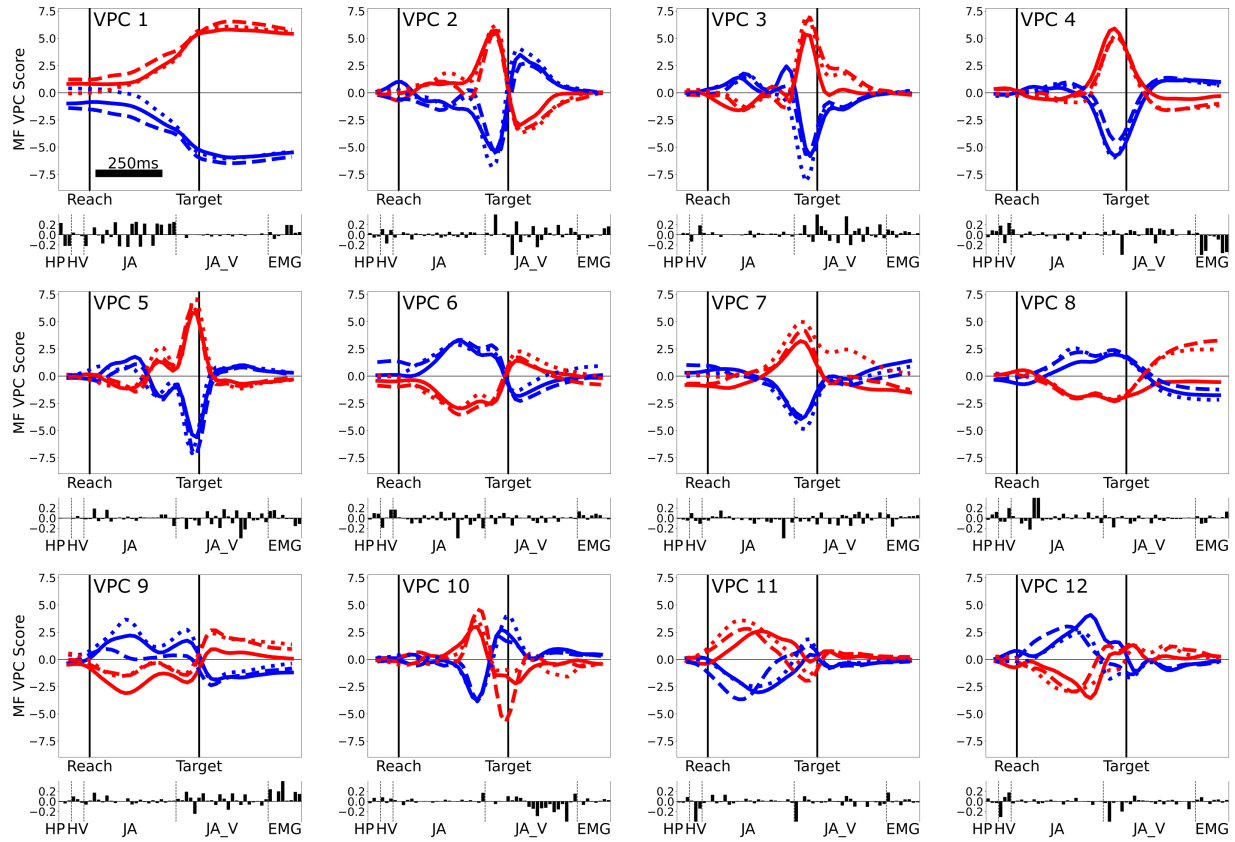

Figure 5.7: **Varimax PCA of the MFs in the Grip Affordance Experiment, Monkey R.** Trial-averaged scores in the first 12 VPCs. Blue: Power Grasps. Red: Pinch Grasps. Solid lines: simple objects. Dashed lines: compound single-grip objects. Dotted lines: compound multi-grasp object. Bar graph insets below each VPC score plot denote the loading vector corresponding to the VPC.

To directly compare the inter-condition separation across the MF PCs, the Euclidean distance in MF PC space, D_{MFPC}, was calculated for each pair of conditions, as in Equation 4.2 in Section 4.1. The MF PC distances D_{MFPC} are shown in Figure 5.8 and the time-averaged MF PC distances $\overline{D}_{\mathrm{MFPC}}$ are shown in Figure 5.9 for all subjects.

In general, the largest distances were observed between Power Grasps and Pinch Grasps (purple trace). This distance peaked around the time of target contact and maintained a moderate level during the target hold period. The peak around target contact was mostly due to differences in joint angular velocities, which diverged maximally at that time.

Condition pairs for which the same grasp was made on different objects were separable in MF PC space, though the distances between these same-grip-type conditions were generally much smaller than those observed between Power Grasps and Pinch Grasps. Despite being relatively small, these differences were significantly larger than expected within-condition variability in every case (Figure 5.9 stars). These distances reflected the small differences in the hand paths for reaches to the different objects, the small differences in hand postures used to grasp the different objects, and the differences observed in EMGs when grasping different objects. The exact patterns of within-grasp separation varied somewhat between subjects. Though small, these differences were notable because the graspable portions were physically the same across objects. Based on $\overline{D}_{\mathrm{MFPC}}$ values, the ratio of average Power Grasp vs. Pinch Grasp difference (Figure 5.9, purple bar) to average within-grasp differences (Figure 5.9, turquoise and orange bars) was 3.60, 4.33, 5.86, 4.40 for Monkey R, Monkey I, Monkey T right hand and Monkey T left hand, respectively. That is, Power Grasps evoked largely different hand posture and muscle activity compared to Pinch Grasps. Power Grasps (and Pinch Grasps) executed on the different objects were very similar in terms of behavior, but small, significant differences were observed.

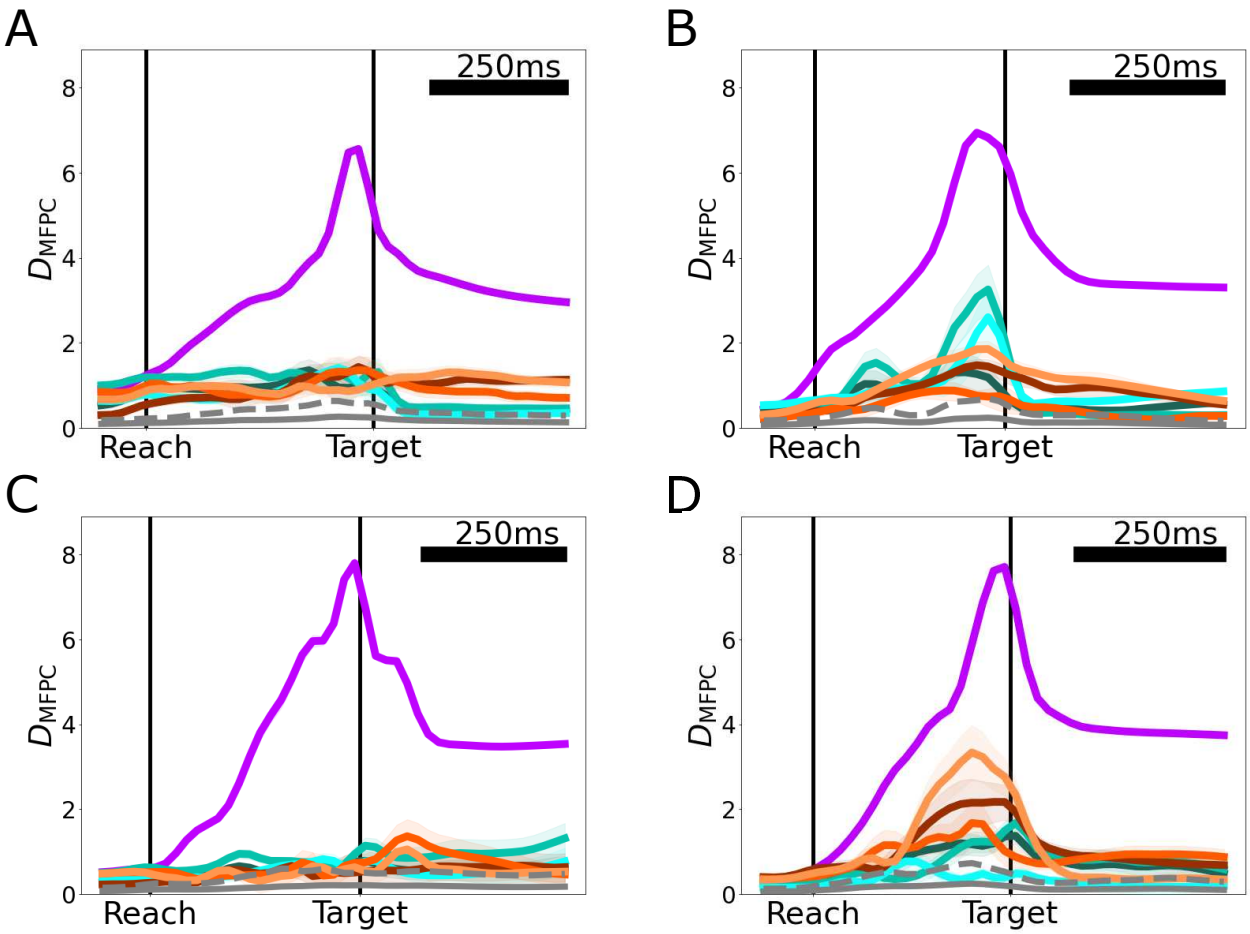

Figure 5.8: **Scaled Euclidean inter-condition distances between pairs of trial-averaged MF PC scores in the Grip Affordance Experiment.** Distances were calculated in the 99% MF PC space. A: Monkey R. B: Monkey I. C: Monkey T right hand. D: Monkey T left hand. Purple: Power Grasps vs. Pinch Grasps. Turquoise colors: Power Grasps on different objects. Orange colors: Pinch Grasps on different objects. Dark turquoise and orange: objects differed in perceived affordances. Medium turquoise and orange: objects differed in learned affordances. Light turquoise and orange: objects differed in perceived and learned affordances. Gray: mean and upper 95% one-sided confidence interval of within-condition variability. 95% confidence intervals are bootstrap intervals, trials resampled 10000 times.

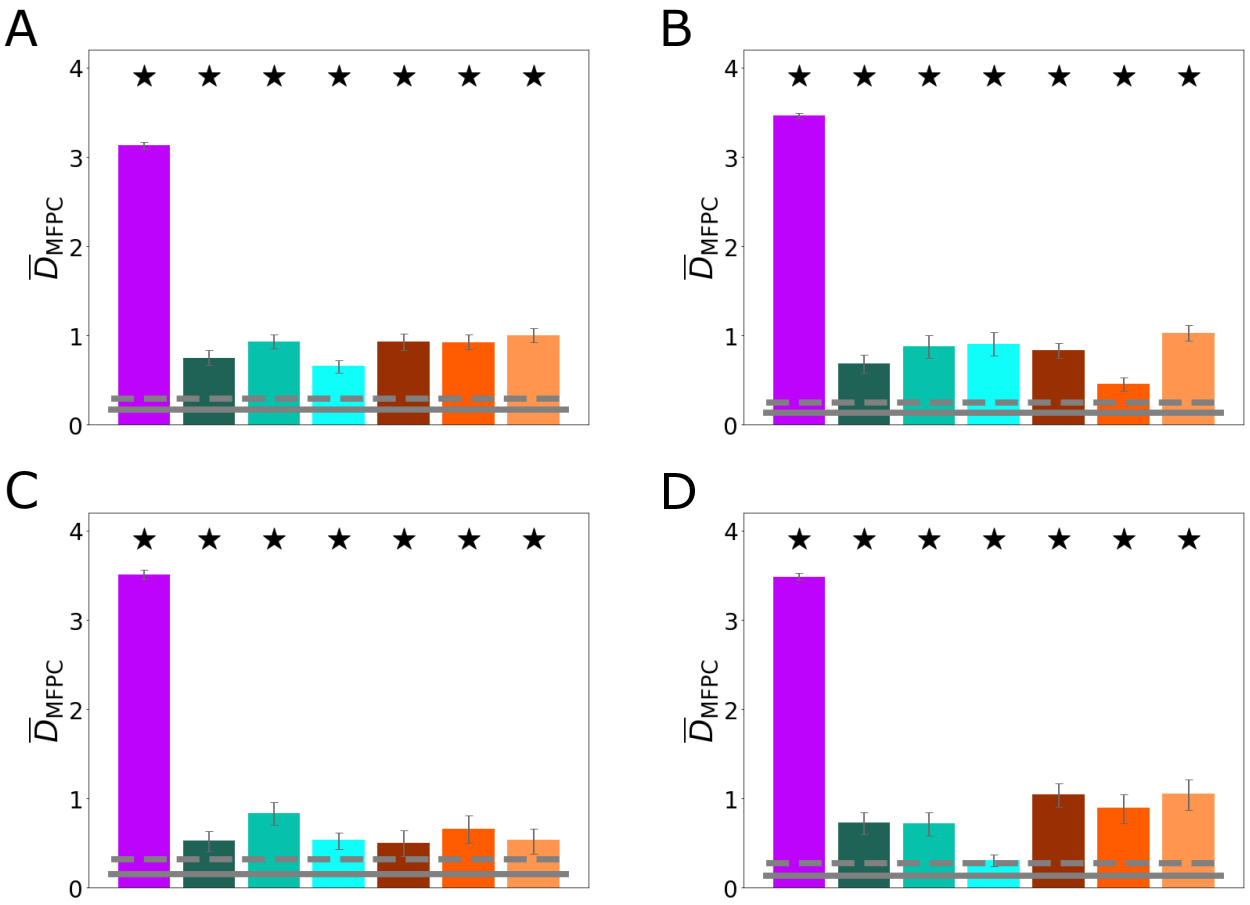

Figure 5.9: **Mean scaled Euclidean inter-condition distances between pairs of trial-averaged MF PC scores in the Grip Affordance Experiment.** Distances were calculated in the 99% MF PC space and averaged over time. A: Monkey R. B: Monkey I. C: Monkey T right hand. D: Monkey T left hand. Star: $\overline{D}_{\mathrm{MFPC},i,j}$ significantly greater than within condition $\overline{D}_{\mathrm{MFPC}}$ variability ($p < 0.05$, one-sided bootstrap interval). Purple: Power Grasps vs. Pinch Grasps. Turquoise colors: Power Grasps on different objects. Orange colors: Pinch Grasps on different objects. Dark turquoise and orange: objects differed in perceived affordances. Medium turquoise and orange: objects differed in learned affordances. Light turquoise and orange: objects differed in perceived and learned affordances. Gray: mean and upper 95% one-sided confidence interval of within-condition variability. 95% confidence intervals are bootstrap intervals, trials resampled 10000 times.

5.3 M1 Neural Activity Differences Across Conditions

This section describes the neural activity in M1 recorded during the Grip Affordance Experiment. M1 neural activity was highly divergent when comparing Power Grasps to Pinch Grasps. Some variability was also observed when comparing conditions in which the same grasp was made on different objects in both individual unit FRs and population activity. These within-grasp distances were relatively larger than the corresponding within-grasp differences in MFs.

After excluding channels with crosstalk and low FR units (see Section A.4.4), a total of 108, 97, 31 and 57 units were analyzed from M1 in Monkey R, Monkey I, Monkey T left hemisphere and Monkey T right hemisphere, respectively. These units consisted of both multi-unit spiking activity and well-isolated single-units.

The FRs of individual units showed a range of different activity patterns. The trial-averaged FRs of four example units are plotted in Figure 5.10.

Monkey R Unit 44.1 (Figure 5.10 A) represents a unit which differentiated only between grip types. This unit had the same FR profile for all Pinch Grasps regardless of the object being grasped. The same held true for Power Grasps, save for two brief periods where Power Grasps for the compound-multigrasp object evoked slightly different FRs vs. Power Grasps on the other objects.

Panels B-D of Figure 5.10 show units which displayed different mean FRs for Power Grasps and Pinch Grasps in general, and also different mean FRs between different object conditions, even when the required grasp was the same for the different objects. Monkey R Unit 86.3 separated objects within power grasps during the reach and grasp periods. Monkey T left hemisphere Unit 14.2 separated objects within Pinch Grasps during the reach and around the time of target contact. Monkey I Unit 87.1 separated objects within both grip types during the pre-movement period and during the reach. These three units were representative of a pattern that was observed in many individual units: Power Grasps and Pinch Grasps evoked generally different FR profiles, with object identity modulating one or both underlying grasp-specific profiles during certain restricted time periods.

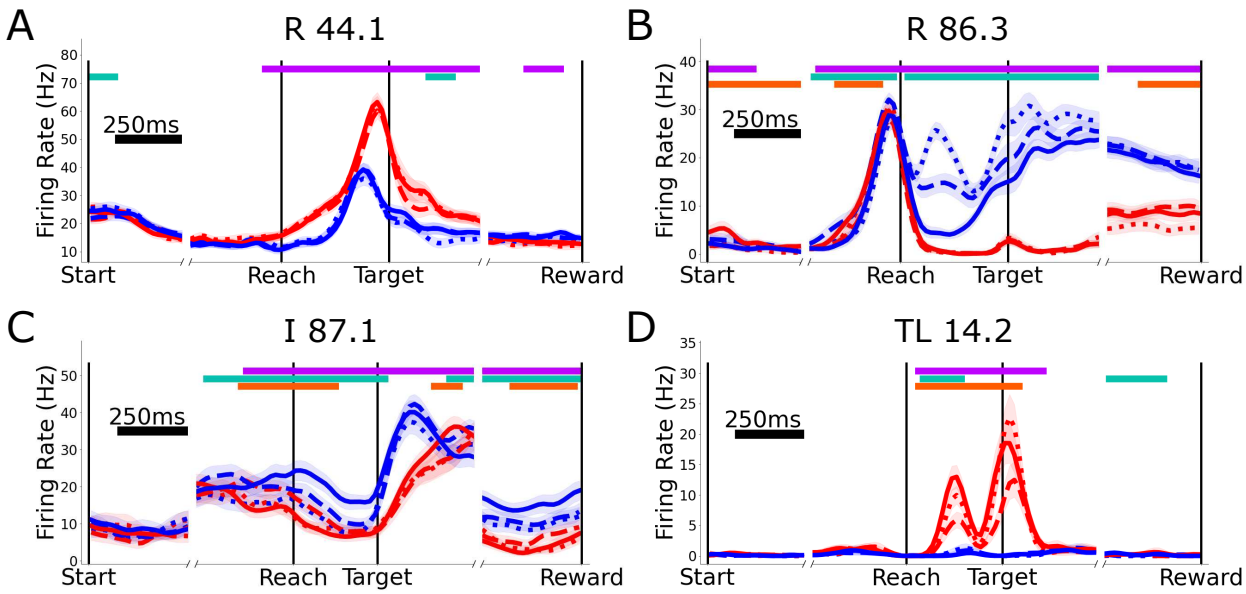

Figure 5.10: **Trial-averaged FRs of four example units during the Grip Affordance Experiment.** A: Monkey R Unit 44.1. B: Monkey R Unit 86.1. C: Monkey I Unit 87.1, D: Monkey T left hemisphere Unit 14.2. Blue: Power Grasp, Red: Pinch Grasp. Solid lines: simple objects. Dashed lines: compound single-grip objects. Dotted lines: compound multi-grasp object. Purple horizontal bars: at least one Power Grasp vs. Pinch Grasp pair significantly different. Turquoise horizontal bars: at least one pair of Power Grasps on different objects significantly different. Orange horizontal bars: at least one pair of Pinch Grasps made on different objects (permutation test of difference in mean FRs, n=10000, $p < 0.01$).

To determine the prevalence of separability of conditions in the FRs of individual units, permutation tests for a difference in mean FRs (n=10000, $p < 0.01$) were performed at each time point between each pair of conditions for each unit. The percentage of units displaying significant modulation (significantly different mean FRs) for each pair of conditions is shown in Figure 5.11 for all subjects.

For Monkey R and Monkey T right hemisphere (Figure 5.11 A and D), the number of neurons with concurrent significant modulations between Power Grasps and Pinch Grasps rose steadily during the pre-movement period, peaking around target contact. For Monkey T left hemisphere (Figure 5.11 C), this peak occurred earlier, in the middle of the reach, whereas for Monkey I (Figure 5.11 B), the peak occurred later, after target contact. The number of neurons concurrently modulated for any within-grasp condition pair was relatively more consistent across the timecourse of the trials, and reached a lower peak of only about 30% for any single within-grasp condition pair. Monkey T left hemisphere had overall lower incidence of within-grasp modulation.

Figure 5.11 portrays the number of neurons with concurrent significant modulation for each condition pair. To visualize the number of individual units with any significant modulation over the whole timecourse of the trial, Venn diagrams were constructed which tabulated the occurrence of significant inter-condition modulation for at least 100 ms (5 timepoints). These diagrams are shown for all subjects in Figure 5.12. To visualize the number of individual units showing sustained tuning, further diagrams were constructed which tabulate instances of inter-condition modulation which lasted at least 500 ms (25 timepoints). These diagrams are shown in Figure 5.13.

For all subjects, a majority of units were significantly modulated for at least one same-grasp condition pair (conditions for which the same grasp was made on different objects) for at least 100 ms. Relatively fewer units showed sustained significant modulation for same-grasp condition pairs, compared to the number of units that showed significant modulation between Power Grasps and Pinch Grasps (Figures 5.12 and 5.13 turquoise and orange circles vs. purple circles). This indicates that same-grasp modulation was often transitory, occurring only at certain times in the trials in individual units. Across all subjects, the great majority

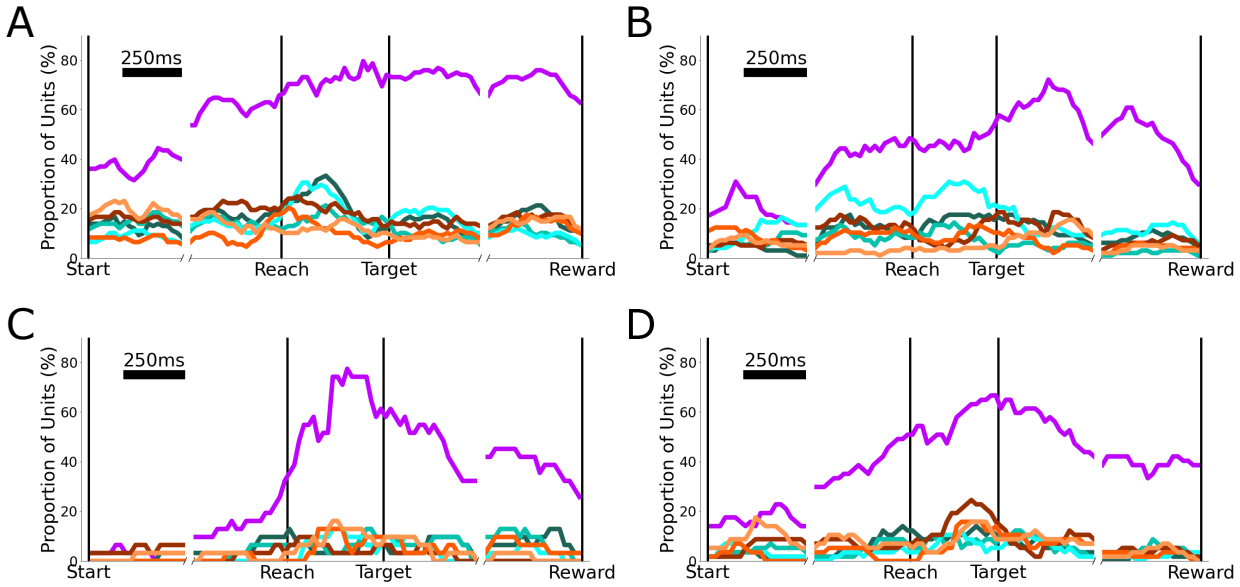

Figure 5.11: **Percentage of units with significantly modulated activity for each pair of conditions in the Grip Affordance Experiment.** Percentage of units with significant modulation for each pair of conditions at each time point ($p < 0.01$, permutation test, 10000 shuffles). A: Monkey R. B: Monkey I. C: Monkey T left hemisphere. D: Monkey T right hemisphere. Purple: any Power Grasp vs. Pinch Grasp. Turquoise colors: Power Grasps on different objects. Orange colors: Pinch Grasps on different objects. Dark turquoise and orange: objects differed in perceived affordances. Medium turquoise and orange: objects differed in learned affordances. Light turquoise and orange: objects differed in perceived and learned affordances.

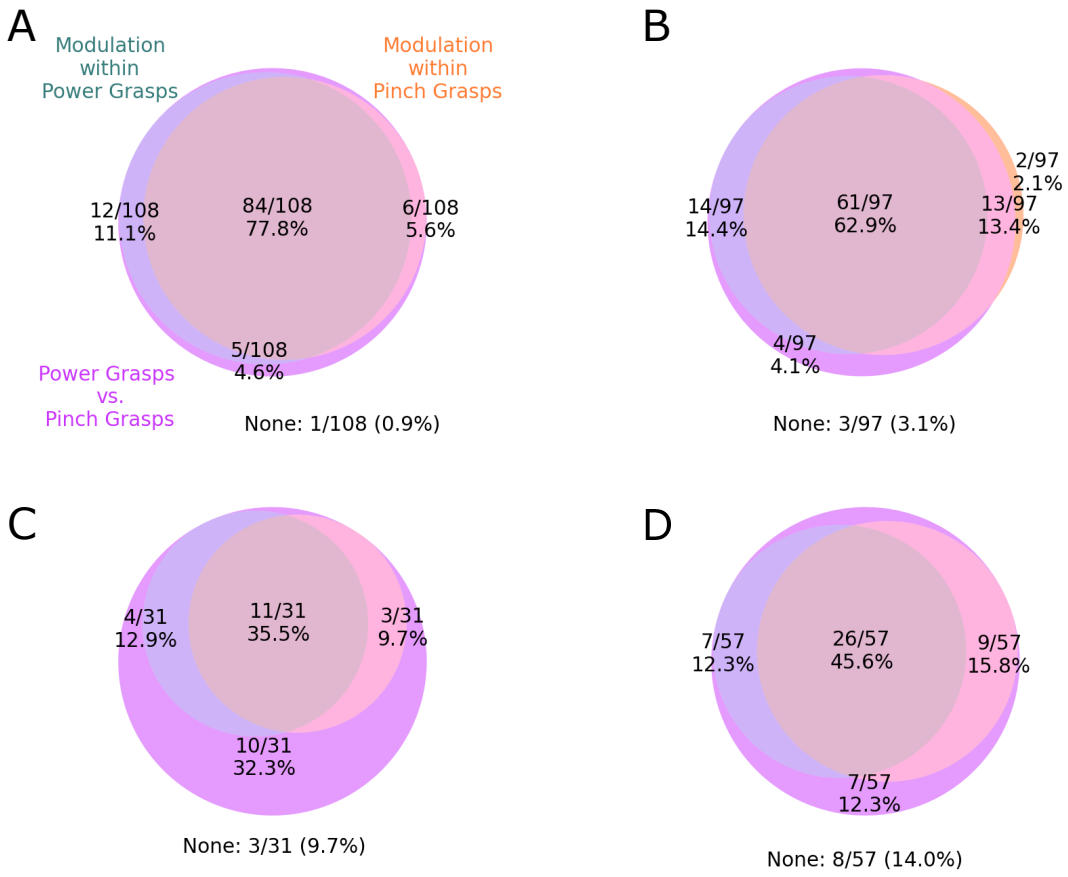

Figure 5.12: **Number of units with ≥ 100 ms of significantly modulated activity, Grip Affordance Experiment.** A: Monkey R. B: Monkey I. C: Monkey T left hemisphere. D: Monkey T right hemisphere. Purple circles: any Power Grasp condition significantly different from any Pinch Grasp condition. Turquoise circles: any significant tuning between Power Grasps on different objects. Orange circles: any significant tuning between Pinch Grasps on different objects. Significant differences were determined by permutation test, 10000 shuffles, $p < 0.01$

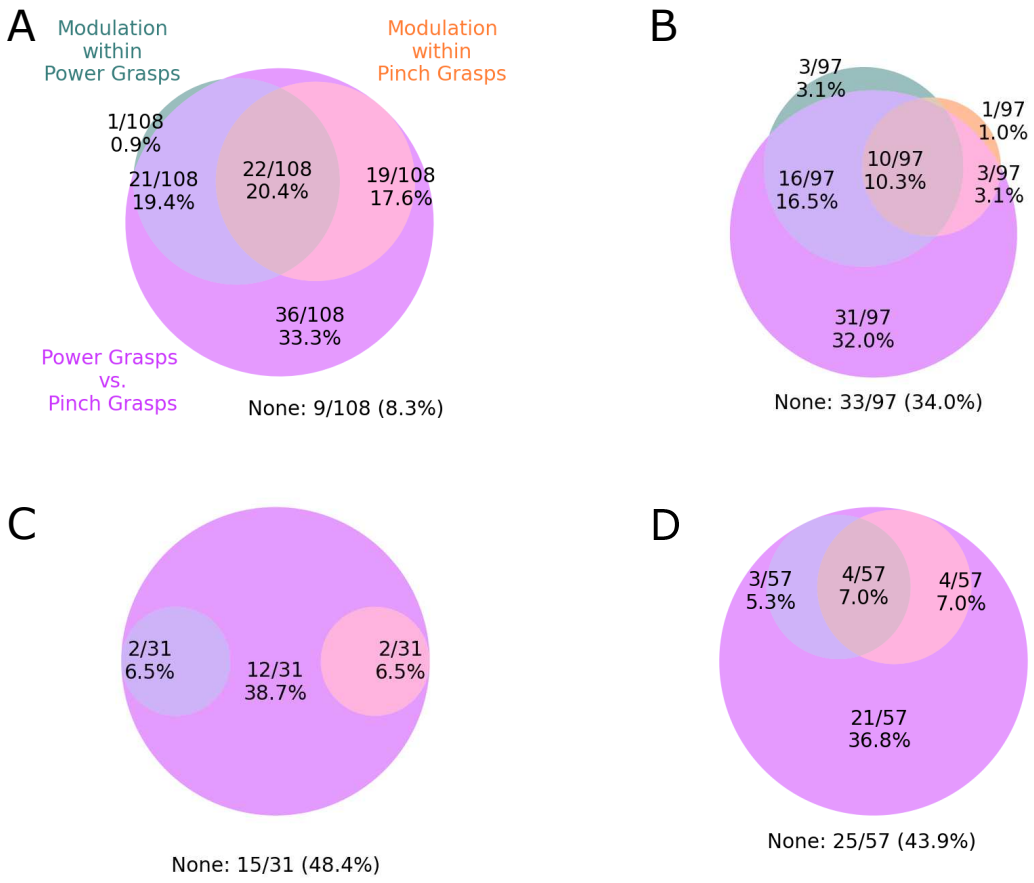

Figure 5.13: **Number of units with $\geq$ 500 ms of significantly modulated activity, Grip Affordance Experiment.** A: Monkey R. B: Monkey I. C: Monkey T left hemisphere. D: Monkey T right hemisphere. Purple circles: any Power Grasp condition significantly different from any Pinch Grasp condition. Turquoise circles: any significant tuning between Power Grasps on different objects. Orange circles: any significant tuning between Pinch Grasps on different objects. Significant differences were determined by permutation test, 10000 shuffles, $p < 0.01$

of units which had any same-grasp modulation were also modulated between at least one Power Grasp vs. Pinch Grasp condition pair, suggesting that modulation for object-related differences co-occurred with grasp type related modulation in individual units.

To examine the patterns of FR variability in the neural population as a whole, varimax PCA was performed on the FRs, as in Section 4.3. The number of PCs accounting for 99% of the variance was 42, 47, 24 and 35 for Monkey R, Monkey I, Monkey T left hemisphere and Monkey T right hemisphere, respectively. The scores of the top 16 FR VPCs are plotted in Figure 5.14 for Monkey R, with the scores for each condition plotted separately.

The predominant source of variance in the FR VPCs was separation between Power Grasps and Pinch Grasps in general. However, within-grasp separation was present in many of the of the VPCs, especially during the early reach period for Power Grasps made on the different objects for Monkey R (5.14 VPCs 2, 4 and 5).

To visualize the magnitude of inter-condition modulation in the population FRs over time, the Euclidean distances between each pair of conditions was calculated. This distance was first calculated in full FR space, treating the FR of each unit as a separate dimension. This distance, deemed the population modulation Δ was calculated by combining the individual unit modulations, δ according to Equations 4.3 and 4.4 in Section 4.3. The resulting Δ values are plotted in Figure 5.15.

For Monkey R and Monkey T both hemispheres, large population modulation in neural space was observed between Power Grasps and Pinch Grasps in general, peaking around the time of target contact. For Monkey I, the between-grasp population modulation was less pronounced and occurred later in the trials. For all subjects, within-grasp population modulation was relatively small, yet consistent across the timecourse of the trials.

For more direct comparison with the inter-condition distances in MF PC space D_{MFPC}, the inter-condition distances were also calculated in FR PC space, according to equation 4.5 in Section 4.3. The FR PC distances D_{FRPC} are shown in Figure 5.16 and the time-averaged FR PC distances $\overline{D}_{\mathrm{FRPC}}$ are shown in Figure 5.17 for all subjects.

The inter-condition distances in FR PC space showed largely the same trend as the population modulation findings. Time-averaged within-grasp distances (Figure 5.17 turquoise and orange bars) were relatively small compared to time-averaged between-grasp

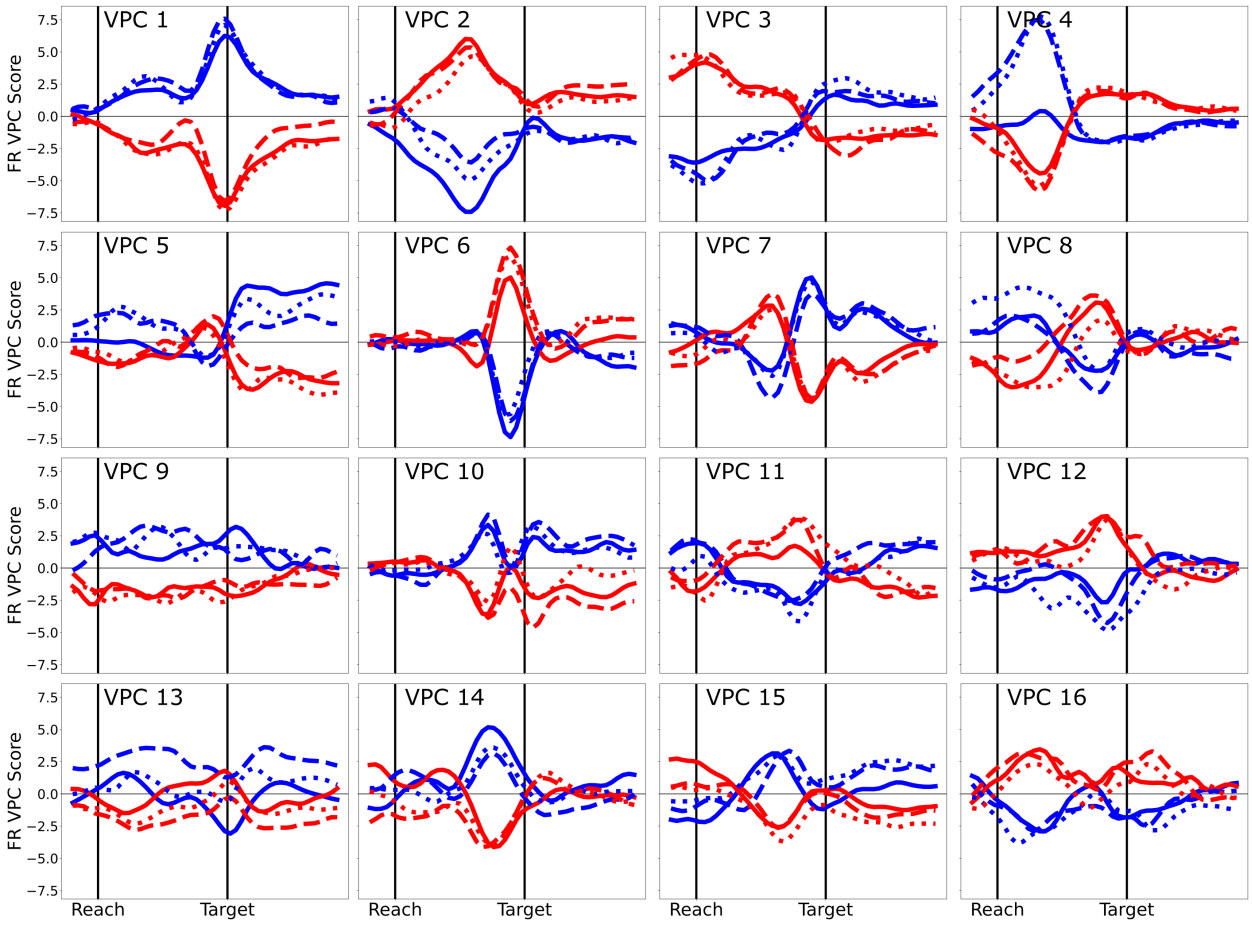

Figure 5.14: **Varimax PCA of the FRs in the Grip Affordance Experiment, Monkey R.** Scores in the top 16 FR VPCs. Blue: Power Grasp, Red: Pinch Grasp. Solid lines: simple objects. Dashed lines: compound single-grip objects. Dotted lines: compound multi-grasp object.

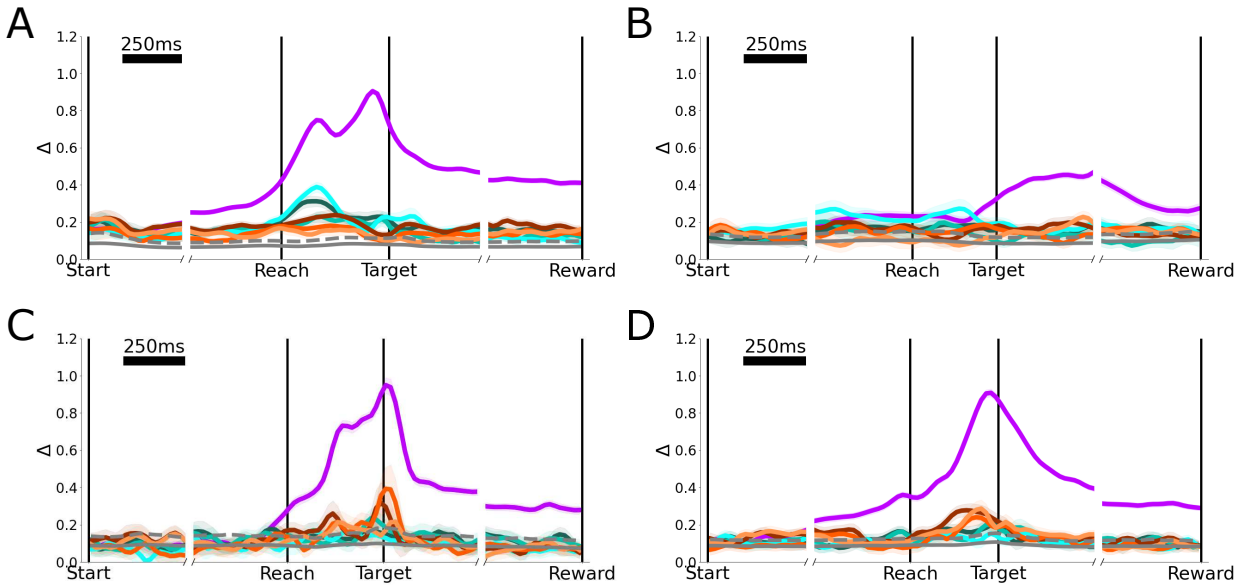

Figure 5.15: **Population modulation Δ and for pairs of conditions in the Grip Affordance Experiment.** A: Monkey R. B: Monkey I. C: Monkey T left hemisphere. D: Monkey T right hemisphere. Purple: Power Grasps vs. Pinch Grasps. Turquoise colors: Power Grasps on different objects. Orange colors: Pinch Grasps on different objects. Dark turquoise and orange: objects differed in perceived affordances. Medium turquoise and orange: objects differed in learned affordances. Light turquoise and orange: objects differed in perceived and learned affordances. Gray: mean and upper 95% one-sided confidence interval of within-condition variability.

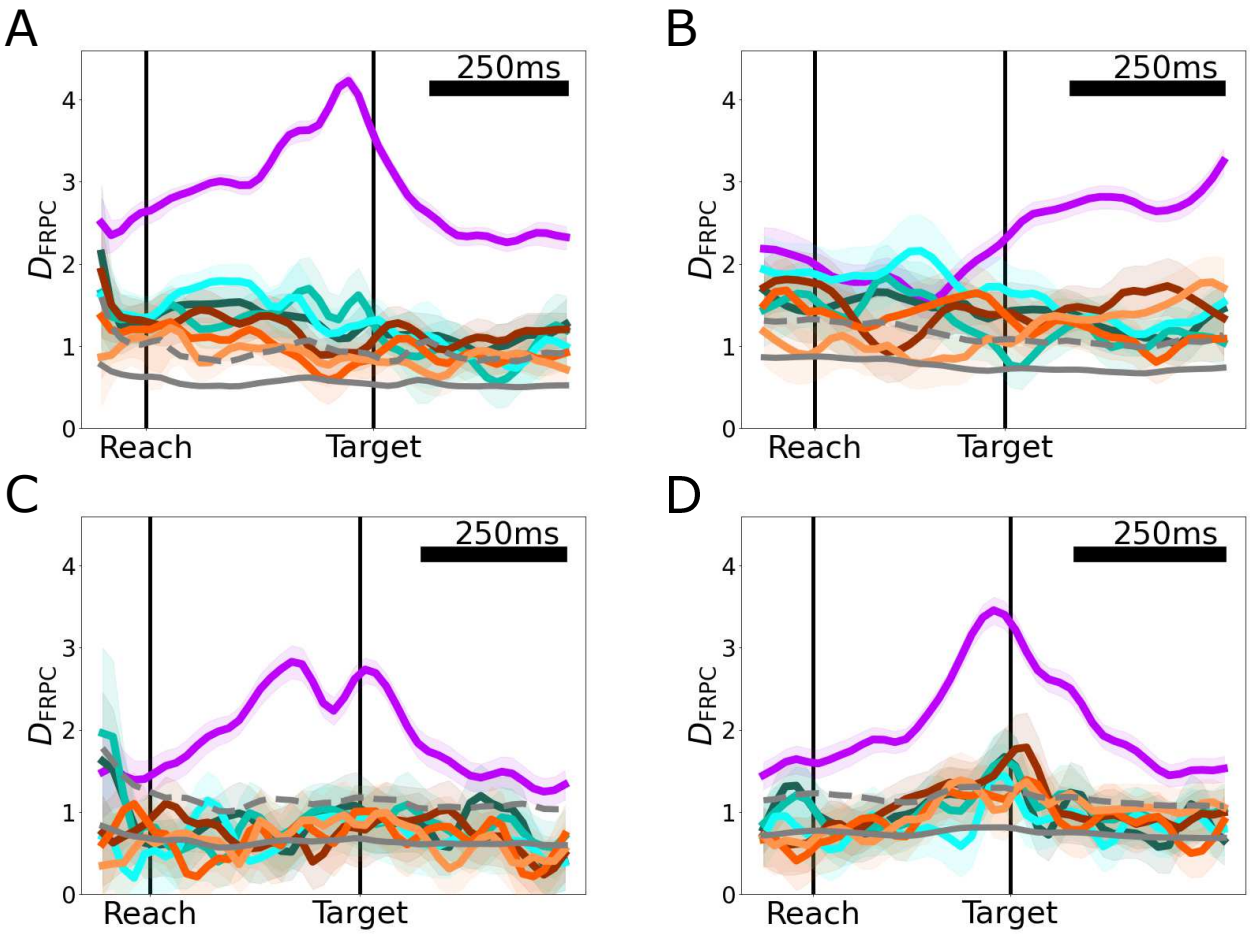

Figure 5.16: **Scaled Euclidean inter-condition distances between pairs of trial-averaged FR PC scores in the Grip Affordance Experiment.** Distances were calculated in the 99% FR PC space. A: Monkey R. B: Monkey I. C: Monkey T left hemisphere. D: Monkey T right hemisphere. Star: $\overline{D}_{\mathrm{FRPC},i,j}$ significantly greater than within condition $\overline{D}_{\mathrm{FRPC}}$ variability ($p < 0.05$, one-sided bootstrap interval). Purple: Power Grasps vs. Pinch Grasps. Turquoise colors: Power Grasps on different objects. Orange colors: Pinch Grasps on different objects. Dark turquoise and orange: objects differed in perceived affordances. Medium turquoise and orange: objects differed in learned affordances. Light turquoise and orange: objects differed in perceived and learned affordances. Gray: mean and upper 95% one-sided confidence interval of within-condition variability. 95% confidence intervals (shaded regions or error bars) are bootstrap intervals, trials resampled 10000 times.

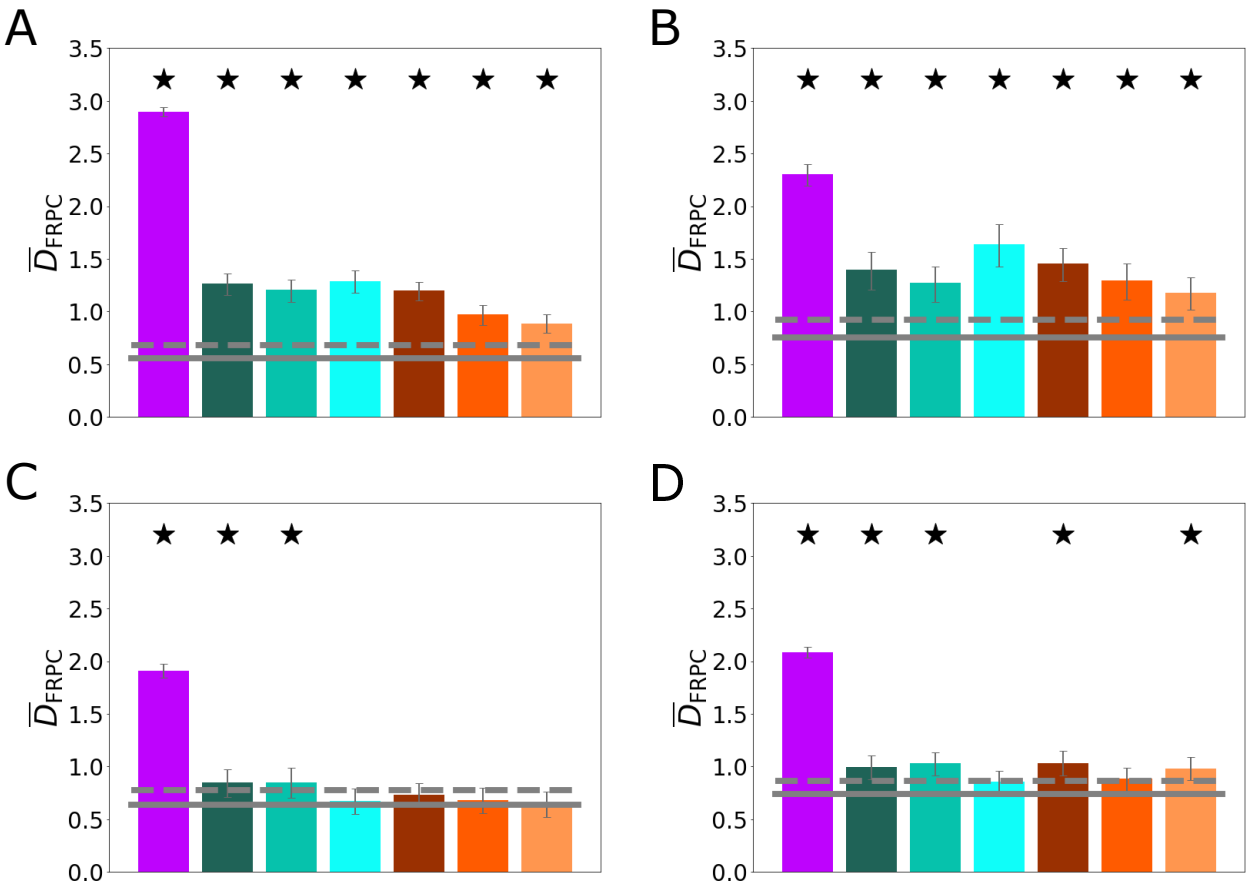

Figure 5.17: **Time-averaged scaled Euclidean inter-condition distances between pairs of trial-averaged FR PC scores in the Grip Affordance Experiment.** Distances were calculated in the 99% FR PC space and averaged over time. A: Monkey R. B: Monkey I. C: Monkey T left hemisphere. D: Monkey T right hemisphere. Star: $\overline{D}_{\mathrm{FRPC},i,j}$ significantly greater than within condition $\overline{D}_{\mathrm{FRPC}}$ variability ($p < 0.05$, one-sided bootstrap interval). Purple: Power Grasps vs. Pinch Grasps. Turquoise colors: Power Grasps on different objects. Orange colors: Pinch Grasps on different objects. Dark turquoise and orange: objects differed in perceived affordances. Medium turquoise and orange: objects differed in learned affordances. Light turquoise and orange: objects differed in perceived and learned affordances. Gray: mean and upper 95% one-sided confidence interval of within-condition variability. 95% confidence intervals (shaded regions or error bars) are bootstrap intervals, trials resampled 10000 times.

distances (Figure 5.17 purple bar). However, though small, these within-grasp neural distances were frequently significantly greater than within-condition $\overline{D}_{\mathrm{FRPC}}$ variability. Every condition pair $\overline{D}_{\mathrm{FRPC}}$ was significantly greater than within-condition variability for Monkey R and Monkey I, while only select pairings were significant in Monkey T. This threshold was likely a conservative one, as the within-condition variability estimate identified the maximal within-condition variability across all conditions. Further analysis with permutation tests suggested that every condition pair $\overline{D}_{\mathrm{FRPC}}$ was significant for all subjects. As in the MFs, the existence of these small but consistent significant within-grasp neural differences was somewhat unexpected, as the behaviors were very similar for the same grasps made on different objects and overall behavioral requirements were constant across such conditions.

On average, the ratio of Power Grasp vs. Pinch Grasp FR PC distances to within-grasp FR PC distances was 2.55, 1.67, 2.58 and 2.16 for Monkey R, Monkey I, Monkey T left hemisphere and Monkey T right hemisphere. Notably, these ratios were smaller than the between-grasp to within-grasp ratios observed for distances in MF PC space. That is, within-grasp distances were relatively larger in FR PC space than in MF PC space, when compared to Power Grasp vs. Pinch Grasp distances. This finding suggests the possibility that M1 neural activity could instantiate contextual encoding of the perceived or learned grip affordances of the object being grasped. In section 5.4, evidence for such explicit grip affordance encoding is considered.

5.4 Evidence for Contextual Grip Affordance Encoding

The analyses of Sections 5.2 and 5.3 revealed that both MFs and FRs were significantly different for conditions in which the same grasp was performed on objects with different perceived or learned grip affordances. The neural differences for these same-grasp, different-context condition pairs were relatively larger than the behavioral differences. Relative to mean Power Grasp vs. Pinch Grasp distances, mean FR PC distances $\overline{D}_{\mathrm{FRPC}}$ for same-grasp condition pairs were 1.47, 2.76, 2.33 and 2.35 times as large as the corresponding mean MF

PC distances $\overline{D}_{\text{MRPC}}$ on average for Monkey R, Monkey I, Monkey T left hemisphere and Monkey T right hemisphere respectively. This disparity in the relative sizes of neural and behavioral distances can be visualized using MDS, as shown in Figure 5.18.

This relative disparity in the separation of same-grasp conditions in FRs as compared to MFs suggests that the neural differences observed between these conditions may not only reflect encoding of MF differences, but may also additionally constitute encoding of the perceived and learned grip affordance differences.

In this section, evidence is considered for the presence of context encoding related to the perceived or learned grip affordances of the object being grasped. In Section 4.4, it was shown that neural variability between reaches made in two different object contexts (object present or object absent) exceeded what could be accounted for by linear neural tuning to MFs. Here, a similar question is asked: does neural variability between conditions for which the same grasp was made on different objects (objects with different perceived or learned grip affordances) exceed that which can be accounted for by linear neural tuning to MFs? Such excessive neural variability can be considered a signature of grip affordance encoding in M1. Evidence for grip affordance encoding is presented first from an encoding perspective (Section 5.4.1), then from a decoding perspective (Section 5.4.2).

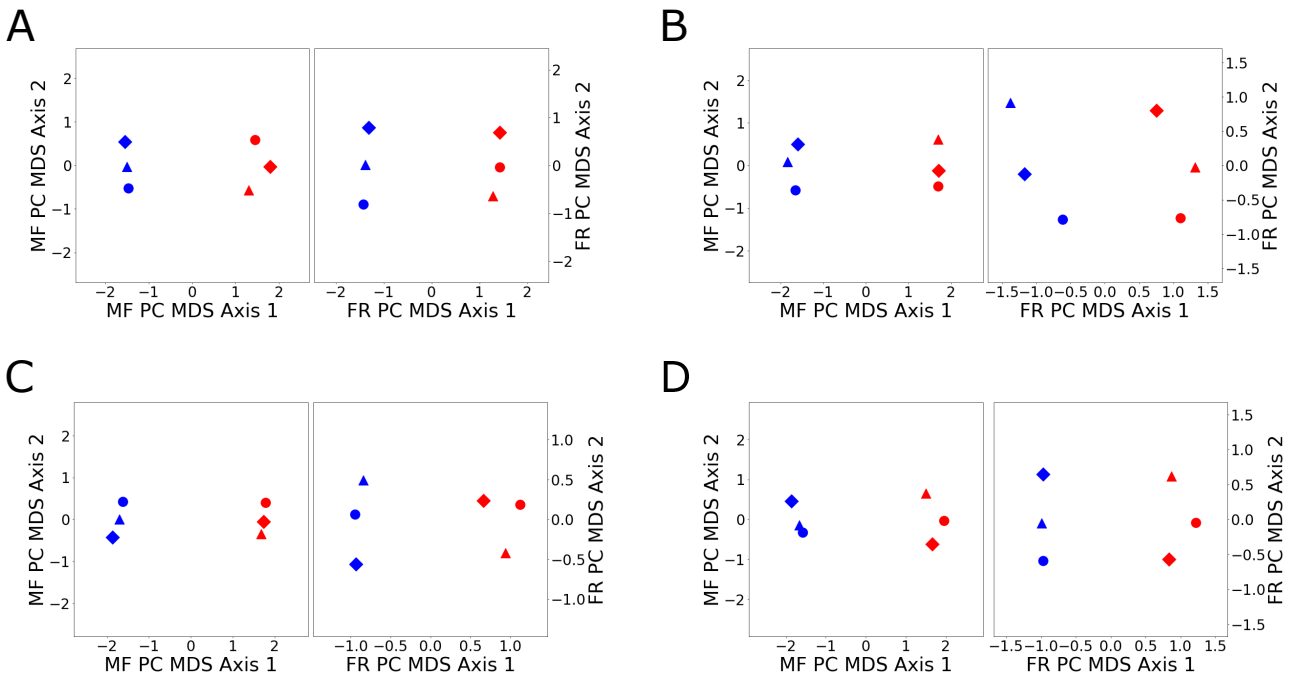

Figure 5.18: **MDS of MF PC and FR PC inter-condition distances in the Grip Affordance Experiment.** A: Monkey R. B: Monkey I. C: Monkey T left hemisphere. D: Monkey T right hemisphere. Left-hand plots: MDS of MF PC distances. Right-hand plots: MDS of FR PC distances. Blue markers: Power Grasps. Red markers: Pinch Grasps. Circles: simple objects. Triangles: compound single-grasp objects. Diamonds: compound multi-grasp object. Plots were rotated to align the mean of all Pinch Grasps with the x-axis, and scaled so that the MF PC and FR PC distances between mean Power Grasp and mean Pinch Grasp were visually equal.

5.4.1 Encoding Perspective

Given the base hypothesis that M1 neural activity is simply and directly related to movements and muscle activity, FRs were first modeled as linear combinations of lagged MF PC scores, as in equation 4.7 in Section 4.4.1. As in Section 4.4.1, PCA was performed on the full matrix of normalized lagged MFs for each subject, and the top PCs explaining 99% of the variance were extracted, resulting in 31, 25, 30 and 21 MF PCs for Monkey R, Monkey I, Monkey T left hemisphere and Monkey T right hemisphere, respectively. The linear MF PC neural tuning models were fit via regression. The resulting trial-averaged regression R^2_{TA} values are shown in Figure 5.19.

The R^2_{TA} distributions suggest that M1 units were generally well-fit by linear combinations of MF PC scores when considering trial-averaged FRs and predicted FRs. Monkey R exhibited the strongest tuning on average. Monkey I had lower a incidence of well-tuned units than the other subjects.

As described in Section 5.2, small but consistent significant differences were observed in the MF PC scores when the same grasps were made on different objects (Figure 5.8 turquoise and orange traces). Relatively larger differences were observed in the FR PC scores between these same-grasp conditions (Figure 5.16 turquoise and orange traces). We hypothesize that, along with MF encoding, M1 units encode the perceived or learned grip affordances of the object that is grasped. This encoding is defined by FR modulations between same-grasp conditions that exceed what can be accounted for by a linear MF tuning model alone, resulting in "extralinear modulation."

To test the hypothesis of grip affordance encoding in M1 units, the extralinear modulation (modulation beyond that which can be accounted for by linear movement tuning), ξ, was calculated for each condition pair for each unit, as in Equations 4.9–4.11 in Section 4.4.1. The extralinear modulation was defined as the modulation in FRs δ minus the modulation in predicted FRs $\hat{\delta}$ generated from the linear FR to MF PC score tuning models. The time-averaged extralinear modulations $\overline{\xi}$ were calculated for each condition pair for each unit by averaging each ξ over the entire peri-movement period.

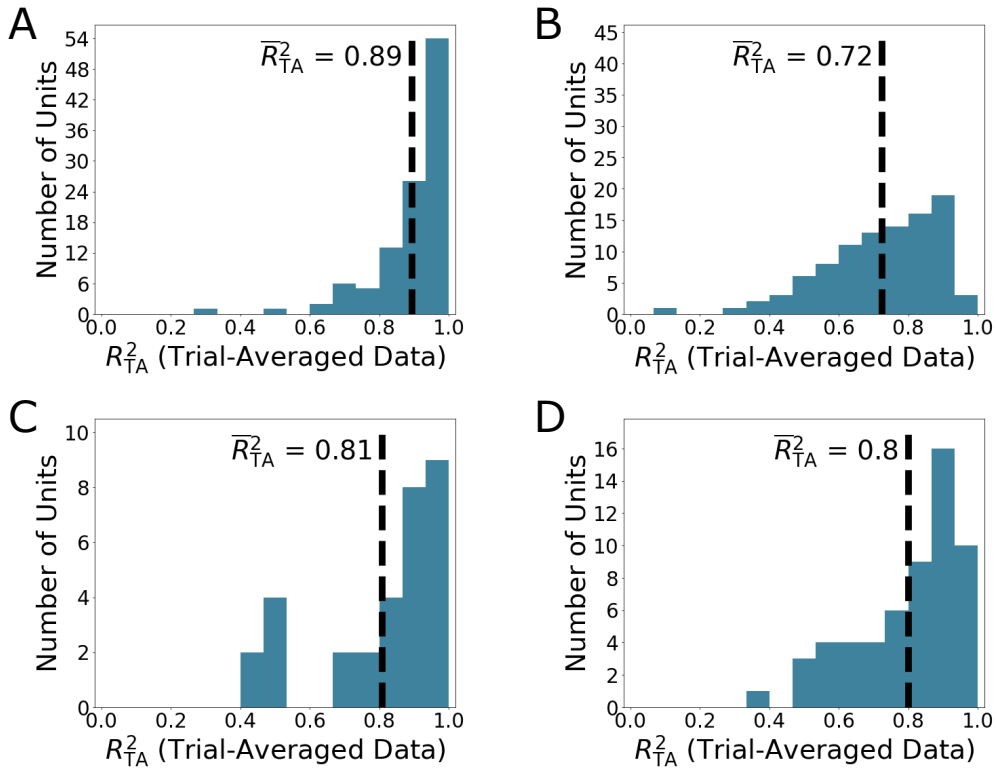

Figure 5.19: **Regression R^2_{TA} distributions for the linear tuning of unit FRs to MF PCs in the Use Affordance Experiment.** A: Monkey R. B: Monkey I. C: Monkey T left hemisphere. D: Monkey T right hemisphere. R^2_{TA} were obtained from trial-averaged neural data and predictions (trial-to-trial variability excluded). Black dashed lines: mean values.

Similarly to the analyses of Section 4.4.1, a unit was considered "grip affordance encoding" if an instance of $\overline{\xi}$ for a same-grasp, different object condition pair was significantly greater than within-condition $\overline{\xi}$ variability at the $p < 0.05$ level. A unit was further considered "robustly grip affordance encoding" if a same-grasp, different object condition pair $\overline{\xi}$ was both significantly greater than within-condition $\overline{\xi}$ variability *and* significantly greater than mean $\overline{\xi}$ for Power Grasps vs. Pinch Grasps at the $p < 0.05$ level. These thresholds are both considered to be conservative, as the within-condition variability estimate identified the highest within-condition variability across all conditions, and Power Grasps and Pinch Grasps evoked relatively very different behaviors.

Table 5.1 displays the percentage of units displaying significant and robust grip affordance encoding, with occurrences of perceived grip affordance encoding and learned grip affordance encoding presented separately within each grip type. Perceived grip affordance encoding refers to extralinear modulation between conditions in which the same grasp was made on a simple object and the corresponding compound single-grasp object. Learned grip affordance encoding refers to extralinear modulation between conditions in which the same grasp was made on a compound single-grasp object and the compound multi-grasp object. Perceived and learned grip affordance encoding refers to extralinear modulation between conditions in which the same grasp was made on a simple object and the compound multi-grasp object.

A small to moderate number grip affordance encoding units were observed in all subjects. About 13–17% of units in Monkey T and Monkey I and 32.4% of units in Monkey R showed evidence of significant grip affordance encoding for at least one same-grasp, different object condition pair. Most of these units also qualified as robustly grip affordance encoding for all subjects. No clear preference for perceived or learned grip affordance encoding was observed, nor was there an obvious preference for grip affordance encoding with in either grip type.

To measure the strength of grip affordance encoding at the population level, population extralinear modulation ξ^{pop} was calculated according to Equation 4.12 in Section 4.4.1. The time-averaged population extralinear modulation $\overline{\xi}^{\text{pop}}$ for each condition pair was also calculated by averaging each ξ^{pop} over time in the peri-movement period. The population extralinear modulation results are shown in Figure 5.20 and the time-averaged population extralinear modulation results are shown in Figure 5.21.

Table 5.1: **Percentage of units displaying significant and robust grip affordance encoding based on magnitude of extralinear modulation.** Unit n is considered significantly grip affordance encoding if an instance of $\overline{\xi}_{\text{SameGrasp,DifferentObject},n}$ is significantly greater than within-condition $\overline{\xi}$ variability. Unit n is further considered robustly affordance encoding if an instance of $\overline{\xi}_{\text{SameGrasp,DifferentObject},n}$ is significantly greater than $\overline{\xi}_{\text{PowerGrasp,PinchGrasp},n}$ ($p < 0.05$ bootstrap one-sided interval). P: difference in perceived grip affordances. L: difference in learned grip affordances. P+L: difference in both perceived and learned grip affordances. "Any" grip affordance encoding was assessed at the $p < 0.0083$ level ($p < 0.05$ Bonferroni-corrected for six comparisons).

		Significant Grip Affordance Encoding						
		Power Grasp			**Pinch Grasp**			**Any**
Subject	**Area**	**P**	**L**	**P+L**	**P**	**L**	**P+L**	
Monkey R	M1	20.4%	11.1%	22.2%	11.1%	5.6%	4.6%	32.4%
Monkey I	M1	13.4%	10.3%	20.6%	6.2%	8.2%	3.1%	16.5%
Monkey T	M1 Left	9.7%	3.2%	3.2%	6.5%	9.7%	9.7%	12.9%
Monkey T	M1 Right	10.5%	10.5%	8.8%	10.5%	7.0%	7.0%	15.8%

		Robust Grip Affordance Encoding						
		Power Grasp			**Pinch Grasp**			**Any**
Subject	**Area**	**P**	**L**	**P+L**	**P**	**L**	**P+L**	
Monkey R	M1	15.7%	8.3%	15.7%	10.2%	4.6%	2.8%	25.9%
Monkey I	M1	13.4%	10.3%	20.6%	5.2%	7.2%	2.1%	15.5%
Monkey T	M1 Left	6.5%	3.2%	3.2%	6.5%	6.5%	6.5%	9.7%
Monkey T	M1 Right	8.8%	8.8%	7.0%	8.8%	3.5%	5.3%	12.3%

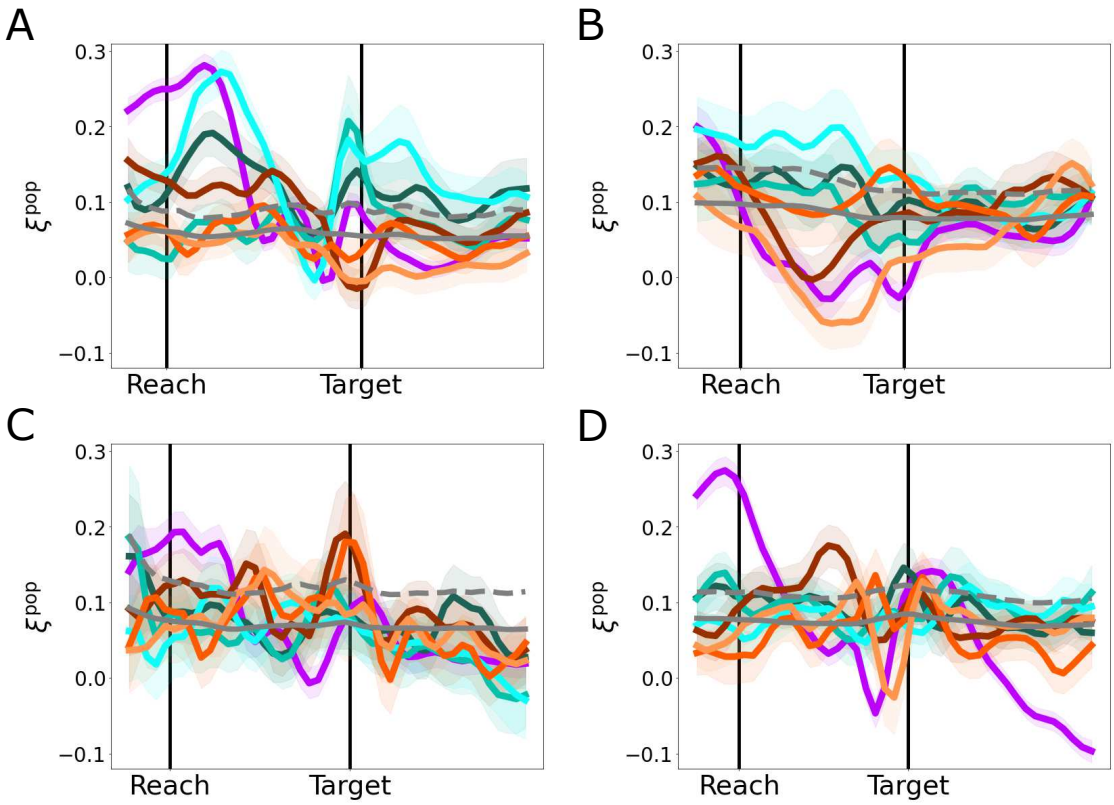

Figure 5.20: **Population extralinear modulation ξ^{pop} for each condition pair in the Grip Affordance Experiment.** A: Monkey R. B: Monkey I. C: Monkey T left hemisphere. D: Monkey T right hemisphere. Purple: Power Grasps vs. Pinch Grasps. Turquoise colors: Power Grasps on different objects. Orange colors: Pinch Grasps on different objects. Dark turquoise and orange: objects differed in perceived affordances. Medium turquoise and orange: objects differed in learned affordances. Light turquoise and orange: objects differed in perceived and learned affordances. Gray: mean and upper 95% one-sided confidence interval of within-condition variability. 95% confidence intervals: bootstrap intervals, trials resampled 10000 times.

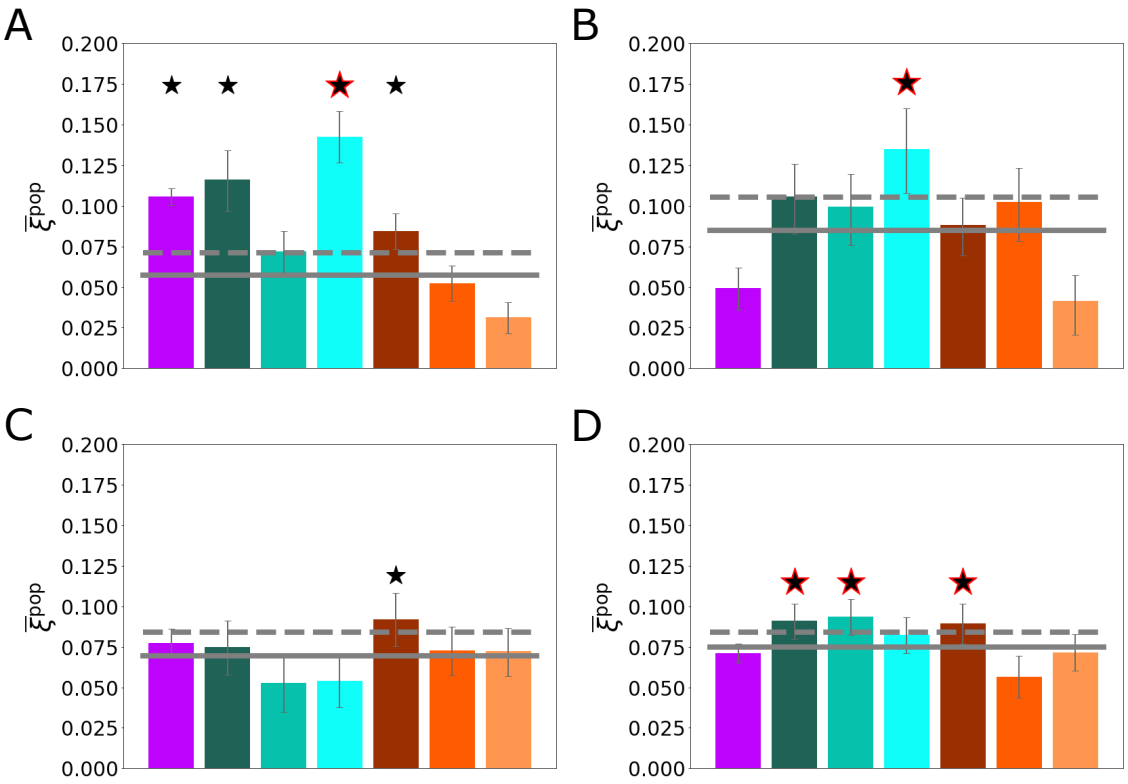

Figure 5.21: **Mean population extralinear modulation $\overline{\xi}^{pop}$ for each condition pair in the Grip Affordance Experiment.** A: Monkey R. B: Monkey I. C: Monkey T left hemisphere. D: Monkey T right hemisphere. Black star: $\overline{\xi}^{pop}_{i,j}$ significantly greater than within-condition $\overline{\xi}^{pop}$ variability. Black and red star: $\overline{\xi}^{pop}_{i,j}$ additionally significantly greater than mean $\overline{\xi}^{pop}_{\text{PowerGrasp,PinchGrasp}}$ ($p < 0.05$, one-sided bootstrap interval). Purple: Power Grasps vs. Pinch Grasps. Turquoise colors: Power Grasps on different objects. Orange colors: Pinch Grasps on different objects. Dark turquoise and orange: objects differed in perceived affordances. Medium turquoise and orange: objects differed in learned affordances. Light turquoise and orange: objects differed in perceived and learned affordances. Gray: mean and upper 95% one-sided confidence interval of within-condition variability. 95% confidence intervals: bootstrap intervals, trials resampled 10000 times.

Significant grip affordance encoding for at least one same-grasp, different object condition pair was observed at the population level for all subjects. Additionally, robust population grip affordance encoding was observed for at least one same-grasp, different object condition pair in all subjects except Monkey T left hemisphere. These effects were generally only present in one or a few same-grasp condition pairs. Both perceived and learned grip affordance differences were encoded, and grip affordance encoding was present within both grip types. The sizes of these effects were relatively small compared to the extralinear modulation observed related to object presence in the Object Presence Experiment, but were nonetheless present in all subjects.

The extralinear modulation analysis suggests the presence of a small grip affordance encoding signal in individual M1 units and in M1 population activity, in that when two objects that differed by their perceived or learned grip affordances were grasped using the same grasp, neural modulations were observed which exceeded what would be expected from linear encoding of MFs alone. The following section presents a similar analysis from a decoding perspective.

5.4.2 Decoding Perspective

The extralinear modulation analyses approach the question of grip affordance encoding from an "encoding" perspective, in that a linear MF PC encoding model was built for each unit, and the modulation of individual units were interrogated for evidence of grip affordance encoding. The problem can also be approached from a "decoding" perspective. As in section 4.4.2, null space analyses were performed to isolate the components of neural activity that were related to or linearly independent from MFs.

For the null space analyses, PCA was performed on trial-averaged FRs and trial-averaged lagged MFs of the peri-movement period to generate mFR PC scores and mMF PC scores. The top mMF PCs explaining 99% of the mMF variance were used, resulting in 13, 12, 13 and 11 mMR PCs for Monkey R, Monkey I, Monkey T left hemisphere and Monkey T right hemisphere respectively. The number of mFR PCs was set to twice the number of mMF PCs, to produce null and potent spaces of equal dimension.

The mMF PC scores were then regressed against the mFR PC scores as in equation 4.13 in Section 4.4.2. The estimated weights matrix $\hat{\mathbf{B}}$ was decomposed to produce $\hat{\mathbf{B}}_{\text{potent}}$ and $\hat{\mathbf{B}}_{\text{null}}$, which where then used to calculate $\hat{\mathbf{F}}_{\text{potent}}$ and $\hat{\mathbf{F}}_{\text{null}}$, the components of neural activity in the potent and null spaces. $\hat{\mathbf{F}}_{\text{potent}}$ describes the neural activity that can be linearly projected through $\mathbf{B}$ to decode mMF PCs, while $\hat{\mathbf{F}}_{\text{null}}$ describes the activity for which projection through $\mathbf{B}$ results in zero (see Section A.6.4 for more details).

For these analyses, context encoding is defined as neural modulation which is not linearly related to MFs. Thus, such grip affordance encoding would manifest as separation between same-grasp conditions in the null space. To characterize this null space separation, the variance due to each condition pair $V_{i,j,t}$ was calculated at each time point for the null space, according to Equation 4.18 as in Section 4.4.2. The total variance in the null space, $\overline{V}_{i,j}$ was also calculated by averaging $V_{i,j,t}$ over the peri-movement period. These values are displayed in Figures 5.22 and 5.23.

For all same-grasp condition pairs, null space variance was well above within-condition estimated null space variance. However, these same-grasp null space variances were always lower than the null space variance observed between Power Grasps and Pinch Grasps. This suggests that grip affordance encoding may be present, but relatively small. Given that neural separation between same-grasp condition pairs was small in general (Figure 5.16), the effect may be present but small in magnitude.

To determine the proportion of the full neural variance which occurred in the null space for each condition pair, the null space proportion by time $\pi_{i,j,t}$ and total null space proportion $\Pi_{i,j}$ were calculated for each condition pair according to Equation 4.20 in Section 5.4.2. These measures are shown in Figures 5.24 and 5.25.

The majority of neural variance due to Power Grasp vs. Pinch Grasp pairs occurred in the potent space (outside of the null space), whereas the majority of neural variance due to same-grasp condition pairs occurred in the null space for all same-grasp condition pairs across subjects (Figure 5.25 purple colors vs. turquoise and orange colors). This further suggests that the neural separations between same-grasp conditions were partially unrelated to MFs and thus constitute additional encoding of perceived and learned grip affordance differences, though the actual magnitudes of these effects were small.

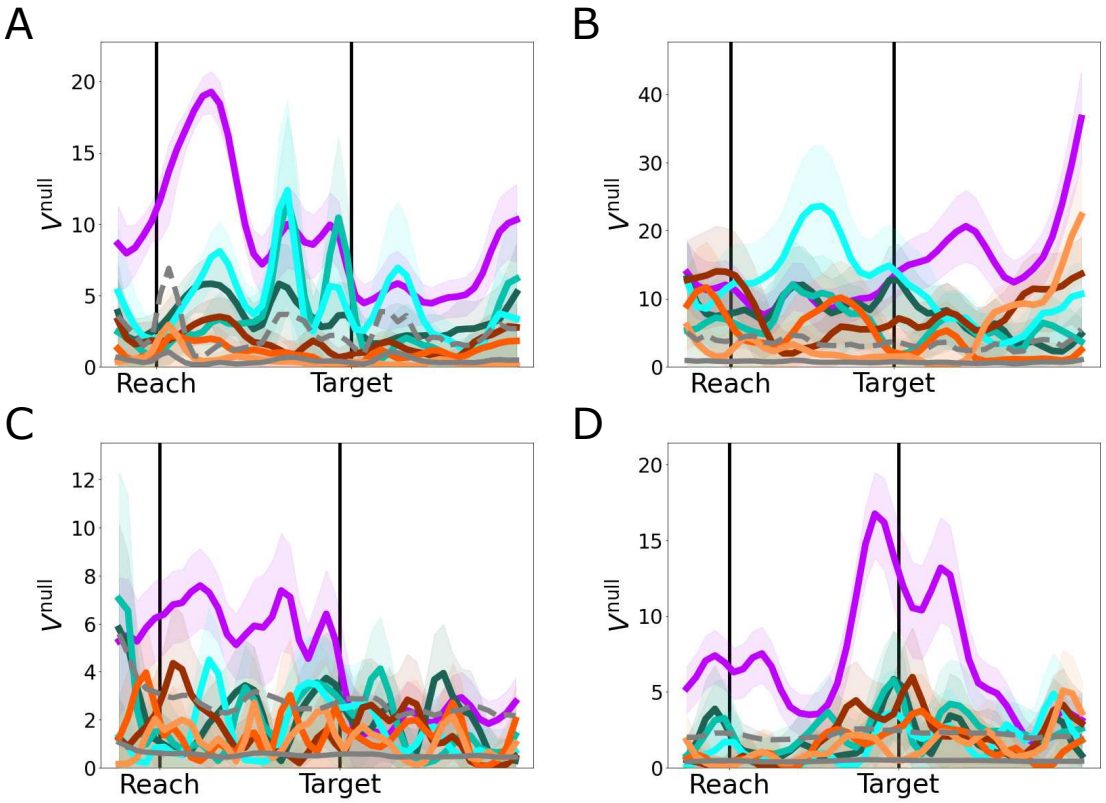

Figure 5.22: **Variances due to each condition pair in the null space.** A: Monkey R. B: Monkey I. C: Monkey T left hemisphere. D: Monkey T right hemisphere. Purple: Power Grasps vs. Pinch Grasps. Turquoise colors: Power Grasps on different objects. Orange colors: Pinch Grasps on different objects. Dark turquoise and orange: objects differed in perceived affordances. Medium turquoise and orange: objects differed in learned affordances. Light turquoise and orange: objects differed in perceived and learned affordances. Gray: mean and upper 95% one-sided confidence interval of within-condition variability. 95% confidence intervals: bootstrap intervals, trials resampled 10000 times.

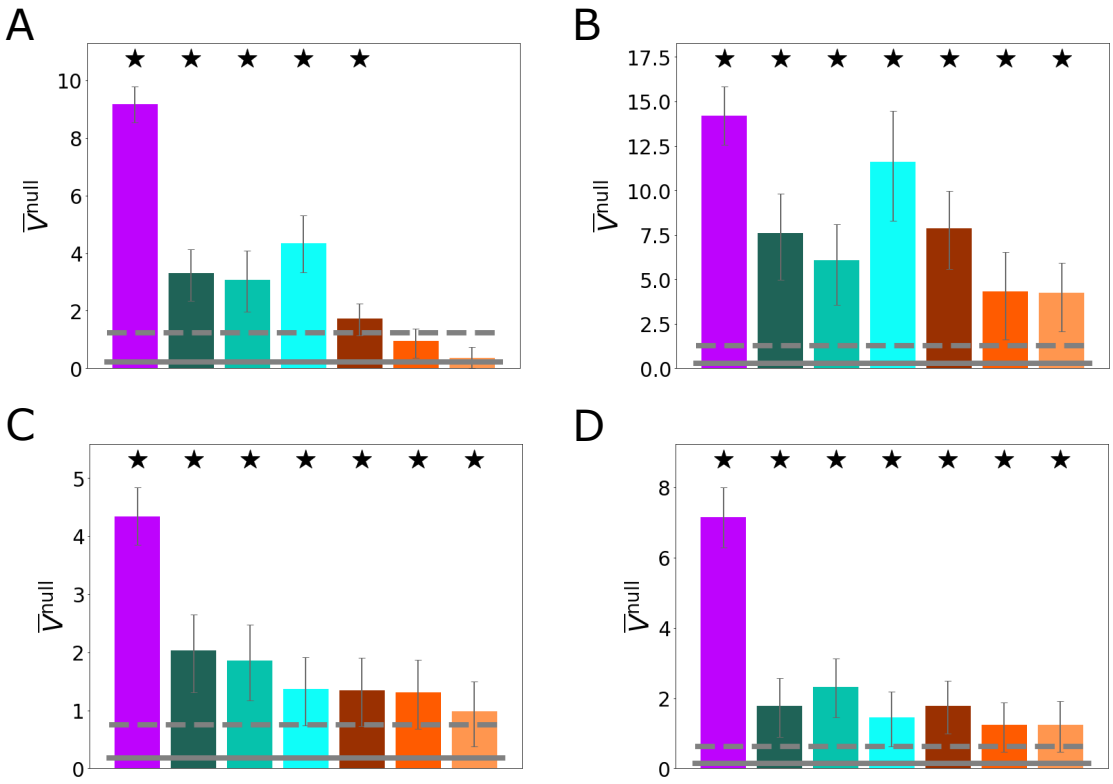

Figure 5.23: **Variances due to each condition pair in the null space.** A: Monkey R. B: Monkey I. C: Monkey T left hemisphere. D: Monkey T right hemisphere. Star: $\overline{V}^{\text{null}}_{i,j}$ significantly greater than within-condition $\overline{V}^{\text{null}}$ variability ($p < 0.05$, one-sided bootstrap interval). Purple: Power Grasps vs. Pinch Grasps. Turquoise colors: Power Grasps on different objects. Orange colors: Pinch Grasps on different objects. Dark turquoise and orange: objects differed in perceived affordances. Medium turquoise and orange: objects differed in learned affordances. Light turquoise and orange: objects differed in perceived and learned affordances. Gray: mean and upper 95% one-sided confidence interval of within-condition variability. 95% confidence intervals: bootstrap intervals, trials resampled 10000 times.

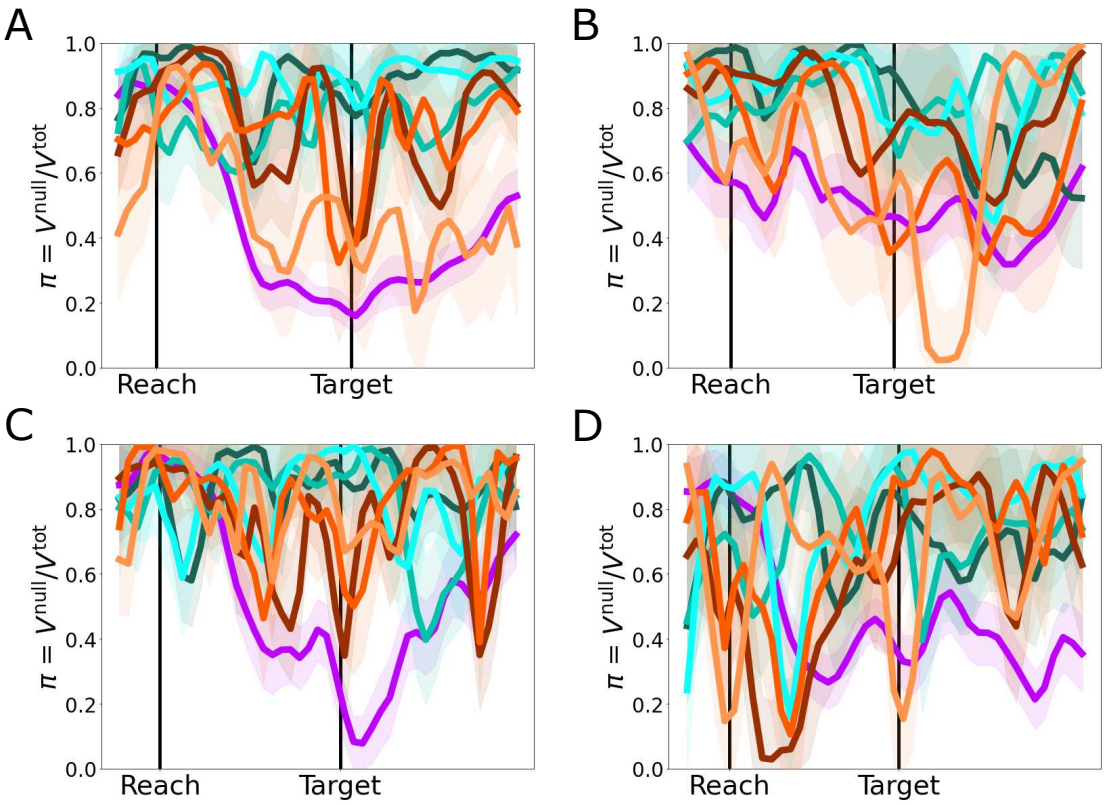

Figure 5.24: **Proportion of full inter-condition variance which occurred in the null space over time π.** A: Monkey R. B: Monkey I. C: Monkey T left hemisphere. D: Monkey T right hemisphere. Purple: Power Grasps vs. Pinch Grasps. Turquoise colors: Power Grasps on different objects. Orange colors: Pinch Grasps on different objects. Dark turquoise and orange: objects differed in perceived affordances. Medium turquoise and orange: objects differed in learned affordances. Light turquoise and orange: objects differed in perceived and learned affordances. Gray: mean and upper 95% one-sided confidence interval of within-condition variability. 95% confidence intervals: bootstrap intervals, trials resampled 10000 times.

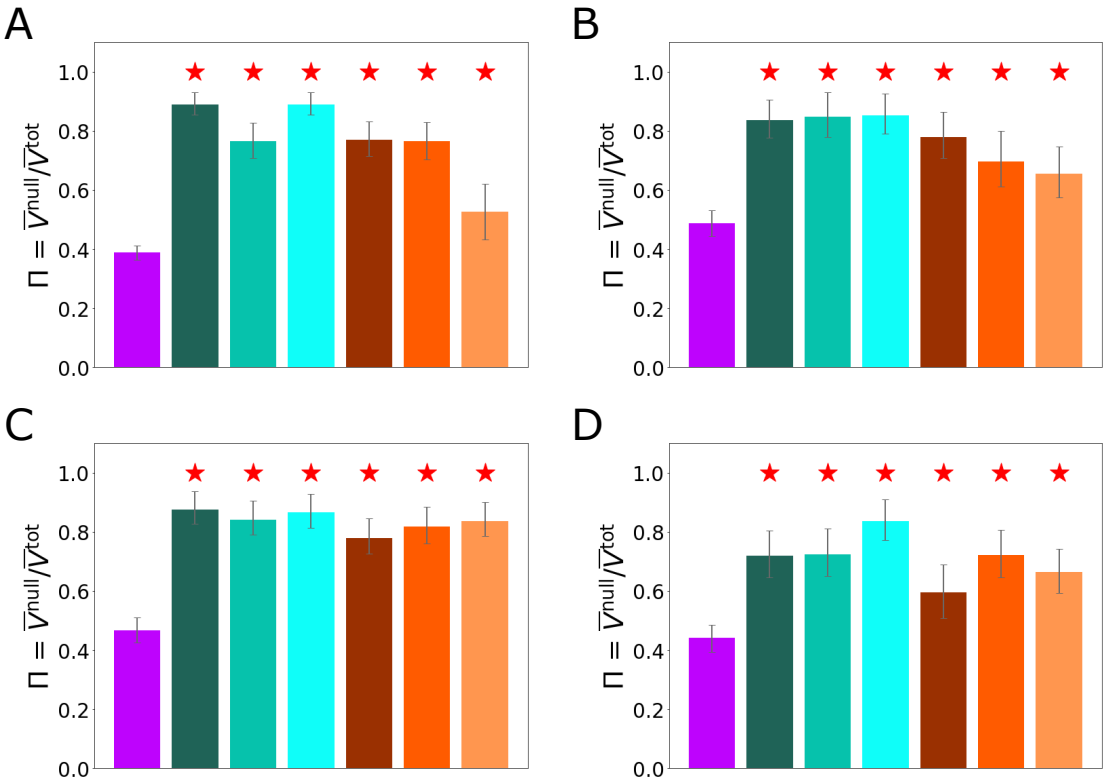

Figure 5.25: **Proportion of full inter-condition variance which occurred in the null space over time Π.** A: Monkey R. B: Monkey I. C: Monkey T left hemisphere. D: Monkey T right hemisphere. Red star: $\Pi_{i,j}$ significantly greater than $\Pi_{\text{PowerGrasp,PinchGrasp}}$ ($p < 0.05$, one-sided bootstrap interval). Purple: Power Grasps vs. Pinch Grasps. Turquoise colors: Power Grasps on different objects. Orange colors: Pinch Grasps on different objects. Dark turquoise and orange: objects differed in perceived affordances. Medium turquoise and orange: objects differed in learned affordances. Light turquoise and orange: objects differed in perceived and learned affordances. Gray: mean and upper 95% one-sided confidence interval of within-condition variability. 95% confidence intervals: bootstrap intervals, trials resampled 10000 times.

Taken together, the results of the extralinear modulation analyses and the null space analyses suggest that grip affordance encoding was present in M1 but was small in magnitude. Encoding of perceived grip affordance differences and learned grip affordance differences were both present. Grip affordance encoding was evident within both Power Grasps and Pinch Grasps. In the next section, different encoding models are compared to confirm the presence of grip affordance information unit FRs, to compare the incidence of perceived vs. learned grip affordance encoding and to investigate the potential interactions between grip affordance encoding and MF encoding.

5.5 Interaction of Grip Affordance and MF Encoding

In Section 5.4, evidence for grip affordance encoding in M1 individual units and populations was presented in terms of the FR modulation that exceeded linear tuning to MFs. In this section, the relation between FRs and MFs is explored with regards to the small but evident grip affordance encoding. Specifically, we ask if grip affordance was encoded concurrently with MF encoding, and whether grip affordance encoding had an additive or interactive effect when present.

As in Section 4.5, several different linear models were constructed and compared. The baseline model, the "MF only" model, related individual unit FRs to only MF PC scores, as in Equation 4.22 in Section 4.5, reproduced below:

$$f_{n,t} = \beta_{0,n} + \sum_{p=1}^{N_{\mathrm{M}}} (\beta_{p,n} s_{p,t+\tau}) + \epsilon \tag{5.1}$$

where $f_{n,t}$ is the normalized FR of unit n at time t, β are constant weights, $s_{p,t+\tau}$ is MF PC score s at time $t+\tau$, and ϵ is a Gaussian noise term, $\epsilon \sim \mathcal{N}(0, \sigma^2)$. As in Section 5.4, τ was set to 40 ms. This model assumes a fixed linear tuning to movements which ignores context.

The next candidate models, direct grip affordance encoding models, described unit FRs as linear combinations of MF PC scores along with indicator variables denoting the different grip affordance context of the object being grasped. These models allowed a different mean FR for

each grip affordance context, assuming that grip affordances were encoded directly in FRs. Three different direct grip affordance encoding models were built to model direct encoding of perceived grip affordances, learned grip affordances or both. The "Direct perceived grip affordance encoding" model is defined in Equation 5.2:

$$f_{n,t} = \beta_{0,n} + \sum_{p=1}^{N_{\mathrm{M}}} \beta_{p,n} s_{p,t+\tau} + \beta_{c,n}^{c} c + \epsilon \tag{5.2}$$

$$c = 0 \text{ for simple objects}$$

$$c = 1 \text{ for compound single-grasp and compound multi-grasp objects}$$

The "Direct learned grip affordance encoding" model is defined in Equation 5.3:

$$f_{n,t} = \beta_{0,n} + \sum_{p=1}^{N_{\mathrm{M}}} \beta_{p,n} s_{p,t+\tau} + \beta_{c,n}^{c} c + \epsilon \tag{5.3}$$

$$c = 0 \text{ for simple objects and compound single-grasp objects}$$

$$c = 1 \text{ for compound multi-grasp objects}$$

The "Direct perceived and learned grip affordance encoding" model is defined in Equation 5.4:

$$f_{n,t} = \beta_{0,n} + \sum_{p=1}^{N_{\mathrm{M}}} \beta_{p,n} s_{p,t+\tau} + \beta_{c1,n}^{c1} c1 + \beta_{c2,n}^{c2} c2 + \epsilon \tag{5.4}$$

$$c1 = 0,\ c2 = 0 \text{ for simple objects}$$

$$c1 = 1,\ c2 = 0 \text{ for compound single-grasp objects}$$

$$c1 = 1,\ c2 = 1 \text{ for compound multi-grasp objects}$$

The final candidate models, interactive grip affordance encoding models, described unit FRs as combinations of MF PC scores along with indicator variables and interaction terms. These models allowed the tuning coefficients to MF PC scores to change depending on the object

context. Again, three different interactive models were built to model interactive encoding of perceived grip affordances, learned grip affordances or both. The "Interactive perceived grip affordance encoding" model is defined in Equation 5.5:

$$f_{n,t} = \beta_{0,n} + \sum_{p=1}^{N_{\mathrm{M}}} \left(\beta_{p,n} s_{p,t+\tau}\right) + \beta_{0,n}^{c} c + \sum_{p=1}^{N_{\mathrm{M}}} \left(\beta_{p,n}^{c} c s_{p,t+\tau}\right) + \epsilon \tag{5.5}$$

$$c = 0 \text{ for simple objects}$$

$$c = 1 \text{ for compound single-grasp and compound multi-grasp objects}$$

The "Interactive learned grip affordance encoding" model is defined in Equation 5.6:

$$f_{n,t} = \beta_{0,n} + \sum_{p=1}^{N_{\mathrm{M}}} \left(\beta_{p,n} s_{p,t+\tau}\right) + \beta_{0,n}^{c} c + \sum_{p=1}^{N_{\mathrm{M}}} \left(\beta_{p,n}^{c} c s_{p,t+\tau}\right) + \epsilon \tag{5.6}$$

$$c = 0 \text{ for simple objects and compound single-grasp objects}$$

$$c = 1 \text{ for compound multi-grasp objects}$$

The "Interactive perceived and learned grip affordance encoding" model is defined in Equation 5.7:

$$f_{n,t} = \beta_{0,n} + \sum_{p=1}^{N_{\mathrm{M}}} \left(\beta_{p,n} s_{p,t+\tau}\right) + \beta_{0,n}^{c1} c1 + \sum_{p=1}^{N_{\mathrm{M}}} \left(\beta_{p,n}^{c1} c1 s_{p,t+\tau}\right) + \beta_{0,n}^{c2} c2 + \sum_{p=1}^{N_{\mathrm{M}}} \left(\beta_{p,n}^{c2} c2 s_{p,t+\tau}\right) + \epsilon \tag{5.7}$$

$$c1 = 0,\ c2 = 0 \text{ for simple objects}$$

$$c1 = 1,\ c2 = 0 \text{ for compound single-grasp objects}$$

$$c1 = 1,\ c2 = 1 \text{ for compound multi-grasp objects}$$

In order to evaluate these models, each was fit separately with linear regression, using the full dataset of FRs f and MF PC scores s. The trial-averaged R^2 values, R^2_{TA} were then calculated for each model and each unit (see Section A.6.3 for details). R^2_{TA} was used instead of full R^2 in order to focus on the ability of the models to fit task-relevant activity, rather than trial-to-trial variability. Table 5.2 displays the mean and median R^2_{TA} values for each model and the R^2_{TA} values for all units and improvement in R^2_{TA} for the different models are plotted in Figures 5.26 and 5.27.

Table 5.2: **Mean R^2_{TA} for the MF Only, Direct and Interactive models, Grip Affordance Experiment.** P: perceived grip affordance encoding. L: learned grip affordance encoding. P+L: both perceived and learned grip affordance encoding.

			Direct			**Interactive**		
Subject	**Area**	**MF Only**	**P**	**L**	**P+L**	**P**	**L**	**P+L**
Monkey R	M1	0.89	0.90	0.90	0.90	0.92	0.92	0.94
Monkey I	M1	0.72	0.74	0.74	0.75	0.79	0.79	0.84
Monkey T	M1 Left	0.81	0.81	0.81	0.82	0.85	0.84	0.88
Monkey T	M1 Right	0.80	0.80	0.81	0.81	0.83	0.83	0.86

R^2_{TA} increases were modest for all subjects when adding direct grip affordance encoding. Though R^2_{TA} increases were larger for interactive grip affordance encoding models, these models also featured many more parameters.

Due to the fact that R^2_{TA} is bounded at 1, and also always increases when adding more model parameters, it alone does not make a sufficient measure for model selection. As a more concrete measure, the Bayesian Information Criterion (BIC) was calculated for each model and each unit (see Section A.6.3). Model selection proceeded by choosing the model with the lowest BIC. The BIC was chosen over other similar measures such as the Akaike Information Criterion or likelihood ratio, as the BIC penalizes the number of parameters more heavily and is thus more conservative. The number of units that had minimum BIC for each of the models is reported in Table 5.3 and shown in Figure 5.28

According to the BIC measure, the majority of units in all subjects were better fit by models which incorporated object context information. As in Section 4.5, chance levels of model selection frequency were estimated by re-fitting models with object labels shuffled across trials, repeated 100 times. For all subjects, MF Only models were selected at much lower rates than would be expected by chance, and Interactive models were selected at much higher rates than would be expected by chance, especially in Monkey R. Models which

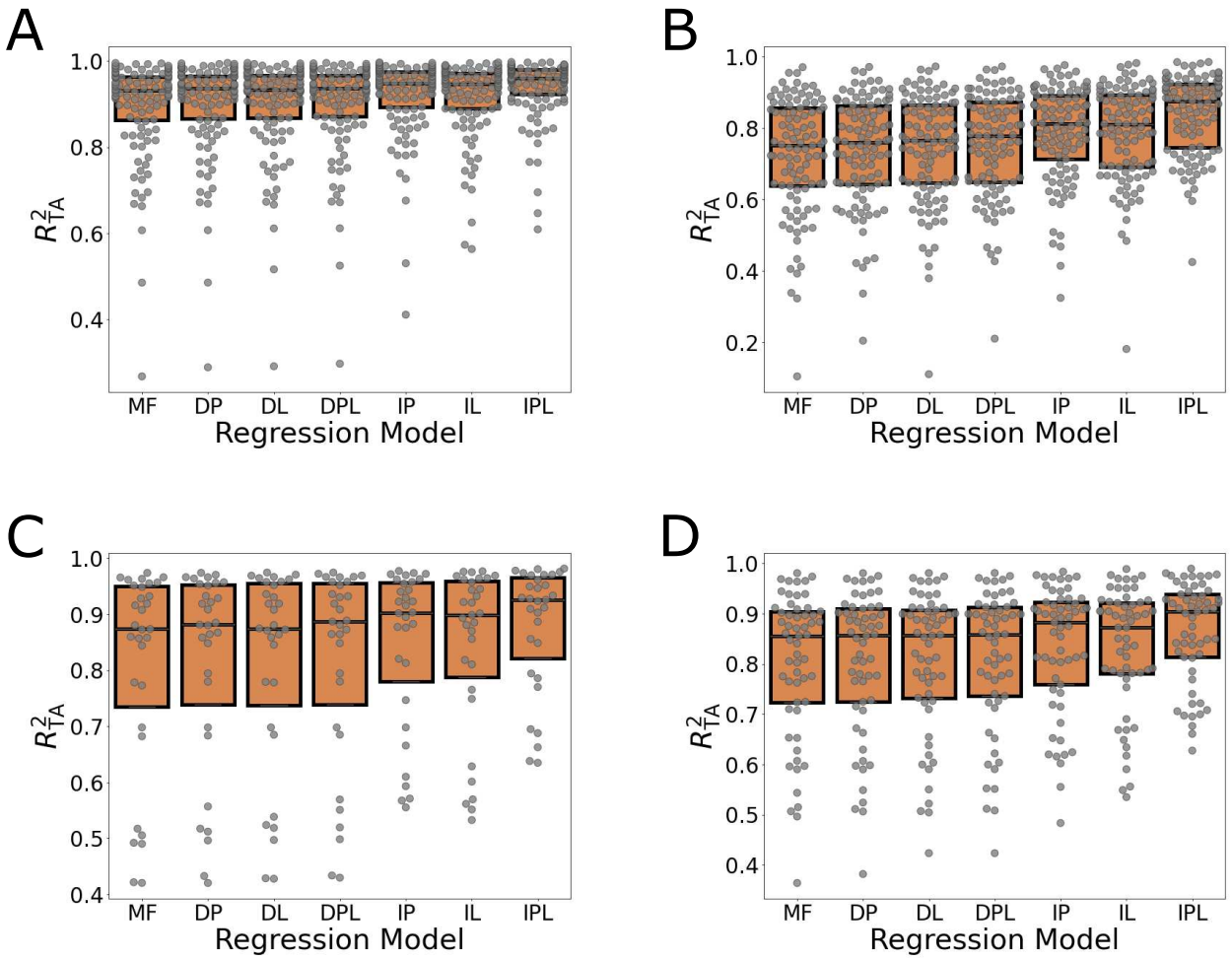

Figure 5.26: R^2_{TA} **for the MF Only, Direct, and Interactive models, Grip Affordance Experiment.** A: Monkey R. B: Monkey I. C: Monkey T left hemisphere. D: Monkey T right hemisphere. R^2_{TA} values for each unit for each model. Gray circles: individual unit R^2_{TA} values. Boxplots denote the median and interquartile range. MF: MF Only model. D: direct grip affordance encoding models. I: interactive grip affordance encoding models. P: perceived grip affordance, L: learned grip affordance.

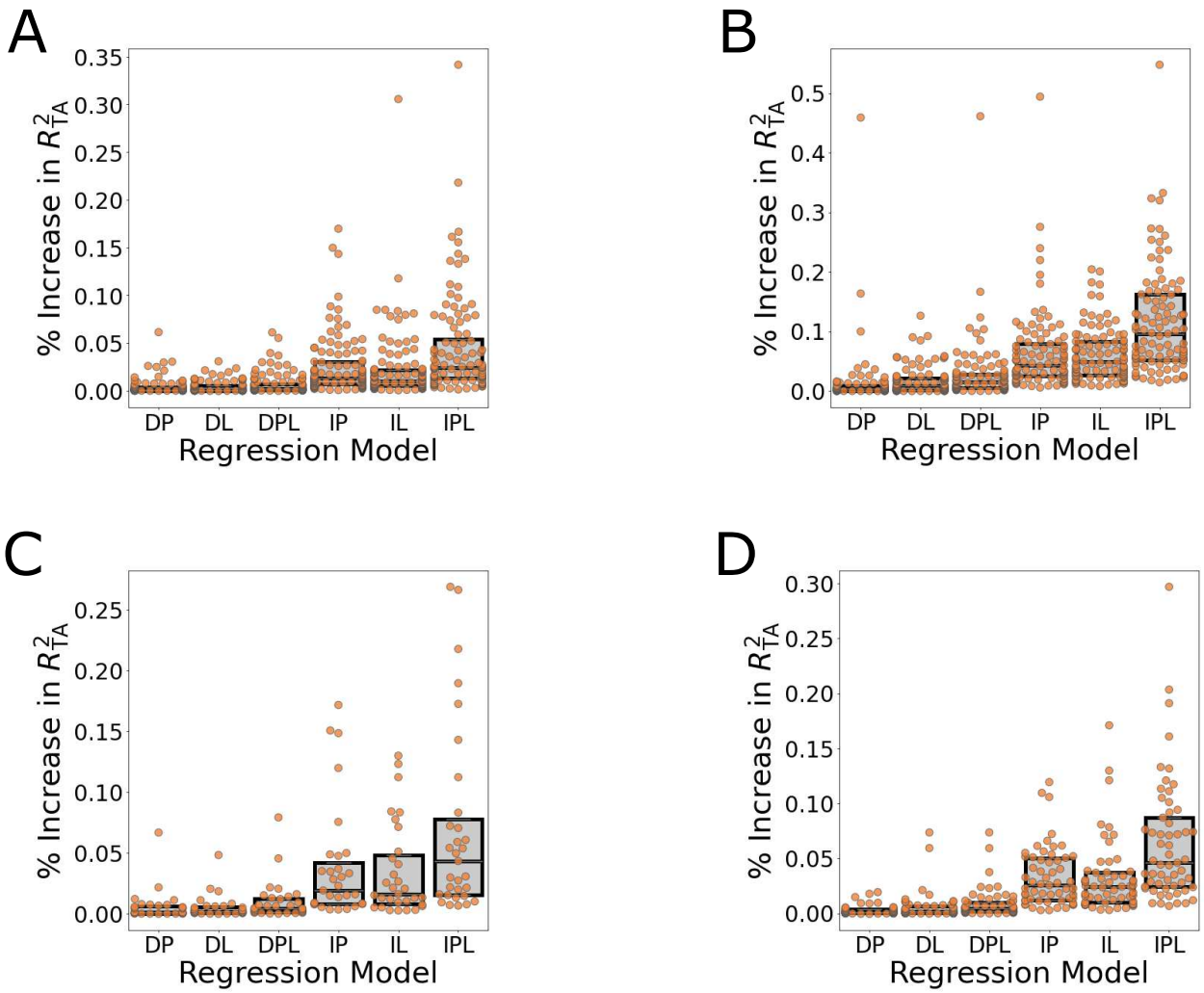

Figure 5.27: R^2_{TA} **increases for the MF Only, Direct, and Interactive models, Grip Affordance Experiment.** A: Monkey R. B: Monkey I. C: Monkey T left hemisphere. D: Monkey T right hemisphere. R^2_{TA} increases for the Direct and Interactive models vs. the MF Only model. Orange circles: individual unit R^2_{TA} increases. Boxplots denote the median and interquartile range. MF: MF Only model. D: direct grip affordance encoding models. I: interactive grip affordance encoding models. P: perceived grip affordance, L: learned grip affordance.

Table 5.3: **The proportion of units which were best fit by the MF Only, Direct and Interactive models according to BIC, Grip Affordance Experiment.** The model for which BIC was minimal was selected as the best model for each unit. P: perceived grip affordance encoding. L: learned grip affordance encoding. P+L: both perceived and learned grip affordance encoding.

			Direct			**Interactive**		
Subject	**Area**	**MF Only**	**P**	**L**	**P+L**	**P**	**L**	**P+L**
Monkey R	M1	9.3%	4.6%	7.4%	7.4%	9.3%	5.6%	56.5%
Monkey I	M1	10.3%	12.4%	21.6%	11.3%	16.5%	6.2%	21.6%
Monkey T	M1 Left	22.6%	16.1%	12.9%	9.7%	9.7%	9.7%	19.4%
Monkey T	M1 Right	15.8%	8.8%	12.3%	8.8%	14.0%	8.8%	31.6%

featured Direct or Indirect encoding of grip affordance factors were selected for 90.7, 89.6, 77.4 and 84.2% of units for Monkey R, Monkey I, Monkey T left hemisphere and Monkey T right hemisphere respectively (chance levels: 41.4, 37.3, 35.8 and 32.8%). Models which featured Interactive grip affordance encoding were selected for 71.2, 44.3, 38.7 and 54.3% of units for Monkey R, Monkey I, Monkey T left hemisphere and Monkey T right hemisphere respectively (chance levels: 4.3, 0.8, 2.6 and 2.4%).

For Monkey R and Monkey T right hemisphere, the Interactive perceived and learned grip affordance encoding model was the single model which best fit the most number of units. For Monkey I and Monkey T left hemisphere, direct grip affordance encoding was more prevalent. As in Section 5.4, there was no clear predominance of perceived grip affordance encoding over learned grip affordance encoding, and many individual units were best fit by models that incorporated direct or interactive encoding of both perceived and learned grip affordance differences.

The selection of models with Interactive grip affordance encoding suggests that many units changed their relations to MFs when objects with different grip affordances were

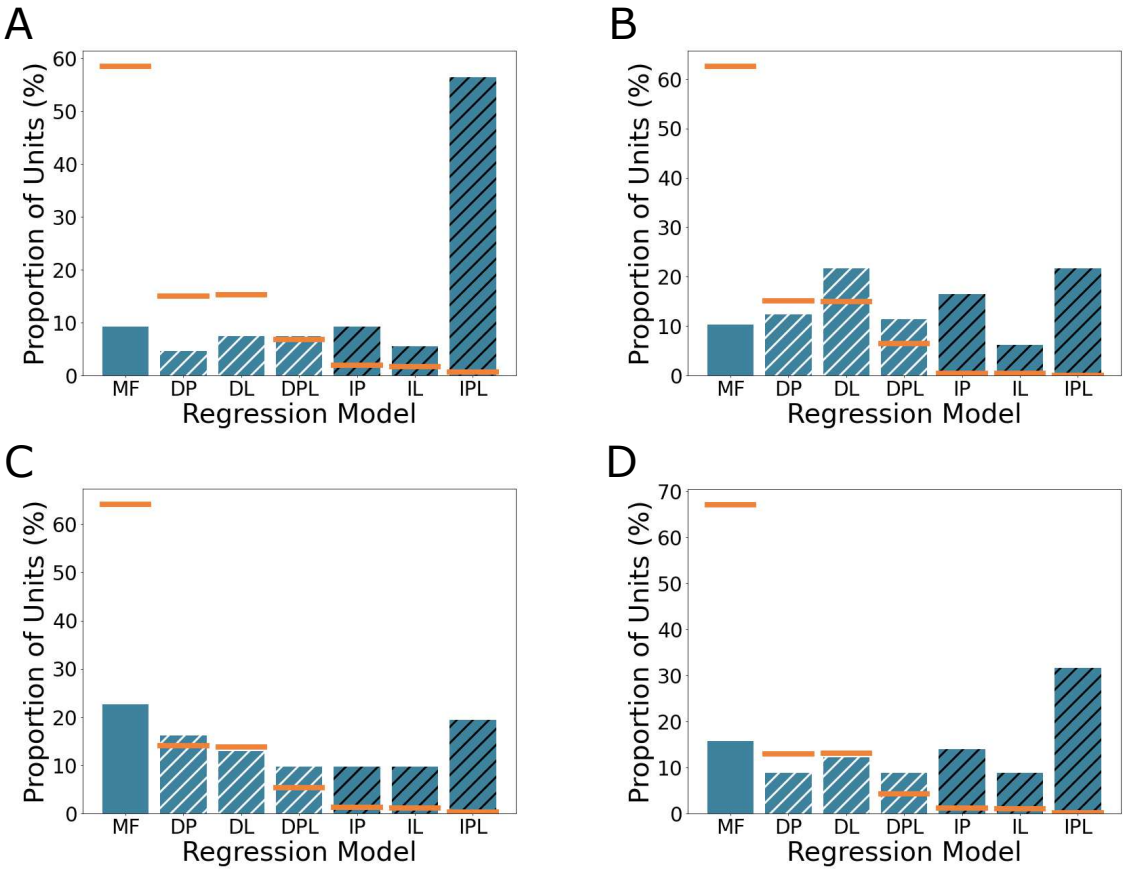

Figure 5.28: **The proportion of units for which each model was the best, according to BIC, Grip Affordance Experiment.** The model for which BIC was minimal was selected as the best model for each unit. A: Monkey R. B: Monkey I. C: Monkey T left hemisphere. D: Monkey T right hemisphere. MF: MF Only model. D, white hatches: direct grip affordance encoding models. I, black hatches: interactive grip affordance encoding models. P: perceived grip affordance, L: learned grip affordance. Orange lines: chance levels of selecting each model, generated by shuffling object context labels 100 times.

grasped. To assess the size of these effects, the angular distance between tuning coefficient vectors Θ were calculated as in Equation 4.25 in Section 4.5 only for units which preferred Interactive grip affordance encoding models. This resulted in average angular distances of 10.2, 18.2, 8.1 and 9.9 degrees for Monkey R, Monkey I, Monkey T left hemisphere and Monkey T right hemisphere respectively. These relatively small Θ values suggest that any grip affordance context related MF tuning coefficient changes were small in magnitude.

These results suggest that grip affordance encoding was prevalent in many individual units in all subjects, and was often interactive with MF encoding. These model fitting analyses identified grip affordance encoding in many more units than did the extralinear modulation analyses of Section 5.4. This implies that grip affordance may have been present in many units, but very small in magnitude. Interactive grip affordance encoding should negatively impact across-context MF decoding, but the small size of the grip affordance encoding effect suggests that this impact may be small. The next section directly addresses the performance of MF decoders in the different object contexts.

5.6 Impact of Grip Affordance on MF Decoding

Successful implementation of an upper limb motor neuroprosthesis requires consistent decoding across different contexts. A neuroprosthetic MF decoder must be able to decode intended grasping movements made on objects that were not used for training the decoder. One way that these objects could differ is in their perceived or learned grip affordances. In this section, various decoders were built to determine the impact of grip affordance encoding in M1 on MF decoding from M1 across different object contexts (objects with different perceived or learned grip affordances).

As in Section 4.6, decoders were built to approximate the approach used in the recent upper limb neuroprosthetic studies of Wodlinger et al and Clanton [119, 437]. The decoding framework is defined in Equation 4.26 in Section 4.6. Details of decoder fitting and cross-validation are provided in Section A.6.5. First, decoders were built and tested on all data

from the Grip Affordance Experiment to decode each normalized MF independently. These decoders were evaluated using 10-fold cross-validation, with RMSE as the goodness of fit measure. The performance of the full decoders are presented in Figure 5.29.

Full decoding results were qualitatively similar to the results for the Object Presence Experiment in Section 4.6. In general, proximal joint angles and hand positions were decoded better than distal joint angles. Hand positions and joint angles were decoded better than hand velocities and joint angular velocities. EMGs were decoded at a level intermediate between joint angles and joint angular velocities, with little difference between proximal and distal EMGs.

To measure the potential effects of grip affordance encoding signals on across-context decoding, 4 different data partitions were used for training separate decoders:

1. The "All Data" decoder, trained on data from all conditions.
2. The "Simple Object" decoder, trained on data from Power Grasps made on the Simple Power Object and Pinch Grasps made on the Simple Pinch Object.
3. The "Compound Single-Grasp Object" decoder, trained on data from Power Grasps made on the Compound Power Object and Pinch Grasps made on the Compound Pinch Object.
4. The "Compound Multi-Grasp Object" decoder, trained on data from Power Grasps and Pinch Grasps made on the Compound Multi-Grasp Object.

Each decoder was tested by decoding data in 3 partitions: the Simple Object data, the Compound Single-Grasp Object data, and the Compound Multi-Grasp Object data. Thus, decoding was performed with full data, within contexts or across contexts. For example, training a decoder on Simple Object data and testing on Simple Object data represented a case of within-context decoding. Training a decoder on Simple Object data and testing on Compound Multi-Grasp data constituted a case of across-context decoding. All decoders were fit and evaluated using 10-fold cross-validation. The resulting decoding RMSEs are presented in Figure 5.30.

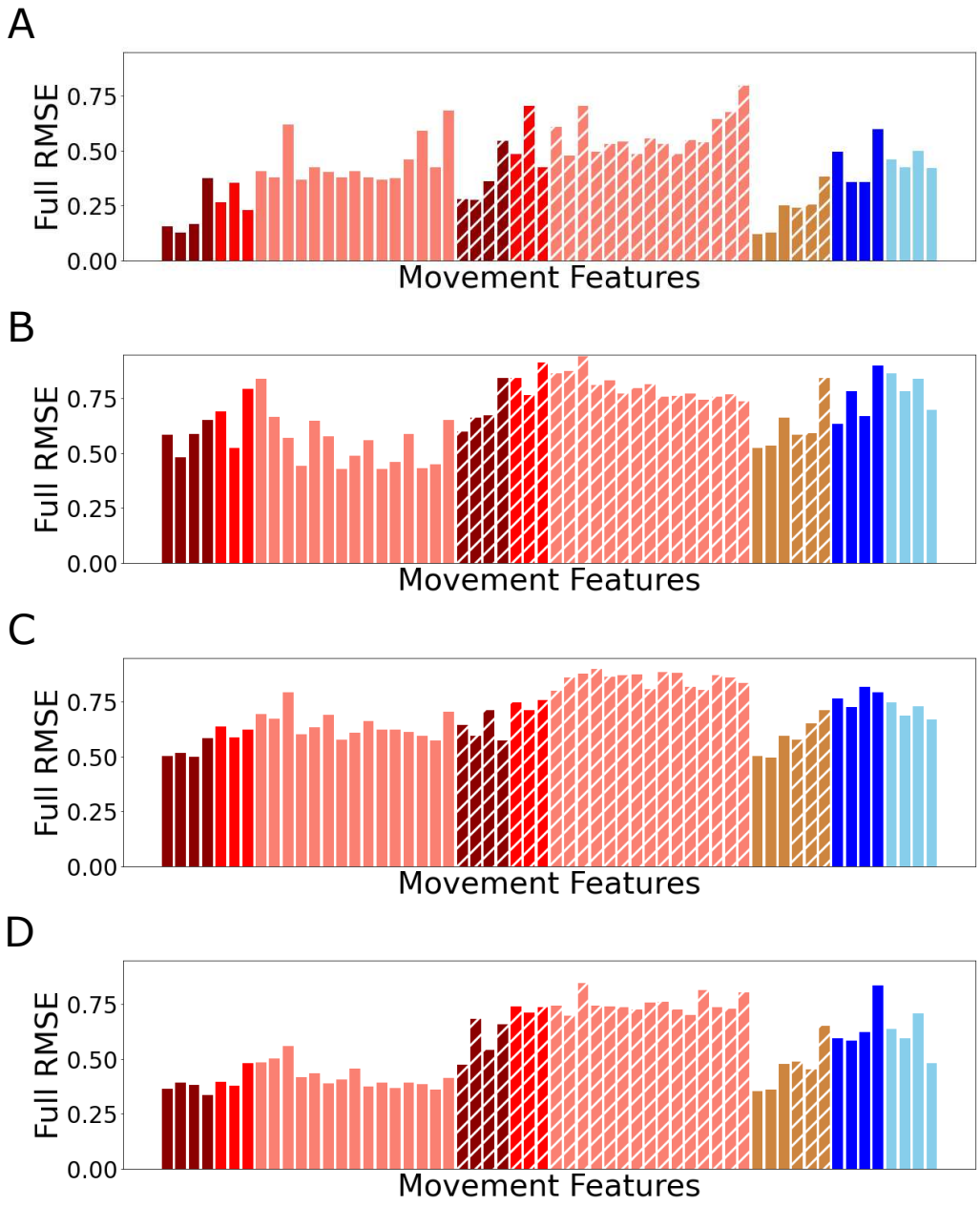

Figure 5.29: **Decoder performance in terms of RMSE when decoding normalized MFs using all data** A Monkey R. B Monkey I. C: Monkey T left hemisphere. D: Monkey T right hemisphere. Each bar is a different normalized MF. Hatched bars are velocities. Dark red: shoulder and elbow joint angles and joint angular velocities, Red: wrist joint angles and joint angular velocities, Light red: finger joint angles and joint angular velocities, Tan: hand positions and velocities, Dark blue: proximal EMG, Light blue: distal EMG

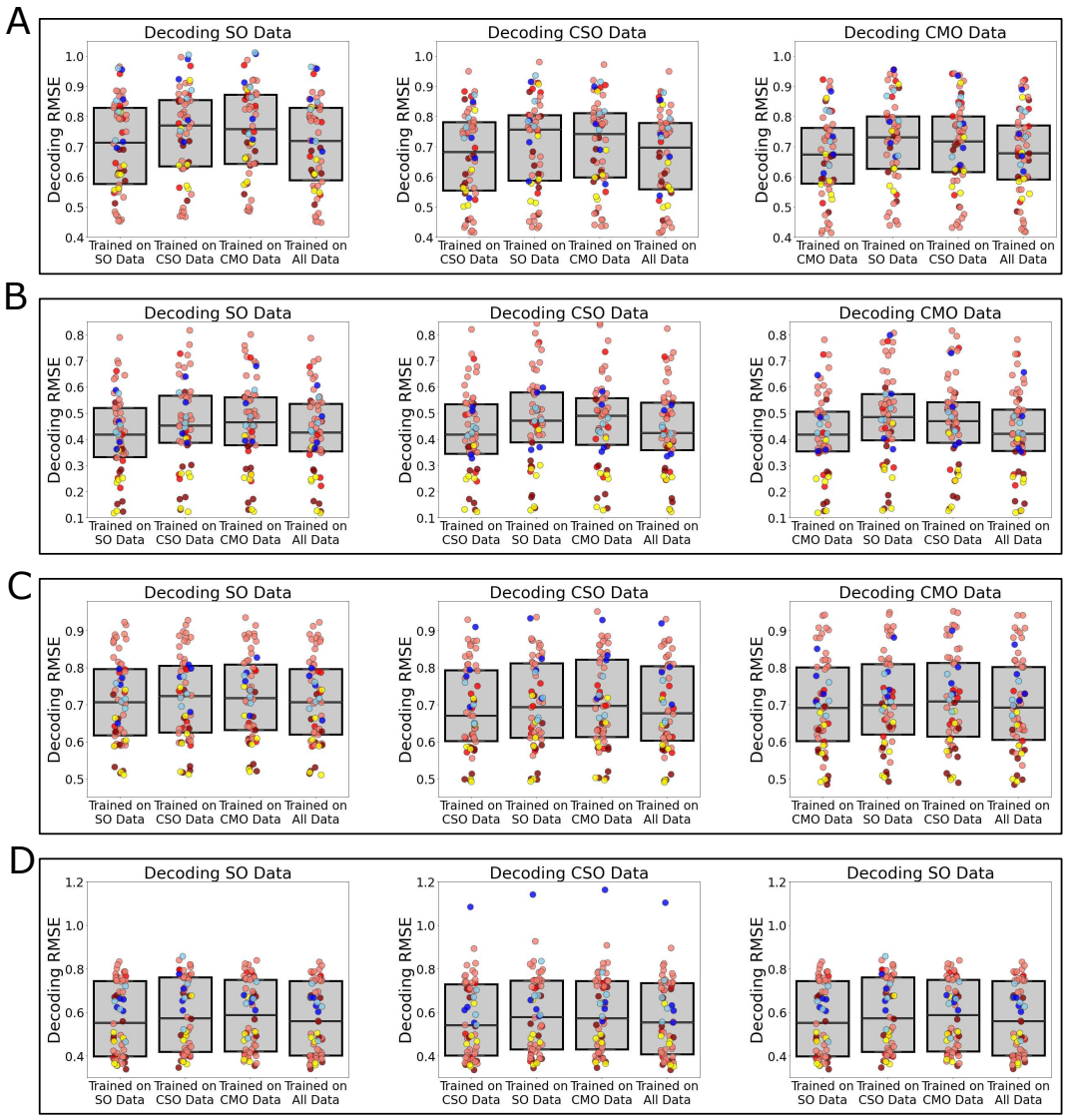

Figure 5.30: **Decoder performance in terms of RMSE when decoding within and across contexts, Grip Affordance Experiment.** A: Monkey R. B: Monkey I. C: Monkey T left hemisphere. D: Monkey T right hemisphere. SO: Simple Objects. CSO: Compound Single-Grasp Objects. CMO: Compound Multi-Grasp Object. Box plots represent the median and interquartile range for all decoded MFs. Colored circles reach represent the RMSE for a single decoded MF. Red circles: joint angles and joint angular velocities. Yellow circles: hand positions and hand velocities. Blue circles: EMG. Lighter colors indicate distal MFs, darker colors are proximal MFs.

Only modest decreases in performance were observed when decoding between contexts as compared to decoding within contexts. Performance of decoders trained on full data were close to within-context decoders. Perceived and learned grip affordance differences both affected decoder performance at approximately the same level.

For a more concise expression of decoder performance within and between contexts, all within-context RMSEs were combined by the square root of the square and average of within-context RMSE values. This was also done for between-context decoder RMSEs and full decoder RMSEs. These averaged RMSE results are presented in Figure 5.31

To measure the impact of decoding across contexts or using full data decoders compared to within-context decoders, the percent change in RMSE was calculated for across-context and full data decoders compared to the within-context decoder values. These percentage RMSE increases, averaged across all MFs, are presented in Table 5.4

As seen by the overall decoder RMSE increases, only modest performance decreases were observed for across-context decoders. However, nearly all of the within-context decoder performance was recovered by training decoders using the full dataset. Thus, grip affordance encoding presented only a small impediment to decoders when attempting to decode grasps on objects with different grip affordances than those used in the training dataset. Decoder performance can be recovered by including all the different object contexts in the training dataset.

Thus far the grip affordance encoding signal in M1 has been shown to be consistent but small in magnitude, with only minor impact on decoding performance. In the next section, the information content of the grip affordance encoding signal is examined in terms of the relation of the grip affordance encoding signal to the afforded but unused grasp.

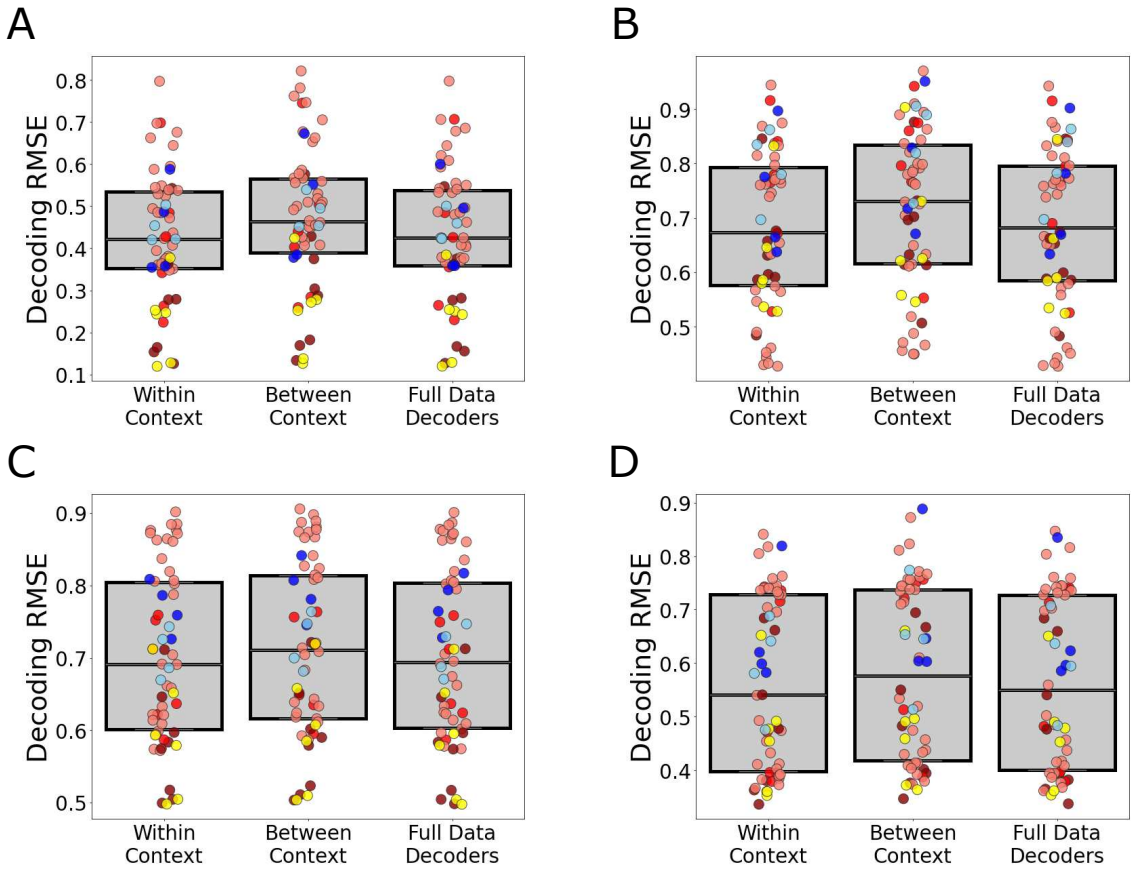

Figure 5.31: **Combined decoder RMSEs for within-context, between-context and full data decoders, Grip Affordance Experiment.** A: Monkey R. B: Monkey I. C: Monkey T left hemisphere. D: Monkey T right hemisphere. Box plots represent the median and interquartile range for all decoded MFs. Colored circles reach represent the RMSE for a single decoded MF. Red circles: joint angles and joint angular velocities. Yellow circles: hand positions and hand velocities. Blue circles: EMG. Lighter colors indicate distal MFs, darker colors are proximal MFs.

Table 5.4: **Percent increase in RMSE for across-context and full data decoders, compared to within-context decoders.**

Subject	**Area**	**Across-context**	**Full Data**
Monkey R	M1	11.1%	2.0%
Monkey I	M1	6.0%	0.5%
Monkey T	M1 Left	1.7%	0.2%
Monkey T	M1 Right	3.7%	0.5%

5.7 Relation of Grip Affordance and Grasp Encoding

The previous sections have focused on assessing the magnitudes of the differences in behavior and neural activity during similar grasps on objects with differences in perceived and learned grip affordances, and on what portion of neural differences may reflect encoding of MF differences or contextual encoding of grip affordances. In this section, the relation of grip affordance dependent differences and grasp encoding is examined in more detail. Specifically, we ask if the presence of a perceived or learned grip affordance biases behavior and neural activity toward the behavior or neural activity associated with the unused afforded grip type. Only weak evidence is found for such biasing occurring in the early preparatory period in neural activity.

Examples of such behavioral biasing have been observed in humans. In one study by Gentilucci in 2002 [362], subjects grasped identically shaped sticks attached to different objects. Although the graspable portions of the objects were the same, the ungrasped portions of the object differed. It was found that when the ungrasped portion of the object was large, the subjects exhibited larger grip apertures, suggesting that behavior may have been biased toward behavior associated with the affordances of the large, ungrasped portion of the object. The analyses of this section are designed to determine if similar effects were obtained in both behavior and neural activity when perceived or learned grip affordances were present but ungrasped.

As an illustration of this concept, we first consider the case of Power Grasps made on the Simple Power Object and Power Grasps made on the Compound Power Object. The Simple Power Object had only a singe perceived grip affordance for Power Grasps. The Compound Power Object had two perceived grip affordances, for Power Grasps or Pinch Grasps. The results of Sections 5.2 and 5.3 showed that behavior and neural activity were significantly different for Power Grasps made on the Simple Power Object and the Compound Power Object. Here, we investigate the hypothesis that the presence of the perceived Pinch Grasp affordance biases the behavior and neural activity during Power Grasps made on the Compound Power Object toward the behavior and neural activity associated with Pinch Grasps relative to the behavior and neural activity observed during

Power Grasps made on the Simple Power Object. Such biasing could reflect "automatic activation" of the representation of the perceived Pinch Grasp affordance. That is, when a Pinch Grasp affordance is perceived, it may activate the neural representation associated with Pinch Grasps, even when a Pinch Grasp is not actually performed. Such a pattern would constitute a "pro-affordance bias." Conversely, a cognitive, purposeful avoidance of the unused Pinch Grasp affordance could bias neural activity away from the Pinch Grasp representation. This would constitute an "anti-affordance bias." Finally, the encoding of the perceived Pinch Grasp affordance could act independently of the Pinch Grasp representation, which would represent "no affordance bias."

To characterize these potential biases in behavior and neural activity due to perceived grip affordances, the perceived affordance shifts S^{MFPC} and S^{FRPC} were calculated according to Equations 5.8–5.11.

$$S^{\mathrm{mMFPC}}_{\mathrm{PinchPerceived},t} = \frac{(M_{\mathrm{PinchGrasp,SpO},t} - M_{\mathrm{PowerGrasp,SPO},t}) \cdot (M_{\mathrm{PowerGrasp,CPO},t} - M_{\mathrm{PowerGrasp,SPO},t})}{\|M_{\mathrm{PinchGrasp,SpO},t} - M_{\mathrm{PowerGrasp,SPO},t}\|^2} \tag{5.8}$$

$$S^{\mathrm{mMFPC}}_{\mathrm{PowerPerceived},t} = \frac{(M_{\mathrm{PowerGrasp,SpO},t} - M_{\mathrm{PinchGrasp,SpO},t}) \cdot (M_{\mathrm{PinchGrasp,CpO},t} - M_{\mathrm{PinchGrasp,SpO},t})}{\|M_{\mathrm{PowerGrasp,SPO},t} - M_{\mathrm{PinchGrasp,SpO},t}\|^2} \tag{5.9}$$

$$S^{\mathrm{mFRPC}}_{\mathrm{PinchPerceived},t} = \frac{(F_{\mathrm{PinchGrasp,SpO},t} - F_{\mathrm{PowerGrasp,SPO},t}) \cdot (F_{\mathrm{PowerGrasp,CPO},t} - F_{\mathrm{PowerGrasp,SPO},t})}{\|F_{\mathrm{PinchGrasp,SpO},t} - F_{\mathrm{PowerGrasp,SPO},t}\|^2} \tag{5.10}$$

$$S^{\mathrm{mFRPC}}_{\mathrm{PowerPerceived},t} = \frac{(F_{\mathrm{PowerGrasp,SpO},t} - F_{\mathrm{PinchGrasp,SpO},t}) \cdot (F_{\mathrm{PinchGrasp,CpO},t} - F_{\mathrm{PinchGrasp,SpO},t})}{\|F_{\mathrm{PowerGrasp,SPO},t} - F_{\mathrm{PinchGrasp,SpO},t}\|^2} \tag{5.11}$$

where $M_{i,t}$ is the vector of mMF PC scores for condition i at time t, $F_{i,t}$ is the vector of mFR PC scores for condition i at time t, SPO is the Simple Power Object, SpO is the Simple Pinch Object, CPO is the Compound Power Object, CpO is the Compound Pinch Object, $\cdot$ denotes the vector dot product operation and $\|\|$ denotes the vector norm operation. These

perceived affordance shifts measure the direction effect of the presence of a perceived grip affordance. A positive value of $S^{\text{mMFPC}}_{\text{PinchPerceived}}$ would indicate that the behavior observed for Power Grasps on the Compound Power Object (which featured a perceived Pinch Grasp affordance) was biased toward the behavior observed for Pinch Grasps on the Simple Pinch Object, relative to Power Grasps on the Simple Power Object. A negative value would indicate that behavior was biased away from the perceived Pinch Grasp affordance. A value approximately equal to zero indicates that the observed behavioral difference was unrelated to the Pinch Grasp affordance.

Affordance shift values were also calculated with respect to learned grip affordances, according to Equations 5.12–5.15.

$$S^{\text{mMFPC}}_{\text{PinchLearned},t} = \frac{(M_{\text{PinchGrasp,CMO},t} - M_{\text{PowerGrasp,CPO},t}) \cdot (M_{\text{PowerGrasp,CMO},t} - M_{\text{PowerGrasp,CPO},t})}{\|M_{\text{PinchGrasp,CMO},t} - M_{\text{PowerGrasp,CPO},t}\|^2} \tag{5.12}$$

$$S^{\text{mMFPC}}_{\text{PowerLearned},t} = \frac{(M_{\text{PowerGrasp,CMO},t} - M_{\text{PinchGrasp,CpO},t}) \cdot (M_{\text{PinchGrasp,CMO},t} - M_{\text{PinchGrasp,CpO},t})}{\|M_{\text{PowerGrasp,CMO},t} - M_{\text{PinchGrasp,CpO},t}\|^2} \tag{5.13}$$

$$S^{\text{mFRPC}}_{\text{PinchLearned},t} = \frac{(F_{\text{PinchGrasp,CMO},t} - F_{\text{PowerGrasp,CPO},t}) \cdot (F_{\text{PowerGrasp,CMO},t} - F_{\text{PowerGrasp,CPO},t})}{\|F_{\text{PinchGrasp,CMO},t} - F_{\text{PowerGrasp,CPO},t}\|^2} \tag{5.14}$$

$$S^{\text{mFRPC}}_{\text{PowerLearned},t} = \frac{(F_{\text{PowerGrasp,CMO},t} - F_{\text{PinchGrasp,CpO},t}) \cdot (F_{\text{PinchGrasp,CMO},t} - F_{\text{PinchGrasp,CpO},t})}{\|F_{\text{PowerGrasp,CMO},t} - F_{\text{PinchGrasp,CpO},t}\|^2} \tag{5.15}$$

where CMO denotes the Compound Multi-Grasp Object. The learned affordance shifts measured the directional impact of the presence of a learned grip affordance. A positive value indicates that behavior or neural activity is shifted towards the behavior or neural activity associated with the learned but unused grip affordance.

Additionally, the analyses of Section 5.4 showed that M1 encoded perceived and learned grip affordances in that neural modulation for same-grasp, different-context conditions was

greater than could be explained by linear tuning to MFs. To determine whether this grip affordance encoding signal also contained evidence for automatic activation of perceived and learned grip affordances, the affordance shifts were also calculated in null space neural activity. The null space neural activity was the component of neural activity that could not linearly combined to decode mMF PC scores. The null space affordance shifts were calculated according to Equations 5.16–5.19.

$$S^{\text{null}}_{\text{PinchPerceived},t} = \frac{\left(\hat{F}^{\text{null}}_{\text{PinchGrasp,SpO},t} - \hat{F}^{\text{null}}_{\text{PowerGrasp,SPO},t}\right) \cdot \left(\hat{F}^{\text{null}}_{\text{PowerGrasp,CPO},t} - \hat{F}^{\text{null}}_{\text{PowerGrasp,SPO},t}\right)}{\|\hat{F}^{\text{null}}_{\text{PinchGrasp,SpO},t} - \hat{F}^{\text{null}}_{\text{PowerGrasp,SPO},t}\|^2} \tag{5.16}$$

$$S^{\text{null}}_{\text{PowerPerceived},t} = \frac{\left(\hat{F}^{\text{null}}_{\text{PowerGrasp,SpO},t} - \hat{F}^{\text{null}}_{\text{PinchGrasp,SpO},t}\right) \cdot \left(\hat{F}^{\text{null}}_{\text{PinchGrasp,CpO},t} - \hat{F}^{\text{null}}_{\text{PinchGrasp,SpO},t}\right)}{\|\hat{F}^{\text{null}}_{\text{PowerGrasp,SpO},t} - \hat{F}^{\text{null}}_{\text{PinchGrasp,SpO},t}\|^2} \tag{5.17}$$

$$S^{\text{null}}_{\text{PinchLearned},t} = \frac{\left(\hat{F}^{\text{null}}_{\text{PinchGrasp,CMO},t} - \hat{F}^{\text{null}}_{\text{PowerGrasp,CPO},t}\right) \cdot \left(\hat{F}^{\text{null}}_{\text{PowerGrasp,CMO},t} - \hat{F}^{\text{null}}_{\text{PowerGrasp,CPO},t}\right)}{\|\hat{F}^{\text{null}}_{\text{PinchGrasp,CMO},t} - \hat{F}^{\text{null}}_{\text{PowerGrasp,CPO},t}\|^2} \tag{5.18}$$

$$S^{\text{null}}_{\text{PowerLearned},t} = \frac{\left(\hat{F}^{\text{null}}_{\text{PowerGrasp,CMO},t} - \hat{F}^{\text{null}}_{\text{PinchGrasp,CpO},t}\right) \cdot \left(\hat{F}^{\text{null}}_{\text{PinchGrasp,CMO},t} - \hat{F}^{\text{null}}_{\text{PinchGrasp,CpO},t}\right)}{\|\hat{F}^{\text{null}}_{\text{PowerGrasp,CMO},t} - \hat{F}^{\text{null}}_{\text{PinchGrasp,CpO},t}\|^2} \tag{5.19}$$

where $\hat{F}^{\text{null}}$ is the vector of null space neural activity for condition i at time t, calculated according to Equation 4.15.

The three potential affordance bias scenarios for the perceived pinch grip affordance are depicted schematically in Figure 5.32.

The affordance shifts calculated in mMF PC space, mFR PC space and null space neural activity are portrayed in Figures 5.33, 5.34 and 5.35.

Positive affordance shift values, indicating a pro-affordance bias, were evident in mMF PC space before the reach for all subjects. This reflects the finding that subjects exhibited a

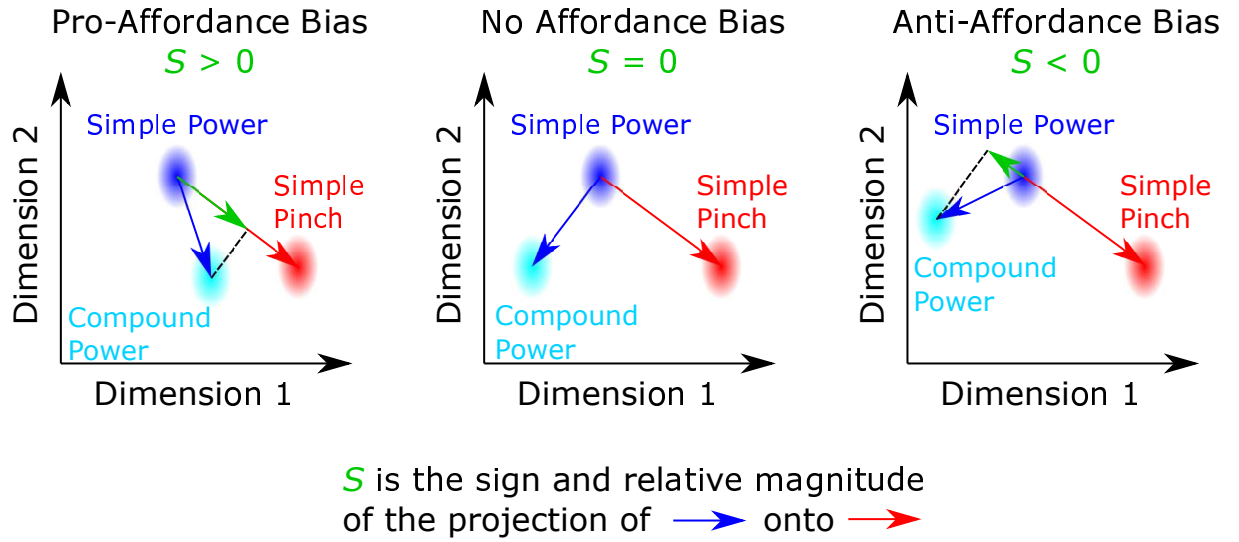

Figure 5.32: **Schematic illustration of three potential forms of grip affordance bias for perceived pinch grip affordance.** Ellipses represent distributions of behavior or neural activity for different conditions. Blue ellipse: Power Grasp, Simple Power Object. Light blue ellipse: Power Grasp, Compound Power Object. Red ellipse: Pinch Grasp, Simple Pinch Object. Blue vector: vector between Power Grasp, Simple Power Object and Power Grasp, Compound Power Object. Red vector: vector between Power Grasp, Simple Power Object and Pinch Grasp, Simple Pinch Object. Green vector: the projection of the blue vector onto the red vector. The affordance shift is the magnitude of the green vector divided by the magnitude of the red vector, with the sign positive when the green and red vector are aligned, and negative when the green and red vector are opposed. Dimensions could correspond to mMF PC scores for S^{mMFPC}, mFR PC scores for S^{mFRPC} and null space neural dimensions for S^{null}. The diagram shows affordance bias scenarios relative to perceived pinch grip at a single time point; S was also calculated relative to perceived power grips, learned pinch grips and learned power grips.

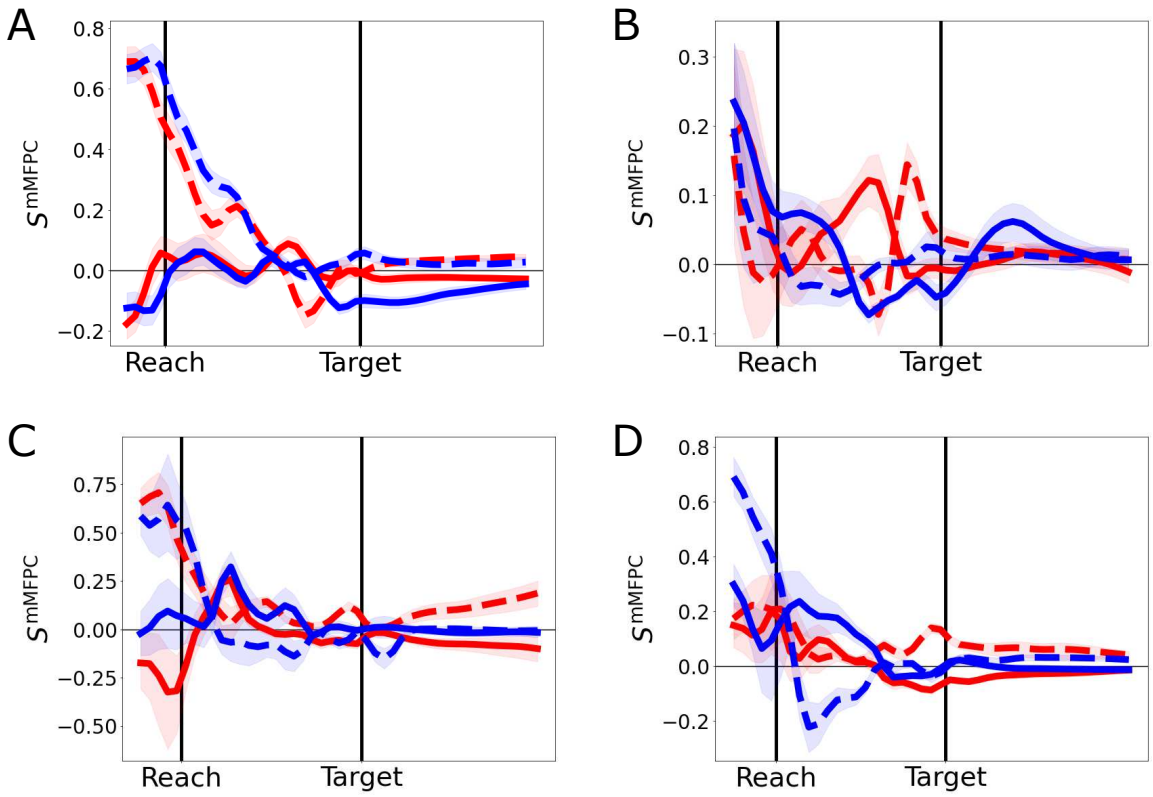

Figure 5.33: **Affordance shifts S^{mMFPC} for the Grip Affordance Experiment.** Affordance shifts calculated in the 99% mMF PC space. A: Monkey R. B: Monkey I. C: Monkey T left hemisphere. D: Monkey T right hemisphere. Blue: shifts for Power Grasp affordances, Red: shifts for Pinch Grasp affordances. Solid lines: perceived affordances. Dashed lines: learned affordances. Shaded 95% confidence intervals are bootstrap intervals, trials resampled 10000 times.

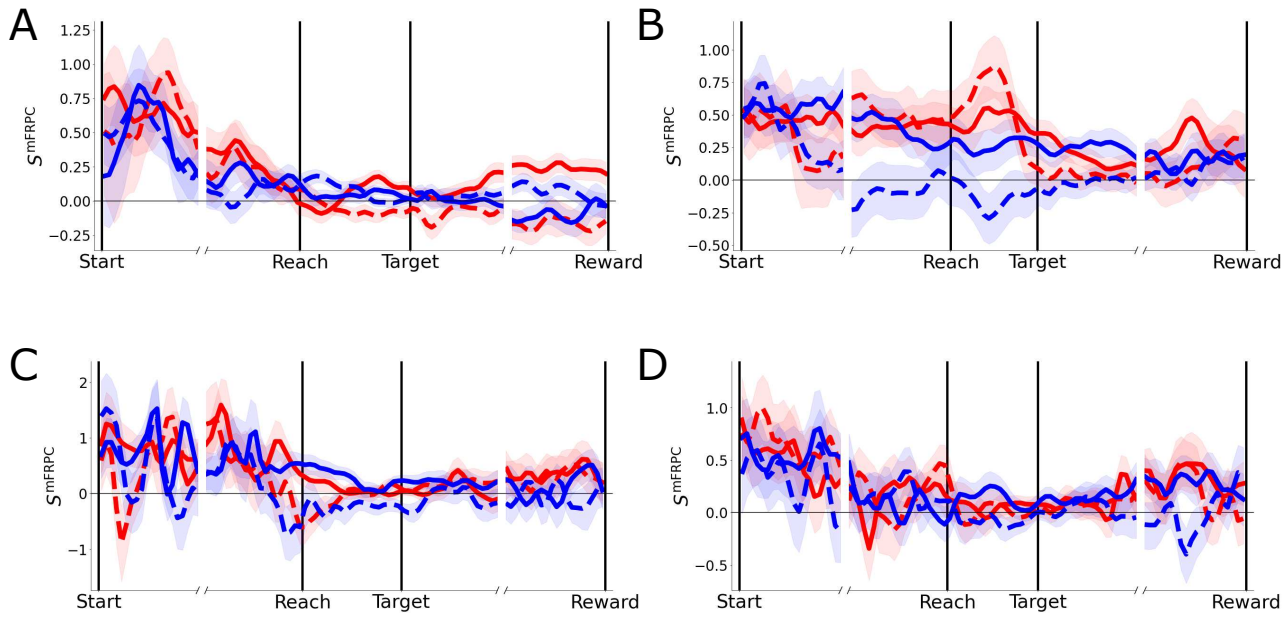

Figure 5.34: **Affordance shifts S^{mFRPC} for the Grip Affordance Experiment.** Affordance shifts calculated in the 99% mFR PC space. A: Monkey R. B: Monkey I. C: Monkey T left hemisphere. D: Monkey T right hemisphere. Blue: shifts for Power Grasp affordances, Red: shifts for Pinch Grasp affordances. Solid lines: perceived affordances. Dashed lines: learned affordances. Shaded 95% confidence intervals are bootstrap intervals, trials resampled 10000 times.

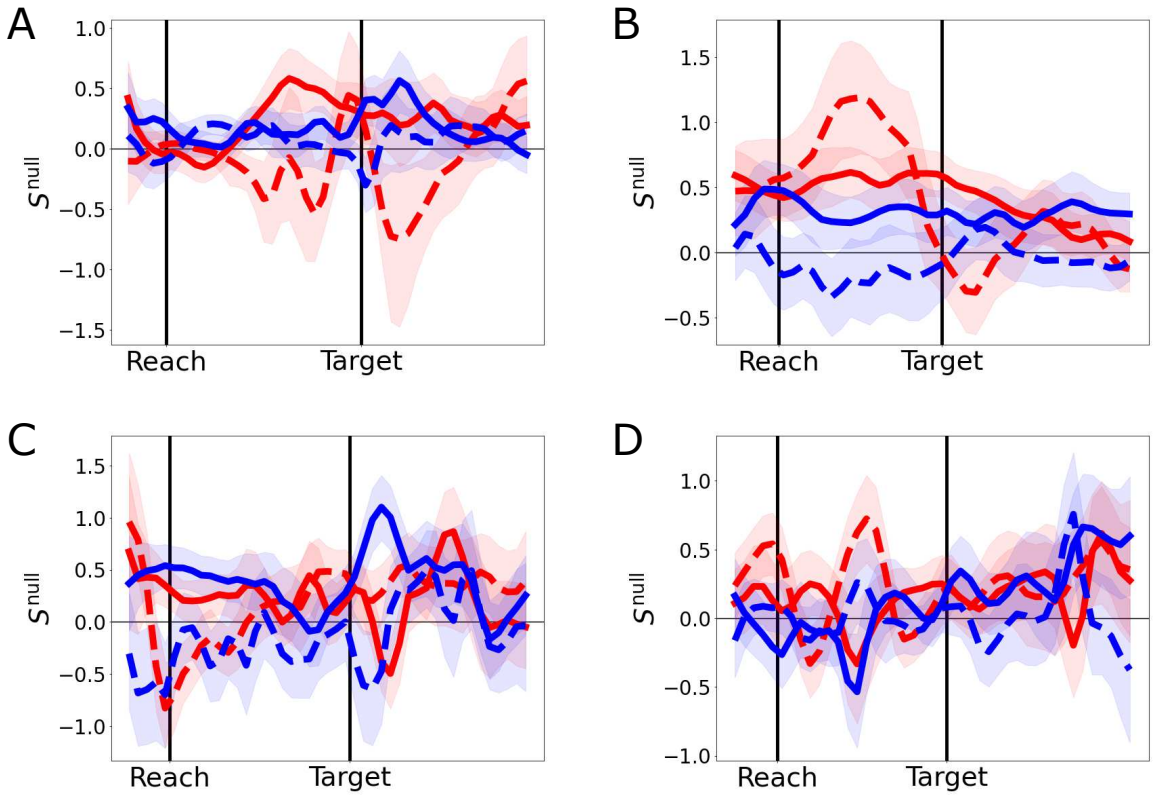

Figure 5.35: **Affordance shifts S^{null} for the Grip Affordance Experiment.** Affordance shifts calculated in null space neural activity. A: Monkey R. B: Monkey I. C: Monkey T left hemisphere. D: Monkey T right hemisphere. Blue: shifts for Power Grasp affordances, Red: shifts for Pinch Grasp affordances. Solid lines: perceived affordances. Dashed lines: learned affordances. Shaded 95% confidence intervals are bootstrap intervals, trials resampled 10000 times.

slightly different start button posture for objects that were only grasped with a Power Grasp and objects that were only grasped with a Pinch Grasp, and exhibited an intermediate posture for trials featuring the Compound Multi-Grasp Object (see Figure 5.4). However, mMF PC affordance shifts were near zero and showed no consistent pattern otherwise during the movement.

In the mFR PC space, affordance shift values were generally positive at the very earliest portions of the trial. As the different objects were presented in different blocks (see 3.2.1), background M1 activity appears to weakly reflected a bias toward the perceived and learned, but unused grip affordances. However, mFR PC affordance shifts were inconsistent between subjects and often near zero during the immediate pre-movement period and throughout the movement, indicating that neural differences observed during the movement were unrelated to encoding of the perceived or learned grip affordances.

Finally, null space affordance shifts showed no consistent pattern and were most frequently not significantly different from zero. This indicates that the component of neural activity specifically related to the encoding of grip affordance differences, though sometimes significant (see Section 5.4) did not encode these grip affordances in a way that related to the representation of the perceived or learned, but unused grip affordance.

In summary, the results presented in this chapter suggest that grip affordance encoding was present in M1, but was small in magnitude. Subjects exhibited very similar but nonetheless consistently significantly different MFs when executing the same grasp on objects with different perceived and learned grip affordances (Section 5.2). Same-grasp conditions were also separable in neural activity, with transient separations in individual FRs and consistent, moderate separation in neural populations. Separation between same-grasp conditions in neural activity was relatively larger than the separation between same-grasp conditions in MFs, relative to the separation between Power Grasps and Pinch Grasps (Section 5.3). The extralinear modulation analyses revealed that grip affordance encoding was evident in a moderate number of individual neurons as well as at the population level for all subjects, in that perceived and learned grip affordance differences evoked neural modulation that could not be fully accounted for by linear encoding of MFs, though this grip affordance encoding signal was small in magnitude (Section 5.4).

Regression model comparisons revealed that grip affordance encoding was evident in many units. For different units, grip affordances were encoded directly in unit FRs or were encoded in an interactive manner with MF encoding (Section 5.5). Grip affordance encoding had only a minor impact on MF decoding, which could be compensated for by including trials for all different objects in the decoder training data set (Section 5.6). Finally, object-dependent background and early preparatory activity may carry information related to the afforded but unused grasp movement.

6.0 Results — Use Affordance Experiment — M1

Results from the Object Presence Experiment, described in Chapter 4, revealed the significant differences in behavior and large differences in neural activity when reaches were performed in the presence or absence of an object, as well as strong explicit encoding of object presence in M1. Results from the Grip Affordance Experiment, described in Chapter 5, revealed subtle but significant changes in behavior and somewhat larger changes in neural activity when objects with different perceived or learned grip affordances were grasped in the same way, and also revealed weak but significant grip affordance encoding in M1. In this chapter, we seek to determine if behavior and M1 neural activity change when grasping objects with different learned use affordances, and whether M1 neural activity additionally encodes object context related to the learned uses of different objects.

The Use Affordance Experiment was deigned to study how behavior and neural activity differ when the same grasps are performed on objects with different learned uses. Many objects, especially tools, have specific uses that are learned through experience. Often, objects with different uses may be shaped similarly and afford similar grasps. For instance, screwdrivers and awls have very similar shapes. They are both grasped using a full hand power grasp around the handle. However, screwdrivers are associated with a rotational twisting motion around the long axis, whereas awls are associated with a forward motion along the long axis. That is, screwdrivers and awls have different learned use affordances; screwdrivers afford screwing and awls afford puncturing.

In the Use Affordance Experiment, we ask whether behavior and M1 neural activity depend on the difference in learned use affordances between two objects, even when the objects are grasped in the same manner and with the same goal.

Two objects were designed and built for this experiment. In a preliminary session, both objects were mechanically fixed in place, and subjects grasped both objects. After this initial session, one object remained mechanically fixed in place, while the other object was released and allowed to slide vertically on guide rods. Subjects were trained to lift the movable object. That is, they learned a new use affordance for only the movable object. In a final

session after this learning occurred, subjects simply grasped and held both objects, or lifted the movable object on some trials. Throughout the sessions, kinematics, muscle activity and neural activity were recorded. In this section, results from the experiment are presented for Monkey R, Monkey I and Monkey T right hemisphere, from which M1 neural data were recorded during the Use Affordance Experiment. Neural data were always recorded from the hemisphere contralateral to the hand used in the task. Results for this experiment from Monkey T PMV and AIP are presented in Section 7.

The main findings of this chapter are summarized as follows. Subjects grasped two identically shaped objects, with two different grip types each, in two sessions: the pre-learning session and the post-learning session. In the pre-learning session, objects were both mechanically fixed in place and differed only by color. In the second session, one object was released while the other remained fixed. Subjects grasped and held both objects, and also grasped and lifted the mobile object. Thus in the pre-learning session, objects had only superficial differences, whereas in the post-learning session, the objects further differed by their learned use affordances. Subtle yet significant differences were observed in behavior for grasps on the objects in the pre-learning session, though the objects differed only by color. Larger behavioral differences were observed for the same grasps executed on the two objects in the post-learning session, after a new use affordance was learned for one object. M1 neural activity also differed for the same grasps executed on the different objects even in the pre-learning session, though differences were larger in the post-learning session. Neural activity differentiated same-grasp conditions to a relatively greater extent than did the MFs. The separation between same-grasp conditions in individual unit FRs and population neural activity was mostly accounted for by fixed linear tuning to MFs, and only weak evidence was observed for explicit encoding of object context in both sessions in M1. Nevertheless, object context was found to be encoded directly in individual unit FRs in some cases, and encoded interactively with MFs in other cases. Object context had little impact on the ability to decode MFs from M1 FRs with a simple linear model. Grasping without lifting the movable object evoked behavior and neural activity that was heavily biased toward the behavior and neural activity associated with subsequent grasping and lifting the movable object, relative to the neural activity associated with grasping the fixed object.

Section 6.1 contains a detailed description of each subject's behavior during the different task conditions of the Use Affordance Experiment. The behavior is described in terms of the observed movement features (MFs), comprised of 22 joint angles and joint angular velocities of the arm, wrist and fingers, 3D hand position and hand velocity, and EMG from eight muscle groups. Section 6.2 characterizes the differences in the MFs observed in the different task conditions. Section 6.3 describes the single unit and population level M1 neural firing rate (FR) responses recorded during the experiment, highlighting the differences in neural activity between same-grasp conditions where present. Section 6.4 concerns the relation between the M1 FRs and the MFs, with specific focus on the evidence for sporadic and weak object context encoding in M1, defined as neural modulation beyond that which can be accounted for by fixed linear tuning to MFs. Section 6.5 compares regression models with direct or interactive object context information. Section 6.6 characterizes the impact of the object context encoding signal on decoding accuracy. Finally, section 6.7 explores the possibility that the differences in behavior and neural activity for power grasps in the post-learning session was related to the learned use action afforded by the movable object.

6.1 Behavioral Results of the Grip Affordance Experiment

For each subject, two sessions were analyzed: a "pre-learning" session and a "post-learning" session. In each session, subjects grasped two objects which were the same shape but different colors. In the pre-learning session, both objects were mechanically fixed in place and subjects grasped and held each object with either a power or a precision grip, resulting in the following 4 task conditions:

1. Power Grasp and Hold, Object 1 (Fixed)
2. Pinch Grasp and Hold, Object 1 (Fixed)
3. Power Grasp and Hold, Object 2 (Fixed)
4. Pinch Grasp and Hold, Object 2 (Fixed)

After the pre-learning session, Object 1 remained mechanically fixed in place while Object 2 was released and allowed to slide vertically on steel guide rods. Subjects learned to lift Object 2 on cue, after grasping it with a Power Grasp. Once this new use was learned for Object 2 and subjects could consistently execute lifts as well as grasps Object 2, data of the post-learning session were recorded. In the post-learning session, subjects repeated all of the task conditions from the pre-learning session, and also performed a Power Grasp and Lift action with Object 2. This resulted in the following 5 task conditions:

1. Power Grasp and Hold, Object 1 (Fixed)
2. Pinch Grasp and Hold, Object 1 (Fixed)
3. Power Grasp and Hold, Object 2 (Movable)
4. Pinch Grasp and Hold, Object 2 (Movable)
5. Power Grasp and Lift, Object 2 (Movable)

All subjects performed 140 repetitions of each task condition, resulting in 560 trials for the pre-learning session and 700 trials for the post-learning session.

For the remainder of this section, Power Grasp and Hold trials are referred to as "Power Hold," Pinch Grasp and Hold trials are referred to as "Pinch Hold" and Power Grasp and Lift trials are referred to as "Power Lift."

The objects of the Use Affordance Experiment are shown in Figure 6.1.

The objects were designed to elicit identical grasps of each type for the grasp-and-hold conditions. To accomplish this, the objects were designed and fabricated to the same dimensions, using CNC milling and 3D printing (see Section A.2.1). The objects were instrumented with force sensors to detect correct and incorrect grasps. Object lifting was tracked using a string potentiometer attached to the object base (Figure 6.2).

All subjects were able to quickly learn the lifting behavior after Object 2 was released. All subjects were able to lift the object without assistance on the first day of training with the movable object, and were consistently able to lift the object on cue within a few sessions. More details of the behavioral training are provided in Section A.3. Figure 6.2 shows single frames of Monkey T performing each of the 5 task conditions of the post-learning session.

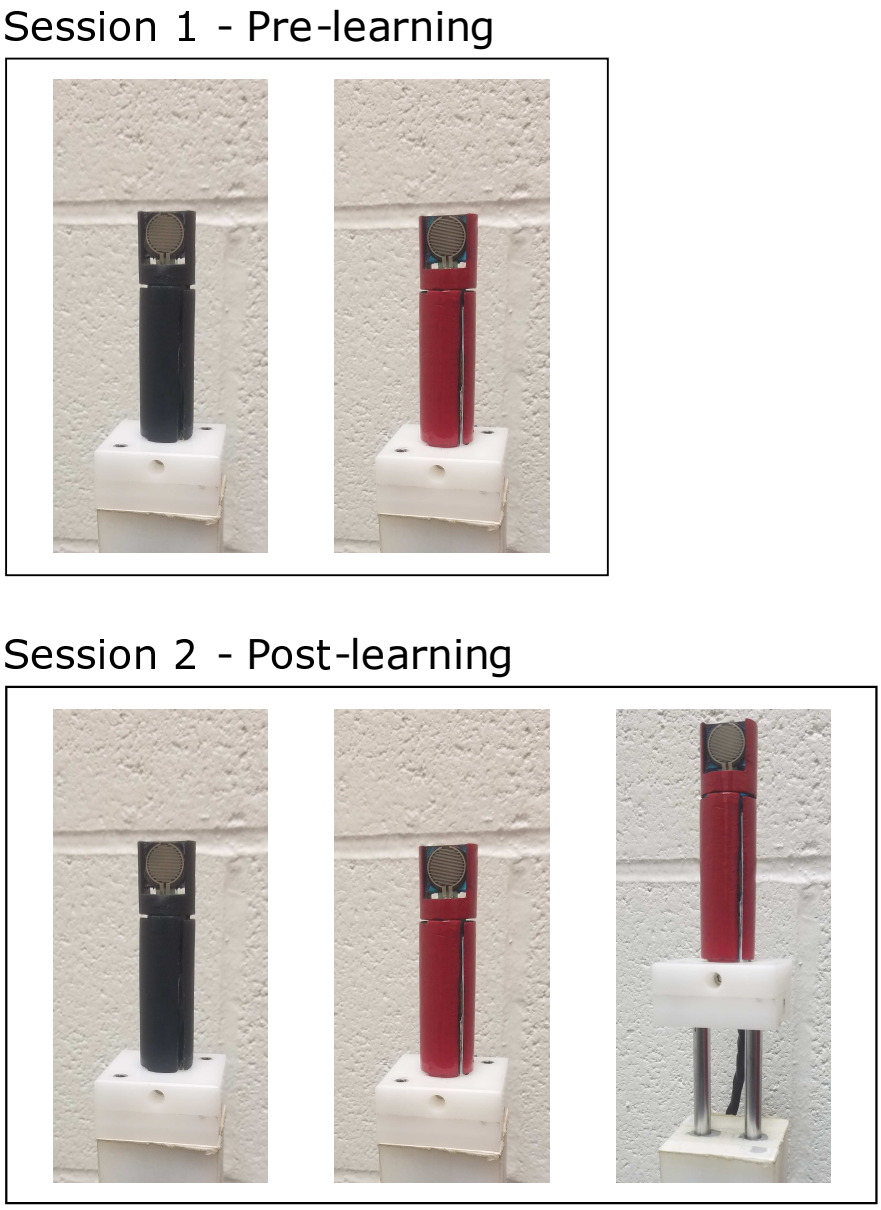

Figure 6.1: **Objects used in the Use Affordance Experiment.** Black object: Object 1. Blue object: Object 2. During the pre-learning session, both objects were mechanically fixed in place. During the post-learning session, Object 1 remained fixed in place and Object 2 was released and allowed to slide vertically. In both sessions, both objects were grasped and held with a Power Grasp or a Pinch Grasp. In the post-learning session, an additional condition was added for which the subject grasped Object 2 with a Power Grasp, held it, and then lifted it.

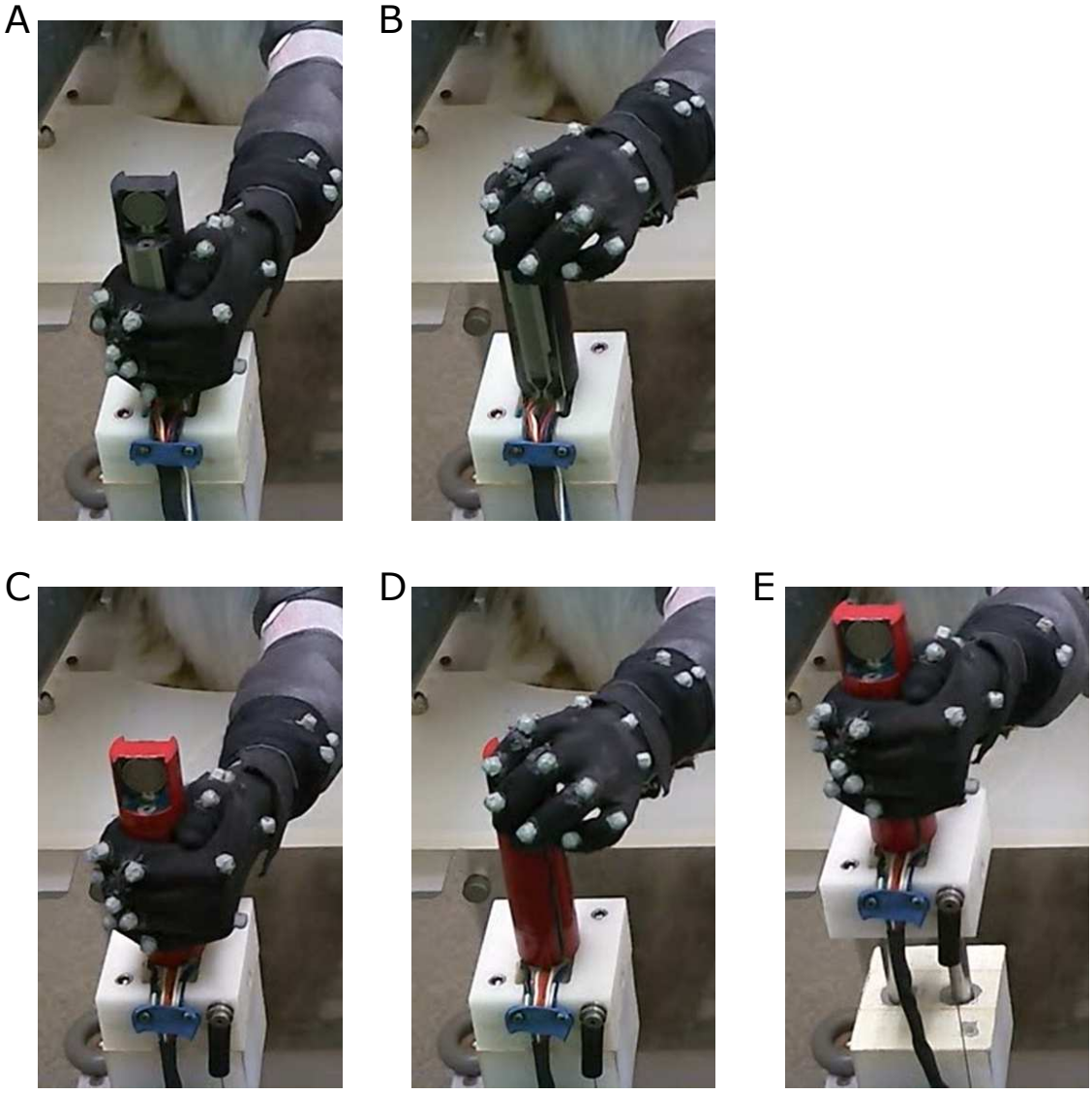

Figure 6.2: **Still frames of video recording of Monkey T performing the task conditions during the post-learning session in the Use Affordance Experiment.** Black object: Object 1. Red object: Object 2. A: Power Hold, Object 1 (Fixed). B: Pinch Hold, Object 1 (Fixed). C: Power Hold, Object 2 (Movable). D: Pinch Hold, Object 2 (Movable). E: Power Lift, Object 2 (Movable).

Trial structure was similar to that employed in the Object Presence Experiment and the Grip Affordance Experiment. The subject started each trial with its hand on the start button near waist. At this time, the subject was cued as to the required behavior (Power Hold, Pinch Hold, or Power Lift). After 800–1200 ms, a go cue was presented, and the subject reached forward to grasp the object. For Power Grasp conditions, the subject grasped the vertical cylindrical portion of the object with a whole-hand grip, opposing digits 2–5 against the palm. For the Pinch Grasp conditions, the subject grasped the tab at the top of the object by opposing digit 2 against the thumb. For the grasp and hold trials, the subject was required to maintain the grasp for 800–1200 ms to receive a reward.

For the Power Lift trials, subjects were required to perform a Power Grasp, maintain the grasp for 800–1200 ms without lifting the object, then, after a cue, lift the object vertically at least 2.5 cm to receive a reward. For Monkey I, the required hold time was only 500 ms, after which the lift cue was delivered. Lift trials were denoted with a triangle on the feedback monitor which remained present throughout the trials, and which provided feedback about the required and actual lift distance during the lift phase. Trials were automatically aborted if any inappropriate force sensor was activated. Grasp-and-hold trials were aborted if the object was lifted at any time, and Power Lift trials were aborted if the object was lifted early. Power Hold trials on Object 2 (the movable object) were excluded from analysis if a lift was erroneously performed after the reward was delivered, which rarely occurred. Subjects only ever lifted Object 2 using a Power Grasp, and never with a Pinch Grasp. Section 3.2 contains more details of the task timing and visual feedback.

The objects were presented in blocks, and objects were changed between blocks by the experimenter, out of view of the subject. For Object 1 blocks in both the pre- and post-learning sessions, Power Hold and Pinch Hold trials were presented in an interleaved pseudorandom fashion. For Object 2 blocks in the pre-learning session, Power Hold and Pinch Hold trials were presented in an interleaved pseudorandom fashion. For Object 2 blocks in the post-learning session, Power Hold, Pinch Hold, and Power Lift trials were presented in an interleaved psuedorandom fashion. Block schedule structure is described further in Section 3.2.1.

For all conditions, the Reach Start time was defined as the time point of the first kinematic sample in which the hand velocity exceeded 1 mm/s for a sustained period. The Target Contact time was defined by the initial uptick of the appropriate force sensors. For lift trials, the lift time was defined by the initial uptick of the lift sensor potentiometer. See Section A.4.5 for more details of data alignment to task epochs.

The subjects exhibited somewhat different reach times (the time between Reach Start and Target Contact) for different grasps, and reach times varied between trials. Power Grasp reach times were shorter than Pinch Grasp reach times on average. In order to compare across conditions and across trials, trials were resampled at variable rates within the reach period to produce an equal number of samples for each trial (see Section A.4.5 for details).

Trial-averaged hand positions and hand velocities are shown in Figure 6.3 for Monkey R for both the pre-learning session and the post-learning session. Positions were calculated relative to the hand position on the start button. The trial-averaged values were calculated by averaging the values at each time point across all 140 trials for each condition. The hand position was defined as the average x-y-z coordinates of markers HAN1, HAN2, HAN3 and HAN4 (see Section A.4.1). The coordinate axes corresponded to the workspace as follows: positive X pointed to the right of the subject, positive Y pointed forward from the subject and positive Z pointed upward.

Different hand trajectories were observed for all Power Grasps vs. all Pinch Grasps, due to the different locations of the graspable portions of the object and the different hand speeds during the reach period. Some overshoot was observed in the hand Z-position, as the subject lifted its hand off the start button and brought it back down to make contact with the object. In the pre-learning session, the hand positions were very similar when the same grasps were made on the different objects (Figure 6.3 A, solid vs. dashed lines). In the post-learning session, the hand trajectories were slightly different for the same grasps made on the different objects, especially in the hand Z-position and Z-velocity. During the target hold period, the hand Z-position was slightly lower for the Power Hold and Power Lift trials on Object 2 (the movable object), compared to Power Hold trials on Object 1 (the fixed object). During the early reach period, the hand Z-velocity was slightly higher for Pinch Hold trials on Object 2, compared to Pinch Hold Trials on Object 1.

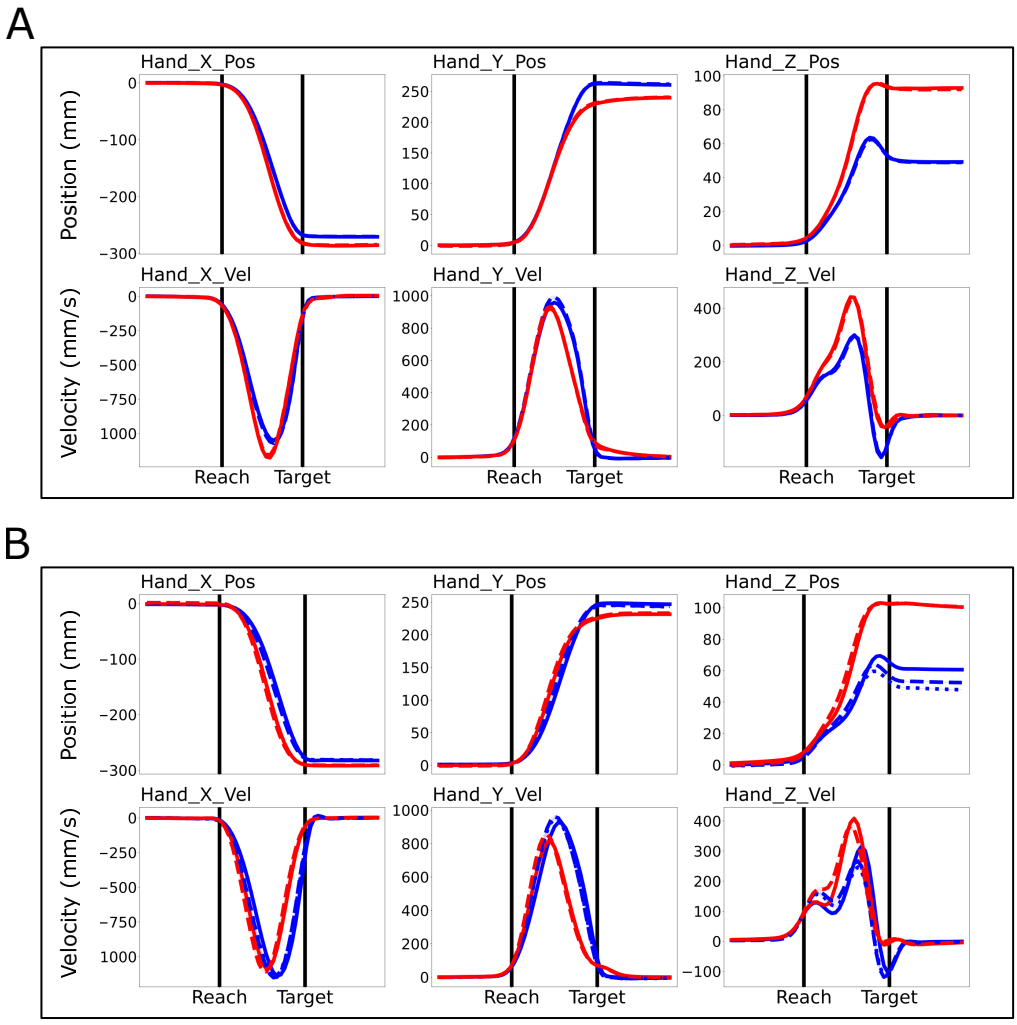

Figure 6.3: **Trial-averaged hand positions and velocities for Monkey R in the pre- and post-learning sessions of the Use Affordance Experiment.** Hand positions are relative to the mean hand position 400 ms before Reach Start. A: Pre-learning session. B: Post-learning session. Solid blue lines: Power Hold, Object 1. Solid red lines: Pinch Hold, Object 1. Dashed blue lines: Power Hold, Object 2. Dashed red lines: Pinch Hold, Object 2. Dotted blue line: Power Lift, Object 2.

Trial-averaged joint angle trajectories of the arm are presented in Figure 6.4 for both the pre- and post-learning sessions for Monkey R. The finger joint angles for Monkey R for the pre- and post-learning sessions are presented in Figures 6.5 and 6.6.

Overall, arm and hand joint angle trajectories were dissimilar for all Power Grasps vs. all Pinch Grasps. In the pre-learning session, small within-grasp differences were observed in the elbow flexion, wrist flexion and wrist abduction angles when the same grasps were performed on the two different objects. Arm and wrist joint angles were more consistent within grasps in the post-learning session.

In the pre-learning session, digit 2–5 PIP flexion and digit 4 and 5 MCP flexion were slightly higher for Pinch Grasps made on Object 1 compared to Pinch Grasps made on Object 2. Power Grasps made on the two objects were highly consistent in the finger joint angles, excepting some small differences in digits 2 and 3 PIP flexion.

In the post-learning session, Pinch Grasp finger joint angles were more consistent between the two objects. Larger differences were observed between Power Grasps made on the two objects. Digit 2–5 MCP and PIP flexion was greater when grasping Object 1 (the fixed object) with a Power Grasp, compared to Power Grasps on Object 2 (the movable object), even for the Power Hold trials on Object 2, when no lift action was performed. In addition, the digits were more spread apart for Power Grasps on Object 1 compared to Power Grasps on Object 2. Power Lift trials were associated with even less digit flexion and digit spreading. Finger joint angles for Power Hold trials on Object 2 were intermediate between Power Hold Trials on Object 1 and Power Lift trials on Object 2, though they were more similar to Power Lift trials in general.

Trial-averaged muscle activity recorded from surface EMG electrodes are shown in Figure 6.7 for both the pre- and post-learning sessions for Monkey R. Details of surface EMG data collection are presented in Section A.4.2.

As with the kinematics, the largest differences in EMGs were observed between all Power Grasps and all Pinch Grasps. In the pre-learning session, Power Grasps were highly consistent between the two objects. Pinch Grasps made on Object 2 elicited slightly lower EMGs in the pectoralis, deltoid, triceps, biceps and wrist extensors compared to Pinch Grasps made on Object 1.

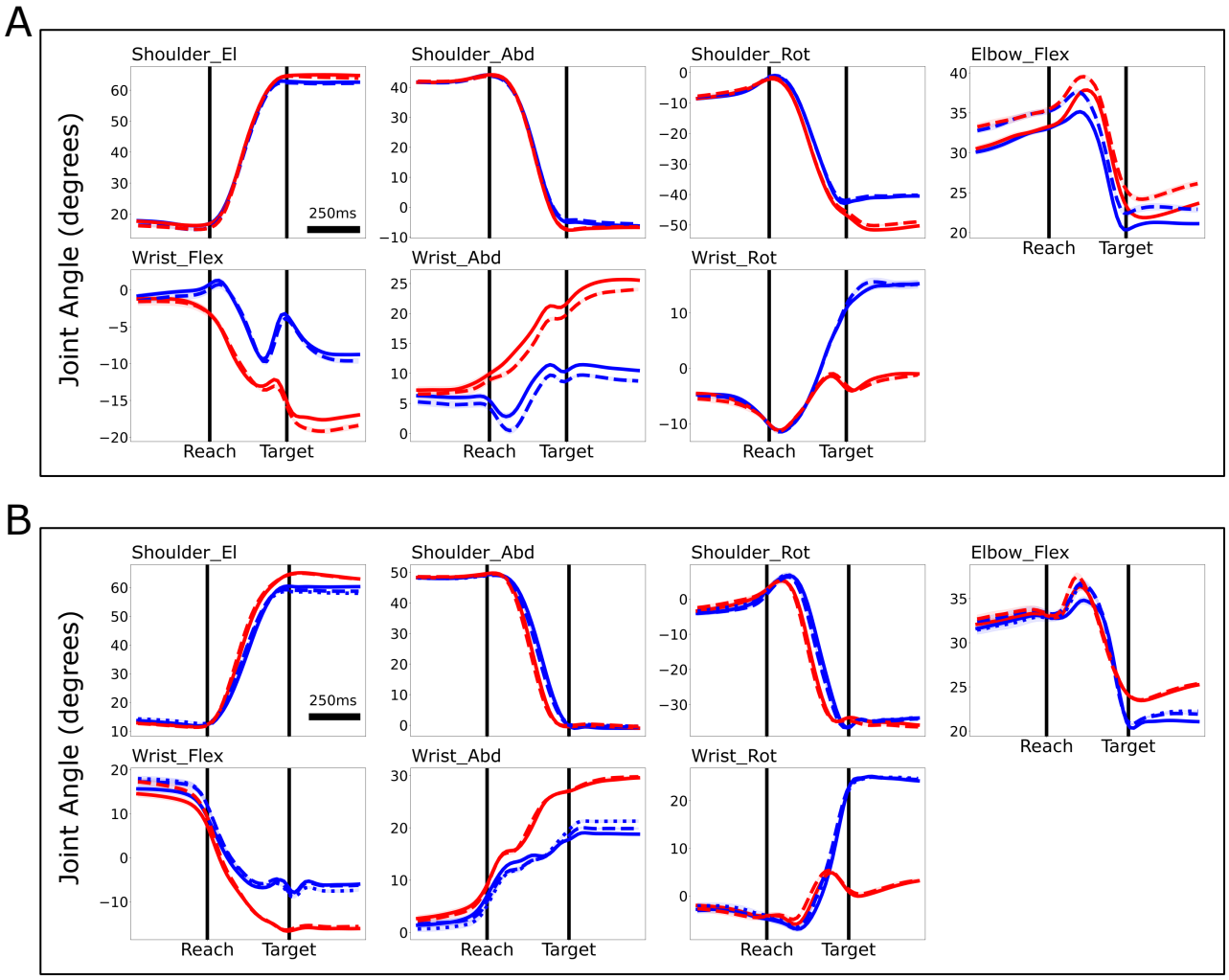

Figure 6.4: **Trial-averaged arm joint angle trajectories for Monkey R in the pre- and post-learning sessions of the Use Affordance Experiment.** A: Pre-learning session. B: Post-learning session. Solid blue lines: Power Hold, Object 1. Solid red lines: Pinch Hold, Object 1. Dashed blue lines: Power Hold, Object 2. Dashed red lines: Pinch Hold, Object 2. Dotted blue line: Power Lift, Object 2. El: elevation, Abd: abduction, Rot: rotation, Flex: flexion.

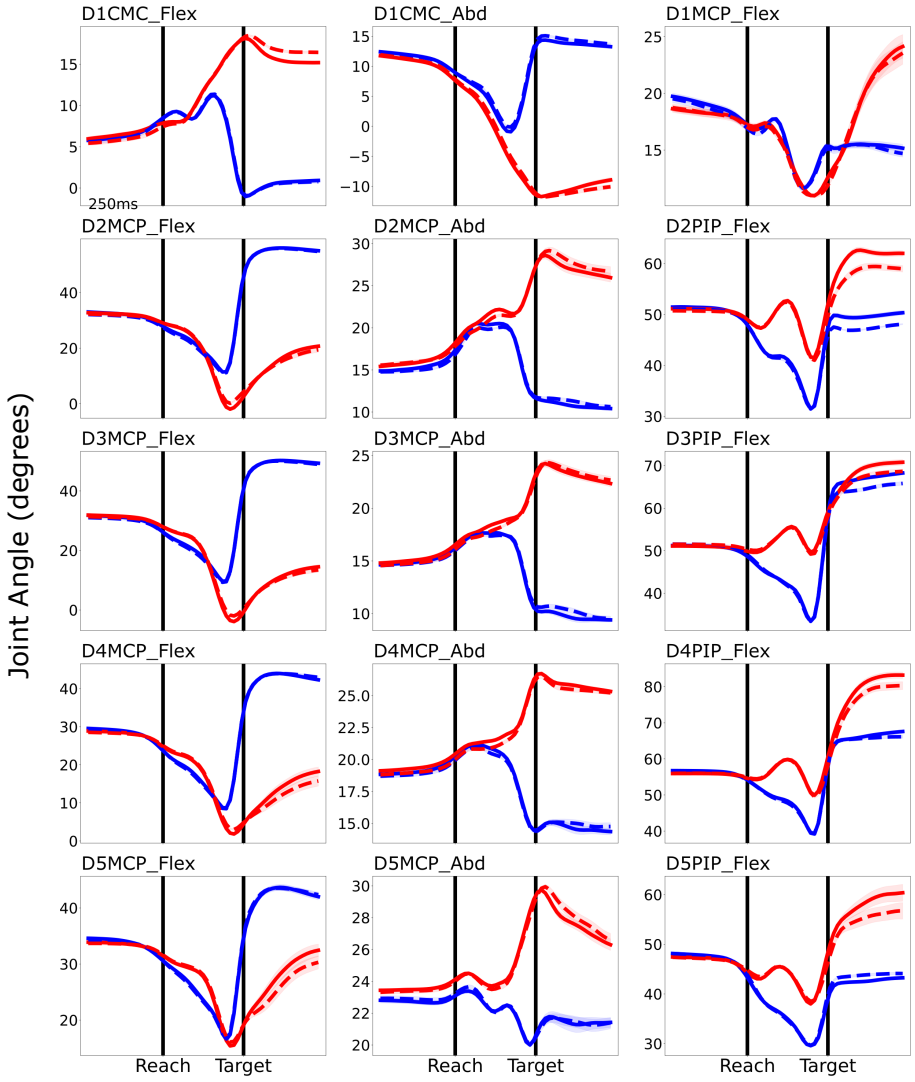

Figure 6.5: **Trial-averaged finger joint angle trajectories for Monkey R in the pre-learning session of the Use Affordance Experiment.** Solid blue lines: Power Hold, Object 1. Solid red lines: Pinch Hold, Object 1. Dashed blue lines: Power Hold, Object 2. Dashed red lines: Pinch Hold, Object 2. CMC: carpometacarpal joint, MCP: metacarpophalangeal joint, PIP: proximal interphalangeal joint. Flex: flexion, Abd: abduction.

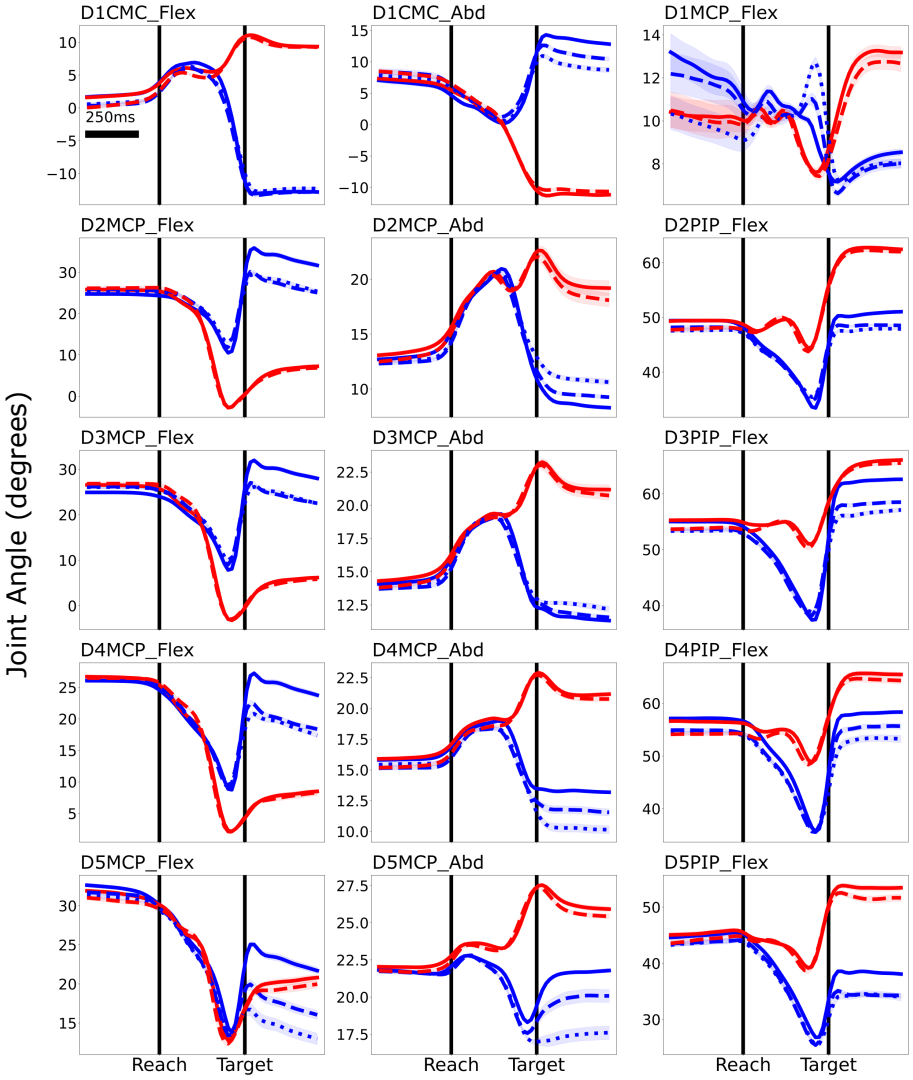

Figure 6.6: **Trial-averaged finger joint angle trajectories for Monkey R in the post-learning session of the Use Affordance Experiment.** Solid blue lines: Power Hold, Object 1. Solid red lines: Pinch Hold, Object 1. Dashed blue lines: Power Hold, Object 2. Dashed red lines: Pinch Hold, Object 2. Dotted blue lines: Power Lift, Object 2. CMC: carpometacarpal joint, MCP: metacarpophalangeal joint, PIP: proximal interphalangeal joint. Flex: flexion, Abd: abduction.

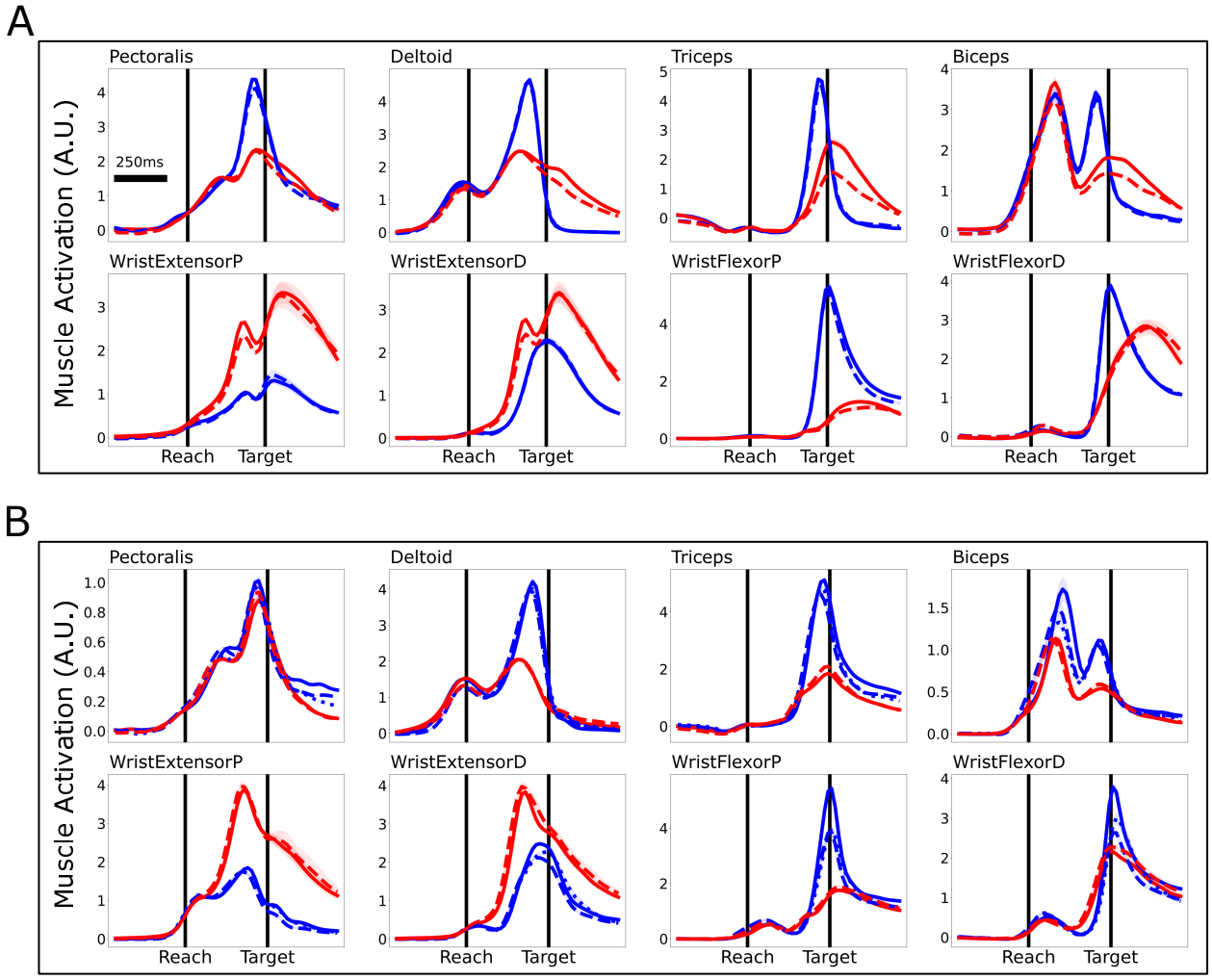

Figure 6.7: **Trial-averaged EMG muscle activations in the pre- and post-learning sessions the Use Affordance Experiment.** EMG values are relative to the mean EMG values 400 ms before Reach Start. A: Pre-learning session. B: Post-learning session. Solid blue lines: Power Hold, Object 1. Solid red lines: Pinch Hold, Object 1. Dashed blue lines: Power Hold, Object 2. Dashed red lines: Pinch Hold, Object 2. Dotted blue lines: Power Lift, Object 2. P: proximal, D: distal.

In the post-learning session, Pinch Grasps were more consistent between the two objects. Power Grasps made on Object 2 elicited slightly lower EMGs in the pectoralis, triceps, biceps and forearm muscles compared to Power Grasps made on Object 1. In general, EMGs for Power Hold trials on Object 2 were more similar to EMGs for Power Lift trials made on Object 2.

Patterns of variability in the MFs were qualitatively consistent across the subjects. In all subjects, the largest separations in MFs were between all Power Grasps and all Pinch Grasps. All subjects displayed slight differences in MFs when executing the same grasps on different objects, even during the pre-learning sessions. Such differences were unexpected, as during the pre-learning sessions the objects were identical other than their color. In the post-learning sessions, larger MF differences were observed between Power Grasps made on the different objects for Monkey R and Monkey T, though less so for Monkey I. For all subjects, the MFs for the Power Hold trials on Object 2 (the movable object) were more similar to the Power Lift trials on Object 2 compared to the Power Hold trials on Object 1, even though the required behaviors for Power Hold were the same for both objects. This indicates that slightly different Power Hold behaviors were observed for the two objects after learning the lift affordance for Object 2, even when Object 2 was not lifted. The next section contains direct comparisons of MFs in the different conditions in order to characterize the size of the grip-type dependent and object-dependent variability in MFs.

6.2 Movement Feature Differences Across Conditions

The goal of the experimental design of the Use Affordance Experiment was to elicit very similar grasps on objects which were at first identical in all but color (pre-learning session), and later, which differed in terms of the learned use affordances of the objects (post-learning session). The analyses in this section describe the relative differences observed in the MFs for the various conditions of the Use Affordance Experiment.

To measure the differences in MFs between different conditions, the Euclidean distance between each pair of conditions was calculated at each time point in subsets of MFs. The

MF subsets were the same as in Chapters 4 and 5, and inter-condition distances in the MF subsets were calculated according to equation 4.1 in Section 4.3. The resulting MF subset distances are shown in 6.8 for both the pre- and post-learning sessions for Monkey R.

Across the MF subsets, the largest distances were observed between Power Grasps and Pinch Grasps. Power Grasp vs. Pinch Grasp distances differed slightly between the pre- and post-learning sessions due to the differences in the placements of the kinematic tracking markers and EMG electrodes on the subject in the two sessions. In all MF subsets, distances between Power Grasps were generally very small in the pre-learning session and increased for the post-learning session. The Power Hold (Object 2) vs. Power Lift (Object 2) distances (Figure 6.8 light turquoise traces) were the lowest of the within-Power-Grasp distances, indicating that the subject used similar hand posture and muscle activity for all Power Grasps on Object 2 after learning the lifting use affordance, even when the object was not lifted. Distances between the Pinch Grasps made on the different objects increased in hand position and hand speed during the reach between the pre- and post-learning sessions, but decreased in EMG.

In order to characterize inter-condition distances across all of the MFs together, the 58 trial-averaged, centered MFs were combined in a dimensionally-reduced form using Principal Components Analysis (PCA) with varimax rotation, as in Sections 4.3 and 5.3. For Monkey R, 12 PCs (14 PCs) explained 99% of the variance in trial-averaged, centered MFs for the pre-learning session (post-learning session). The first 12 MF VPC scores and VPC loadings are shown in Figure 6.9 for the pre-learning session and Figure 6.10 for the post-learning session, with each condition plotted separately. VPCs are sorted by amount of variance explained.

The largest separations in VPCs were between Power Grasps and Pinch Grasps. In the pre-learning session, small separations were observed between same-grasp conditions for both Pinch Grasps and Power Grasps made on the different objects. Separations between Power Grasps were more prominent in the post-learning session, as they were larger in magnitude and present in more of the VPCs compared to the pre-learning session. In general, within-grasp separations were confined to specific time periods in specific VPCs.

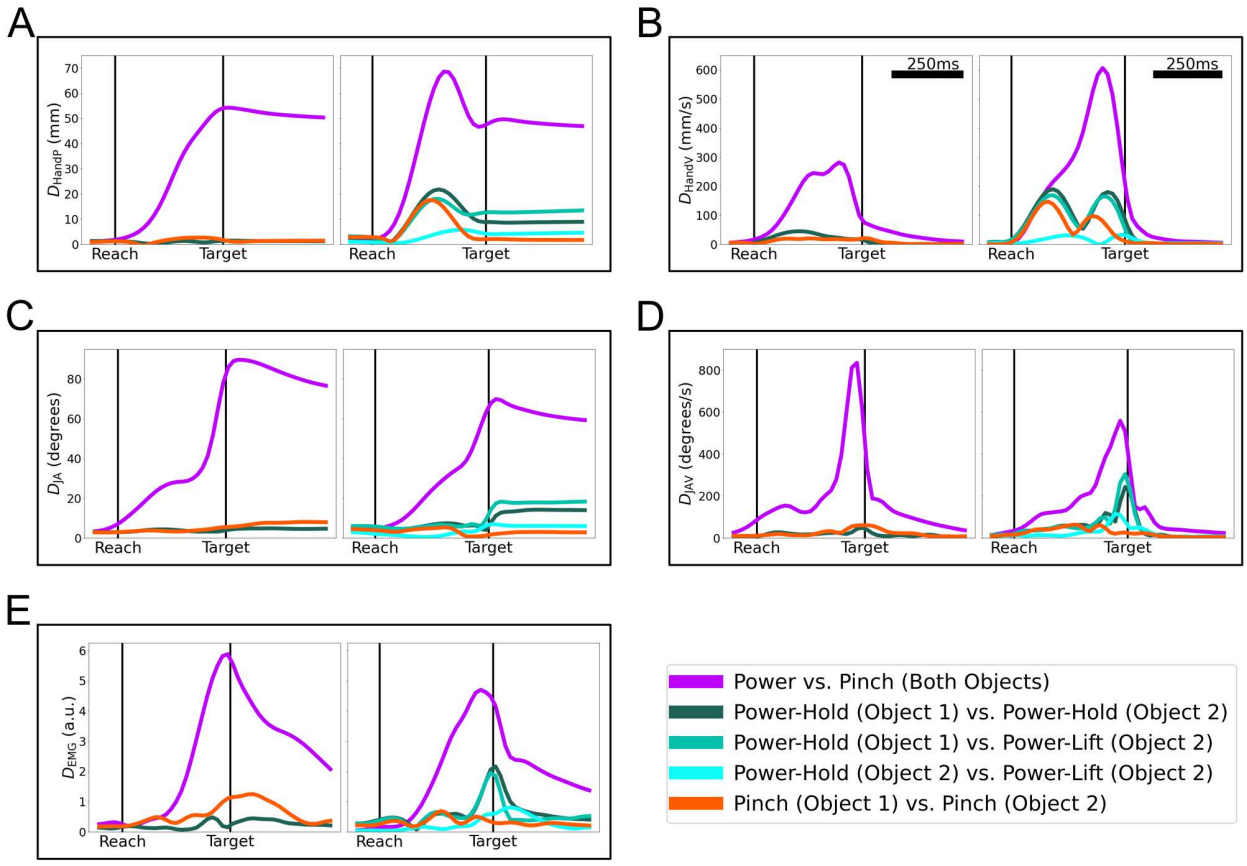

Figure 6.8: **Inter-condition distances in MF subsets for Monkey R in the pre- and post-learning sessions of the Use Affordance Experiment** A: distances in hand position. B: distances in hand velocity. C: distances in joint angles. D: distances in joint angular velocities. E: distances in EMGs. Left-hand plots: pre-learning session. Right-hand plots: post-learning session.

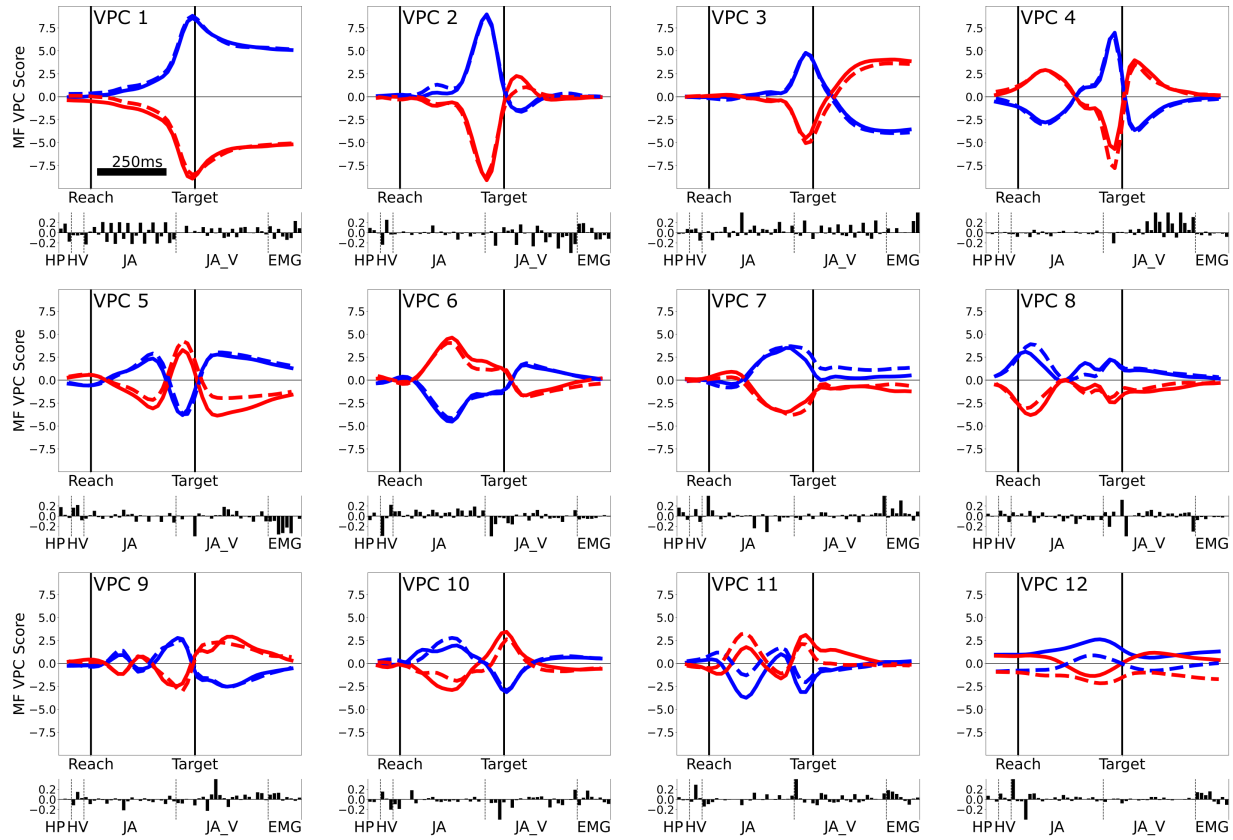

Figure 6.9: **Varimax PCA of the MFs in the pre-learning session of the Use Affordance Experiment, Monkey R.** Trial-averaged scores in the first 12 VPCs. Solid blue lines: Power Hold, Object 1. Solid red lines: Pinch Hold, Object 1. Dashed blue lines: Power Hold, Object 2. Dashed red lines: Pinch Hold, Object 2. Bar graph insets below each VPC score plot denote the loading vector corresponding to the VPC.

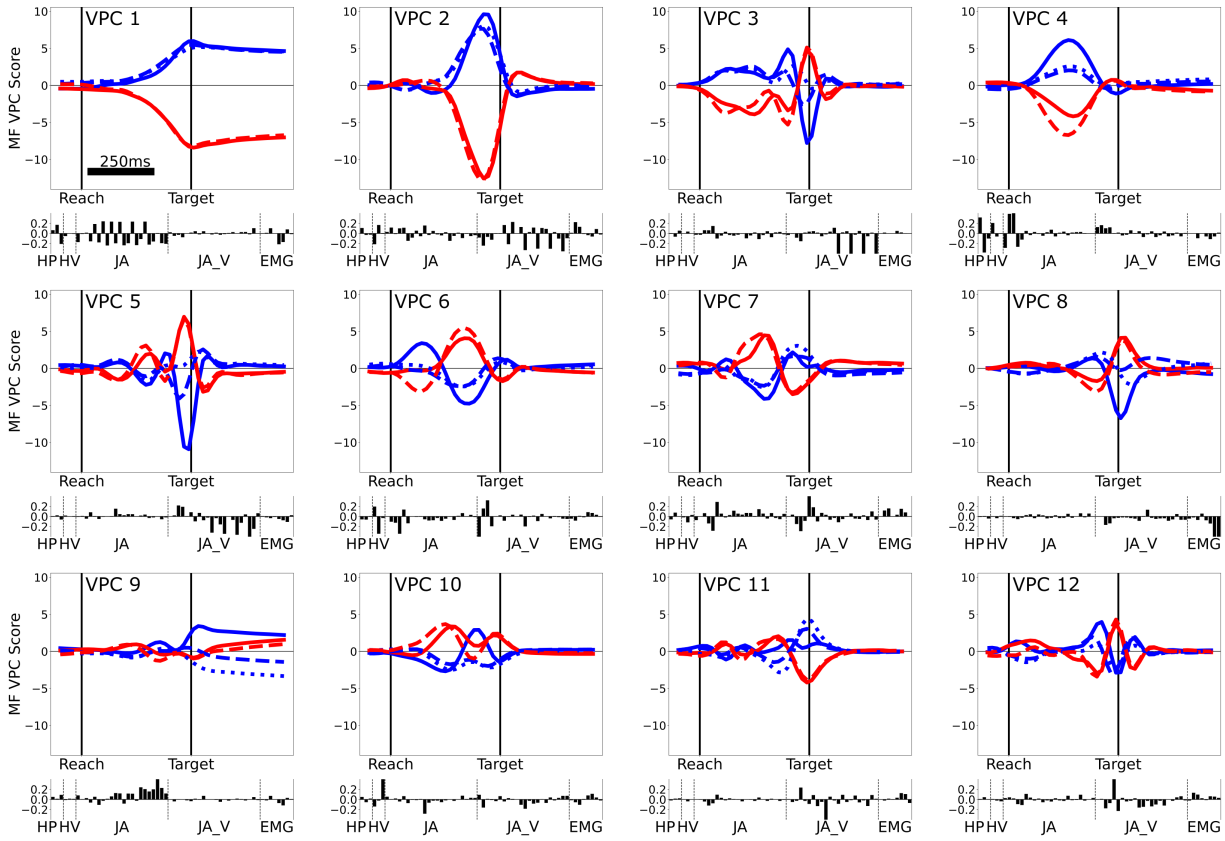

Figure 6.10: **Varimax PCA of the MFs in the post-learning session of the Use Affordance Experiment, Monkey R.** Trial-averaged scores in the first 12 VPCs. Solid blue lines: Power Hold, Object 1. Solid red lines: Pinch Hold, Object 1. Dashed blue lines: Power Hold, Object 2. Dashed red lines: Pinch Hold, Object 2. Dotted blue lines: Power Lift, Object 2. Bar graph insets below each VPC score plot denote the loading vector corresponding to the VPC.

To directly compare the inter-condition separation across the MF PCs, the Euclidean distance in MF PC space, D_{MFPC}, was calculated for each pair of conditions, as in Equation 4.2 in Section 4.1. The MF PC distances D_{MFPC} are shown in Figure 6.11 and the time-averaged MF PC distances $\overline{D}_{\mathrm{MFPC}}$ are shown in Figure 6.12 for both the pre- and post-learning sessions for all subjects.

Again, the largest distances were observed between Power Grasps and Pinch Grasps (Figure 6.11, purple trace). These distances peaked around the time of target contact and maintained a moderate level during the target hold period. Relatively small distances were observed between condition pairs in which the same grasp was performed on different objects, even in the pre-learning sessions. These within-grasp distances persisted or increased in the post-learning session for all subjects. For every condition pair, MF distances $\overline{D}_{\mathrm{MFPC}}$ were significantly greater than expected within-condition variation in $\overline{D}_{\mathrm{MFPC}}$ (Figure 6.12 stars), even during the pre-learning session when objects only differed in their color.

For Monkey I, Power Hold trials diverged from the Power Lift trials rapidly after target contact, due to the shorter hold period for Power Lift trials for Monkey I. In the post-learning session, the Power Hold (Object 2) and Power Lift (Object 2) were the closest within-Power-Grasp condition pair, (Figure 6.11 light turquoise vs. dark and medium turquoise). This indicates that the MFs for the Power Hold trials on Object 2 were more similar to the Power Lift trials on Object 2, compared to the Power Hold trials on Object 1, even though the object was not lifted.

The MF PC distances varied slightly in magnitude in the pre- and post-learning sessions. This was likely due to differences in the MF recording setup in each session. To accommodate these differences and provide a more consistent measure of the size of within-grasp distances, the size of within grasp distances were calculated relative to the average Power Grasp vs. Pinch Grasp distance. These values were calculated by dividing the mean MFPC distance $\overline{D}_{\mathrm{MFPC}}$ for either Power Hold (Object 1) vs. Power Hold (Object 2) (Figure 6.12 dark turquoise bars) or Pinch Hold (Object 1) vs. Pinch Hold (Object 2) (Figure 6.12 orange bars) by the average of the $\overline{D}_{\mathrm{MFPC}}$ for the two Power Grasp vs. Pinch Grasp condition pairs (Figure 6.12 purple bar). In order to make more direct comparisons of the variance due only to the grasp and hold trials in the pre- and post-learning sessions,

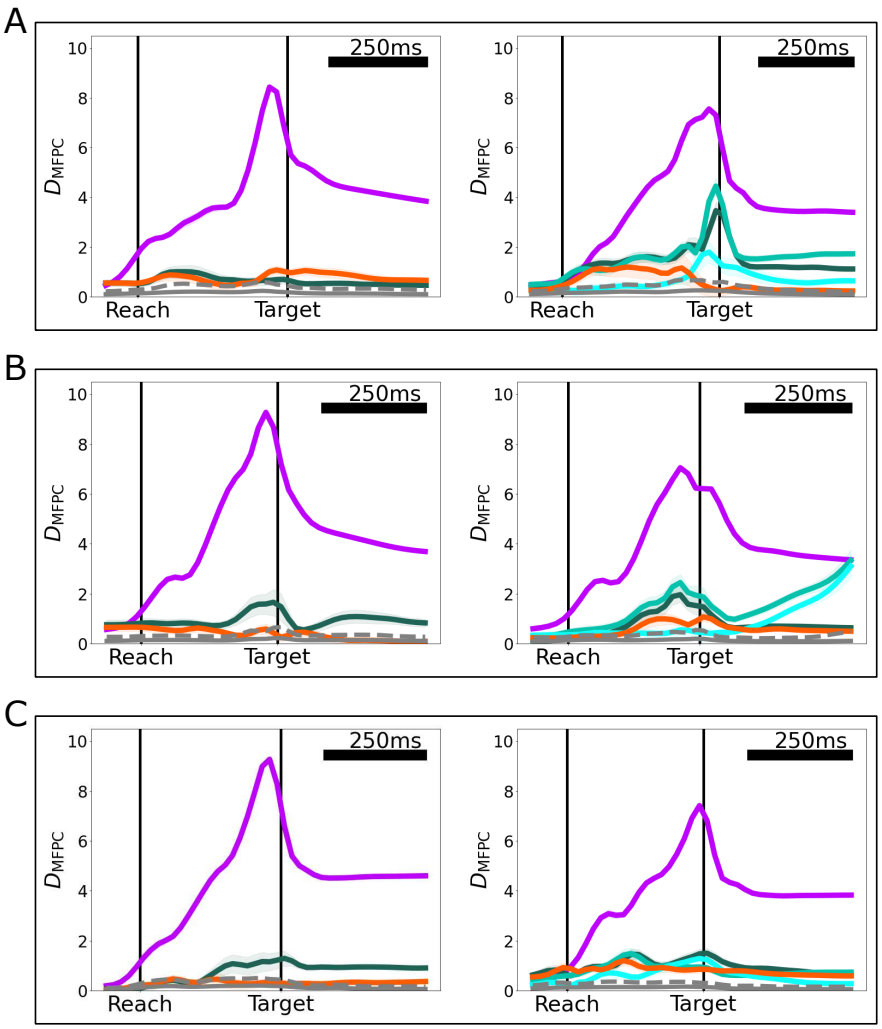

Figure 6.11: **Scaled Euclidean inter-condition distances between pairs of trial-averaged MF PC scores in the pre- and post-learning sessions of the Use Affordance Experiment.** Distances were calculated in the 99% MF PC space. A: Monkey R. B: Monkey I. C: Monkey T. Purple: mean Power Hold vs. Pinch Hold for Objects 1 and 2. Dark turquoise: Power Hold, Object 1 vs. Power Hold, Object 2. Medium turquoise: Power Hold, Object 1 vs. Power Lift, Object 2. Light turquoise: Power Hold, Object 2 vs. Power Lift, Object 2. Orange: Pinch Hold, Object 1 vs. Pinch Hold, Object 2. Gray: mean and upper 95% one-sided confidence interval of within-condition variability. 95% confidence intervals are bootstrap intervals, trials resampled 10000 times.

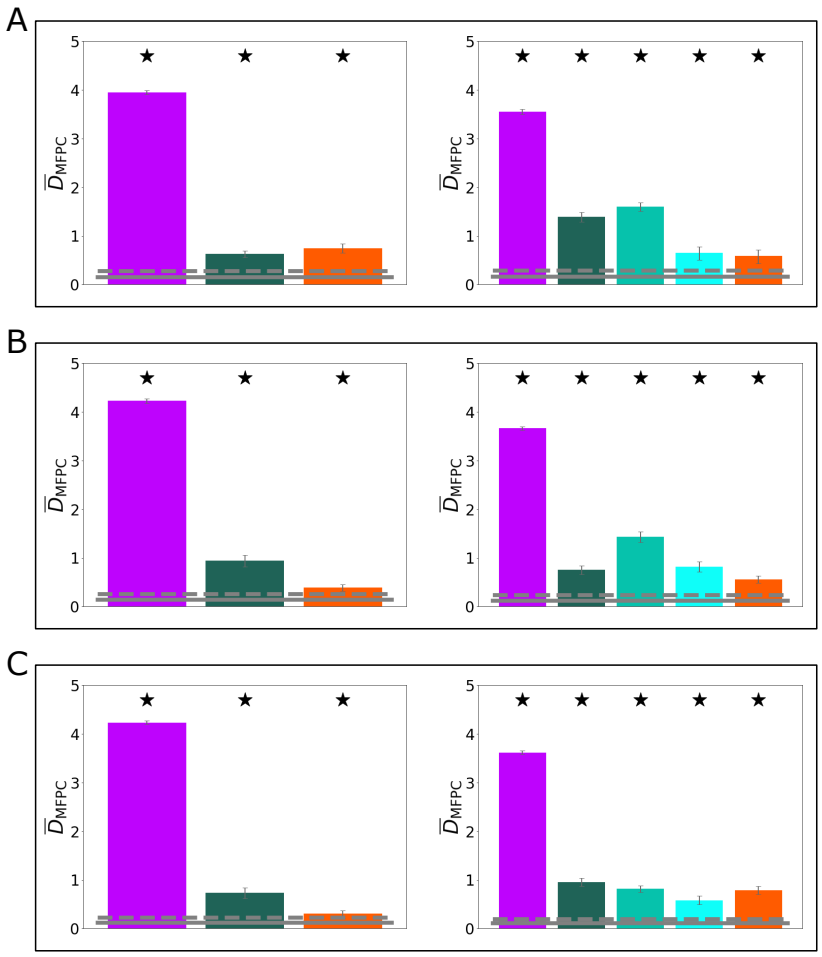

Figure 6.12: **Mean scaled Euclidean inter-condition distances between pairs of trial-averaged MF PC scores in the pre- and post-learning sessions of the Use Affordance Experiment.** Distances were calculated in the 99% MF PC space and averaged over time. A: Monkey R. B: Monkey I. C: Monkey T. Star: $\overline{D}_{\mathrm{MFPC},i,j}$ significantly greater than within condition $\overline{D}_{\mathrm{MFPC}}$ variability ($p < 0.05$, one-sided bootstrap interval). Purple: mean Power Hold vs. Pinch Hold for Objects 1 and 2. Dark turquoise: Power Hold, Object 1 vs. Power Hold, Object 2. Medium turquoise: Power Hold, Object 1 vs. Power Lift, Object 2. Light turquoise: Power Hold, Object 2 vs. Power Lift, Object 2. Orange: Pinch Hold, Object 1 vs. Pinch Hold, Object 2. Gray: mean and upper 95% one-sided confidence interval of within-condition variability. 95% confidence intervals are bootstrap intervals, trials resampled 10000 times.

the MF PCs were recalculated for the post-learning session excluding the Power Lift trials. These recalculated MF PCs were then used to calculate the proportional effect sizes. These proportional effect sizes are presented in Table 6.1.

Table 6.1: **Proportional size of within-grasp MF PC distances for the pre- and post-learning sessions in the Use Affordance Experiment.** Proportional effect sizes were calculated by dividing $\overline{D}_{\mathrm{MFPC}}$ for same-behavior, different-object condition pairs by the average $\overline{D}_{\mathrm{MFPC}}$ for Power Grasp vs. Pinch Grasp condition pairs.

		Pre-learning		**Post-learning**	
Subject	**Area**	**Power**	**Pinch**	**Power**	**Pinch**
Monkey R	M1	0.16	0.19	0.40	0.17
Monkey I	M1	0.22	0.09	0.23	0.17
Monkey T	M1 Right	0.17	0.07	0.26	0.21

For all subjects, the proportional sizes of the MF PC distances between same-grasp trials performed on the different objects increased from the pre-learning session to the post-learning session by a factor of 1.62, 1.29 and 1.96 on average for Monkey R, Monkey I and Monkey T. For Monkey I, this increase was nominal in Power Grasps.

Though small, these within-grasp differences were significant, and notable because the objects were identical other than color for the pre-learning session. For the post-learning session, the objects only differed by color and by the learned use affordance for Object 2. However, MFPC differences were observed even when the required behaviors (grasp and hold) were the same for the two objects. These differences were generally proportionally larger after the use affordance had been learned for Object 2.

6.3 M1 Neural Activity Differences Across Conditions

This section describes the neural activity in M1 recorded during the Use Affordance Experiment. M1 neural activity was highly divergent when comparing Power Grasps to Pinch Grasps. Some variability was also observed when comparing conditions in which the same grasp was made on different objects in both individual unit FRs and population activity.

After excluding channels with crosstalk and low FR units (see Section A.4.4), a total of 106 (113), 86 (60) and 58 (52) units were analyzed for Monkey R, Monkey I and Monkey T respectively for the pre-learning (post-learning) session. These units consisted of both multi-unit spiking activity and well-isolated single-units.

The FRs of individual units showed a diversity of different activity patterns. In some cases, individual units were recorded in both the pre- and post-learning sessions. These instances were identified using an algorithm developed by Fraser and Schwartz (2012) [439], which uses pairwise cross-correlograms, autocorrelograms, waveform shapes and mean FRs to track units that were present in multiple recording sessions. In some instances, units which showed little difference in FRs for same-grasp conditions in the pre-learning session had different FRs for same-grasp conditions in the post-learning period, suggesting potential encoding of the learned use affordance. Three examples of such units are shown in Figure 6.13.

For each of the example neurons displayed in Figure 6.13, little to no significant FR differences were observed between Power Hold, Object 1 trials and Power Hold, Object 2 trials in the pre-learning session (Figure 6.13 left-hand plots, solid blue vs. dashed blue traces). Significant differences between Power Hold trials on the different objects appeared in the post-learning session (Figure 6.13 right-hand plots, solid blue vs. dashed blue traces and turquoise horizontal bars at top). For Monkey R Unit 95.1, these FR differences occurred in the pre-movement and reach periods. For Monkey I Unit 20.1, the FR differences occurred in the pre-movement period. For Monkey T Unit 16.1, the FR differences occurred after target contact. Notably, for all of these example units units also displayed FR modulation related to execution of the lifting action (Figure 6.13 right-hand plots, dotted blue traces).

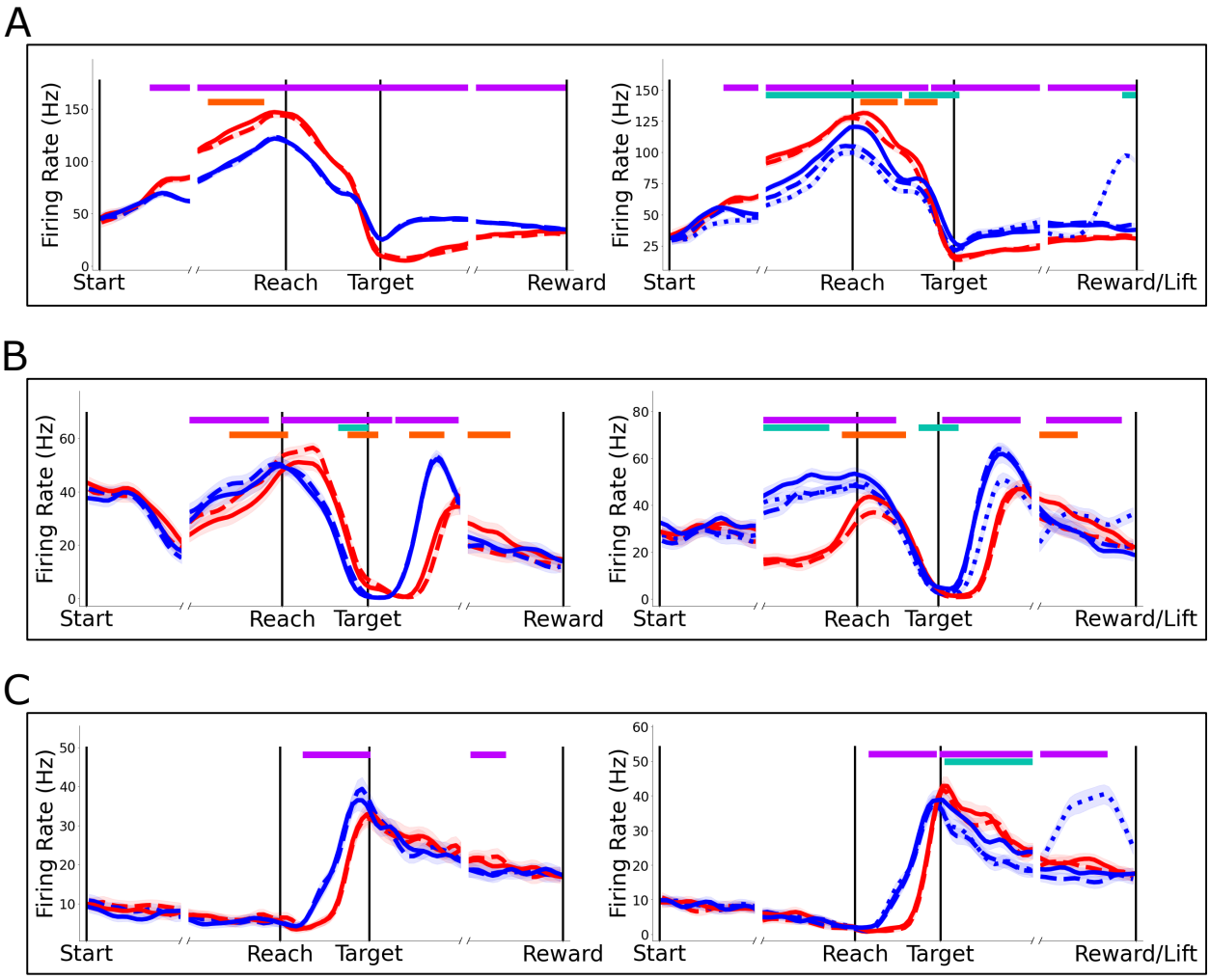

Figure 6.13: **Trial-averaged FRs of 3 example units recorded in the pre- and post-learning sessions of the Use Affordance Experiment.** A: Monkey R Unit 95.1. B: Monkey I Unit 20.1. C: Monkey T Unit 16.1. Left-hand plots: pre-learning session. Right-hand plots: post-learning session. Solid blue lines: Power Hold, Object 1. Solid red lines: Pinch Hold, Object 1. Dashed blue lines: Power Hold, Object 2. Dashed red lines: Pinch Hold, Object 2. Dotted blue lines: Power Lift, Object 2. Purple horizontal bars: at least one Power Grasp vs. Pinch Grasp pair significantly different. Turquoise horizontal bars: Power Hold, Object 1 significantly different from Power Hold, Object 2. Orange horizontal bars: Pinch Hold, Object 1 significantly different from Pinch Hold, Object 2 (permutation test of difference in mean FRs, n=10000, $p < 0.01$).

These units exemplify common patterns in individual unit FRs in the Use Affordance Experiment. Where they occurred, within-grasp FR differences were generally small compared to between-grasp differences. Within-grasp FR differences generally manifested as a modulation of the FR trajectory for the underlying grasp, as opposed to manifesting as a large change in MF trajectory timecourse. Within-grasp FR differences were typically constrained to specific temporal periods in individual units.

To determine the prevalence of separability of conditions in the FRs of individual units, permutation tests for a difference in mean FRs (n=10000, $p < 0.01$) were performed at each time point between each pair of conditions for each unit. The percentage of neurons displaying concurrent significant modulation (significantly different mean FRs) for each pair of conditions is shown in Figure 6.14 for all subjects.

For all subjects, the percentage of units which were concurrently significantly modulated for Power Grasps vs. Pinch Grasps was consistently high across the pre- and post-learning sessions (Figure 6.14 purple traces). Only a small percentage of units were concurrently significantly modulated for condition pairs in which the same grasp was executed on different objects in the pre-learning session. In the post-learning session, relatively more units were concurrently significantly modulated for the Power Hold (Object 1) vs. Power Hold (Object 2) condition pair (Figure 6.14 dark turquoise traces), though this percentage remained relatively low. Conversely, the percentage of units which were concurrently significantly modulated for the Pinch Hold (Object 1) vs. Pinch Hold (Object 2) condition pair (Figure 6.14 orange traces) were similar between the pre- and post-learning sessions. In the post-learning sessions, preparatory activity immediately preceding the lifting action was evident as the number of units significantly modulated for Power Hold vs. Power Lift pairs (Figure 6.14 medium and light turquoise traces) increased towards the end of the trials. This lifting preparatory activity began during the reach period for Monkey R, after target contact for Monkey I and only just before the lift cue for Monkey T right hemsiphere.

Figure 6.14 portrays the number of neurons with concurrent significant modulation for each condition pair. To visualize the number of individual units with any significant modulation over the whole timecourse of the trial, Venn diagrams were constructed which tabulated the occurrence of significant inter-condition modulation for at least 100 ms (5

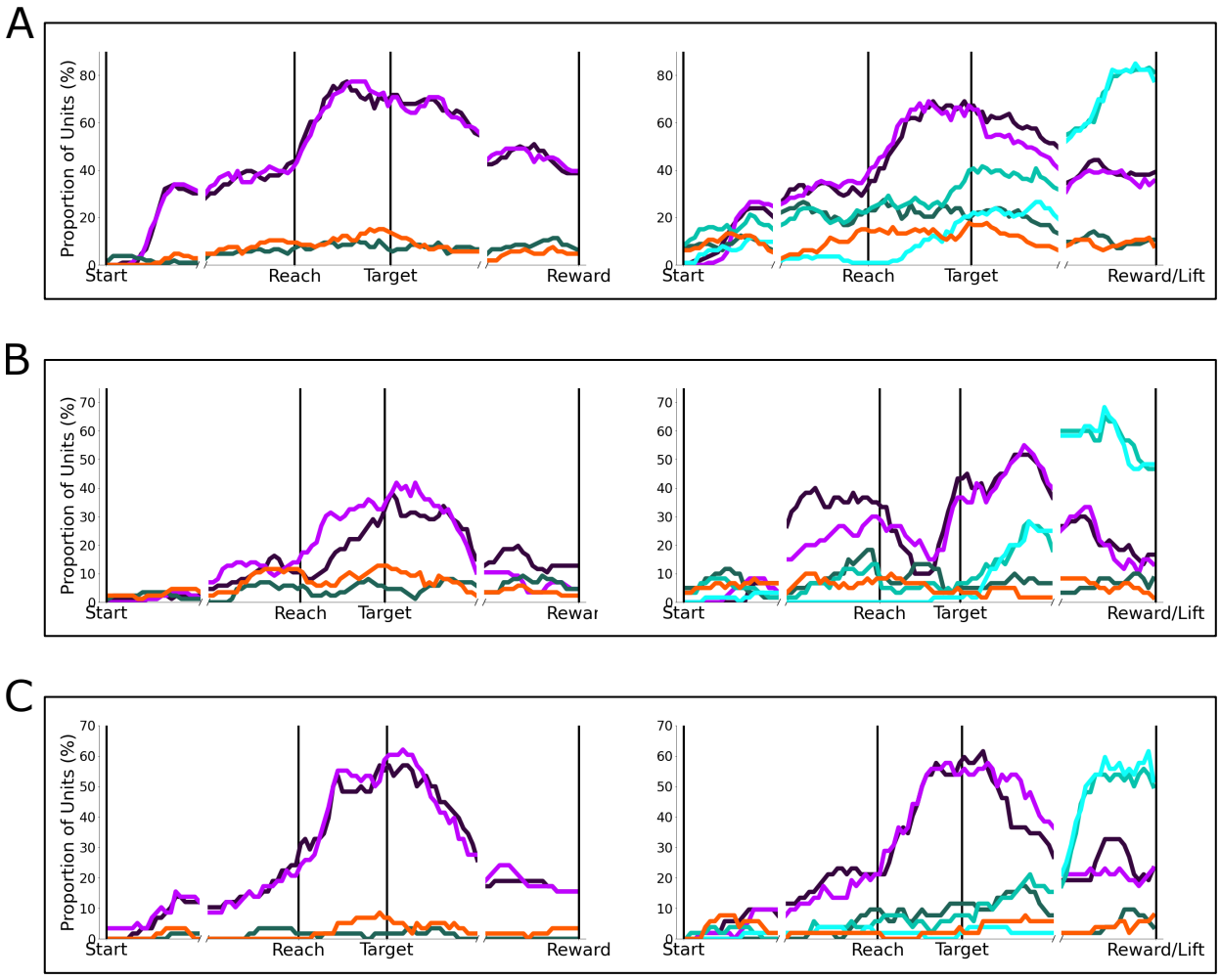

Figure 6.14: **Percentage of units with significantly modulated activity for each pair of conditions in the pre- and post-learning sessions of the Use Affordance Experiment.** Percentage of units with significant modulation for each pair of conditions at each time point ($p < 0.01$, permutation test, 10000 shuffles). A: Monkey R. B: Monkey I. C: Monkey T. Left-hand plots: pre-learning session. Right-hand plots: post-learning session. Purple: any Power Hold vs. any Pinch Hold. Dark turquoise: Power Hold, Object 1 vs. Power Hold, Object 2. Medium turquoise: Power Hold, Object 1 vs. Power Lift, Object 2. Light turquoise: Power Hold, Object 2 vs. Power Lift, Object 2. Orange: Pinch Hold, Object 1 vs. Pinch Hold, Object 2.

timepoints). These diagrams are shown for all subjects in Figure 6.15. To visualize the number of individual units showing sustained tuning, further diagrams were constructed which tabulate instance of inter-condition modulation which lasted at least 500 ms (25 timepoints). These diagrams are shown in Figure 6.16. The Venn diagrams excluded modulation related to Power Lift trials.

For all subjects, the number of units displaying $\geq$ 100 ms of significant modulation between conditions in which the same grasp was executed on different objects increased between the pre-learning and post-learning sessions. Additionally, for all subjects the number of units with short-term modulation between Pinch Grasps was greater than the number of units with short-term modulation between Power Grasps during the pre-learning session. This relationship switched for the post-learning session. The great majority of units which displayed short-term within-grasp modulation were also modulated between Power Grasps and Pinch Grasps.

The number of units displaying $\geq$ 500 ms of significant modulation for same-grasp conditions was much lower than the number of units displaying $\geq$ 100 ms of significant modulation. This suggests that within-grasp modulation was transitory and constrained to only certain time periods in each individual unit.

To examine the patterns of FR variability in the neural population as a whole, varimax PCA was performed on the FRs, as in Sections 4.3 and 5.3. The number of PCs accounting for 99% of the variance was 25 (36), 33 (32) and 26 (30) for Monkey R, Monkey I and Monkey T, respectively in the pre-learning (post-learning) session. The scores of the top 16 FR VPCs are plotted in Figure 6.17 for the pre-learning session and in Figure 6.18 for the post-learning session for Monkey R, with the scores for each condition plotted separately.

As in the MF VPCs, the largest source of separation in FR VPCs was the difference between all Power Grasps and all Pinch Grasps (Figures 6.17 and 6.18 blue traces vs. red traces). In the pre-learning session, moderate separation was observed between conditions in which the same grasp was made on different objects (Figure 6.17 solid vs. dashed traces). This within-grasp variance was more prevalent between the two Pinch Grasp conditions.

In the post learning session, within-grasp separation was more prevalent between the Power Grasp conditions. This within-grasp separation was apparent in many FR VPCs.

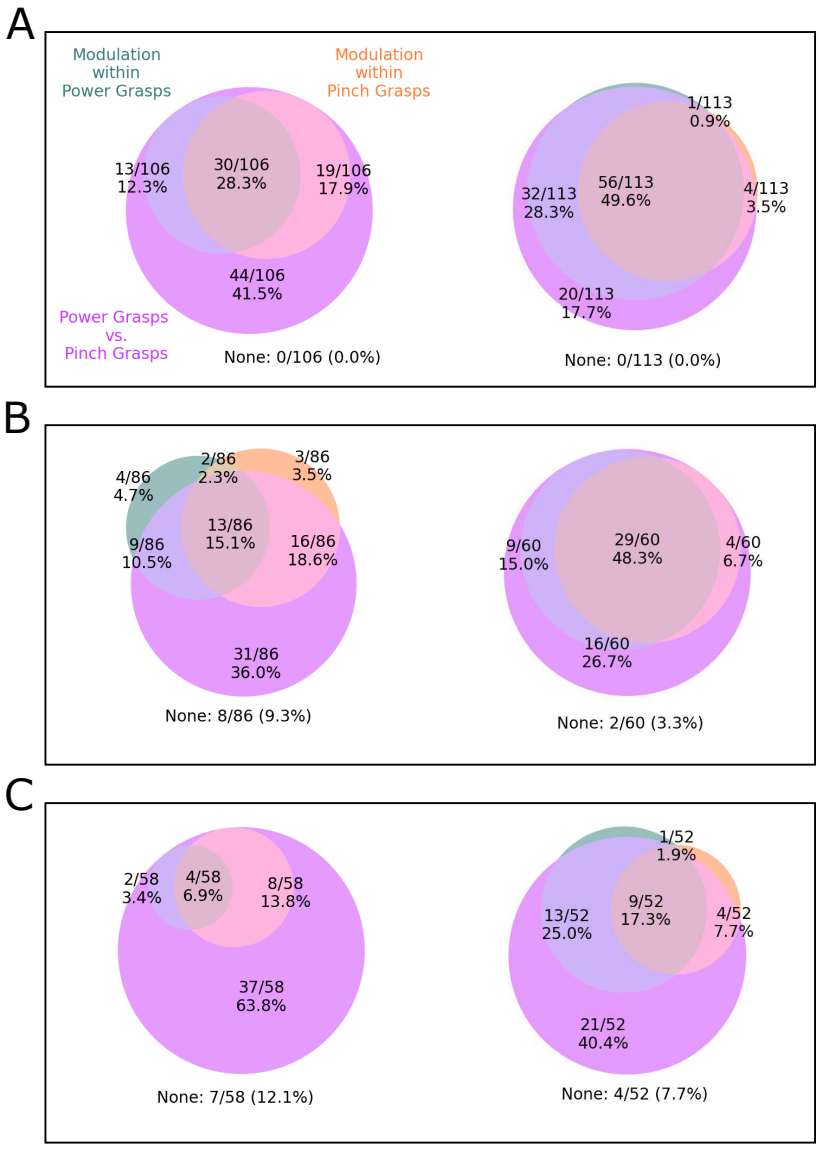

Figure 6.15: **Number of units with $\geq$ 100 ms of significantly modulated activity, Use Affordance Experiment.** A: Monkey R. B: Monkey I. C: Monkey T. Left-hand plots: pre-learning session. Right-hand plots: post-learning session. Purple circles: any Power Grasp condition significantly different from any Pinch Grasp condition. Turquoise circles: Power Hold, Object 1 significantly different from Power Hold, Object 2. Orange circles: Pinch Hold, Object 1 significantly different from Pinch Hold, Object 2. Significant differences were determined by permutation test, 10000 shuffles, $p < 0.01$

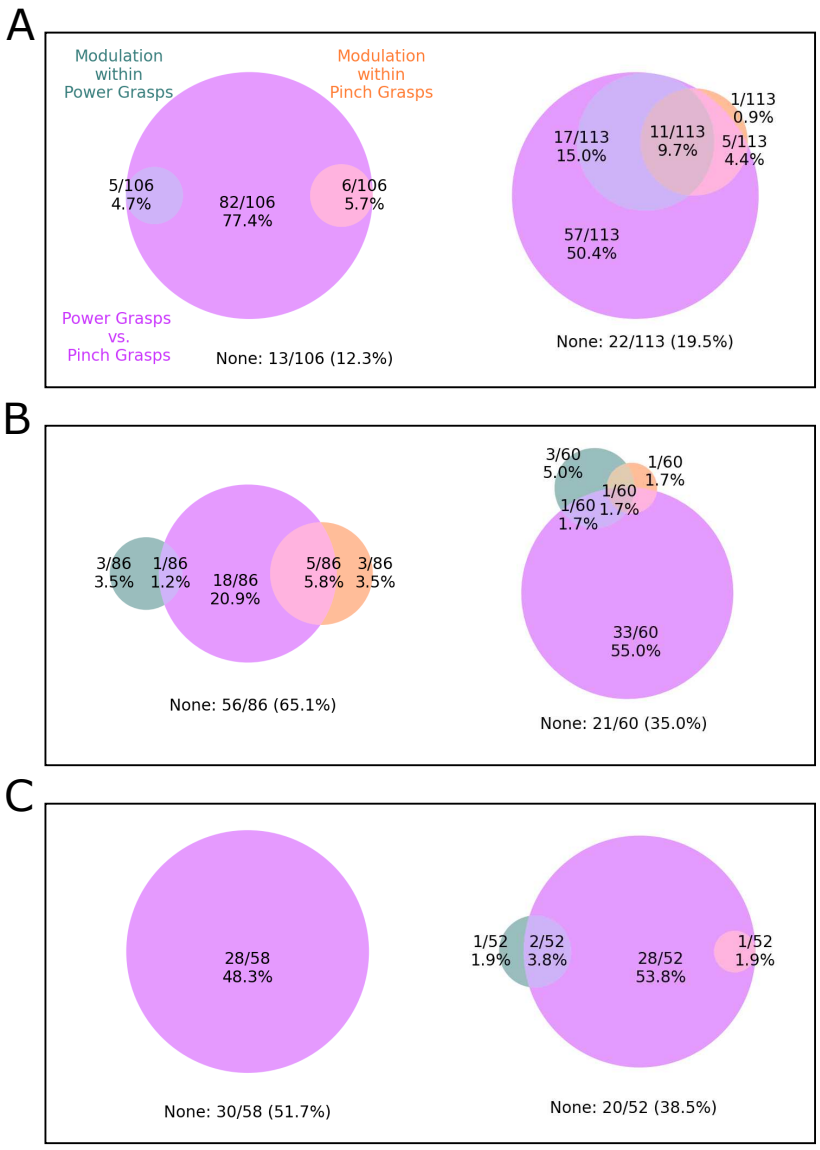

Figure 6.16: **Number of units with $\geq$ 500 ms of significantly modulated activity, Use Affordance Experiment.** A: Monkey R. B: Monkey I. C: Monkey T. Left-hand plots: pre-learning session. Right-hand plots: post-learning session. Purple circles: any Power Grasp condition significantly different from any Pinch Grasp condition. Turquoise circles: Power Hold, Object 1 significantly different from Power Hold, Object 2. Orange circles: Pinch Hold, Object 1 significantly different from Pinch Hold, Object 2. Significant differences were determined by permutation test, 10000 shuffles, $p < 0.01$

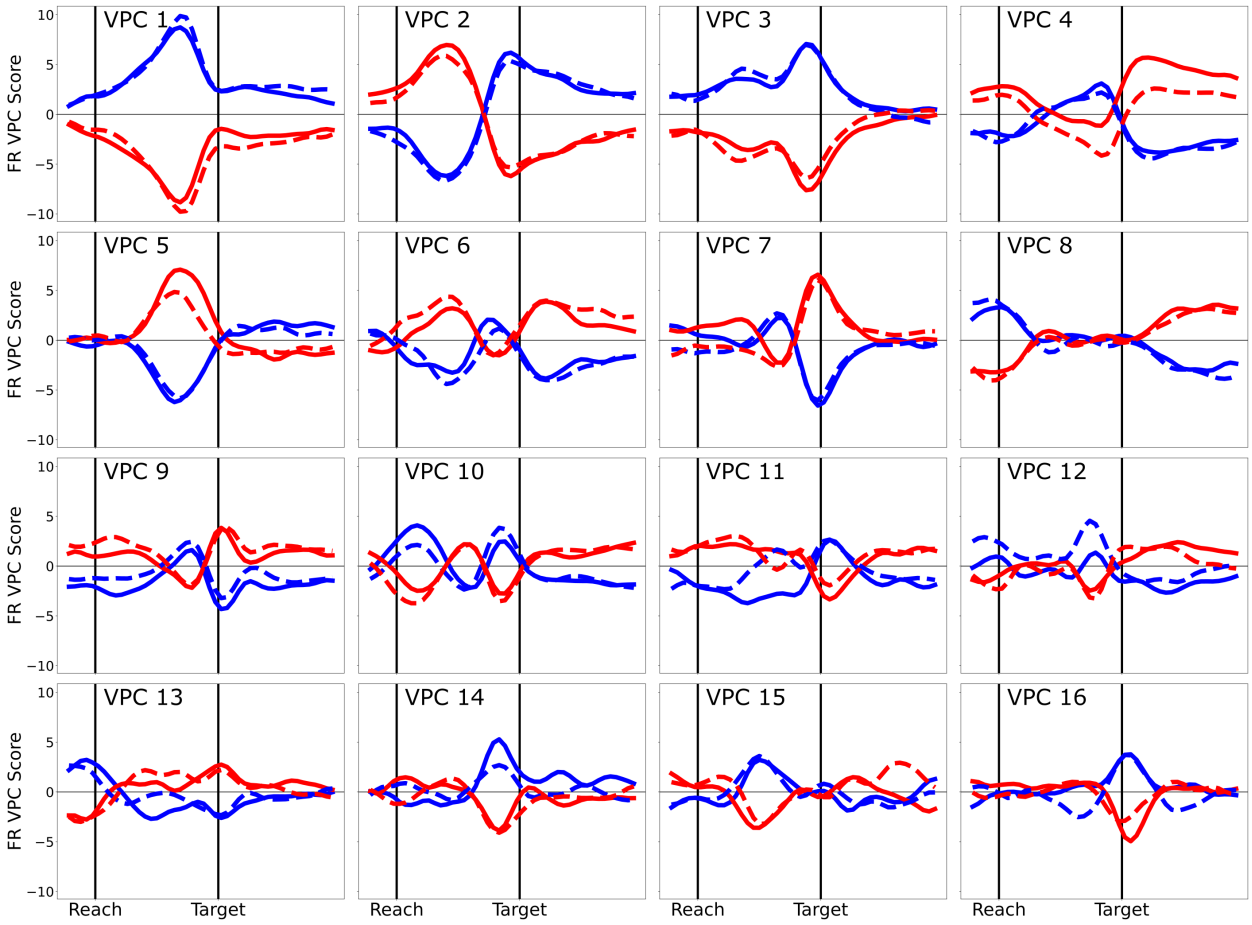

Figure 6.17: **Varimax PCA of the FRs in the pre-learning session of the Use Affordance Experiment, Monkey R.** Scores in the top 16 FR VPCs. Solid blue lines: Power Hold, Object 1. Solid red lines: Pinch Hold, Object 1. Dashed blue lines: Power Hold, Object 2. Dashed red lines: Pinch Hold, Object 2. Dotted blue lines: Power Lift, Object 2.

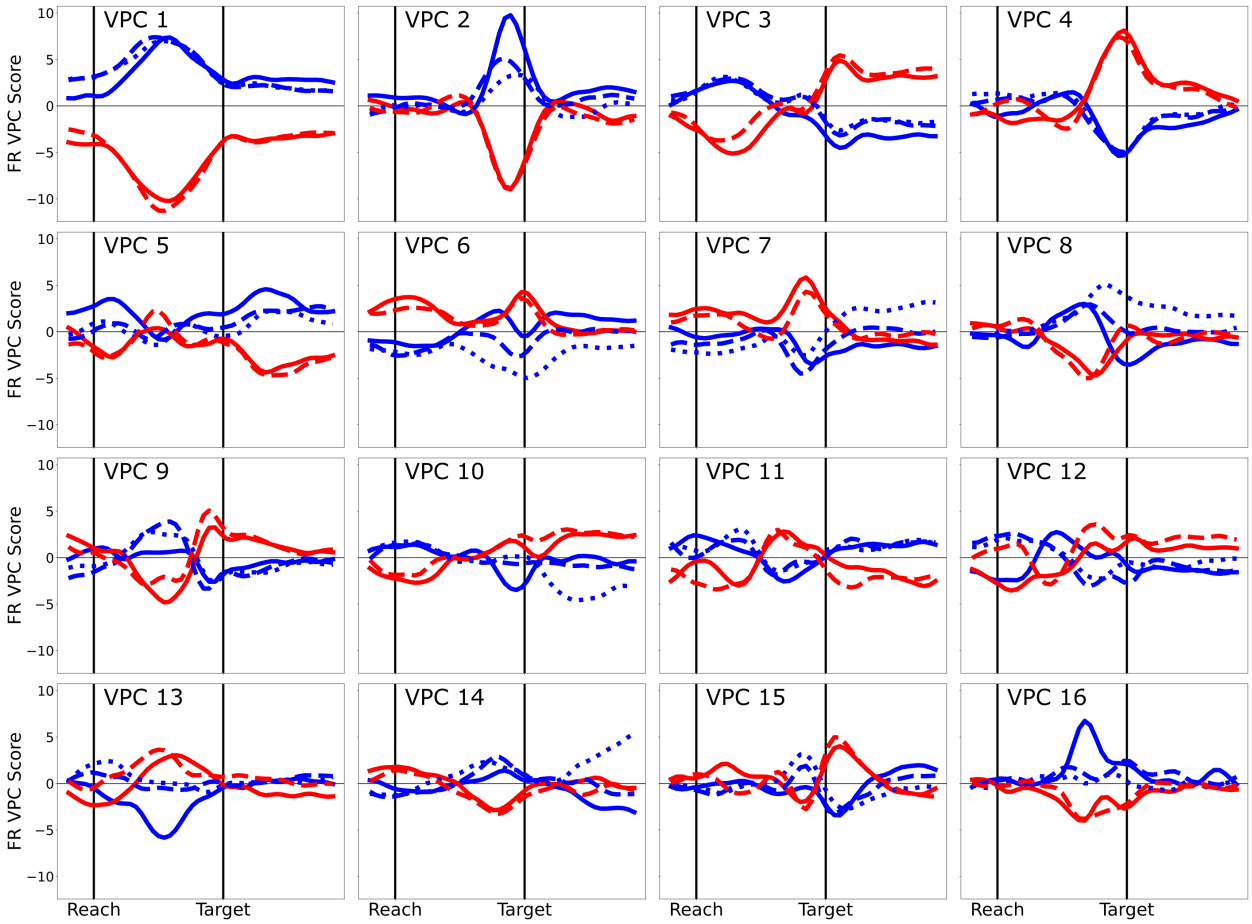

Figure 6.18: **Varimax PCA of the FRs in the post-learning session of the Use Affordance Experiment, Monkey R.** Scores in the top 16 FR VPCs. Solid blue lines: Power Hold, Object 1. Solid red lines: Pinch Hold, Object 1. Dashed blue lines: Power Hold, Object 2. Dashed red lines: Pinch Hold, Object 2. Dotted blue lines: Power Lift, Object 2.

The Power Lift condition was further separated from the two Power Hold conditions in several FR VPCs (notably FR VPCs 6, 7, 8 10 and 14). In other FR VPCs, the two Power Grasps on Object 2 were grouped together, and were separate from the Power Grasp for Object 1 (notably, FR VPCs 1, 2, 3, 5, 9, 13 and 16).

To visualize the magnitude of inter-condition modulation in the population FRs over time, the Euclidean distances between each pair of conditions was calculated. This distance was first calculated in full FR space, treating the FR of each unit as a separate dimension. This distance, deemed the population modulation Δ was calculated by combining the individual unit modulations, δ according to Equations 4.3 and 4.4 in Section 4.3. The resulting Δ values are plotted in Figure 6.19.

The patterns in population modulation (Figure 6.19) were similar to those observed in the percentage of significantly modulated units (Figure 6.14). As in Section 5.3, magnitude of population modulation was lower in general for Monkey I compared to the other subjects.

For more direct comparison with the inter-condition distances in MF PC space D_{MFPC}, the inter-condition distances were also calculated in FR PC space, according to Equation 4.5 in Section 4.3. The FR PC distances D_{FRPC} are shown in Figure 6.20 and the time-averaged FR PC distances $\overline{D}_{\mathrm{FRPC}}$ are shown in Figure 6.21 for both the pre- and post-learning sessions for all subjects.

For all subjects, distances in FR PC space were largest for Power Grasp vs. Pinch Grasp pairs. Except for Power Hold, Object 1 vs. Power Hold Object 2 for Monkey T in the pre-learning session, $\overline{D}_{\mathrm{FRPC}}$ for every same-behavior, different object condition pair was significantly greater than expected within-condition variability in $\overline{D}_{\mathrm{FRPC}}$ (Figure 6.21, stars). For all subjects, the Power Hold, Object 2 and Power Lift, Object 2 conditions were the most similar Power Grasp conditions in FR PCs of the post-learning session throughout the reach period until the Target Contact time (Figure 6.20 light turquoise traces). After target contact, lift trials diverged from hold trials.

Due to differences in the sampled neural population between the pre- and post-learning sessions, the overall magnitude of modulation may have shifted between the sessions. In order to compare the size of effects in the pre-learning session vs. the post-learning session, the proportional size of within-grasp modulation was calculated by dividing the

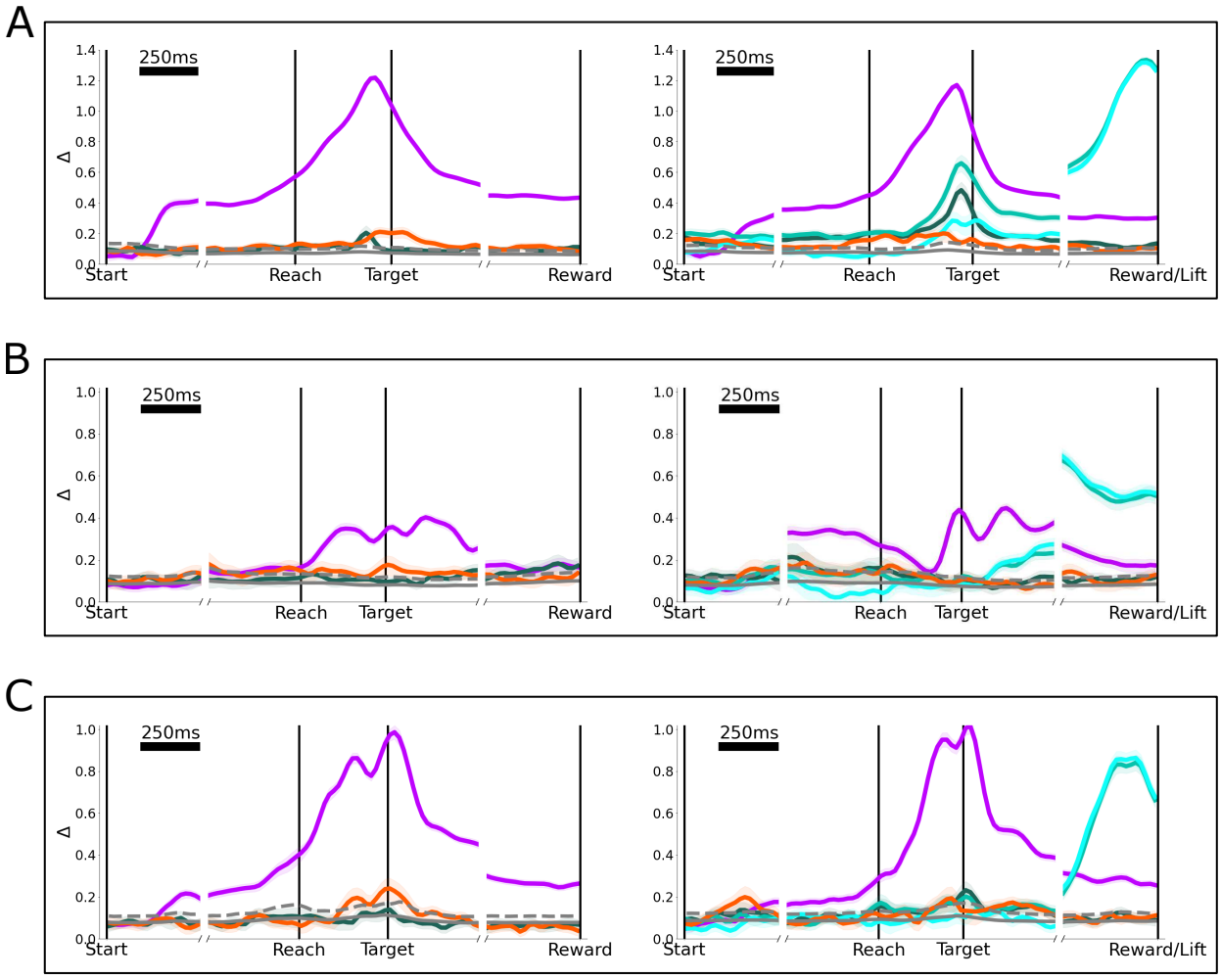

Figure 6.19: **Population modulation Δ and for pairs of conditions in pre- and post-learning sessions of the Use Affordance Experiment.** A: Monkey R. B: Monkey I. C: Monkey T. Left-hand plots: pre-learning session. Right-hand plots: post-learning session. Purple: mean Power Hold vs. Pinch Hold for Objects 1 and 2. Dark turquoise: Power Hold, Object 1 vs. Power Hold, Object 2. Medium turquoise: Power Hold, Object 1 vs. Power Lift, Object 2. Light turquoise: Power Hold, Object 2 vs. Power Lift, Object 2. Orange: Pinch Hold, Object 1 vs. Pinch Hold, Object 2. Gray: mean and upper 95% one-sided confidence interval of within-condition variability.

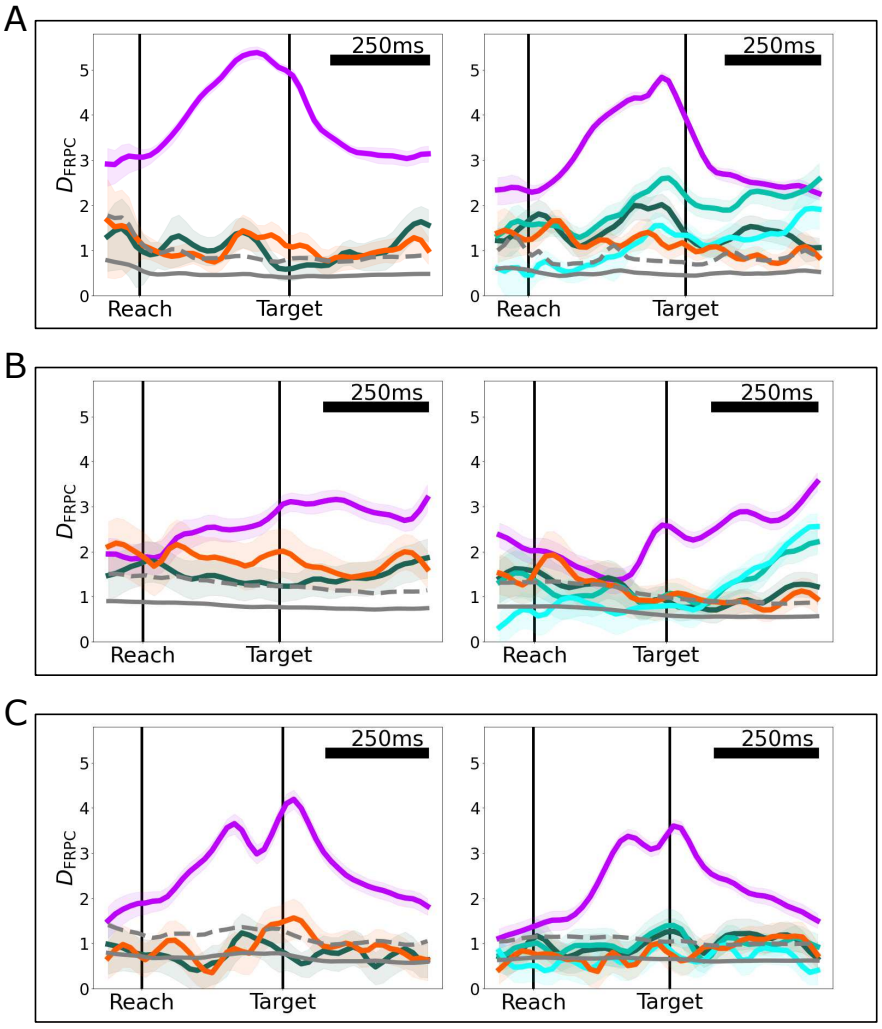

Figure 6.20: **Scaled Euclidean inter-condition distances between pairs of trial-averaged FR PC scores in the Use Affordance Experiment.** Distances were calculated in the 99% FR PC Space. A: Monkey R. B: Monkey I. C: Monkey T. Left-hand plots: pre-learning session. Right-hand plots: post-learning session. Purple: mean Power Hold vs. Pinch Hold for Objects 1 and 2. Dark turquoise: Power Hold, Object 1 vs. Power Hold, Object 2. Medium turquoise: Power Hold, Object 1 vs. Power Lift, Object 2. Light turquoise: Power Hold, Object 2 vs. Power Lift, Object 2. Orange: Pinch Hold, Object 1 vs. Pinch Hold, Object 2. Gray: mean and upper 95% one-sided confidence interval of within-condition variability. 95% confidence intervals (shaded regions or error bars) are bootstrap intervals, trials resampled 10000 times.

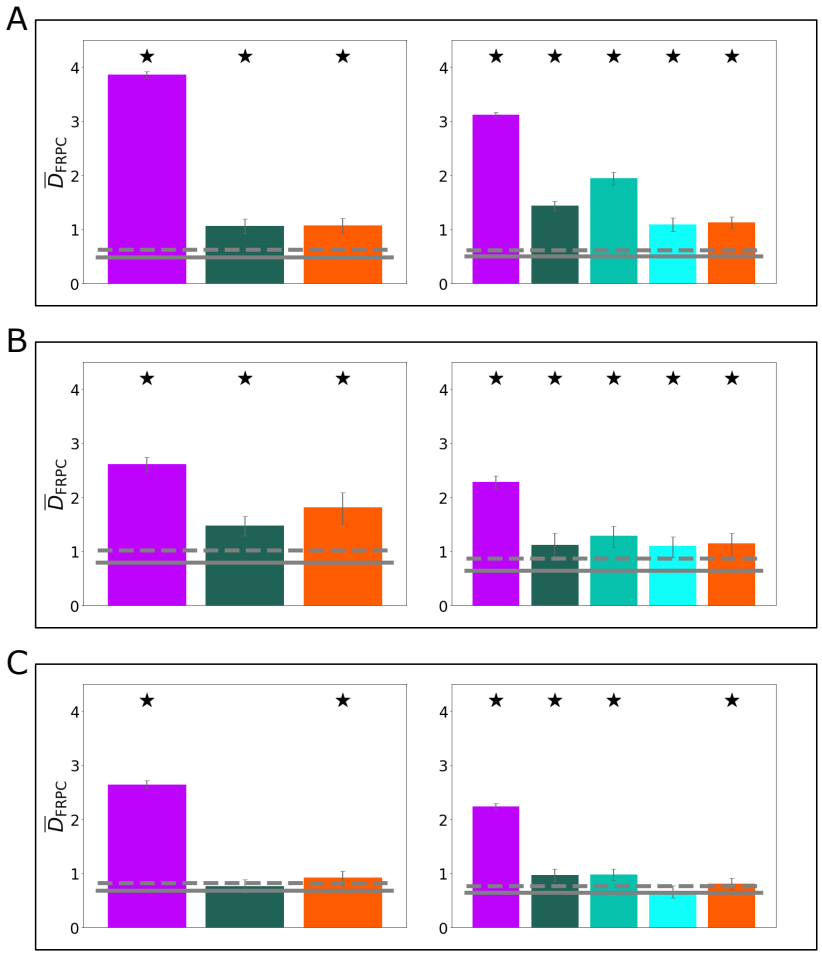

Figure 6.21: **Time-averaged scaled Euclidean inter-condition distances between pairs of trial-averaged FR PC scores in the Use Affordance Experiment.** Distances were calculated in the 99% FR PC Space. A: Monkey R. B: Monkey I. C: Monkey T. Left-hand plots: pre-learning session. Right-hand plots: post-learning session. Star: $\overline{D}_{\mathrm{FRPC},i,j}$ significantly greater than within condition $\overline{D}_{\mathrm{FRPC}}$ variability ($p < 0.05$, one-sided bootstrap interval). Purple: mean Power Hold vs. Pinch Hold for Objects 1 and 2. Dark turquoise: Power Hold, Object 1 vs. Power Hold, Object 2. Medium turquoise: Power Hold, Object 1 vs. Power Lift, Object 2. Light turquoise: Power Hold, Object 2 vs. Power Lift, Object 2. Orange: Pinch Hold, Object 1 vs. Pinch Hold, Object 2. Gray: mean and upper 95% one-sided confidence interval of within-condition variability. 95% confidence intervals (shaded regions or error bars) are bootstrap intervals, trials resampled 10000 times.

within-grasp distances by the mean between-grasp distances, as in Section 6.2. For these calculations, FR PCs were recalculated in the post-learning sessions, excluding Power Lift, Object 2 trials to further facilitate direct comparison between the sessions. These proportional effect sizes are shown in Table 6.2.

Table 6.2: **Proportional size of within-grasp FR PC distances for the pre- and post-learning sessions in the Use Affordance Experiment.** Proportional effect sizes were calculated by dividing $\overline{D}_{\mathrm{FRPC}}$ for same-behavior condition pairs by the average $\overline{D}_{\mathrm{FRPC}}$ for Power Grasp vs./ Pinch Grasp.

		Pre-learning		**Post-learning**	
Subject	**Area**	**Power**	**Pinch**	**Power**	**Pinch**
Monkey R	M1	0.28	0.28	0.49	0.37
Monkey I	M1	0.57	0.70	0.50	0.51
Monkey T	M1 Right	0.29	0.35	0.45	0.37

For Monkey R and Monkey T, the proportional size of the Power Hold, Object 1 vs. Power Hold, Object 2 distances increased between the pre-learning session and the post-learning session. However, for Monkey I, this proportional distance decreased between the pre-learning and post-learning session. The FR PC proportional effect sizes of the post-learning session were 1.54, 0.80 and 1.28 times the proportional effect sizes of the pre-learning session on average for Monkey R, Monkey I and Monkey T.

The proportional within-grasp distances were larger in FR PCs than in MF PCs, for both the pre-learning and post-learning sessions. This neural separation between conditions for which the behaviors were very similar may reflect encoding of the learned use affordances of the object, or of contextual object differences in general. In the next section, evidence for such object context encoding is considered.

6.4 Evidence for Object Context Encoding

The analyses of Sections 6.2 and 6.3 revealed that both MFs and FRs were significantly different for conditions in which the same grasp was performed on objects of different color (in the pre-learning session) or on objects with different learned use affordances (in the post-learning session). The neural differences for these same-grasp, different-context condition pairs were relatively larger than the behavioral differences. Relative to mean Power Grasp vs. Pinch Grasp distances, mean FR PC distances $\overline{D}_{\mathrm{FRPC}}$ for same-grasp condition pairs were 1.60, 5.08 and 3.26 times as large as the corresponding mean MF PC distances $\overline{D}_{\mathrm{FRPC}}$ in the pre-learning session, and 1.73, 2.62 and 1.74 times as large in the post-learning session for Monkey R, Monkey I and Monkey T respectively. This disparity in the relative sizes of neural and behavioral distances can be visualized using MDS, as shown in Figure 5.18.

This relative disparity in the separation of same-grasp conditions in FRs as compared to MFs suggests the possibility that the neural differences observed between these conditions not only reflect encoding of MF differences, but may also additionally constitute encoding of the perceived and learned grip affordance differences.

In this section, evidence is considered for the presence of context encoding related to the learned use affordances of the object being grasped. Context encoding is here defined as neural variation between conditions in which the same action was performed in different contexts beyond what can be accounted for by linear neural tuning to MFs. In Section 4.4, M1 neural activity was shown to contain strong context encoding related to the context of whether or not an object was present. In Section 5.4, M1 neural activity was shown to contain weak context encoding related to the perceived and learned grip affordance of different grasped objects. In this section, evidence is considered for context encoding in M1 related to the learned use affordances of grasped objects. Evidence for object context encoding is presented first from an encoding perspective (Section 6.4.1), then from a decoding perspective (Section 6.4.2). In summary, the analyses of this section show that M1 contextual encoding of object color and learned object use affordance was negligible in size, sporadic and inconsistent between subjects.

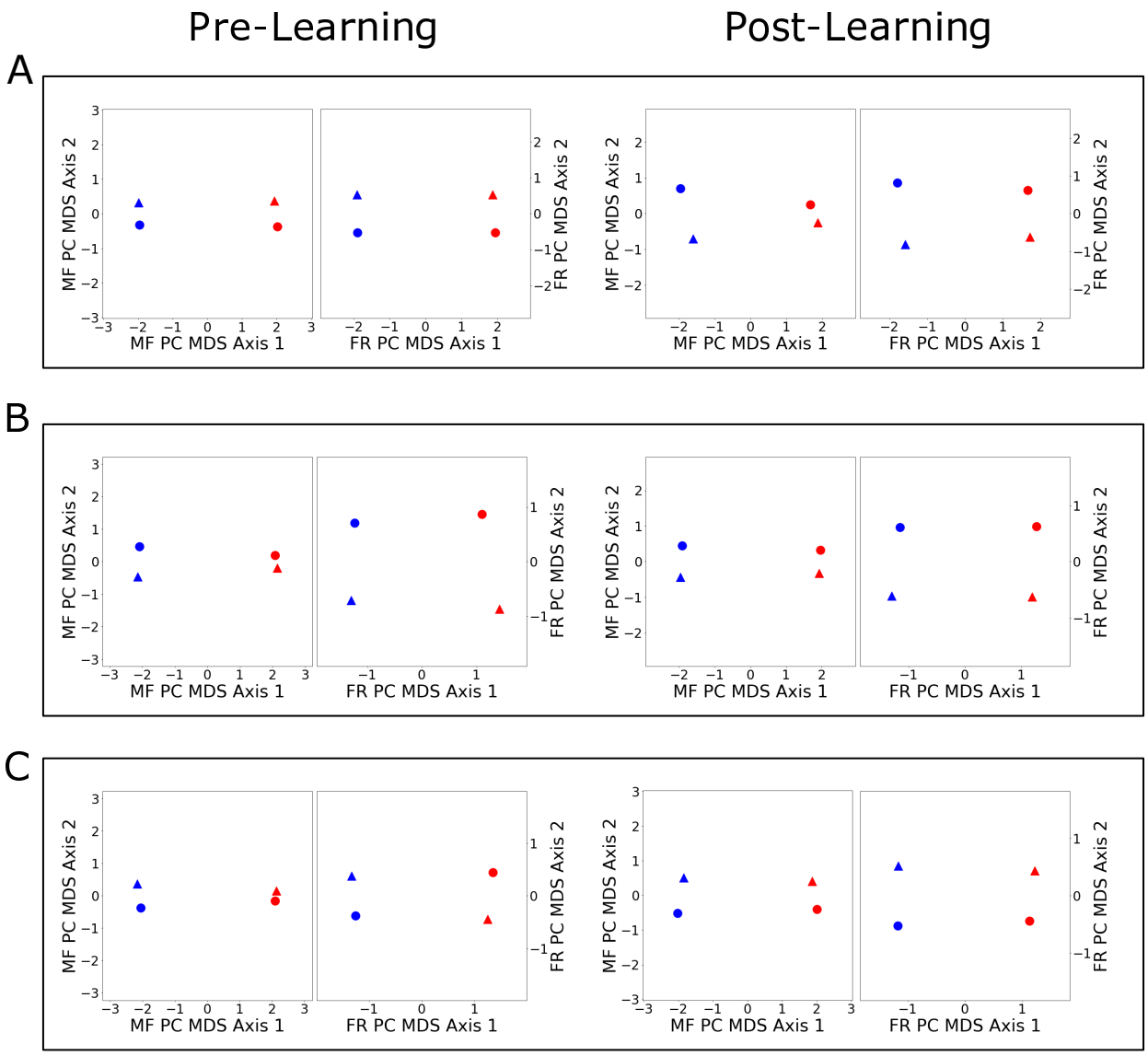

Figure 6.22: **MDS of MF PC and FR PC inter-condition distances in the Use Affordance Experiment.** A: Monkey R. B: Monkey I. C: Monkey T. Left-hand plots: MDS of MF PC distances. Right-hand plots: MDS of FR PC distances. Blue markers: Power Hold. Red markers: Pinch Hold. Circles: Object 1. Triangles: Object 2. Power Lift trials are excluded from this plot. Plots were rotated to align the mean of both Pinch Hold conditions with the x-axis, and scaled so that the MF PC and FR PC distances between mean Power Hold and mean Pinch Hold were visually equal.

For the following analyses, the Power Lift, Object 2 trials were excluded from analysis. This was done in order to focus only on conditions in which the same grasp and hold actions were performed on the different objects. Thus the four conditions that are analyzed in both the pre- and post-learning sessions are:

1. Power Hold, Object 1
2. Pinch Hold, Object 1
3. Power Hold, Object 2
4. Pinch Hold, Object 2

6.4.1 Encoding Perspective

Given the base hypothesis that M1 neural activity is simply and directly related to movements or muscle activity, FRs were first modeled as linear combinations of MF PCs, as in equation 4.7 in Section 4.4.1. As in Section 4.4.1 and 5.4.1, PCA was performed on the full matrix of normalized lagged MFs for each subject, and the top PCs explaining 99% of the variance were extracted, resulting in 29 (28), 22 (23) and 17 (19) MF PCs for Monkey R, Monkey I and Monkey T respectively for the pre-learning (post-learning) session. The linear MF PC neural tuning models were fit via regression. The resulting trial-averaged regression R^2_{TA} values are shown in Figure 6.23.

The R^2_{TA} distributions suggest that M1 units were well-modeled by linear combinations of MF PCs in general when considering trial-averaged data. Monkey R exhibited the strongest tuning on average, followed by Monkey T, then Monkey I. The mean R^2_{TA} values did not change substantially between the pre- and post-learning sessions.

As described in Section 6.2, small but consistent and significant differences were observed in the MF PC scores when the same grasp and hold actions were performed on the different objects (Figure 6.11, dark turquoise and orange traces), in both the pre- and post-learning sessions. Relatively larger differences were observed in the FR PC scores for these condition pairs (Figure 6.22). We hypothesized that M1 units may encode the learned use affordance differences of the objects, or simply the perceived color difference of the objects, along with

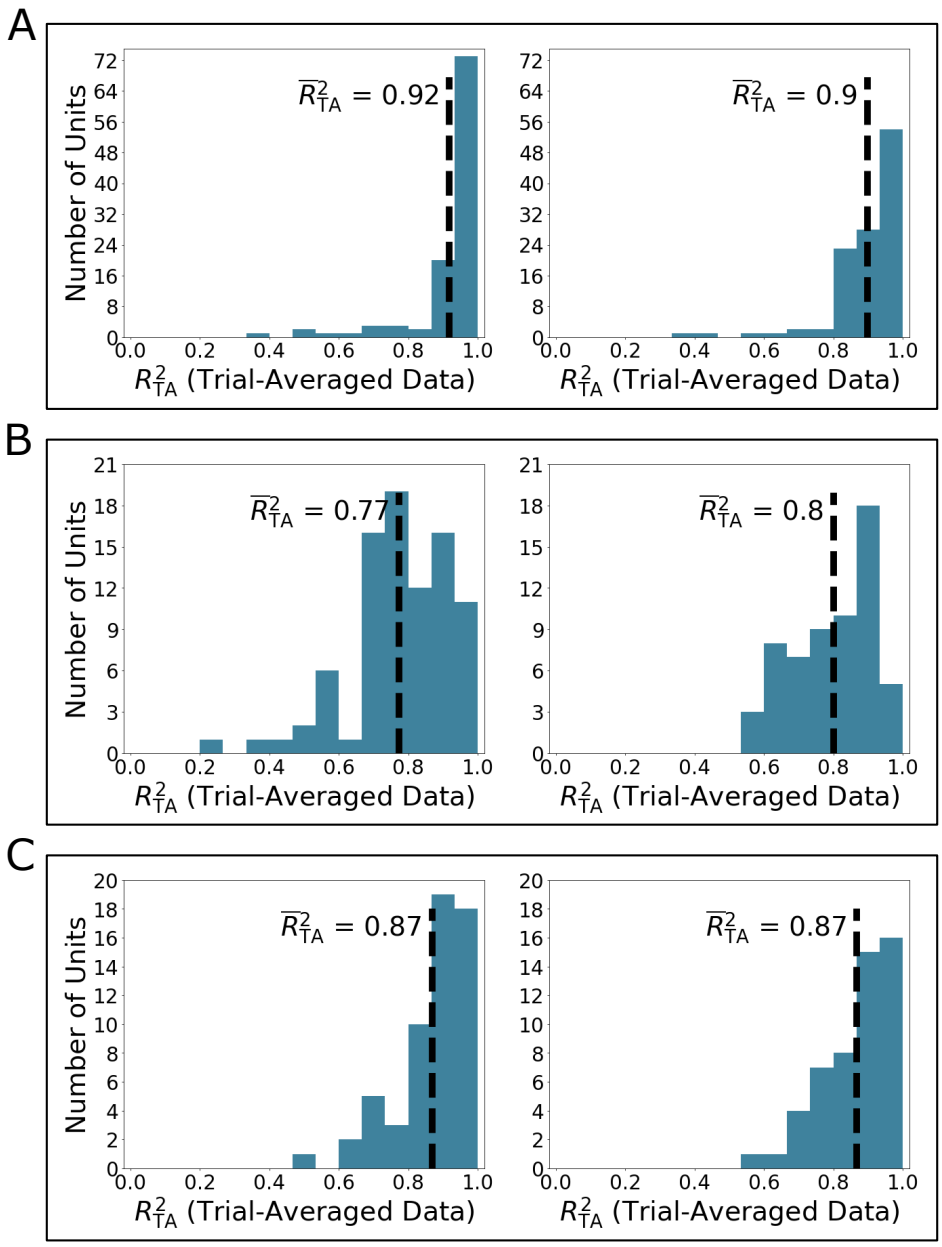

Figure 6.23: **Regression R^2_{TA} distributions for the linear tuning of unit FRs to MF PCs in the pre- and post-learning sessions of the Use Affordance Experiment.** A: Monkey R. B: Monkey I. C: Monkey T. Left-hand plots: pre-learning session. Right-hand plots: post-learning session. R^2_{TA} were obtained from trial-averaged neural data and predictions (trial-to-trial variability excluded). Black dashed lines: mean values.

MF encoding. In that case, the FR modulations between same-grasp conditions would exceed what can be accounted for by a linear tuning model alone, resulting in "extralinear modulation."

To test the hypothesis of use affordance related encoding in M1 units, the extralinear modulation (modulation beyond that which can be accounted for by linear movement tuning), ξ, was calculated for each condition pair for each unit, as in Equations 4.9–4.11 in Section 4.4.1. The extralinear modulation was defined as the modulation in FRs δ minus the modulation in predicted FRs $\hat{\delta}$ generated from the linear FR to MF PC tuning models. The time-averaged extralinear modulations $\overline{\xi}$ were calculated by averaging each ξ over the entire peri-movement period.

As in Section 4.4.1 and Section 4.4.2, a unit was considered context encoding if $\overline{\xi}$ for a same-grasp condition pair was significantly greater than expected within-condition $\overline{\xi}$ variation, and was further considered robustly context encoding if that same-grasp $\overline{\xi}$ was additionally greater than mean $\overline{\xi}$ for Power Grasp vs. Pinch Grasp ($p < 0.05$, bootstrapped one-sided interval, trials resampled 10000 times).

Table 6.3 displays the percentage of units with significant object context tuning in the pre- and post-learning sessions.

Only a small number of individual units showed evidence for significant or robust context encoding in either the pre- or post-learning sessions within either grip type. The only instances of context encoding for which over 10% of units were sensitive were within both grip types in the post-learning session in Monkey R, suggesting a potential minor encoding of use affordance in Monkey R M1. For Monkey I and Monkey T, 8.6 and 9.3% of units displayed some evidence of context encoding between Pinch Grasps in the pre-learning session. This suggests a very minor potential encoding of color difference in these subjects, restricted only to the Pinch Grasps of the pre-learning session.

As noted in Section 6.4, some individual units were recorded in both the pre- and post-learning sessions, as identified by the unit tracking algorithm developed by Fraser and Schwartz [439]. To determine the frequency of use affordance encoding related to the learning of the lift action in individual units, the occurrence of object context encoding in

Table 6.3: **Percentage of object context encoding units based on magnitude of extralinear modulation.** Unit n is considered significantly context encoding if an instance of $\overline{\xi}_{\text{SameGrasp,DifferentObject},n}$ is significantly greater than within-condition $\overline{\xi}$ variability. Unit n is further considered robustly context encoding if an instance of $\overline{\xi}_{\text{SameGrasp,DifferentObject},n}$ is significantly greater than $\overline{\xi}_{\text{PowerGrasp,PinchGrasp},n}$ ($p < 0.05$ bootstrap one-sided interval). Power: object context encoding observed for Power Hold, Object 1 vs. Power Hold, Object 2. Pinch: object context encoding observed for Pinch Hold, Object 1 vs. Pinch Hold, Object 2.

		Significant Context Encoding			
		Pre-learning		**Post-learning**	
Subject	**Area**	**Power**	**Pinch**	**Power**	**Pinch**
Monkey R	M1	2.8%	4.7%	11.5%	11.5%
Monkey I	M1	0.0%	9.3%	3.3%	0.0%
Monkey T	M1 Right	1.7%	8.6%	3.8%	1.9%

		Robust Context Encoding			
		Pre-learning		**Post-learning**	
Subject	**Area**	**Power**	**Pinch**	**Power**	**Pinch**
Monkey R	M1	1.9%	3.8%	8.8%	8.8%
Monkey I	M1	0.0%	7.0%	3.3%	0.0%
Monkey T	M1 Right	0.0%	5.2%	3.8%	1.9%

these tracked units was tabulated across the pre- and post-learning sessions. The percentage of tracked units displaying object context encoding in only one, both, or neither of the pre- and post-learning sessions is shown in Table 6.4.

Only a small percentage of units showed any evidence of context encoding in the two categories. As in the units as a whole, the only notable effects were in Monkey R, where a small increase was observed associated with the learning of the use affordance, and in Monkey I, where some potential color encoding units were observed only with respect to Pinch Grasps in the pre-learning session.

The individual unit extralinear modulation results were inconsistent between subjects and small in terms of the number of units displaying the effect. To measure the strength of object presence encoding at the population level, population extralinear modulation ξ^{pop} was calculated according to Equation 4.12 in Section 4.4.1. The time-averaged population extralinear modulation $\overline{\xi}^{\text{pop}}$ for each condition pair was also calculated by averaging each ξ^{pop} over time in the peri-movement period. The population extralinear modulation results are shown in Figure 6.24 and the time-averaged population extralinear modulation results are shown in Figure 6.25 for both the pre- and post-learning sessions.

The only within-grasp condition pair $\overline{\xi}$ which qualified as showing evidence of robust context encoding was Pinch Hold, Object 1 vs. Pinch Hold, Object 2 for Monkey I in the pre-learning session (Figure 6.25 B, left hand plot, orange bar). Additionally, Monkey R showed evidence of significant object context encoding for both grip types in the post-learning session only. These results suggest that context encoding related to the color of the objects or the learned use affordances of the objects were very small where present and were inconsistent between subjects. Similar analyses and conclusions are presented in the following section, approaching the question of context encoding from a "decoding" perspective.

Table 6.4: **Frequency of object context encoding in units recorded in both the pre- and post-learning sessions of the Use Affordance Experiment, based on magnitude of extralinear modulation.** Unit n is considered object presence encoding if an instance of $\overline{\xi}_{\text{SameGrasp,DifferentObject},n}$ is significantly greater than both $\overline{\xi}_{\text{PowerGrasp,PinchGrasp},n}$ $p < 0.05$ (bootstrap one-sided interval, trials resampled 10000 times). Power Grasps: object context encoding due to extralinear modulation for Power Hold, Object 1 vs. Power Hold, Object 2. Pinch Grasps: object context encoding due to extralinear modulation for Pinch Hold, Object 1 vs. Pinch Hold, Object 2. # Tracked Units: number of tracked units, with the number of units recorded in the pre- and post-learning sessions in parentheses. Pre Only: object context encoding observed in the pre-learning session but not the post-learning session. Post Only: object context encoding observed in the post-learning session but not the pre-learning session. Both: object context encoding observed in both the pre- and post-learning sessions. Neither: object context encoding observed in neither the pre- nor post-learning session.

Power Grasps					
Subject	**Area**	**# Tracked Units**	**Pre Only**	**Post Only**	**Both**
Monkey R	M1	67 (106, 113)	1.5%	11.9%	1.5%
Monkey I	M1	49 (86, 60)	0.0%	4.1%	0.0%
Monkey T	M1 Right	35 (58, 52)	0.0%	5.7%	0.0%

Pinch Grasps					
Subject	**Area**	**# Tracked Units**	**Pre Only**	**Post Only**	**Both**
Monkey R	M1	67 (106, 113)	4.5%	11.9%	3.0%
Monkey I	M1	49 (86, 60)	14.3%	0.0%	0.0%
Monkey T	M1 Right	35 (58, 52)	5.7%	0.0%	2.9%

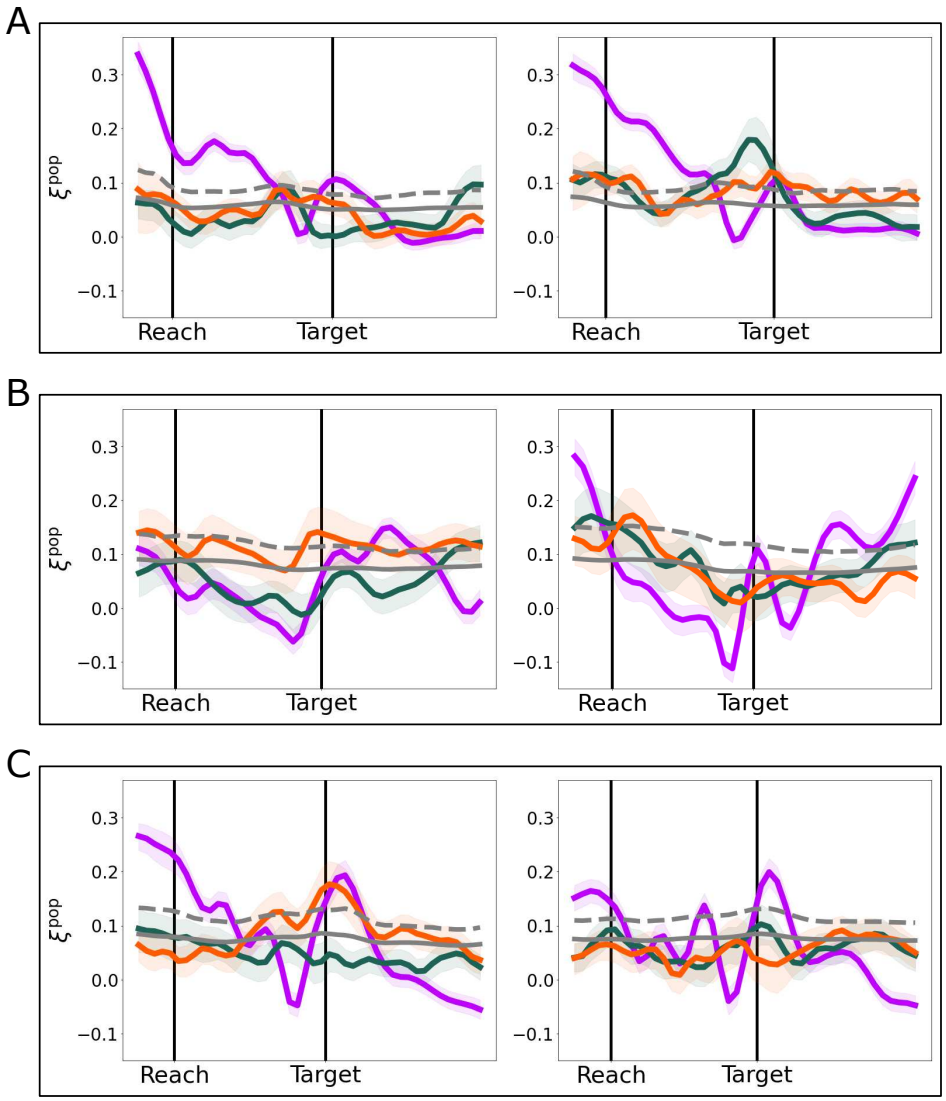

Figure 6.24: **Population extralinear modulation ξ^{pop} for each condition pair in the pre- and post-learning sessions of the Use Affordance Experiment.** A: Monkey R. B: Monkey I. C: Monkey T. Purple: Power Hold vs. Pinch Hold for Objects 1 and 2. Dark turquoise: Power Hold, Object 1 vs. Power Hold, Object 2. Orange: Pinch Hold, Object 1 vs. Pinch Hold, Object 2. Gray: mean and upper 95% one-sided confidence interval of within-condition variability. 95% confidence intervals: bootstrap intervals, trials resampled 10000 times.

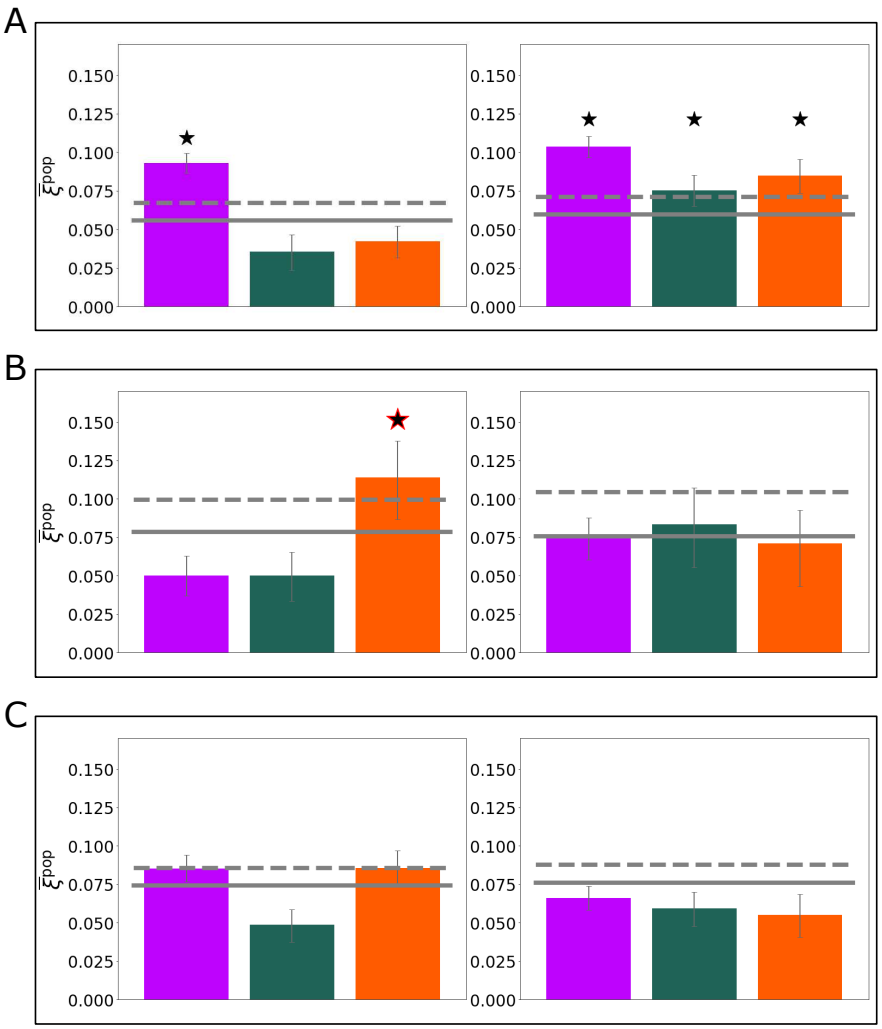

Figure 6.25: **Mean population extralinear modulation $\overline{\xi}^{\text{pop}}$ for each condition pair in the pre- and post-learning sessions of the Use Affordance Experiment.** A: Monkey R. B: Monkey I. C: Monkey T. Left-hand plots: pre-learning session. Right-hand plots: post-learning session. Black star: $\overline{\xi}^{\text{pop}}_{i,j}$ significantly greater than within-condition $\overline{\xi}^{\text{pop}}$ variability. Black and red star: $\overline{\xi}^{\text{pop}}_{i,j}$ additionally significantly greater than mean $\overline{\xi}^{\text{pop}}_{\text{PowerGrasp,PinchGrasp}}$ ($p < 0.05$, one-sided bootstrap interval). Purple: mean Power Hold vs. Pinch Hold for Objects 1 and 2. Dark turquoise: Power Hold, Object 1 vs. Power Hold, Object 2. Orange: Pinch Hold, Object 1 vs. Pinch Hold, Object 2. Gray: mean and upper 95% one-sided confidence interval of within-condition variability. 95% confidence intervals: bootstrap intervals, trials resampled 10000 times.

6.4.2 Decoding Perspective

The extralinear modulation analyses approach the question of object context encoding from an "encoding" perspective, in that a linear MF PC encoding model was built for each unit, and the modulation of individual units were interrogated for evidence of object presence encoding. The problem can also be approached from a "decoding" perspective. As in section 4.4.2, null space analyses were performed to isolate the components of neural activity that were related to or linearly unrelated to MFs. as in Section 6.4.2, Power Lift, Object 2 trials were excluded from these analyses.

For the null space analyses, PCA was performed on FRs and trial-averaged lagged MFs of the peri-movement period to generate the mFR PC scores and mMF PC scores. The top mMF PCs explaining 99% of the variance were used, resulting in 11 (12), 11 (11) and 10 (10) mMF PCs for Monkey R, Monkey I and Monkey T respectively for the pre-learning session (post-learning session). The number of mFR PCs was set to twice the number of mMFs PCs, to produce null and potent spaces of equal dimension.

The mMF PC scores were then regressed against the mFR PC scores as in equation 4.13 in Section 4.4.2. The estimated weights matrix $\hat{\mathbf{B}}$ was decomposed to produce $\hat{\mathbf{B}}_{\text{potent}}$ and $\hat{\mathbf{B}}_{\text{null}}$, which where then used to calculate $\hat{\mathbf{F}}_{\text{potent}}$ and $\hat{\mathbf{F}}_{\text{null}}$, the components of neural activity in the potent and null spaces. $\hat{\mathbf{F}}_{\text{potent}}$ describes the neural activity that can be linearly projected through $\mathbf{B}$ to decode mMF PCs, while $\hat{\mathbf{F}}_{\text{null}}$ describes the activity for which projection through $\mathbf{B}$ results in 0 (see Section A.6.4 for more details).

For these analyses, object context encoding is defined as neural modulation which is not linearly related to MFs. Thus, such object context encoding would manifest as separation between same-grasp conditions in the null space. To characterize this null space separation, the variance due to each condition pair $V_{i,j,t}$ was calculated at each time point for the null space, according to Equation 4.18 as in Section 4.4.2. The time-averaged variance in the null space, $\overline{V}_{i,j}$ was also calculated by averaging $V_{i,j,t}$ over the peri-movement period. These values are displayed in Figures 6.26 and 6.27 for both the pre- and post-learning sessions.

For all condition pairs except Power Hold, Object 1 vs. Power Hold Object 2 in Monkey T in the pre-learning session, null space variance $\overline{V}^{\text{null}}$ exceeded expected within-condition

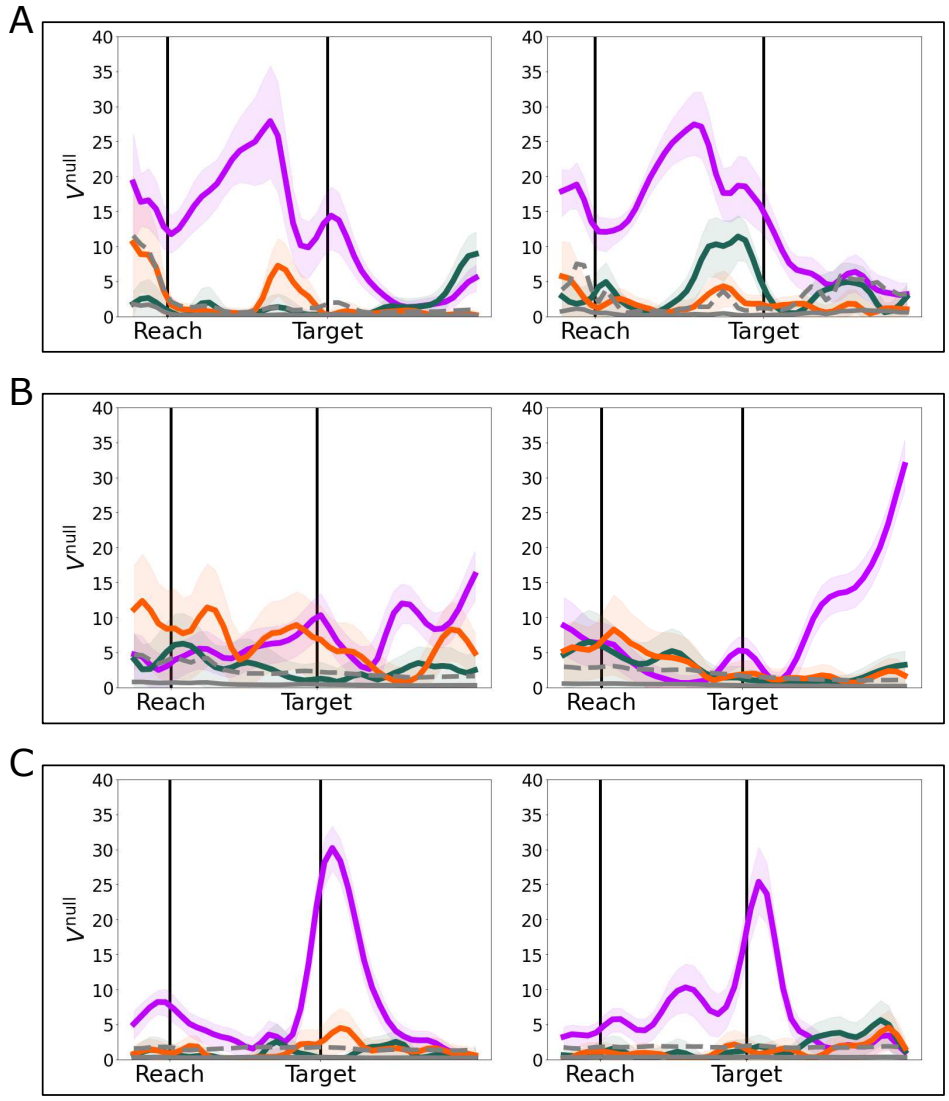

Figure 6.26: **Variances due to each condition pair in the null space for the pre- and post-learning sessions of the Use Affordance Experiment.** A: Monkey R. B: Monkey I. C: Monkey T left right hemisphere. Left-hand plots: pre-learning session. Right-hand plots: post-learning session. Purple: mean Power Hold vs. Pinch Hold for Objects 1 and 2. Dark turquoise: Power Hold, Object 1 vs. Power Hold, Object 2. Orange: Pinch Hold, Object 1 vs. Pinch Hold, Object 2. Gray: mean and upper 95% one-sided confidence interval of within-condition variability. 95% confidence intervals: bootstrap intervals, trials resampled 10000 times.

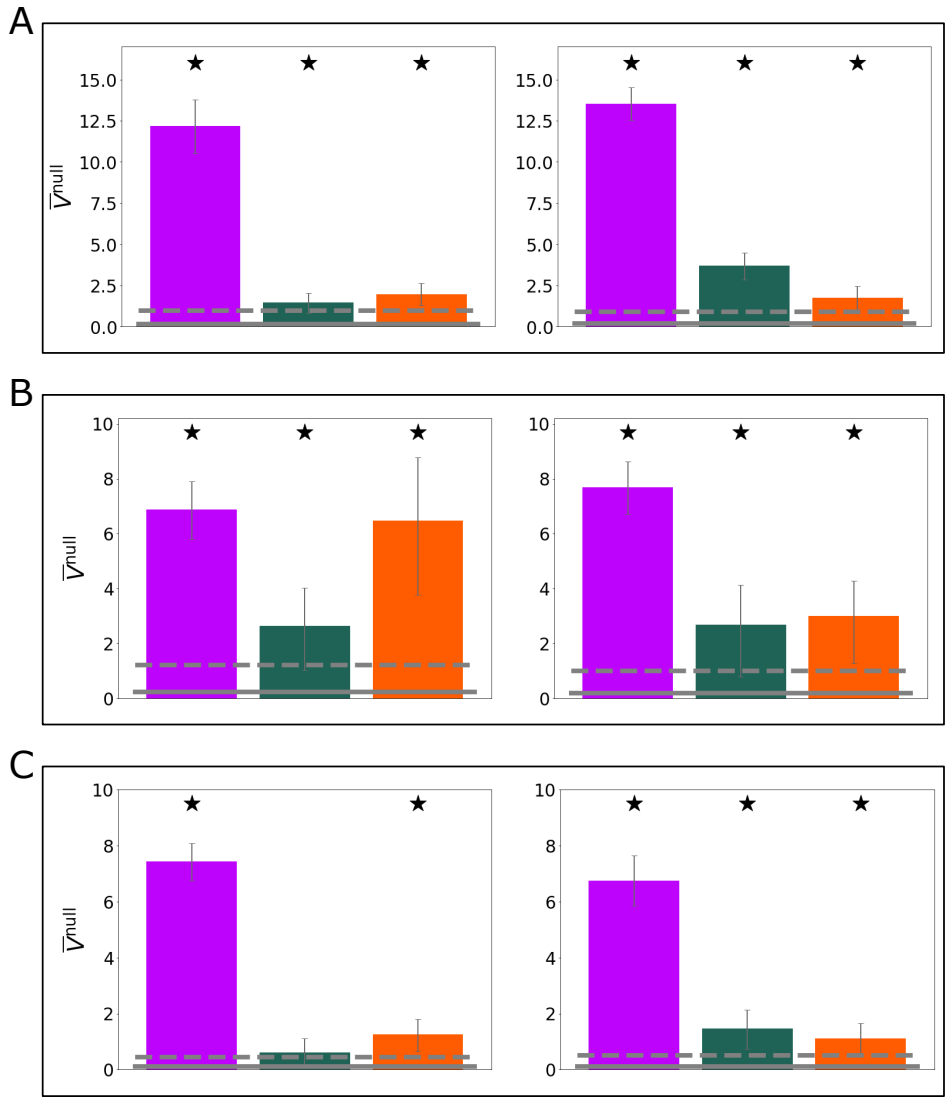

Figure 6.27: **Variances due to each condition pair in the null space for the pre- and post-learning sessions of the Use Affordance Experiment.** A: Monkey R. B: Monkey I. C: Monkey T. Left-hand plots: pre-learning session. Right-hand plots: post-learning session. Star: $\overline{V}^{\text{null}}_{i,j}$ significantly greater than within-condition $\overline{V}^{\text{null}}$ variability ($p < 0.05$, one-sided bootstrap interval). Purple: mean Power Hold vs. Pinch Hold for Objects 1 and 2. Dark turquoise: Power Hold, Object 1 vs. Power Hold, Object 2. Orange: Pinch Hold, Object 1 vs. Pinch Hold, Object 2. Gray: mean and upper 95% one-sided confidence interval of within-condition variability. 95% confidence intervals: bootstrap intervals, trials resampled 10000 times.

$\overline{V}^{\text{null}}$ variance. However, null space variances were generally very small in magnitude. One exception was Monkey I Pinch Hold Object 1 vs. Pinch Hold Object 2 which may reflect encoding of color difference for that specific subject and grasp.

To determine the proportion of the full neural variance which occurred in the null space for each condition pair, the null space proportion by time $\pi_{i,j,t}$ and total null space proportions $\Pi_{i,j}$ were calculated for each condition pair according to Equation 4.20 in Section 6.4.2. These measures are shown in Figures 6.28 and 6.29 for both the pre- and post-learning sessions.

For all subjects, neural variance due to same-grasp condition pairs occurred mostly in the null space. Contrastingly, less than half of variance due to Power Grasp vs. Pinch Grasp occurred in the null space (except for Monkey I in the post-learning session). This suggests that the neural differences observed for same-grasp, different object conditions were largely not linearly related to movements, and thus may have constituted encoding of object context, but as shown by the extralinear modulation and null space variance analyses, the actual magnitude of these object context encoding effects were very small.

The findings of the extralinear modulation and null space analyses were that context encoding related to object color differences and learned object use affordance differences may have been present at a very low level in M1 individual units and populations. However, results were sporadic and inconsistent between subjects. In the following section, further evidence for potential context encoding in single units is considered different regression models. These models are compared to determine if and how this object context encoding signal is represented in individual M1 units, and if the context encoding signal interacts with MF PC encoding.

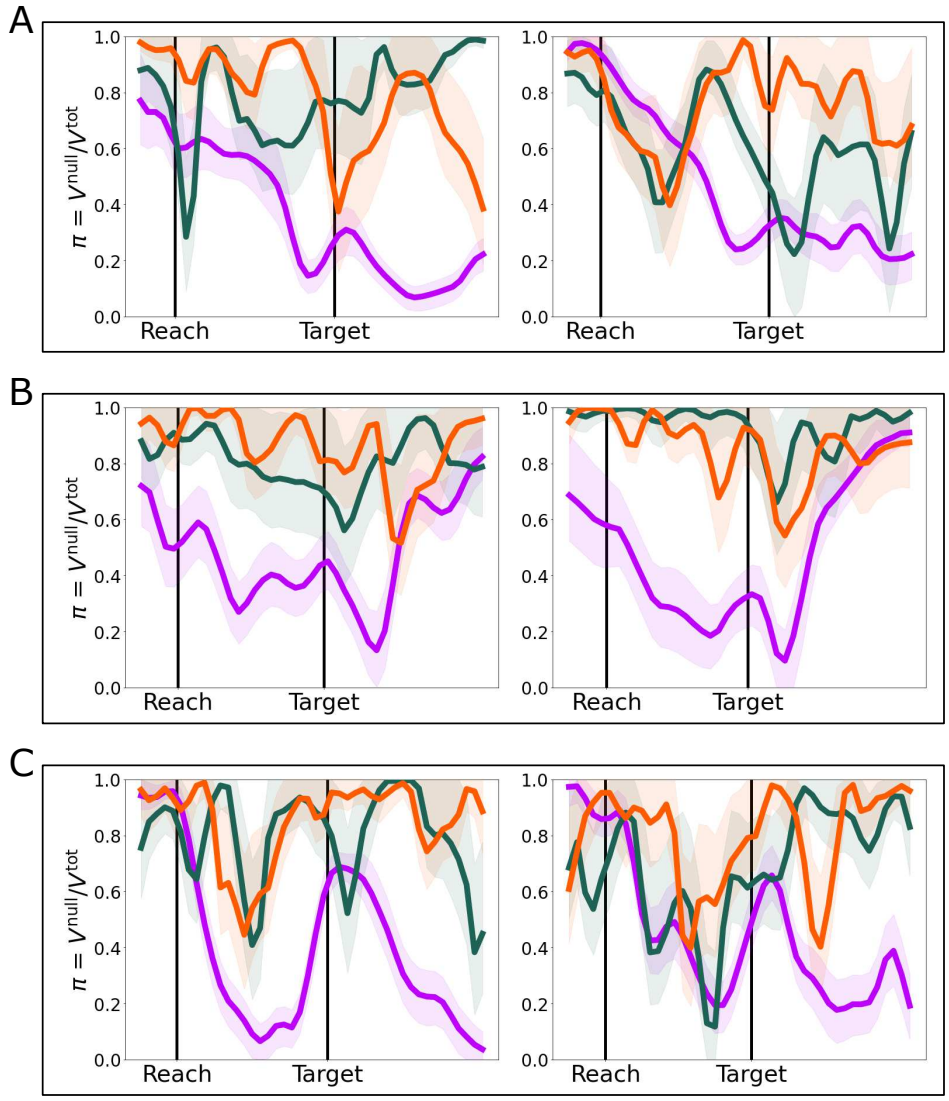

Figure 6.28: **Proportion of full inter-condition variance which occurred in the null space over time for the pre- and post-learning sessions of the Use Affordance Experiment.** A: Monkey R. B: Monkey I. C: Monkey T. Left-hand plots: pre-learning session. Right-hand plots: post-learning session. Purple: mean Power Hold vs. Pinch Hold for Objects 1 and 2. Dark turquoise: Power Hold, Object 1 vs. Power Hold, Object 2. Orange: Pinch Hold, Object 1 vs. Pinch Hold, Object 2. Gray: mean and upper 95% one-sided confidence interval of within-condition variability. 95% confidence intervals: bootstrap intervals, trials resampled 10000 times.

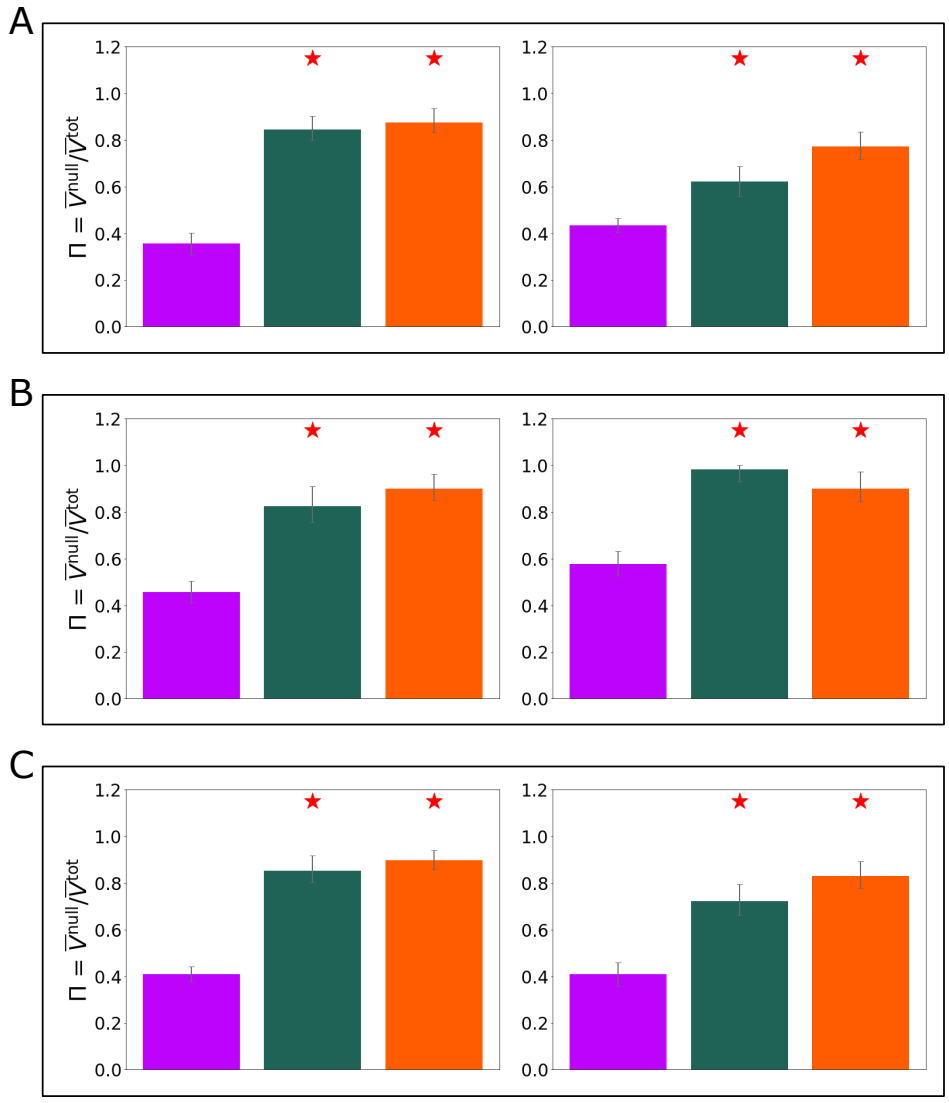

Figure 6.29: **Proportion of full inter-condition variance which occurred in the null space over time for the pre- and post-learning sessions of the Use Affordance Experiment.** A: Monkey R. B: Monkey I. C: Monkey T. Left-hand plots: pre-learning session. Right-hand plots: post-learning session. Red star: $\overline{\Pi}_{i,j}$ significantly greater than $\overline{\Pi}_{\text{PowerGrasp,PinchGrasp}}$ ($p < 0.05$, one-sided bootstrap interval). Purple: mean Power Hold vs. Pinch Hold for Objects 1 and 2. Dark turquoise: Power Hold, Object 1 vs. Power Hold, Object 2. Orange: Pinch Hold, Object 1 vs. Pinch Hold, Object 2. Gray: mean and upper 95% one-sided confidence interval of within-condition variability. 95% confidence intervals: bootstrap intervals, trials resampled 10000 times.

6.5 Interaction of Object Context and MF Encoding

In Section 6.4, object context encoding in M1 individual units and populations was discussed in terms of the FR modulation that exceeded linear tuning to MFs. In this section, the relation between FRs and MFs is explored in relation to the object context encoding. Specifically, we ask if object context was encoded concurrently with MF encoding, and whether object context encoding had an additive or interactive effect when present. For these analyses, as in Section 6.4, Power Lift, Object 2 trials were excluded.

As in Section 4.5, several different linear models were constructed and compared. The baseline model, the "MF only" model, related individual unit FRs to only MF PC scores, as in Equation 4.22 in Section 4.5, reproduced below:

$$f_{n,t} = \beta_{0,n} + \sum_{p=1}^{N_{\mathrm{M}}} (\beta_{p,n} s_{p,t+\tau}) + \epsilon \tag{6.1}$$

where $f_{n,t}$ is the normalized FR of unit n at time t, β are constant weights, $s_{p,t+\tau}$ is MF PC score s at time $t+\tau$, and ϵ is a Gaussian noise term, $\epsilon \sim \mathcal{N}(0, \sigma^2)$. As in Section 6.4, τ was set to 40 ms. This model assumes a fixed linear tuning to movements which ignores context.

The next candidate models, direct object context encoding models, described unit FRs as linear combinations of MF PC scores along with indicator variables denoting which object was grasped. These models allowed a different mean FR for each object context, assuming that object context was encoded directly in FRs. The "Direct object context encoding" model is defined in Equation 6.2:

$$f_{n,t} = \beta_{0,n} + \sum_{p=1}^{N_{\mathrm{M}}} \beta_{p,n} s_{p,t+\tau} + \beta^{c}_{c,n} c + \epsilon \tag{6.2}$$

$$c = 0 \text{ for Object 1}$$

$$c = 1 \text{ for Object 2}$$

The final candidate models, interactive object context encoding models, described unit FRs as linear combinations of MF PC scores and indicator variables and interaction terms. These models allowed the MF PC score tuning coefficients to change depending on the which object was grasped. The "Interactive object context encoding" model is defined in Equation 6.3:

$$f_{n,t} = \beta_{0,n} + \sum_{p=1}^{N_{\mathrm{M}}} \left(\beta_{p,n} s_{p,t+\tau}\right) + \beta^{c}_{0,n} c + \sum_{p=1}^{N_{\mathrm{M}}} \left(\beta^{c}_{p,n} c s_{p,t+\tau}\right) + \epsilon \tag{6.3}$$

$$c = 0 \text{ for Object 1}$$

$$c = 1 \text{ for Object 2}$$

In order to evaluate these models, each was fit separately with linear regression, using the full dataset of FRs f and MF PC scores s. All candidate models were fit separately for the pre-learning session and the post-learning session. The trial-averaged R^2 values, R^2_{TA} were then calculated for each model and each unit (see Section A.6.3 for details). R^2_{TA} was used instead of full R^2 in order to focus on the ability of the models to fit task-relevant activity, rather than trial-to-trial variability. The R^2_{TA} values for all units for the different models are plotted in Figure 6.30, for both the pre- and post-learning sessions.

R^2_{TA} increases were modest for all subjects when adding direct object context encoding, in both the pre- and post-learning sessions. Though R^2_{TA} increases were larger for interactive object context encoding models, these models also featured many more parameters.

Due to the fact that R^2_{TA} is bounded at 1, and also always increases when adding more model parameters, it alone does not make a sufficient measure for model selection. As a more concrete measure, the Bayesian Information Criterion (BIC) was calculated for each model and each unit (see Section A.6.3). Model selection proceeded by choosing the model with the lowest BIC. The BIC was chosen over other similar measures such as the Akaike Information Criterion or likelihood ratio, as the BIC penalizes the number of parameters more heavily and is thus more conservative. The number of units that had minimum BIC for each of the models is shown in Figure 6.31 for both the pre- and post-learning sessions.

Model selection results were different for the different subjects. For Monkey R, in both the pre- and post-learning sessions, the majority of units were best fit by models which

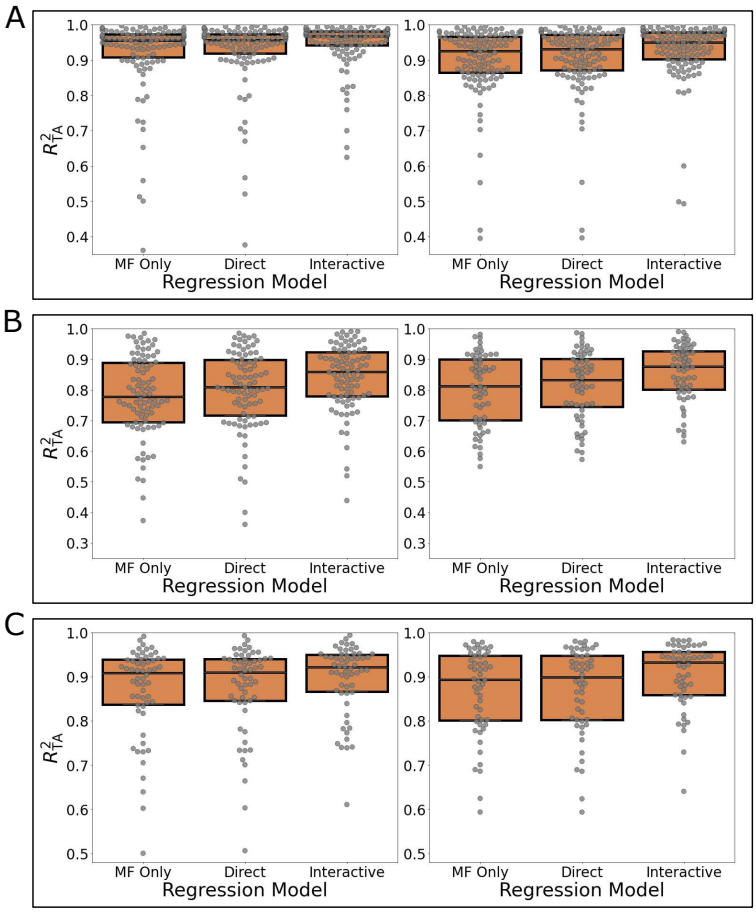

Figure 6.30: R^2_{TA} **values for the MF Only, Direct, and Interactive models in the pre- and post-learning sessions of the Use Affordance Experiment.** A: Monkey R. B: Monkey I. C: Monkey T. Left-hand plots: pre-learning session. Right-hand plots: post-learning session. Gray circles: individual unit R^2_{TA} values. Boxplots denote the median and interquartile range.

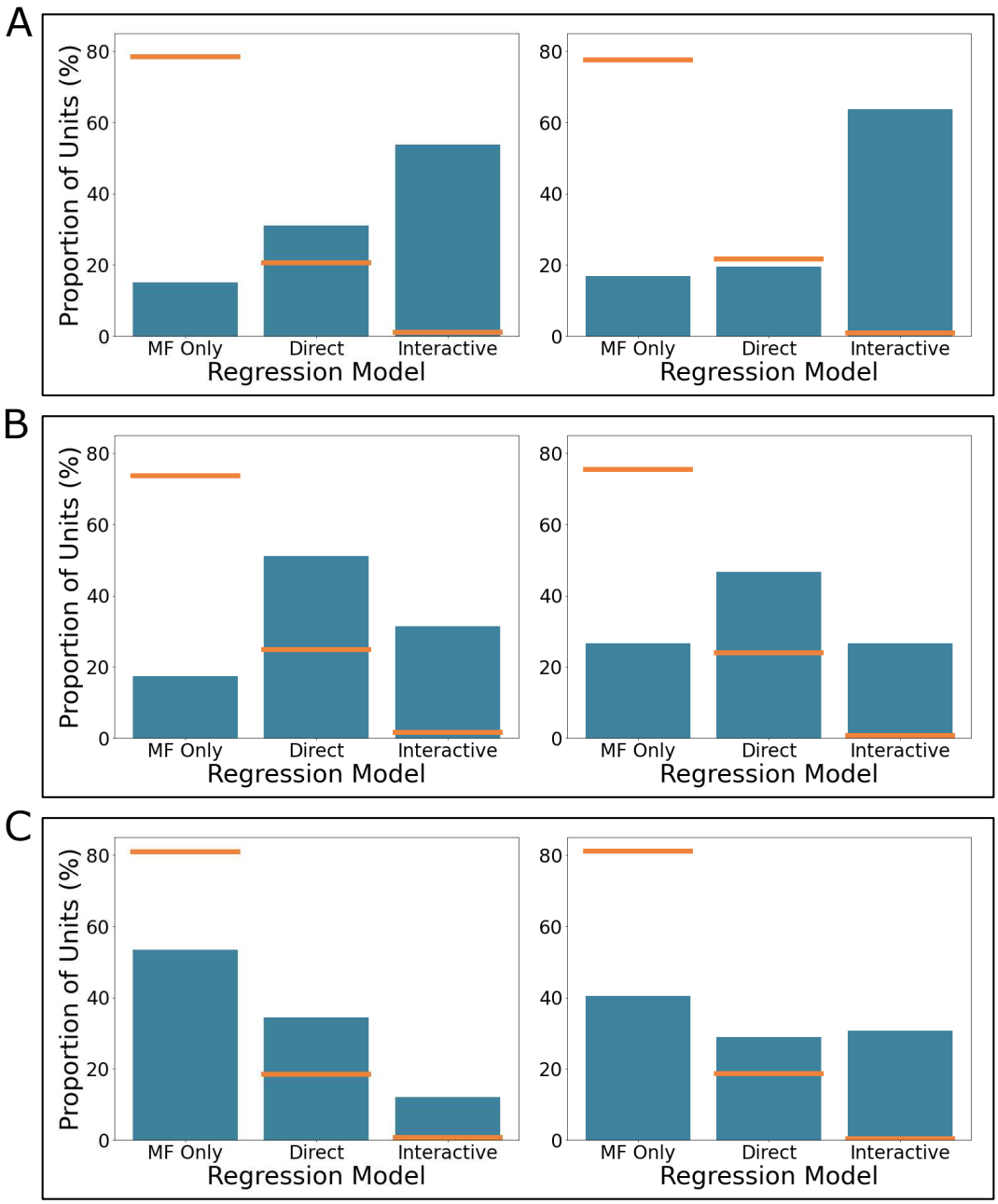

Figure 6.31: **The proportion of units for which each model was the best, according to BIC for the pre- and post-learning sessions of the Use Affordance Experiment.** The model for which BIC was minimal was selected as the best model for each unit. A: Monkey R. B: Monkey I. C: Monkey T. Left-hand plots: pre-learning session. Right-hand plots: post-learning session. Orange lines: chance levels of selecting each model, generated by shuffling object context labels 100 times.

included contextual information, with Interactive encoding predominant over Direct encoding. Interactive object context encoding was even more prominent in the post-learning session compared to Direct object context encoding.

For Monkey I, in both the pre- and post-learning sessions, the majority of units were best fit by models which included contextual information, with direct object context encoding predominant over interactive object context encoding. A greater percentage of units were better fit by models without contextual information in the post-learning period compared to the pre-learning period.

For Monkey T, in the pre-learning session, the majority of units were best fit by models without contextual information, whereas in the post-learning session, the majority of units were best fit by models with contextual information. In the pre-learning session, direct object context encoding was more prevalent compared to interactive object context encoding. In the post-learning session, the number of units displaying interactive object context encoding increased relative to the pre-learning session.

As in Sections 4.5 and 5.5, baseline chance levels of model selection for each type were estimated by refitting models on datasets with object labels shuffled across trials (Figure 6.31 orange lines). For all subjects, MF Only models were selected at lower rates than expected by chance, and Interactive models were selected at higher rates than expected by chance in both sessions.

In the pre-learning sessions, models which featured Direct or Indirect encoding of grip affordance factors were selected for 84.9, 82.6 and 46.6% of units for Monkey R, Monkey I and Monkey T respectively (chance levels: 27.4, 26.4 and 19.1%). Models which featured Interactive grip affordance encoding were selected for 53.8, 31.4 and 12.1% of units for Monkey R, Monkey I and Monkey T respectively (chance levels: 1.1, 1.6 and 0.7%).

In the post-learning sessions, models which featured Direct or Indirect encoding of grip affordance factors were selected for 83.2, 73.3 and 59.6% of units for Monkey R, Monkey I and Monkey T respectively (chance levels: 22.4, 24.7 and 18.9%). Models which featured Interactive grip affordance encoding were selected for 63.7, 26.7 and 30.8% of units for Monkey R, Monkey I and Monkey T respectively (chance levels: 0.9, 0.6 and 0.3%).

The selection of models with Interactive grip affordance encoding suggests that units changed their relations to MFs when the different objects were grasped. To assess the size of these effects, the angular distance between tuning coefficient vectors Θ were calculated as in Equation 4.25 in Section 4.5 only for units which preferred Interactive grip affordance encoding models. This resulted in average angular distances of 9.5, 16.4 and 6.3 degrees for Monkey R, Monkey I and Monkey T respectively in the pre-learning session and 10.8, 13.3 and 9.9 degrees for Monkey R, Monkey I and Monkey T respectively in the post-learning session. These relatively small Θ values suggest that any color or use affordance context related MF tuning coefficient changes were very small in magnitude.

These model fitting results suggest that object context encoding was present in many more individual units than were identified by the extralinear modulation analyses of Section 6.5 in both the pre- and post-learning sessions. The context encoding was often interactive with MF encoding, especially for Monkey R. The number of units with Interactive context encoding increased from the pre-learning session to the post-learning session for Monkey R and Monkey T, but decreased for Monkey I. The broad disparity between the results for the model fitting analyses and the extralinear modulation analyses, which were likely more conservative, suggest that object context encoding beyond encoding of MF differences was present in many individual units, but at a very low level. Interactive object context encoding should negatively impact across-context MF decoding, but the small size of these effects suggest that this impact may be small. The next section directly addresses the performance of MF decoders in the different object contexts.

6.6 Impact of Object Context on MF Decoding

Successful implementation of an upper limb motor neuroprosthesis requires consistent decoding across different contexts. A neuroprosthetic MF decoder must be able to decode intended grasping movements made on objects that were not used for training the decoder. One way that these objects could differ is in their learned use affordances, or in aspects not related to motor performance, such as color. In this section, various decoders were built to

determine the impact of object context encoding in M1 on MF decoding from M1 across different object contexts (objects with different colors or different learned use affordances). For these analyses, as in Sections 6.4 and 6.5, the Power Lift trials were excluded from analysis.

As in Sections 4.6 and 5.6, decoders were built to approximate the approach used in the recent upper limb neuroprosthetic studies of Wodlinger et al and Clanton [119, 437]. The decoding framework is defined in Equation 4.26 in Section 4.6. Details of decoder fitting and cross-validation are provided in Section A.6.5. First, decoders were built and tested on all data from the Use Affordance Experiment to decode each normalized MF independently. These decoders were evaluated using 10-fold cross-validation, with RMSE as the goodness of fit measure.

In both the pre- and post-learning sessions, the performance of the full decoders were qualitatively similar to those presented in Sections 4.6 and 5.6; the proximal kinematics were decoded more accurately than distal kinematics, Joint angles and hand positions were decoded more accurately than joint angular velocities and hand velocities, and EMGs were decoded at a level intermediate between joint angles and joint angular velocities.

To test the effect of context encoding on across-context decoding, three different data partitions were used for training separate decoders:

1. The "All Data" decoder, trained on data from all conditions.
2. The "Object 1" decoder, trained on data from Power Hold trials and Pinch Hold trials executed on Object 1
3. The "Object 2" decoder, trained on data from Power Hold trials and Pinch Hold trials executed on Object 2

Decoders were constructed and tested separately for the pre- and post-learning sessions. Each decoder was tested by decoding data for either Object 1 or Object 2. Thus, decoding was performed with the full data decoder, within-contexts, or across contexts. For example, training a decoder on Object 1 data and testing on Object 1 data represented a case of within-context decoding. Training a decoder on Object 1 data and testing on Object 2 data

represented a case of across-context decoding. All decoders were fit and evaluated using 10-fold cross-validation. The resulting decoding RMSEs are presented in Figure 6.32 for the pre-learning session, and in Figure 6.33 for the post-learning session.

For all subjects, in both the pre- and post-learning sessions, decoding across contexts resulted in only a small increase in RMSE (decrease in performance) compared to decoding within contexts. Decoding with full data decoders resulted in performance similar to that observed for the within-context decoders.

To measure the impact of decoding across contexts or using full data decoders compared to within-context decoders, the percent change in RMSE was calculated for across-context and full data decoders compared to the within-context decoder values. These percentage RMSE increases, averaged across all MFs, are presented in Table 6.5

As seen by the overall percent RMSE increases, only modest performance decreases were observed for across-context decoders vs. within-context decoders. For Monkey R and Monkey T, across-context decoder performance decreases were larger in the post-learning session, though only by a very small amount. For all subjects, decoding using the full data decoders resulted in negligible performance decreases. Thus, grasping objects that differ in color or in learned use affordance presents only a minor challenge for decoders when the grasped objects were not in the training set, but decoding performance can be recovered by including all of the different objects in the training datastet.

Thus far, object context encoding in M1 related to differences in object color and learned use affordances has been shown to be consistent but small in magnitude, with only minor impact on decoding performance. In the next section, the information content of the use affordance encoding signal is examined in terms of the relation of the use affordance signal to the activity observed on trials when the object was actually lifted.

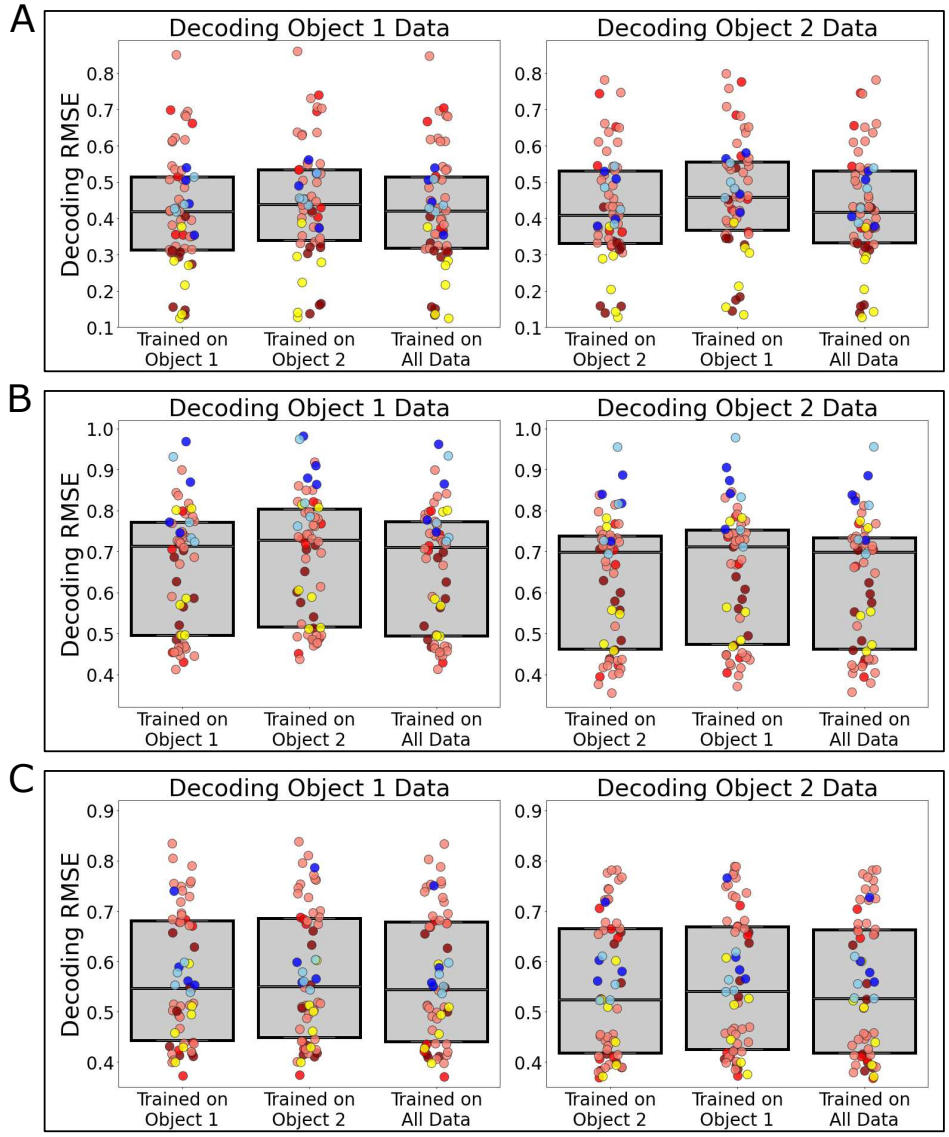

Figure 6.32: **Decoder performance in terms of RMSE when decoding within and across contexts for the pre-learning session of the Use Affordance Experiment.** A: Monkey R. B: Monkey I. C: Monkey T. Box plots represent the median and interquartile range for all decoded MFs. Colored circles reach represent the RMSE for a single decoded MF. Red circles: joint angles and joint angular velocities. Yellow circles: hand positions and hand velocities. Blue circles: EMG. Lighter colors indicate distal MFs, darker colors are proximal MFs.

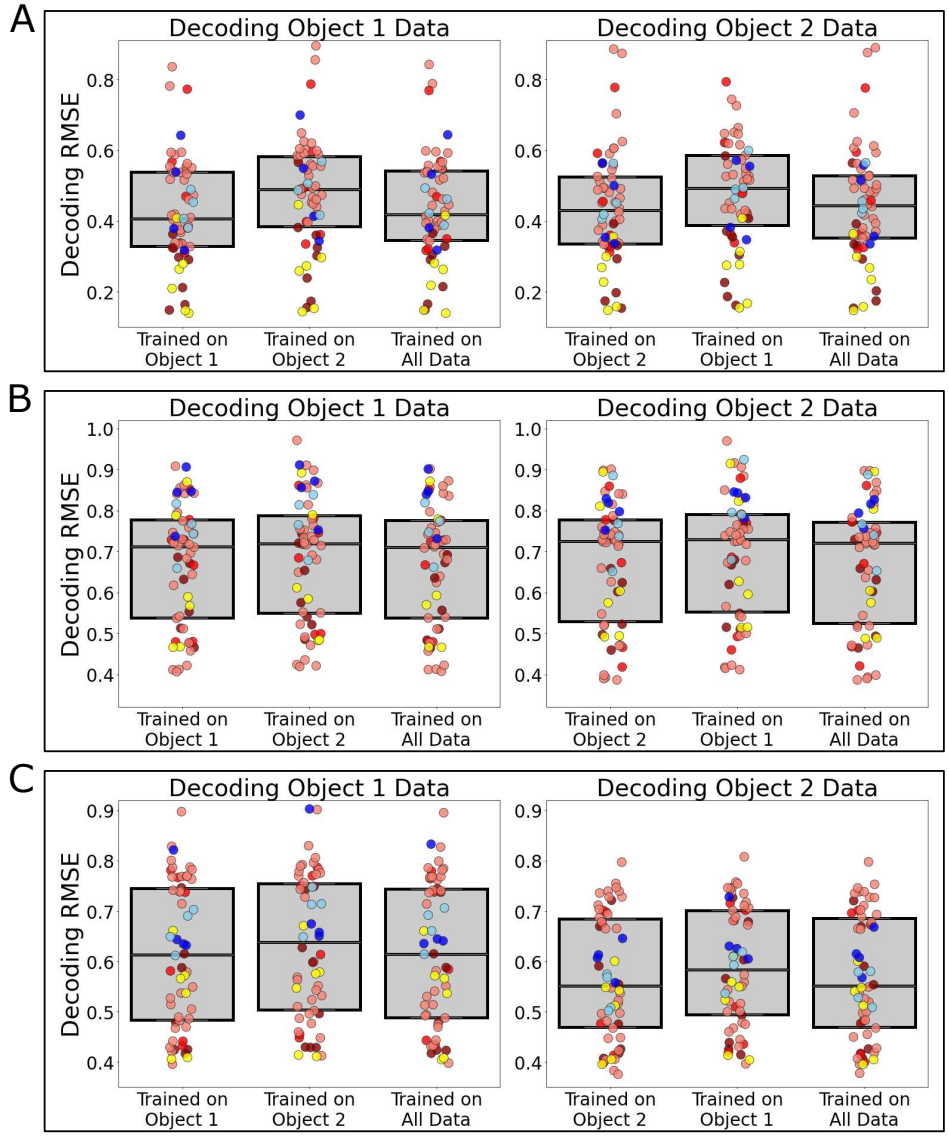

Figure 6.33: **Decoder performance in terms of RMSE when decoding within and across contexts for the post-learning session of the Use Affordance Experiment.** A: Monkey R. B: Monkey I. C: Monkey T. Box plots represent the median and interquartile range for all decoded MFs. Colored circles reach represent the RMSE for a single decoded MF. Red circles: joint angles and joint angular velocities. Yellow circles: hand positions and hand velocities. Blue circles: EMG. Lighter colors indicate distal MFs, darker colors are proximal MFs.

Table 6.5: **Percent increase in RMSE for across-context and full data decoders, compared to within-context decoders.**

		Pre-learning Session		**Post-learning Session**	
Subject	**Area**	**Across-context**	**Full Data**	**Across-context**	**Full Data**
Monkey R	M1	7.7%	0.6%	12.2%	1.7%
Monkey I	M1	3.2%	-0.2%	3.2%	0.0%
Monkey T	M1 Right	1.1%	-0.2%	3.5%	0.4%

6.7 Relation of Use Affordance and Use Action Encoding

The previous sections have focused on assessing the magnitudes of the differences in behavior and neural activity during similar grasps on objects with different learned use affordances, and on what portion of the neural differences may reflect encoding of MF differences or contextual encoding of the learned use affordance. In this section, the relation of use affordance related differences and the encoding of the use action itself is examined in more detail. Specifically, we ask if the behavior and neural activity when grasping to hold the object with the learned lifting affordance was biased toward the behavior and neural activity observed when that object was subsequently lifted, relative to the behavior and neural activity observed when the mechanically fixed object was grasped and held. Only data from the post-learning session are considered in this section.

Human behavioral studies have found that objects are grasped differently when they have a known use. A study by Creem in 2001 [432] found that humans spontaneously grasped tools in the way that corresponds to their known use (by the handle), even when no explicit grasp instruction was given and when such a grasp resulted in an uncomfortable arm posture. In this section, we seek evidence of similar use-knowledge related changes in both grasp behavior and neural activity.

The analyses of Sections 6.2 and 6.3 showed that significant differences were observed in behavior and neural activity in M1 for grasps made on an object with no learned use affordance grasps made on the object with the learned use affordance of lifting. Here, we ask if these differences reflect a biasing of grasp behavior and neural activity toward behavior and neural activity observed on trials when the movable object was actually lifted.

Three potential "affordance bias" scenarios are considered.

The first, "pro-affordance bias," describes the scenario in which Power Hold, Object 2 behavior and neural activity is biased toward Power Lift, Object 2 behavior and neural activity relative to Power Hold, Object 1 behavior and neural neural activity. Such pro-affordance bias could reflect "automatic activation" of preparatory activity related to the lifting action. The second affordance bias scenario considered was that of "anti-affordance bias." In that case, Power Hold, Object 2 behavior and neural activity would be biased away

from Power Lift, Object 2 neural activity relative to Power Hold, Object 1 neural activity. This could result from "suppression" of preparatory neural activity related to the unused lifting movement. The final affordance bias scenario considered was that of "no affordance bias." In that case, neural and behavioral differences would be unrelated to the learned lifting action. These affordance biases were only considered for Power Grasps made on the two objects, as that was the only grasp used for lifting Object 2.

To characterize these biases in neural activity, the affordance shifts S^{mMFPC} and S^{mFRPC} were calculated in the 99% mMF PC and mFR PC spaces, according to Equations 6.4 and 6.5.

$$S_t^{\text{mMFPC}} = \frac{(M_{\text{PowerLift,O2},t} - M_{\text{PowerHold,O1},t}) \cdot (M_{\text{PowerHold,O2},t} - M_{\text{PowerHold,O1},t})}{\|M_{\text{PowerLift,O2},t} - M_{\text{PowerHold,O1},t}\|^2} \tag{6.4}$$

$$S_t^{\text{mFRPC}} = \frac{(F_{\text{PowerLift,O2},t} - F_{\text{PowerHold,O1},t}) \cdot (F_{\text{PowerHold,O2},t} - F_{\text{PowerHold,O1},t})}{\|F_{\text{PowerLift,O2},t} - F_{\text{PowerHold,O1},t}\|^2} \tag{6.5}$$

where $M_{i,t}$ is the vector of mMF PC scores for condition i at time t, $F_{i,t}$ is the vector of mFR PC scores for condition i at time t, O1 denotes Object 1 and O2 denotes Object 2.

In addition, affordance shifts were calculated in null space neural activity, the component of neural activity that could not be linearly combined to decode mMF PC scores. The null space affordance shift was calculated according to Equation 6.6.

$$S_t^{\text{mFRPC}} = \frac{\left(\hat{F}^{\text{null}}_{\text{PowerLift,O2},t} - \hat{F}^{\text{null}}_{\text{PowerHold,O1},t}\right) \cdot \left(\hat{F}^{\text{null}}_{\text{PowerHold,O2},t} - \hat{F}^{\text{null}}_{\text{PowerHold,O1},t}\right)}{\|\hat{F}^{\text{null}}_{\text{PowerLift,O2},t} - \hat{F}^{\text{null}}_{\text{PowerHold,O1},t}\|^2} \tag{6.6}$$

where $\hat{F}^{\text{null}}_{i,t}$ is the vector of null space neural activity for condition i at time t, as calculated in Equation 4.15.

The potential affordance bias scenarios are depicted schematically in Figure 6.34.

The affordance shifts calculated in mMF PC space, mFR PC space and null space neural activity are portrayed in Figures 6.35, 6.36 and 6.37.

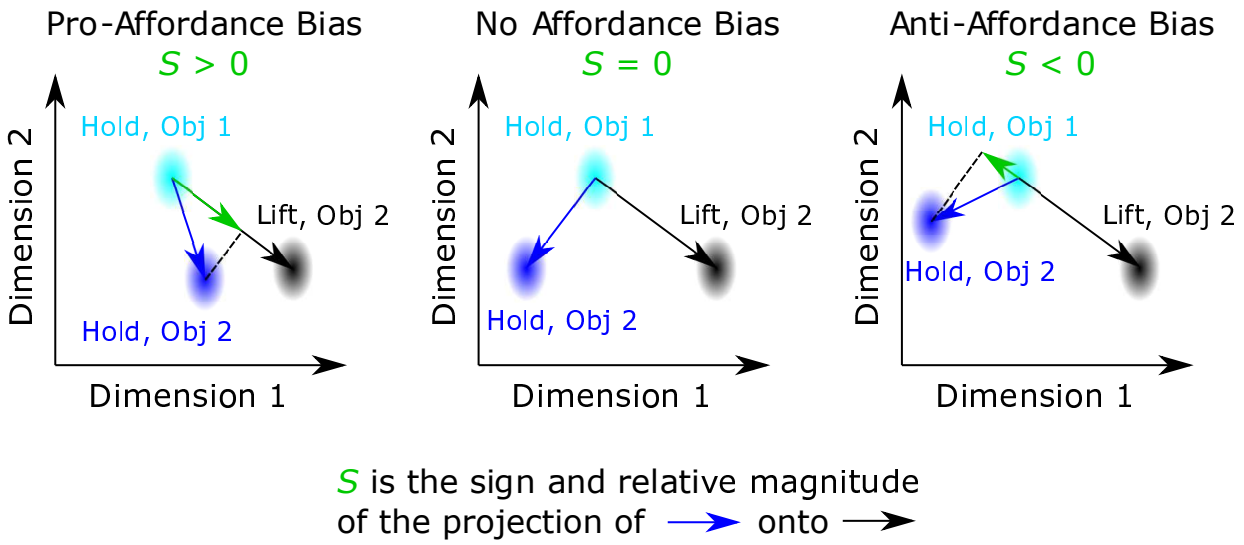

Figure 6.34: **Schematic illustration of three potential forms of use affordance bias.** Ellipses represent distributions of behavior or neural activity for different conditions. Light blue ellipse: Power Hold, Object 1. Blue ellipse: Power Hold, Object 2. Black ellipse: Power Lift, Object 2. Blue vector: vector between Power Hold, Object 1 and Power Hold, Object 2. Black vector: vector between Power Hold, Object 1 and Power Lift, Object 2. Green vector: the projection of the blue vector onto the black vector. The affordance shift is the magnitude of the green vector divided by the magnitude of the black vector, with the sign positive when the green and black vector are aligned, and negative when the green and black vector are opposed. Dimensions could correspond to mMF PC scores for S^{mMFPC}, mFR PC scores for S^{mFRPC} and null space neural dimensions for S^{null}. The diagram shows affordance bias scenarios relative to the learned use affordance at a single time point.

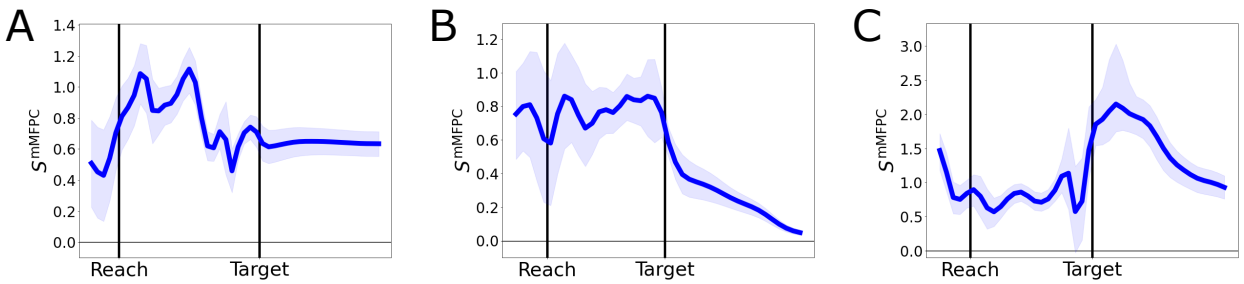

Figure 6.35: **Affordance shifts S^{mMFPC} for the Use Affordance Experiment.** Affordance shifts calculated in the 99% mMF PC space. A: Monkey R. B: Monkey I. C: Monkey T right hemisphere. Shaded 95% confidence intervals are bootstrap intervals, trials resampled 10000 times.

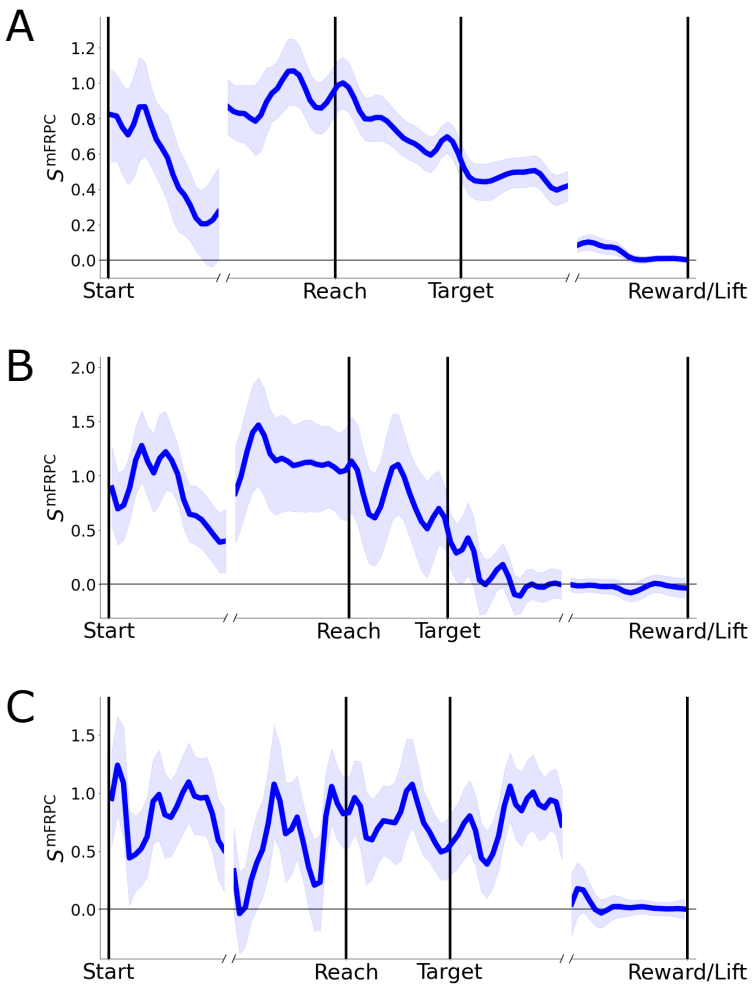

Figure 6.36: **Affordance shifts S^{mFRPC} for the Use Affordance Experiment.** Affordance shifts calculated in the 99% mFR PC space. A: Monkey R. B: Monkey I. C: Monkey T right hemisphere. Shaded 95% confidence intervals are bootstrap intervals, trials resampled 10000 times.

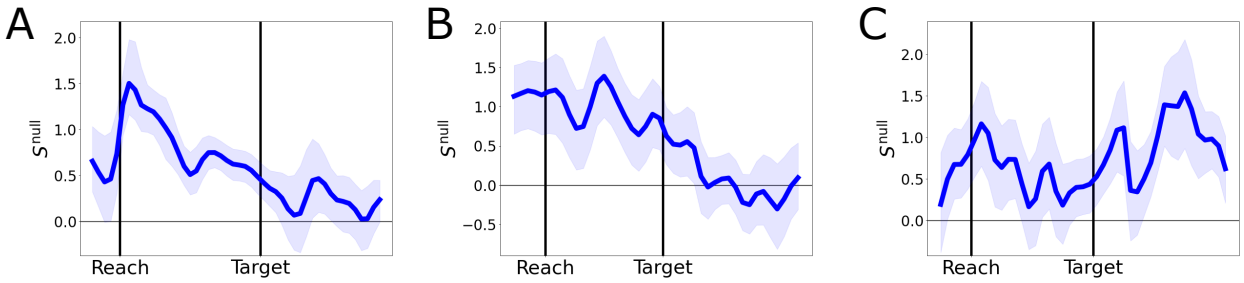

Figure 6.37: **Affordance shifts S^{null} for the Use Affordance Experiment.** Affordance shifts calculated in the null space neural activity. A: Monkey R. B: Monkey I. C: Monkey T right hemisphere. Shaded 95% confidence intervals are bootstrap intervals, trials resampled 10000 times.

Large positive S^{mMFPC} values were observed throughout the movement periods, indicating that behavior for Power Hold trials on Object 2 was similar to behavior observed during Power Lift trials on Object 2 for all subjects. That is, the grasping behavior used to grasp and hold the movable object was similar to the grasp behavior used to actually lift it. This affordance shift rapidly declined after target contact for Monkey I, reflecting the fact that Monkey I had a shorter hold period for Power Lift trials.

Large positive S^{mFRPC} values were observed starting at the earliest portions of the preparatory periods and throughout movement for all subjects. This indicates that, although the magnitude of neural separation for Power Hold, Object 1 and Power Hold, Object 2 was very small at the start of trials (see Figure 6.19), this separation already reflected the learned use affordance of the movable object. The affordance shift values decreased about 100 ms after the cue presentation in all subjects, perhaps reflecting processing of the cue information as to whether the trial would entail a lift action or not, as all Object 2 trials were presented in the same block (see Section 3.2.1). The mFR PC affordance shifts were near zero during the late hold period, as at this time, neural activity diverged for Power Lift trials in preparation for the lifting action.

Finally, positive S^{null} values were observed for all subjects for the early movement period. This indicates that the neural activity that was not directly linearly related to mMF PC scores was also biased toward Power Lift, Object 2 neural activity for Power Hold, Object 2 trials. This positive shift decreased after target contact for Monkey R and Monkey I, but remained positive for Monkey T right hemisphere.

The occurrence of pro-affordance bias in mMF PC scores, mFR PC scores and null space neural activity support but do not definitively confirm the hypothesis that the motor representation of the use action afforded by Object 2 was automatically activated in the presence of the object, even when it was not lifted. These results are discussed further in Section 8.

In summary, the results presented in this chapter suggest that object context encoding related to object color differences and object learned use affordance differences was present in M1, but was small in magnitude. Subjects grasped two objects that differed only by color in the pre-learning session, and by color and learned use affordances in the post-

learning session. Subjects exhibited very similar MFs when executing the same grasps on the two objects, though small but consistent and significant differences were observed between these same-grasp conditions (Section 6.2). Same-grasp conditions were separable in neural activity, with transient separations in individual FRs and consistent, moderate separations in neural populations. The separations between same-grasp conditions were proportionally larger in FRs than in MFs (Section 6.3). The neural population modulation due to same-grasp conditions was mostly explained by linear tuning to MFs, and as such, evidence for explicit encoding of object context in M1 population activity was weak and inconsistent between subjects (Section 6.4). Object context was frequently encoded both directly in FRs and in an interactive fashion with MF encoding in individual neurons, though again the size of this effect was small (Section 6.5). The object context encoding signal had only a minor impact on MF decoding when decoding grasps across object contexts, which could be compensated for by including grasps on both objects in the decoder training set (Section 6.6). Finally, the object use affordance related behavioral and neural differences manifested as a biasing of Power Hold, Object 2 behavior and neural activity toward Power Lift, Object 2 neural activity relative to Power Hold, Object 1 neural activity. This was consistent with partial automatic activation of the preparatory neural activity associated with the lifting action.

7.0 Results — Object Context Encoding in PMV and AIP

The results in Chapters 4, 5 and 6 reveal the presence of object context encoding in primary motor cortex (M1), in that neural activity in M1 differed for very similar behaviors made in different object contexts. This object context encoding was relatively small during reach-to-grasp actions (Chapters 5 and 6) and relatively large during reaches with or without a graspable object present (Chapter 4). As this object context encoding was not directly related to movements or muscle activity, its presence in M1 was unexpected. Thus, a natural question arises: what is the cortical source of object context related information in M1?

M1 receives input from an array of premotor cortical areas [40, 41, 307] (see Section 2.2). One of these premotor areas, the ventral premotor cortex (PMV), is particularly active for grasping and manipulation actions (see Section 2.3). Along with its bi-directional M1 connections, PMV is also strongly interconnected with the anterior intraparietal cortex (AIP), which contains a more visual representation of graspable objects (see Section 2.4). M1, PMV and AIP constitute essential nodes of the "cortical grasp network," as described by Jeannerod [255], which has been theorized to implement a visuomotor transformation which transforms visual information about objects to a grasping movement command (see Section 2.5).

Neural activity in PMV and AIP has been shown to encode object differences based on object shape and grip affordances (see Sections 2.3 and 2.4). Nevertheless, explicit object context encoding remains largely unstudied in these areas. In this section, the encoding of object context is explored as related to object presence or absence, learned or perceived grip affordances, superficial color differences, and learned use affordances. Evidence is also considered as to whether PMV and AIP are the source of object context information in M1.

To explore these questions, neural spiking activity in PMV and AIP was recorded simultaneously with M1 activity in Monkey T. Recording in PMV and AIP was accomplished with floating microelectrode arrays (FMAs, Microprobes for Life Science, Gaithersburg, MD), implanted using a novel electrode planning, alignment and implantation procedure, described in Section A.1.2. PMV and AIP data were collected

from both the left and right hemispheres of Monkey T. A separate implant procedure was performed for each hemisphere. After each implant, neural data were recorded during the 3 experiments previously described: the Object Presence Experiment, the Grip Affordance Experiment, and the Use Affordance Experiment. The tasks were always performed with the hand contralateral to the neural implants. Thus, Monkey T performed all experiments twice; once with the right hand and once with the left hand. The results presented in this section describe neural data obtained during the same sessions as described for Monkey T M1 data in Chapters 4, 5 and 6. Additionally, PMV and AIP data are presented for Monkey T left hemisphere for the Object Presence and Use Affordance Experiment, for which M1 data was not recorded due to a damaged M1 array pedestal.

The analyses presented in this section pertain to neural activity recorded during the Object Presence Experiment, Grip Affordance Experiment and Use Affordance Experiment. The behavioral tasks for each experiment are described in detail in Sections 4.1, 5.1 and 6.1. Due to the lower number of units recorded in PMV and AIP compared to M1, as well as the fact that PMV and AIP units were only recorded in a single subject, the findings presented in this section are preliminary.

The main findings of this chapter are summarized as follows. Units in PMV and AIP were recorded along with M1 units in Monkey T during execution of the Object Presence Experiment, the Grip Affordance Experiment and the Use Affordance Experiment. PMV and AIP unit activity was qualitatively similar to M1 unit activity, though PMV and AIP units had lower FRs, and a higher prevalence of preparatory activity. Modulation for grip type and object context were observed at similar levels in M1, PMV and AIP, though in a few cases, PMV and AIP units displayed extreme modulation for differences in object context. Fitting of linear MF encoding models and MF decoding from population activity revealed that PMV and AIP neural activity was related to MFs at a level comparable to, but somewhat lower than M1. Extralinear modulation analyses revealed object presence encoding and grip affordance encoding in PMV and AIP at levels similar to that observed in M1. PMV was found to preferentially encode object context for Power Grasp, Object 1 vs. Power Grasp, Object 2 in the Use Affordance Experiment post-learning session, suggesting a special role for PMV in storing and processing learned use affordance information. One

PMV area and both AIP areas also strongly encoded object presence during the preparatory period. The timecourses of grip type, object presence and grip affordance related modulation suggest that these factors may be encoded sequentially in AIP, PMV and M1 in a feedforward manner. Finally, affordance shifts related to object presence and learned use affordance were observed in PMV and AIP that were similar to those observed in M1, suggesting that the representations of actions afforded by an object may be automatically activated in these areas.

Section 7.1 contains descriptions of individual unit FRs in PMV and AIP units, as well as population PMV and AIP activity patterns. Section 7.2 discusses the relation of PMV and AIP to MFs, with comparisons to M1. Section 7.3 presents evidence for object context encoding in PMV and AIP based on extralinear modulation, and also describes preparatory activity in PMV and AIP related to object context differences. In Section 7.4, the timecourses of modulation due to movement-related or contextual factors are compared in M1, PMV and AIP. Section 7.5 concerns the affordance related biases in neural activity of PMV and AIP observed in the three experiments.

7.1 Single Unit and Population Activity in PMV and AIP

Single units and multi-units were successfully recorded from both left and right hemisphere PMV and AIP in Monkey T. Two 32-channel FMAs were implanted in each area. For M1 recordings, a single 96-channel Utah Array (Blackrock Microsystems, Salt Lake City, UT) was implanted in each hemisphere. Details of the implantation methods are presented in Section A.1. Given the lower number of electrodes, cortical morphology and relative paucity of large pyramidal neurons in PMV and AIP, fewer units were recorded and analyzed from PMV and AIP compared to M1. The number of units recorded in each area for each experiment and each subject is displayed in Table 7.1. In several cases, unit yields were impacted by array mechanical failures (see Section A.1.2.7 for details).

Table 7.1: **Unit yields in all brain areas for each subject in the Object Presence Experiment, Grip Affordance Experiment and Use Affordance Experiment.** OPE: Object Presence Experiment. GAE: Grip Affordance Experiment. UAE Pre: Use Affordance Experiment, pre-learning session. UAE Post: Use Affordance Experiment, post-learning session. Asterisks denote implants for which some mechanical array failure occurred, limiting unit yields (see Section A.1.2.7). Blank cells indicate sessions for which neural data were not recorded.

			Number of Units Analyzed			
Subject	**Area**	**Arrays**	**OPE**	**GAE**	**UAE Pre**	**UAE Post**
Monkey R	M1	2x Utah	124	108	106	113
Monkey I	M1	1x Utah		97	86	60
Monkey T	M1 Left	1x Utah*		31		
Monkey T	M1 Right	1x Utah	57	57	58	52
Monkey T	PMV Left	2x FMA*	10	16	12	7
Monkey T	PMV Right	2x FMA	28	30	38	35
Monkey T	AIP Left	2x FMA*	10	21	16	1
Monkey T	AIP Right	2x FMA*	15	9	5	19

In general, PMV and AIP individual unit responses, although qualitatively similar to M1 unit responses, differed in several ways. PMV and AIP units tended to have lower FRs than M1 units. The distributions of mean firing rates for the 3 cortical areas are shown in Figure 7.1.

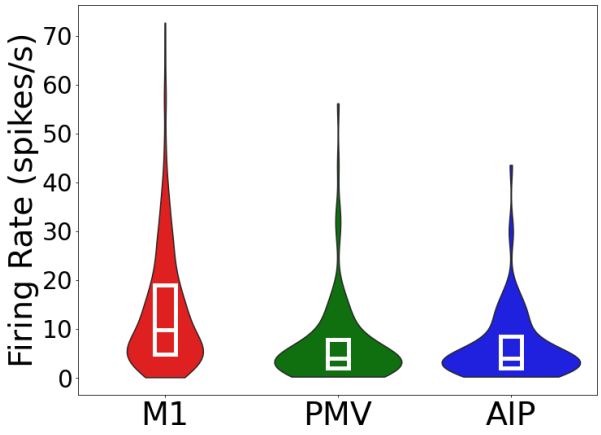

Figure 7.1: **Mean FR distributions for M1, PMV and AIP units across all experiments and subjects.** Red: M1. Green: PMV. Blue: AIP. Violin plots display frequency distribution of mean FRs. Box plots (white) depict medians and interquartile ranges.

Individual unit FRs in PMV and AIP were qualitatively similar to FRs of M1 units in that they were modulated over the courses of the reach-to-grasp actions and often displayed different FRs for Power Grips and Pinch Grips in the three experiments. This is consistent with previous research that posits the involvement of PMV and AIP in grasp action selection during movement preparation. Individual PMV and AIP units were often active during the preparatory period, but strong modulation in FRs was observed throughout the movement period as well, often coincident with grasp onset. The FR profiles of several examples of PMV and AIP units that were significantly modulated for Power Grasps vs. Pinch Grasps are displayed in Figure 7.2.

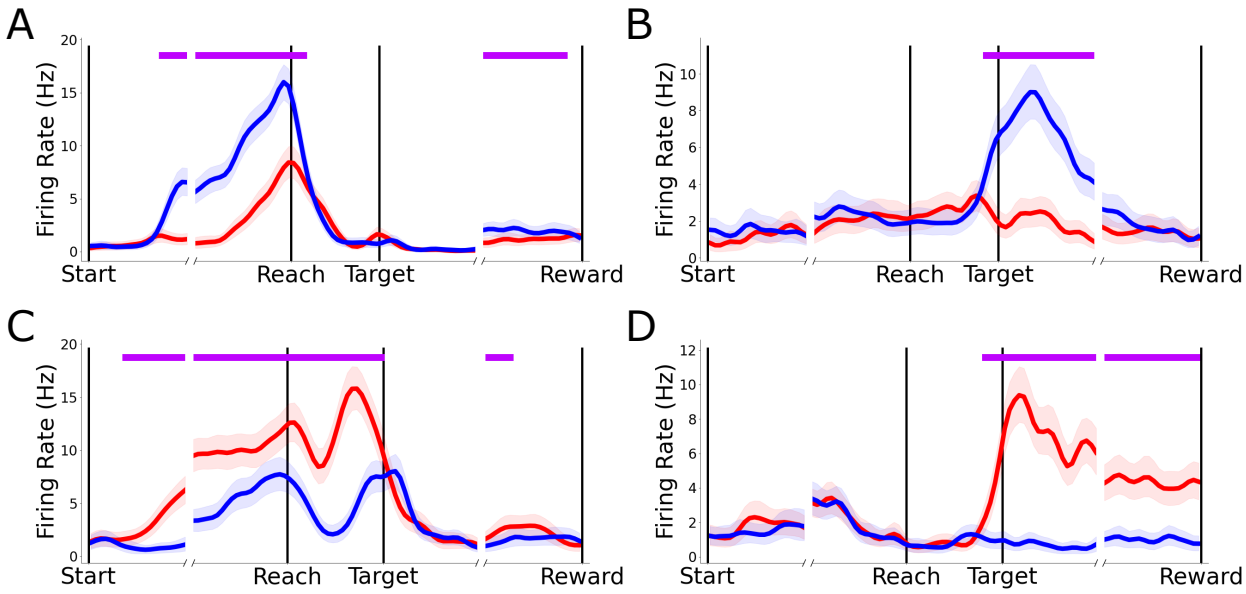

Figure 7.2: **Example units from PMV and AIP with significant FR modulation for Power Grasps vs. Pinch Grasps.** A: Monkey T PMV right hemisphere unit 154.2 in the Use Affordance Experiment post-learning session. B: Monkey T PMV left hemisphere unit 118.1 in the Use Affordance Experiment pre-learning session. C: Monkey T AIP left hemisphere unit 186.2 in the Grip Affordance Experiment. D: Monkey T AIP right hemisphere unit 166.1 in the Object Presence Experiment. Blue traces: mean FRs for all Power Grasp trials. Red traces: mean FRs for all Pinch Grasp trials. Purple bars at top denote time points when Power Grasp mean FR was significantly different from Pinch Grasp mean FR, $p < 0.01$, permutation test, labels shuffled 10000 times. Power Grasp and Lift trials were excluded in B, and Object Reach and No-Object Reach trials were excluded in D.

The units in Figure 7.2 illustrate the ubiquity and diversity of grasp-related FR modulation in PMV and AIP units. Figure 7.2 A displays a PMV unit that had preparatory grasp-related FR modulation, with a preference for Power Grasps, and low FRs throughout the late reach and target hold periods. Figure 7.2 C displays an AIP unit with similar preparatory grasp-related FR modulation, but with preference for Pinch Grasps. Figure 7.2 B displays a PMV unit with grasp-related FR modulation coinciding with grasp onset, with a preference for Power Grasps. Figure 7.2 D displays n AIP unit with similar grasp-related FR modulation around grasp onset, but with a preference for Pinch Grasp.

Both preparatory and motor-coincident grasp-related FR modulation patterns were observed in PMV and AIP units, as well as preferences for power or pinch grasps. The units shown in Figure 7.2 exemplify a common pattern in PMV and AIP: for many units, FRs were modulated only during a specific time period, and had very low FRs at other times. However, individual unit responses were diverse in PMV and AIP. Many units were modulated by the task in general, but did not display modulation between different conditions. For other units, grasp-related modulation was not restricted to only the preparatory or grasp phases and spanned across whole trials.

Significant FR modulations for conditions in which the same basic behavior was executed in different object contexts were also frequently observed in PMV and AIP. In a few cases, extreme examples of context-related FR modulation were observed in PMV or AIP units which surpassed any such FR modulation observed in M1 units. For example, the FRs of an AIP unit which displayed strong object-presence dependent modulation in the Object Presence Experiment is displayed in Figure 7.3.

The unit depicted in Figure 7.3 was almost completely quiescent for all conditions in which an object was present, including the Object Reach condition. Conversely, the unit was active and temporally modulated for entire No-Object Reach trials, despite the behavior being very similar for Object Reach trials and No-Object Reach trials. Such stark object-presence related modulation was not present in M1 units or most PMV and AIP units.

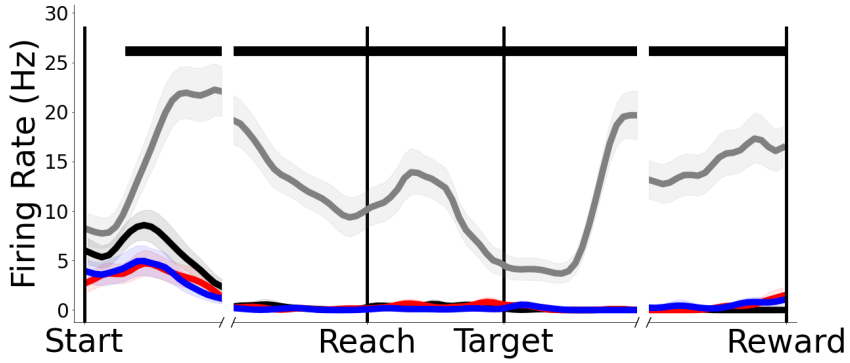

Figure 7.3: **Example AIP unit with strong object-presence dependent FR modulation in the Object Presence Experiment.** Monkey T AIP left hemisphere unit 169.1. Blue trace: Power Grasp. Red trace: Pinch Grasp. Black trace: Object Reach. Gray trace: No-Object Reach. Black bar: mean FRs significantly different between Object Reach and No-Object Reach ($p < 0.01$, permutation test, labels shuffled 10000 times).

The FRs of a PMV unit and an AIP unit which displayed strong within-grasp modulation in the Grip Affordance Experiment are displayed in Figure 7.4.

Figure 7.4 A displays a PMV unit with context-related FR modulation in the preparatory and reach periods. During grasp cue presentation, a burst of activity was observed for only the Compound Multigrasp Object and the Compound Pinch Object. During the reach period, a relatively large increase in FRs was observed for Pinch Grasps executed on compound objects, while the FR for Pinch Grasps on the Simple Pinch Object remained close to 0. Figure 7.4 B depicts a unit which displayed significantly different FR trajectories for Pinch Grasps on the Simple Pinch Object and Pinch Grasps on the compound objects throughout the entire timecourse of the trial. This unit was almost entirely quiescent during Power Grasp trials. These units represent the most extreme cases of within-grasp modulation observed in the Grip Affordance Experiment. In the majority of M1 units which displayed object-related within-grasp FR modulation, this modulation typically manifested as transient, small differences in FRs without changing the overall shape of the FR timecourse (Figure 5.10). However, for the units depicted in Figure 7.4, different objects induced large changes in FR patterns.

The FRs of 2 PMV units which displayed strong within-rasp modulation in the post-learning session of the Use Affordance Experiment are displayed in Figure 7.5.

The PMV unit in Figure 7.5 A displayed lower FRs for all grasps on Object 2 (dashed traces) compared to grasps on Object 1 (solid traces) during the preparatory period. The unit in Figure 7.5 displayed similar object-related FR modulation, but during the time around grasp onset and target contact. This modulation occurred in the post-learning session of the Use Affordance Experiment, after which the lifting action had been learned, associated with Object 2. Such clear, consistent object-related FR modulation was not observed in M1 or AIP and was rarely observed in other PMV units.

The Venn diagrams in Figure 7.6 illustrate the prevalence of sustained significant modulation for grip type and for object context in all M1, PMV and AIP units. Units were combined across all experiments for which units from each area were recorded. Sustained significant modulation was defined as $>$ 500 ms (25 timepoints) of statistically significant difference in mean FRs between 2 conditions. Units were labeled "Power Grasp vs. Pinch

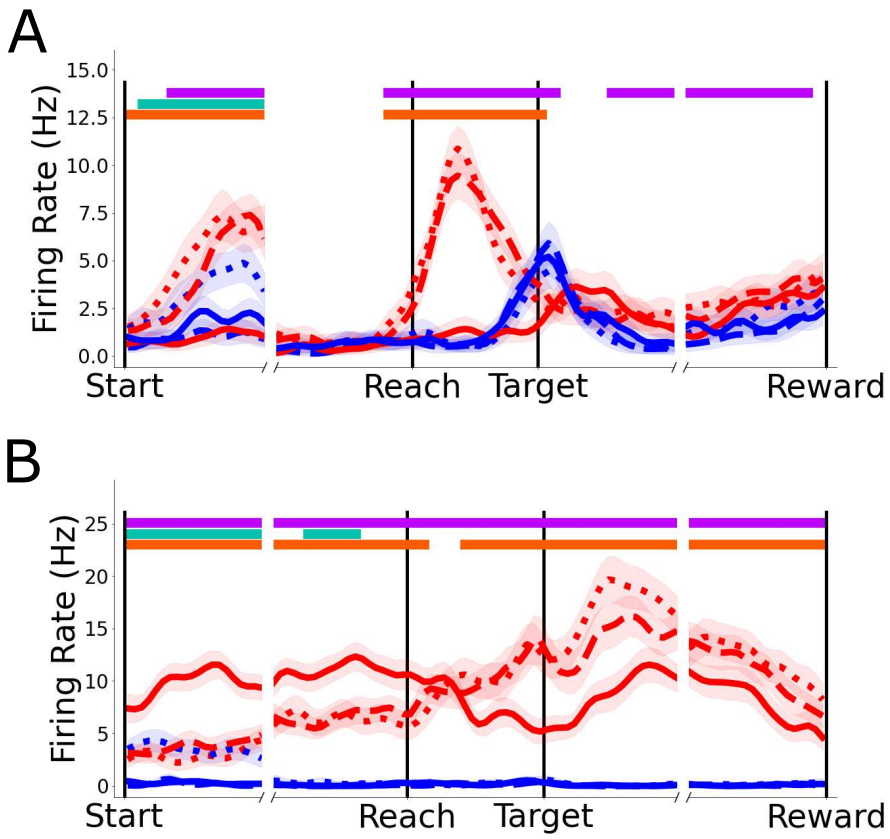

Figure 7.4: **Example PMV and AIP units with strong within-grasp FR modulation in the Grip Affordance Experiment.** A: Monkey T PMV right hemisphere unit 133.1. B: Monkey T AIP left hemisphere 190.1. Blue traces: Power Grasps. Red traces: Pinch Grasps. Solid traces: simple objects. Dashed traces: compound single-grasp objects. Dotted traces: compound multi-grasp object. Purple bars: mean FRs significantly different between any Power Grasp and any Pinch Grasp. Turquoise bars: mean FRs significantly different between any Power Grasps on different objects. Orange bars: mean FRs significantly different between any Pinch Grasps on different objects ($p < 0.01$, permutation tests, labels shuffled 10000 times).

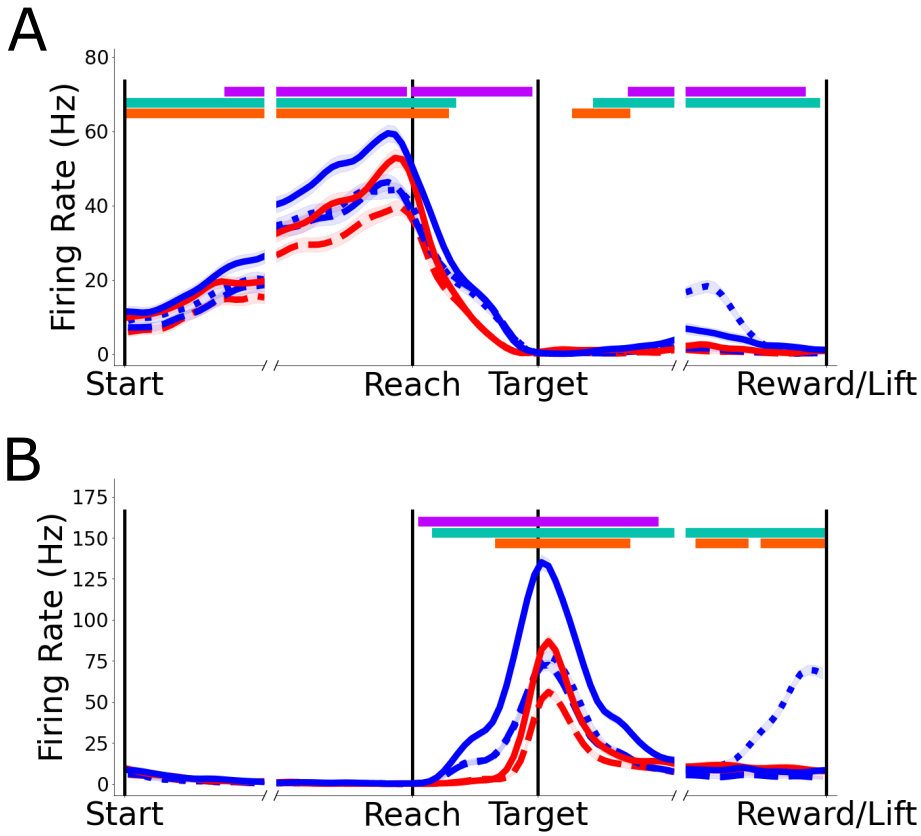

Figure 7.5: **Example PMV units with strong within-grasp FR modulation in the post-learning session of the Use Affordance Experiment.** A: Monkey T PMV right hemisphere unit 125.1. B: Monkey T PMV right hemisphere unit 105.1. Blue traces: Power Grasps. Red traces: Pinch Grasps. Solid traces: grasp and hold trials, Object 1. Dashed traces: grasp and hold trials, Object 2. Dotted blue trace: Power Grasp and Lift trials, Object 2. Purple bars: mean FRs significantly different between any Power Grasp and any Pinch Grasp. Turquoise bars: mean FRs significantly different for Power Grasp and Hold, Object 1 vs. Power Grasp and Hold, Object 2. Orange bars: mean FRs significantly different for Pinch Grasp and Hold, Object 1 vs. Pinch Grasp and Hold, Object 2 ($p < 0.01$, permutation tests, labels shuffled 10000 times).

Grasp" if sustained significant modulation was observed between any Power Grasp vs. Pinch Grasp condition pair. Units were labeled "Same Behavior Different Object Context" if sustained significant modulation was observed between any condition pair in which the same behavior was performed in different object contexts (e.g. Object Reach vs. No-Object Reach in the Object Presence Experiment; Pinch Grasp, Simple Pinch Object vs. Pinch Grasp, Compound Pinch Object in the Grip Affordance Experiment; Power Grasp, Object 1 vs. Power Grasp, Object 2 in the Use Affordance Experiment).

Sustained significant modulation for both grip type and object context was observed in all cortical areas. The great majority of Monkey R M1 units showed sustained significant modulation for one or both of grip type and object context. For the other M1 areas and PMV areas, about half of units showed sustained significant modulation for one or both, and in AIP a lower percentage was observed. Overall, all areas displayed about the same proportion of object context modulation to grip type modulation.

To examine the general timecourses of FRs in PMV and AIP units, the trial-averaged normalized FRs were calculated across all units in each PMV and AIP area, as was done for M1 units in Section 4.3 Figure 4.14. The mean PMV and AIP FR timecourses are displayed in Figure 7.7 for the Object Presence Experiment. Averaged normalized FRs are shown only for the Object Presence Experiment, as this experiment included all of the fundamental behaviors used in all experiments: Power Grasps, Pinch Grasps, and Reaches.

Monkey T PMV left hemisphere and AIP right hemisphere (Figure 7.7 A and D) showed evidence of preparatory and motor-related activity, as FRs were high during the preparatory period and around the time of grasp onset and target hold. For these areas, a general decrease of FRs was observed during the early and mid reach periods. Monkey T PMV right hemisphere and AIP left hemisphere (Figure 7.7 B and C) showed more strictly grasp-related activity, as FRs were low during the preparatory period and early reach, but increased around the time of target contact. Monkey T PMV right hemisphere (Figure 7.7 B) especially had global mean FR patterns very similar to those observed in M1 (Figure 4.14). All areas showed generally higher firing rates for Pinch Grasps vs. Power Grasps, a pattern that was observed in most of the PMV and AIP populations.

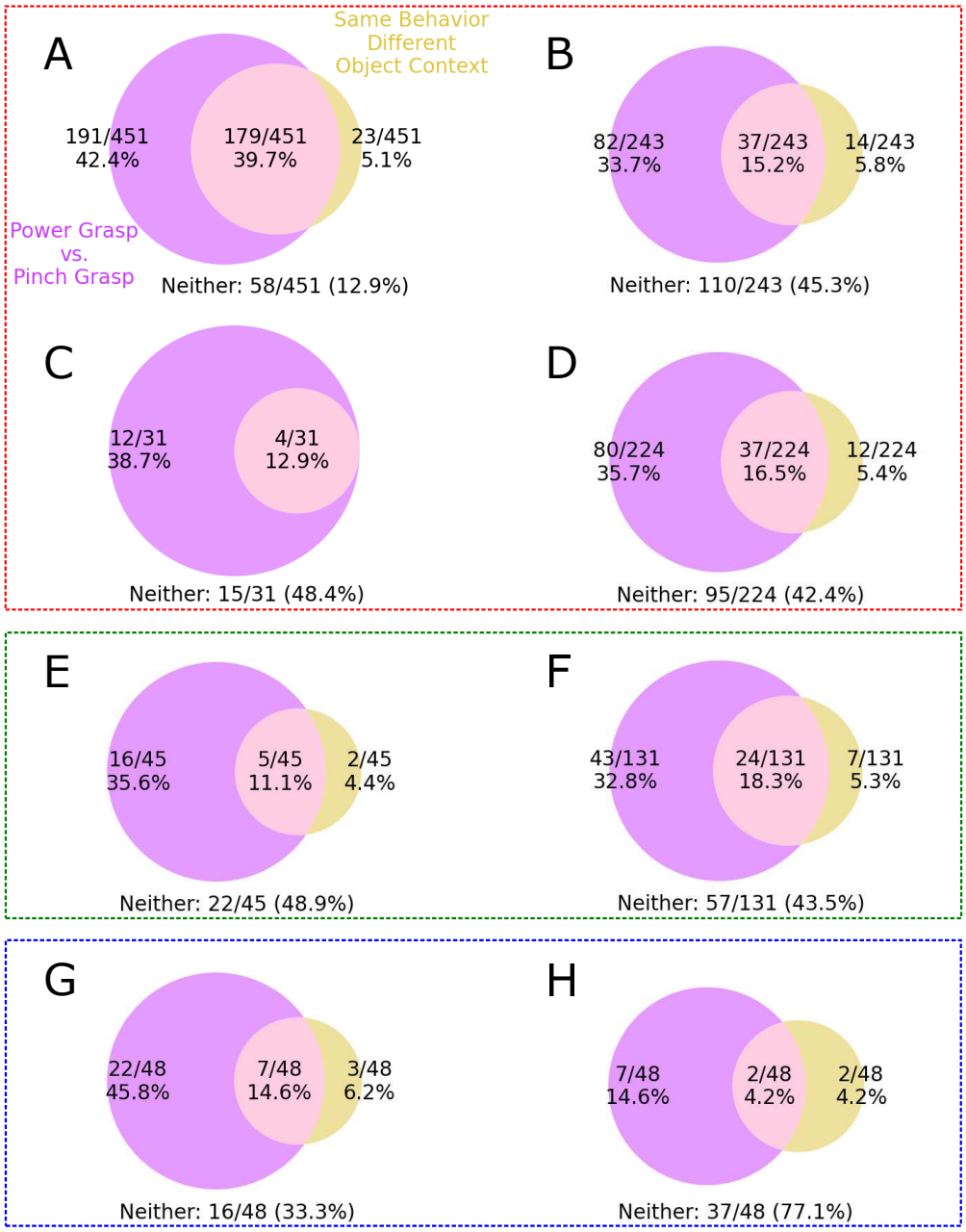

Figure 7.6: **Occurrence of sustained significant modulation for grip type and object context in M1, PMV and AIP.** Red: M1. Green: PMV. Blue: AIP. A: Monkey R M1. B: Monkey I M1. C: Monkey T left hemisphere M1. D: Monkey T right hemisphere M1. E: Monkey T left hemisphere PMV. F: Monkey T right hemisphere PMV. G: Monkey T left hemisphere AIP. H: Monkey T right hemisphere AIP.

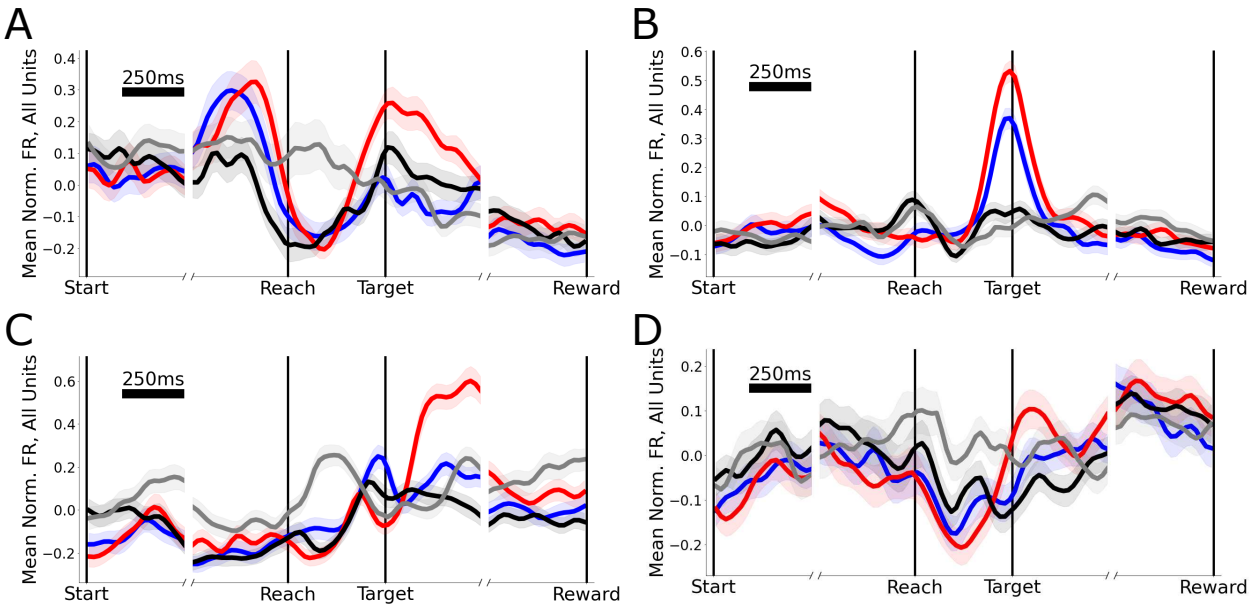

Figure 7.7: **Mean normalized FRs of all PMV and AIP units for the conditions of the Object Presence Experiment.** A: Monkey T PMV left hemisphere. B: Monkey T PMV right hemisphere. C: Monkey T AIP left hemisphere. D: Monkey T AIP right hemisphere. Blue: Power Grasp. Red: Pinch Grasp. Black: Object Reach. Gray: No-Object Reach.

The mean normalized FRs of Figure 7.7 also reveal that PMV and AIP units were active not only for reach-to-grasp conditions, but also for reach-only conditions, even when the object was not present in the workspace (Figure 7.7 gray traces). While PMV and AIP have been primarily studied in the context of grasping, recent studies have identified cortical connectivity between PMV and AIP and other parietal and premotor areas with reach-related activity [290], as well as neural activity related to reaches in PMV and AIP [234].

To examine the prevalence of reaching related activity in PMV and AIP in more detail, the number of units which preferred each of the conditions in the Object Presence Experiment are plotted in Figure 7.8.

Surprisingly, many units in PMV and AIP displayed the highest firing rates for the reach conditions of the Object Presence Experiment. In both AIP areas, the No-Object Reach condition, for which the object was absent, was the single most commonly preferred condition among individual units. This further confirms that PMV and AIP are related not only to grasp but also to reaches made in space with no object present.

The FR patterns observed in PMV and AIP units suggest that these areas may encode both MFs and object context. The relation of PMV and AIP units FRs to MFs is explored in Section 7.2, and the possibility of object context encoding in PMV and AIP is explored in Section 7.3.

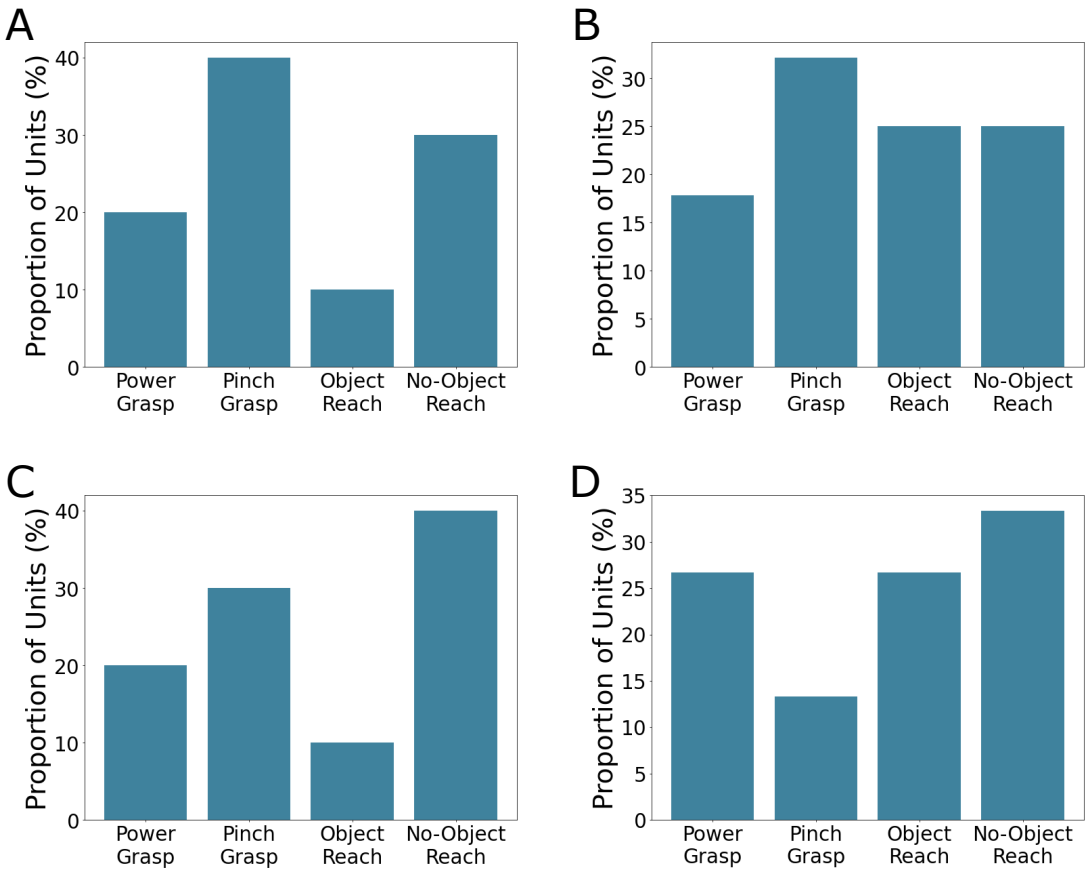

Figure 7.8: **Preferred conditions of individual PMV and AIP units in the Object Presence experiment.** Bars portray the percentage of units which displayed the highest mean peri-movement FRs for each condition. A: Monkey T left hemisphere PMV. B: Monkey T right hemisphere PMV. C: Monkey T left hemisphere AIP. D: Monkey T right hemisphere AIP.

7.2 Relation of PMV and AIP Neural Activity to MFs

Much of the early studies in PMV and AIP focused on the neural responses in these areas during the presentation of and preparation for grasping of different objects (see Sections 2.3 and 2.4). More recent studies have shown that grasp-related hand and finger kinematics can be decoded from PMV and AIP neural activity at levels comparable to decoding from M1 neural activity (e.g. [163]). In this section, the relation between PMV and AIP neural activity and MFs is interrogated in terms of MF encoding in PMV and AIP unit FRs, as well as the ability to decode MFs from PMV and AIP population activity.

To determine the extent of MF encoding in PMV and AIP individual units, unit FRs were regressed against MF PC scores, assuming a linear model. MF PCss were calculated as in Sections 4.4, 5.4 and 6.4, using all normalized lagged MFs in the peri-movement period and selecting the top MF PCs explaining 99% of the MF variance. The linear model for regression was the same as in Equation 4.7, reproduced below:

$$f_{n,t} = \beta_{0,n} + \sum_{p=1}^{N_{\text{MFPC}}} (\beta_{p,n} s_{p,t+\tau}) + \epsilon \tag{7.1}$$

where $f_{n,t}$ is the FR of unit n at time t, β are constant weights, N_{MFPC} is the number of MF PCs, $s_{p,t+\tau}$ is the score of MF PC p at time $t+\tau$ and ϵ is a Gaussian noise term. As for the M1 models, τ was set to a value of 40 ms.

The regression parameters β were estimated using linear regression. Models were estimated for each PMV and AIP unit in each experiment. These estimated models were then used to produce predicted FRs. Regression R^2 values were calculated for each model. To compare across subjects and cortical areas, R^2 values from all units across all experiments were combined for each subject and each cortical area. The distributions of R^2 values are shown in Figure 7.9.

The highest mean R^2 value was observed for Monkey R M1 units, which featured a relatively large number of units with high R^2s. Monkey T left and right hemisphere M1 units displayed the second and third highest mean R^2s. However, the mean R^2 values for Monkey T left and right hemisphere PMV and left hemisphere AIP were comparable to the

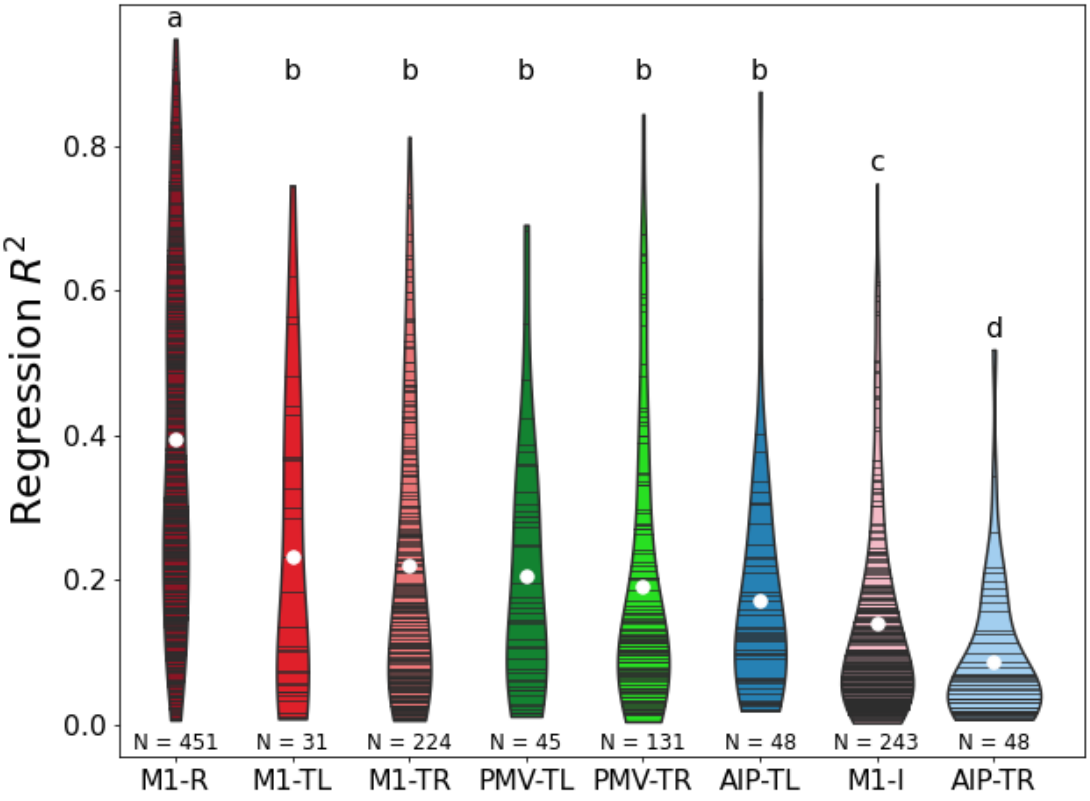

Figure 7.9: **Regression R^2 values for FR tuning to MF PC scores in M1, PMV and AIP.** Each violin plot depicts the distribution of R^2 values across all recorded units in all experiments for each cortical area. Columns are ordered by decreasing mean R^2. Reds: M1 units. Greens: PMV units. Blues: AIP units. Black lines: individual unit R^2 values from a single experiment. White markers: mean R^2 values for each area across all units and all experiments. Lower case letters denote significant differences in mean R^2 values between cortical areas; distributions with the same letter label were not significantly different ($p < 0.05$, permutation test, labels shuffled 10000 times).

R^2s observed in Monkey T left and right hemisphere M1. The mean R^2 was not significantly different for Monkey T left or right hemisphere M1, left or right hemisphere PMV or left hemisphere AIP ($p > 0.05$, permutation test, labels shuffled 10000 times). Monkey I M1 displayed significantly lower mean R^2 than the M1 areas of the other subjects, as well as Monkey T left and right hemisphere PMV and left hemisphere AIP. The lowest mean R^2 was observed for Monkey T right hemisphere AIP, which was significantly less than the mean R^2s of all other areas.

To further elucidate the relationship of PMV and AIP units to MFs, decoders were built to decode normalized MFs from linear combinations of unit FRs. Decoders were constructed as in Sections 4.6, 5.6 and 6.6, with the model of 4.26, reproduced below:

$$y_{m,t} = \boldsymbol{W}_m \boldsymbol{X}_t \tag{7.2}$$

where $y_{m,t}$ is the value of normalized MF m at time t (normalized over the full data set), W_m is a vector of weights, and X_t is a vector of FRs. The FRs X_t were calculated as in previous studies [119, 437] by binning spike counts in 30 ms bins and combining the last 15 bins ocurring before time t using an exponential filter with decay constant 0.95. The decoders were trained and tested on data from the peri-movement period only. Regression weights W_m were fit using ridge regression, with a fixed λ value of 0.02 for all models.

In order to accommodate the different numbers of units recorded in each area for each experiment, decoders were built using restricted numbers of units. This was accomplished by selecting up to 1000 random subsets of units of size $N_{\text{restricted}}$, with no repeats, and constructing and testing decoders with each subset using 10-fold cross validation. Performance was measured using RMSE values, combined across all folds, subsets and MFs, generating a single RMSE for each cortical area, for each $N_{\text{restricted}}$, for each experiment. This allowed comparison of decoder performances in each cortical area for decoders built with equal numbers of predictors. The decoding performance of the restricted-unit decoders are shown in Figure 7.10.

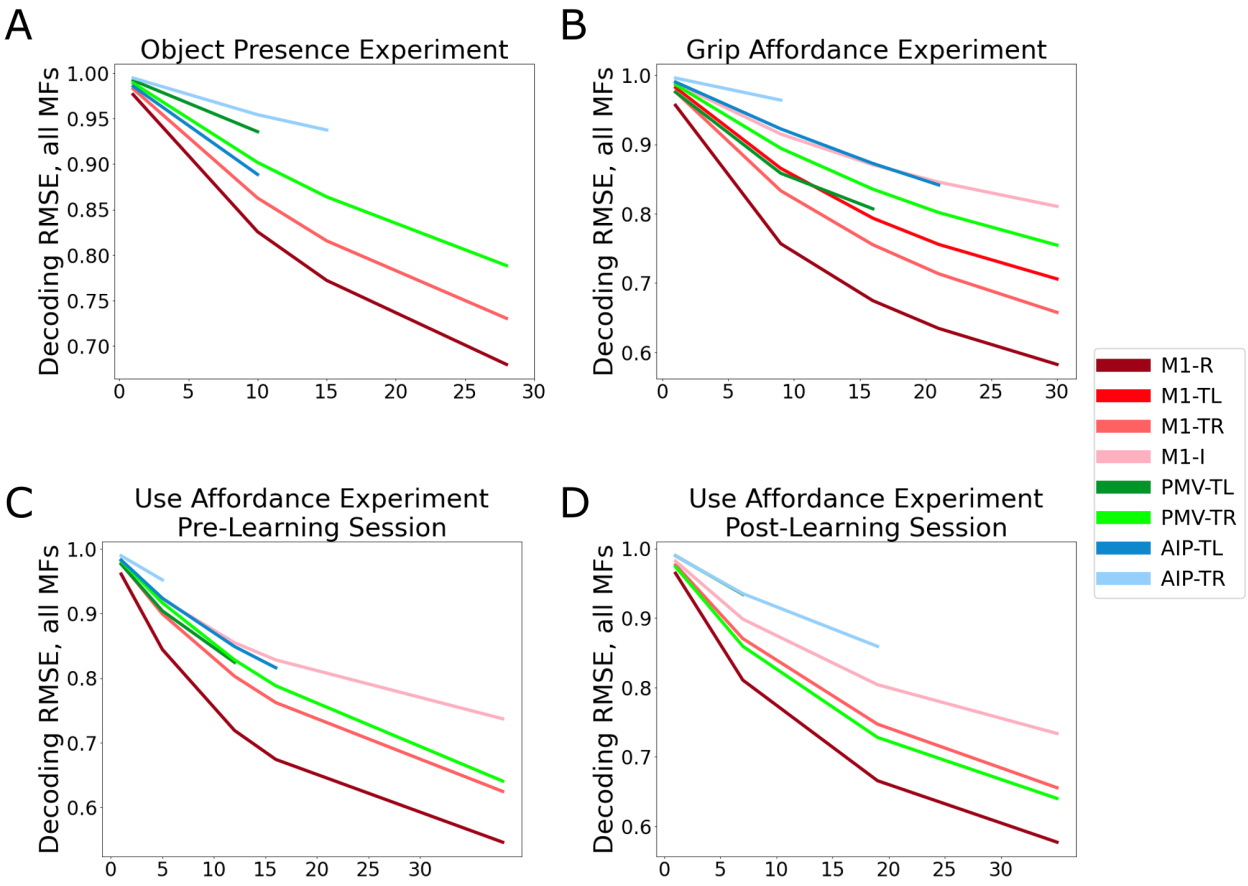

Figure 7.10: **MF Decoding Performance in M1, PMV and AIP.**

In general, the best MF decoding performances (lowest RMSEs) were observed for Monkey R M1. Decoder performances were comparable for Monkey T left and right hemisphere M1, left and right hemisphere PMV and left hemisphere AIP. Decoder performance for Monkey I M1 and Monkey T right hemisphere AIP were consistently low.

The regression and decoding results in PMV and AIP reveal that PMV and AIP unit FRs encode MF-related information at levels comparable to that observed in M1. This is congruent with other recent studies of M1, PMV and AIP activity during grasping [163]. In the subsequent section, evidence is considered for the presence of object context encoding in PMV and AIP in addition to MF encoding.

7.3 Evidence for Object Context Encoding in PMV and AIP

The results of Section 7.1 reveal that many PMV and AIP units were significantly modulated for conditions in which the same reaching or grasping behavior was performed in different object contexts (Figure 7.6). In some cases, this within-behavior modulation was large in magnitude (Figures 7.3–7.5). However, as noted in Sections 4.2, 5.2 and 6.2, small but consistent differences were observed in the MFs when comparing trials for same behavior, different object context condition pairs. Given the consistent relationship between PMV and AIP neural activity and MFs, as explored in the previous section, the object-context related neural modulation could reflect explicit encoding of object context, beyond linear encoding of MFs.

To determine if the neural modulation in PMV and AIP constituted object context encoding as opposed to just MF encoding, the extralinear modulation for PMV and AIP units and neural populations was calculated. This analysis was identical to that performed for M1 units and populations in Sections 4.4.1, 5.4.1 and 6.4.1. The extralinear modulation measures the amount of FR population modulation that exceeds what can be accounted for by linear tuning to MF PC scores.

The extralinear modulation ξ was first calculated for each individual unit, as in Equation 4.11. For each unit, ξ is defined as the absolute difference in mean FRs for two

conditions minus the absolute difference in mean predicted FRs, generated from the linear FR tuning to MF PC scores model described in Section 7.2. A unit was considered "object context encoding" if $\overline{\xi}$ for a same behavior, different object context condition pair exceeded estimated within-condition $\overline{\xi}$ variability at the $p < 0.05$ level (one-sided bootstrap interval, trials resampled 10000 times), as in Sections 4.4.1, 5.4.1 and 6.4.1. Table 7.2 displays the percentage of object context encoding PMV and AIP units found in each experiment. The percentages of object context encoding M1 units are included for reference.

Table 7.2: **Percentage of units with significant object context encoding in M1, PMV and AIP in each experiment.** OPE: Object Presence Experiment. GAE: Grip Affordance Experiment. UAE Pre: Use Affordance Experiment, pre-learning session. UAE Post: Use Affordance Experiment, post-learning session. For the Object Presence Experiment, the percentage of units which encode object presence is displayed. For the Grip Affordance and Use Affordance Experiments, the percentage of units which showed any within-grip object context encoding is displayed. Blank cells indicate sessions for which neural data were not recorded. * For Monkey T left hemisphere AIP, only 1 unit was recorded in the Use Affordance Experiment post-learning session.

		% of Object Context Encoding Units			
Subject	**Area**	**OPE**	**GAE**	**UAE Pre**	**UAE Post**
Monkey R	M1	39.5%	32.4%	5.7%	17.7%
Monkey I	M1		16.5%	5.8%	3.3%
Monkey T	M1 Left		12.9%		
Monkey T	M1 Right	24.6%	15.8%	6.9%	3.8%
Monkey T	PMV Left	20.0%	6.25%	0.0%	42.9%
Monkey T	PMV Right	10.7%	16.7%	2.6%	11.4%
Monkey T	AIP Left	20.0%	14.3%	0.0%	0.0%*
Monkey T	AIP Right	6.7%	22.2%	0.0%	0.0%

The percentages of object context encoding units were consistent across brain areas, with some key exceptions. Monkey T right hemisphere PMV and AIP displayed less frequent object presence encoding than other areas, at 10.7 and 6.7% of units respectively, compared to 20–40% in the other areas. The percentage of units encoding learned or perceived grip affordance differences was consistent in all areas, except for Monkey T left hemisphere PMV, which featured a markedly lower percentage of grip affordance encoding units. Monkey T left hemisphere PMV featured a remarkably high percentage of units encoding object context in the Use Affordance Experiment post-learning session.

In order to evaluate the magnitudes of the various object context encoding effects in PMV and AIP populations, the population extralinear modulations ξ^{pop} were calculated according to Equation 4.12. The population extralinear modulation ξ^{pop} is a measure of the separation between FRs for each condition pair in neural state space minus the separation between predicted FRs generated from linear FR to MF PC score tuning models. The time-averaged population extralinear modulation $\overline{\xi}^{\text{pop}}$ results for all cortical areas across all experiments are displayed in Figure 7.11

As in Sections 4.4.1, 5.4.1 and 6.4.1, a neural population was considered "significantly object context encoding" if $\overline{\xi}^{\text{pop}}$ for a same behavior, different object context condition pair was significantly greater than estimated within-condition $\overline{\xi}^{\text{pop}}$ variation. A neural population was further considered "robustly object context encoding" if $\overline{\xi}^{\text{pop}}$ for a same behavior, different object context condition pair was significantly greater than within-condition variation *and* significantly greater than mean $\overline{\xi}^{\text{pop}}$ for Power Grasps vs. Pinch Grasps ($p < 0.05$, one-sided bootstrap interval, trials resampled 10000 times). The occurrence of population-level significant and robust object context encoding in all cortical areas is further summarized in Table 7.3

Significant object presence encoding was observed at the population level in all areas except Monkey T right hemisphere AIP. Moreover, in areas where encoding of object presence was significant, it was also robust except in Monkey T right hemisphere PMV. This suggests that object presence encoding was a powerful driver of activity in all M1 populations and left hemisphere PMV and AIP. These areas all strongly encoded the contextual factor of whether or not the object was present, beyond linear encoding of MF differences.

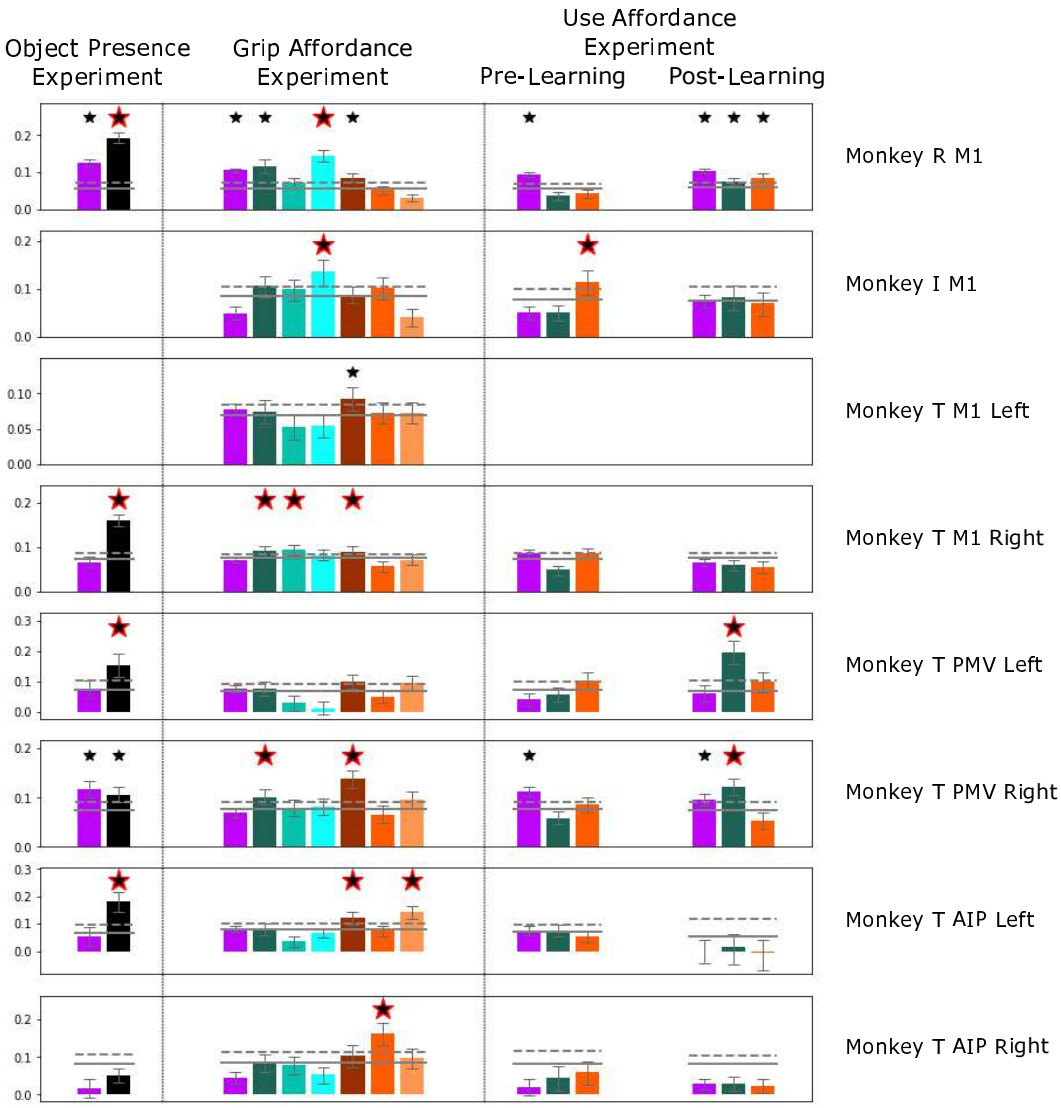

Figure 7.11: **Time-averaged population extralinear modulation $\overline{\xi}^{\text{pop}}$ in M1, PMV and AIP for all experiments.** Purple bars: Power Grasps vs. Pinch Grasps. Black bars: Object Reach vs. No-Object Reach. Turquoise bars: Power Grasps on different objects. Orange bars: Pinch Grasps on different objects. Black star: $\overline{\xi}^{\text{pop}}_{i,j}$ significantly greater than within-condition $\overline{\xi}^{\text{pop}}$ variability. Black and red star: $\overline{\xi}^{\text{pop}}_{i,j}$ additionally significantly greater than mean $\overline{\xi}^{\text{pop}}_{\text{PowerGrasp,PinchGrasp}}$ ($p < 0.05$, one-sided bootstrap interval). Gray: mean and upper 95% one-sided confidence interval of within-condition variability. Error bars are bootstrap 95% confidence intervals.

Table 7.3: **Occurrence of population-level object context encoding in M1, PMV and AIP.** Green cells: significant population-level object context encoding was present. Asterisk: Robust population-level object context encoding was present. Gray cells: population-level object context encoding was not present. Blank cells indicate sessions for which neural data were not recorded. OPE: Object Presence Experiment. GAE: Grip Affordance Experiment. UAE Pre: Use Affordance Experiment, pre-learning session. UAE Post: Use Affordance Experiment, post-learning session. Population-level object context encoding was defined as at least one $\overline{\xi}^{\text{pop}}$ for a same behavior different object context condition pair significantly greater than estimated within-condition $\overline{\xi}^{\text{pop}}$ at the $p < 0.05$ level (one-sided bootstrap intervals, trials resampled 10000 times). Robust population-level object context encoding required that the same behavior different object context $\overline{\xi}^{\text{pop}}$ was also significantly greater than mean $\overline{\xi}^{\text{pop}}$ for Power Grasps vs. Pinch Grasps.

Subject	**Area**	**OPE**	**GAE**	**UAE Pre**	**UAE Post**
Monkey R	M1	*	*		
Monkey I	M1		*	*	
Monkey T	M1 Left				
Monkey T	M1 Right	*	*		
Monkey T	PMV Left	*			*
Monkey T	PMV Right		*		*
Monkey T	AIP Left	*	*		
Monkey T	AIP Right		*		

Significant grip affordance encoding was observed at the population level in all areas except Monkey T left hemisphere PMV. Moreover, in all areas where grip affordance encoding was significant, it was also robust except in Monkey T left hemisphere M1. Where present, grip affordance encoding was moderate in size, and was restricted to only one or a few same-grasp different object condition pairs.

In the Use Affordance Experiment pre-learning session, significant, robust population-level object context encoding was observed only in Monkey I M1 with respect to extralinear modulation for Pinch Grasp, Object 1 vs. Pinch Grasp Object 2 (Figure 7.11 orange bars, middle right column). However, in the post-learning session of the Use Affordance Experiment, significant, robust object context encoding was present only in Monkey T left hemisphere PMV and right hemisphere PMV. These effects were driven by extralinear modulations for Power Grasp, Object 1 vs. Power Grasp, Object 2, which were large in both PMV areas, especially Monkey T left hemisphere PMV (Figure 7.11 turquoise bars, far right column). This increase in object context encoding between Power Grasps coincided with the learning of the lifting use affordance for Object 2, which was associated only with Power Grasps. Thus, these results suggest a special role for PMV in encoding the learned use affordance of Object 2. Monkey R M1 also encoded object context during the Use Affordance Experiment post-learning session but at a lower level.

In Sections 4.5, 5.5 and 6.5, the interaction between object context encoding and MF encoding in individual unit FRs was explored. Object context was found to be encoded both directly in unit FRs or interactively with MFs for most units. To determine whether object context encoding was instantiated similarly in PMV and AIP units, multiple encoding models were fit and tested. These models described MF Only encoding (as in Equation 4.22), MF encoding with Direct object context encoding (Equations 4.23, 5.3, 5.2, 5.4 and 6.2), and Interactive MF and object context encoding (Equations 4.24, 5.6, 5.5, 5.7 and 6.3). The models were compared using the Bayes' Information Criterion (BIC). The distribution of units for which the best models were MF only encoding, MF encoding with additive, direct object context encoding or interactive MF and object context encoding are displayed in Figure 7.12, with results combined across experiments.

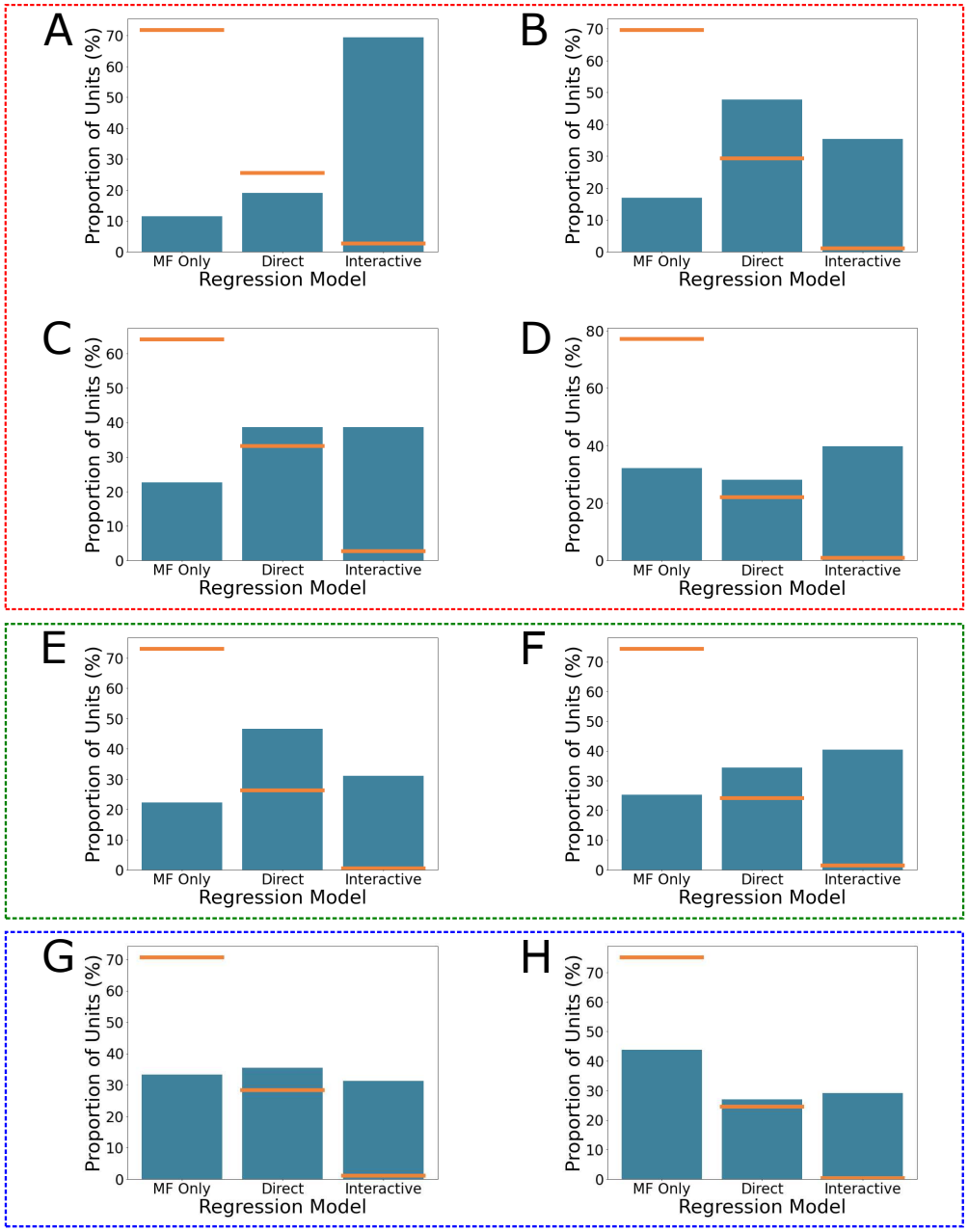

Figure 7.12: **Occurrence of direct and indirect object context encoding in M1, PMV and AIP.** Red: M1. Green: PMV. Blue: AIP. A: Monkey R M1. B: Monkey I M1. C: Monkey T left hemisphere M1. D: Monkey T right hemisphere M1. E: Monkey T left hemisphere PMV. F: Monkey T right hemisphere PMV. G: Monkey T left hemisphere AIP. H: Monkey T right hemisphere AIP. Orange lines: chance levels of selecting each model, generated by shuffling object context labels 100 times.

To ensure that model selection results reflected actual encoding of object context and were not simply a result of arbitrarily dividing the data into subsets, baseline frequencies of model selection were calculated by fitting the MF Only, Direct and Interactive models on datasets in which the object context labels for whole trials were randomly shuffled. The BICs of these shuffled-label models were compared to estimate the chance level of selecting each type of model. This procedure was repeated 100 times for each session to generate the average baseline chance frequencies of selecting each model (Figure 7.12 orange lines). In all areas, MF Only encoding was selected at rates much lower than chance levels, and Interactive context encoding was selected at rates much higher than chance levels.

Overall, the balance of MF Only encoding and Direct and Interactive object context encoding was similar across all areas in all experiments. For all areas, the majority of units were best fit by encoding models which included some form of object context information. For all areas except Monkey R M1, the number of units best fit by models with Direct object context encoding was similar to the number of units best fit by models with Interactive object context encoding. In Monkey R M1, Interactive object context encoding was much more prevalent. These results suggest that object presence encoding was actually present in many more units than identified by the extralinear modulation analyses, but at a subtle and small level. Additionally, context encoding was very often interactive with MF encoding in all areas.

The analyses presented thus far in this section describe the evidence for object context encoding in PMV and AIP in the peri-movement period only. PMV and AIP have historically been noted for their preparatory and visual-responsive encoding of grasps and objects [223, 224,254,271,274,274,351] (see Sections 2.3 and 2.4). The mean normalized FR trajectories of Figure 7.7 suggest that PMV and AIP units were modulated during the preparatory period in the current experiments.

To interrogate the presence of object context encoding during the preparatory, pre-movement period, the time-averaged population modulation $\overline{\Delta}^{\text{prep}}$ was calculated in each area during the preparatory period (from 200 ms after the start of the trial to 100 ms before Reach Start). The population modulation is the scaled Euclidean distance in neural state space between mean FRs for all units in two conditions. $\overline{\Delta}^{\text{prep}}$ is shown for all areas,

for all experiments in Figure 7.13. Instances in which $\overline{\Delta}^{\text{prep}}$ for same-behavior, different object context condition pairs were significantly greater than estimated within-condition $\overline{\Delta}^{\text{prep}}$ are highlighted with a black star. Instances in which $\overline{\Delta}^{\text{prep}}$ for same-behavior, different object context condition pairs were additionally significantly greater than $\overline{\Delta}^{\text{prep}}$ for Power Grasps vs. Pinch Grasps are highlighted with a black and red star.

Significant preparatory modulations related to grip type (Power Grasp vs. Pinch Grasp) were observed in all areas across all experiments, except in Monkey T right hemisphere in AIP, where it was never observed, and in Monkey T left hemisphere AIP, where it was not observed during the Object Presence Experiment. The absence of preparatory grip type modulation in the AIP regions may reflect the fact that the objects were often a single object which was grasped in multiple ways, and thus had the same visual appearance. AIP may be more related to the visual percept of the object than to how it is grasped. Alternatively, this lack of preparatory grip type modulation may have just been due to the low number of units recorded in these areas.

Significant preparatory modulations relative to object presence were observed in all areas, further confirming that object presence or absence was a strong driver of activity throughout the frontoparietal grasp network. Moreover, in Monkey T left hemisphere PMV and both AIP areas, preparatory modulation for object presence was greater in magnitude than modulation for grip type. This highlights the relative importance of object presence or absence in these areas, especially during preparatory activity.

Significant preparatory modulation related to perceived and learned grip affordance differences were observed for at least one same-grasp, different object condition pair in all areas except Monkey T right hemisphere AIP. These effects were moderate in size.

Significant preparatory modulations related to object color differences (in the Use Affordance Experiment pre-learning session) were present only in Monkey R M1, Monkey I M1 and Monkey T left hemisphere PMV. These preparatory modulations were small in size and were most often observed within Pinch Grasp conditions.

In the Use Affordance Experiment, preparatory modulations related to object context were observed in all areas except Monkey I M1 and Monkey T right hemisphere AIP. Notably,

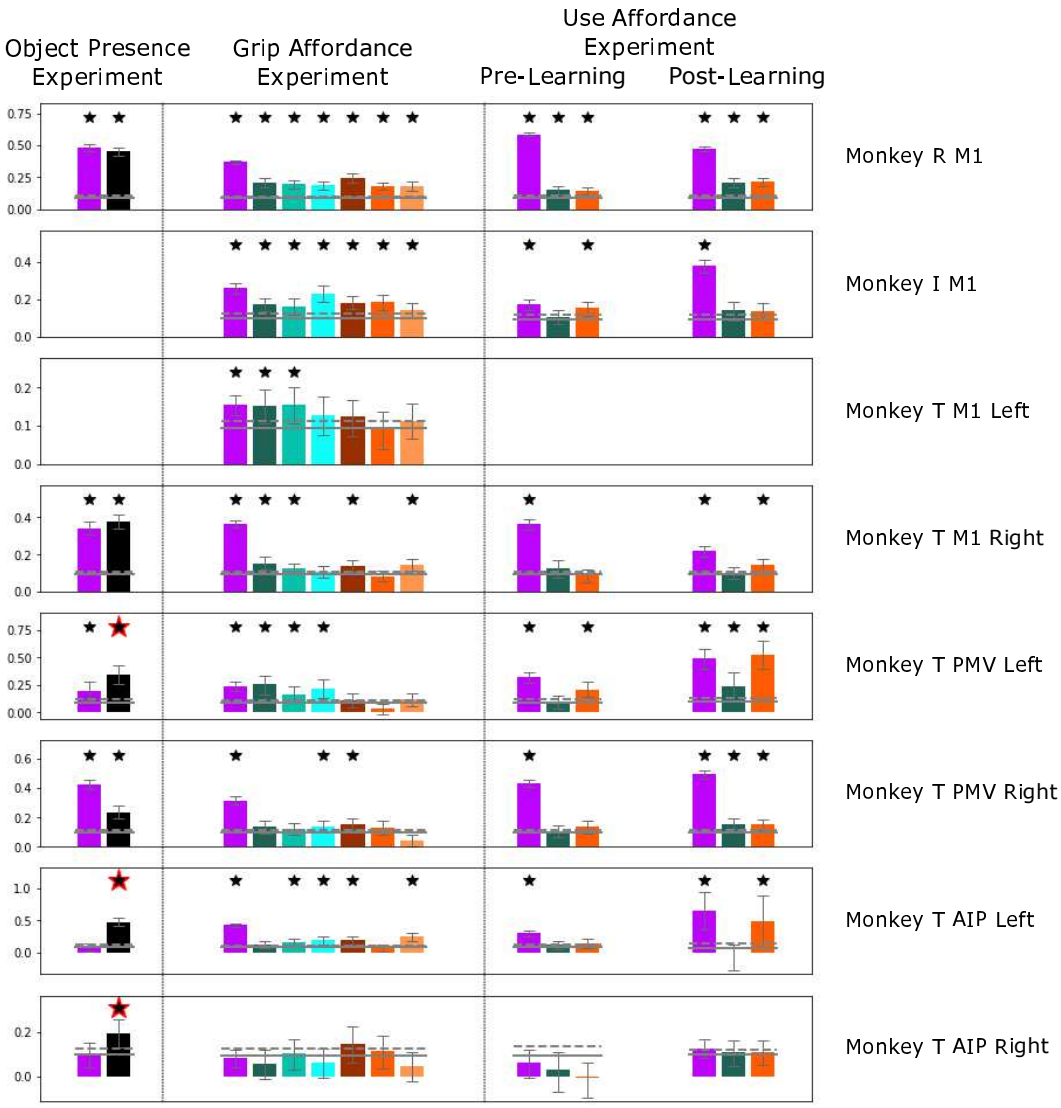

Figure 7.13: **Time-averaged preparatory population modulation $\overline{\Delta}^{\text{prep}}$ in M1, PMV and AIP for all experiments.** Purple bars: Power Grasps vs. Pinch Grasps. Black bars: Object Reach vs. No-Object Reach. Turquoise bars: Power Grasps on different objects. Orange bars: Pinch Grasps on different objects. Black star: $\overline{\Delta}^{\text{prep}}_{i,j}$ significantly greater than within-condition $\overline{\Delta}^{\text{prep}}$ variability. Black and red star: $\overline{\Delta}^{\text{prep}}_{i,j}$ additionally significantly greater than mean $\overline{\Delta}^{\text{prep}}_{\text{PowerGrasp,PinchGrasp}}$ ($p < 0.05$, one-sided bootstrap interval). Gray: mean and upper 95% one-sided confidence interval of within-condition variability. Error bars are bootstrap 95% confidence intervals.

in Monkey R M1, and both PMV areas of Monkey T, this preparatory modulation was observed for Power grasps, for which context encoding during movement was also observed (Figure 7.11). Nevertheless, these effects were relatively small.

In the next section, the timing of the preparatory and movement related activity in M1, PMV and AIP are compared directly.

7.4 Sequential Activation of AIP, PMV and M1

The results of the previous section support the existence of object context encoding in M1, PMV and AIP in both the preparatory period and the peri-movement period. While bidirectional projections exist between M1, PMV and AIP, the AIP-PMV-M1 grasp network is often framed as an essentially feedforward network which implements a visuomotor transformation [255]. In support of this feedforward network structure, electrical stimulation in PMV has been found to have direct modulatory influence on M1 corticospinal output [314–316] and AIP modulation of M1 corticospinal output is dependent on PMV [320] (see Section 2.5 for further discussion).

To investigate the possibility of direct connectivity between units recorded in the different cortical areas, the noise correlations (correlations between FRs after subtraction of FR trial averages) between each pair of units was calculated for sessions in which M1, PMV and AIP data were simultaneously recorded. Pairwise noise correlations were universally low (< 0.05), indicating that no recorded units strongly and directly influenced other recorded units. This was unsurprising, given the large number of neurons in these cortical areas, the relatively sparse sampling obtained by the implanted electrodes and the relatively low number of units recorded in PMV and AIP.

To investigate the possibility of feedforward flow of grip type or object context information at a population level, the time-courses of population modulation Δ were compared over the courses of full trials. The Δ trajectories for Power Grasps vs. Pinch Grasps, averaged across all Power Grasp vs. Pinch Grasp condition pairs for all experiments, are shown in Figure 7.14 for the areas which were simultaneously recorded

(Monkey T left and right hemisphere M1, PMV and AIP). The Δ, Power Grasp vs. Pinch Grasp values for each area were normalized to the maximum Δ values observed in each area over the whole trial.

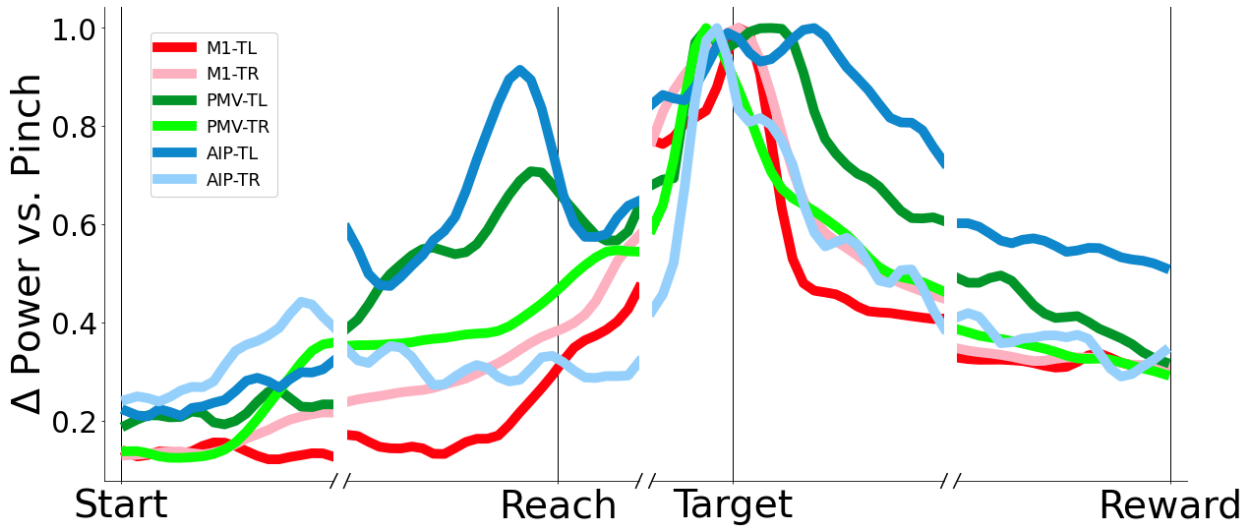

Figure 7.14: **Population modulation Δ timecourses in M1, PMV and AIP for Power Grasps vs. Pinch Grasps across all experiments.** Data from Monkey T. Red traces: M1. Green traces: PMV. Blue traces: AIP. Dark colors: left hemisphere areas. Light colors: right hemisphere areas.

Population modulation Δ related to the intended grip type (Power Grasps vs. Pinch Grasps across all experiments) arose first in AIP, followed by PMV and then M1. In the left hemisphere areas, grip type Δ arose first in AIP during the start button hold period, with a subsequent peak before movement onset (Figure 7.14 dark blue trace). Left hemisphere PMV grip type Δ tightly followed AIP Δ, with a pre-movement modulation peak occurring about 20ms (one sample) after the AIP pre-movement peak (Figure 7.14 dark green trace). In the right hemisphere areas, a small increase in grip type Δ was observed first in AIP about 200 ms after trial start. This was closely followed by a small rise in grip type Δ in right hemisphere PMV (Figure 7.14 light green trace). In all PMV and AIP areas, a second,

stronger peak of grip type Δ was observed at the time of Target Contact. By contrast, left hemisphere M1 displayed little grip type Δ during the preparatory period, with Δ rising just before Reach Start and peaking around the time of Target Contact. In right hemisphere M1, grip type Δ slowly increased during the pre-movement period, with a steeper uptick during the reach and a peak around the time of Target Contact.

The grip type population modulation timecourses suggest that grip type information may flow sequentially from AIP to PMV to M1. To determine if object context information was also relayed in a sequential, feedforward manner, the timecourses of population modulation Δ for various same-behavior, different object context comparisons were calculated. The timecourses of Δ for Object Reach vs. No-Object Reach are displayed in Figure 7.15 for Monkey T in the Object Presence Experiment. Again, Δ for each area was normalized to the maximum value observed in each area over the whole trial.

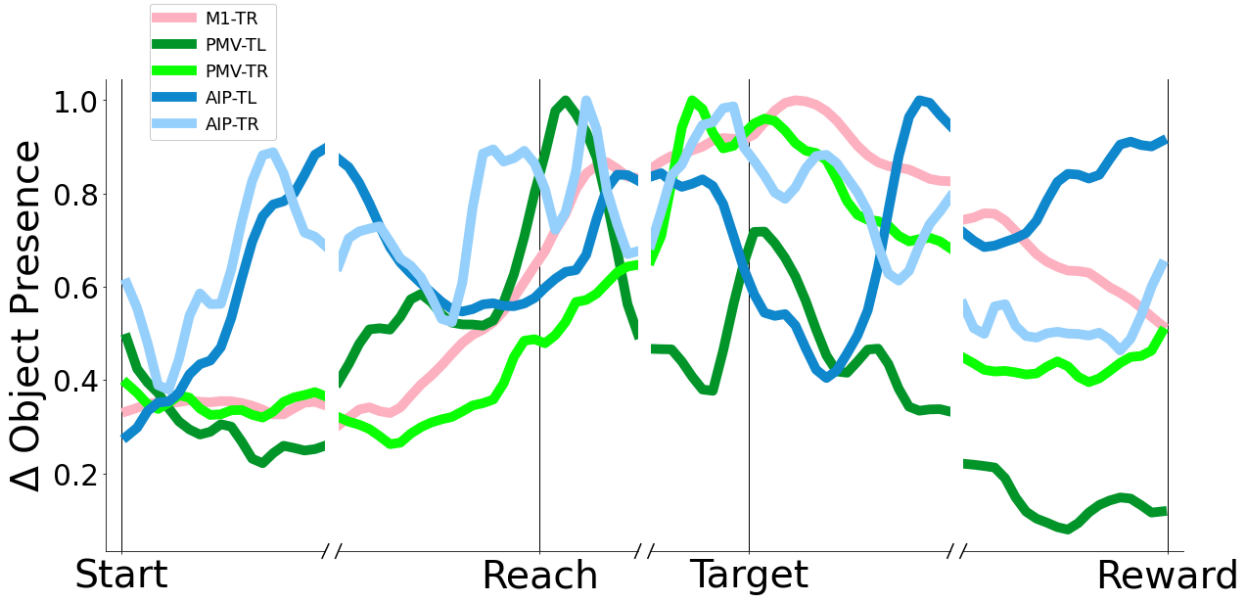

Figure 7.15: **Population modulation Δ timecourses in M1, PMV and AIP for Object Reach vs. No-Object Reach in the Object Presence Experiment.** Data from Monkey T. Red traces: M1. Green traces: PMV. Blue traces: AIP. Dark colors: left hemisphere areas. Light colors: right hemisphere areas.

Population modulation Δ related to object presence (Object Reach vs. No-Object Reach in the Object Presence Experiment) was again observed first in AIP, then in PMV and M1, though right hemisphere PMV Δ lagged right hemisphere M1 Δ. In both right and left hemisphere AIP, object presence Δ rose rapidly just after the start of the trials, exhibiting a peak during the start button hold period (Figure 7.15, dark and light blue traces). Object presence Δ was sustained throughout the movements in AIP. Left hemisphere PMV also displayed an early rise in object presence Δ, starting at least 400ms before Reach Start and peaking just after the start of the reach, with a second, smaller peak around the time of Target Contact (Figure 7.15). In right hemisphere M1, object presence Δ arose more slowly during the pre-movement period, with a steady increase to a peak just after Target Contact (Figure 7.15 light red trace).

The timecourses of object presence Δ suggest that contextual information related to object presence may flow sequentially from AIP to PMV to M1. To determine if object context information related to grip affordances were also encoded sequentially in AIP, PMV and M1, the timecourses of Δ from the Grip Affordance Experiment were calculated. The average timecourses of Δ for Pinch Grasp condition pairs made on objects with different perceived and learned grip affordances are displayed in Figure 7.16. The three Δ values for the three Pinch Grasp, different object condition pairs were averaged to produce a single Δ timecourse for each area. The Δ between Pinch Grasps values in each area were normalized to the maximum values observed over the course of the trial.

Once again, population modulation Δ related to perceived and learned grip affordance differences of objects that were grasped with a Pinch Grip was observed first in AIP and PMV, and later in M1. Both left and right hemisphere AIP displayed a rapid increase in Δ between Pinch Grasps at the start of the trial, with right hemisphere PMV displaying a similar, but slightly later early increase in Δ between Pinch Grasps. Left hemisphere PMV displayed a gradual increase in Δ between Pinch Grasps during the pre-movement period, with a peak around the time of movement onset and a larger peak at the time of Target Contact. During the reach, Δ between Pinch Grasps in right hemisphere PMV preceded Δ between Pinch Grasps in right hemisphere M1 by about 40ms (two samples). The main Δ

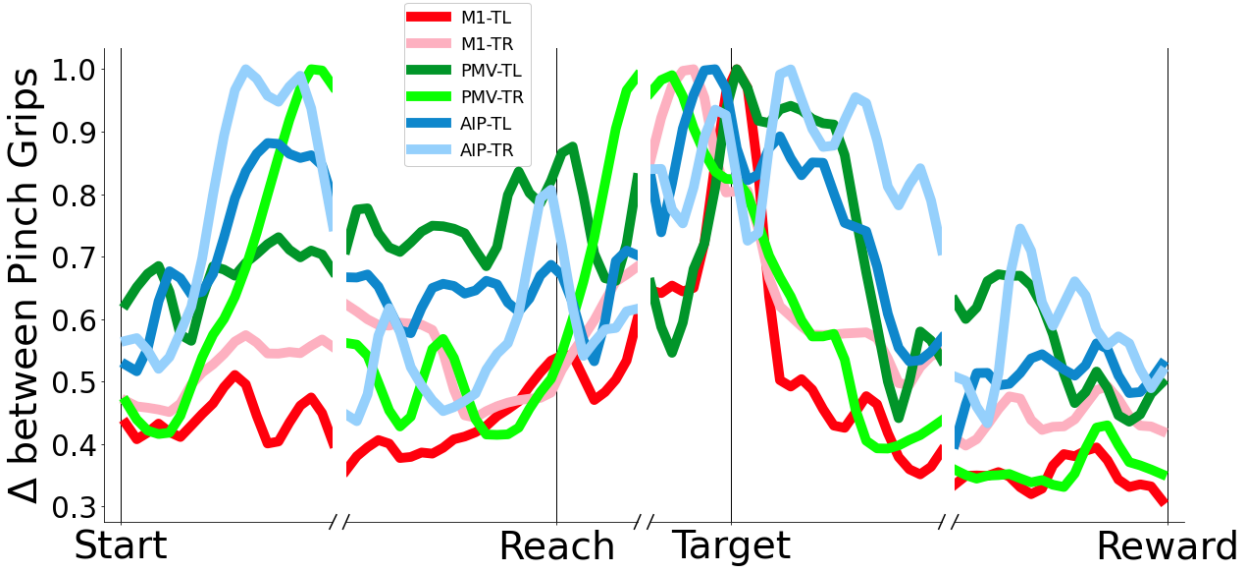

Figure 7.16: **Population modulation Δ timecourses in M1, PMV and AIP for Pinch Grasps executed on objects with different perceived or learned grip affordances in the Grip Affordance Experiment.** Data from Monkey T. Red traces: M1. Green traces: PMV. Blue traces: AIP. Dark colors: left hemisphere areas. Light colors: right hemisphere areas.

peak in left hemisphere M1 occurred slightly later still, at the time of object contact. The timing of Δ between Pinch Grasps suggests that grip affordance information may proceed sequentially from AIP to PMV to M1.

The timecourses of Δ for Power Grasp vs. Pinch Grasp in all experiments, for Object Reach vs. No-Object Reach in the Object Presence Experiment and for Pinch Grasps made on different objects in the Grip Affordance Experiment suggest that grip type, object presence context and grip affordance context may all be sequentially processed in AIP, then PMV, then M1. Δ between power grasps in the Grip Affordance Experiment, and for the same grasp, different object condition pairs of the Use Affordance Experiment were not examined, as object context encoding was rarer for these condition pairs, and was not detected in all three cortical areas (see Figure 7.11 and Table 7.3).

7.5 Automatic Activation of Affordances in PMV and AIP

In Sections 4.7, 5.7 and 6.7, the M1 neural differences observed between different object context were examined for evidence that they may constitute "automatic activation" of an object's grasp or use affordances when those affordances are present but not utilized. In the Object Presence Experiment, evidence was found that behavior and neural activity during Object Reach trials were biased toward the behavior and neural activity observed during grasps of that object, relative to the behavior and neural activity observed during No-Object Reaches. This suggests the possibility that the motor representations of the grasp actions afforded by the object were partially activated when the object was present. In the Grip Affordance Experiment, pro-affordance biases were present only in very early neural activity, suggesting that the presence of a perceived or learned, but unused grip affordance drove background activity in M1 toward the activity observed when that grip affordance was actually acted upon. In the Use Affordance Experiment, strong pro-affordance biases were present in behavior and M1 neural activity, suggesting that the representation of the lift action was activated for grasps of the movable object, even when it was not lifted.

In this section, evidence is presented for similar affordance biases in PMV and AIP neural activity. To measure these affordance biases, the neural affordance shifts S^{mFRPC} were calculated in mFR PC space, defined as the scores in the PCA dimensions capturing 99% of trial-averaged FR variance. The shifts were calculated for each of the three experiments. Object Presence Experiment S^{mFRPC} values were calculated according to Equations 4.29 and 4.30, Grip Affordance Experiment S^{mFRPC} values were calculated according to Equations 5.11–5.14, and Use Affordance Experiment S^{mFRPC} values were calculated according to Equation 6.5. Null space analyses were not performed for PMV and AIP neural activity, as the lower number of units recorded in these areas did not provide sufficient dimensionality to decompose further and still retain useful information.

The Object Presence Experiment affordance shifts in PMV and AIP are presented in Figure 7.17.

Object Presence related neural affordance shifts were generally positive in all areas throughout the preparatory and reach periods, indicating that object presence drove neural activity toward the neural activity observed during trials in which the object was grasped. In left hemisphere PMV and right hemisphere AIP (Figure 7.17 A and D), this affordance shift was near zero after target acquisition, but in right hemisphere PMV and left hemisphere AIP (Figure 7.17 B and C), the affordance shift value remained high throughout the target hold period.

The Grip Affordance Experiment affordance shifts in PMV and AIP are presented in Figure 7.18.

No consistent pattern of positive or negative affordance bias was observed related to perceived or learned grip affordances in any area.

The Use Affordance Experiment affordance shifts in PMV and AIP are presented in Figure 7.19.

Positive affordance shift values were observed in both PMV areas and right hemisphere AIP. Insufficient data were obtained from left hemisphere AIP for these analyses. The pro-affordance shift related to the unused use affordance was present in all areas even at the start of the trial. In all areas, a transient decrease in affordance shift was observed about 40ms after cue presentation in left hemisphere AIP and about 60ms after cue presentation in left

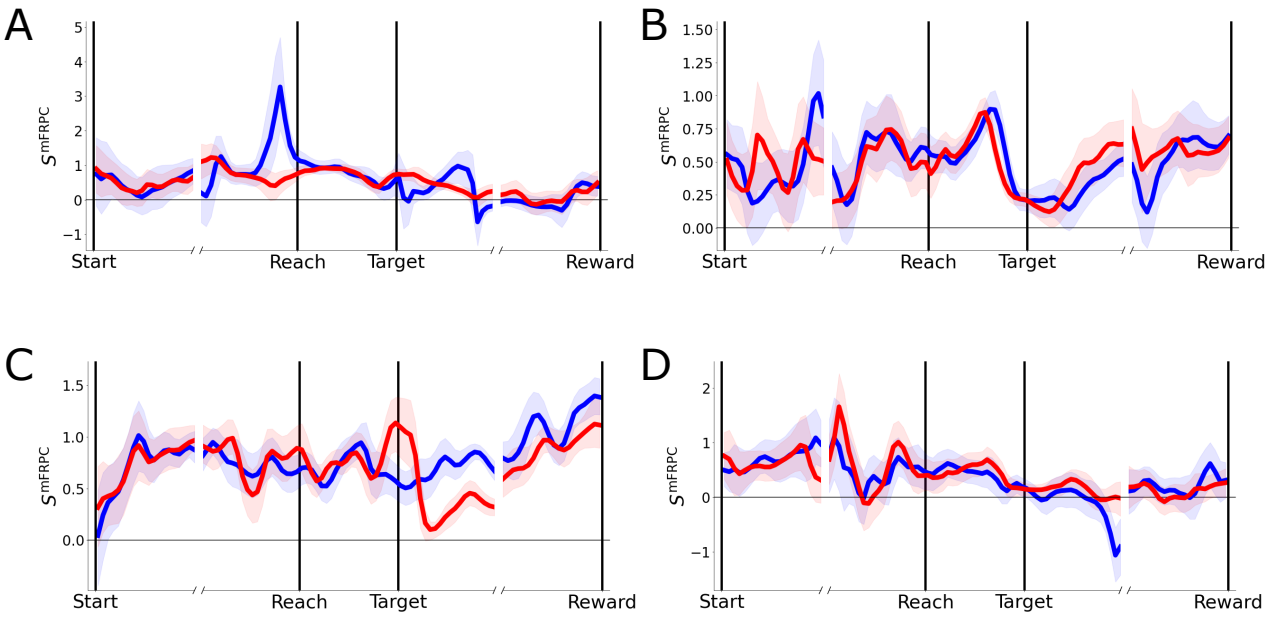

Figure 7.17: **PMV and AIP Affordance Shifts S^{mFRPC} in the Object Presence Experiment.** Affordance shifts were calculated in the 99% mFR PC space. A: Monkey T left hemisphere PMV. B: Monkey T right hemisphere PMV. C: Monkey T left hemisphere AIP. D: Monkey T right hemisphere AIP. Blue: shifts relative to Power Grasp, Red: shifts relative to Pinch Grasp. Shaded 95% confidence intervals are bootstrap intervals, trials resampled 10000 times.

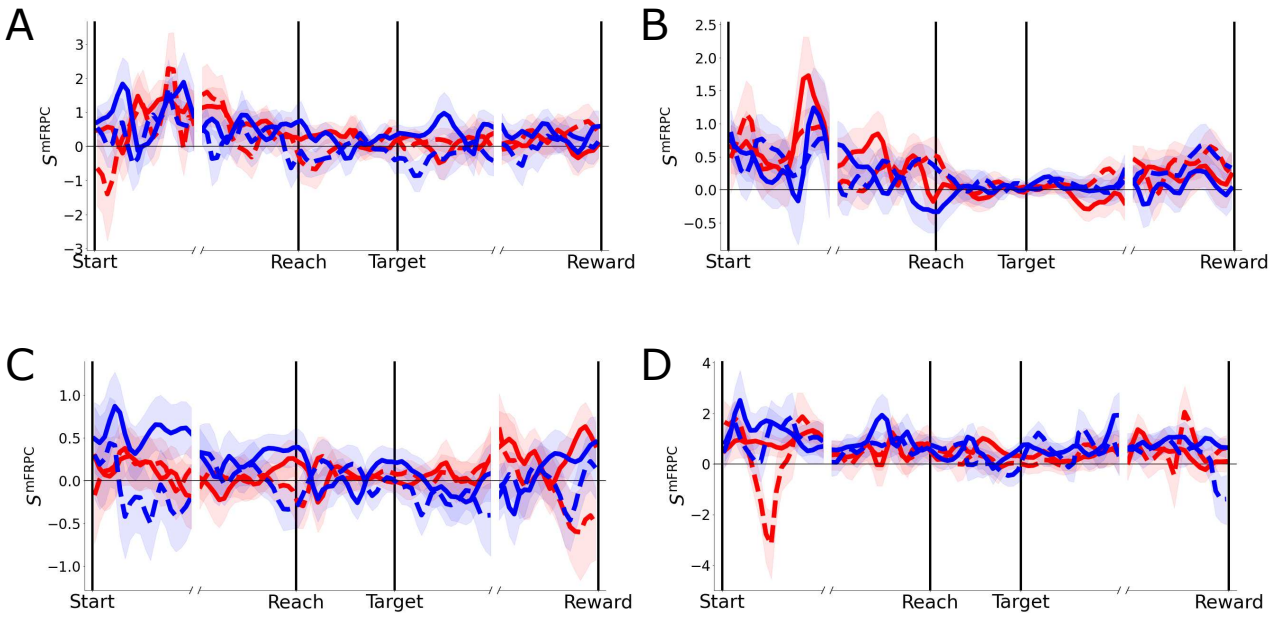

Figure 7.18: **PMV and AIP Affordance Shifts S^{mFRPC} in the Grip Affordance Experiment.** Affordance shifts were calculated in the 99% mFR PC space. A: Monkey T left hemisphere PMV. B: Monkey T right hemisphere PMV. C: Monkey T left hemisphere AIP. D: Monkey T right hemisphere AIP. Blue: shifts for Power Grasp affordances, Red: shifts for Pinch Grasp affordances. Solid lines: perceived affordances. Dashed lines: learned affordances. Shaded 95% confidence intervals are bootstrap intervals, trials resampled 10000 times.

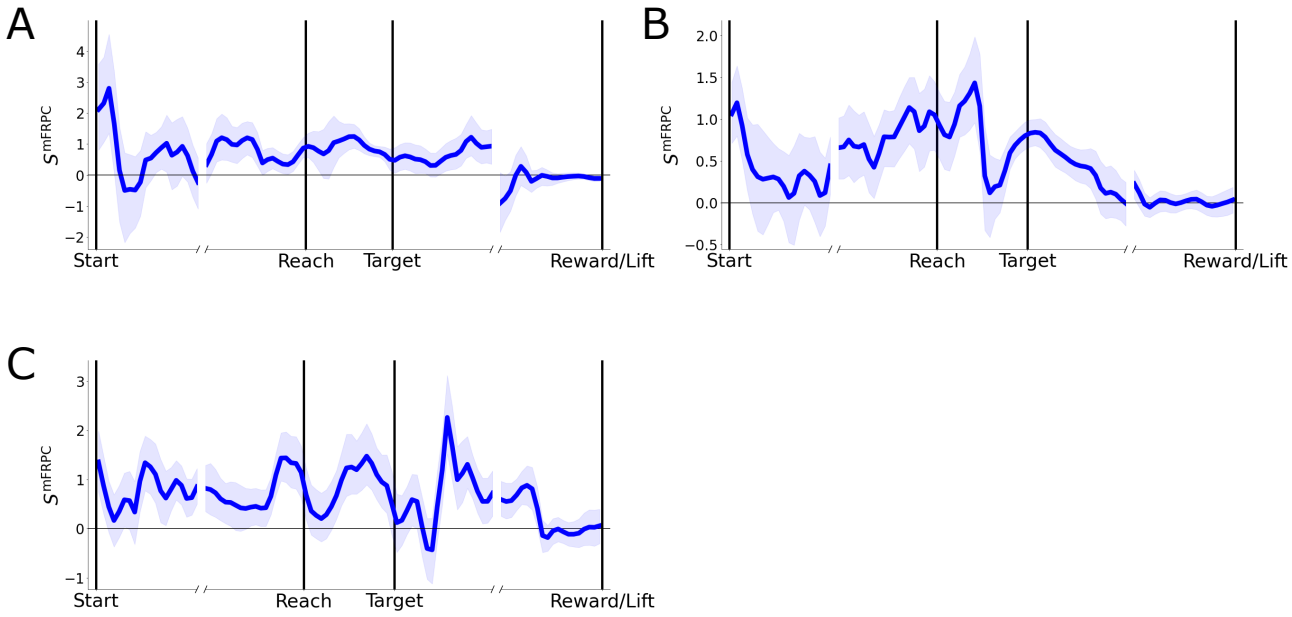

Figure 7.19: **PMV and AIP Affordance Shifts S^{mFRPC} in the Use Affordance Experiment.** Affordance shifts were calculated in the 99% mFR PC space. A: Monkey T left hemisphere PMV. B: Monkey T right hemisphere PMV. C: Monkey T right hemisphere AIP. Shaded 95% confidence intervals are bootstrap intervals, trials resampled 10000 times.

and right hemisphere PMV, perhaps reflecting processing of the cue information related to whether or not the trial would entail a lift action. Similar transient decreases in affordance shift related to the learned use affordance were also observed in M1, but at a slightly later time. The relative timing of these effects further supports the hierarchical organization of object affordance processing from AIP to PMV to M1.

The positive affordance shifts observed during the Object Presence Experiment and the Use Affordance Experiment support, but do not definitively confirm, the hypothesis that the PMV and AIP representations of an object's grasp and learned use affordances can be partially automatically activated when that object is presented.

In summary, cortical areas PMV and AIP were identified as potential sources of the object context encoding signal in M1. PMV and AIP units were recorded in Monkey T simultaneously with M1 units during execution of the Object Presence Experiment, the Grip Affordance Experiment and the Use Affordance Experiment. PMV and AIP unit activity was modulated by grip type as well as object context at similar levels to M1 units. A few PMV and AIP units displayed extreme object context related modulations, though levels of sustained modulation for contextual factors and for grip type were similar to those observed in M1 (Section 7.1). PMV and AIP unit FRs were found to be partially related to MFs, as linear MF encoding model fits in PMV and AIP were comparable to those observed in M1, and the ability to decode MFs from PMV and AIP population activity was generally only slightly worse than that observed in M1 (Section 7.2). Based on the magnitude of observed extralinear modulation, object presence and perceived and learned grip affordances were robustly encoded in PMV and AIP areas at levels similar to that observed in M1. In the Use Affordance Experiment, only PMV populations robustly encoded the learned use affordance in the post-learning session, suggesting a special role for PMV in linking learned use affordance knowledge to action. Left hemisphere PMV and both AIP areas also displayed strong object presence related modulations in the preparatory period which exceeded preparatory grip type modulations (Section 7.3). The timecourses of population modulation in the different cortical areas suggest that grip type, object presence and grip affordance information may proceed sequentially from AIP to PMV to M1 as the movement is prepared and executed (Section 7.4). Neural activity in PMV and AIP reflected potential

automatic activation of the representations of an object's grasp affordances when the object was present in the workspace, and of the representations of an object's learned use affordance when an object was acted upon but not manipulated.

8.0 Discussion

The three experiments of this dissertation, the Object Presence Experiment, the Grip Affordance Experiment and the Use Affordance Experiment are discussed below. Section 8.1 contains a summary and discussion of the main findings of the three experiments. Section 8.2 describes additional control analyses which were performed to verify certain results. Section 8.3 contains a discussion of the limitations of the experimental design and implications for interpretation of the results. Section 8.4 contains suggestions for future work based on the findings of the three experiments. Section 8.5 presents a final conclusion.

8.1 Summary and Discussion of Results

Each of the three experiments was designed to investigate the effect of an object-related contextual factor on behavior and on neural activity in the frontoparietal grasp network regions M1, PMV and AIP. The Object Presence Experiment was designed to study the effect of object presence or absence on reaching behavior and associated neural activity. The Grip Affordance and Use Affordance Experiments were designed to investigate the effect of object identity on behavior and neural activity for similar grasping movements. In the Grip Affordance Experiment, object identity was defined by the perceived and learned grip affordance of different objects. In the Use Affordance Experiment, object identity was defined by superficial differences in color between two objects, and subsequently, after a learning period, by the learned use affordance differences of the two objects. All three experiments featured pairs of conditions for which the subjects performed movements with the same overall requirements in different object contexts.

In all three experiments, behavior, in terms of MFs, differed significantly in different object contexts. These differences were observed despite the overall task requirements being held constant across contexts. In the Object Presence Experiment, the reach target for Object Reach trials (for which the object was present) was the same as the reach target

for No-Object Reach trials (for which the object was absent). Despite this, significantly different MFs were observed between the two reaches. In the Grip Affordance Experiment, the exact same physical portions of objects were grasped while they were presented alone or assembled into different compound objects. Despite this, differences were observed in MFs for grasps made on the different objects. In the Use Affordance Experiment pre-learning session objects were shaped the same and differed only by color. Yet differences in grasp MFs were observed when the two different objects were grasped. In the Use Affordance Experiment post-learning session, a novel use affordance was learned for one object. When both objects were required to be only grasped and held, grasp MFs differed to a greater extent than in the pre-learning session, especially for power grasps, which were associated with the learned use of the movable object.

The differences in MFs were associated with proportionately larger differences in neural activity. Significant differences were observed in single units and neural populations in M1, PMV and AIP for task conditions in which the behavioral requirements remained constant but object-related contextual factors differed. As arm and hand movement is ultimately controlled by the brain, a portion of these neural differences was related to the production of the context-dependent MFs. However, a portion of the neural differences could not be accounted for by a linear relation to MFs, and thus constituted explicit encoding of the object context. This object context encoding manifested as differentiation in neural activity which was larger than what would be expected if neural activity in the frontoparietal grasp network was simply and linearly related to the production of movements and muscle activity. The encoding of object presence or absence was found to be large in magnitude in all brain areas. The encoding of perceived and learned grip affordance differences in the Grip Affordance Experiment was found to be moderate in all brain areas. The encoding of learned use affordance in the Use Affordance Experiment was found to be negligible in M1 and AIP, but prominent in PMV.

Different linear encoding models were built and fit to investigate the structure of object context encoding in individual units. These models fit FRs of individual units to only linear combinations of MFs or could also contain indicator variables denoting the object context, and interaction terms between indicator variables and MFs. Evaluation of these models

revealed that object contextual factors were often encoded directly in individual unit FRs or in an interactive manner with MFs. This implies that the linear relationship between neural activity and MFs changed depending on the object context. Interactive context encoding was most prevalent for object presence encoding, but was also found for encoding of perceived and learned grip affordances and learned use affordance.

This interactive context encoding has important implications for the design of BCI-controlled neuroprosthetic systems. To be useful, these systems must ultimately allow users to command movements of the neuroprosthesis in a wide array of possible situations. This requires that neural decoders be able to accurately decode movement intentions in different contexts. Object presence encoding was found to have a particularly detrimental impact on MF decoding from M1 neural activity, as training a decoder with the object present resulted in poor performance when decoding movements made when the object was absent, and vice-versa. A multi-layer decoder scheme in which context-specific decoders were layered with an object presence classifier was found to increase decoder performance using data from M1 alone. Contextual changes in object identity (grip affordances and learned use affordances) did not have substantial impact on decoder performance, likely due to the smaller sizes of these effects overall.

The context-related changes in behavior and neural activity were analyzed to determine if they carried information about object affordances. When an object was present, behavior and neural activity during preparation and early movement were biased toward the behavior and neural activity associated with the grasps afforded by that object, even when it was not actually grasped. When a perceived or learned grip affordance was present, background neural activity in M1 was found to be weakly biased toward neural activity associated with the afforded grip. When an object with a known use affordance was grasped, behavior and neural activity was biased toward the behavior and neural activity associated with the use of that object, even when it was not actually used. These effects are consistent with the hypothesis that when object affordances in the environment are perceived, they are automatically processed in dorsal stream brain areas and the associated motor representations are activated, though other interpretations are possible.

Some evidence was found that object related contextual information was first processed in AIP and PMV, and subsequently transmitted to M1. These "higher order" brain areas contained units which were strongly modulated by object contextual factors to an extent that was not observed in M1. Object Presence in particular was found to be a strong driver of PMV and AIP neural activity, especially in the preparatory period. Learned use affordance difference was encoded very strongly in PMV, but not M1 or AIP, suggesting that PMV is preferentially involved in the storage and processing of object use knowledge. The relative timecourses of object context related neural modulation in M1, PMV and AIP is consistent with a sequential organization in which context-related information flows from AIP to PMV to M1.

Interpretation of Context-Dependent MF Differences

The context-related behavioral differences were possible because task requirements could be achieved with a range of possible behaviors. For example, in the reach conditions of the Object Presence Experiment, subjects were rewarded as long as the mean hand position entered the initial 3 cm target sphere and remained within the subsequent 6 cm hold sphere in space. The hand and arm posture were unconstrained, as long as the mean hand position requirements were met. For the grasping conditions in all experiments, hand posture, arm position and muscle activity were similarly unconstrained, as long as the required force sensors of the objects were activated.

Many of the context-dependent differences in MFs were small, especially in the Grip Affordance Experiment and Use Affordance Experiment pre-learning session, and were likely only detected due to the high trial counts obtained in the experiments.

There are many possible reasons for the behavioral differences observed in the different object contexts of the three experiments. One potential explanation is that behavior reflected pragmatic solutions in certain situations. For example, the hand was lifted slightly higher when compound objects were grasped with a power grasp compared to when simple objects were grasped with a power grasp. This may have reflected the monkeys actively avoiding

the pinch grasp tab portion of the compound objects, leaving a larger margin of error so that they did not accidentally contact it during the reach. Behavioral differences for reaches with and without the object present may have also reflected object avoidance.

The object presence related differences in reach behavior could have resulted from different feedback control strategies employed in the two reaches. For both types of reaches, the feedback circle displayed on the monitor in front of the subjects provided information about the proximity of the hand to the target sphere. However, when the object was present, it provided an additional spatial cue as to the location of the reach target sphere. When the object was present, the subjects could control their reach using both visual feedback from the feedback monitor and visual perception of the distance between the hand and the object.

Behavioral differences could have also reflected implicit preparation for potential actions afforded by the objects. This was most evident in the Use Affordance Experiment, where the movable object was grasped as if it would be lifted, even in trials when it was not required to be lifted. Since the entire movement sequence was cued at the start of the trial, subjects presumably knew they would not have to lift the object, and yet still behaved as though they were ready to do so. Such preparation of possible actions could be advantageous in a naturalistic setting, where behavior is controlled flexibly in real time in response to a continuous flow of sensory input and internal drives, as opposed to a constrained laboratory setting where behavior is dictated and highly controlled.

Pragmatic explanations are more difficult to apply to other observed contextual differences in MFs. For instances, in the pre-learning session of the Use Affordance Experiment, objects differed substantially only in their color. Yet, small but significant differences in MFs were observed for grasps on the two objects. Such color-dependent changes in grasp behavior has been observed in humans, and could be related to the color of the object causing it to be perceived as larger or smaller than it actually was [377].

Alternatively, the context-related differences in behavior may not have been related to any specific aspect of the task, but may instead have been signatures of the neural encoding of contextual differences. This possibility is further discussed below.

Interpretation of Context-Dependent Differences in Neural Activity

Many of the context-dependent changes in neural activity were small relative to underlying neural variability, especially in the grip affordance experiment and Use Affordance Experiment pre-learning session, and were likely only detected due to the high trial counts obtained in the experiments.

In some cases, contextual object differences pragmatically required different movements. Some of the neural differences observed in different object contexts could thus have been related to the direct control of these different movements.

Neural differences for reaches in the presence or absence of an object may have been related to the differences in visual feedback in the two conditions. The visual perception of the hand relative to the object provided an additional source of feedback for targeting the reach. AIP and PMV in particular have been implicated in visually guided control of movement [218, 238, 440] and M1 activity has been found to change for different visual feedback conditions [406].

Neural activity may also have reflected explicit encoding of object context. Evidence for such context encoding was found in the current data; neural activity was sometimes markedly different for very similar behaviors. Such differences in neural activity are possible because of the redundancy in the cortical motor system. Grasp-related cortical areas contain many millions of neurons, while the hand is controlled by tens of muscles. Additionally, projections from cortex to the spinal cord are complex; each corticospinal neuron projects to multiple sites in the spinal cord and each motoneuron receives input from many different cortical and spinal neurons. Because of this multiplicity in the nervous system, the mapping from neural activity to behavior is not one-to-one but many-to-one; multiple different patterns of neural activity can generate similar movements.

There are several reasons why having separate neural representations of similar movements made in different contexts could be advantageous. Naturalistic grasping behavior is extremely flexible and very similar grasping actions can be followed by different subsequent behavior (for example grasping a hammer to pound nails vs. grasping a screwdriver to twist screws). Neurally distinct representations of the initial motor acts

could facilitate generation of different subsequent behavioral sequences. Similarly, distinct representations of similar grasping actions made on different objects could allow for subsequent modification of one representation while leaving the other intact.

Thus, context encoding may constitute a neural strategy for optimally satisfying a mixture of immediate and more abstract goals. The motor cortical neural activity patterns for two similar behaviors made in different contexts are constrained by the fact that they must lead to the production of successful immediate behavior. Due to the redundancy of the motor system, this immediate behavioral goal does not fully constrain neural activity, and additional context-related changes in neural activity may satisfy other less immediate goals such as the implicit preparation of potential actions that are known to be rewarding, or more abstract goals such as maximizing separation between neural representations to maintain the potential for flexible behavior in unknown future circumstances.

Special Role of PMV in Encoding Learned Use Affordance

In the Use Affordance Experiment post-learning session, the only areas that robustly encoded learned use affordance were left and right hemisphere PMV in Monkey T. This use affordance encoding was restricted to conditions in which the objects were grasped with a power grasp, which was the grip type associated with the learned use of the movable object. These effects appeared only in the post-learning session, and thus coincided with the learning of the lifting affordance for the movable object. While significant neural differences for the same grasping behaviors performed on the two objects were found in M1 and AIP, these differences were largely accounted for by linear relation to MFs. In contrast, the encoding of use affordance context in PMV was large and exceeded what could be expected from MF encoding, especially in left hemisphere PMV.

The finding of strong use affordance encoding only in PMV may reflect the unique cortical connectivity of PMV. PMV is strongly interconnected with prefrontal cortical areas such as area 46 [202–204, 206]. These prefrontal areas may be involved in linking arbitrary contextual sensory cues to objects in order to produce appropriate learned

behaviors [441–443]. Learning the new use of the movable object entailed linking its color to the relatively abstract knowledge that it could be manipulated in a certain way. Thus PMV may constitute the node in the frontoparietal grasp network in which contextual sensory information is linked to stored object use knowledge.

PMV has been theorized to consist of multiple different sub-areas with distinct cortical connectivity [253] and cytoarchitecture [204, 252]. F5a, which is located more laterally in the bank of the arcuate sulcus, is thought to be related more to sensory information and cognitive processing, while F5p, which is located more medially in the bank of the arcuate sulcus, is thought to be more directly related to movement [116,163,228,251]. Based on these distinctions, one might hypothesize that object use affordance encoding would preferentially occur in F5a.

The current results show mixed support for this hypothesis. In left hemisphere PMV, the area that displayed the strongest use affordance encoding, neurons were only recorded from F5p. The array which corresponded with F5a was damaged during surgery and thus the two regions could not be compared in left hemisphere PMV. This suggests that F5p also participates in more cognitive, abstract processing. However, in right hemisphere PMV, all of the individual units which significantly encoded use affordance were recorded on the lateral array, corresponding with F5a. The array in F5p of the right hemisphere featured no use affordance encoding units. Thus, results from right hemisphere PMV do support the cognitive-motor distinction between F5a and F5p.

Interpretation of Affordance Shift Analyses

In the Object Presence Experiment, it was found that when the object was present, behavior and neural activity were biased toward the behavior and neural activity associated with grasps afforded by the object. In the Use Affordance Experiment, behavior and neural activity for trials in which the movable object was grasped and held were similar to behavior and neural activity observed on trials when that object was actually lifted, relative to grasps on the fixed object. In the Grip Affordance Experiment, background neural activity in M1

for conditions where a perceived or learned grip affordance was present was weakly biased toward trials in which that affordance was actually utilized.

These findings support the hypothesis that affordances in the environment are automatically processed in the motor system. This can be interpreted as implicit preparation for afforded potential behaviors. Such automatic preparation would likely be advantageous in naturalistic settings where behavior must be generated rapidly based on sensory cues. Automatic activation of afforded action representations is also supported by human behavioral and brain imaging research (see Section 2.5.2).

Interestingly, for the Object Presence and Use Affordance Experiments, the affordance shifts in the null space neural activity were only present during the movement period and disappeared during the target hold phase. This suggests that object affordances may have only been processed when they were potentially relevant for action, during hand approach toward the object. These effects could also be related to the differential control of movement and posture in the motor system [407], differential relation of neural activity to movement over the course of grasping movements [419] or the fact that somatosensory touch feedback information influenced M1 after object contact.

Also notable was that the affordance shift observed during the preparatory period of the Use Affordance Experiment transiently decreased after the cue was presented informing the subject if the object was required to be lifted or simply held on that trial. This transient decrease occurred sequentially in AIP, PMV and M1. The tight linkage of this transient modulation to the onset of the use cue further implies that this shift in neural activity was related to the learned use affordance of the object.

The observed biases in behavior and neural activity could be interpreted in other ways. In the object presence experiment, the similarity of neural activity and behavior during trials in which the object was present may have reflected that the hand was visually controlled in relation to the object during conditions in which it was present, but the hand was controlled using memory and the abstract feedback display when the object was absent. In the Use Affordance Experiment, the subject may have simply habitually learned to grasp the movable object differently, and this was reflected in behavior and neural activity. Finally, the effects could have represented explicit, rather than implicit

preparation of afforded movements. Subjects may have been intentionally preparing movements that were not necessary on certain trials. However, this explanation is unlikely, as spurious lifts of the movable object on hold trials and spurious grasps of the object on object reach trials were rare.

Differences in the Methods for Identifying Object Context Encoding

Three different methods, the extralinear modulation analysis, the direct/interactive context encoding model fitting analysis and the null space analysis, were employed to identify object context encoding, defined as object context related modulations in neural activity that exceeded the amount that could be accounted for by linear relation MFs. These methods were employed in order to determine what amount of neural difference in different contexts actually corresponded to the contextual difference, rather than behavioral differences in the two contexts. Many extant studies which purport to find neural differences related to context (e.g. [239–241, 351, 421, 425, 426]) did not monitor the behavior in detail and are thus unable to make such a distinction.

Two of these methods, the extralinear modulation analysis and the direct/interactive context encoding model fitting analysis, operated from an encoding perspective in that individual unit FRs were fit with linear MF encoding models. The third, the null space analysis, operated from a decoding perspective in that combinations of MFs were fit by combinations of unit FRs. These methods differed in their ability to identify signatures of neural activity that was unrelated to movement.

In the extralinear modulation analysis, MF encoding models were fit to individual unit FRs and the structure of the residuals was analyzed to determine if the separation between certain pairs of conditions was not fully captured by the MF encoding models. This evaluation could be performed on a single unit basis or on a population level by combining across units. As each individual unit was fit separately, this allowed for each unit's idiosyncratic representation of movement features to be subtracted away. As the entirety of a unit's relation to MFs was captured with a single model, this method was likely

unreliable at specific timepoints and for specific conditions, but on average was able to identify large fluctuations in neural activity that were beyond what would be expected by linear relation to MFs, and was likely thus a conservative measure.

The direct/interactive model fitting analysis also involved fitting encoding models to individual unit FRs. Three types of models were tested; ones that fit neural activity using only combinations of MFs, ones that featured indicator variables denoting object context, or ones that featured indicator variables and indicator variable-MF interaction terms. The model fits were evaluated and selected based on BIC. This method was found to be highly sensitive. Often, more complex models were selected even when they produced only marginal increases in R^2. Context label shuffle controls showed that these models would often spuriously identify direct context encoding, but identification of interactive context encoding was more likely to reflect a real effect. However, as evidenced by the angular distances between context-specific tuning coefficient vectors, small interactive effects were sometimes identified as significant, especially in the Grip Affordance Experiment and Use Affordance Experiment.

For the null space analysis, combinations of MFs were fit by combinations of FRs. This model allowed only coordinated patterns of neural activity to be related to MFs, and thus was unlikely to account for the idiosyncratic ways in which individual units related to MFs. Thus, "null space" neural activity likely still contained neural variability that was actually representative of MF differences. This is reflected by the fact that the power grasp vs. pinch grasp comparisons generated high null space variance. In addition, the null space analysis used trial-averaged data and thus was unable to utilize the trial-to-trial variability in MFs and neural activity to better estimate the neural relation to MFs.

As the extralinear modulation analysis was found to be conservative, yet still able to capture each individual unit's activity patterns to isolate MF-related and context-related neural activity, it was selected as the main measure used to identify the presence of context encoding.

The ability of the extralinear analysis to account for movement related activity is evidenced by the finding that only very low extralinear modulation was found for the power grasp vs. pinch grasp comparison. The extralinear modulation for these condition

pairs, which featured large movement differences and evoked large neural differences, were only above chance levels in Monkey R M1 and Monkey T right hemisphere PMV. These areas had very strong preparatory activity as well as strong movement tuning, and thus the preparatory was likely correctly identified as extralinear modulation.

All of these methods relied on fitting single models across all of the available data to estimate neural relation to MFs. Thus, the performance of each method would likely improve if applied over a greater range of behavior and neural activity across more varied movements.

Context Encoding vs. Non-Linear MF Encoding

The findings of the context encoding analyses were interpreted as revealing linear encoding of MFs concurrent with encoding of contextual factors. An alternative interpretation of these findings is that non-linear MF encoding was present. This could be described as a mapping where certain local regions in neural state space all map to similar MFs, and other regions that are relatively close in neural state space map to different MFs. The two descriptions are not incompatible. Context encoding describes differences in neural activity as encoding both MFs and additional cognitive factors, while non-linear MF encoding describes neural activity as only relating to MFs, albeit in a non-linear, complex way. It could be that one interpretation is more conducive to construction of BCI neural decoders and to understanding neural activity in general. Further experimentation and close examination of such effects across a wide range of behaviors will be necessary to determine this. Preliminary examination of non-linear MF encoding was performed by fitting simple non-linear models (see Section 8.2).

Interactive Context Encoding vs. Transient Direct Context Encoding

The finding that units were often best fit by models with context indicator variable and MF interaction terms was interpreted as meaning that the relation between neural activity and MFs can change across contexts. This interpretation is backed up by findings that even corticomotoneurons are flexible in their influence on their targeted muscles across contexts [52, 378, 379, 411] (see Section 2.7 for discussion of contextual changes in the relation of neural activity to movement). Based on the angular distances between MF tuning coefficient vectors, these MF tuning changes were moderate in the Object Presence Experiment and small in the Grip Affordance Experiment and Use Affordance Experiment.

However, given the structure of the task, these findings could also reflect transient direct context encoding. In the three experiments of this dissertation, often only a single action was performed in each context. Thus, MFs were very consistent for that context. A transient direct encoding of context would manifest as a change in neural activity during only one part of that behavior. As the MFs during that part of the behavior were very consistent, this would be mathematically equivalent to observing a change in the neural correlation with behavior at that time. These two potential encoding schemes could be disambiguated by evoking a wider range of behavior in each context.

Context-Detecting MF Decoder

In the Object Presence Experiment, decoding analyses revealed that the object presence encoding effect, if unaccounted for, had a detrimental impact on the ability to accurately decode MFs across contexts. To address this problem, a multi-layer decoder architecture was proposed and tested. This method used an object presence classifier to appropriately combine the output from two context-specific decoders trained separately in each context. These results suggest that contextual factors, especially object presence, will need to be accounted for by neural decoders, and that such accounting can be achieved with modified decoder implementation.

Similar context-detecting decoders have been found to be useful in other decoding situations. Classification of movement state vs. rest state to gate a kinematic decoder has been found to greatly decrease instances of spurious unintended movement decoding during rest periods [166, 169, 403]. When decoding monkey locomotion, decoding improved when separate decoders were constructed for forward and backward walking and appropriately switched between [161]. Non-linear combinations of local linear decoders were found to perform better than single fixed linear decoders, and approached the performance of fully nonlinear decoders for decoding hand position [164].

Interpretation of Context Encoding in a Dynamical Systems Framework

Recently, it has been proposed that M1 may be best described as a dynamical system which generates patterns that are appropriate for driving muscle activity [126]. Based on this dynamical systems perspective, M1 activity has been found to have relatively high "divergence" compared to supplementary motor area in a study by Russo et al [444]. This means that in M1, similar initial neural activity patterns can lead to multiple different subsequent activity patterns. Conversely, low divergence was observed in supplementary motor area, in that separate patterns of neural activity were typically preceded by distinct patterns of neural activity. The authors suggest that this low divergence in supplementary motor area is related to the monitoring of the representation of the task-related contextual factor of how much time has elapsed.

The context encoding observed in this dissertation can be interpreted as lowering the divergence in M1 neural activity. The effect of context encoding was to separate neural activity patterns for similar movements made in different contexts. This may facilitate the subsequent generation of distinct movement patterns.

8.2 Additional Controls

The neural, kinematic and EMG data used for analyses were resampled at 20 Hz and smoothed with a 30 ms width Gaussian kernel. Analyses were repeated over a range of different resampling frequencies and smoothing kernels. In all cases, results did not qualitatively change.

Significant differences in mean FRs of individual units were identified using permutation tests. Other methods were tried, such as the t-test and the Mann-Whitney U test. Very similar results were obtained in all cases.

For the MF PC inter-condition distances, FR PC inter-condition distances and extralinear modulation, significance was determined by the observed value significantly exceeding overall estimated within-condition variability. This within-condition variability was estimated over all conditions in each experiment. Permutation tests were applied as an alternative measure of significance for these calculated statistics. The permutation tests resulted in somewhat higher frequency of identification of significant differences. As the within-condition variability comparison was found to be more conservative and more interpretable, it was chosen as the main analysis used in the presentation of the results.

As noted in the results of the Object Presence Experiment, some of the object presence effect may have been related to inclusion of grasp trials in the context of "object present." Thus, encoding model analyses and decoding analyses were repeated using only reach trials, excluding grasp trials. The object presence encoding effect was still observed in these analyses (Sections 4.5 and 4.6).

Several analyses required fitting encoding models by regressing unit FRs on MF PC scores. Though MF PCs explaining 99% of MF variance were used, there could have been additional meaningful information in the higher order MF dimensions. To test this possibility, encoding models were also fit using the full set of MF PCs capturing all of the recorded MF variance. Results were almost identical when using the full vs. 99% MF PC space.

Neuronal spike counts are often observed to have Poisson-like statistics. As such, linear models may theoretically be better estimated by using square root transformed FRs as the

regressands, as the noise will be more normally distributed [445]. To test this, encoding model analyses were repeated using square root transformed FRs. All results were found to be qualitatively similar to those obtained when using standard FRs.

The encoding models were built using MFs that were lagged at a constant 40 ms relative to FRs. This single value was chosen for it's simplicity and applicability across MFs and brain areas. Performing the model fits using MF data at a range of different lags, or calculating optimal lags for each MF, did not qualitatively change any of the findings of the analyses.

Neural activity may have reflected non-linear tuning to MFs as opposed to encoding of object context. As a cursory test of such a possibility, simple non-linear MF encoding models were tested which featured additional squared or cubed MF terms. While these models did improve overall model fits, FRs were still most often better fit by models which included these non-linear terms *and* object context information, suggesting that the object context encoding effects were robust.

Recent studies have suggested that the relation between M1 neural activity and MFs may change over the different phases of a movement [405, 419, 446]. Thus, the extralinear modulation observed for contextual differences may have been partially related to unaccounted for temporal changes in tuning. To test this possibility, encoding models were fit which allowed coefficients to change across four periods of the task; the pre-movement/reach initiation phase, the mid-reach phase, the target contact phase and the target hold phase. While these models did improve fits, context encoding was still detected at similar levels to those obtained with single fixed linear encoding models.

The direct/interactive context encoding model fit analyses used BIC as a measure to select the best model based on model likelihood estimates. To determine whether this model selection likely identified actual object context encoding effects as opposed to spurious effects resulting from arbitrarily dividing the data into partitions, the model fit analyses were repeated while shuffling the object context labels across trials. Several different shuffling strategies were tried to determine the effect of subdividing the data in different ways. Shuffling the trial labels randomly resulted in some spurious identification of direct context encoding, but rare spurious identification of interactive context encoding. These shuffles are presented in Figures 4.30, 4.31, 5.28, 6.31 and 7.12. Shuffling the trial

labels in a manner linked to time over the course of the session resulted in somewhat higher incidence of spurious context encoding identification. Labeling the first halves of each block as one context and the second halves of each block as the other context resulted in higher spurious identification of direct context encoding, but not interactive context encoding. Labeling the first half of each session as one context and the second half as the other context resulted in a much higher incidence of spurious identification of both direct and interactive context encoding. This further justifies the use of the balanced block presentation schedule (see Section 3.2.1), which was designed to avoid such effects. Thus, some of the identified direct and interactive object context encoding may have been spurious, but likely predominately reflected actual encoding of context information.

8.3 Limitations

The experiments and analyses performed for this dissertation were limited in several important ways.

First, the experiments involved relatively low numbers of conditions presented in blocks. This design was consciously chosen in order to obtain very high trial counts in each condition. As the context-dependent effects were expected to be small in size, maximizing the trial count allowed greater statistical power to accurately identify and characterize small but significant effects.

However, the presentation of the task conditions in blocks had several disadvantages. Differences in behavior and neural activity observed between blocks may have reflected temporal drift in relevant factors such as alertness, motivation and thirst. The blocks were presented in a balanced fashion to attempt to compensate for such drifts, but nevertheless they could have affected the results.

It is also possible that the kinematic markers and EMG electrodes may have slightly shifted position between blocks. The balanced block presentation schedule would lessen the impact of such drift in kinematic and EMG monitoring. Similarly, micromotion of the arrays in the brain could result in changes in the neural signal over time. To address this

potentiality, neural signals were carefully examined during off-line sorting for evidence of temporal drift, and were excluded if the magnitude of the recorded spikes became so low that they were not reliably recorded.

In many studies of grasp related neural activity, especially in AIP, objects were changed randomly in a darkened room and presented by illuminating the object at the start of the trial. This allows study of the initial visual perception of the object (e.g. [116,225,279]). Such an object presentation strategy would likely have been ineffectual in the current experiments given that the object remained the same throughout the task presentation bock, so the subject would already know what object was in the workspace. Given that the objects were presented in blocks, and that we were more interested in studying effects during movement, such visual presentation of objects was not utilized.

The analyses of PMV and AIP neural activity were limited by low unit yields, especially in AIP. This was partially due to limitations of the novel array alignment and insertion procedure utilized to implant PMV and AIP. Many of these limitations were addressed between the first and second implant procedures (see Section A.1.2.7).

The low number of conditions in each experiment limited the interpretability of certain analyses. For example, as noted in Section 8.1, interactive context encoding could not be disambiguated from transient direct context encoding. Additionally, encoding models relating neural activity to MFs likely suffered from overfitting of the limited and stereotyped behaviors in the experiments. This was especially apparent for the decoding analysis of reach trials only in Section 4.6. In that case, the performance of context-specific decoders and the single fixed linear decoder may have reflected overfitting of the similar but consistently different reaching behaviors observed for the reaches with and without an object present.

To produce the results presented in this dissertation, only a single session was analyzed from each subject in each experiment. This was done to avoid the potential influence of day-to-day fluctuations in neural activity and to compare neural activity and behavior directly recorded in the same experiment to ensure that findings of differences in different task conditions were robust. Additionally, processing of the kinematic data was highly labor intensive and thus obtaining accurate kinematic tracking in multiple sessions was not possible given time constraints.

Context encoding effects were defined as neural activity that was unexplained by linear relation to movement features. However, this analysis was naturally limited by which movement features were recorded. While we attempted to record a wide range of kinematics of the arm and hand, the recording of EMG was limited by the nature of surface EMG recordings and by the relatively low channel count (eight) compared to the number of muscles involved in reaching and grasping behaviors (over 40). Thus, it is possible that some of the neural variability that was identified as encoding of object context may have reflected differences in unrecorded movement features, such as the intrinsic hand muscles. It is also possible that this excessive neural variability encoded aspects of the movement features that were not considered (e.g. higher-order kinematic terms such as acceleration and jerk).

The Object Presence Experiment was designed to reproduce and elaborate on recent human BCI studies [119, 410]. In these studies, paralyzed humans attempted to grasp an object, or attempted to pantomime grasp movements in empty space. In the current experiments, the kinematic tracking system was incapable of accurately tracking the finger joint angles in real time. This limitation, combined with the limited cognitive abilities of macaques, meant that the subjects could not be trained to perform realistic pantomimed grasping movements. Subjects could only be trained to perform reaches with or without an object present. Thus, only indirect comparisons to the human studies are possible.

The force sensors used to instrument the objects were relatively low-cost, consumer grade sensors. They were found to give slightly inconsistent readings. Thus they were inappropriate for accurately measuring the actual grip forces exerted on the objects. Additionally, the object dimensions may have differed slightly between different objects, causing the force sensitivity to be different for different objects. To accomodate these limitations, the grasp force thresholds were set at very low values and the objects were adjusted so that even the slightest touch of the object caused the force threshold to be greatly exceeded. It was assumed that objects were grasped with approximately the same force. However, there may have been differences in the grip forces exerted on objects that could not be accurately assessed and accounted for. This would have only affected the results of the Use Affordance Experiment, as that was the only experiment where two distinct objects were grapsed.

The objects used in the experiments were manufactured using 3D printing and CNC manufacturing techniques. This resulted in very consistent objects, but nevertheless very small variations in object dimensions across objects may have existed. This would have affected only results from the Use Affordance Experiment, in which two physically distinct objects were grasped.

8.4 Future Directions

The experiments of this dissertation were designed to examine very specific effects, and were thus quite limited, as discussed in the previous section. Future experiments could expand the findings of these studies in numerous ways.

There are many additional ways in which object context could be varied. Objects could be linked to greater or lesser reward values, or could differ in weight or texture. An object could be learned to be used as a tool, as opposed to simply being manipulated, as in the Use Affordance Experiment. Tool use learning has been shown to evoke broad structural [26–28] and functional [24, 25, 29] changes in grasp-related cortical areas. It is likely that tool use knowledge would also be encoded as a contextual factor in the frontoparietal grasp network even when the tool is simply grasped and not used.

The portion of M1 that was recorded for these experiments was located on the convexity of the precentral gyrus. However, most of the corticomotoneurons of M1 are located in the bank of the central sulcus [49]. Thus, neural activity in the bank of the central sulcus may be even more closely related to behavior. It would be illuminating to determine whether contextual encoding signals could also be identified in this sulcal M1.

For various reasons, the unit yields obtained in PMV and AIP were limited in the current experiments. This limited the potential analyses of neural activity in these areas. Simultaneous recording of a greater number of units in these areas using denser microelectrode arrays could enable more interesting analyses. The information flow between AIP, PMV and M1 could be characterized in greater detail, with methods such as communication subspace identification using reduced rank regression [447].

Context encoding effects could be characterized in much greater detail with a larger number of different of trial conditions within each context. The current experiments often included only a single trial condition in each context. Presenting the different objects at multiple spatial locations and requiring reaches to multiple spatial locations with no object present would help elucidate the interaction between object context and reach kinematic encoding. Additionally, observing a consistent contextual effect in multiple behaviors performed in two different context would more robustly verify the presence of context encoding. Additionally, decoding analyses would be more robust and applicable to actual BCI design.

In the current experiments, object context effects were mostly studied during movement. However, AIP and PMV and known to contain visually responsive neurons. Presentation of objects by rapid illumination, passively viewing objects without acting and tracking eye gaze would allow the possible identification of object context effects in visual activity in these areas.

PMV and the inferior parietal lobule are known to contain mirror neurons which encode both performed and observed grasping actions. While cursory investigations were able to identify some mirror neuron activity in PMV and AIP (data not shown), mirror neuron activity was not studied in detail. Future experiments in which subjects both observe and perform actions in different object contexts could determine of object context encoding occurs also in mirror neuron activity.

8.5 Conclusion

The data presented herein reveal that reaching and grasping behavior and neural activity in the frontoparietal grasp network are significantly influenced by object affordance related contextual factors. Three experiments were designed to study behavioral and neural changes due to the contextual factors of object presence and object identity, in terms of perceived and learned grip affordances and learned use affordances. Reaching and grasping kinematics and EMG differed significantly when movements with the same requirements were performed in

different object contexts. These behavioral differences were accompanied by proportionately larger differences in neural activity in M1, PMV and AIP. Neural differences related to object presence and grip affordances often exceeded what could be accounted for by linear relation to movement features, and thus constituted explicit object context encoding. Encoding of learned use affordance was found only in PMV, suggesting a special role for PMV in processing object use knowledge. These effects, especially as related to object presence, have implications for neuroprosthetic decoding across different contexts. When an object was acted upon, behavior and neural activity was biased toward the behavior and neural activity associated with the actions afforded by the object, even when those actions were not actually performed. This suggests that grip and use affordances may be automatically processed and implicitly prepared in the frontoparietal grasp network. We posit that the encoding of object context exploits the redundancy in the cortical motor system to separate the representations of similar movements made in different contexts, facilitating greater flexibility in grasp and object use behavior.

Appendix — Detailed Methods

This appendix contains detailed descriptions of the experimental methods employed in the course of this dissertation work. Section A.1 describes the surgical implantation of the two types of microelectrode arrays used to record neural data, with Section A.1.1 describing the implantation of Utah arrays in M1, and Section A.1.2 describing the novel method that was devised for positioning and implanting FMAs in PMV and AIP. Section A.2 describes the design and fabrication of the various graspable objects used in the experiments. Section A.3 describes the behavioral training procedures used to achieve the high levels of performance observed in the behavioral tasks. Section A.4 describes the data acquisition and preprocessing steps for each of the data streams (Sections A.4.1 – A.4.4), and describes the alignment and resampling procedures used to synchronize the data streams (Section A.4.5). Section A.4.6 describes the data structures that were used for subsequent statistical analyses. Section A.5 describes the modular software used to control the task in real time. Section A.6 contains descriptions of the statistical methods employed in producing the results in Chapters 4–7.

All surgical procedures, animal training and care were performed under the auspices, guidelines and requirements of the University of Pittsburgh Institutional Animal Care and Use Committee (IACUC) and the United States Food and Drug Administration (FDA). Animal care and some surgical procedures were performed with assistance from the University of Pittsburgh Department of Labaratory Animal Resources (DLAR).

A.1 Surgical Methods

The following procedure was used for all microelectrode array implant surgeries. All surgeries were performed in asceptic conditions with sterilized equipment. Anesthesia was initially induced with ketamine HCl (15 mg/kg IM) delivered in the home cage. Before surgery, the monkey was administered glycopyrrolate (0.004 mg/kg IM) to reduce salivation,

cefazolin (25 mg/kg IM) as a prophylactic antibiotic, and dexamethasone (0.2 mg/kg IM) to reduce brain swelling. The head and lower hindlimbs were then shaved before transporting the animal to the surgical suite.

Upon arrival in the operating room, the subject was induced into a deeper anesthetic state by administering 3–5% isoflurane through a snout mask. The subject was then intubated and ventilation was initiated while confirming proper placement of the endotracheal tube using a stethoscope. Anesthesia was maintained with 2–3% isoflurane throughout the procedure. Vital signs were monitored via a pulse oximeter placed on the subject's hand and a rectal thermometer. A hot water pad and warm air blower were used to maintain healthy body temperature. An intravenous drip was placed in the hindlimb to provide dextrose saline throughout the procedure at a rate of one drop per 10 seconds.

The monkey's head was placed in a stereotaxic frame (Kopf Instruments, Tujunga, CA). The scalp, ears, ear bars and stereotaxic frame were disinfected with iodine and isopropyl alcohol. Sterile drapes were placed over the head and body with a window cut out over the scalp.

A large incision was made in the scalp over the hemisphere of interest. Cranial muscles were retracted, and the underlying skull scraped clean. A craniotomy was then opened over the targeted cortical areas, based on a standardized offset from the centerline and ear bars in the cases of Monkey I and Monkey R, or based on measurements from the MRI image in Monkey T (Section A.1.2). A durotomy was performed to reveal the cortical surface over the desired areas.

Microelectrode arrays were then implanted in the cortex. Monkey I was implanted with one Utah Array (Blackrock Microsystems, Salt Lake City, UT) in M1. Monkey R was implanted with two Utah arrays in M1. Each hemisphere of Monkey T was implanted with one Utah Array in M1 and four FMAs (Microprobes for Life Science, Gaithersburg, MD) with two of the FMAs in PMV and two in AIP. The two hemispheres of Monkey T were implanted in two separate surgeries six months apart. Utah Array implantation procedures are described in Section A.1.1 and FMA planning and implantation procedures are described in Section A.1.2.

After array insertion, artificial dura was placed over the arrays and tucked under the dural margins. The dura was then sutured closed over the artificial dura. The bone flap was thinned using a surgical drill so as not to apply pressure to the arrays, then placed over the craniotomy and secured in place with titanium bone straps and bone screws. The margins around the bone flap were filled with bone dust collected during the initial craniotomy. The skin was then sutured closed.

The subject was then removed from the stereotaxic frame, extubated and taken off of the intravenous drip. Immediately post-procedure, subjects were administered buprenorphine (0.01 mg/kg IM) for analgesia, cefazolin (25 mg/kg IM) as an antibiotic and dexamethasone (0.2 mg/kg IM) to continue to reduce brain swelling. Subjects were then returned to the home cage and monitored until alert and receptive to food and water. All subjects recovered to full alertness in one to two hours. Monkeys I and R recovered full function immediately, while Monkey T displayed temporary weakness in the limbs contralateral to the implanted hemisphere, which resolved after about one week in both cases.

Following each major surgery, subjects were administered buprenorphine (0.01 mg/kg IM) twice daily for three days, cefazolin (25 mg/kg IM) twice daily for seven days and dexamethasone (0.2–0.07 mg/kg IM, decreasing dose) twice daily for seven days. The suture margins around the skin implants were cleaned regularly and monitored for any sign of infection.

A.1.1 Utah Arrays

Utah Arrays were purchased from Blackrock Microsystems. All Utah Arrays were placed in M1 and were configured as a standard 10 by 10 square of 1.5 mm platinum-tipped electrodes spaced 400 µm apart (96 recording electrodes). Monkey I received one array in left hemisphere M1, Monkey R received two arrays in left hemisphere M1, and Monkey T received one array in left hemisphere M1 and one array in right hemisphere M1 in two separate surgeries. Each Utah Array insertion surgery followed the same general procedure.

After the craniotomy (Section A.1), the connector pedestal was positioned on the skull and secured provisionally with one to two titanium self-drilling bone screws. The wire bundle

was manipulated so as to place the array over the desired cortex with minimal tension, and held in place temporarily with bone wax. Array placement was based on visually identified anatomical landmarks, targeting the M1 hand and arm area on the convexity of the precentral gyrus, at the mediolateral level of the spur of the arcuate sulcus.

Utah Arrays were inserted using the Blackrock Microsystems pneumatic array inserter, with a pulse width setting of 3.0 and insertion pressure setting of 17.5. The inserter was positioned manually over the array using an articulating, locking multi-joint arm (Manfrotto, Ramsey, NJ), and lowered with a manual microdrive (Narishige International, Amityville, NY) until just above the array and perpendicular to the cortical surface. Insertion was carefully timed to coincide with a systolic pulse. The ground wires from the Utah Array pedestals were tucked under the dural margins. After the craniotomy was closed, the pedestals were fully secured with bone screws and bone straps, and all bone wax was removed.

A.1.2 Novel FMA Implant Procedure

The portion of M1 located on the convexity of the precentral gyrus is easily accessible on the cortical surface. Thus, a flat microelectrode array such as the standard Utah Array could be used to record from M1. By contrast, PMV is located in the posterior bank of the lower limb of the arcuate sulcus and AIP is located in the lateral bank of the anterior extent of the intraparietal sulcus. In order to chronically record from these sulcal areas, a microelectrode array with longer and customizable shanks was required.

The Floating Microelectrode Array (FMA), manufactured by Microprobes for Life Science (Gaithersburg, MD), was chosen for this purpose. In order to successfully record from PMV and AIP, the FMAs must be precisely positioned in the cortex relative to sulcal morphology that is not readily visible on the brain surface. Many current solutions for array implant targeting, such as infrared marker motion tracking stereotaxic systems, are prohibitively expensive. Simpler methods such as setting the insertion angle by hand using rotational micromanipulators and assuming the sulci are approximately perpendicular to the brain surface are slow, inaccurate and prone to human error.

In order to accurately and rapidly insert the FMAs at relatively low cost, a novel insertion procedure was devised which utilized structural magnetic resonance imaging (MRI), computer-aided design (CAD) software, computer numeric controlled (CNC) milling and 3D printing. This procedure was used to implant FMAs in both hemispheres of Monkey T in two separate surgeries. The following sections describe components of this procedure: the design of the FMAs (Section A.1.2.1), the computer-aided planning of the FMA implant locations and the design and fabrication of custom inserter aligners (Section A.1.2.2), the FMA insertion surgical procedure (Section A.1.2.3), the implantation results (Section A.1.2.4), the design and fabrication of an FMA connector pedestal (Section A.1.2.5), and the fabrication of a 3D skull model for surgical planning (Section A.1.2.6). The final section contains a discussion of limitations of the method, and design improvements that were made between the two iterations of the procedure (Section A.1.2.7).

A.1.2.1 FMA Electrode Configurations

The FMA is an array of customizable length platinum/iridium microwires bonded into a flat ceramic substrate, which is attached to a flexible, coated gold wire bundle that allows the array to "float" on the cortical surface. Four FMAs were implanted in each hemisphere of Monkey T: two in PMV of each hemisphere and two in AIP of each hemisphere, for a total of eight implants. The left and right hemisphere procedures were performed separately about six months apart.

All implanted FMAs contained four rows of nine electrodes, for a total of 36 shanks, with 400 µm inter-electrode spacing. The lengths of the FMA electrode shanks are shown in Table A1 for "standard" FMAs and Table A2 for the "short" FMA. Standard FMAs were used for all implants except the right hemisphere anterior AIP implant. The "short" FMA was designed in order to conform to the shape of the gray matter in the right hemisphere anterior intraparietal sulcus (see Section A.1.2.7). The electrode lengths were staggered to reduce the number of wires simultaneously penetrating the cortical surface during insertion in order to reduce cortical puckering.

Table A1: **Electrode shank lengths for the standard FMA.** Rows of cells correspond to rows of electrodes on the array. Red-colored electrodes had impedance of 0.01 MΩ, all other electrodes had impedance of 0.5 MΩ.

Electrode Length (mm)								
7.1	6.3	7.1	6.3	7.1	6.3	7.1	6.3	6.0
5.0	4.7	5.5	4.7	5.5	4.7	5.5	4.7	5.5
3.9	3.1	3.9	3.1	3.9	3.1	3.9	3.1	3.0
3.0	1.5	2.3	1.5	2.3	1.5	2.3	1.5	2.3

Table A2: **Electrode shank lengths for the short FMA.** This array was implanted in Monkey T right hemisphere anterior AIP. Rows of cells correspond to rows of electrodes on the array. Red-colored electrodes had impedance of 0.01 MΩ, all other electrodes had impedance of 0.5 MΩ.

Electrode Length (mm)								
5.2	6.2	5.7	6.2	5.7	6.2	5.7	5.2	4.7
4.0	4.7	5.2	4.7	5.2	4.7	5.2	4.7	5.2
3.9	3.1	3.9	3.1	3.9	3.1	3.9	3.1	3.0
3.0	1.5	2.3	1.5	2.3	1.5	2.3	1.5	2.3

A.1.2.2 Array Positioning and Insertion Guide Design

The Utah Arrays could be positioned satisfactorily in M1 by visualizing anatomical landmarks on the cortical surface. The deep sulcal morphology of areas PMV and AIP can not be determined from the visual features of the brain surface alone, and thus accurately implanting FMAs in these areas is more difficult. Other researchers typically insert FMAs by visualizing the cortical surface and attempting to insert the arrays perpendicular to the general curve of the cortical surface in the appropriate region. This is accomplished by positioning the inserter by hand using a rotationally adjustable stereotaxic manipulator arm [personal communications].

As more reliable, precise, rapid placement of the FMAs was desired, a novel FMA positioning procedure was devised and implemented. In summary, 3D information from a structural MRI was imported into CAD software in order to plan the final implanted array location in the cortex. The stereotaxic frame components were also modeled in the CAD software, to obtain the positions and angles of the arrays relative to the stereotaxic bars. Inserter aligners were then modeled and 3D printed which allowed for rapid and reliable alignment of the inserter microdrive along each FMA implantation axis during surgery.

The first step was to obtain a structural MRI of the brain. The subject was sedated with ketamine HCl (15 mg/kg IM), intubated and placed on ventilation. Anesthesia was maintained using 2–3% isoflurane. The subject was then mounted in a plastic MRI-compatible stereotaxic frame, of the same dimensions as the metal frame used during surgery. Scans were performed with an Allegra 3 Tesla MRI scanner (Siemens, Munich, Germany). Three 3D MPRAGE structural series T1 weighted images were combined by taking the arithmetic mean to produce the final image. A coronal view from the resulting image is shown in Figure A1.

The MRI image was then segmented using ITK-SNAP software [448] in order to extract surfaces pertaining to the white matter, gray matter, sulci, skull, and stereotaxic frame ear bars. The results of this segmentation are displayed in Figure A2

3D surface information generated by segmentation of the MRI was exported in .stl format. These surfaces were then imported into the CAD program SolidWorks (Dassault

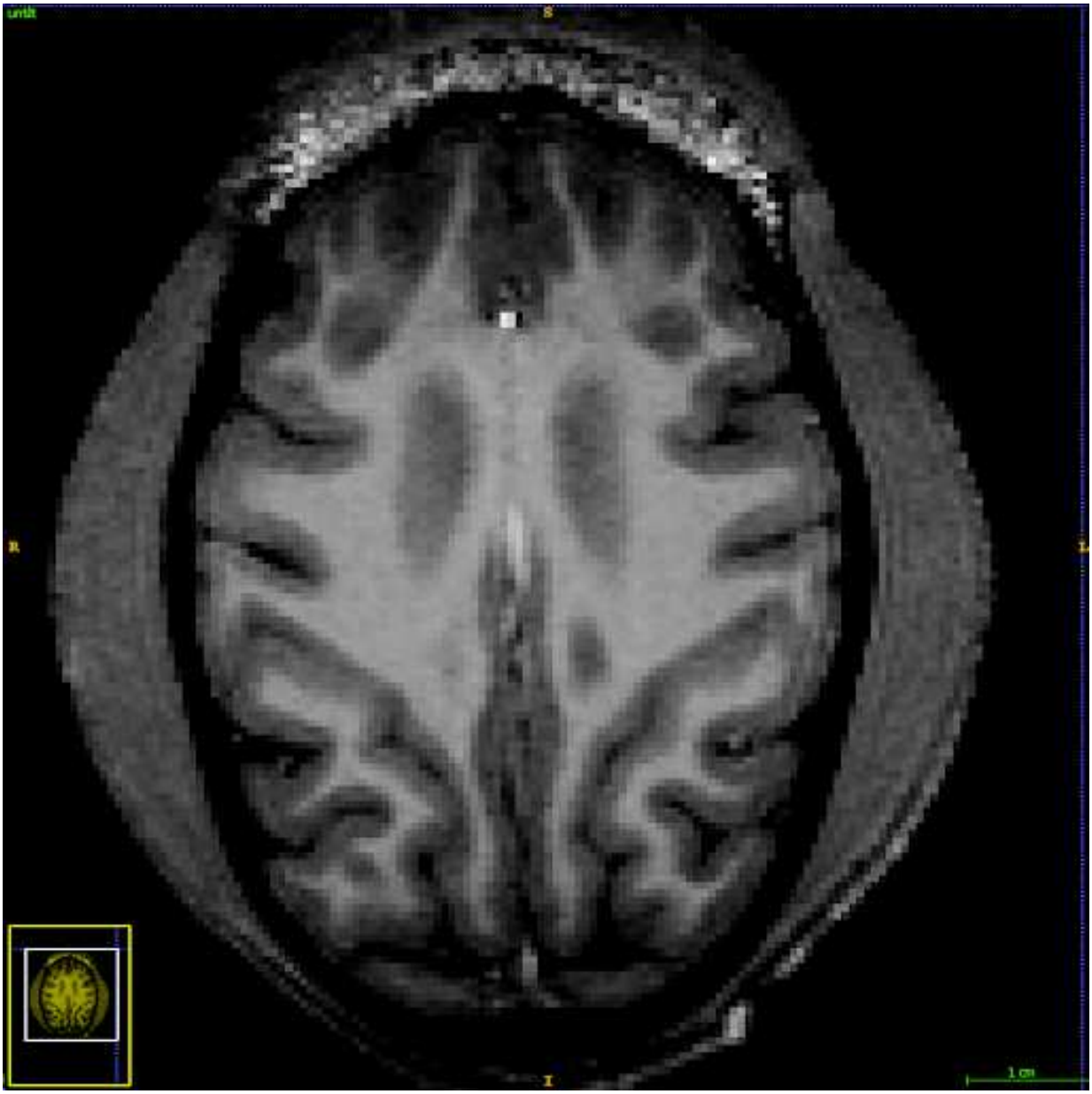

Figure A1: **Structural MRI of Monkey T, coronal view.** Screenshot from ITK-SNAP software [448].

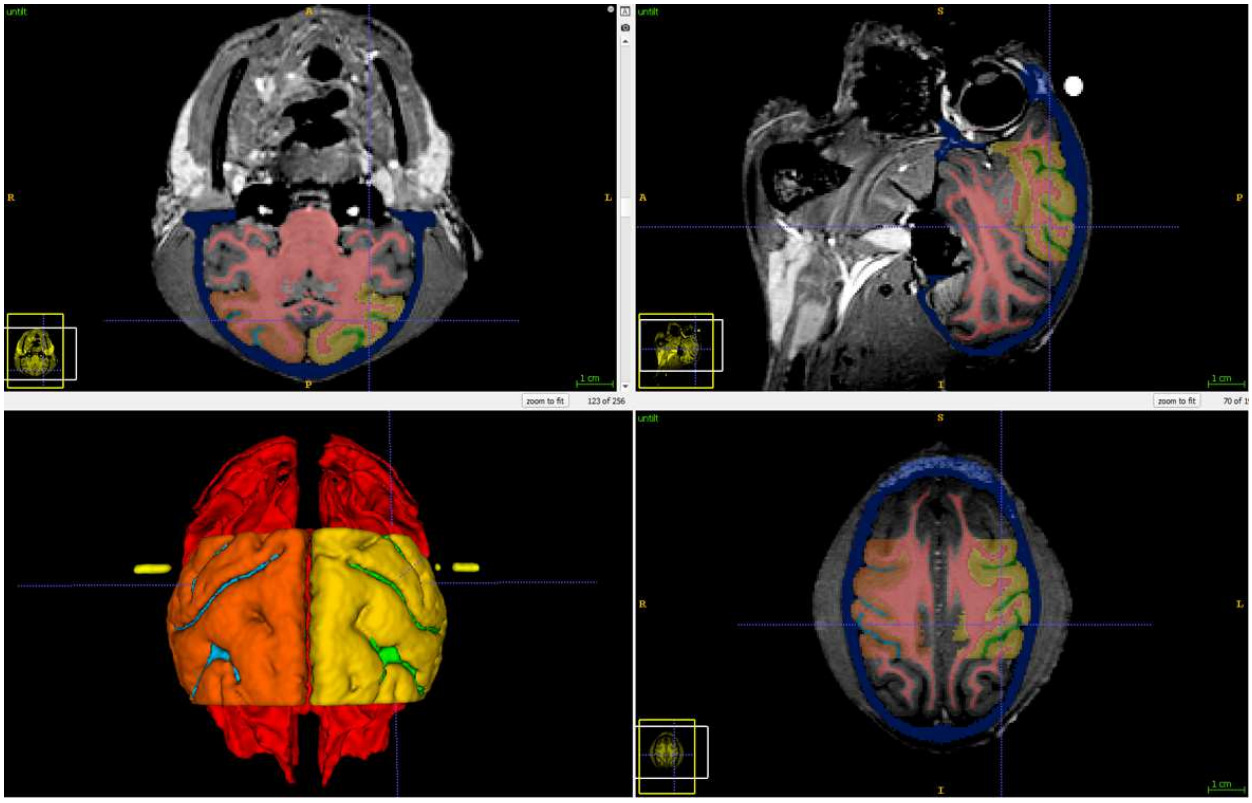

Figure A2: **Segmentation of MRI image of Monkey T.** Screenshot from ITK-SNAP software [448]. Red: white matter, Orange: right hemisphere gray matter, Cyan: right hemisphere sulci, Dark yellow: left hemisphere gray matter, Green: left hemisphere sulci, Dark blue: skull, Bright yellow: ear bars.

Systémes, Waltham, MA). The surfaces were aligned with a coordinate system centered on the ear bar centroids and the midline of the brain, rotated such that the eye cup bars were horizontal. The FMAs were also modeled in the SolidWorks environment, and positioned such that the array backs were flush with the cortical surface, and all electrode tips lay within the desired gray matter areas. The PMV arrays were positioned in the anterior bank of the arcuate sulcus, immediately lateral to the spur. The AIP FMAs were positioned in the lateral bank of the intraparietal sulcus at the anterior terminus of the sulcus. The craniotomies were also planned in SolidWorks by finding the coordinates of the craniotomy corners that would grant adequate access to the appropriate brain areas. The Solidworks model of the array placements is shown in Figure A3.

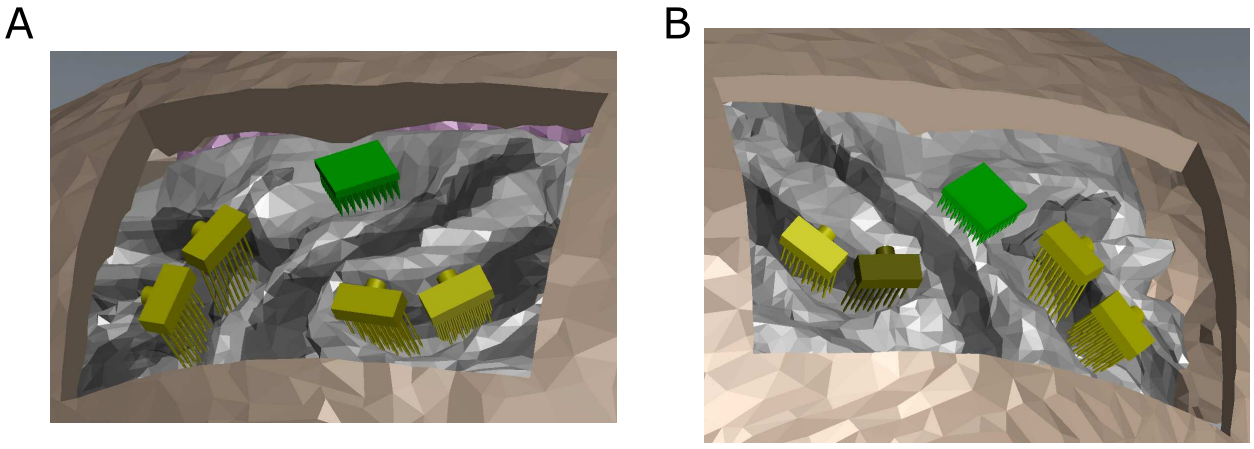

Figure A3: **CAD model with arrays virtually placed in the brain.** Screenshot from SolidWorks software. A: left hemisphere, B: right hemisphere. The gray matter was removed from this image in order to show the electrode arrays. Tan: skull, Light gray: white matter, Dark gray: sulci, Green: Utah Arrays, Yellow: standard FMAs, Dark yellow: short FMA.

The stereotaxic frame was also modeled in the CAD environment to obtain the desired coordinates of each array relative to the stereotaxic bars. This is depicted in Figure A4

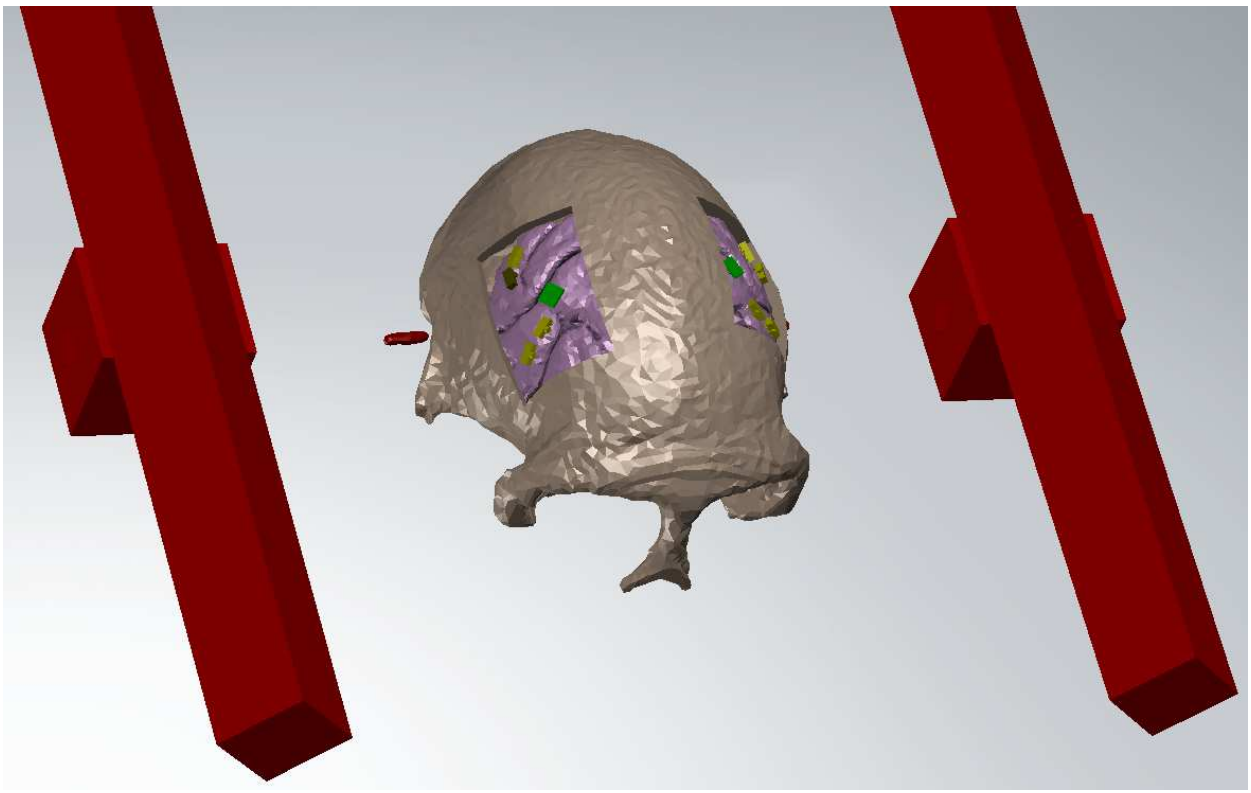

Figure A4: **CAD model with stereotaxic bars modeled relative to the subject's head.** Screenshot from SolidWorks software. Tan: skull, Pink: gray matter, Green: Utah Arrays, Yellow: standard FMAs, Dark yellow: short FMA, Red: stereotaxic frame and ear bars.

The stereotaxic calibrator plate was also modeled in the CAD environment. In order to allow for rapid alignment of the array inserter along the insertion axis of each FMA, physical inserter aligners were designed in the CAD environment. These aligners were designed to fit securely on the calibrator plate. The aligners contained holes that were concentric with the insertion axis of each FMA. The holes in the aligners were designed to fit a steel alignment rod which was of similar diameter to the FMA inserter microdrive housing. A unique inserter aligner was designed for each hemisphere. The aligners are depicted in the CAD software in Figure A5.

The inserter aligners were then 3D printed. Each aligner was printed as solid, monolithic piece for added structural integrity and to avoid warping or sagging. The left hemisphere aligner was printed using a Form 1+ SLA 3D printer (Formlabs, Somerville, MA) and the right hemisphere aligner was printed using an Ultimaker 2+ FFF 3D printer (Ultimaker, Waltham, MA) (see Section A.1.2.7). The printed pieces are shown in Figure A6.

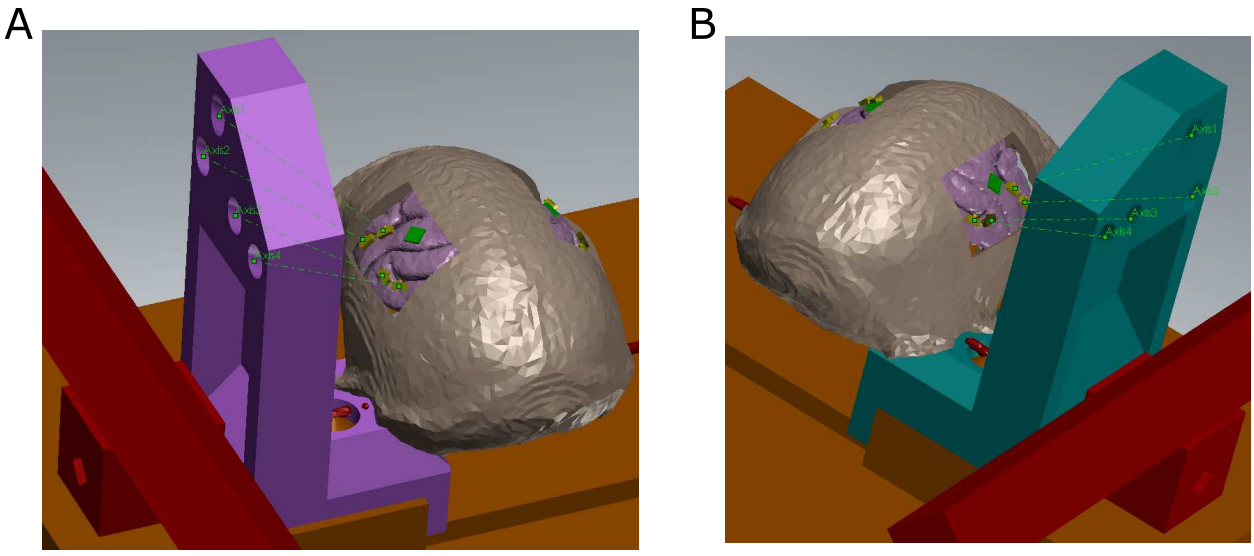

Figure A5: **CAD model of FMA inserter aligners on the stereotaxic calibration plate.** Screenshots from SolidWorks software. A: left hemisphere, B: right hemisphere. Purple and Teal: inserter aligners, Green dashed lines: FMA insertion axes, Tan: skull, Pink: gray matter, Green: Utah Arrays, Yellow: standard FMAs, Dark yellow: short FMA, Red: stereotaxic frame and ear bars, Orange: stereotaxic calibrator plate.

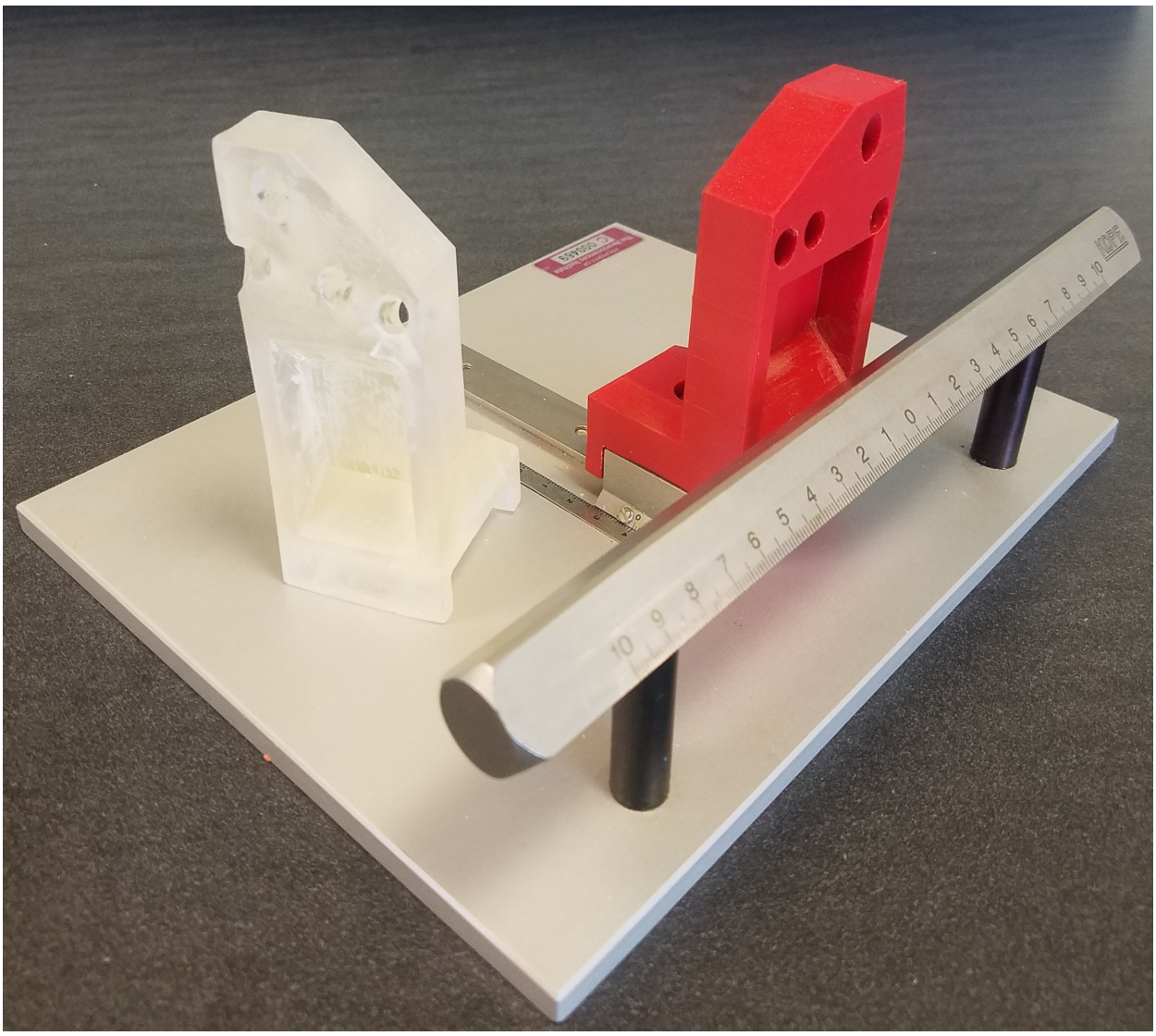

Figure A6: **3D printed FMA inserter aligners on the stereotaxic calibration plate.** White/translucent piece: left hemisphere inserter aligner, Red piece: right hemisphere inserter aligner. The right hemisphere inserter aligner is mounted on the stereotaxic calibration plate as it would be during surgery.

A.1.2.3 Surgical Procedure

Before each FMA implant surgery, the inserter aligners, alignment rod, stereotaxic calibration plate and manipulator arm were all sterilized. The same manipulator arm was used for the Utah Array and FMA inserters. At the start of surgery, the appropriate aligner was mounted on the stereotaxic calibrator plate as in Figure A6. During surgery, the alignment and insertion procedure for each FMA implant was as follows.

First, the manipulator arm was clamped on to the stereotaxic calibrator plate bar, and the anteroposterior position was noted. The aligner rod was then inserted through the shaft clamp on the manipulator arm, and through the appropriate FMA insertion axis alignment hole in the inserter aligner. The shaft clamp was then secured to the alignment rod, and the entire manipulator arm was locked securely in place. The alignment rod was then removed, and the manipulator arm was removed from the stereotaxic calibrator plate bar, keeping the manipulator arm locked in the established configuration. The FMA inserter microdrive was then placed in the shaft clamp of the manipulator arm, and the whole arm was mounted on the surgical stereotaxic frame bar at the same AP position as recorded from the calibrator plate. The FMA was then affixed to the inserter microdrive tip for implantation. The alignment and insertion stages of this procedure are depicted in Figure A7.

While the angle of insertion was locked in place after alignment, the anteroposterior and mediolateral position could be adjusted by sliding the manipulator along the stereotaxic frame bar or by adjusting the micromanipulator on the distal end of the manipulator arm, respectively. This allowed for fine adjustments in position before insertion. Most of the arrays were adjusted a small amount ($\sim$2mm anterior) in order to achieve the desired positions as planned in the CAD environment or to avoid visible blood vessels. The amount of adjustment was consistent across arrays. This positional error could have been caused by differences in the MRI compatible stereotaxic frame and the surgical stereotaxic frame, warping of the MRI image, or growth of the monkey during the time between the MRI image acquisition and surgery.

The FMAs were inserted using a computer controlled microdrive with a 3D printed vacuum tip (NeuroNexus, Ann Arbor, MI) (Figure A7 B) as follows. The FMA was affixed

A

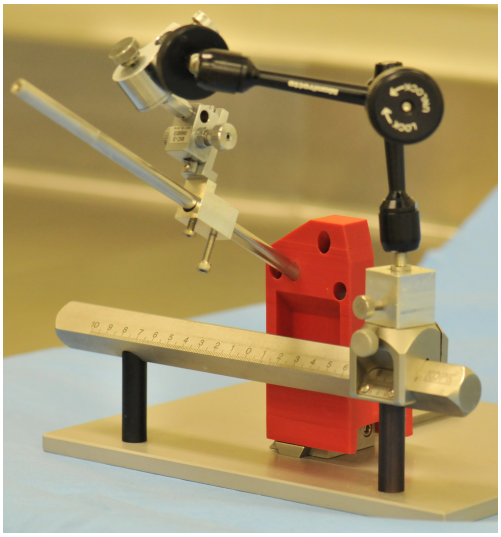

B

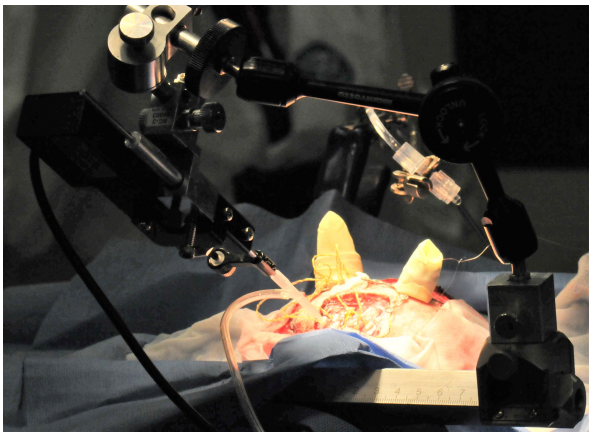

Figure A7: **FMA inserter alignment procedure during surgery.** A: alignment of the manipulator arm using the alignment rod, with the inserter aligner mounted on the stereotaxic calibration plate. B: insertion of an FMA, with the inserter microdrive mounted in the manipulator arm in place of the alignment rod and the entire assembly mounted on the surgical stereotaxic frame.

to the vacuum tip, and lowered until close to the cortical surface. Insertion then proceeded by advancing the microdrive at a rate of 1mm/min for 1 minute, then holding position for 1 minute to allow for any cortical puckering to resolve. This sequence was repeated until the array backing was flush with the cortical surface. At the final depth, the inserter tip suction was disengaged and the inserter was held in place for 1 minute. The microdrive was then retracted.

A.1.2.4 Insertion Results

All FMAs were implanted successfully. Figure A8 shows the final array placements in the brain (Panels A and B), compared with the planned placements in the CAD model (Panels C and D).

Unit yields over time are plotted in Figure A9 for each array. The unit yield for an array was defined as the number of units sorted online (N_{Units}) divided by the number of electrodes on that array ($N_{\text{Electrodes}}$).

Units were readily detectable a few days after implantation on all FMAs, save for the left hemisphere lateral PMV FMA as the wire bundle connecting the FMA to the pedestal was damaged during surgery (see Section A.1.2.7). Contrastingly, no units were detectable on the M1 Utah Arrays until about two weeks after surgery. From ∼20 days post-implant on, unit yields for the Utah Arrays and FMAs were comparable, and unit yields on all intact arrays remained stable. In general, unit yields were higher in the right hemisphere (Figure A9 B) compared to the left hemisphere (Figure A9 A). The left hemisphere anterior AIP FMA performed markedly worse than all other FMAs (Figure A9 A, dark blue trace). Potential reasons for the hemispheric difference in yields, the poor performance of the left hemisphere lateral AIP FMA are discussed in Section A.1.2.7. In a few cases, array components were damaged after implantation, causing unit yields to drop (Figure A9, stars). These array failures are discussed in Section A.1.2.7.

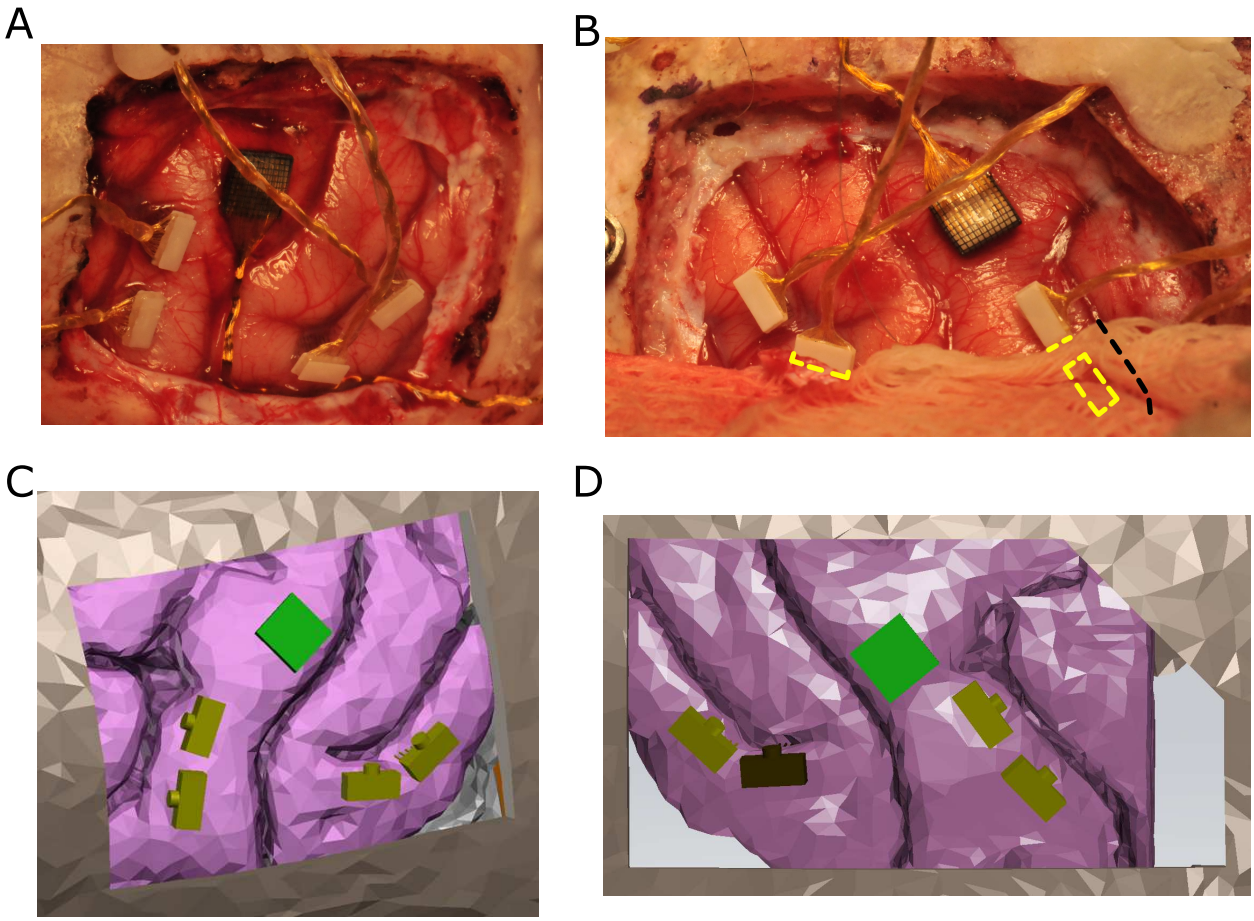

Figure A8: **Comparison of actual inserted array positions and array positions planned in CAD software.** A, B: final array positions after insertion. C, D: array positions as planned in SolidWorks. A, C: left hemisphere. B, D: right hemisphere. B: sulcus (black dashed line) and array edges (yellow dashed lines) that were obscured by gauze in the photograph were estimated by reference to other photographs from the surgery.

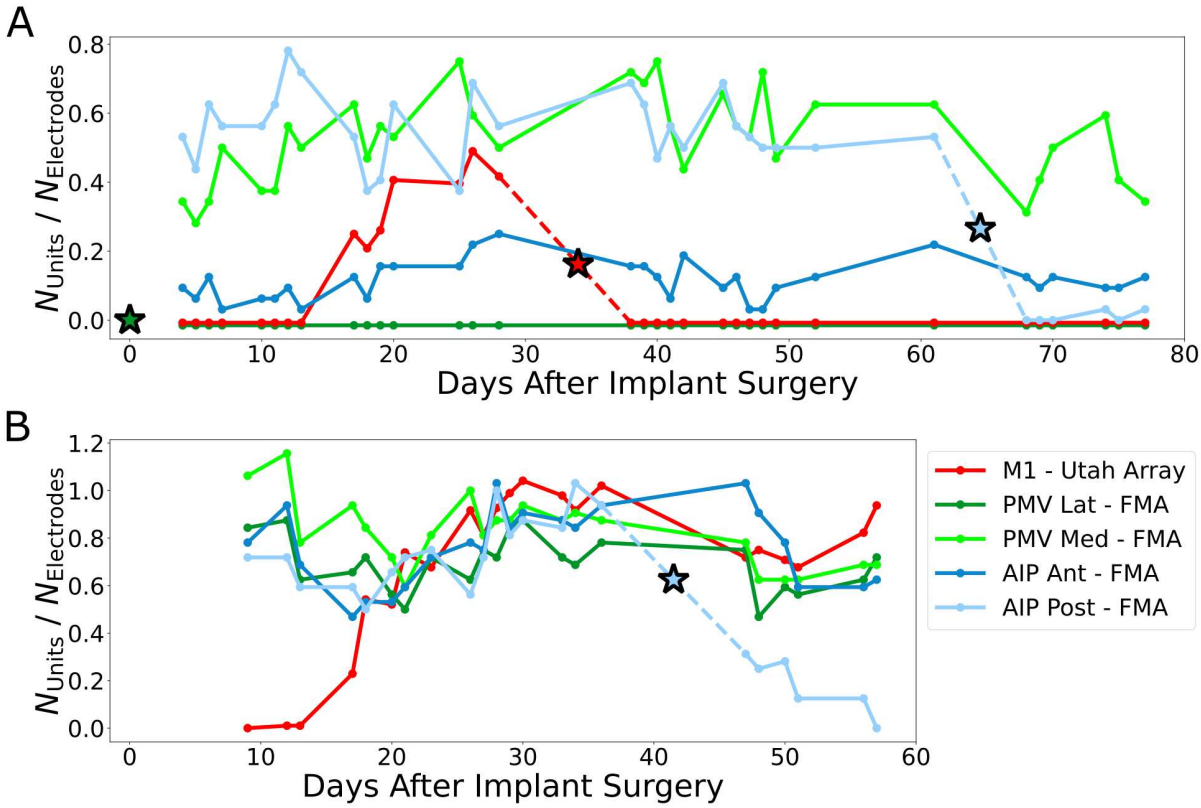

Figure A9: **Utah Array and FMA unit yields over time, Monkey T.** A: left hemisphere, B: right hemisphere. Stars: approximate time at which an array component sustained damage, hindering further recordings.

A.1.2.5 Pedestal Design and Fabrication

Individual FMAs are typically shipped from the manufacturer as standalone components, with the FMA attached via a coated gold wire bundle to a small 36-pin connector (Omnetics, Minneapolis, MN). In order to protect and provide stable access to these connectors, a connector housing pedestal was designed and fabricated. The pedestal was designed with slots to hold the connectors with enough inter-connector spacing to allow for interfacing with the headstage pre-amplifiers (see Section A.4.4). The pedestal was designed with four legs containing holes which were used to mount the pedestal directly to the skull with bone screws. The pedestal leg dimensions were designed such that they would be flexible enough to conform to the curvature of the skull, but robust enough to withstand any interactions from the monkey or its cage mates or any accidental impacts.

The pedestal was machined from a single monolithic piece of grade 2 titanium (McMaster-Carr, Santa Fe Springs, CA) using a CNC Mini Mill (Haas, Oxnard, CA). The empty pedestal was sent to Microprobes for Life Science for final assembly with the four FMAs. After conclusion of the left hemisphere recordings, the pedestal was explanted, disassembled, sterilized and reused for the right hemisphere implant. The pedestal is shown in Figure A10.

The CNC mill was also used to machine a headstage protector and a low profile cap, both made of Delrin plastic (DuPont de Nemours, Wilmington, DE). The headstage protector attached to the top of the pedestal to protect the headstages and cables during recording (Figure A11 D). The low profile cap attached to the top of the pedestal to cover and protect the FMA connectors when not in use (Figure A10 B).

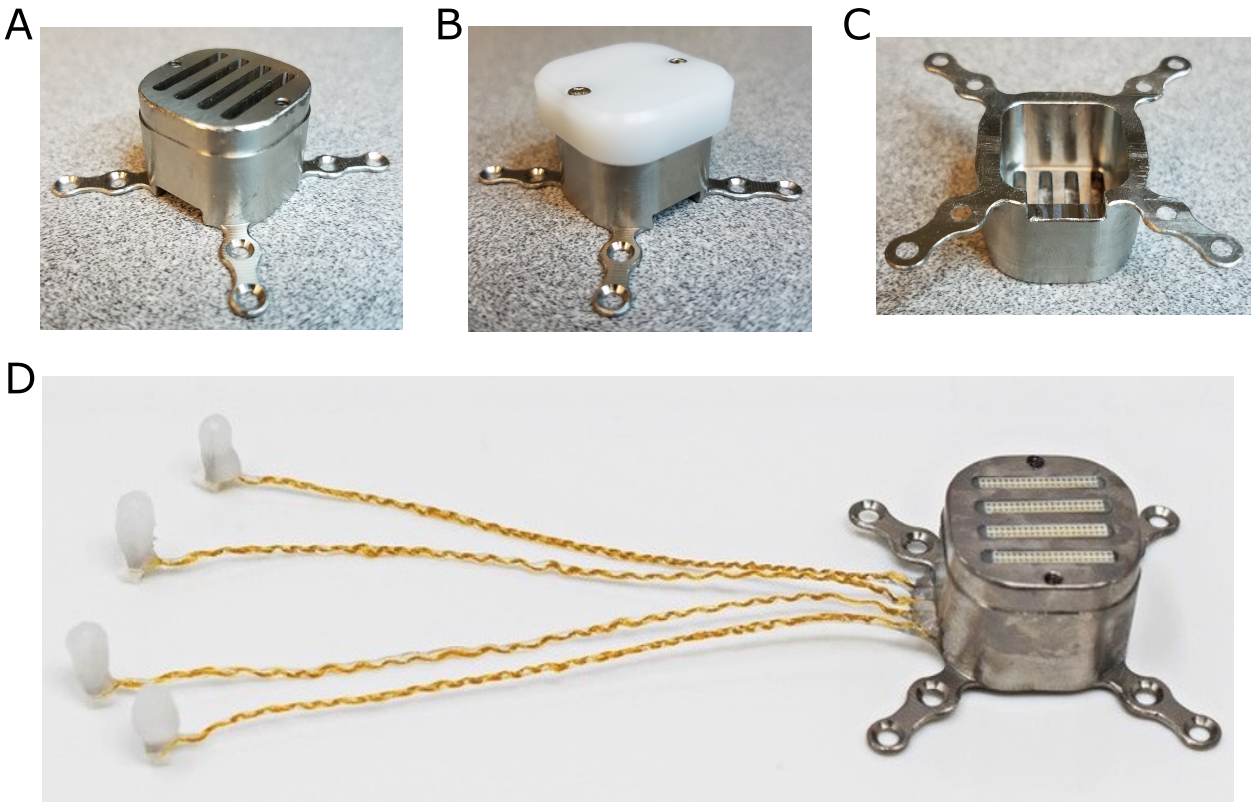

Figure A10: **Titanium FMA connector pedestal.** A: top view of the pedestal. B: pedestal with protective cap. C: bottom view of the pedestal. D: fully assembled pedestal with FMAs installed.

A.1.2.6 3D Printed Skull Model

The 3D skull surface information obtained from the MRI image was used to print a model of the skull using the Form 1+ SLA 3D printer. This model served as a testbed for pedestal and craniotomy placements, and for choosing appropriate bone screws. The skull model was sterilized and used as a reference during the implant surgeries. The model with mock pedestals attached is shown in Figure A11.

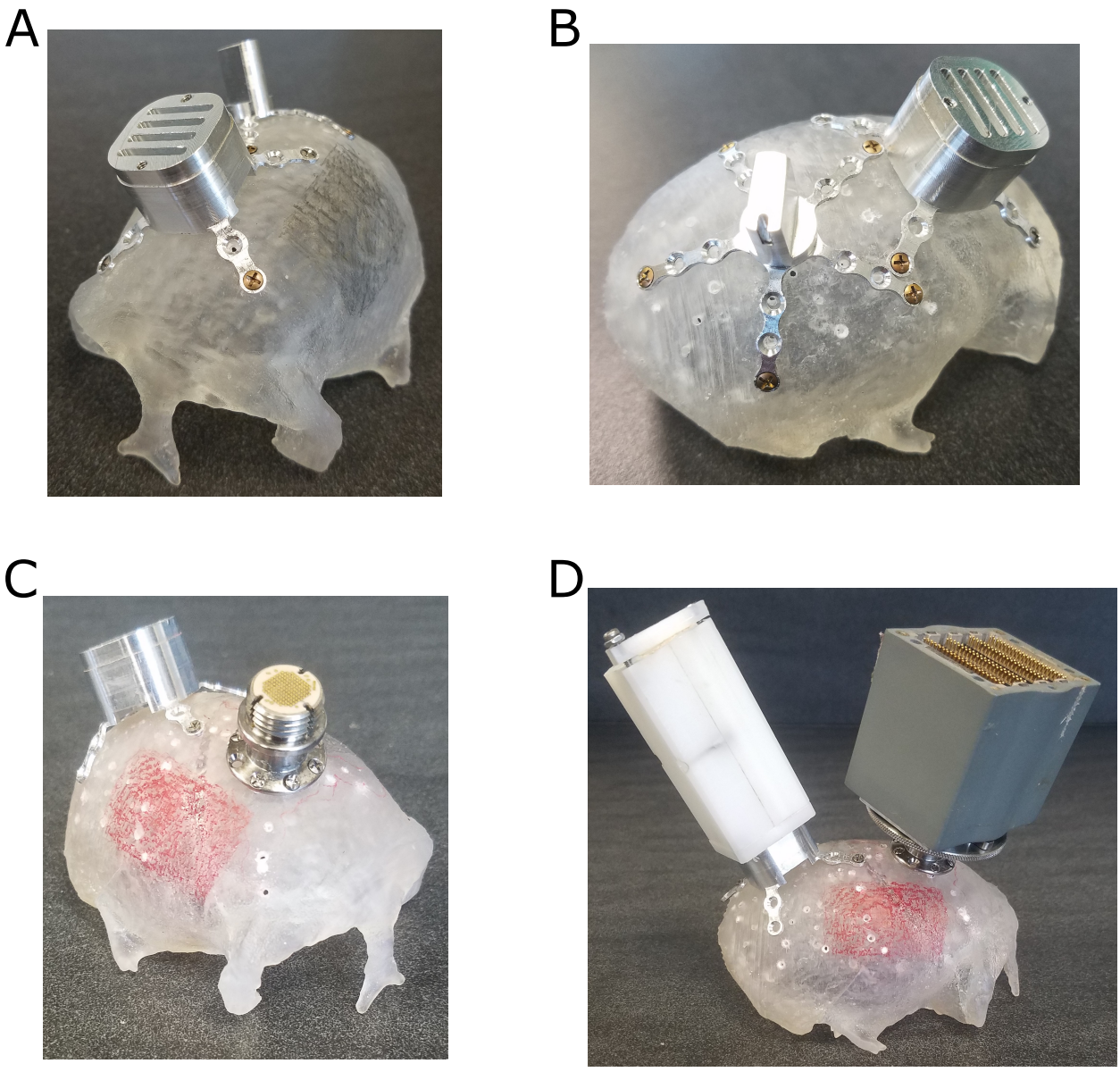

Figure A11: **3D printed skull model with mock pedestals.** A: front view, left hemisphere implant configuration, black shading is approximate craniotomy location. B: side view, left hemisphere implant configuration. C: front view, right hemisphere implant configuration, red shading is approximate craniotomy location. D: side view, right hemisphere configuration. Dark gray box: Blackrock Microsystems headstage connector, White box: custom-machined FMA headstage protector.

A.1.2.7 Limitations and Design Modifications

Several problems were encountered during implementation of the novel FMA implant procedure. Most of these difficulties occurred during the first (left hemisphere) implantation, and were resolved by design and equipment modifications before the second (right hemisphere) implantation. These difficulties and their solutions are discussed below.

Premature CARBOWAX FMA Coating Dissolution

After assembly into the connector pedestal, the FMAs were delivered from the manufacturer with water soluble CARBOWAX (Dow, Midland, MI) covering and protecting the delicate electrodes (Figure A10 D). This covering was dissolved using heated saline, as shown in Figure A12, before each FMA insertion. During the left hemisphere surgery, the CARBOWAX was discovered to have partially dissolved prematurely. This was most likely attributable to the method used to sterilize the FMAs.

The entire array assemblies were sterilized before surgery using ethyline oxide. For the left hemisphere implant, ethylene oxide sterilization was performed at 100 °F. This caused partial degredation of the CARBOWAX, exposing some of the electrode tips. Though care was taken not to touch the exposed tips, some damage may have occurred. For the right hemisphere implant, ethylene oxide sterilization was performed at room temperature. This preserved the integrity of the CARBOWAX coating until it was properly dissolved during surgery. The premature exposure of the electrode tips may have contributed to the generally lower unit yields of the left hemisphere FMAs (Figure A9).

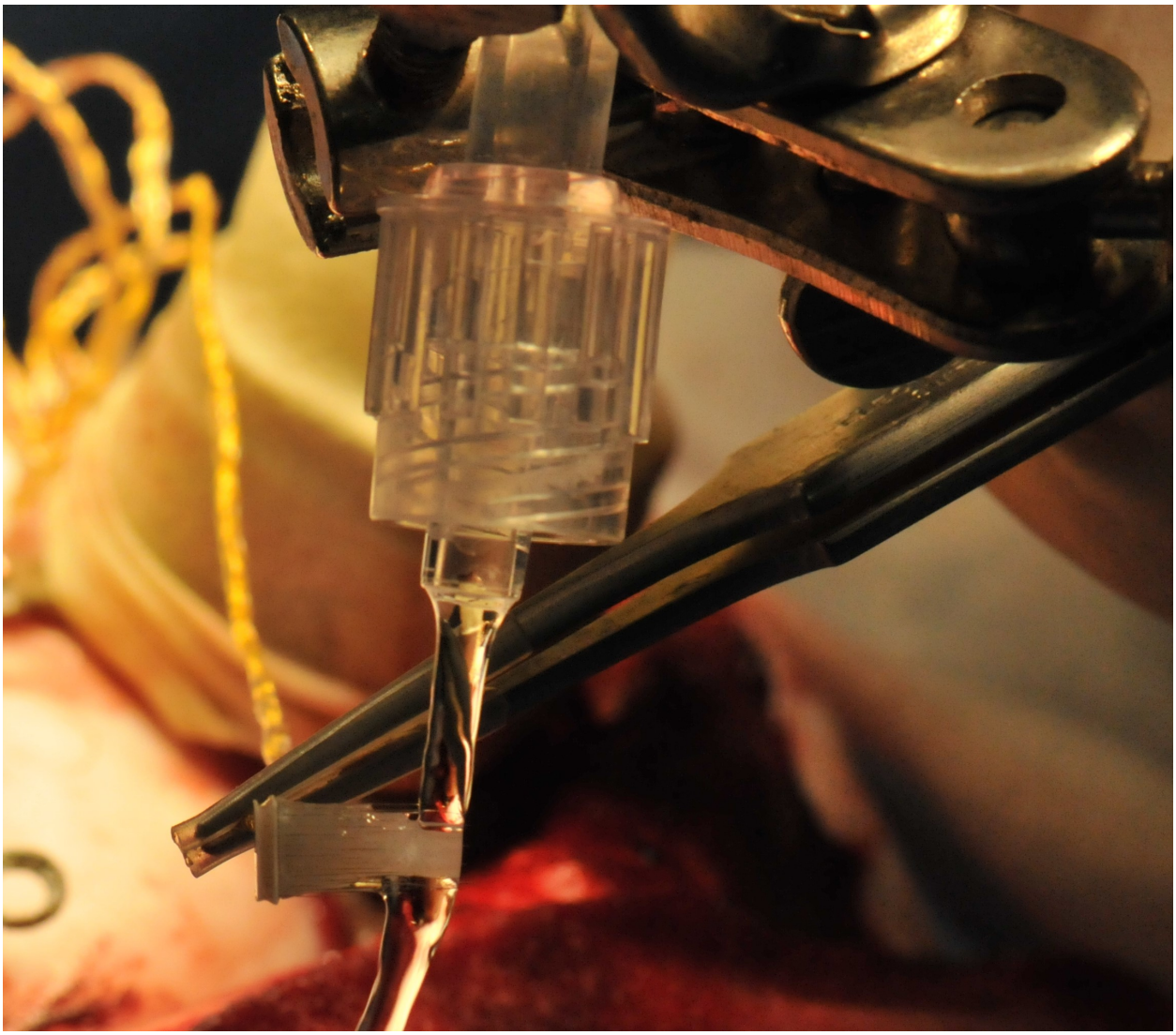

Figure A12: **Dissolution of the CARBOWAX FMA protective coating using heated saline during the left hemisphere FMA implant procedure.**

Inadequate Inserter Tip Suction

The computer-controlled inserter microdrive utilized a hollow, 3D printed suction tip (Figure A7 B, white tip with tube, bottom center). Suction was applied through this tip using a pump, in order to securely hold the FMAs for insertion. For the left hemisphere surgery, the Blackrock Microsystems Utah Array inserter base unit was used to provide suction. This suction enabled only a weak attachment between the inserter tip and FMA. In order to provide more secure attachment, a small amount of petroleum jelly was applied to the array backings before placing them against the inserter tip. Though this allowed the arrays to stick to the inserter tip, the arrays may still have moved relative to the inserter tip during insertion, and the petroleum may have created additional outward forces on the FMAs when the inserter microdrive was retracted after insertion.

For the right hemisphere surgery, a more powerful, medical-grade suction pump, the Schuco-Vac S330A Suction Aspirator (Allied Healthcare Products, St. Louis, MO), was used to provide suction for the inserter tip. Owing to this stronger suction, the right hemisphere arrays were likely inserted with less motion of the arrays relative to the inserter tip, and with cleaner detachment when the inserter was retracted. The inadequate suction during the left hemisphere surgery may have contributed to the relatively lower unit yields observed in the left hemisphere FMAs (Figure A9).

Left Hemisphere Lateral PMV FMA Wire Bundle Severed During Closure

During placement of the titanium bone strap used to close the craniotomy, the screwdriver slipped off of the bone screw and severed the delicate wire bundle attaching the left hemisphere lateral PMV FMA to the connector pedestal, causing total loss of the signals from that array (Figure A9 A dark green trace and star). This accident was attributed to the use of the wrong screwdriver head, which did not securely lock into the bone screw head. For the right hemisphere surgery, the correct screwdriver was utilized and no such errors occurred.

Left Hemisphere Utah Array Pedestal Failure

Between 34 and 35 days after implantation, the left hemisphere Utah Array pedestal, obtained from Blackrock Microsystems, suffered catastrophic failure while Monkey T was in the home cage. The pedestal was an untested prototype, manufactured using 3D printed titanium. This resulted in weak points around the bone screw holes in the pedestal legs, which caused the legs to fracture near the base of the pedestal. This resulted in complete loss of the signals from the Utah Array in the left hemisphere (Figure A9 A red trace and star). To avoid this problem for the right hemisphere implant, a standard Utah Array pedestal was used, along with additional custom titanium bone straps to secure the pedestal to the skull.

Left Hemisphere Posterior AIP FMA Wire Bundle Damage at Pedestal Base

Between 61 and 68 days after implantation, the left hemisphere posterior AIP FMA became damaged and all signals from the array were lost. Careful examination while the subject was sedated revealed that the wire bundle connecting the FMA to the connector pedestal had severed near the pedestal base. This damage was attributed to the presence of a small gap between the pedestal base and the skull beneath the wire bundle exit port.

The FMA connector pedestal was designed with a relatively broad, flat base. This resulted in a small gap between the pedestal base and the skull when the flat pedestal was affixed to the curved skull surface. The gap can be seen in Figure A13 A (green arrow).

This gap allowed the wire bundles to move toward the skull relative to the pedestal base. The pedestal interior was filled with a rigid epoxy and the wire bundles outside the pedestal were covered with a flexible coating. The difference in material stiffness led to excessive strain in the wire bundles when the wire bundles near the pedestal base were moved. Due to downward pressure, either from the skin pulled around the pedestal or from the subject grooming the area, the wire bundles of the left hemisphere implant were displaced near the pedestal base, severing the left hemisphere posterior AIP FMA wire bundle.

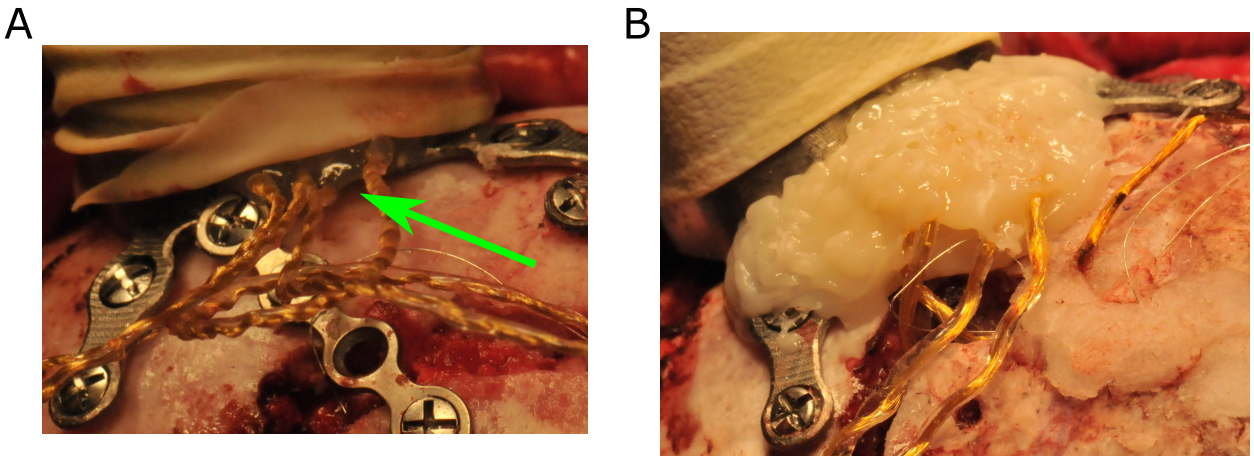

Figure A13: **Gap between wire bundles and skull near the FMA connector pedestal base.** A: left hemisphere implant, with green arrow highlighting the wire bundle gap. B: right hemisphere implant, with UV curable dental cement (off-white material) filling the wire bundle gap and encasing the top of the wire bundles.

In order to prevent motion of the wire bundles near the pedestal base for the right hemisphere implant, the gap beneath the wire bundles was filled with UV curable dental cement. Additionally, dental cement was built up over the tops of the wire bundles to fully encase and protect them. This encasement can be seen in Figure A13 B (off-white material). This method successfully protected the wire bundles for the duration of the right hemisphere implantation period of about two months.

While care was taken to smooth the surface of the dental cement, the surface remained rough. This caused the skin to gradually retract from the area. A potential future solution would be to devise a better method for smoothing the top of the dental cement to avoid foreign body reaction. A more rigorous solution would be to obviate the need for dental cement by modifying the pedestal design. The 3D skull surface information could be used to design the pedestal such that the pedestal base was curved to conform to the shape of the skull. This would eliminate the gap under the wire bundles, but would necessitate

precise pre-surgical planning of the placement of the pedestal with less potential for positional adjustment during surgery. Fabricating a pedestal with a curved base would also require a more complex machining and assembly process.

Right Hemisphere Posterior AIP FMA Wire Bundle Damage

Between 36 and 47 days after implantation, the right hemisphere posterior AIP FMA wire bundle became partially damaged, resulting in a markedly reduced unit yield (Figure A9 B light blue trace and star). This damage was attributed to the fact that the wire bundle under ran a suture line near the anterior Utah Array pedestal. The wire bundle likely became damaged through mechanical interaction with the skin or with the pedestal bone strap hardware. This may have been exacerbated by the monkey grooming the area.

The FMA wire bundles were flexible but also delicate. In addition, relatively long wire bundles were used (90 mm for the left hemisphere surgery, 70 mm for the right hemisphere surgery). This allowed for easier manipulation of the wire bundles during surgery, but caused the wire bundles to be susceptible to damage afterward. Future FMA implant procedures should utilize shorter wire bundles, and better wire bundle placement, ensuring the wire bundles traverse underneath intact portions of skin or muscle. Wire bundle routing could be accomplished using guides that attach to the skull with bone screws.

Poor Performance of Left Hemisphere Anterior AIP FMA

The left hemisphere anterior AIP FMA yielded markedly fewer units than all other intact FMAs (Figure A9 A dark blue trace). This lower performance may have been due to a combination of factors, including the premature dissolution of the CARBOWAX coatings and the inadequate inserter tip suction in the left hemisphere surgery. Another reason may have been inadequate compensation for the cortical morphology in the implanted location.

In both hemispheres, the anterior AIP FMA was implanted very close to the terminus of the intraparietal sulcus. The sulcal depth decreased as the cortex flattened near the tip of the sulcus. The left hemisphere anterior AIP FMA was of the standard, long length (Table A1). While planning the array placement in CAD software, the electrode tips could be placed in the cortex, but many tips lay very close to the white matter tracts beneath the cortex. Thus, any positional or angular error in implantation may have resulted in some of the electrode tips being implanted into white matter instead of cortex. These electrodes would not yield any distinguishable unit activity.

For the right hemisphere implant, a unique FMA was designed with shorter electrodes (Table A2). This shorter configuration provided better conformation to the underlying cortical morphology, with a larger margin between planned electrode tip locations and white matter. The right hemisphere anterior AIP short FMA had unit yields very similar to the other intact FMAs (Figure A9 B dark blue trace).

Brittle Left Hemisphere Inserter Aligner

The left hemisphere inserter aligner was printed using the Form 1+ SLA 3D printer, using the "Clear" resin. This printer uses an ultraviolet laser to cure a liquid polymer resin layer by layer into a solid piece. This material was found to be overly brittle. During surgery, inserting and removing the alignment rod caused small fractures around two of the alignment holes in the inserter aligner (see Figure A6, white/translucent object, left-most and right-most alignment holes). While the inserter aligner remained functional, the potential for greater damage during use encouraged a change in the fabrication method for the right hemisphere procedure.

The right hemisphere inserter aligner was thus printed using the Ultimaker 2+ FFF 3D printer. This printer extrudes molten plastic filament through a nozzle layer by layer to create a solid piece. This method produced a less brittle final result, with a small sacrifice in build tolerance. The right hemisphere inserter aligner remained undamaged throughout the right hemisphere procedure.

General Limitations

As noted in Section A.1.2.3, the manipulator arm was designed to allow for positional adjustments in the anteroposterior axis and the mediolateral axis. However, manual adjustments in the angle of insertion, if necessary, would be difficult, inaccurate and approximate.

While the long axis of insertion was determined using the inserter aligners, the rotational angle around the long axis was unconstrained. This angle was set by hand by adjusting each FMA while affixed to the inserter microdrive suction tip to match the planned FMA orientations as closely as possible. As this adjustment was approximate, the FMA orientations likely deviated a small amount from the planned orientations.

The locking manipulator arm was very rigid in the locked configuration. Despite this rigidity, errors may have been introduced by deformation of the arm when transferring it from the stereotaxic calibration plate to the surgical stereotaxic frame, or when attaching the inserter microdrive. Such errors would be difficult to detect and measure.

Positional and rotational errors may have also been introduced in reconciling the MRI image with the actual subject. These errors could result from warping of the MRI image, or dimensional and material property differences between the MRI compatible plastic stereotaxic frame and the steel surgical stereotaxic frame. Growth and maturation of the subject in the time period between MRI scanning and surgery could also have introduced errors. This type of error was the likely reason for the need to adjust the FMA implant positions slightly anterior (Section A.1.2.3).

The inserter aligner 3D printing process may have also introduced errors. The 3D printers used to create the inserter aligners are relatively low-cost, consumer grade systems. The final 3D printed product may be warped relative to the digital model due to unpredictable defects in the printing processes, such as clouding of the resin tank in the Form 1+ printer, or clogging of the print nozzle in the Ultimaker 2+ printer.

Successful placements of the FMAs were determined by visual inspection of the array locations during surgery (Figure A8) and the presence of distinguishable units (Figure A9). In addition, the signals from these areas were functionally related to the grasping tasks

(Section 7), and some evidence for mirror neuron activity was detected (data not shown). Marking the electrode tracks and performing histology would allow for more detailed evaluation of the success of the procedure.

Finally, this method relied on anatomical landmarks to identify the desired brain areas. While this is a common method in macaque neuroscience, inter-subject differences in functional brain anatomy may exist. More accurate estimations of the locations of the targeted cortical areas could be achieved using methods such as intracortical microstimulation or functional magnetic resonance imaging (fMRI) in combination with a behavioral task.

In conclusion, despite limitations, the novel FMA implant planning, alignment and insertion procedure proved largely successful. The 3D printed inserter aligners allowed for rapid, accurate insertion of the FMAs in the desired cortical locations. The inserter aligners and manipulator arm represent a low-cost solution which allows for rapid sequential insertion of multiple arrays and enables translational adjustments in the final array position. The connector pedestal enabled chronic, stable recordings over a period of months. The 3D printed skull model facilitated the planning of pedestal placements and craniotomies. Several difficulties and design flaws were identified and improved upon between the two implant procedures.

A.2 Object Design and Fabrication

The graspable objects were designed to meet several requirements. First, the objects must afford specific, repeatable grasps. Second, the objects must be instrumented with force sensors in order to detect grasps and object contact. Third, for experiments where multiple objects were to be grasped, the objects must be as similar as possible, with the only difference between objects being the color of the objects such that they can be readily identified by the subjects. Fourth, the objects must be durable and robust enough to retain functionality after repeated unpredictable interactions from the macaque subjects.

Several iterations of objects were designed and fabricated until all of the design requirements were satisfied. The final design and fabrication methods are discussed below for the compound objects used in the Object Presence Experiment and Use Affordance Experiment (Section A.2.1) and for the modular objects used in the Grip Affordance Experiment (Section A.2.2).

A.2.1 Compound Objects for the Object Presence Experiment and the Use Affordance Experiment

The Object Presence Experiment and the Use Affordance Experiment utilized the same basic object design. These objects were designed to afford both a power grasp and a pinch grasp. To accomplish this, objects were designed with a cylindrical vertical central "power grasp portion" below a "pinch grasp portion" tab. The final object is shown in Figure A14 A. Multiple different colored objects of the same design were fabricated (see Figure 4.1 and Figure 6.1) The objects were designed in SolidWorks. CAD models of the objects are shown in Figure A14 B and C.

In order to detect grasps, force sensing resistors (FSRs; see Section A.4.3 for details) were affixed to the objects in different locations. To detect pinch grasps, the FSRs were affixed directly to the front and back of the pinch tab. The front pinch grasp FSR is visible in Figure A14 A. This method was feasible as the pinch tab surfaces were small and flat.

In order to detect power grasps, a different approach was required. Affixing the FSRs directly to the curved surface of the cylindrical power grasp portions resulted in non-zero signals when the sensors were unloaded, drift in sensor baseline over time and inconsistent signals when grasped. In a previous thesis study, Sagi Perel constructed instrumented objects by affixing FSRs to the surface of objects, gluing small beads to the FSRs, and encasing the object in heat shrink tubing [118]. This method was inappropriate for the current experiments as the bead would create an irregular surface which could differ between objects. In order to create objects that were identically shaped, the FSRs were affixed underneath flexible flaps on either side of the cylindrical power grasp portion of the objects. This allowed

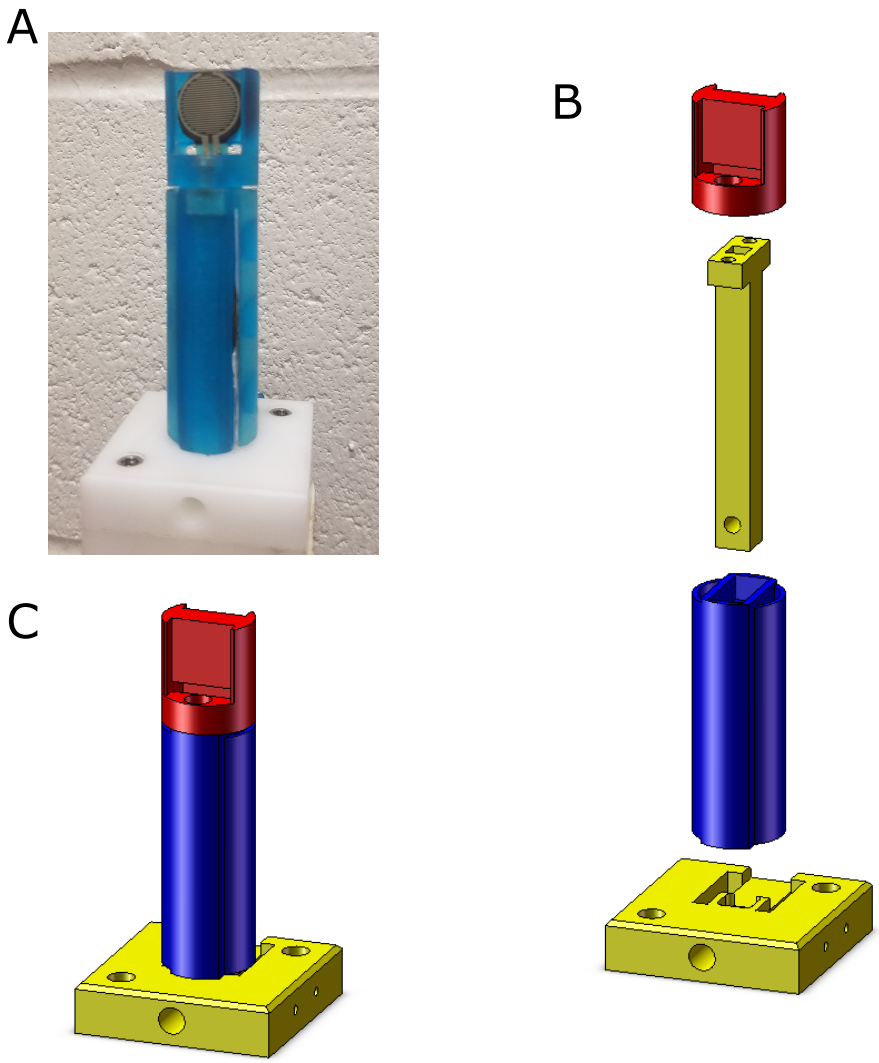

Figure A14: **Design of compound objects for the Object Presence Experiment and Use Affordance Experiment.** A: final fabricated object. B: exploded view of the object showing the components. C: assembled object in CAD software. Blue: power grasp portion, Red: pinch grasp portion, Yellow: structural components. B, C: screenshots from SolidWorks software.

the FSRs to lie flat. The flaps deflected inward and pressed on the FSRs when the object was grasped with a power grasp. Detailed CAD models of the power grasp portion showing these flexible flaps are depicted in Figure A15.

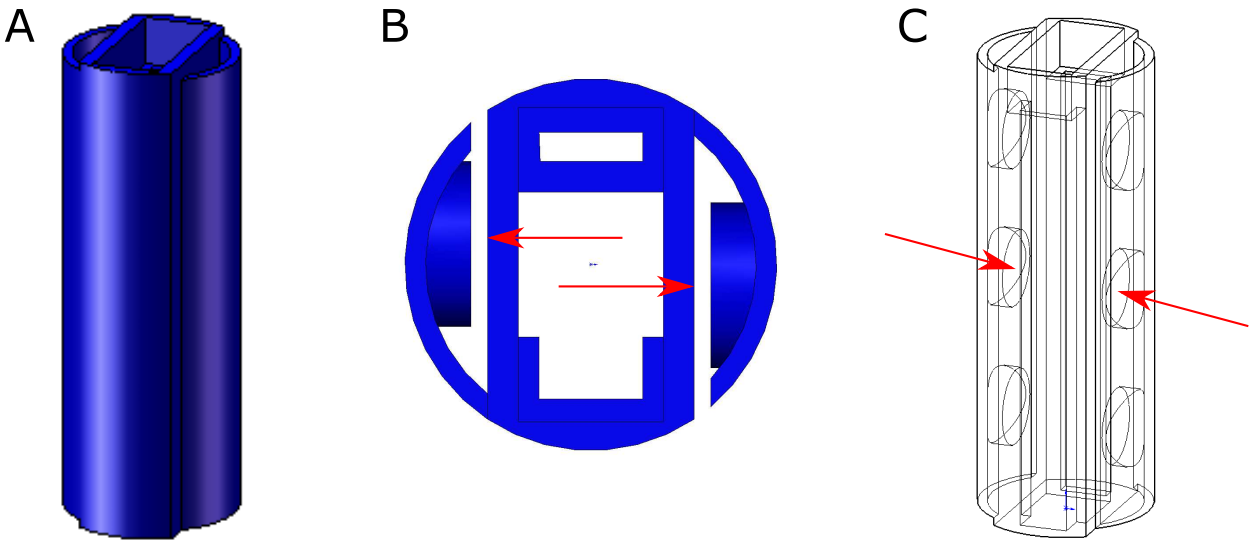

Figure A15: **Detailed view of the design of the power grasp portion of the compound object.** Screenshots from SolidWorks software. A: the power grasp portion. B: top-down view of the power grasp portion. C: skeleton view of the power grasp portion showing internal structure. Red arrows indicate FSR locations.

The power grasp portion was designed with a hollow center to accommodate a structural core and to allow space for the wired connections to the pinch grasp FSRs. An additional strip-style FSR was affixed directly to the back of the black object used in the Object Presence Experiment in order to detect any aberrant object contact during the Object Reach condition (Figure 4.1). This sensor was important for the training phase of the Object Presence task (see Section A.3), but was rarely activated after the task had been learned.

The compound objects were fabricated with a combination of CNC milling and 3D printing. The graspable portions (red and blue in Figure A14 B and C) were printed using the Form 1+ 3D printer. The structural core and base (yellow in Figure A14) were

machined from Delrin plastic using the Haas Mini Mill. These structural parts were made from Delrin for added strength and durability, as subjects often exerted high forces on the objects during training.

The objects were mounted on a rigid aluminum frame in the experiment room (80/20, Columbia City, IN). For the Use Affordance Experiment, the mobile object was mounted on two steel vertical guide rods in ball bearing sleeves in the object mount, allowing the object to move vertically.

A.2.2 Modular Objects for the Grip Affordance Experiment

For the Grip Affordance Experiment, a set of modular objects was designed and fabricated. These objects could afford a power grasp, a pinch grasp, or both. The power grasp portion was identical to that used in the other two experiments and was 3D printed, with a machined Delrin core. The pinch grip tab was located on the side of the object, and was machined from Delrin. A small plate was attached to the side of the pinch grip tab to prevent the subject from using the palm to activate the front pinch grip FSR.

The modular design allowed the exact same physical grasp portion to be used for the different conditions in the Grip Affordance Experiment, by assembling the modular parts in different ways. The objects were differentiated by changing the color of an LED embedded in the objects. The assembled objects used in the Grip Affordance Experiment are shown in Figure 5.1. The modular pieces are shown in Figure A16.

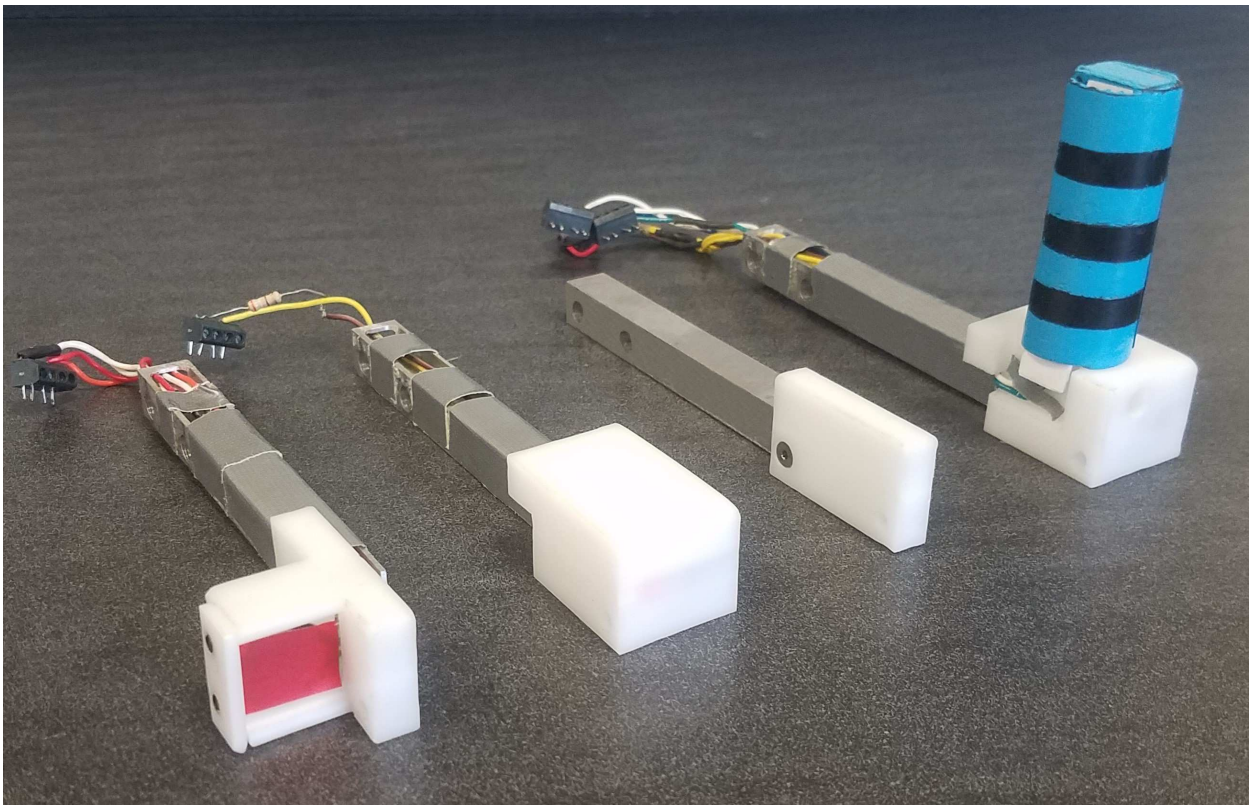

Figure A16: **Modular object components used in the Grip Affordance Experiment.** The object components could be assembled in different ways to form the various objects used in the Grip Affordance Experiment. (Figure 5.1).

A.3 Behavioral Training

All training was accomplished using positive reinforcement. The monkeys were water restricted, and water was used as the primary reward, with supplemental dried fruit used occasionally. Subjects always received at least 15 mL/kg of water per day, either through training or supplementation, and were granted free access to water for at least two days every week.

Each monkey was fitted with a metal collar and trained to accept restraint via a pole attached to the collar. The monkey was then trained to sit upright in a primate chair with limbs restrained. The monkey was then acclimated to the experimental room and apparatus.

The first behavioral task was pressing the start button. The experimenter manually guided the monkey's hand to press the button in the initial training sessions. Subjects were automatically rewarded for each button press. Rewards were delivered via a drink tube attached to the primate chair. The flow of water through the drink tube was gated by a solenoid, controlled automatically by the Dragonfly software module `RewardModule` (see A.5). A characteristic success sound was played in conjunction with reward delivery, controlled by the Dragonfly software module `sound_maker` (see A.5).

The next step in training was to grasp the object. Subjects were given a small reward for pressing the button, and a large reward for grasping the object. The success sound was played after each successful step. Subjects were initially guided to grasp the object through demonstration and assistance. The experimenter then left the room and the subject was rewarded for any object touch, gradually requiring a complete grasp. The reward for pressing the button was gradually decreased until subjects were only rewarded for grasping the object, while the success sound was still played for both actions. The movement time limit was gradually decreased, and required hold time was gradually increased until the desired timing was achieved. Power grasps were learned first, followed by pinch grasps.

Training for the Use Affordance Experiment proceeded in a similar manner to grasp training. All subjects learned to lift the object after demonstration and assistance within a few sessions.

For the Object Presence Experiment, monkeys learned the No-Object Reach condition before the Object Reach condition. The target radius was initially set very large such that any forward motion away from the start button would be rewarded. This was gradually decreased to the final values of a 3cm radius initial target sphere and a 6cm radius hold target sphere. These were the smallest targets which could be reliably achieved by all subjects. Monkeys were then trained on the Object Reach condition. The experiment was carefully monitored and any trial in which the object was touched in any way was aborted, and the task was automatically aborted by activation of any of the FSRs. Subjects eventually learned to reach toward but not contact the object.

Once subjects could reliably perform the tasks, rewards were made smaller and randomized. The randomized reward size followed an exponential distribution. This technique encouraged subjects to complete more trials, while delivering the same amount of water on average. In addition, dried fruit was sometimes given between experiment blocks to encourage higher trial counts.

A.4 Data Acquisition and Preprocessing

This section contains in-depth descriptions of the hardware and software used to collect and align the various data streams involved in the experiments. Section A.4.1 concerns the kinematic data, Section A.4.2 concerns the EMG data, Section A.4.3 concerns behavioral state detection (object FSRs, lift sensor and start button), Section A.4.4 concerns the neural data, Section A.4.5 concerns the temporal alignment and resampling of the data, and Section A.4.6 contains a description of the resulting data structure which served as input to the custom data analysis software.

A.4.1 Kinematics

Kinematic data were acquired using a passive marker infrared motion tracking system (Vicon, Oxford, UK). Images were captured with 11 Vicon MX cameras positioned around the experiment room. The cameras captured data at a rate of 100 frames per second. A subset of these cameras is shown in Figure A17.

Data from the cameras were streamed to a PC via the Vicon MX Ultranet system, and processed using Vicon Nexus 2 software. Before each session, cameras were calibrated using a Vicon calibration wand until all cameras reported low errors, and the world coordinate system was set using a Vicon calibration L-plate. The world coordinates (WLD) were set such that $\mathrm{WLD_X}$ pointed to the right of the subject, $\mathrm{WLD_Y}$ pointed forward from the subject, and $\mathrm{WLD_Z}$ pointed upward.

The subject's arm, hand and finger positions were tracked using infrared-reflective markers. Markers were built by wrapping small beads with infrared-reflective tape. They were then assembled into an upper arm plate, a lower arm plate, and a tracking glove. The plates were constructed by gluing a triangle of markers to a plastic sheet, which was then secured to the subject using a strap of elastic fabric with hook-and-loop fasteners. The tracking glove was constructed by gluing markers directly to a custom-sewn glove made from elastic fabric. The tracking garments are shown in Figure A18 with marker names labeled, and the marker reconstructions in the Vicon Nexus software are shown in Figure A19. Markers can be seen on Monkey R in Figure 3.1.

Markers on the tracking glove were placed directly above specific finger joints, with the exception of marker HAN1, which was placed in the center of the dorsum of the hand, near the wrist. Marker HAN2 was placed on the digit 2 metacarpophalangeal (MCP) joint. Marker HAN3 was placed on the digit 5 MCP joint. Marker HAN4 was placed on the thumb carpo-metacarpal (CMC) joint. Marker D1PR was placed on the thumb MCP joint. Marker D1DI was placed on the thumb interphalangeal (IP) joint. Markers D2PR–D5PR were placed on the proximal interphalangeal (PIP) joints of digits 2–5. Markers D2DI–D5DI were placed on the distal interphalangeal (DIP) joints of digits 2–5.

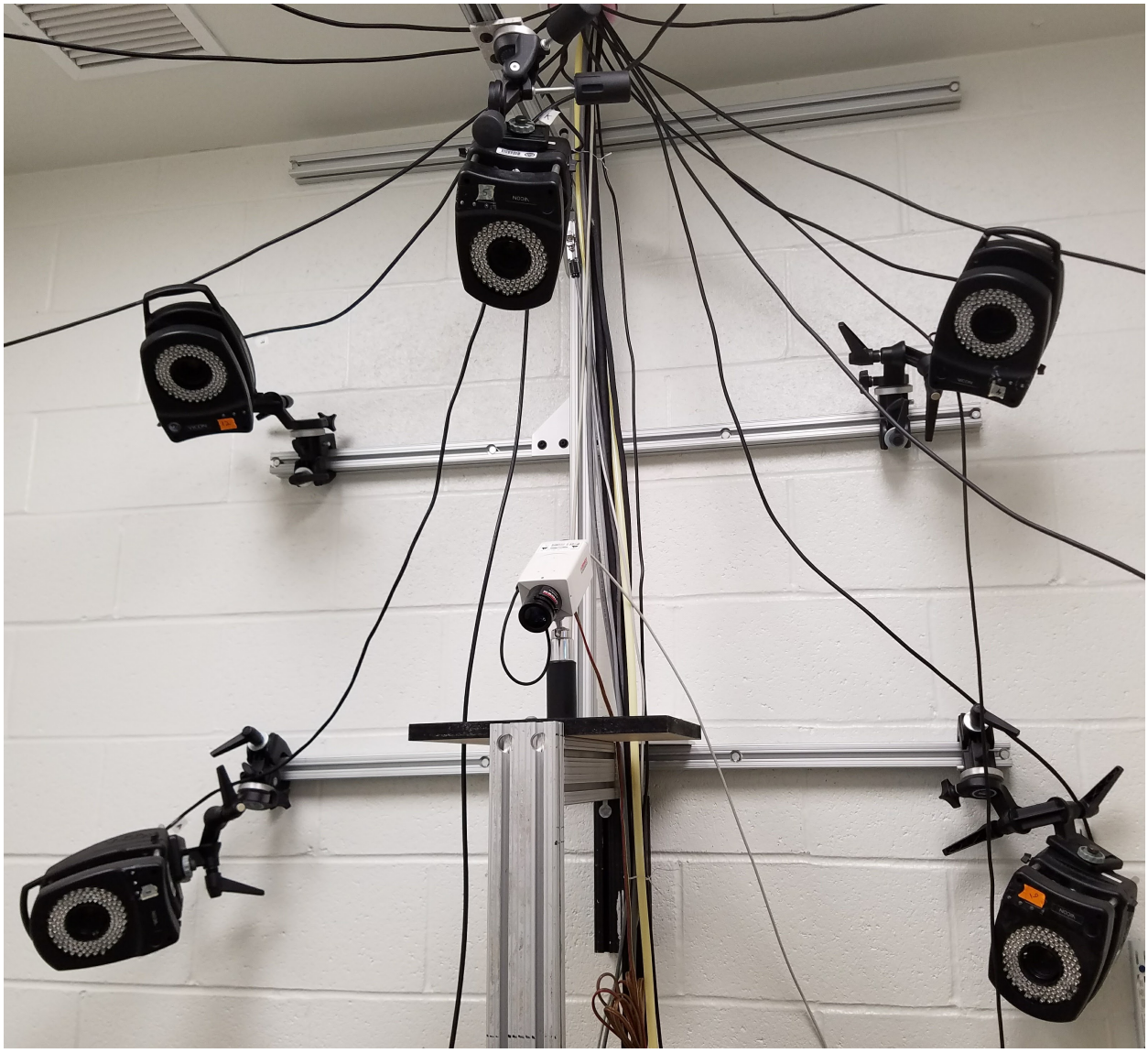

Figure A17: **Motion tracking cameras in the experiment room.** 5 of the 11 cameras are shown. At center is an infrared CCTV camera used for monitoring the experiment remotely.

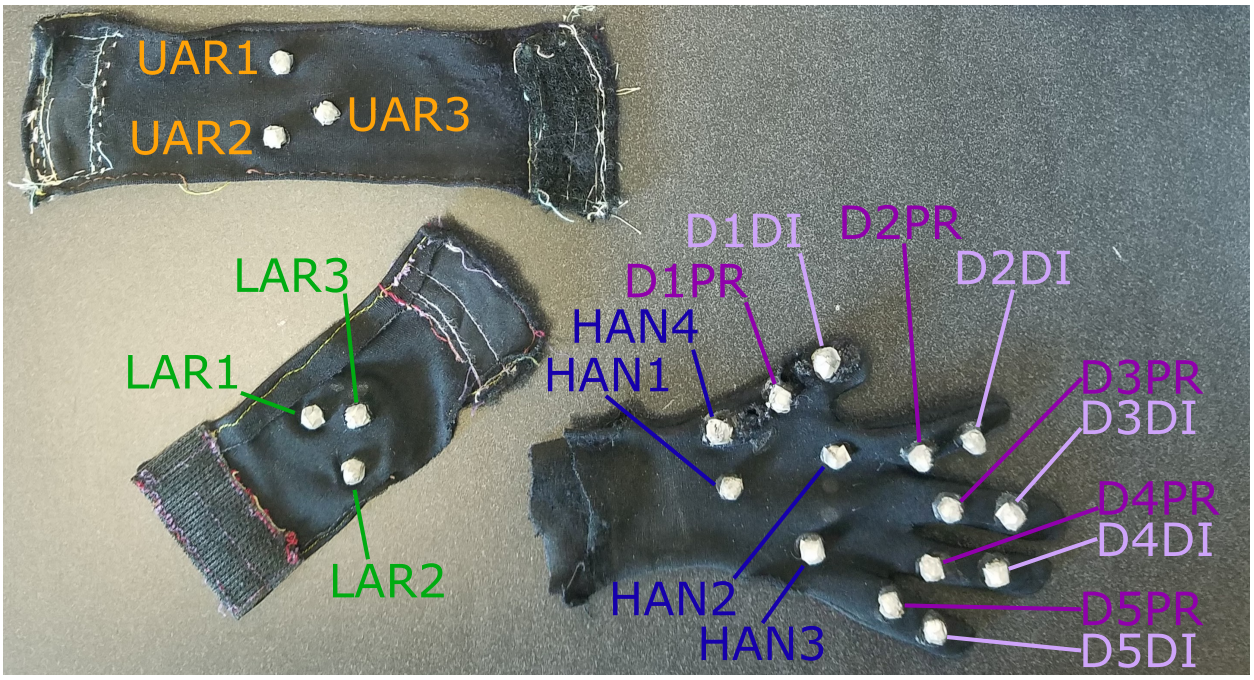

Figure A18: **Motion tracking marker garments.** Garments shown were made for Monkey T right arm and hand.

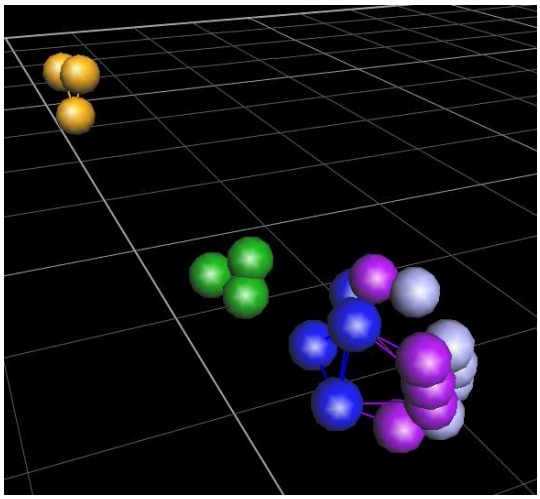

Figure A19: **Motion tracking marker reconstructions.** Screenshot from Vicon Nexus software. Subject was performing a power grasp.

The Nexus software reconstructed marker positions based on individual camera images and camera positions as estimated during calibration. The software also attempted to label the markers based on a kinematic model. Despite extensive parameter tuning for the reconstruction and labeling algorithms, the initial labeled reconstructions contained many errors. These errors typically manifested as missing markers, spurious reconstructions where no marker was present, and mislabeling. Errors were especially prominent in the finger markers around the time of object contact.

A multi-stage process was implemented to fix errors in marker reconstruction and to correct mislabeled markers. This process utilized the tools within the Nexus software as well as custom software written in MATLAB. The processing stages proceeded as follows:

1. Initial files containing labeled reconstructions were generated using the Nexus "Reconstruct and Label" data pipeline.
2. In the Nexus software, gross mislabeling of upper arm, lower arm and hand markers were identified and manually fixed.
3. In the automated custom software, suspected spurious markers were unlabeled and mislabeled upper arm, lower arm and hand markers were relabeled in the right order.
4. In the Nexus software, unlabeled spurious markers were manually deleted, unlabeled true markers were manually labeled and gaps in the upper arm, lower arm and hand marker trajectories were filled manually.
5. In the automated custom software, frames in which finger markers were mislabeled were either fixed automatically or marked for manual checking.
6. In the Nexus software, gaps in the finger marker trajectories were manually filled and mislabeled finger markers were manually relabeled.
7. In the automated custom software, markers were scanned and frames containing suspected errors were marked for manual checking.
8. In the Nexus software, marked frames were checked manually and any remaining errors were fixed.
9. Steps (7) and (8) were repeated until no more errors could be identified.

The custom software worked by performing a series of checks to ensure that markers were in a sensible configuration. For example, the custom software checked that the finger markers proceeded in the correct order from digit 2 to digit 4, and that proximal digit markers lay between hand markers and distal digit markers. The software attempted to fix labeling errors automatically using brute force label switching and repeated checking. When the software could not automatically fix the labeling, it printed the indices of problematic frames to a text file so that they could be checked manually. In the Nexus software, gaps were primarily filled using "spline fill" for short gaps ($\leq$ 9 frames), "pattern fill" for longer gaps ($\leq$ 250 frames) and "rigid body fill" for the longest gaps ($>$ 250 frames). This multi-stage process, though arduous and time-consuming, resulted in accurate, gapless estimations of marker positions.

Joint angles were extracted from marker positions by constructing coordinate frames for each limb segment and finding angles between appropriate coordinate frame axes. This method was selected for its interpretability and consistency, though it does not provide a completely accurate estimate of the true joint angles. Other, more complicated methods such as fitting to a virtual musculoskeletal model, were found to be inconsistent.

The limb segment coordinate frames were constructed according to Table A3. In general, the x-axis corresponded to the long axis of the limb segment pointing away from the trunk, the y-axis pointed along the transverse axis of the limb segment in the plane of the markers on that segment, and the z-axis pointed out from the limb segment perpendicular to the plane of the markers on that segment. Only the x-axis was constructed for the proximal and distal finger segments.

The joint angles were computed by finding the angles between appropriate limb segment axes, according to the equations in Table A4. World coordinate axes, $\mathrm{WLD_X}$, $\mathrm{WLD_Y}$ and $\mathrm{WLD_Z}$, were specified by the motion tracking calibration procedure and corresponded to right of the subject, forward from the subject, and upwards, respectively.

Thumb interphalangeal (IP) joint and digits 2–5 distal interphalangeal (DIP) joint flexions were not calculated as markers could not be tracked reliably on the finger tips. The unrecorded DIP flexion angles were likely highly correlated with PIP flexion angles.

In addition to the 22 joint angles of the arm, hand and fingers, the 3D Endpoint Position was also calculated at each time point by averaging the x, y, z positions of the HAN1, HAN2,

Table A3: **Calculation of limb segment coordinate frames from marker positions.** Marker names denote the x, y, z position vector of the marker. These coordinate frames were calculated for every video frame. The symbol "×" denotes the cross-product operation, and symbols ‖‖ denote the vector norm operation.

Axis	**Calculation Method**
$\mathrm{UAR_X}$	$\frac{\mathrm{UAR2-UAR1}}{\|\mathrm{UAR2-UAR1}\|}$
$\mathrm{UAR_Z}$	$\mathrm{UAR_X} \times \frac{\mathrm{UAR3-UAR1}}{\|\mathrm{UAR3-UAR1}\|}$
$\mathrm{UAR_Y}$	$\mathrm{UAR_Z} \times \mathrm{UAR_X}$
$\mathrm{LAR_X}$	$\frac{\mathrm{LAR2-LAR1}}{\|\mathrm{LAR2-LAR1}\|}$
$\mathrm{LAR_Z}$	$\mathrm{LAR_X} \times \frac{\mathrm{LAR3-LAR1}}{\|\mathrm{LAR3-LAR1}\|}$
$\mathrm{LAR_Y}$	$\mathrm{LAR_Z} \times \mathrm{LAR_X}$
$\mathrm{HAN_X}$	$\frac{(1/3)(2(\mathrm{HAN2})+\mathrm{HAN3})-\mathrm{HAN1}}{\|(1/3)(2(\mathrm{HAN2})+\mathrm{HAN3})-\mathrm{HAN1}\|}$
$\mathrm{HAN_Z}$	$\mathrm{HAN_X} \times \frac{\mathrm{HAN2-HAN1}}{\|\mathrm{HAN2-HAN1}\|}$
$\mathrm{HAN_Y}$	$\mathrm{HAN_Z} \times \mathrm{HAN_X}$
$\mathrm{D1P_X}$	$\frac{\mathrm{D1PR-HAN4}}{\|\mathrm{D1PR-HAN4}\|}$
$\mathrm{D2P_X}$	$\frac{\mathrm{D2PR-HAN2}}{\|\mathrm{D2PR-HAN2}\|}$
$\mathrm{D3P_X}$	$\frac{\mathrm{D3PR}-(1/3)(2(\mathrm{HAN2})+\mathrm{HAN3})}{\|\mathrm{D3PR}-(1/3)(2(\mathrm{HAN2})+\mathrm{HAN3})\|}$
$\mathrm{D4P_X}$	$\frac{\mathrm{D4PR}-(1/3)(\mathrm{HAN2}+2(\mathrm{HAN3}))}{\|\mathrm{D4PR}-(1/3)(\mathrm{HAN2}+2(\mathrm{HAN3}))\|}$
$\mathrm{D5P_X}$	$\frac{\mathrm{D5PR-HAN3}}{\|\mathrm{D5PR-HAN3}\|}$
$\mathrm{D1D_X}$	$\frac{\mathrm{D1DI-D1PR}}{\|\mathrm{D1DI-D1PR}\|}$
$\mathrm{D2D_X}$	$\frac{\mathrm{D2DI-D2PR}}{\|\mathrm{D2DI-D2PR}\|}$
$\mathrm{D3D_X}$	$\frac{\mathrm{D3DI-D3PR}}{\|\mathrm{D3DI-D3PR}\|}$
$\mathrm{D4D_X}$	$\frac{\mathrm{D4DI-D4PR}}{\|\mathrm{D4DI-D4PR}\|}$
$\mathrm{D5D_X}$	$\frac{\mathrm{D5DI-D5PR}}{\|\mathrm{D5DI-D5PR}\|}$

Table A4: **Calculation of joint angles from limb segment coordinate frame axes.** $\angle(\text{Axis}_1, \text{Axis}_2)$ denotes the angle between Axis_1 and Axis_2, calculated by the inverse cosine of the dot product, with "Sign" denoting the axis used to determine the sign of the angle based on the right-hand rule; "+" indicates the joint angle value was always positive. Digits 2–5 MCP_Flex, MCP_Abd and PIP_Flex (last 3 rows) were all calculated the same way, replacing "#" with the appropriate digit number. El: elevation, Abd: abduction, Rot: rotation, Flex: flexion, CMC: carpometacarpal joint, MCP: metacarpophalangeal joint, PIP: proximal interphalangeal joint.

Joint	**Calculation Method**	**Sign**
Shoulder_El	$\angle(-\text{WLD}_\text{Z}$, UAR_X projected onto the WLD_YZ plane)	WLD_X
Shoulder_Abd	$\angle(\text{UAR}_\text{X}$, UAR_X projected onto the WLD_YZ plane)	$-\text{WLD}_\text{Y}$
Shoulder_Rot	$\angle(\text{UAR}_\text{Y}$, $\text{WLD}_\text{Y'}$ after rotation to align $-\text{WLD}_\text{Z}$ with UAR_X)	UAR_X
Elbow_Flex	$\angle(\text{UAR}_\text{X}$, $\text{LAR}_\text{X})$	UAR_Z
Wrist_Flex	$\angle(\text{LAR}_\text{X}$, HAN_X projected onto the LAR_XZ plane)	LAR_Y
Wrist_Abd	$\angle(\text{HAN}_\text{X}$, HAN_X projected onto the LAR_XZ plane)	LAR_Z
Wrist_Rot	$\angle(\text{LAR}_\text{Y}$, $\text{UAR}_\text{Y'}$ after rotation to align UAR_X with LAR_X)	LAR_X
D1CMC_Flex	$\angle(\text{HAN}_\text{X}$, D1P_X projected onto the HAN_XZ plane)	HAN_Y
D1CMC_Abd	$\angle(\text{D1P}_\text{X}$, D1P_X projected onto the HAN_XZ plane)	HAN_Z
D1MCP_Flex	$\angle(\text{D1D}_\text{X}$, $\text{D1P}_\text{X})$	+
D#MCP_Flex	$\angle(\text{HAN}_\text{X}$, $\text{D\#P}_\text{X}$ projected onto the HAN_XZ plane)	HAN_Y
D#MCP_Abd	$\angle(\text{D\#P}_\text{X}$, $\text{D\#P}_\text{X}$ projected onto the HAN_XZ plane)	$-\text{HAN}_\text{Z}$
D#PIP_Flex	$\angle(\text{D\#D}_\text{X}$, $\text{D\#P}_\text{X})$	+

HAN3 and HAN4 markers. joint angular velocities and endpoint velocities were calculated by taking the difference between sequential values using the `diff` function in MATLAB, multiplying by the sample frequency (0.01) and interpolating the resulting values at the original sample time points.

For all experiments, the motion tracking data were recorded and saved for offline preprocessing. For the Object Reach and No-Object Reach conditions in the Object Presence Experiment, the endpoint position was also streamed in real time for use in control of the behavioral task. This was accomplished with custom MATLAB software. This software constituted a Dragonfly module, `ViconStream` (see Section A.5), and was based on the DataStream SDK provided by Vicon.

The `ViconStream` module worked by calculating the current hand position as the average of the HAN1, HAN2, HAN3 and HAN4 markers for each frame, then calculating 1/[(current hand position) - (target hand position)] and sending the resulting value out as a Dragonfly message, `VICON_STREAM_DATA` for use in task judging and feedback (see Section A.5). The target hand position was calculated as the average hand position from the Hold B period of successful trials from both Power Grasp and Pinch Grasp conditions. The target hand positions were obtained from a single Vicon motion capture file captured during a Power Grasp/Pinch Grasp block from the Object Presence Experiment. Monkey I, Monkey R, Monkey T right hand and Monkey T left hand target hand positions were calculated from Vicon files `0090404.c3d`, `0024601.c3d`, `0043103.c3d` and `0051804.c3d` respectively.

A.4.2 EMG

Surface EMG activity from muscles in the shoulder and arm were recorded throughout all experiments. Data were collected with an AMT-8 8 Channel EMG System (Bortec Biomedical, Calgary, Canada). The AMT-8 system consisted of a battery-powered portable unit with wired connections to EMG electrodes and a main amplifier unit. The alligator-style electrode connection clips were replaced with button-style connectors for additional stability. Data from the amplifier were collected and stored using an ADLINK DAQ-2208

Analog Input Card (ADLINK, Taipei, Taiwan). EMG recording was controlled using the MATLAB Dragonfly module `FSREMG` (see Section A.5). EMG data were collected and stored at a sample rate of 5 kHz.

Two types of electrodes were used to obtain EMG. MedGel ECG Pediatric Foam Electrodes (Medline Industries, Northfield, IL) were used for the lower arm, biceps and triceps in all subjects and the deltoid in Monkey T. Red Dot Monitoring Electrodes (3M, Saint Paul, MN) were used for deltoid and pectoralis in Monkeys I and R, trapezius in Monkey T, and the reference electrode in all subjects. A small amount of Spectra 360 Electrode Gel (Parker Laboratories, Fairfield, NJ) was applied to each electrode. Electrodes were secured by loosely wrapping the arm with black foam M Wrap Underwrap (Mueller Sports Medicine, Prairie du Sac, WI). This wrap can be seen in Figure 3.1. The more adhesive Red Dot electrodes were used on areas that could not be wrapped with the M Wrap. The subjects' arms were shaved regularly to improve electrode adhesion.

The signal for each EMG channel was the differential voltage between two adjacent electrodes relative to the reference electrode. The reference electrode was placed on the trunk, at the bottom of the rib cage. Electrode placements were selected to maximize coverage of task-relevant muscles, while accommodating electrode size. Photographs of the EMG electrode locations on Monkey T's left arm are shown in Figure A20.

The shoulder and upper arm electrodes were placed so as to record from a single muscle. The lower arm electrodes likely recorded activity from several underlying muscles. The EMG channel names and likely underlying muscles are listed in Table A5. For Monkey T, the trapezius was recorded instead of pectoralis as Monkey T did not tolerate the pectoralis electrodes. Pectoralis electrode placement can be seen on Monkey R in Figure 3.1.

The resulting EMG signals were of good quality with low noise. The signals occasionally contained small heartbeat artifacts, especially on the pectoralis electrodes. These artifacts were generally small relative to the EMG signal.

After collection, EMG signals were preprocessed in the following steps. The signals were high-pass filtered with a first-order IIR Butterworth filter with a corner frequency of 100 Hz. The resulting signals were rectified by taking the absolute value. Finally, the signals were low-pass filtered with an IIR Butterworth filter of order 4 and cutoff frequency of 30 Hz.

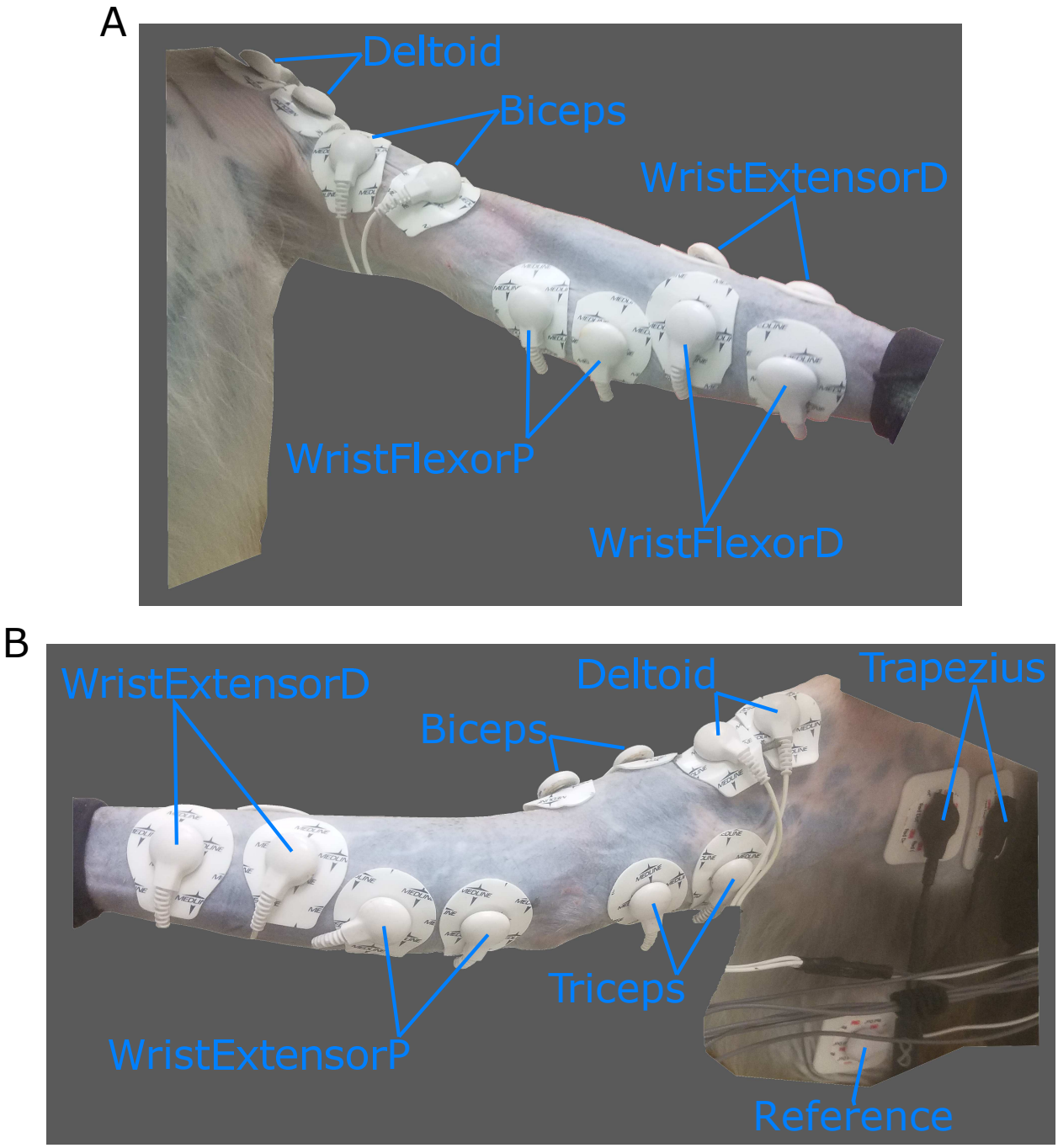

Figure A20: **EMG electrode locations, Monkey T left arm.** A: anterior view, B: posterior view.

Table A5: **EMG Channel Names and Likely Underlying Muscles.**

EMG #	**Subjects**	**EMG Name**	**Underlying Muscles**
1	I and R	Pectoralis	pectoralis
1	T	Trapezius	trapezius
2	All	Deltoid	deltoid
3	All	Triceps	triceps
4	All	Biceps	biceps
5	All	WristExtensorP	extensor carpi ulnaris extensor digitorum comunis anconeus
6	All	WristExtensorD	extensor digitorum comunis extensor carpi radialis brevis abductor pollicis longus extensor pollicis brevis extensor pollicis longus
7	All	WristFlexorP	flexor carpi radialis flexor carpi ulnaris pronator teres palmaris longus flexor digitorum superficialis
8	All	WristFlexorD	brachioradialis flexor pollicis longus flexor digitorum superficialis

A.4.3 Start Button, Force Sensors and Lift Sensor

Start Button

The start button consisted of a simple pushbutton electromechanical switch. The signal from the start button was collected using an Arduino MEGA microcontroller (Arduino, Somerville, MA). The start button signal was monitored by the Dragonfly modules `carduinoIO` and `SimpleJudge`, which sent the Dragonfly signal `START_BUTTON_PRESSED` when the button was depressed, and `START_BUTTON_RELEASED` when the button was released (see Section A.5).

Force Sensors and Lift Sensor

Force sensing was accomplished using force sensing resistors (FSRs). The grasp FSRs were FSR 402 0.5 inch diameter force sensors, and the extra touch detection FSR used in the Object Presence Experiment was an FSR 408 strip-style force sensor (Interlink Electronics, Camarillo, CA). All FSRs were wired according to the diagram in Figure A21. The FSR circuit was a simple voltage divider with an input voltage of 5 V in series with the FSR and a 1 kΩ resistor. The FSR ranged from ∞ Ω to 0 Ω as the FSR was compressed, and thus the output signal from the FSR circuit ranged from 0 V to 5 V.

For the Use Affordance Experiment, vertical object displacement was measured using an SP1-50 linear position tranducer (TE Connectivity, Schaffhausen, Switzerland). The SP1-50 is a rotational "string" potentiometer attached to a spring-loaded spool holding a cable. The cable was secured to the object and the housing of the SP1-50 was secured to the frame below the object. The SP1-50 contains a voltage divider, and thus outputs a signal in the range from 0 V to the input voltage (5 V in this case), increasing as the cable is extended when the object is lifted. The SP1-50 cable can be seen attached to the back of the movable object of the Use Affordance Experiment in Figure 6.2.

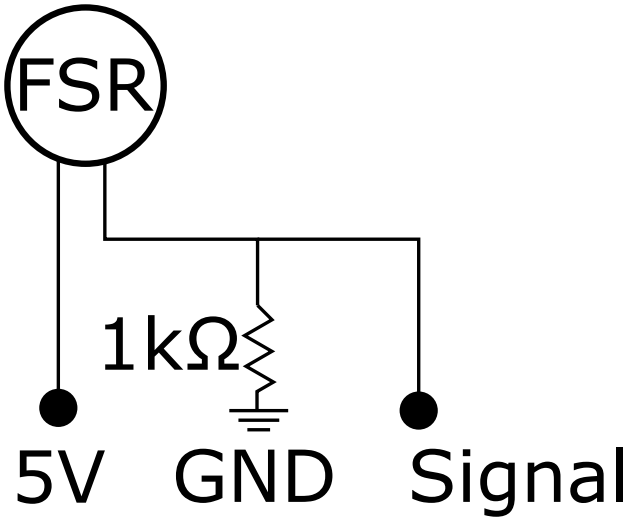

Figure A21: **Force sensing resistor (FSR) circuit diagram.**

Data from all FSRs and the lift sensor were collected using the same DAQ-2208 card that was used for EMG collection (Section A.4.2). The input 5 V and ground for all of the FSRs and lift sensor were also provided by the DAQ-2208 card. Data collection and storage was controlled by the Dragonfly module `FSREMG` (see Section A.5). These data were collected at a rate of 5 kHz.

For online task control, the signals from the FSRs and lift sensor were collected and broadcast by the Dragonfly module `FSREMG`. This was used to automatically confirm object grasp and object lift, or to automatically detect incorrect grasps in order to abort trials. The module sent the average FSR or lift sensor signal from the last 50 samples as the Dragonfly message `FORCE_SENSOR_DATA` (see Section A.5).

A.4.4 Neural Data

Neural spiking data were recorded from microelectrode arrays implanted in the cortex (see Section A.1). Each array was connected to a skull-mounted pedestal which housed a connector. Pre-amplifier headstages were used to interface with these pedestal connectors. For the Utah arrays, Plexon M HST/CereStage 96 headstages were used and for the

FMAs, Plexon F3 HST/32o25-GEN3-36P-G1 headstages were used (Plexon, Dallas, TX). The signals from the headstages were then amplified with the Plexon DigiAmp Digitizing Amplifier, which amplified and digitized the signals at 40 kHz and 16-bit resolution. These signals were then sent to the Plexon OmniPlex Neural Data Acquisition System, which then interfaced with a PC.

Neural signals were processed in Plexon OmniPlex software. The signals were high-pass filtered at 200 Hz. Signals were initially referenced to a wire connected to the outside of the pedestals. Each channel was then additionally digitally referenced to a channel on the same array which showed no spiking activity. The digital referencing was critical for reducing the small but persistent noise generated from the EMG recording system.

A threshold was set on each channel at a value of -3.5 standard deviations of voltage, based on a 10-second recording taken while the subject was at rest at the beginning of each session. For each channel, each time the filtered signal crossed the threshold, a 0.8 ms long snippet of the filtered signal was extracted and displayed. This allowed action potential spikes to be easily viewed.

Spikes were sorted online on each channel using the "lines" method, which sorts snippets based on whether they intersect user-defined line segments in the snippet window. Online spike sorting was performed quickly and non-judiciously, as the main purpose of online spike sorting was to mark channels for later careful offline spike sorting. The snippet data from each channel were saved for offline processing.

The neural data from all files in a single session were combined and analyzed using Plexon Offline Sorter software. Any large noise artifacts were manually identified and rejected. Spikes were sorted manually in the software using the "lines" method and by identifying clusters in the 2D snippet PCA space. Spikes that were sorted together were considered a "unit." Spikes were tracked across time to accommodate drifts in spike magnitude over the course of the sessions. If a unit's spikes became too small to distinguish from background activity at any point in the recording, the unit was rejected. Multiple units were sometimes identified on a single channel, where the waveforms of two distinct units could be clearly separated. When two units could not be reliably separated, they were sorted together into a "multi-unit".

Spikes from an individual unit sometimes occurred on multiple channels due to crosstalk. This could be due to a single neuron being recorded by multiple electrodes, but was more likely due to a short-circuit in the array or connector hardware. In order to identify these instances, the spike times on each pair of channels were compared. For each channel pair, if 75% or more of spikes on a channel ocurred within 1 ms of a spike on the other channel, the channel with fewer overall spikes was excluded from further analysis.

Single units representing the spikes from a single neuron were also identified by calculating the number of inter-spike intervals that were less than 1 ms. Units with 0 inter-spike intervals less than 1 ms were labeled as single units. In general, activity of single units was not markedly different from activity of multi-units. In the results presented in Chapters 4–7, "units" refers to both multi-units and single units.

The final output of the neural recording and sorting steps were spike times labeled with the channel and unit numbers where they occurred.

A.4.5 Data Alignment, Resampling and Smoothing

The kinematic, EMG, FSR, neural and Dragonfly message data (see A.5) were all recorded in different clocks as they were recorded on separate computer systems. A "sync pulse" was employed to synchronize these signals. This 5 V pulse was sent using a PCIe-8361 Device for PXI Remote Control (National Instruments, Austin, TX), controlled by the Dragonfly module `SyncModule` (see Section A.5). The `SyncModule` module also sent a Dragonfly message, `SYNC_PULSE` every time the voltage pulse was sent. A sync pulse was sent at the start of each trial, or 30 seconds after the last pulse. This sync pulse was recorded as an analog signal in each of the data acquisition systems.

The timestamps for all data were converted into the clock of the computer running the `SyncModule` module. This was done by regressing the `SYNC_PULSE` message send times against the time stamps when the signal was first detected by the system to be synchornized. These timestamps were adjusted by one half sample, assuming that the pulse arrived halfway between samples. The data timestamps were then converted by multiplying by the slope and adding the offset that were calculated via regression.

After synchronization, all data were smoothed and resampled at time points relative to certain task events. Data were resampled at 20 ms intervals in three windows:

1. from the time that the start button was pressed to 400 ms after the start button was pressed
2. from 400 ms before reach start to 400 ms after target contact
3. from 400 ms before the reward was delivered (or before the lift cue for the Power Lift condition in the Use Affordance Experiment) to the time that the reward was delivered (or the time of the lift cue for the Power Lift condition in the Use Affordance Experiment)

The start button press time was determined from the send time of the `START_PAD_PRESSED` message (see A.5). The reach time was the time of the first kinematic sample in which the hand velocity surpassed and remained above 1 mm/s for at least 250 ms. The target contact time was the time of the first FSR sample in which one of the grasp FSRs surpassed the contact threshold. The contact threshold was determined as 5 times the maximum FSR value observed during the pre-movement period minus 4 times the mean FSR value during the pre-movement period. For the Object Reach and No-Object Reach conditions in the Object Presence Experiment, target contact time was the time of the first kinematic sample for which the hand position fell inside the target sphere. The reward time was the send time of the `GIVE_REWARD` message (see Section A.5).

The reach times (the time between reach start and target contact) were variable between trials and between condition types. In order to achieve a constant number of samples during the reach, data falling within the reach period were resampled at a variable. First, the average reach time was calculated across all trials in a single session. This average reach time was then divided by 20 ms, and the resulting value rounded to the nearest integer to determine the number of samples for the reach period, $N_{\text{ReachSamples}}$. Then, for the reach period of each trial, $N_{\text{ReachSamples}}$ time points evenly spaced between the reach start time and target contact time were used for resampling each of the data streams.

The kinematic, FSR and EMG data were resampled and smoothed at the appropriate time points by convolving the raw signals with a Gaussian kernel with standard deviation 30 ms. Neural firing rates for each unit were calculated at each time point by binning spike

times in 1 ms bins, multiplying these counts by 1000 to convert to units of spikes per second, and convolving with a Gaussian kernel with standard deviation 30 ms. Lagged versions of the kinematics and EMG were also calculated at time points 40 ms after the standard time points for use in the regression (Section A.6.3) and null space (Section A.6.4) analyses.

Firing rates for use in decoding analyses were also calculated at each standard time point. This was done in a manner similar to the method used by Wodlinger et al 2014 [119] and Clanton 2011 [437]. At each time point, for each unit, spikes were binned in 15 30 ms bins occurring before that time point. Counts were multiplied by 33.33 to convert to units of spikes per second and multiplied by an exponential function with decay constant 0.95.

A.4.6 Data Structure

The preprocessing stages outlined above were performed using custom MATLAB software. This section describes the resulting data structures. Below, the fields of the data structures are listed in bold font, along with a description of the contents of each field in italic font. The MATLAB data structures are described, but all of the statistical analyses were performed in Python by converting the MATLAB structures to Python-compatible structures using the `mat73` and `numpy` packages. All data plots in this dissertation were created in Python using the `matplotlib` and `seaborn` packages.

Data fields in alphabetical order:

EMG

$[N_{\text{Sample}} \times N_{\text{EMG}} \times N_{\text{Trial}}]$ *matrix of preprocessed surface EMG measurements.*

emgID

$[N_{\text{EMG}} \times 1]$ *cell array of EMG channel names.*

EMGlag

$[N_{\text{Sample}} \times N_{\text{EMG}} \times N_{\text{Trial}}]$ *matrix of preprocessed surface EMG measurements at time points 40 ms after the standard time points.*

EP

$[N_{\text{Sample}} \times 3 \times N_{\text{Trial}}]$ *matrix of preprocessed 3D endpoint positions.*

EPlag

$[N_{\text{Sample}} \times 3 \times N_{\text{Trial}}]$ *matrix of preprocessed 3D endpoint positions at time points 40 ms after the standard time points.*

EPV

$[N_{\text{Sample}} \times 3 \times N_{\text{Trial}}]$ *matrix of preprocessed 3D endpoint velocities.*

EPVlag

$[N_{\text{Sample}} \times 3 \times N_{\text{Trial}}]$ *matrix of preprocessed 3D endpoint velocities at time points 40 ms after the standard time points.*

Experiment

String describing which experiment the data are from.

FF

$[N_{\text{Sample}} \times N_{\text{Sensors}} \times N_{\text{Trial}}]$ *matrix of FSR and lift sensor values.*

FFlag

$[N_{\text{Sample}} \times N_{\text{Sensors}} \times N_{\text{Trial}}]$ *matrix of FSR and lift sensor values at time points 40 ms after the standard time points.*

fixed_lag

Float describing the temporal shift of the lagged data fields, in seconds.

forceID

$[N_{\text{Sensors}} \times 1]$ *cell array of FSR and lift sensor names.*

FFlag

$[N_{\text{Sample}} \times N_{\text{Sensors}} \times N_{\text{Trial}}]$ *matrix of FSR and lift sensor values at time points 40 ms after the standard time points.*

FR

$[N_{\text{Sample}} \times N_{\text{Units}} \times N_{\text{Trial}}]$ *matrix of preprocessed firing rates.*

FRD

$[N_{\text{Sample}} \times N_{\text{Units}} \times N_{\text{Trial}}]$ *matrix of preprocessed firing rates for decoding.*

JA

$[N_{\text{Sample}} \times N_{\text{Joints}} \times N_{\text{Trial}}]$ *matrix of preprocessed joint angles.*

JAlag

$[N_{\text{Sample}} \times N_{\text{Joints}} \times N_{\text{Trial}}]$ *matrix of preprocessed joint angles at time points 40 ms after the standard time points.*

JAV

$[N_{\text{Sample}} \times N_{\text{Joints}} \times N_{\text{Trial}}]$ *matrix of preprocessed joint angular velocities.*

JAVlag

$[N_{\text{Sample}} \times N_{\text{Joints}} \times N_{\text{Trial}}]$ *matrix of preprocessed joint angular velocities at time points 40 ms after the standard time points.*

jointID

$[N_{\text{Joints}} \times 1]$ *cell array of joint names.*

Monkey

String describing which subject the data are from.

nfixbin

The number of samples in each 400 ms time window.

nvarbin

The number of samples in the reach period time window.

pshortisi

$[N_{\text{Units}} \times 1]$ *array containing the proportion of inter-spike intervals that are shorter than 1 ms, for each unit.*

resolution

The sample frequency of the resampled data points in ms.

Session

The number of the session from which the data were collected.

smoothkern

String describing the smoothing kernel used to smooth kinematic, force and EMG data, and to calculate the FRs.

spikeID

$[N_{\text{Units}} \times 2]$ *array of unit channel numbers and unit indices.*

task_map

$[N_{\text{Trials}} \times 1]$ *array of integers denoting the task condition of each trial.*

task_types

$[N_{\text{Conditions}} \times 1]$ *cell array of condition names.*

trial_no

$[N_{\text{Trials}} \times 1]$ *array of trial numbers.*

vardt

$[N_{\text{Trials}} \times 1]$ *array of variable rate sample frequencies for the reach period windows in ms.*

A.5 Modular Task Automation Software

The custom software used to control and automate the behavioral tasks was comprised of multiple modules across three computers. These modules controlled a variety of functions, such as task phase progression, visual task feedback, reward delivery and data acquisition. In order to coordinate the modules, the modular messaging software Dragonfly (`https://dragonflymessaging.org/`) was employed.

The Dragonfly software allows software modules written in different languages and running on different computers to communicate seamlessly at high speed by sending messages through a central hub module. The software also logs the messages and message data, along with send and receive timestamps, for later analysis.

Below is a list of the critical modules which comprised the task control software, with brief descriptions of the module functions and the messages sent or received by the module.

`MessageManager`

Core Dragonfly module to which all other modules connect, and which collates and forwards all messages.

`QuickLogger`

Core Dragonfly module which records all message data and message metadata for offline analysis.

`ApplicationControl`

Python module which starts and stops other modules at the beginning and end of the session.

`Executive`

MATLAB task control module which dictates the progression of task states. Receives `START_PAD_PRESSED`, `START_PAD_RELEASED`, `JUDGE_VERDICT`. *Sends* `GIVE_REWARD`.

`SampleGenerator`

Python module which sends a message every 20 ms that serves as a clock to trigger other modules.

`SyncModule`

C++ module which sends the hardware sync pulse for data alignment and triggers the Vicon and Plexon systems to begin and pause recording. Sends `SYNC_PULSE`.

`SimpleJudge`

MATLAB module which judges whether certain task progression criteria have been met, such as the start button being pressed. Receives `INPUT_DOF_DATA`. *Sends* `START_PAD_PRESSED`, `START_PAD_RELEASED`.

`GatingForceJudge`

MATLAB module which judges whether certain task progression criteria have been met, such as activation of the grasp FSRs or positioning the hand within the target sphere. Receives `FSR_DATA`, `VICON_STREAM_DATA`. *Sends* `JUDGE_VERDICT`.

`FSREMG`

MATLAB module which controls data collection from the FSRs and EMG system. Sends `FSR_DATA`.

`ViconStream`

MATLAB module which streams hand position relative to the target hand position, for use in real-time task judging during the Object Presence Experiment. Sends `VICON_STREAM_DATA`.

`ColorCueDisplay`

Python module which controls the visual feedback shown to the subject. Receives `FSR_DATA`, `VICON_STREAM_DATA`.

`RewardModule`

Python module which controls the solenoid that opens to deliver the reward to the subject. Receives `GIVE_REWARD`.

`sound_maker`

C# module that plays a sound upon successful completion of certain task phases.

`VideoLogger`

Python module which controls the video monitoring of the task.

A.6 Statistical Analyses

This section describes the statistical analyses used to generate the results of Chapters 4–7. All statistical analyses were performed in Python.

A.6.1 Principal Components Analysis

Principal Components Analysis (PCA) can be used to find an orthonormal basis in which the axes (Principal Components, PCs) are ranked according to amount of data variance which occurs along each axis. Each PC represents an eigenvector of the covariance matrix of the input data. PCA can be used for dimensionality reduction by considering only the top-ranked PCs that explain most of the data variance.

Varimax PCA was used to visualize MF and FR variation (Sections 4.2, 4.3, 5.2, 5.3, 6.2 and 6.3). The procedure is explained here for MFs, but the same method was applied to the FRs, substituting FRs for MFs and N_{Units} for N_{MF}. As a first step, the MFs in the peri-movement period (100 ms before reach start to 400ms after target contact) were first trial-averaged by taking the mean MFs across all trials within each condition. The condition-independent MF timecourses were then removed (data were centered across time) by subtracting the mean over all conditions for each MF at each time point. The MFs were then normalized by dividing each MF by its standard deviation. This resulted in a $[(N_{\text{MoveSamples}} * N_{\text{Conditions}}) \times N_{\text{MF}}]$ matrix of trial-averaged, centered MFs which was then used as the input to the PCA algorithm.

PCA was performed using the `PCA` function of the Python `statsmodels` package, with arguments `standardize = 'False'`, `demean = 'False'`, `method = 'eig'`.

The cumulative variance explained was found by calculating the cumulative sum of the ranked covariance matrix eigenvalues divided by the sum of all eigenvalues. The smallest number (N_{PC}) of eigenvalues for which the cumulative variance explained was > 0.99 were selected, and the corresponding eigenvectors (components) were assembled into a $[N_{\text{MF}} \times N_{\text{PC}}]$ principal component (PC) matrix.

Varimax rotation was then applied to this component matrix. The varimax method applies a rotation to the components which seeks to maximize the variance of the squared component loading values, while preserving orthogonality of components. The effect of varimax is to reduce the number of large loading values in each component, allowing for easier interpretation. Varimax rotation was performed using a custom iterative function in Python, resulting in the rotated varimax principal components matrix (VPCs). The VPC scores were then computed by projecting the trial-averaged, centered MFs through the VPC matrix. The VPCs were ranked by descending variance of VPC scores. The VPC scores and VPC components are shown in Figures 4.10, 4.11, 5.7, 6.9 and 6.10 for the MFs, and the VPC scores for the FRs are shown in Figures 4.17, 4.18, 5.14, 6.17 and 6.18.

The inter-condition distances in MF PC space and FR PC space displayed in Figures 4.12, 4.20, 5.8, 5.9, 5.16, 5.17, 6.11, 6.12, 6.20 and 6.21 were calculated using PC scores generated using the method described above, but excluding the varimax step.

PCA was also used to reduce the dimensionality of MFs and produce uncorrelated features for the regressions of Sections 4.4.1, 4.5, 5.4.1, 5.5, 6.4.1, 6.5, 7.2 and 7.3. For this purpose, lagged MFs (occurring 40ms after the standard time points) from the peri-movement period were normalized by subtracting the mean and dividing by the standard deviation of each MF. Unlike the varimax PCA above, MFs were not trial-meaned nor were they centered at each time point. This produced a $[(N_{\text{MoveSamples}} * N_{\text{Trials}}) \times N_{\text{MF}}]$ matrix of normalized, lagged MFs which were used as the input to the PCA algorithm.

PCA was then performed as above, and the top covariance matrix eigenvectors (components) explaining 99% of the data variance were extracted to produce the PC matrix. The PC scores were then computed by projecting the normalized MFs through this PC matrix. These scores then used for regression (see Section A.6.3).

Finally, PCA was also used to reduce the dimensionality of the lagged MFs and the FRs of the peri-movement period for the null space analyses of Sections 4.4.2, 5.4.2 and 6.4.2. For this purpose, the lagged MFs and the FRs were trial-averaged, resulting in a $[(N_{\text{MoveSamples}} * N_{\text{Conditions}}) \times 58]$ lagged mMF matrix and a $[(N_{\text{MoveSamples}} * N_{\text{Conditions}}) \times N_{\text{Units}}]$ mFR matrix which where then normalized and used as inputs to the `PCA` function. The smallest number of mMF PCs (covariance matrix eigenvectors) accounting for at least 99%

of lagged MF variance were chosen to construct the mMF PC score matrix, and twice this number of mFR PCs were chosen to construct the mFR PC score matrix. The number of mFR PCs was chosen to be twice of the number of mMF PCs so that the potent and null spaces would have equal dimensionality. These matrices were then used for the null space analyses detailed in Section A.6.4.

A.6.2 Permutation Tests

Significant differences in mean FRs between conditions were detected using permutation tests (Sections 4.3, 5.3, 6.3 and 7.1). The permutation test is a non-parametric alternative for the common t-test. The permutation test leverages randomized resampling to estimate the distribution of a test statistic (in this case, the difference in mean FRs) under the null hypothesis (in this case, that the mean FRs were equal).

At each time point, for each pair of conditions, the ($N_{\text{Trials}}/N_{\text{Conditions}}$) FR values from condition i were compared against the ($N_{\text{Trials}}/N_{\text{Conditions}}$) FR values from condition j. The empirical difference in means was first calculated as:

$$d_{i,j} = \overline{f}_i - \overline{f}_j \tag{A.1}$$

The permuted mean difference was then calculated by randomly shuffling the condition labels of the FR values, generating $f^*_{i,q}$ and $f^*_{j,q}$. The permuted mean difference for iteration q is then calculated as:

$$d^*_{i,j,q} = \overline{f^*}_{i,q} - \overline{f^*}_{j,q} \tag{A.2}$$

This procedure was repeated 10000 times to generate a distribution of permuted mean differences $\boldsymbol{d^*_{i,j}}$. This distribution approximates the distribution of mean differences under the null hypothesis that the mean difference is equal to 0.

A p-value, $p_{i,j}$, was then generated by counting the number of instances of permuted mean differences $\boldsymbol{d^*_{i,j}}$ that were more extreme than the empirical mean difference $d_{i,j}$ and dividing by the number of permutations:

$$p_{i,j} = \frac{\min\left[\#(\boldsymbol{d^*_{i,j}} > d_{i,j}),\ \#(\boldsymbol{d^*_{i,j}} < d_{i,j})\right]}{10000} \tag{A.3}$$

This p-value approximates the likelihood of observing the empirical difference in means, $d_{i,j}$ under the null hypothesis that the actual underlying difference in means is equal to 0.

This procedure was repeated for each time point, for each pair of conditions, for each unit to produce the data plotted in Figures 4.16, 5.11 and 6.14.

Paired permutation tests were used to compare decoder performances in Section 4.6. The paired permutation test is a non-parametric alternative to the paired-sample t-test for difference in means. The paired permutation test is performed similarly to the permutation test, but instead of shuffling all data labels, each group is forced to contain only one data point from each pair. This is accomplished by switching pair labels of each pair with a probability of 0.5 for each iteration to generate the null distribution of mean differences. As in the permutation test, the null distribution of mean differences is compared against the empirical mean difference to generate a p-value.

A.6.3 Encoding Model Regression

For encoding analyses, multiple linear regression was used to estimate encoding weights for predicting FRs from lagged MF PC scores and context-related indicator variables. Only data from the peri-movement period were used, with MF data lagging FR data by 40 ms. The calculation of MF PC scores is detailed in Section A.6.1. The formulation for the regression was:

$$\mathbf{Q} = \mathbf{P}\boldsymbol{\beta} + \epsilon \tag{A.4}$$

where $\mathbf{Q}$ is a $[N_{\text{Ttot}} \times N_{\text{Units}}]$ matrix of normalized FRs, $\mathbf{P}$ is a $[N_{\text{Ttot}} \times N_{\text{Predictors}}]$ matrix of predictors, consisting of lagged MF PCs, indicator variables and interaction terms, $\boldsymbol{\beta}$ is a $[N_{\text{Predictors}} \times N_{\text{Units}}]$ matrix of regression weights, and ϵ is a multivariate Gaussian noise

term. Each column of $\mathbf{Q}$ corresponds to the normalized FR of a unit, f, as in Equation 4.22. Thus, this matrix form is equivalent to regressing each individual FR on the predictor matrix P. The calculation of the PC scores is described in section A.6.1.

The predictor matrix took 3 different forms, the "MF Only" model, the "Direct" model, and the "Interactive" model (see Sections 4.5, 5.5 and 6.5). For the "MF Only" model, the predictor matrix $\mathbf{P}$ contained $(N_{\mathrm{MFPC}} + 1)$ columns: the N_{MFPC} lagged MF PC scores and a column of 1s. Thus in the "MF Only" model, the columns of $\boldsymbol{\beta}$ constitute each unit's "preferred direction" in MF PC space. For the "Direct" model, the predictor matrix $\mathbf{P}$ contained $(N_{\mathrm{MFPC}} + 2)$ columns: the N_{MFPC} lagged MF PC scores, a column of 1s and an indicator variable column which contained 1s for samples from trials in one object context, and 0s for samples from trials in the other object context. For the "Interactive" model, the predictor matrix $\mathbf{P}$ contained $(2 * N_{\mathrm{MFPC}} + 2)$ columns: the N_{MFPC} lagged MF PC scores, a column of 1s, the indicator variable column, and N_{MFPC} interaction term columns which contained the lagged MF PC scores for samples from one object context and 0s for samples from the other object context. Equations 4.22, 4.23 and 4.24 describe these 3 models in terms of predicting a single unit firing rate f, whereas for the actual calculations, the matrix formulations were used to predict all firing rates, $\mathbf{Q}$, simultaneously.

The regression weight matrix, $\boldsymbol{\beta}$, was estimated using the following formula:

$$\hat{\boldsymbol{\beta}} = (\mathbf{P}^{\mathrm{T}}\mathbf{P})^{-1}\mathbf{P}^{\mathrm{T}}\mathbf{Q} \tag{A.5}$$

Where $\mathbf{P}^{\mathrm{T}}$ is the transpose of matrix $\mathbf{P}$, and $()^{-1}$ denotes the matrix inverse operation. This method was viable as the lagged MF PCs were linearly independent.

In order to calculate goodness of fit metrics for each model, the predicted FRs, $\hat{\mathbf{Q}}$ and the residuals, $\mathbf{E}$ were calculated as:

$$\hat{\mathbf{Q}} = \mathbf{P}\hat{\boldsymbol{\beta}} \tag{A.6}$$

$$\mathbf{E} = \mathbf{Q} - \hat{\mathbf{Q}} \tag{A.7}$$

For each column k of $\mathbf{Q}$ (i.e. for each unit k), the residual sum of squares, SSE_k, the standard deviation of residuals, σ_k, and the total sum of squares, SST_k were calculated as:

$$\mathrm{SSE}_k = \sum_{t=1}^{N_{\mathrm{Ttot}}} (E_{t,k})^2 \tag{A.8}$$

$$\sigma_k = \frac{\mathrm{SSE}_k}{N_{\mathrm{Ttot}} - 1} \tag{A.9}$$

$$\mathrm{SST}_k = \sum_{t=1}^{N_{\mathrm{Ttot}}} (Q_{t,k})^2 \tag{A.10}$$

where $E_{t,k}$ is the entry of $\mathbf{E}$ in row t and column k, and $Q_{t,k}$ is the entry of $\mathbf{Q}$ in row t and column k.

The regression R_k^2 values, the estimated log-likelihood of the model, $\log(\hat{L}_k)$ and the Bayes Information Criterion, BIC_k, for each unit k were then calculated as:

$$R_k^2 = 1 - \frac{\mathrm{SSE}_k}{\mathrm{SST}_k} \tag{A.11}$$

$$\log(\hat{L}_k) = -\frac{N_{\mathrm{Ttot}}}{2}\log(2\pi) - \frac{N_{\mathrm{Ttot}}}{2}\log(\sigma_k^2) - \frac{1}{2\sigma_k^2}\mathrm{SSE}_k \tag{A.12}$$

$$\mathrm{BIC}_k = (N_{\mathrm{Predictors}} + 1)\log(N_{\mathrm{Ttot}}) - 2\log(\hat{L}_k) \tag{A.13}$$

Finally, the trial-averaged $R_{\mathrm{TA},k}^2$ were calculated. To do so, the trial-averaged FRs, $\mathbf{Q}_{\mathrm{TA}}$ and trial-averaged predicted FRs, $\hat{\mathbf{Q}}_{\mathrm{TA}}$ were calculated by averaging $\mathbf{Q}$ and $\hat{\mathbf{Q}}$ over all trials within each condition. The resulting $\mathbf{Q}_{\mathrm{TA}}$ and $\hat{\mathbf{Q}}_{\mathrm{TA}}$ were of dimension $[(N_{\mathrm{MoveSamples}} * N_{\mathrm{Conditions}}) \times N_{\mathrm{Units}}]$. The $R_{\mathrm{TA},k}^2$ values were then calculated as the squared Pearson's correlation coefficient of $\mathbf{Q}_{\mathrm{TA}}$ and $\hat{\mathbf{Q}}_{\mathrm{TA}}$:

$$R_{\mathrm{TA},k}^2 = \mathrm{cor}(\mathbf{Q}_{\mathrm{TA},:,k}, \hat{\mathbf{Q}}_{\mathrm{TA},:,k})^2 \tag{A.14}$$

where $\mathbf{Q}_{\mathrm{TA},:,k}$ denotes a vector containing all entries of $\mathbf{Q}_{\mathrm{TA}}$ in column k (all trial-averaged FRs of unit k), and $\mathbf{Q}_{\mathrm{TA},:,k}$ denotes a vector containing all entries of $\hat{\mathbf{Q}}_{\mathrm{TA}}$ in column k (all trial-averaged predicted FRs of unit k). The Pearson's correlation coefficient calculation

was performed using the `corrcoef` function of the Python package `numpy`. The measure $R^2_{\mathrm{TA},k}$ provides a measure of goodness of fit of the model for unit k that ignores trial-to-trial variability, which was generally large (see Figure 4.22).

A.6.4 Null Space Analyses

The null space analyses in this dissertation were inspired by the work of Kaufman et al 2014 [132]. While Kaufman et al regressed neural activity against only muscle activity, here the neural activity was regressed against linear combinations of all of the recorded MFs, including joint angles, joint angular velocities, hand positions, hand velocities and muscle activity.

The first step of the null space analysis was to reduce the dimensionality of trial-averaged FRs and trial-averaged lagged MFs, as detailed in Section A.6.1. Whereas the regressions of Section A.6.3 modeled FRs as linear combinations of MF PC scores (encoding perspective), the regressions for the null space analyses modeled mMF PC scores as linear combinations of mFR PC scores (decoding perspective), according to the following equation:

$$\mathbf{M} = \mathbf{F}\mathbf{B} + \epsilon \tag{A.15}$$

where $\mathbf{M}$ is a $[(N_{\mathrm{MoveSamples}} * N_{\mathrm{Conditions}}) \times N_{\mathrm{mMFPC}}]$ matrix of lagged mMF PC scores, $\mathbf{F}$ is a $[(N_{\mathrm{MoveSamples}} * N_{\mathrm{Conditions}}) \times N_{\mathrm{mFRPC}}]$ matrix of lagged mFR PC scores and $\mathbf{B}$ is a $[N_{\mathrm{mFRPC}} \times N_{\mathrm{mMFPC}}]$ matrix of regression weights. Unlike the predictor matrix $\mathbf{P}$ in Section A.6.3, $\mathbf{F}$ did not contain a column of 1s and thus $\mathbf{B}$ did not contain a constant offset term. The regression weight matrix $\mathbf{B}$ was estimated as:

$$\hat{\mathbf{B}} = (\mathbf{F}^{\mathrm{T}}\mathbf{F})^{-1}\mathbf{F}^{\mathrm{T}}\mathbf{M} \tag{A.16}$$

resulting in the $[N_{\mathrm{mFRPC}} \times N_{\mathrm{mMFPC}}]$ matrix $\hat{\mathbf{B}}$. As described in Section A.6.1, the number of mFR PCs and mMF PCs were selected such that:

$$N_{\mathrm{mFRPC}} = 2N_{\mathrm{mMFPC}} \tag{A.17}$$

Accordingly, $\hat{\mathbf{B}}$ was of rank N_{mMFPC}, whereas the full mFR PC matrix was of rank $2N_{\text{mMFPC}}$. Thus, the row space of $\hat{\mathbf{B}}$ describes the N_{mMFPC}-dimensional subspace of neural activity $\mathbf{F}$ which can be linearly combined to decode the mMF PCs (the "potent space"), and the null space of $\hat{\mathbf{B}}$ describes the N_{mMFPC}-dimensional subspace of neural activity $\mathbf{F}$ which in an mMF PC decode of 0 (the "null space").

Singular Value Decomposition (SVD) was used to decompose $\hat{\mathbf{B}}$ to find the row space $\hat{\mathbf{B}}_{\text{potent}}$ and the null space $\hat{\mathbf{B}}_{\text{null}}$:

$$\text{SVD}(\hat{\mathbf{B}}^{\text{T}}) = \mathbf{USV}^{\text{T}} \tag{A.18}$$

$$\hat{\mathbf{B}}_{\text{potent}}^{\text{T}} = \text{first } N_{\text{mMFPC}} \text{ rows of } \mathbf{V}^{\text{T}} \tag{A.19}$$

$$\hat{\mathbf{B}}_{\text{null}}^{\text{T}} = \text{last } N_{\text{mMFPC}} \text{ rows of } \mathbf{V}^{\text{T}} \tag{A.20}$$

SVD was performed using the `linalg.svd` function of the Python `numpy` package. The neural activity $\mathbf{F}$ can then be partitioned into potent space activity $\hat{\mathbf{F}}_{\text{potent}}$ and null space activity $\hat{\mathbf{F}}_{\text{null}}$ by projecting through $\hat{\mathbf{B}}_{\text{potent}}$ and $\hat{\mathbf{B}}_{\text{null}}$ respectively:

$$\hat{\mathbf{F}}_{\text{potent}} = \mathbf{F}\hat{\mathbf{B}}_{\text{potent}} \tag{A.21}$$

$$\hat{\mathbf{F}}_{\text{null}} = \mathbf{F}\hat{\mathbf{B}}_{\text{null}} \tag{A.22}$$

The resulting $\hat{\mathbf{F}}_{\text{potent}}$ is the neural activity that can be linearly decoded to produce the mMF PC scores and $\hat{\mathbf{F}}_{\text{null}}$ is the neural activity that is linearly unrelated to mMF PC scores. As $\mathbf{V}^{\text{T}}$ is a unitary matrix, and $\hat{\mathbf{B}}_{\text{potent}}$ and $\hat{\mathbf{B}}_{\text{null}}$ span orthogonal subspaces, variance in the total mFR PC space $\mathbf{F}$ is equal to the sum of variances in the two subspaces $\hat{\mathbf{F}}_{\text{potent}}$ and $\hat{\mathbf{F}}_{\text{null}}$. The potent and null spaces were constructed to have the same dimensionality in order to facilitate direct comparison of variance in the two spaces.

A.6.5 Movement Feature Decoding

The MF decoding analyses in this dissertation were designed to approximate the decoding methods used in recent neuroprosthetic studies [119, 437]. Accordingly, each MF was decoded independently using a linear model combining FRs. The FRs used for decoding were calculated using a sliding exponential filter (see Section A.4.4). While the study of Wodlinger et al [119] first estimated encoding models for each neuron using optimal linear estimation, here we directly decoded normalized MFs from FRs, as the large number of highly correlated MFs recorded for this dissertation (58 vs. 7 or 11 for Wodlinger et al) would likely hinder accurate encoding model construction.

For the MF decoding analyses, a regression framework of the following form was used:

$$\mathbf{Y} = \mathbf{X}\mathbf{W} + \epsilon \tag{A.23}$$

where $\mathbf{Y}$ is a $[(N_{\text{MoveSamples}} * N_{\text{TrainingTrials}}) \times N_{\text{MF}}]$ matrix of normalized MFs, $\mathbf{X}$ is a $[(N_{\text{MoveSamples}} * N_{\text{TrainingTrials}}) \times (N_{\text{Units}} + 1)]$ matrix of normalized decoding FRs (see Section A.4.4) with an added column of 1s, and $\mathbf{W}$ is a $[(N_{\text{Units}} + 1) \times N_{\text{MF}}]$ matrix of ridge regression weights.

The weights matrix $\mathbf{W}$ was estimated with ridge regression, using the `OLS` class from the Python package `statsmodels`. Ridge regression is a regularized version of multiple linear regression which uses a regularization constant, λ to reduce the overall magnitudes of the weight coefficients. This results in biased, but more accurate predictions of novel data.

For each session, a single λ parameter was found using 10-fold cross-validation. To do this, the full set of trials was partitioned into 10 randomized blocks, each containing an equal number of trials from each task condition. For each fold of cross-validation, the model was fit with ridge regression using 9 of the blocks as training data, and tested on the remaining block. The root mean squared error (RMSE) was calculated from the difference between the actual normalized MFs of the test block and the predicted normalized MFs for the test block. This procedure was repeated 10 times, using a different block of trials as the test block each time. A single overall RMSE value was then calculated by taking the square root of the mean squared error averaged across all MFs and the 10 folds. This entire procedure

was repeated for a range of candidate λ values, and the λ value that resulted in the lowest overall RMSE was chosen, and applied to all decoding model estimates for that session. Ridge regression parameters λ ranged from 0.01 to 0.03.

Different decoders were built using either the full dataset from a session, or certain data subsets pertaining to different object contexts. These decoders were then tested on either the same subset used for training, or on a separate test subset.

When training and testing a decoder using the same data subset (e.g. training and testing on only the No-Object Reach data from the Object Presence Experiment), 10-fold cross-validation was used to evaluate decoder performance. The trials in the data subset were partitioned into 10 equal-sized blocks, taking a balanced number of trials from each condition present in the data subset. Then, for each fold, 9 of these blocks were used to train a decoder, and the MFs in the remaining block were predicted. The mean squared error (MSE) between predicted and actual MFs in the test block were then calculated. This procedure was repeated 10 times, testing on a different block each time. A single RMSE value for each MF was then calculated by averaging the 10 MSEs from the 10 folds and taking the square root.

When training on one data subset and testing on another (e.g. training on the Object Reach data and testing on the No-Object Reach data from the Object Presence Experiment), a similar procedure was used. Both the training and testing data subsets were partitioned into 10 blocks as above. A decoder was trained with 9 of the blocks in the training subset. Instead of using the left-out block from the training subset as the test block, one of the blocks from the testing subset was used as the test block. Repeating this procedure produced 10 MSE values for each MF. A single RMSE value for each MF was then calculated by averaging the 10 MSEs from the 10 folds and taking the square root.

For the context-detecting decoders, separate context-specific linear decoders were constructed and trained on data from only a single context. For example, one decoder was trained on only the No-Object Reach data in the Object Presence Experiment, and another decoder was trained on only data from the conditions in which the object was present (Object Reach, Power Grasp and Pinch Grasp conditions). In addition, a classifier was trained to classify the context (i.e. whether the object was present or absent in the Object

Presence Experiment). Classification was accomplished using a Gaussian Naive Bayes classifier, implemented with the `GaussianNB` class of the `sklearn` Python package. Along with binary predictions, the Gaussian Naive Bayes classifier also output the probability of each label. To decode each MF using the context-detecting decoder, the outputs from the two context-specific decoders were multiplied by the probability of each class as output by the classifier, and summed. This decoder architecture is illustrated in Figure 4.37. The context-detecting decoder was evaluated using 10-fold cross-validation, and performance was compared against two perfectly applied context-specific decoders and a single context-blind decoder, all trained and tested using the same cross-validation folds.

A.6.6 Bootstraps

For many of the summary statistics reported in Chapters 4–7, bootstrap methods were employed to estimate confidence intervals and correct for bias in the estimation of the statistics. This was done for the trial-averaged MF values (Figures 4.2–4.7, 5.2–5.5 and 6.3–6.7), MF PC inter-condition distances, D_{MFPC} and $\overline{D}_{\text{MFPC}}$ (Figures 4.12, 5.8, 5.9, 6.11 and 6.12), trial-averaged FRs (Figures 4.13, 5.10, 6.13 and 7.2–7.5), the overall trial-averaged normalized FRs (Figures 4.14 and 7.7), the population modulation Δ and Δ^{prep} (Figures 4.19, 5.15, 6.19, 7.13 and 7.14–7.16), the extralinear modulation ξ and $\overline{\xi}$ (Figure 4.24), the population extralinear modulation ξ^{pop} and $\overline{\xi}^{\text{pop}}$ (Figures 4.25, 5.20, 5.21, 6.24, 6.25 and 7.11), the neural variance in the full, potent and null subspaces V and $\overline{V}$ (Figures 4.26, 4.27, 5.22, 5.23, 6.26 and 6.27), the proportion of total variance in the null space π and Π (Figures 4.28, 5.24, 5.25, 6.28, 6.29), and the affordance shift S (Figures 4.40, 5.33–5.35, 6.35–6.37 and 7.17–7.19).

The bootstrap method is a powerful, general, but computationally intensive non-parametric method for finding confidence intervals for an estimated summary statistic $\hat{\theta}$, and correcting bias in the estimation of the statistic. The bootstrap method uses randomized resampling with replacement to estimate the distribution of the estimated statistic $\hat{\boldsymbol{\theta}}^*$ based on the empirical variation in the sample. The critical assumption of the

bootstrap, the "bootstrap principle," is that the relation of the bootstrapped statistic $\hat{\boldsymbol{\theta}}^*$ to the sample statistic $\hat{\theta}$ approximates the relation of the sample statistic $\hat{\theta}$ to the underlying true value of the statistic θ.

For each of the summary statistics noted above, a similar procedure was used to generate the bootstrap distributions. First, the statistic was estimated from the full data set:

$$\hat{\theta} = h(x) \tag{A.24}$$

where $h(x)$ is a functional of the original data sample x. For example, the calculation of the statistic ξ is shown in Equation 4.11. For each bootstrap iteration b, a new bootstrapped sample x_b^* was constructed by randomly resampling the full sample x with replacement. This resampling was performed in a block fashion, resampling full trials with replacement in order to preserve temporal structure in the data. Each bootstrapped resample x_b^* was the same size as the original sample x, but could contain multiple instances of particular trials, and no instances of other trials. A single bootstrapped statistic estimate was then calculated as:

$$\hat{\theta}_b^* = h(x_b^*) \tag{A.25}$$

This procedure was repeated 10000 times, generating a new bootstrapped sample x_b^* and bootstrapped statistic estimate $\hat{\theta}_b^*$ on each iteration. Random resample indices were generated using the `random.randint` function of the Python package `numpy`. The 10000 bootstrapped statistic estimates thus produced a distribution, $\hat{\boldsymbol{\theta}}^*$.

Given the bootstrapped distribution $\hat{\boldsymbol{\theta}}^*$, the confidence interval CI was calculated as follows:

$$a_1 = (\hat{\boldsymbol{\theta}}^* - \hat{\theta})_{\alpha/2} \tag{A.26}$$

$$a_2 = (\hat{\boldsymbol{\theta}}^* - \hat{\theta})_{1-\alpha/2} \tag{A.27}$$

$$\text{CI} = [\hat{\theta} - a_2,\ \hat{\theta} - a_1] \tag{A.28}$$

where $()_{\alpha/2}$ denotes the $\alpha/2$ quantile and $()_{1-\alpha/2}$ denotes the $1-\alpha/2$ quantile. For all reported statistic confidence intervals, α was set to 0.05, generating two-sided 95% confidence intervals.

The bias in the estimation of the statistic, $\hat{e}$ can also be estimated based on the bootstrapped distribution:

$$\hat{e} = \overline{\hat{\boldsymbol{\theta}}^*} - \hat{\theta} \tag{A.29}$$

This relies on the "bootstrap principle" as stated above, where $\hat{e}$ estimates the "true" bias of the statistic estimate, e:

$$e = \hat{\theta} - \theta \tag{A.30}$$

The bias-corrected statistic $\hat{\theta}_{\mathrm{BC}}$ can then be calculated as:

$$\hat{\theta}_{\mathrm{BC}} = \hat{\theta} - \hat{e} \tag{A.31}$$

For all of the summary statistics noted at the beginning of this session, the bias-corrected statistic and 95% confidence intervals are reported.

The bootstrap method was also used for hypothesis testing in the cases of the mean inter-condition MF PC distances $\overline{D}_{\mathrm{MFPC}}$, the mean inter-condition FR PC distances $\overline{D}_{\mathrm{FRPC}}$, the mean extralinear modulation $\overline{\xi}$, the mean population extralinear modulation $\overline{\xi}^{\mathrm{pop}}$, the total variance in the null space $\overline{V}^{\mathrm{null}}$ and the mean preparatory population modulation $\overline{\Delta}^{\mathrm{prep}}$.

In each of these cases, the hypothesis to be tested was that the statistic in one instance was greater than the statistic in another instance:

$$\hat{\theta}_2 - \hat{\theta}_1 > 0 \tag{A.32}$$

The null hypothesis was thus:

$$\hat{\theta}_2 - \hat{\theta}_1 \leq 0 \tag{A.33}$$

The p-value characterizing the evidence for the null hypothesis is then generated as:

$$p = \frac{\#\left[(2\hat{\theta}_2^* - \hat{\boldsymbol{\theta}}^*{}_2) - (2\hat{\theta}_1^* - \hat{\boldsymbol{\theta}}^*{}_1) \leq 0\right]}{N_{\text{Bootstrap}}} \tag{A.34}$$

that is, the number of bias-corrected bootstrapped statistic differences that were less than or equal to 0, divided by the number of bootstrap iterations (10000). For the tests noted above, the null hypothesis was rejected at $p < 0.05$, or the p-value was reported directly. Such tests were used to detect "robust context encoding" (see Sections 4.4.1, 5.4.1, 6.4.1).

Additionally a bootstrap method was used to estimate the expected within-condition variability of the inter-condition MF PC distances D_{MFPC} and $\overline{D}_{\text{MFPC}}$, the inter-condition FR PC distances D_{FRPC} and $\overline{D}_{\text{FRPC}}$, the population modulation Δ, the extralinear modulations ξ and $\overline{\xi}$, the population extralinear modulations ξ^{pop} and $\overline{\xi}^{\text{pop}}$, the variance in the null space V^{null} and $\overline{V}^{\text{null}}$ and the mean preparatory population modulation $\overline{\Delta}^{\text{prep}}$.

A similar method was used to estimate overall within-condition variability for all of the above estimates. A distribution of 10000 within-condition estimates was generated by calculating the statistic by comparing one random half of trials from a condition to the other half of trials from that same condition. The condition was selected randomly on each iteration, so that all conditions contributed to the final distribution. For each of the 10000 within-condition estimates, an additional 10-iteration bootstrap was performed in order to estimate the bias of each within-condition estimate. While this resulted in highly variable bias estimates on each iteration, when considered together, the 10000 bias estimates yielded a good estimation of bias.

Biases were found to be larger for small values of the estimated statistics, and decreased for larger values. To generate a bias-corrected distribution of within-condition statistic estimates, the biases generated from the 10-iteration bootstraps were fit with a model of the form:

$$\hat{\boldsymbol{e}}_{\text{W}} = \frac{a}{\hat{\boldsymbol{\theta}}_{\text{W}} + b} \tag{A.35}$$

where $\hat{\boldsymbol{e}}_{\mathrm{W}}$ is the distribution of estimated within-condition statistic biases, a and b are fitted parameters and $\hat{\boldsymbol{\theta}}_{\mathrm{W}}$ is the distribution of within-condition statistic estimates. The bias corrected within-condition statistic distribution was then calculated as:

$$\hat{\boldsymbol{\theta}}_{\mathrm{W}}^{\mathrm{BC}} = \hat{\boldsymbol{\theta}}_{\mathrm{W}} - \hat{\boldsymbol{e}}_{\mathrm{W}} \tag{A.36}$$

These bias-corrected within-condition estimate distributions were used for hypothesis testing as described above to determine if a between-condition statistic was significantly greater than expected within-condition variability of that statistic. This was done by generating a p-value according to the following equation:

$$p = \frac{\#\left[(2\hat{\theta}^{*} - \hat{\boldsymbol{\theta}}^{*}) - \hat{\boldsymbol{\theta}}_{\mathrm{W}}^{\mathrm{BC}} \leq 0\right]}{N_{\mathrm{Bootstrap}}} \tag{A.37}$$

Between-condition statistics were considered significantly greater than within-condition statistic variability when $\mathrm{p} < 0.05$.

The mean bias-corrected within-condition statistic estimates $\overline{\hat{\boldsymbol{\theta}}}_{\mathrm{W}}^{\mathrm{BC}}$ and upper 95% confidence bounds $(\hat{\boldsymbol{\theta}}_{\mathrm{W}}^{\mathrm{BC}})_{0.95}$ are also reported as the gray solid and dashed lines in Figures 4.12, 4.19, 4.20, 4.25, 4.26, 4.27, 5.8, 5.9, 5.15, 5.16, 5.17, 5.20, 5.21, 5.22, 5.23, 6.11, 6.12, 6.19, 6.20, 6.21, 6.24, 6.25, 6.26, 6.27, 7.11 and 7.13.

Bibliography

[1] J. R. Napier, "The prehensile movements of the human hand," *The Journal of bone and joint surgery. British volume*, vol. 38, no. 4, pp. 902–913, 1956.

[2] M. Jeannerod, "Intersegmental coodination during reaching at natural visual objects," *Attention and performance*, pp. 153–169, 1981.

[3] M. Jeannerod, "The timing of natural prehension movements," *Journal of motor behavior*, vol. 16, no. 3, pp. 235–254, 1984.

[4] M. Santello and J. F. Soechting, "Gradual molding of the hand to object contours," *Journal of neurophysiology*, vol. 79, no. 3, pp. 1307–1320, 1998.

[5] N. Kamakura, M. Matsuo, H. Ishii, F. Mitsuboshi, and Y. Miura, "Patterns of static prehension in normal hands," *American Journal of Occupational Therapy*, vol. 34, no. 7, pp. 437–445, 1980.

[6] K. H. Kroemer, "Coupling the hand with the handle: an improved notation of touch, grip, and grasp," *Human factors*, vol. 28, no. 3, pp. 337–339, 1986.

[7] L. E. Miller, "Limb movement: getting a handle on grasp," *Current biology*, vol. 14, no. 17, pp. R714–R715, 2004.

[8] M. Santello, M. Flanders, and J. F. Soechting, "Postural hand synergies for tool use," *Journal of neuroscience*, vol. 18, no. 23, pp. 10105–10115, 1998.

[9] C. R. Mason, J. E. Gomez, and T. J. Ebner, "Hand synergies during reach-to-grasp," *Journal of neurophysiology*, vol. 86, no. 6, pp. 2896–2910, 2001.

[10] J. N. Ingram, K. P. Körding, I. S. Howard, and D. M. Wolpert, "The statistics of natural hand movements," *Experimental brain research*, vol. 188, no. 2, pp. 223–236, 2008.

[11] E. Todorov and Z. Ghahramani, "Analysis of the synergies underlying complex hand manipulation," in *The 26th Annual International Conference of the IEEE Engineering in Medicine and Biology Society*, vol. 2, pp. 4637–4640, IEEE, 2004.

[12] M. H. Schieber and M. Santello, "Hand function: peripheral and central constraints on performance," *Journal of applied physiology*, 2004.

[13] N. B. Macfarlane and M. S. Graziano, "Diversity of grip in macaca mulatta," *Experimental brain research*, vol. 197, no. 3, pp. 255–268, 2009.

[14] L. Sartori, A. C. Ciani, M. Bulgheroni, and U. Castiello, "Reaching and grasping behavior in macaca fascicularis: a kinematic study," *Experimental brain research*, vol. 224, no. 1, pp. 119–124, 2013.

[15] C. R. Mason, L. S. Theverapperuma, C. M. Hendrix, and T. J. Ebner, "Monkey hand postural synergies during reach-to-grasp in the absence of vision of the hand and object," *Journal of neurophysiology*, vol. 91, no. 6, pp. 2826–2837, 2004.

[16] C. E. Vargas-Irwin, G. Shakhnarovich, P. Yadollahpour, J. M. Mislow, M. J. Black, and J. P. Donoghue, "Decoding complete reach and grasp actions from local primary motor cortex populations," *Journal of neuroscience*, vol. 30, no. 29, pp. 9659–9669, 2010.

[17] M. C. Spalding, *Characterizing the correlation between motor cortical neural firing and grasping kinematics*. PhD thesis, University of Pittsburgh, 2010.

[18] S. Schaffelhofer, M. Sartori, H. Scherberger, and D. Farina, "Musculoskeletal representation of a large repertoire of hand grasping actions in primates," *IEEE Transactions on Neural Systems and Rehabilitation Engineering*, vol. 23, no. 2, pp. 210–220, 2014.

[19] T. Brochier, R. L. Spinks, M. A. Umilta, and R. N. Lemon, "Patterns of muscle activity underlying object-specific grasp by the macaque monkey," *Journal of neurophysiology*, vol. 92, no. 3, pp. 1770–1782, 2004.

[20] M. D. Gumert, M. Kluck, and S. Malaivijitnond, "The physical characteristics and usage patterns of stone axe and pounding hammers used by long-tailed macaques in the andaman sea region of thailand," *American Journal of Primatology: Official Journal of the American Society of Primatologists*, vol. 71, no. 7, pp. 594–608, 2009.

[21] A. M. Ducoing and B. Thierry, "Tool-use learning in tonkean macaques (macaca tonkeana)," *Animal cognition*, vol. 8, no. 2, pp. 103–113, 2005.

[22] C. Warden, A. Koch, and H. Fjeld, "Instrumentation in cebus and rhesus monkeys," *The Pedagogical Seminary and Journal of Genetic Psychology*, vol. 56, no. 2, pp. 297–310, 1940.

[23] A. Shurcliff, D. Brown, and F. Stollnitz, "Specificity of training required for solution of a stick problem by rhesus monkeys (macaca mulatta)," *Learning and Motivation*, vol. 2, no. 3, pp. 255–270, 1971.

[24] A. Iriki, M. Tanaka, and Y. Iwamura, "Coding of modified body schema during tool use by macaque postcentral neurones.," *Neuroreport*, vol. 7, no. 14, pp. 2325–2330, 1996.

[25] S. Obayashi, T. Suhara, Y. Nagai, J. Maeda, S. Hihara, and A. Iriki, "Macaque prefrontal activity associated with extensive tool use," *Neuroreport*, vol. 13, no. 17, pp. 2349–2354, 2002.

[26] H. Ishibashi, S. Hihara, M. Takahashi, T. Heike, T. Yokota, and A. Iriki, "Tool-use learning selectively induces expression of brain-derived neurotrophic factor, its receptor trkb, and neurotrophin 3 in the intraparietal multisensorycortex of monkeys," *Cognitive Brain Research*, vol. 14, no. 1, pp. 3–9, 2002.

[27] S. Hihara, T. Notoya, M. Tanaka, S. Ichinose, H. Ojima, S. Obayashi, N. Fujii, and A. Iriki, "Extension of corticocortical afferents into the anterior bank of the intraparietal sulcus by tool-use training in adult monkeys," *Neuropsychologia*, vol. 44, no. 13, pp. 2636–2646, 2006.

[28] M. Quallo, C. Price, K. Ueno, T. Asamizuya, K. Cheng, R. Lemon, and A. Iriki, "Gray and white matter changes associated with tool-use learning in macaque monkeys," *Proceedings of the National Academy of Sciences*, vol. 106, no. 43, pp. 18379–18384, 2009.

[29] M. M. Quallo, A. Kraskov, and R. N. Lemon, "The activity of primary motor cortex corticospinal neurons during tool use by macaque monkeys," *Journal of Neuroscience*, vol. 32, no. 48, pp. 17351–17364, 2012.

[30] K. Brodmann, *Vergleichende Lokalisationslehre der Grosshirnrinde in ihren Prinzipien dargestellt auf Grund des Zellenbaues*. Barth, 1909.

[31] G. Fritsch and E. Hitzig, "Uber die elektrische erregbarkeit des grosshirns," *Archiv fur Anatomie, Physiologie und wissenschaftliche Medizin*, vol. 37, pp. 300–332, 1870.

[32] D. Ferrier, "Experiments on the brain of monkeys.—no. i," *Proceedings of the Royal Society of London*, vol. 23, no. 156-163, pp. 409–430, 1875.

[33] W. Penfield and E. Boldrey, "Somatic motor and sensory representation in the cerebral cortex of man as studied by electrical stimulation," *Brain*, vol. 60, no. 4, pp. 389–443, 1937.

[34] H. Kwan, W. MacKay, J. Murphy, and Y. Wong, "Spatial organization of precentral cortex in awake primates. ii. motor outputs.," *Journal of neurophysiology*, vol. 41, no. 5, pp. 1120–1131, 1978.

[35] K. Sato and J. Tanji, "Digit-muscle responses evoked from multiple intracortical foci in monkey precentral motor cortex," *Journal of Neurophysiology*, vol. 62, no. 4, pp. 959–970, 1989.

[36] M. Godschalk, A. R. Mitz, B. van Duin, and H. van der Burga, "Somatotopy of monkey premotor cortex examined with microstimulation," *Neuroscience research*, vol. 23, no. 3, pp. 269–279, 1995.

[37] L. Fornia, V. Ferpozzi, M. Montagna, M. Rossi, M. Riva, F. Pessina, F. Martinelli Boneschi, P. Borroni, R. N. Lemon, L. Bello, *et al.*, "Functional characterization of the left ventrolateral premotor cortex in humans: a direct electrophysiological approach," *Cerebral Cortex*, vol. 28, no. 1, pp. 167–183, 2018.

[38] M. S. Graziano, C. S. Taylor, and T. Moore, "Complex movements evoked by microstimulation of precentral cortex," *Neuron*, vol. 34, no. 5, pp. 841–851, 2002.

[39] M. S. Graziano, C. S. Taylor, T. Moore, and D. F. Cooke, "The cortical control of movement revisited," *Neuron*, vol. 36, no. 3, pp. 349–362, 2002.

[40] O. A. Gharbawie, I. Stepniewska, H. Qi, and J. H. Kaas, "Multiple parietal–frontal pathways mediate grasping in macaque monkeys," *Journal of Neuroscience*, vol. 31, no. 32, pp. 11660–11677, 2011.

[41] C. Darian-Smith, I. Darian-Smith, K. Burman, and N. Ratcliffe, "Ipsilateral cortical projections to areas 3a, 3b, and 4 in the macaque monkey," *Journal of Comparative Neurology*, vol. 335, no. 2, pp. 200–213, 1993.

[42] J. W. Holsapple, J. B. Preston, and P. L. Strick, "The origin of thalamic inputs to the" hand" representation in the primary motor cortex," *Journal of Neuroscience*, vol. 11, no. 9, pp. 2644–2654, 1991.

[43] H. G. Kuypers, "Central cortical projections to motor and somato-sensory cell groups: an experimental study in the rhesus monkey," *Brain*, vol. 83, no. 1, pp. 161–184, 1960.

[44] K. Toyoshima and H. Sakai, "Exact cortical extent of the origin of the corticospinal tract (cst) and the quantitative contribution to the cst in different cytoarchitectonic areas. a study with horseradish peroxidase in the monkey.," *Journal fur Hirnforschung*, vol. 23, no. 3, p. 257, 1982.

[45] R. Nudo and R. Masterton, "Descending pathways to the spinal cord, iii: Sites of origin of the corticospinal tract," *Journal of Comparative Neurology*, vol. 296, no. 4, pp. 559–583, 1990.

[46] R. P. Dum and P. L. Strick, "The origin of corticospinal projections from the premotor areas in the frontal lobe," *Journal of Neuroscience*, vol. 11, no. 3, pp. 667–689, 1991.

[47] M. P. Galea and I. Darian-Smith, "Multiple corticospinal neuron populations in the macaque monkey are specified by their unique cortical origins, spinal terminations, and connections," *Cerebral cortex*, vol. 4, no. 2, pp. 166–194, 1994.

[48] R. Lemon, "Corticomotoneuronal system," *Encyclopedia of Neuroscience*, pp. 197–202, 2010.

[49] J.-A. Rathelot and P. L. Strick, "Subdivisions of primary motor cortex based on cortico-motoneuronal cells," *Proceedings of the National Academy of Sciences*, vol. 106, no. 3, pp. 918–923, 2009.

[50] E. E. Fetz and P. D. Cheney, "Postspike facilitation of forelimb muscle activity by primate corticomotoneuronal cells," *Journal of neurophysiology*, vol. 44, no. 4, pp. 751–772, 1980.

[51] R. Lemon, G. Mantel, and R. Muir, "Corticospinal facilitation of hand muscles during voluntary movement in the conscious monkey.," *The Journal of physiology*, vol. 381, no. 1, pp. 497–527, 1986.

[52] E. Buys, R. Lemon, G. Mantel, and R. Muir, "Selective facilitation of different hand muscles by single corticospinal neurones in the conscious monkey.," *The Journal of physiology*, vol. 381, no. 1, pp. 529–549, 1986.

[53] B. J. McKiernan, J. K. Marcario, J. H. Karrer, and P. D. Cheney, "Corticomotoneuronal postspike effects in shoulder, elbow, wrist, digit, and intrinsic hand muscles during a reach and prehension task," *Journal of neurophysiology*, vol. 80, no. 4, pp. 1961–1980, 1998.

[54] M. H. Schieber and G. Rivlis, "Partial reconstruction of muscle activity from a pruned network of diverse motor cortex neurons," *Journal of neurophysiology*, vol. 97, no. 1, pp. 70–82, 2007.

[55] R. Porter and R. Lemon, *Corticospinal function and voluntary movement*. Oxford University Press, USA, 1993.

[56] R. N. Lemon, "Descending pathways in motor control," *Annu. Rev. Neurosci.*, vol. 31, pp. 195–218, 2008.

[57] D. G. Lawrence and H. G. Kuypers, "The functional organization of the motor system in the monkey: I. the effects of bilateral pyramidal lesions," *Brain*, vol. 91, no. 1, pp. 1–14, 1968.

[58] R. Passingham, V. Perry, and F. Wilkinson, "The long-term effects of removal of sensorimotor cortex in infant and adult rhesus monkeys," *Brain*, vol. 106, no. 3, pp. 675–705, 1983.

[59] M. Matsumura, T. Sawaguchi, T. Oishi, K. Ueki, and K. Kubota, "Behavioral deficits induced by local injection of bicuculline and muscimol into the primate motor and premotor cortex," *Journal of neurophysiology*, vol. 65, no. 6, pp. 1542–1553, 1991.

[60] K. Kubota, "Motor cortical muscimol injection disrupts forelimb movement in freely moving monkeys," *Neuroreport*, vol. 7, no. 14, pp. 2379–2384, 1996.

[61] T. Brochier, M.-J. Boudreau, M. Paré, and A. M. Smith, "The effects of muscimol inactivation of small regions of motor and somatosensory cortex on independent finger movements and force control in the precision grip," *Experimental brain research*, vol. 128, no. 1-2, pp. 31–40, 1999.

[62] L. Fogassi, V. Gallese, G. Buccino, L. Craighero, L. Fadiga, and G. Rizzolatti, "Cortical mechanism for the visual guidance of hand grasping movements in the monkey: A reversible inactivation study," *Brain*, vol. 124, no. 3, pp. 571–586, 2001.

[63] M. H. Schieber and A. V. Poliakov, "Partial inactivation of the primary motor cortex hand area: effects on individuated finger movements," *Journal of Neuroscience*, vol. 18, no. 21, pp. 9038–9054, 1998.

[64] C. E. Lang and M. H. Schieber, "Differential impairment of individuated finger movements in humans after damage to the motor cortex or the corticospinal tract," *Journal of neurophysiology*, vol. 90, no. 2, pp. 1160–1170, 2003.

[65] K. Nakajima, M. Maier, P. Kirkwood, and R. Lemon, "Striking differences in transmission of corticospinal excitation to upper limb motoneurons in two primate species," *Journal of neurophysiology*, vol. 84, no. 2, pp. 698–709, 2000.

[66] R. N. Lemon and J. Griffiths, "Comparing the function of the corticospinal system in different species: organizational differences for motor specialization?," *Muscle & Nerve: Official Journal of the American Association of Electrodiagnostic Medicine*, vol. 32, no. 3, pp. 261–279, 2005.

[67] M. H. Schieber, "Constraints on somatotopic organization in the primary motor cortex," *Journal of neurophysiology*, vol. 86, no. 5, pp. 2125–2143, 2001.

[68] Y. Shinoda, J.-I. Yokota, and T. Futami, "Divergent projection of individual corticospinal axons to motoneurons of multiple muscles in the monkey," *Neuroscience letters*, vol. 23, no. 1, pp. 7–12, 1981.

[69] D. M. Griffin, H. M. Hudson, A. Belhaj-Saif, B. J. McKiernan, and P. D. Cheney, "Do corticomotoneuronal cells predict target muscle emg activity?," *Journal of neurophysiology*, vol. 99, no. 3, pp. 1169–1986, 2008.

[70] M. C. Park, A. Belhaj-Saif, and P. D. Cheney, "Properties of primary motor cortex output to forelimb muscles in rhesus macaques," *Journal of neurophysiology*, vol. 92, no. 5, pp. 2968–2984, 2004.

[71] M. C. Park, A. Belhaj-Saif, M. Gordon, and P. D. Cheney, "Consistent features in the forelimb representation of primary motor cortex in rhesus macaques," *Journal of Neuroscience*, vol. 21, no. 8, pp. 2784–2792, 2001.

[72] J.-A. Rathelot and P. L. Strick, "Muscle representation in the macaque motor cortex: an anatomical perspective," *Proceedings of the National Academy of Sciences*, vol. 103, no. 21, pp. 8257–8262, 2006.

[73] T. Takei and K. Seki, "Spinal interneurons facilitate coactivation of hand muscles during a precision grip task in monkeys," *Journal of Neuroscience*, vol. 30, no. 50, pp. 17041–17050, 2010.

[74] T. Takei and K. Seki, "Spinal premotor interneurons mediate dynamic and static motor commands for precision grip in monkeys," *Journal of Neuroscience*, vol. 33, no. 20, pp. 8850–8860, 2013.

[75] T. Takei and K. Seki, "Synaptic and functional linkages between spinal premotor interneurons and hand-muscle activity during precision grip," *Frontiers in computational neuroscience*, vol. 7, p. 40, 2013.

[76] W. R. Gowers, *A Manual of Diseases of the Nervous System: Diseases of the nerves and spinal cord*, vol. 1. Blakiston, 1896.

[77] C. G. Phillips and W. M. Landau, "Clinical neuromythology viii upper and lower motor neuron: The little old synecdoche that works," *Neurology*, vol. 40, no. 6, pp. 884–884, 1990.

[78] A. Smith, M.-C. Hepp-Reymond, and U. Wyss, "Relation of activity in precentral cortical neurons to force and rate of force change during isometric contractions of finger muscles," *Experimental Brain Research*, vol. 23, no. 3, pp. 315–332, 1975.

[79] M.-C. Hepp-Reymond, E. J. Hüsler, M. A. Maier, and H.-X. Qi, "Force-related neuronal activity in two regions of the primate ventral premotor cortex," *Canadian journal of physiology and pharmacology*, vol. 72, no. 5, pp. 571–579, 1994.

[80] M.-C. Hepp-Reymond, M. Kirkpatrick-Tanner, L. Gabernet, H.-X. Qi, and B. Weber, "Context-dependent force coding in motor and premotor cortical areas," *Experimental brain research*, vol. 128, no. 1-2, pp. 123–133, 1999.

[81] C. M. Hendrix, C. R. Mason, and T. J. Ebner, "Signaling of grasp dimension and grasp force in dorsal premotor cortex and primary motor cortex neurons during reach to grasp in the monkey," *Journal of Neurophysiology*, vol. 102, no. 1, pp. 132–145, 2009.

[82] R. W. Intveld, B. Dann, J. A. Michaels, and H. Scherberger, "Neural coding of intended and executed grasp force in macaque areas aip, f5, and m1," *Scientific Reports*, vol. 8, no. 1, pp. 1–16, 2018.

[83] J. F. Kalaska, D. Cohen, M. L. Hyde, and M. Prud'Homme, "A comparison of movement direction-related versus load direction-related activity in primate motor cortex, using a two-dimensional reaching task," *Journal of Neuroscience*, vol. 9, no. 6, pp. 2080–2102, 1989.

[84] M. Taira, J. Boline, N. Smyrnis, A. P. Georgopoulos, and J. Ashe, "On the relations between single cell activity in the motor cortex and the direction and magnitude of three-dimensional static isometric force," *Experimental brain research*, vol. 109, no. 3, pp. 367–376, 1996.

[85] L. E. Sergio, C. Hamel-Pâquet, and J. F. Kalaska, "Motor cortex neural correlates of output kinematics and kinetics during isometric-force and arm-reaching tasks," *Journal of neurophysiology*, vol. 94, no. 4, pp. 2353–2378, 2005.

[86] M. M. Morrow and L. E. Miller, "Prediction of muscle activity by populations of sequentially recorded primary motor cortex neurons," *Journal of neurophysiology*, vol. 89, no. 4, pp. 2279–2288, 2003.

[87] B. R. Townsend, L. Paninski, and R. N. Lemon, "Linear encoding of muscle activity in primary motor cortex and cerebellum," *Journal of neurophysiology*, vol. 96, no. 5, pp. 2578–2592, 2006.

[88] R. Holdefer and L. Miller, "Primary motor cortical neurons encode functional muscle synergies," *Experimental Brain Research*, vol. 146, no. 2, pp. 233–243, 2002.

[89] R. Muir and R. Lemon, "Corticospinal neurons with a special role in precision grip," *Brain research*, vol. 261, no. 2, pp. 312–316, 1983.

[90] K. Bennett and R. Lemon, "Corticomotoneuronal contribution to the fractionation of muscle activity during precision grip in the monkey," *Journal of neurophysiology*, vol. 75, no. 5, pp. 1826–1842, 1996.

[91] A. P. Georgopoulos, J. F. Kalaska, R. Caminiti, and J. T. Massey, "On the relations between the direction of two-dimensional arm movements and cell discharge in primate motor cortex," *Journal of Neuroscience*, vol. 2, no. 11, pp. 1527–1537, 1982.

[92] A. B. Schwartz, R. E. Kettner, and A. P. Georgopoulos, "Primate motor cortex and free arm movements to visual targets in three-dimensional space. i. relations between single cell discharge and direction of movement," *Journal of Neuroscience*, vol. 8, no. 8, pp. 2913–2927, 1988.

[93] A. P. Georgopoulos, R. Caminiti, J. F. Kalaska, and J. T. Massey, "Spatial coding of movement: a hypothesis concerning the coding of movement direction by motor cortical populations," *Experimental Brain Research*, vol. 49, no. Suppl. 7, pp. 327–336, 1983.

[94] A. P. Georgopoulos, A. B. Schwartz, and R. E. Kettner, "Neuronal population coding of movement direction," *Science*, vol. 233, no. 4771, pp. 1416–1419, 1986.

[95] A. P. Georgopoulos, R. E. Kettner, and A. B. Schwartz, "Primate motor cortex and free arm movements to visual targets in three-dimensional space. ii. coding of the direction of movement by a neuronal population," *Journal of Neuroscience*, vol. 8, no. 8, pp. 2928–2937, 1988.

[96] Q.-G. Fu, J. I. Suarez, and T. J. Ebner, "Neuronal specification of direction and distance during reaching movements in the superior precentral premotor area and primary motor cortex of monkeys," *Journal of Neurophysiology*, vol. 70, no. 5, pp. 2097–2116, 1993.

[97] D. W. Moran and A. B. Schwartz, "Motor cortical representation of speed and direction during reaching," *Journal of neurophysiology*, vol. 82, no. 5, pp. 2676–2692, 1999.

[98] J. Ashe and A. P. Georgopoulos, "Movement parameters and neural activity in motor cortex and area 5," *Cerebral cortex*, vol. 4, no. 6, pp. 590–600, 1994.

[99] N. G. Hatsopoulos, Q. Xu, and Y. Amit, "Encoding of movement fragments in the motor cortex," *Journal of Neuroscience*, vol. 27, no. 19, pp. 5105–5114, 2007.

[100] T. N. Aflalo and M. S. Graziano, "Partial tuning of motor cortex neurons to final posture in a free-moving paradigm," *Proceedings of the National Academy of Sciences*, vol. 103, no. 8, pp. 2909–2914, 2006.

[101] T. N. Aflalo and M. S. Graziano, "Relationship between unconstrained arm movements and single-neuron firing in the macaque motor cortex," *Journal of Neuroscience*, vol. 27, no. 11, pp. 2760–2780, 2007.

[102] D. W. Cabel, P. Cisek, and S. H. Scott, "Neural activity in primary motor cortex related to mechanical loads applied to the shoulder and elbow during a postural task," *Journal of neurophysiology*, vol. 86, no. 4, pp. 2102–2108, 2001.

[103] W. Wang, S. S. Chan, D. A. Heldman, and D. W. Moran, "Motor cortical representation of position and velocity during reaching," *Journal of neurophysiology*, vol. 97, no. 6, pp. 4258–4270, 2007.

[104] E. Stark, R. Drori, I. Asher, Y. Ben-Shaul, and M. Abeles, "Distinct movement parameters are represented by different neurons in the motor cortex," *European Journal of Neuroscience*, vol. 26, no. 4, pp. 1055–1066, 2007.

[105] W. Wu and N. Hatsopoulos, "Evidence against a single coordinate system representation in the motor cortex," *Experimental brain research*, vol. 175, no. 2, pp. 197–210, 2006.

[106] W. Thach, "Correlation of neural discharge with pattern and force of muscular activity, joint position, and direction of intended next movement in motor cortex and cerebellum," *Journal of neurophysiology*, vol. 41, no. 3, pp. 654–676, 1978.

[107] S. Kakei, D. S. Hoffman, and P. L. Strick, "Muscle and movement representations in the primary motor cortex," *Science*, vol. 285, no. 5436, pp. 2136–2139, 1999.

[108] S. Kakei, D. S. Hoffman, and P. L. Strick, "Sensorimotor transformations in cortical motor areas," *Neuroscience research*, vol. 46, no. 1, pp. 1–10, 2003.

[109] P. Cisek, D. J. Crammond, and J. F. Kalaska, "Neural activity in primary motor and dorsal premotor cortex in reaching tasks with the contralateral versus ipsilateral arm," *Journal of neurophysiology*, vol. 89, no. 2, pp. 922–942, 2003.

[110] S. Kennedy, *Motor cortical activity related to the combined control of force and motion.* PhD thesis, University of Pittsburgh, 2018.

[111] S. D. Kennedy and A. B. Schwartz, "Distributed processing of movement signaling," *Proceedings of the National Academy of Sciences*, vol. 116, no. 52, pp. 26266–26273, 2019.

[112] E. P. Gardner, J. Y. Ro, K. S. Babu, and S. Ghosh, "Neurophysiology of prehension. ii. response diversity in primary somatosensory (si) and motor (mi) cortices," *Journal of neurophysiology*, vol. 97, no. 2, pp. 1656–1670, 2007.

[113] C. A. Porro, M. P. Francescato, V. Cettolo, M. E. Diamond, P. Baraldi, C. Zuiani, M. Bazzocchi, and P. E. Di Prampero, "Primary motor and sensory cortex activation during motor performance and motor imagery: a functional magnetic resonance imaging study," *Journal of Neuroscience*, vol. 16, no. 23, pp. 7688–7698, 1996.

[114] M. Roth, J. Decety, M. Raybaudi, R. Massarelli, C. Delon-Martin, C. Segebarth, S. Morand, A. Gemignani, M. Décorps, and M. Jeannerod, "Possible involvement of primary motor cortex in mentally simulated movement: a functional magnetic resonance imaging study.," *Neuroreport*, vol. 7, no. 7, pp. 1280–1284, 1996.

[115] M. A. Umilta, T. Brochier, R. L. Spinks, and R. N. Lemon, "Simultaneous recording of macaque premotor and primary motor cortex neuronal populations reveals different functional contributions to visuomotor grasp," *Journal of neurophysiology*, vol. 98, no. 1, pp. 488–501, 2007.

[116] S. Schaffelhofer, A. Agudelo-Toro, and H. Scherberger, "Decoding a wide range of hand configurations from macaque motor, premotor, and parietal cortices," *Journal of Neuroscience*, vol. 35, no. 3, pp. 1068–1081, 2015.

[117] T. Brochier and M. A. Umiltà, "Cortical control of grasp in non-human primates," *Current opinion in neurobiology*, vol. 17, no. 6, pp. 637–643, 2007.

[118] S. Perel, *Dynamic functional connectivity between cortex and muscles*. PhD thesis, University of Pittsburgh, 2012.

[119] B. Wodlinger, J. Downey, E. Tyler-Kabara, A. Schwartz, M. Boninger, and J. Collinger, "Ten-dimensional anthropomorphic arm control in a human brain-machine interface: difficulties, solutions, and limitations," *Journal of neural engineering*, vol. 12, no. 1, p. 016011, 2014.

[120] J. M. Goodman, G. A. Tabot, A. S. Lee, A. K. Suresh, A. T. Rajan, N. G. Hatsopoulos, and S. Bensmaia, "Postural representations of the hand in the primate sensorimotor cortex," *Neuron*, vol. 104, no. 5, pp. 1000–1009, 2019.

[121] M. Saleh, K. Takahashi, Y. Amit, and N. G. Hatsopoulos, "Encoding of coordinated grasp trajectories in primary motor cortex," *Journal of Neuroscience*, vol. 30, no. 50, pp. 17079–17090, 2010.

[122] M. Saleh, K. Takahashi, and N. G. Hatsopoulos, "Encoding of coordinated reach and grasp trajectories in primary motor cortex," *Journal of Neuroscience*, vol. 32, no. 4, pp. 1220–1232, 2012.

[123] E. Okorokova, J. M. Goodman, N. Hatsopoulos, and S. J. Bensmaia, "Decoding hand kinematics from population responses in sensorimotor cortex during grasping," *Journal of Neural Engineering*, 2020.

[124] M. Mollazadeh, V. Aggarwal, N. V. Thakor, and M. H. Schieber, "Principal components of hand kinematics and neurophysiological signals in motor cortex during reach to grasp movements," *Journal of neurophysiology*, vol. 112, no. 8, pp. 1857–1870, 2014.

[125] M. M. Churchland and K. V. Shenoy, "Temporal complexity and heterogeneity of single-neuron activity in premotor and motor cortex," *Journal of neurophysiology*, vol. 97, no. 6, pp. 4235–4257, 2007.

[126] K. V. Shenoy, M. Sahani, and M. M. Churchland, "Cortical control of arm movements: a dynamical systems perspective," *Annual review of neuroscience*, vol. 36, 2013.

[127] M. M. Churchland, J. P. Cunningham, M. T. Kaufman, J. D. Foster, P. Nuyujukian, S. I. Ryu, and K. V. Shenoy, "Neural population dynamics during reaching," *Nature*, vol. 487, no. 7405, pp. 51–56, 2012.

[128] A. K. Suresh, J. M. Goodman, E. V. Okorokova, M. Kaufman, N. G. Hatsopoulos, and S. J. Bensmaia, "Neural population dynamics in motor cortex are different for reach and grasp," *Elife*, vol. 9, p. e58848, 2020.

[129] M. H. Schieber, "Dissociating motor cortex from the motor," *The Journal of physiology*, vol. 589, no. 23, pp. 5613–5624, 2011.

[130] G. E. Alexander and M. D. Crutcher, "Functional architecture of basal ganglia circuits: neural substrates of parallel processing," *Trends in neurosciences*, vol. 13, no. 7, pp. 266–271, 1990.

[131] A. P. Georgopoulos, M. Crutcher, and A. Schwartz, "Cognitive spatial-motor processes. 3. motor cortical prediction of movement direction during an instructed delay period.," *Experimental brain research*, vol. 75, no. 1, pp. 183–194, 1989.

[132] M. T. Kaufman, M. M. Churchland, S. I. Ryu, and K. V. Shenoy, "Cortical activity in the null space: permitting preparation without movement," *Nature neuroscience*, vol. 17, no. 3, pp. 440–448, 2014.

[133] G. F. Elsayed, A. H. Lara, M. T. Kaufman, M. M. Churchland, and J. P. Cunningham, "Reorganization between preparatory and movement population responses in motor cortex," *Nature communications*, vol. 7, no. 1, pp. 1–15, 2016.

[134] A. P. Georgopoulos, J. T. Lurito, M. Petrides, A. B. Schwartz, and J. T. Massey, "Mental rotation of the neuronal population vector," *Science*, vol. 243, no. 4888, pp. 234–236, 1989.

[135] M. M. Churchland, J. P. Cunningham, M. T. Kaufman, S. I. Ryu, and K. V. Shenoy, "Cortical preparatory activity: representation of movement or first cog in a dynamical machine?," *Neuron*, vol. 68, no. 3, pp. 387–400, 2010.

[136] E. Fetz, D. Finocchio, M. Baker, and M. Soso, "Sensory and motor responses of precentral cortex cells during comparable passive and active joint movements," *Journal of Neurophysiology*, vol. 43, no. 4, pp. 1070–1089, 1980.

[137] R. N. Lemon and R. Porter, "Afferent input to movement-related precentral neurones in conscious monkeys," *Proceedings of the Royal Society of London. Series B. Biological Sciences*, vol. 194, no. 1116, pp. 313–339, 1976.

[138] R. Lemon, "Functional properties of monkey motor cortex neurones receiving afferent input from the hand and fingers," *The Journal of physiology*, vol. 311, no. 1, pp. 497–519, 1981.

[139] J. Tanji and S. Wise, "Submodality distribution in sensorimotor cortex of the unanesthetized monkey," *Journal of Neurophysiology*, vol. 45, no. 3, pp. 467–481, 1981.

[140] K. E. Schroeder, Z. T. Irwin, A. J. Bullard, D. E. Thompson, J. N. Bentley, W. C. Stacey, P. G. Patil, and C. A. Chestek, "Robust tactile sensory responses in finger area of primate motor cortex relevant to prosthetic control," *Journal of neural engineering*, vol. 14, no. 4, p. 046016, 2017.

[141] P. D. Ganzer, S. C. Colachis 4th, M. A. Schwemmer, D. A. Friedenberg, C. F. Dunlap, C. E. Swiftney, A. F. Jacobowitz, D. J. Weber, M. A. Bockbrader, and G. Sharma,

"Restoring the sense of touch using a sensorimotor demultiplexing neural interface," *Cell*, 2020.

[142] J. Rothwell, M. Traub, B. Day, J. Obeso, P. Thomas, and C. Marsden, "Manual motor performance in a deafferented man," *Brain*, vol. 105, no. 3, pp. 515–542, 1982.

[143] R. J. Nudo, E. J. Plautz, and G. W. Milliken, "Adaptive plasticity in primate motor cortex as a consequence of behavioral experience and neuronal injury," in *Seminars in neuroscience*, vol. 9, pp. 13–23, Elsevier, 1997.

[144] H.-X. Qi, I. Stepniewska, and J. H. Kaas, "Reorganization of primary motor cortex in adult macaque monkeys with long-standing amputations," *Journal of neurophysiology*, vol. 84, no. 4, pp. 2133–2147, 2000.

[145] R. Chen, L. Cohen, and M. Hallett, "Nervous system reorganization following injury," *Neuroscience*, vol. 111, no. 4, pp. 761–773, 2002.

[146] A. Karni, G. Meyer, C. Rey-Hipolito, P. Jezzard, M. M. Adams, R. Turner, and L. G. Ungerleider, "The acquisition of skilled motor performance: fast and slow experience-driven changes in primary motor cortex," *Proceedings of the National Academy of Sciences*, vol. 95, no. 3, pp. 861–868, 1998.

[147] J. N. Sanes and J. P. Donoghue, "Plasticity and primary motor cortex," *Annual review of neuroscience*, vol. 23, no. 1, pp. 393–415, 2000.

[148] C.-S. R. Li, C. Padoa-Schioppa, and E. Bizzi, "Neuronal correlates of motor performance and motor learning in the primary motor cortex of monkeys adapting to an external force field," *Neuron*, vol. 30, no. 2, pp. 593–607, 2001.

[149] J. A. Kleim, T. M. Hogg, P. M. VandenBerg, N. R. Cooper, R. Bruneau, and M. Remple, "Cortical synaptogenesis and motor map reorganization occur during late, but not early, phase of motor skill learning," *Journal of Neuroscience*, vol. 24, no. 3, pp. 628–633, 2004.

[150] B. Jarosiewicz, S. M. Chase, G. W. Fraser, M. Velliste, R. E. Kass, and A. B. Schwartz, "Functional network reorganization during learning in a brain-computer interface paradigm," *Proceedings of the National Academy of Sciences*, vol. 105, no. 49, pp. 19486–19491, 2008.

[151] S. M. Chase, R. E. Kass, and A. B. Schwartz, "Behavioral and neural correlates of visuomotor adaptation observed through a brain-computer interface in primary motor cortex," *Journal of neurophysiology*, vol. 108, no. 2, pp. 624–644, 2012.

[152] X. Zhou, R. N. Tien, S. Ravikumar, and S. M. Chase, "Distinct types of neural reorganization during long-term learning," *Journal of neurophysiology*, vol. 121, no. 4, pp. 1329–1341, 2019.

[153] A. Pascual-Leone, D. Nguyet, L. G. Cohen, J. P. Brasil-Neto, A. Cammarota, and M. Hallett, "Modulation of muscle responses evoked by transcranial magnetic stimulation during the acquisition of new fine motor skills," *Journal of neurophysiology*, vol. 74, no. 3, pp. 1037–1045, 1995.

[154] R. J. Nudo, G. W. Milliken, W. M. Jenkins, and M. M. Merzenich, "Use-dependent alterations of movement representations in primary motor cortex of adult squirrel monkeys," *Journal of Neuroscience*, vol. 16, no. 2, pp. 785–807, 1996.

[155] K. D. Anderson, "Targeting recovery: priorities of the spinal cord-injured population," *Journal of neurotrauma*, vol. 21, no. 10, pp. 1371–1383, 2004.

[156] G. J. Snoek, M. J. IJzerman, H. J. Hermens, D. Maxwell, and F. Biering-Sorensen, "Survey of the needs of patients with spinal cord injury: impact and priority for improvement in hand function in tetraplegics," *Spinal cord*, vol. 42, no. 9, pp. 526–532, 2004.

[157] E. E. Fetz, "Operant conditioning of cortical unit activity," *Science*, vol. 163, no. 3870, pp. 955–958, 1969.

[158] E. E. Fetz and D. V. Finocchio, "Operant conditioning of specific patterns of neural and muscular activity," *Science*, vol. 174, no. 4007, pp. 431–435, 1971.

[159] E. E. Fetz and M. A. Baker, "Operantly conditioned patterns on precentral unit activity and correlated responses in adjacent cells and contralateral muscles.," *Journal of neurophysiology*, vol. 36, no. 2, pp. 179–204, 1973.

[160] L. R. Hochberg, M. D. Serruya, G. M. Friehs, J. A. Mukand, M. Saleh, A. H. Caplan, A. Branner, D. Chen, R. D. Penn, and J. P. Donoghue, "Neuronal ensemble control of prosthetic devices by a human with tetraplegia," *Nature*, vol. 442, no. 7099, pp. 164–171, 2006.

[161] N. Fitzsimmons, M. Lebedev, I. Peikon, and M. A. Nicolelis, "Extracting kinematic parameters for monkey bipedal walking from cortical neuronal ensemble activity," *Frontiers in integrative neuroscience*, vol. 3, p. 3, 2009.

[162] A. K. Bansal, W. Truccolo, C. E. Vargas-Irwin, and J. P. Donoghue, "Decoding 3d reach and grasp from hybrid signals in motor and premotor cortices: spikes, multiunit activity, and local field potentials," *Journal of neurophysiology*, vol. 107, no. 5, pp. 1337–1355, 2012.

[163] V. K. Menz, S. Schaffelhofer, and H. Scherberger, "Representation of continuous hand and arm movements in macaque areas m1, f5, and aip: a comparative decoding study," *Journal of neural engineering*, vol. 12, no. 5, p. 056016, 2015.

[164] S.-P. Kim, J. C. Sanchez, D. Erdogmus, Y. N. Rao, J. Wessberg, J. C. Principe, and M. Nicolelis, "Divide-and-conquer approach for brain machine interfaces: nonlinear mixture of competitive linear models," *Neural Networks*, vol. 16, no. 5-6, pp. 865–871, 2003.

[165] W. Wu, M. J. Black, D. Mumford, Y. Gao, E. Bienenstock, and J. P. Donoghue, "Modeling and decoding motor cortical activity using a switching kalman filter," *IEEE transactions on biomedical engineering*, vol. 51, no. 6, pp. 933–942, 2004.

[166] V. Aggarwal, M. Mollazadeh, A. G. Davidson, M. H. Schieber, and N. V. Thakor, "State-based decoding of hand and finger kinematics using neuronal ensemble and lfp activity during dexterous reach-to-grasp movements," *Journal of neurophysiology*, vol. 109, no. 12, pp. 3067–3081, 2013.

[167] S. B. Hamed, M. H. Schieber, and A. Pouget, "Decoding m1 neurons during multiple finger movements," *Journal of neurophysiology*, vol. 98, no. 1, pp. 327–333, 2007.

[168] S. Acharya, F. Tenore, V. Aggarwal, R. Etienne-Cummings, M. H. Schieber, and N. V. Thakor, "Decoding individuated finger movements using volume-constrained neuronal ensembles in the m1 hand area," *IEEE Transactions on Neural Systems and Rehabilitation Engineering*, vol. 16, no. 1, pp. 15–23, 2008.

[169] V. Aggarwal, S. Acharya, F. Tenore, H.-C. Shin, R. Etienne-Cummings, M. H. Schieber, and N. V. Thakor, "Asynchronous decoding of dexterous finger movements using m1 neurons," *IEEE Transactions on Neural Systems and Rehabilitation Engineering*, vol. 16, no. 1, pp. 3–14, 2008.

[170] A. Jorge, D. A. Royston, E. C. Tyler-Kabara, M. L. Boninger, and J. L. Collinger, "Classification of individual finger movements using intracortical recordings in human motor cortex," *Neurosurgery*, 2020.

[171] D. M. Taylor, S. I. H. Tillery, and A. B. Schwartz, "Direct cortical control of 3d neuroprosthetic devices," *Science*, vol. 296, no. 5574, pp. 1829–1832, 2002.

[172] M. D. Serruya, N. G. Hatsopoulos, L. Paninski, M. R. Fellows, and J. P. Donoghue, "Instant neural control of a movement signal," *Nature*, vol. 416, no. 6877, pp. 141–142, 2002.

[173] J. M. Carmena, M. A. Lebedev, R. E. Crist, J. E. O'Doherty, D. M. Santucci, D. F. Dimitrov, P. G. Patil, C. S. Henriquez, and M. A. Nicolelis, "Learning to control a brain–machine interface for reaching and grasping by primates," *PLoS biol*, vol. 1, no. 2, p. e42, 2003.

[174] J. Wessberg, C. R. Stambaugh, J. D. Kralik, P. D. Beck, M. Laubach, J. K. Chapin, J. Kim, S. J. Biggs, M. A. Srinivasan, and M. A. Nicolelis, "Real-time prediction of hand trajectory by ensembles of cortical neurons in primates," *Nature*, vol. 408, no. 6810, pp. 361–365, 2000.

[175] Z. Irwin, K. Schroeder, P. Vu, A. Bullard, D. Tat, C. Nu, A. Vaskov, S. Nason, D. Thompson, J. Bentley, *et al.*, "Neural control of finger movement via intracortical brain–machine interface," *Journal of neural engineering*, vol. 14, no. 6, p. 066004, 2017.

[176] M. Velliste, S. Perel, M. C. Spalding, A. S. Whitford, and A. B. Schwartz, "Cortical control of a prosthetic arm for self-feeding," *Nature*, vol. 453, no. 7198, pp. 1098–1101, 2008.

[177] C. Ethier, E. R. Oby, M. J. Bauman, and L. E. Miller, "Restoration of grasp following paralysis through brain-controlled stimulation of muscles," *Nature*, vol. 485, no. 7398, pp. 368–371, 2012.

[178] S.-P. Kim, J. D. Simeral, L. R. Hochberg, J. P. Donoghue, and M. J. Black, "Neural control of computer cursor velocity by decoding motor cortical spiking activity in humans with tetraplegia," *Journal of neural engineering*, vol. 5, no. 4, p. 455, 2008.

[179] V. Gilja, C. Pandarinath, C. H. Blabe, P. Nuyujukian, J. D. Simeral, A. A. Sarma, B. L. Sorice, J. A. Perge, B. Jarosiewicz, L. R. Hochberg, *et al.*, "Clinical translation

of a high-performance neural prosthesis," *Nature medicine*, vol. 21, no. 10, p. 1142, 2015.

[180] S.-P. Kim, J. D. Simeral, L. R. Hochberg, J. P. Donoghue, G. M. Friehs, and M. J. Black, "Point-and-click cursor control with an intracortical neural interface system by humans with tetraplegia," *IEEE transactions on neural systems and rehabilitation engineering*, vol. 19, no. 2, pp. 193–203, 2011.

[181] J. Simeral, S.-P. Kim, M. Black, J. Donoghue, and L. Hochberg, "Neural control of cursor trajectory and click by a human with tetraplegia 1000 days after implant of an intracortical microelectrode array," *Journal of neural engineering*, vol. 8, no. 2, p. 025027, 2011.

[182] R. Vinjamuri, D. J. Weber, Z.-H. Mao, J. L. Collinger, A. D. Degenhart, J. W. Kelly, M. L. Boninger, E. C. Tyler-Kabara, and W. Wang, "Toward synergy-based brain-machine interfaces," *IEEE Transactions on Information Technology in Biomedicine*, vol. 15, no. 5, pp. 726–736, 2011.

[183] L. R. Hochberg, D. Bacher, B. Jarosiewicz, N. Y. Masse, J. D. Simeral, J. Vogel, S. Haddadin, J. Liu, S. S. Cash, P. Van Der Smagt, *et al.*, "Reach and grasp by people with tetraplegia using a neurally controlled robotic arm," *Nature*, vol. 485, no. 7398, pp. 372–375, 2012.

[184] J. L. Collinger, B. Wodlinger, J. E. Downey, W. Wang, E. C. Tyler-Kabara, D. J. Weber, A. J. McMorland, M. Velliste, M. L. Boninger, and A. B. Schwartz, "High-performance neuroprosthetic control by an individual with tetraplegia," *The Lancet*, vol. 381, no. 9866, pp. 557–564, 2013.

[185] J. E. Downey, J. M. Weiss, S. N. Flesher, Z. C. Thumser, P. D. Marasco, M. L. Boninger, R. A. Gaunt, and J. L. Collinger, "Implicit grasp force representation in human motor cortical recordings," *Frontiers in neuroscience*, vol. 12, p. 801, 2018.

[186] C. E. Bouton, A. Shaikhouni, N. V. Annetta, M. A. Bockbrader, D. A. Friedenberg, D. M. Nielson, G. Sharma, P. B. Sederberg, B. C. Glenn, W. J. Mysiw, *et al.*, "Restoring cortical control of functional movement in a human with quadriplegia," *Nature*, vol. 533, no. 7602, pp. 247–250, 2016.

[187] A. B. Ajiboye, F. R. Willett, D. R. Young, W. D. Memberg, B. A. Murphy, J. P. Miller, B. L. Walter, J. A. Sweet, H. A. Hoyen, M. W. Keith, *et al.*, "Restoration of reaching and grasping movements through brain-controlled muscle stimulation in

a person with tetraplegia: a proof-of-concept demonstration," *The Lancet*, vol. 389, no. 10081, pp. 1821–1830, 2017.

[188] S. C. Colachis IV, M. A. Bockbrader, M. Zhang, D. A. Friedenberg, N. V. Annetta, M. A. Schwemmer, N. D. Skomrock, W. J. Mysiw, A. R. Rezai, H. S. Bresler, *et al.*, "Dexterous control of seven functional hand movements using cortically-controlled transcutaneous muscle stimulation in a person with tetraplegia," *Frontiers in Neuroscience*, vol. 12, p. 208, 2018.

[189] M. Bockbrader, N. Annetta, D. Friedenberg, M. Schwemmer, N. Skomrock, S. Colachis IV, M. Zhang, C. Bouton, A. Rezai, G. Sharma, *et al.*, "Clinically significant gains in skillful grasp coordination by an individual with tetraplegia using an implanted brain-computer interface with forearm transcutaneous muscle stimulation," *Archives of Physical Medicine and Rehabilitation*, vol. 100, no. 7, pp. 1201–1217, 2019.

[190] J. E. O'Doherty, M. A. Lebedev, P. J. Ifft, K. Z. Zhuang, S. Shokur, H. Bleuler, and M. A. Nicolelis, "Active tactile exploration using a brain–machine–brain interface," *Nature*, vol. 479, no. 7372, pp. 228–231, 2011.

[191] S. N. Flesher, J. E. Downey, J. M. Weiss, C. L. Hughes, A. J. Herrera, E. C. Tyler-Kabara, M. L. Boninger, J. L. Collinger, and R. A. Gaunt, "Restored tactile sensation improves neuroprosthetic arm control," *bioRxiv*, p. 653428, 2019.

[192] K. Ganguly and J. M. Carmena, "Emergence of a stable cortical map for neuroprosthetic control," *PLoS Biol*, vol. 7, no. 7, p. e1000153, 2009.

[193] K. Ganguly, D. F. Dimitrov, J. D. Wallis, and J. M. Carmena, "Reversible large-scale modification of cortical networks during neuroprosthetic control," *Nature neuroscience*, vol. 14, no. 5, p. 662, 2011.

[194] P. T. Sadtler, K. M. Quick, M. D. Golub, S. M. Chase, S. I. Ryu, E. C. Tyler-Kabara, M. Y. Byron, and A. P. Batista, "Neural constraints on learning," *Nature*, vol. 512, no. 7515, pp. 423–426, 2014.

[195] K. E. Schroeder and C. A. Chestek, "Intracortical brain-machine interfaces advance sensorimotor neuroscience," *Frontiers in neuroscience*, vol. 10, p. 291, 2016.

[196] R. A. Andersen, E. J. Hwang, and G. H. Mulliken, "Cognitive neural prosthetics," *Annual review of psychology*, vol. 61, pp. 169–190, 2010.

[197] T. Aflalo, S. Kellis, C. Klaes, B. Lee, Y. Shi, K. Pejsa, K. Shanfield, S. Hayes-Jackson, M. Aisen, C. Heck, *et al.*, "Decoding motor imagery from the posterior parietal cortex of a tetraplegic human," *Science*, vol. 348, no. 6237, pp. 906–910, 2015.

[198] R. A. Andersen, T. Aflalo, and S. Kellis, "From thought to action: The brain–machine interface in posterior parietal cortex," *Proceedings of the National Academy of Sciences*, vol. 116, no. 52, pp. 26274–26279, 2019.

[199] J. F. Fulton, "A note on the definition of the "motor" and "premotor" areas," *Brain*, vol. 58, no. 2, pp. 311–316, 1935.

[200] M. Matelli, G. Luppino, and G. Rizzolatti, "Patterns of cytochrome oxidase activity in the frontal agranular cortex of the macaque monkey," *Behavioural brain research*, vol. 18, no. 2, pp. 125–136, 1985.

[201] S. H. Johnson-Frey, "The neural bases of complex tool use in humans," *Trends in cognitive sciences*, vol. 8, no. 2, pp. 71–78, 2004.

[202] R. P. Dum and P. L. Strick, "Frontal lobe inputs to the digit representations of the motor areas on the lateral surface of the hemisphere," *Journal of Neuroscience*, vol. 25, no. 6, pp. 1375–1386, 2005.

[203] M. Matelli, R. Camarda, M. Glickstein, and G. Rizzolatti, "Afferent and efferent projections of the inferior area 6 in the macaque monkey," *Journal of Comparative Neurology*, vol. 251, no. 3, pp. 281–298, 1986.

[204] H. Barbas and D. Pandya, "Architecture and frontal cortical connections of the premotor cortex (area 6) in the rhesus monkey," *Journal of comparative neurology*, vol. 256, no. 2, pp. 211–228, 1987.

[205] K. Kurata, "Corticocortical inputs to the dorsal and ventral aspects of the premotor cortex of macaque monkeys," *Neuroscience research*, vol. 12, no. 1, pp. 263–280, 1991.

[206] M.-T. Lu, J. B. Preston, and P. L. Strick, "Interconnections between the prefrontal cortex and the premotor areas in the frontal lobe," *Journal of Comparative Neurology*, vol. 341, no. 3, pp. 375–392, 1994.

[207] S. Ghosh and R. Gattera, "A comparison of the ipsilateral cortical projections to the dorsal and ventral subdivisions of the macaque premotor cortex," *Somatosensory & motor research*, vol. 12, no. 3-4, pp. 359–378, 1995.

[208] S. Bruni, M. Gerbella, L. Bonini, E. Borra, G. Coudé, P. F. Ferrari, L. Fogassi, M. Maranesi, F. Rodà, L. Simone, *et al.*, "Cortical and subcortical connections of parietal and premotor nodes of the monkey hand mirror neuron network," *Brain Structure and Function*, vol. 223, no. 4, pp. 1713–1729, 2018.

[209] A. M. Martino and P. L. Strick, "Corticospinal projections originate from the arcuate premotor area," *Brain research*, vol. 404, no. 1-2, pp. 307–312, 1987.

[210] S.-Q. He, R. P. Dum, and P. L. Strick, "Topographic organization of corticospinal projections from the frontal lobe: motor areas on the lateral surface of the hemisphere," *Journal of Neuroscience*, vol. 13, no. 3, pp. 952–980, 1993.

[211] R. P. Dum and P. L. Strick, "Motor areas in the frontal lobe of the primate," *Physiology & behavior*, vol. 77, no. 4-5, pp. 677–682, 2002.

[212] S. P. Wise, "The ventral premotor cortex, corticospinal region c, and the origin of primates," *Cortex*, vol. 42, no. 4, pp. 521–524, 2006.

[213] E. Borra, A. Belmalih, M. Gerbella, S. Rozzi, and G. Luppino, "Projections of the hand field of the macaque ventral premotor area f5 to the brainstem and spinal cord," *Journal of Comparative Neurology*, vol. 518, no. 13, pp. 2570–2591, 2010.

[214] G. Rizzolatti, R. Camarda, L. Fogassi, M. Gentilucci, G. Luppino, and M. Matelli, "Functional organization of inferior area 6 in the macaque monkey," *Experimental brain research*, vol. 71, no. 3, pp. 491–507, 1988.

[215] E. Stark, I. Asher, and M. Abeles, "Encoding of reach and grasp by single neurons in premotor cortex is independent of recording site," *Journal of neurophysiology*, vol. 97, no. 5, pp. 3351–3364, 2007.

[216] E. Schmidlin, T. Brochier, M. A. Maier, P. A. Kirkwood, and R. N. Lemon, "Pronounced reduction of digit motor responses evoked from macaque ventral premotor cortex after reversible inactivation of the primary motor cortex hand area," *Journal of Neuroscience*, vol. 28, no. 22, pp. 5772–5783, 2008.

[217] K. Takahashi, M. D. Best, N. Huh, K. A. Brown, A. A. Tobaa, and N. G. Hatsopoulos, "Encoding of both reaching and grasping kinematics in dorsal and ventral premotor cortices," *Journal of Neuroscience*, vol. 37, no. 7, pp. 1733–1746, 2017.

[218] U. Halsband and R. Passingham, "The role of premotor and parietal cortex in the direction of action," *Brain research*, vol. 240, no. 2, pp. 368–372, 1982.

[219] M. Davare, M. Andres, G. Cosnard, J.-L. Thonnard, and E. Olivier, "Dissociating the role of ventral and dorsal premotor cortex in precision grasping," *Journal of Neuroscience*, vol. 26, no. 8, pp. 2260–2268, 2006.

[220] G. Rizzolatti, C. Scandolara, M. Matelli, and M. Gentilucci, "Afferent properties of periarcuate neurons in macaque monkeys. i. somatosensory responses," *Behavioural brain research*, vol. 2, no. 2, pp. 125–146, 1981.

[221] G. Rizzolatti, C. Scandolara, M. Matelli, and M. Gentilucci, "Afferent properties of periarcuate neurons in macaque monkeys. ii. visual responses," *Behavioural brain research*, vol. 2, no. 2, pp. 147–163, 1981.

[222] G. Rizzolatti, M. Gentilucci, L. Fogassi, G. Luppino, M. Matelli, and S. Ponzoni-Maggi, "Neurons related to goal-directed motor acts in inferior area 6 of the macaque monkey," *Experimental Brain Research*, vol. 67, no. 1, pp. 220–224, 1987.

[223] A. Murata, L. Fadiga, L. Fogassi, V. Gallese, V. Raos, and G. Rizzolatti, "Object representation in the ventral premotor cortex (area f5) of the monkey," *Journal of neurophysiology*, vol. 78, no. 4, pp. 2226–2230, 1997.

[224] V. Raos, M.-A. Umiltá, A. Murata, L. Fogassi, and V. Gallese, "Functional properties of grasping-related neurons in the ventral premotor area f5 of the macaque monkey," *Journal of neurophysiology*, vol. 95, no. 2, pp. 709–729, 2006.

[225] M.-C. Fluet, M. A. Baumann, and H. Scherberger, "Context-specific grasp movement representation in macaque ventral premotor cortex," *Journal of Neuroscience*, vol. 30, no. 45, pp. 15175–15184, 2010.

[226] J. Carpaneto, M. Umiltà, L. Fogassi, A. Murata, V. Gallese, S. Micera, and V. Raos, "Decoding the activity of grasping neurons recorded from the ventral premotor area f5 of the macaque monkey," *Neuroscience*, vol. 188, pp. 80–94, 2011.

[227] J. Grèzes, J. L. Armony, J. Rowe, and R. E. Passingham, "Activations related to "mirror" and "canonical" neurones in the human brain: an fmri study," *Neuroimage*, vol. 18, no. 4, pp. 928–937, 2003.

[228] S. Schaffelhofer and H. Scherberger, "Object vision to hand action in macaque parietal, premotor, and motor cortices," *Elife*, vol. 5, p. e15278, 2016.

[229] B. R. Townsend, E. Subasi, and H. Scherberger, "Grasp movement decoding from premotor and parietal cortex," *Journal of Neuroscience*, vol. 31, no. 40, pp. 14386–14398, 2011.

[230] T. Theys, P. Pani, J. van Loon, J. Goffin, and P. Janssen, "Selectivity for three-dimensional shape and grasping-related activity in the macaque ventral premotor cortex," *Journal of Neuroscience*, vol. 32, no. 35, pp. 12038–12050, 2012.

[231] M. Maranesi, L. Bonini, and L. Fogassi, "Cortical processing of object affordances for self and others' action," *Frontiers in psychology*, vol. 5, p. 538, 2014.

[232] A. J. Suminski, P. Mardoum, T. P. Lillicrap, and N. G. Hatsopoulos, "Temporal evolution of both premotor and motor cortical tuning properties reflect changes in limb biomechanics," *Journal of neurophysiology*, vol. 113, no. 7, pp. 2812–2823, 2015.

[233] W. Wu and N. G. Hatsopoulos, "Coordinate system representations of movement direction in the premotor cortex," *Experimental brain research*, vol. 176, no. 4, pp. 652–657, 2007.

[234] S. J. Lehmann and H. Scherberger, "Reach and gaze representations in macaque parietal and premotor grasp areas," *Journal of Neuroscience*, vol. 33, no. 16, pp. 7038–7049, 2013.

[235] A. B. Schwartz, D. W. Moran, and G. A. Reina, "Differential representation of perception and action in the frontal cortex," *Science*, vol. 303, no. 5656, pp. 380–383, 2004.

[236] T. Ochiai, H. Mushiake, and J. Tanji, "Involvement of the ventral premotor cortex in controlling image motion of the hand during performance of a target-capturing task," *Cerebral Cortex*, vol. 15, no. 7, pp. 929–937, 2005.

[237] S. Kakei, D. S. Hoffman, and P. L. Strick, "Direction of action is represented in the ventral premotor cortex," *Nature neuroscience*, vol. 4, no. 10, pp. 1020–1025, 2001.

[238] H. Mushiake, M. Inase, and J. Tanji, "Neuronal activity in the primate premotor, supplementary, and precentral motor cortex during visually guided and internally

determined sequential movements," *Journal of neurophysiology*, vol. 66, no. 3, pp. 705–718, 1991.

[239] L. Bonini, S. Rozzi, F. U. Serventi, L. Simone, P. F. Ferrari, and L. Fogassi, "Ventral premotor and inferior parietal cortices make distinct contribution to action organization and intention understanding," *Cerebral Cortex*, vol. 20, no. 6, pp. 1372–1385, 2010.

[240] L. Bonini, F. U. Serventi, L. Simone, S. Rozzi, P. F. Ferrari, and L. Fogassi, "Grasping neurons of monkey parietal and premotor cortices encode action goals at distinct levels of abstraction during complex action sequences," *Journal of Neuroscience*, vol. 31, no. 15, pp. 5876–5886, 2011.

[241] S. Bruni, V. Giorgetti, L. Fogassi, and L. Bonini, "Multimodal encoding of goal-directed actions in monkey ventral premotor grasping neurons," *Cerebral Cortex*, vol. 27, no. 1, pp. 522–533, 2017.

[242] K. Kurata and J. Tanji, "Premotor cortex neurons in macaques: activity before distal and proximal forelimb movements," *Journal of Neuroscience*, vol. 6, no. 2, pp. 403–411, 1986.

[243] G. Di Pellegrino, L. Fadiga, L. Fogassi, V. Gallese, and G. Rizzolatti, "Understanding motor events: a neurophysiological study," *Experimental brain research*, vol. 91, no. 1, pp. 176–180, 1992.

[244] V. Gallese, L. Fadiga, L. Fogassi, and G. Rizzolatti, "Action recognition in the premotor cortex," *Brain*, vol. 119, no. 2, pp. 593–609, 1996.

[245] G. Rizzolatti, L. Fadiga, V. Gallese, and L. Fogassi, "Premotor cortex and the recognition of motor actions," *Cognitive brain research*, vol. 3, no. 2, pp. 131–141, 1996.

[246] G. Rizzolatti and M. A. Arbib, "Language within our grasp," *Trends in neurosciences*, vol. 21, no. 5, pp. 188–194, 1998.

[247] G. Rizzolatti and G. Luppino, "The cortical motor system," *Neuron*, vol. 31, no. 6, pp. 889–901, 2001.

[248] A. Kraskov, N. Dancause, M. M. Quallo, S. Shepherd, and R. N. Lemon, "Corticospinal neurons in macaque ventral premotor cortex with mirror properties:

a potential mechanism for action suppression?," *Neuron*, vol. 64, no. 6, pp. 922–930, 2009.

[249] M. J. Rochat, F. Caruana, A. Jezzini, I. Intskirveli, F. Grammont, V. Gallese, G. Rizzolatti, M. A. Umiltà, *et al.*, "Responses of mirror neurons in area f5 to hand and tool grasping observation," *Experimental brain research*, vol. 204, no. 4, pp. 605–616, 2010.

[250] L. Bonini, M. Maranesi, A. Livi, L. Fogassi, and G. Rizzolatti, "Space-dependent representation of objects and other's action in monkey ventral premotor grasping neurons," *Journal of Neuroscience*, vol. 34, no. 11, pp. 4108–4119, 2014.

[251] K. Kurata, "Hierarchical organization within the ventral premotor cortex of the macaque monkey," *Neuroscience*, vol. 382, pp. 127–143, 2018.

[252] A. Belmalih, E. Borra, M. Contini, M. Gerbella, S. Rozzi, and G. Luppino, "Multimodal architectonic subdivision of the rostral part (area f5) of the macaque ventral premotor cortex," *Journal of Comparative Neurology*, vol. 512, no. 2, pp. 183–217, 2009.

[253] M. Gerbella, A. Belmalih, E. Borra, S. Rozzi, and G. Luppino, "Cortical connections of the anterior (f5a) subdivision of the macaque ventral premotor area f5," *Brain Structure and Function*, vol. 216, no. 1, pp. 43–65, 2011.

[254] H. Sakata and M. Taira, "Parietal control of hand action," *Current opinion in neurobiology*, vol. 4, no. 6, pp. 847–856, 1994.

[255] M. Jeannerod, M. A. Arbib, G. Rizzolatti, and H. Sakata, "Grasping objects: the cortical mechanisms of visuomotor transformation," *Trends in neurosciences*, vol. 18, no. 7, pp. 314–320, 1995.

[256] C. A. Buneo and R. A. Andersen, "The posterior parietal cortex: sensorimotor interface for the planning and online control of visually guided movements," *Neuropsychologia*, vol. 44, no. 13, pp. 2594–2606, 2006.

[257] C. Grefkes and G. R. Fink, "The functional organization of the intraparietal sulcus in humans and monkeys," *Journal of anatomy*, vol. 207, no. 1, pp. 3–17, 2005.

[258] E. Borra, A. Belmalih, R. Calzavara, M. Gerbella, A. Murata, S. Rozzi, and G. Luppino, "Cortical connections of the macaque anterior intraparietal (aip) area," *Cerebral Cortex*, vol. 18, no. 5, pp. 1094–1111, 2008.

[259] J.-A. Rathelot, R. P. Dum, and P. L. Strick, "Posterior parietal cortex contains a command apparatus for hand movements," *Proceedings of the National Academy of Sciences*, vol. 114, no. 16, pp. 4255–4260, 2017.

[260] S. Faugier-Grimaud, C. Frenois, and D. G. Stein, "Effects of posterior parietal lesions on visually guided behavior in monkeys," *Neuropsychologia*, vol. 16, no. 2, pp. 151–168, 1978.

[261] V. Gallese, A. Murata, M. Kaseda, N. Niki, and H. Sakata, "Deficit of hand preshaping after muscimol injection in monkey parietal cortex.," *Neuroreport: An International Journal for the Rapid Communication of Research in Neuroscience*, 1994.

[262] F. Binkofski, C. Dohle, S. Posse, K. M. Stephan, H. Hefter, R. J. Seitz, and H.-J. Freund, "Human anterior intraparietal area subserves prehension: a combined lesion and functional mri activation study," *Neurology*, vol. 50, no. 5, pp. 1253–1259, 1998.

[263] M.-T. Perenin and A. Vighetto, "Optic ataxia: A specific disruption in visuomotor mechanisms: I. different aspects of the deficit in reaching for objects," *Brain*, vol. 111, no. 3, pp. 643–674, 1988.

[264] M. Jeannerod, J. Decety, and F. Michel, "Impairment of grasping movements following a bilateral posterior parietal lesion," *Neuropsychologia*, vol. 32, no. 4, pp. 369–380, 1994.

[265] M. Davare, J. C. Rothwell, and R. N. Lemon, "Causal connectivity between the human anterior intraparietal area and premotor cortex during grasp," *Current Biology*, vol. 20, no. 2, pp. 176–181, 2010.

[266] M. Davare, M. Andres, E. Clerget, J.-L. Thonnard, and E. Olivier, "Temporal dissociation between hand shaping and grip force scaling in the anterior intraparietal area," *Journal of Neuroscience*, vol. 27, no. 15, pp. 3974–3980, 2007.

[267] N. J. Rice, E. Tunik, and S. T. Grafton, "The anterior intraparietal sulcus mediates grasp execution, independent of requirement to update: new insights from transcranial magnetic stimulation," *Journal of Neuroscience*, vol. 26, no. 31, pp. 8176–8182, 2006.

[268] E. Tunik, S. H. Frey, and S. T. Grafton, "Virtual lesions of the anterior intraparietal area disrupt goal-dependent on-line adjustments of grasp," *Nature neuroscience*, vol. 8, no. 4, pp. 505–511, 2005.

[269] M. Dafotakis, R. Sparing, S. B. Eickhoff, G. R. Fink, and D. A. Nowak, "On the role of the ventral premotor cortex and anterior intraparietal area for predictive and reactive scaling of grip force," *Brain research*, vol. 1228, pp. 73–80, 2008.

[270] V. B. Mountcastle, J. Lynch, A. Georgopoulos, H. Sakata, and C. Acuna, "Posterior parietal association cortex of the monkey: command functions for operations within extrapersonal space," *Journal of neurophysiology*, vol. 38, no. 4, pp. 871–908, 1975.

[271] M. Taira, S. Mine, A. Georgopoulos, A. Murata, and H. Sakata, "Parietal cortex neurons of the monkey related to the visual guidance of hand movement," *Experimental brain research*, vol. 83, no. 1, pp. 29–36, 1990.

[272] H. Sakata, M. Taira, A. Murata, and S. Mine, "Neural mechanisms of visual guidance of hand action in the parietal cortex of the monkey," *Cerebral Cortex*, vol. 5, no. 5, pp. 429–438, 1995.

[273] A. Murata, V. Gallese, G. Luppino, M. Kaseda, and H. Sakata, "Selectivity for the shape, size, and orientation of objects for grasping in neurons of monkey parietal area aip," *Journal of neurophysiology*, vol. 83, no. 5, pp. 2580–2601, 2000.

[274] A. Murata, V. Gallese, M. Kaseda, and H. Sakata, "Parietal neurons related to memory-guided hand manipulation," *Journal of Neurophysiology*, vol. 75, no. 5, pp. 2180–2186, 1996.

[275] S. Srivastava, G. A. Orban, P. A. De Mazière, and P. Janssen, "A distinct representation of three-dimensional shape in macaque anterior intraparietal area: fast, metric, and coarse," *Journal of Neuroscience*, vol. 29, no. 34, pp. 10613–10626, 2009.

[276] T. Theys, S. Srivastava, J. van Loon, J. Goffin, and P. Janssen, "Selectivity for three-dimensional contours and surfaces in the anterior intraparietal area," *Journal of Neurophysiology*, vol. 107, no. 3, pp. 995–1008, 2012.

[277] M. C. Romero, I. C. Van Dromme, and P. Janssen, "The role of binocular disparity in stereoscopic images of objects in the macaque anterior intraparietal area," *PLoS One*, vol. 8, no. 2, p. e55340, 2013.

[278] M. C. Romero, P. Pani, and P. Janssen, "Coding of shape features in the macaque anterior intraparietal area," *Journal of Neuroscience*, vol. 34, no. 11, pp. 4006–4021, 2014.

[279] M. A. Baumann, M.-C. Fluet, and H. Scherberger, "Context-specific grasp movement representation in the macaque anterior intraparietal area," *Journal of Neuroscience*, vol. 29, no. 20, pp. 6436–6448, 2009.

[280] C. Grefkes, P. H. Weiss, K. Zilles, and G. R. Fink, "Crossmodal processing of object features in human anterior intraparietal cortex: an fmri study implies equivalencies between humans and monkeys," *Neuron*, vol. 35, no. 1, pp. 173–184, 2002.

[281] E. P. Gardner, K. S. Babu, S. D. Reitzen, S. Ghosh, A. S. Brown, J. Chen, A. L. Hall, M. D. Herzlinger, J. B. Kohlenstein, and J. Y. Ro, "Neurophysiology of prehension. i. posterior parietal cortex and object-oriented hand behaviors," *Journal of Neurophysiology*, vol. 97, no. 1, pp. 387–406, 2007.

[282] R. I. Rumiati, P. H. Weiss, T. Shallice, G. Ottoboni, J. Noth, K. Zilles, and G. R. Fink, "Neural basis of pantomiming the use of visually presented objects," *Neuroimage*, vol. 21, no. 4, pp. 1224–1231, 2004.

[283] K. F. Valyear, C. Cavina-Pratesi, A. J. Stiglick, and J. C. Culham, "Does tool-related fmri activity within the intraparietal sulcus reflect the plan to grasp?," *Neuroimage*, vol. 36, pp. T94–T108, 2007.

[284] L. G. Ungerleider, "Two cortical visual systems," *Analysis of visual behavior*, pp. 549–586, 1982.

[285] M. A. Goodale and D. A. Milner, "Separate visual pathways for perception and action," *Trends in Neurosciences*, vol. 15, no. 1, pp. 20–25, 1992.

[286] M. A. Goodale, J. P. Meenan, H. H. Bülthoff, D. A. Nicolle, K. J. Murphy, and C. I. Racicot, "Separate neural pathways for the visual analysis of object shape in perception and prehension," *Current Biology*, vol. 4, no. 7, pp. 604–610, 1994.

[287] O. A. Gharbawie, I. Stepniewska, and J. H. Kaas, "Cortical connections of functional zones in posterior parietal cortex and frontal cortex motor regions in new world monkeys," *Cerebral cortex*, vol. 21, no. 9, pp. 1981–2002, 2011.

[288] J. H. Kaas, O. A. Gharbawie, and I. Stepniewska, "Cortical networks for ethologically relevant behaviors in primates," *American journal of primatology*, vol. 75, no. 5, pp. 407–414, 2013.

[289] S. T. Grafton, "The cognitive neuroscience of prehension: recent developments," *Experimental brain research*, vol. 204, no. 4, pp. 475–491, 2010.

[290] E. Borra, M. Gerbella, S. Rozzi, and G. Luppino, "The macaque lateral grasping network: a neural substrate for generating purposeful hand actions," *Neuroscience & Biobehavioral Reviews*, vol. 75, pp. 65–90, 2017.

[291] K. Nelissen and W. Vanduffel, "Grasping-related functional magnetic resonance imaging brain responses in the macaque monkey," *Journal of Neuroscience*, vol. 31, no. 22, pp. 8220–8229, 2011.

[292] K. Nelissen, P. A. Fiave, and W. Vanduffel, "Decoding grasping movements from the parieto-frontal reaching circuit in the nonhuman primate," *Cerebral Cortex*, vol. 28, no. 4, pp. 1245–1259, 2018.

[293] J. C. Culham, S. L. Danckert, J. F. De Souza, J. S. Gati, R. S. Menon, and M. A. Goodale, "Visually guided grasping produces fmri activation in dorsal but not ventral stream brain areas," *Experimental brain research*, vol. 153, no. 2, pp. 180–189, 2003.

[294] C. Cavina-Pratesi, S. Monaco, P. Fattori, C. Galletti, T. D. McAdam, D. J. Quinlan, M. A. Goodale, and J. C. Culham, "Functional magnetic resonance imaging reveals the neural substrates of arm transport and grip formation in reach-to-grasp actions in humans," *Journal of Neuroscience*, vol. 30, no. 31, pp. 10306–10323, 2010.

[295] R. P. Grol, M. C. Bosch, M. E. Hulscher, M. P. Eccles, and M. Wensing, "Planning and studying improvement in patient care: the use of theoretical perspectives," *The Milbank Quarterly*, vol. 85, no. 1, pp. 93–138, 2007.

[296] F. Binkofski, G. Buccino, K. M. Stephan, G. Rizzolatti, R. J. Seitz, and H.-J. Freund, "A parieto-premotor network for object manipulation: evidence from neuroimaging," *Experimental Brain Research*, vol. 128, no. 1-2, pp. 210–213, 1999.

[297] H. H. Ehrsson, A. Fagergren, T. Jonsson, G. Westling, R. S. Johansson, and H. Forssberg, "Cortical activity in precision-versus power-grip tasks: an fmri study," *Journal of neurophysiology*, vol. 83, no. 1, pp. 528–536, 2000.

[298] H. H. Ehrsson, A. Fagergren, and H. Forssberg, "Differential fronto-parietal activation depending on force used in a precision grip task: an fmri study," *Journal of neurophysiology*, vol. 85, no. 6, pp. 2613–2623, 2001.

[299] J. Decety, D. Perani, M. Jeannerod, V. Bettinardi, B. Tadary, R. Woods, J. C. Mazziotta, and F. Fazio, "Mapping motor representations with positron emission tomography," *Nature*, vol. 371, no. 6498, pp. 600–602, 1994.

[300] S. T. Grafton, M. A. Arbib, L. Fadiga, and G. Rizzolatti, "Localization of grasp representations in humans by positron emission tomography," *Experimental brain research*, vol. 112, no. 1, pp. 103–111, 1996.

[301] L. J. Buxbaum, K. M. Kyle, K. Tang, and J. A. Detre, "Neural substrates of knowledge of hand postures for object grasping and functional object use: Evidence from fmri," *Brain research*, vol. 1117, no. 1, pp. 175–185, 2006.

[302] R. Ishibashi, G. Pobric, S. Saito, and M. A. Lambon Ralph, "The neural network for tool-related cognition: an activation likelihood estimation meta-analysis of 70 neuroimaging contrasts," *Cognitive Neuropsychology*, vol. 33, no. 3-4, pp. 241–256, 2016.

[303] M. L. Kellenbach, M. Brett, and K. Patterson, "Actions speak louder than functions: the importance of manipulability and action in tool representation," *Journal of cognitive neuroscience*, vol. 15, no. 1, pp. 30–46, 2003.

[304] J. W. Lewis, "Cortical networks related to human use of tools," *The neuroscientist*, vol. 12, no. 3, pp. 211–231, 2006.

[305] M. Godschalk, R. N. Lemon, H. G. Kuypers, and H. Ronday, "Cortical afferents and efferents of monkey postarcuate area: an anatomical and electrophysiological study," *Experimental Brain Research*, vol. 56, no. 3, pp. 410–424, 1984.

[306] M. Matsumura and K. Kubota, "Cortical projection to hand-arm motor area from post-arcuate area in macaque monkeys: a histological study of retrograde transport of horseradish peroxidase," *Neuroscience letters*, vol. 11, no. 3, pp. 241–246, 1979.

[307] K. F. Muakkassa and P. L. Strick, "Frontal lobe inputs to primate motor cortex: evidence for four somatotopically organized 'premotor'areas," *Brain research*, vol. 177, no. 1, pp. 176–182, 1979.

[308] S. Ghosh, C. Brinkman, and R. Porter, "A quantitative study of the distribution of neurons projecting to the precentral motor cortex in the monkey (m. fascicularis)," *Journal of Comparative Neurology*, vol. 259, no. 3, pp. 424–444, 1987.

[309] H. Tokuno and J. Tanji, "Input organization of distal and proximal forelimb areas in the monkey primary motor cortex: a retrograde double labeling study," *Journal of Comparative Neurology*, vol. 333, no. 2, pp. 199–209, 1993.

[310] S. Ghosh and R. Porter, "Corticocortical synaptic influences on morphologically identified pyramidal neurones in the motor cortex of the monkey.," *The Journal of Physiology*, vol. 400, no. 1, pp. 617–629, 1988.

[311] H. Tokuno and A. Nambu, "Organization of nonprimary motor cortical inputs on pyramidal and nonpyramidal tract neurons of primary motor cortex: an electrophysiological study in the macaque monkey," *Cerebral cortex*, vol. 10, no. 1, pp. 58–68, 2000.

[312] A. Kraskov, G. Prabhu, M. M. Quallo, R. N. Lemon, and T. Brochier, "Ventral premotor–motor cortex interactions in the macaque monkey during grasp: response of single neurons to intracortical microstimulation," *Journal of Neuroscience*, vol. 31, no. 24, pp. 8812–8821, 2011.

[313] M.-H. Boudrias, R. L. McPherson, S. B. Frost, and P. D. Cheney, "Output properties and organization of the forelimb representation of motor areas on the lateral aspect of the hemisphere in rhesus macaques," *Cerebral cortex*, vol. 20, no. 1, pp. 169–186, 2010.

[314] G. Cerri, H. Shimazu, M. Maier, and R. Lemon, "Facilitation from ventral premotor cortex of primary motor cortex outputs to macaque hand muscles," *Journal of neurophysiology*, vol. 90, no. 2, pp. 832–842, 2003.

[315] H. Shimazu, M. A. Maier, G. Cerri, P. A. Kirkwood, and R. N. Lemon, "Macaque ventral premotor cortex exerts powerful facilitation of motor cortex outputs to upper limb motoneurons.," *Journal of Neuroscience*, vol. 24, no. 5, pp. 1200–1211, 2004.

[316] G. Prabhu, H. Shimazu, G. Cerri, T. Brochier, R. L. Spinks, M. A. Maier, and R. N. Lemon, "Modulation of primary motor cortex outputs from ventral premotor cortex during visually guided grasp in the macaque monkey," *The Journal of physiology*, vol. 587, no. 5, pp. 1057–1069, 2009.

[317] M. Davare, R. Lemon, and E. Olivier, "Selective modulation of interactions between ventral premotor cortex and primary motor cortex during precision grasping in humans," *The Journal of physiology*, vol. 586, no. 11, pp. 2735–2742, 2008.

[318] M. Davare, K. Montague, E. Olivier, J. C. Rothwell, and R. N. Lemon, "Ventral premotor to primary motor cortical interactions during object-driven grasp in humans," *Cortex*, vol. 45, no. 9, pp. 1050–1057, 2009.

[319] L. Verhagen, H. C. Dijkerman, W. P. Medendorp, and I. Toni, "Cortical dynamics of sensorimotor integration during grasp planning," *Journal of Neuroscience*, vol. 32, no. 13, pp. 4508–4519, 2012.

[320] G. Koch, M. Cercignani, C. Pecchioli, V. Versace, M. Oliveri, C. Caltagirone, J. Rothwell, and M. Bozzali, "In vivo definition of parieto-motor connections involved in planning of grasping movements," *Neuroimage*, vol. 51, no. 1, pp. 300–312, 2010.

[321] T. Theys, P. Pani, J. van Loon, J. Goffin, and P. Janssen, "Three-dimensional shape coding in grasping circuits: a comparison between the anterior intraparietal area and ventral premotor area f5a," *Journal of cognitive neuroscience*, vol. 25, no. 3, pp. 352–364, 2013.

[322] J. J. Gibson, *The ecological approach to visual perception*. Boston, MA, US: Houghton, Mifflin and Company, 1979.

[323] P. Cisek, "Cortical mechanisms of action selection: the affordance competition hypothesis," *Philosophical Transactions of the Royal Society B: Biological Sciences*, vol. 362, no. 1485, pp. 1585–1599, 2007.

[324] P. Cisek and J. F. Kalaska, "Neural correlates of reaching decisions in dorsal premotor cortex: specification of multiple direction choices and final selection of action," *Neuron*, vol. 45, no. 5, pp. 801–814, 2005.

[325] P. Cisek and J. F. Kalaska, "Neural mechanisms for interacting with a world full of action choices," *Annual review of neuroscience*, vol. 33, pp. 269–298, 2010.

[326] S. Thill, D. Caligiore, A. M. Borghi, T. Ziemke, and G. Baldassarre, "Theories and computational models of affordance and mirror systems: an integrative review," *Neuroscience & Biobehavioral Reviews*, vol. 37, no. 3, pp. 491–521, 2013.

[327] A. H. Fagg and M. A. Arbib, "Modeling parietal–premotor interactions in primate control of grasping," *Neural Networks*, vol. 11, no. 7-8, pp. 1277–1303, 1998.

[328] D. Caligiore, A. M. Borghi, D. Parisi, and G. Baldassarre, "Tropicals: A computational embodied neuroscience model of compatibility effects.," *Psychological Review*, vol. 117, no. 4, p. 1188, 2010.

[329] J. R. Simon and J. D. Wolf, "Choice reaction time as a function of angular stimulus-response correspondence and age," *Ergonomics*, vol. 6, no. 1, pp. 99–105, 1963.

[330] M. Tucker and R. Ellis, "The potentiation of grasp types during visual object categorization," *Visual cognition*, vol. 8, no. 6, pp. 769–800, 2001.

[331] L. Craighero, L. Fadiga, G. Rizzolatti, and C. Umiltà, "Action for perception: a motor-visual attentional effect.," *Journal of experimental psychology: Human perception and performance*, vol. 25, no. 6, p. 1673, 1999.

[332] R. Ellis and M. Tucker, "Micro-affordance: The potentiation of components of action by seen objects," *British journal of psychology*, vol. 91, no. 4, pp. 451–471, 2000.

[333] M. Tucker and R. Ellis, "Action priming by briefly presented objects," *Acta psychologica*, vol. 116, no. 2, pp. 185–203, 2004.

[334] S. Glover, D. A. Rosenbaum, J. Graham, and P. Dixon, "Grasping the meaning of words," *Experimental Brain Research*, vol. 154, no. 1, pp. 103–108, 2004.

[335] Z. Pappas and A. Mack, "Potentiation of action by undetected affordant objects," *Visual Cognition*, vol. 16, no. 7, pp. 892–915, 2008.

[336] K.-W. Chua, D. N. Bub, M. E. Masson, and I. Gauthier, "Grasp representations depend on knowledge and attention.," *Journal of Experimental Psychology: Learning, Memory, and Cognition*, vol. 44, no. 2, p. 268, 2018.

[337] L. Vainio, M. Tucker, and R. Ellis, "Precision and power grip priming by observed grasping," *Brain and Cognition*, vol. 65, no. 2, pp. 195–207, 2007.

[338] L. Craighero, L. Fadiga, C. A. Umiltà, and G. Rizzolatti, "Evidence for visuomotor priming effect," *Neuroreport*, vol. 8, no. 1, pp. 347–349, 1996.

[339] D. N. Bub, M. E. Masson, and R. Kumar, "Time course of motor affordances evoked by pictured objects and words.," *Journal of Experimental Psychology: Human Perception and Performance*, vol. 44, no. 1, p. 53, 2018.

[340] M. Tucker and R. Ellis, "On the relations between seen objects and components of potential actions.," *Journal of Experimental Psychology: Human perception and performance*, vol. 24, no. 3, p. 830, 1998.

[341] L. L. Chao and A. Martin, "Representation of manipulable man-made objects in the dorsal stream," *Neuroimage*, vol. 12, no. 4, pp. 478–484, 2000.

[342] T. Okada, S. Tanaka, T. Nakai, S. Nishizawa, T. Inui, N. Sadato, Y. Yonekura, and J. Konishi, "Naming of animals and tools: a functional magnetic resonance imaging study of categorical differences in the human brain areas commonly used for naming visually presented objects," *Neuroscience letters*, vol. 296, no. 1, pp. 33–36, 2000.

[343] J. Grèzes and J. Decety, "Does visual perception of object afford action? evidence from a neuroimaging study," *Neuropsychologia*, vol. 40, no. 2, pp. 212–222, 2002.

[344] S. H. Creem-Regehr and J. N. Lee, "Neural representations of graspable objects: are tools special?," *Cognitive Brain Research*, vol. 22, no. 3, pp. 457–469, 2005.

[345] M. Tettamanti, F. Conca, A. Falini, and D. Perani, "Unaware processing of tools in the neural system for object-directed action representation," *Journal of Neuroscience*, vol. 37, no. 44, pp. 10712–10724, 2017.

[346] F. Fang and S. He, "Cortical responses to invisible objects in the human dorsal and ventral pathways," *Nature neuroscience*, vol. 8, no. 10, pp. 1380–1385, 2005.

[347] A. Martin, C. L. Wiggs, L. G. Ungerleider, and J. V. Haxby, "Neural correlates of category-specific knowledge," *Nature*, vol. 379, no. 6566, pp. 649–652, 1996.

[348] S. T. Grafton, L. Fadiga, M. A. Arbib, and G. Rizzolatti, "Premotor cortex activation during observation and naming of familiar tools," *Neuroimage*, vol. 6, no. 4, pp. 231–236, 1997.

[349] J. Grèzes, M. Tucker, J. Armony, R. Ellis, and R. E. Passingham, "Objects automatically potentiate action: an fmri study of implicit processing," *European Journal of Neuroscience*, vol. 17, no. 12, pp. 2735–2740, 2003.

[350] L. Bonini, M. Maranesi, A. Livi, L. Fogassi, and G. Rizzolatti, "Ventral premotor neurons encoding representations of action during self and others' inaction," *Current Biology*, vol. 24, no. 14, pp. 1611–1614, 2014.

[351] M. Maranesi, S. Bruni, A. Livi, F. Donnarumma, G. Pezzulo, and L. Bonini, "Differential neural dynamics underling pragmatic and semantic affordance processing in macaque ventral premotor cortex," *Scientific reports*, vol. 9, no. 1, pp. 1–11, 2019.

[352] D. Tkach, J. Reimer, and N. G. Hatsopoulos, "Congruent activity during action and action observation in motor cortex," *Journal of Neuroscience*, vol. 27, no. 48, pp. 13241–13250, 2007.

[353] J. Dushanova and J. Donoghue, "Neurons in primary motor cortex engaged during action observation," *European Journal of Neuroscience*, vol. 31, no. 2, pp. 386–398, 2010.

[354] G. Vigneswaran, R. Philipp, R. N. Lemon, and A. Kraskov, "M1 corticospinal mirror neurons and their role in movement suppression during action observation," *Current Biology*, vol. 23, no. 3, pp. 236–243, 2013.

[355] R. Hari, N. Forss, S. Avikainen, E. Kirveskari, S. Salenius, and G. Rizzolatti, "Activation of human primary motor cortex during action observation: a neuromagnetic study," *Proceedings of the National Academy of Sciences*, vol. 95, no. 25, pp. 15061–15065, 1998.

[356] C. Ansuini, M. Santello, S. Massaccesi, and U. Castiello, "Effects of end-goal on hand shaping," *Journal of neurophysiology*, vol. 95, no. 4, pp. 2456–2465, 2006.

[357] M. Goodale, L. Jakobson, and J. Keillor, "Differences in the visual control of pantomimed and natural grasping movements," *Neuropsychologia*, vol. 32, no. 10, pp. 1159–1178, 1994.

[358] M. Saling, J. Alberts, G. Stelmach, and J. R. Bloedel, "Reach-to-grasp movements during obstacle avoidance," *Experimental brain research*, vol. 118, no. 2, pp. 251–258, 1998.

[359] U. Castiello, "Mechanisms of selection for the control of hand action," *Trends in Cognitive Sciences*, vol. 3, no. 7, pp. 264–271, 1999.

[360] S. Jackson, G. Jackson, and J. Rosicky, "Are non-relevant objects represented in working memory? the effect of non-target objects on reach and grasp kinematics," *Experimental Brain Research*, vol. 102, no. 3, pp. 519–530, 1995.

[361] U. Castiello, "Grasping a fruit: Selection for action.," *Journal of Experimental Psychology: Human Perception and Performance*, vol. 22, no. 3, p. 582, 1996.

[362] M. Gentilucci, "Object motor representation and reaching–grasping control," *Neuropsychologia*, vol. 40, no. 8, pp. 1139–1153, 2002.

[363] M. Gentilucci, F. Benuzzi, L. Bertolani, E. Daprati, and M. Gangitano, "Language and motor control," *Experimental Brain Research*, vol. 133, no. 4, pp. 468–490, 2000.

[364] D. A. Rosenbaum, F. Marchak, H. J. Barnes, J. Vaughan, J. D. Slotta, and M. J. Jorgensen, "Constraints for action selection: Overhand versus underhand grips.," in *Attention and Performance Xiii: Motor Representation and Control*, pp. 321–342, Lawrence Erlbaum Associates, Inc, 1990.

[365] D. A. Rosenbaum and M. J. Jorgensen, "Planning macroscopic aspects of manual control," *Human Movement Science*, vol. 11, no. 1-2, pp. 61–69, 1992.

[366] D. A. Rosenbaum, J. Vaughan, H. J. Barnes, and M. J. Jorgensen, "Time course of movement planning: selection of handgrips for object manipulation.," *Journal of Experimental Psychology: Learning, Memory, and Cognition*, vol. 18, no. 5, p. 1058, 1992.

[367] D. A. Rosenbaum, K. M. Chapman, M. Weigelt, D. J. Weiss, and R. van der Wel, "Cognition, action, and object manipulation.," *Psychological bulletin*, vol. 138, no. 5, p. 924, 2012.

[368] M. Gentilucci, A. Negrotti, and M. Gangitano, "Planning an action," *Experimental Brain Research*, vol. 115, no. 1, pp. 116–128, 1997.

[369] R. G. Cohen and D. A. Rosenbaum, "Where grasps are made reveals how grasps are planned: generation and recall of motor plans," *Experimental Brain Research*, vol. 157, no. 4, pp. 486–495, 2004.

[370] L. Sartori, C. Becchio, B. G. Bara, and U. Castiello, "Does the intention to communicate affect action kinematics?," *Consciousness and cognition*, vol. 18, no. 3, pp. 766–772, 2009.

[371] C. Ansuini, L. Giosa, L. Turella, G. Altoè, and U. Castiello, "An object for an action, the same object for other actions: effects on hand shaping," *Experimental Brain Research*, vol. 185, no. 1, pp. 111–119, 2008.

[372] K. R. Naish, A. T. Reader, C. Houston-Price, A. J. Bremner, and N. P. Holmes, "To eat or not to eat? kinematics and muscle activity of reach-to-grasp movements are influenced by the action goal, but observers do not detect these differences," *Experimental Brain Research*, vol. 225, no. 2, pp. 261–275, 2013.

[373] A. Cavallo, A. Koul, C. Ansuini, F. Capozzi, and C. Becchio, "Decoding intentions from movement kinematics," *Scientific Reports*, vol. 6, no. 1, pp. 1–8, 2016.

[374] M. Soriano, A. Cavallo, A. D'Ausilio, C. Becchio, and L. Fadiga, "Movement kinematics drive chain selection toward intention detection," *Proceedings of the National Academy of Sciences*, vol. 115, no. 41, pp. 10452–10457, 2018.

[375] A. Koul, A. Cavallo, F. Cauda, T. Costa, M. Diano, M. Pontil, and C. Becchio, "Action observation areas represent intentions from subtle kinematic features," *Cerebral Cortex*, vol. 28, no. 7, pp. 2647–2654, 2018.

[376] R. Marteniuk, C. MacKenzie, M. Jeannerod, S. Athenes, and C. Dugas, "Constraints on human arm movement trajectories.," *Canadian Journal of Psychology/Revue canadienne de psychologie*, vol. 41, no. 3, p. 365, 1987.

[377] M. Gentilucci, F. Benuzzi, L. Bertolani, and M. Gangitano, "Influence of stimulus color on the control of reaching-grasping movements," *Experimental brain research*, vol. 137, no. 1, pp. 36–44, 2001.

[378] A. G. Davidson, V. Chan, R. O'Dell, and M. H. Schieber, "Rapid changes in throughput from single motor cortex neurons to muscle activity," *Science*, vol. 318, no. 5858, pp. 1934–1937, 2007.

[379] D. M. Griffin, D. S. Hoffman, and P. L. Strick, "Corticomotoneuronal cells are "functionally tuned"," *Science*, vol. 350, no. 6261, pp. 667–670, 2015.

[380] S. Naufel, J. I. Glaser, K. P. Kording, E. J. Perreault, and L. E. Miller, "A muscle-activity-dependent gain between motor cortex and emg," *Journal of neurophysiology*, vol. 121, no. 1, pp. 61–73, 2019.

[381] A. Jackson, J. Mavoori, and E. E. Fetz, "Correlations between the same motor cortex cells and arm muscles during a trained task, free behavior, and natural sleep in the macaque monkey," *Journal of neurophysiology*, vol. 97, no. 1, pp. 360–374, 2007.

[382] A. Miri, C. L. Warriner, J. S. Seely, G. F. Elsayed, J. P. Cunningham, M. M. Churchland, and T. M. Jessell, "Behaviorally selective engagement of short-latency effector pathways by motor cortex," *Neuron*, vol. 95, no. 3, pp. 683–696, 2017.

[383] Y. Matsuzaka, N. Picard, and P. L. Strick, "Skill representation in the primary motor cortex after long-term practice," *Journal of neurophysiology*, vol. 97, no. 2, pp. 1819–1832, 2007.

[384] N. Picard, Y. Matsuzaka, and P. L. Strick, "Extended practice of a motor skill is associated with reduced metabolic activity in m1," *Nature neuroscience*, vol. 16, no. 9, pp. 1340–1347, 2013.

[385] N. G. Hatsopoulos, L. Paninski, and J. P. Donoghue, "Sequential movement representations based on correlated neuronal activity," *Experimental brain research*, vol. 149, no. 4, pp. 478–486, 2003.

[386] Y. Ben-Shaul, R. Drori, I. Asher, E. Stark, Z. Nadasdy, and M. Abeles, "Neuronal activity in motor cortical areas reflects the sequential context of movement," *Journal of Neurophysiology*, vol. 91, no. 4, pp. 1748–1762, 2004.

[387] X. Lu and J. Ashe, "Anticipatory activity in primary motor cortex codes memorized movement sequences," *Neuron*, vol. 45, no. 6, pp. 967–973, 2005.

[388] A. F. Carpenter, A. P. Georgopoulos, and G. Pellizzer, "Motor cortical encoding of serial order in a context-recall task," *Science*, vol. 283, no. 5408, pp. 1752–1757, 1999.

[389] G. E. Alexander and M. D. Crutcher, "Neural representations of the target (goal) of visually guided arm movements in three motor areas of the monkey," *Journal of neurophysiology*, vol. 64, no. 1, pp. 164–178, 1990.

[390] J. Zhang, A. Riehle, J. Requin, and S. Kornblum, "Dynamics of single neuron activity in monkey primary motor cortex related to sensorimotor transformation," *Journal of Neuroscience*, vol. 17, no. 6, pp. 2227–2246, 1997.

[391] L. Shen and G. E. Alexander, "Neural correlates of a spatial sensory-to-motor transformation in primary motor cortex," *Journal of neurophysiology*, vol. 77, no. 3, pp. 1171–1194, 1997.

[392] S. Wise, S. Moody, K. Blomstrom, and A. Mitz, "Changes in motor cortical activity during visuomotor adaptation," *Experimental Brain Research*, vol. 121, no. 3, pp. 285–299, 1998.

[393] N. Zach, D. Inbar, Y. Grinvald, H. Bergman, and E. Vaadia, "Emergence of novel representations in primary motor cortex and premotor neurons during associative learning," *Journal of Neuroscience*, vol. 28, no. 38, pp. 9545–9556, 2008.

[394] S. H. Scott and J. F. Kalaska, "Changes in motor cortex activity during reaching movements with similar hand paths but different arm postures," *Journal of neurophysiology*, vol. 73, no. 6, pp. 2563–2567, 1995.

[395] S. H. Scott and J. F. Kalaska, "Reaching movements with similar hand paths but different arm orientations. i. activity of individual cells in motor cortex," *Journal of neurophysiology*, vol. 77, no. 2, pp. 826–852, 1997.

[396] R. Caminiti, P. B. Johnson, and A. Urbano, "Making arm movements within different parts of space: dynamic aspects in the primate motor cortex," *Journal of Neuroscience*, vol. 10, no. 7, pp. 2039–2058, 1990.

[397] L. E. Sergio and J. F. Kalaska, "Systematic changes in motor cortex cell activity with arm posture during directional isometric force generation," *Journal of neurophysiology*, vol. 89, no. 1, pp. 212–228, 2003.

[398] R. Paz, T. Boraud, C. Natan, H. Bergman, and E. Vaadia, "Preparatory activity in motor cortex reflects learning of local visuomotor skills," *Nature neuroscience*, vol. 6, no. 8, pp. 882–890, 2003.

[399] P. L. Gribble and S. H. Scott, "Overlap of internal models in motor cortex for mechanical loads during reaching," *Nature*, vol. 417, no. 6892, pp. 938–941, 2002.

[400] M. A. Lebedev, J. M. Carmena, J. E. O'Doherty, M. Zacksenhouse, C. S. Henriquez, J. C. Principe, and M. A. Nicolelis, "Cortical ensemble adaptation to represent velocity of an artificial actuator controlled by a brain-machine interface," *Journal of Neuroscience*, vol. 25, no. 19, pp. 4681–4693, 2005.

[401] R. G. Rasmussen, A. Schwartz, and S. M. Chase, "Dynamic range adaptation in primary motor cortical populations," *Elife*, vol. 6, p. e21409, 2017.

[402] P. J. Ifft, S. Shokur, Z. Li, M. A. Lebedev, and M. A. Nicolelis, "A brain-machine interface enables bimanual arm movements in monkeys," *Science translational medicine*, vol. 5, no. 210, pp. 210ra154–210ra154, 2013.

[403] M. Velliste, S. D. Kennedy, A. B. Schwartz, A. S. Whitford, J.-W. Sohn, and A. J. McMorland, "Motor cortical correlates of arm resting in the context of a reaching task and implications for prosthetic control," *Journal of Neuroscience*, vol. 34, no. 17, pp. 6011–6022, 2014.

[404] N. Kadmon Harpaz, D. Ungarish, N. G. Hatsopoulos, and T. Flash, "Movement decomposition in the primary motor cortex," *Cerebral Cortex*, vol. 29, no. 4, pp. 1619–1633, 2019.

[405] S. Suway, J. Orellana, A. McMorland, G. Fraser, Z. Liu, M. Velliste, S. Chase, R. Kass, and A. Schwartz, "Temporally segmented directionality in the motor cortex," *Cerebral Cortex*, vol. 28, no. 7, pp. 2326–2339, 2018.

[406] S. B. Suway and A. B. Schwartz, "Activity in primary motor cortex related to visual feedback," *Cell Reports*, vol. 29, no. 12, pp. 3872–3884, 2019.

[407] I. Kurtzer, T. M. Herter, and S. H. Scott, "Random change in cortical load representation suggests distinct control of posture and movement," *Nature neuroscience*, vol. 8, no. 4, pp. 498–504, 2005.

[408] G. Kroliczak, C. Cavina-Pratesi, D. Goodman, and J. Culham, "What does the brain do when you fake it? an fmri study of pantomimed and real grasping," *Journal of Neurophysiology*, vol. 97, no. 3, pp. 2410–2422, 2007.

[409] E. Freud, S. N. Macdonald, J. Chen, D. J. Quinlan, M. A. Goodale, and J. C. Culham, "Getting a grip on reality: Grasping movements directed to real objects and images rely on dissociable neural representations," *Cortex*, vol. 98, pp. 34–48, 2018.

[410] J. E. Downey, L. Brane, R. A. Gaunt, E. C. Tyler-Kabara, M. L. Boninger, and J. L. Collinger, "Motor cortical activity changes during neuroprosthetic-controlled object interaction," *Scientific reports*, vol. 7, no. 1, pp. 1–10, 2017.

[411] D. M. Griffin, H. M. Hudson, A. Belhaj-Saif, and P. D. Cheney, "Stability of output effects from motor cortex to forelimb muscles in primates," *Journal of Neuroscience*, vol. 29, no. 6, pp. 1915–1927, 2009.

[412] D. Flament, P. Goldsmith, C. Buckley, and R. Lemon, "Task dependence of responses in first dorsal interosseous muscle to magnetic brain stimulation in man.," *The Journal of Physiology*, vol. 464, no. 1, pp. 361–378, 1993.

[413] M. Tinazzi, S. Farina, S. Tamburin, S. Facchini, A. Fiaschi, D. Restivo, and A. Berardelli, "Task-dependent modulation of excitatory and inhibitory functions within the human primary motor cortex," *Experimental brain research*, vol. 150, no. 2, pp. 222–229, 2003.

[414] N. Kouchtir-Devanne, C. Capaday, F. Cassim, P. Derambure, and H. Devanne, "Task-dependent changes of motor cortical network excitability during precision grip compared to isolated finger contraction," *Journal of Neurophysiology*, vol. 107, no. 5, pp. 1522–1529, 2012.

[415] N. Geevasinga, P. Menon, M. C. Kiernan, and S. Vucic, "Motor cortical function and the precision grip," *Physiological reports*, vol. 2, no. 12, p. e12120, 2014.

[416] L. Cattaneo, M. Voss, T. Brochier, G. Prabhu, D. Wolpert, and R. Lemon, "A cortico-cortical mechanism mediating object-driven grasp in humans," *Proceedings of the National Academy of Sciences*, vol. 102, no. 3, pp. 898–903, 2005.

[417] G. Prabhu, M. Voss, T. Brochier, L. Cattaneo, P. Haggard, and R. Lemon, "Excitability of human motor cortex inputs prior to grasp," *The Journal of physiology*, vol. 581, no. 1, pp. 189–201, 2007.

[418] G. Prabhu, R. Lemon, and P. Haggard, "On-line control of grasping actions: object-specific motor facilitation requires sustained visual input," *Journal of Neuroscience*, vol. 27, no. 46, pp. 12651–12654, 2007.

[419] R. N. Lemon, R. Johansson, and G. Westling, "Corticospinal control during reach, grasp, and precision lift in man," *Journal of Neuroscience*, vol. 15, no. 9, pp. 6145–6156, 1995.

[420] R. J. Smith, A. B. Soares, A. G. Rouse, M. H. Schieber, and N. V. Thakor, "Modeling task-specific neuronal ensembles improves decoding of grasp," *Journal of neural engineering*, vol. 15, no. 3, p. 036006, 2018.

[421] L. Fogassi, P. F. Ferrari, B. Gesierich, S. Rozzi, F. Chersi, and G. Rizzolatti, "Parietal lobe: from action organization to intention understanding," *Science*, vol. 308, no. 5722, pp. 662–667, 2005.

[422] G. Coudé, G. Toschi, F. Festante, M. Bimbi, J. Bonaiuto, and P. F. Ferrari, "Grasping neurons in the ventral premotor cortex of macaques are modulated by social goals," *Journal of cognitive neuroscience*, vol. 31, no. 2, pp. 299–313, 2019.

[423] M. Marangon, S. Jacobs, and S. H. Frey, "Evidence for context sensitivity of grasp representations in human parietal and premotor cortices," *Journal of Neurophysiology*, vol. 105, no. 5, pp. 2536–2546, 2011.

[424] J. P. Gallivan, I. S. Johnsrude, and J. Randall Flanagan, "Planning ahead: object-directed sequential actions decoded from human frontoparietal and occipitotemporal networks," *Cerebral Cortex*, vol. 26, no. 2, pp. 708–730, 2016.

[425] C. E. Vargas-Irwin, L. Franquemont, M. J. Black, and J. P. Donoghue, "Linking objects to actions: encoding of target object and grasping strategy in primate ventral premotor cortex," *Journal of Neuroscience*, vol. 35, no. 30, pp. 10888–10897, 2015.

[426] L. Bonini, F. Ugolotti Serventi, S. Bruni, M. Maranesi, M. Bimbi, L. Simone, S. Rozzi, P. F. Ferrari, and L. Fogassi, "Selectivity for grip type and action goal in macaque inferior parietal and ventral premotor grasping neurons," *Journal of Neurophysiology*, vol. 108, no. 6, pp. 1607–1619, 2012.

[427] S. H. Creem-Regehr, V. Dilda, A. E. Vicchrilli, F. Federer, and J. N. Lee, "The influence of complex action knowledge on representations of novel graspable objects: evidence from functional magnetic resonance imaging," *Journal of the International Neuropsychological Society: JINS*, vol. 13, no. 6, p. 1009, 2007.

[428] M. Umiltà, I. Intskirveli, F. Grammont, M. Rochat, F. Caruana, A. Jezzini, V. Gallese, G. Rizzolatti, *et al.*, "When pliers become fingers in the monkey motor system," *Proceedings of the National Academy of Sciences*, vol. 105, no. 6, pp. 2209–2213, 2008.

[429] P. Van Kan, K. M. Horn, and A. R. Gibson, "The importance of hand use to discharge of interpositus neurones of the monkey.," *The Journal of physiology*, vol. 480, no. 1, pp. 171–190, 1994.

[430] A. Gibson, "Construction of a reach-to-grasp," in *Novartis Foundation Symposium 218 - Sensory Guidance of Movement*, Wiley Online Library, 1998.

[431] A. G. Rouse and M. H. Schieber, "Spatiotemporal distribution of location and object effects in primary motor cortex neurons during reach-to-grasp," *Journal of Neuroscience*, vol. 36, no. 41, pp. 10640–10653, 2016.

[432] S. H. Creem and D. R. Proffitt, "Grasping objects by their handles: a necessary interaction between cognition and action.," *Journal of experimental psychology: Human Perception and Performance*, vol. 27, no. 1, p. 218, 2001.

[433] M. N. Loh, L. Kirsch, J. C. Rothwell, R. N. Lemon, and M. Davare, "Information about the weight of grasped objects from vision and internal models interacts within the primary motor cortex," *Journal of Neuroscience*, vol. 30, no. 20, pp. 6984–6990, 2010.

[434] M. J. McGinley, M. Vinck, J. Reimer, R. Batista-Brito, E. Zagha, C. R. Cadwell, A. S. Tolias, J. A. Cardin, and D. A. McCormick, "Waking state: rapid variations modulate neural and behavioral responses," *Neuron*, vol. 87, no. 6, pp. 1143–1161, 2015.

[435] B. R. Cowley, A. C. Snyder, K. Acar, R. C. Williamson, B. M. Yu, and M. A. Smith, "Slow drift of neural activity as a signature of impulsivity in macaque visual and prefrontal cortex," *Neuron*, vol. 108, no. 3, pp. 551–567, 2020.

[436] W. E. Allen, M. Z. Chen, N. Pichamoorthy, R. H. Tien, M. Pachitariu, L. Luo, and K. Deisseroth, "Thirst regulates motivated behavior through modulation of brainwide neural population dynamics," *Science*, vol. 364, no. 6437, 2019.

[437] S. T. Clanton, *Brain-computer interface control of an anthropomorphic robotic arm*. PhD thesis, Carnegie Mellon University, 2011.

[438] S. B. Suway, *Neural state changes in primate motor cortex during arm movements with distinct control requirements*. PhD thesis, University of Pittsburgh, 2019.

[439] G. W. Fraser and A. B. Schwartz, "Recording from the same neurons chronically in motor cortex," *Journal of neurophysiology*, vol. 107, no. 7, pp. 1970–1978, 2012.

[440] K. Maeda, H. Ishida, K. Nakajima, M. Inase, and A. Murata, "Functional properties of parietal hand manipulation–related neurons and mirror neurons responding to vision

of own hand action," *Journal of cognitive neuroscience*, vol. 27, no. 3, pp. 560–572, 2015.

[441] M. Mishkin and F. J. Manning, "Non-spatial memory after selective prefrontal lesions in monkeys," *Brain research*, vol. 143, no. 2, pp. 313–323, 1978.

[442] R. Passingham, "Delayed matching after selective prefrontal lesions in monkeys (macaca mulatta)," *Brain research*, vol. 92, no. 1, pp. 89–102, 1975.

[443] S. Bruni, V. Giorgetti, L. Bonini, and L. Fogassi, "Processing and integration of contextual information in monkey ventrolateral prefrontal neurons during selection and execution of goal-directed manipulative actions," *Journal of Neuroscience*, vol. 35, no. 34, pp. 11877–11890, 2015.

[444] A. A. Russo, R. Khajeh, S. R. Bittner, S. M. Perkins, J. P. Cunningham, L. Abbott, and M. M. Churchland, "Neural trajectories in the supplementary motor area and motor cortex exhibit distinct geometries, compatible with different classes of computation," *Neuron*, 2020.

[445] J. Kihlberg, J. Herson, and W. Schotz, "Square root transformation revisited," *Journal of the Royal Statistical Society: Series C (Applied Statistics)*, vol. 21, no. 1, pp. 76–81, 1972.

[446] A. G. Rouse and M. H. Schieber, "Condition-dependent neural dimensions progressively shift during reach to grasp," *Cell reports*, vol. 25, no. 11, pp. 3158–3168, 2018.

[447] J. D. Semedo, A. Zandvakili, C. K. Machens, M. Y. Byron, and A. Kohn, "Cortical areas interact through a communication subspace," *Neuron*, vol. 102, no. 1, pp. 249–259, 2019.

[448] P. A. Yushkevich, J. Piven, H. Cody Hazlett, R. Gimpel Smith, S. Ho, J. C. Gee, and G. Gerig, "User-guided 3D active contour segmentation of anatomical structures: Significantly improved efficiency and reliability," *Neuroimage*, vol. 31, no. 3, pp. 1116–1128, 2006.